INAUGURAL – DISSERTATION

zur
Erlangung der Doktorwürde
der Naturwissenschaftlich – Mathematischen
Gesamtfakultät
der Ruprecht – Karls – Universität
Heidelberg

Vorgelegt von
Diplom-Geowissenschaftler Bastian Baecker
aus Bonn – Bad Godesberg

Tag der mündlichen Prüfung: 14. April 2014

Thema

Primordial and other noble gases in micrometeorites

Gutachter: Prof. Dr. Mario Trieloff

              PD Dr. Ulrich Ott

Zusammenfassung

Die vorliegende Arbeit, die im Rahmen des DFG (Deutsche Forschungsgemeinschaft) SPP (Special Priority Program) 1385 "*The First 10 Million Years of the Solar System - a Planetary Materials Approach*" angefertigt wurde, befasst sich mit dem Edelgasgehalt von Mikrometeoriten (MMs) (50µm - 1mm) und deren isotopischer Zusammensetzung. Dabei wurden insbesondere die Gemeinsamkeiten und Unterschiede von MMs zu Meteoriten untersucht. Auch der Einfluss der Erdatmosphäre auf das Edelgasbudget beim Durchgang der MMs war von Interesse. Bei den Untersuchungen lag der Schwerpunkt auf dem Edelgas Xenon in ungeschmolzenen MMs. Dazu musste eine Spezialausführung des Edelgas-Massenspektrometer (MS) "Noblesse" der Firma Nu Instruments in Betrieb genommen, betreut und die Messmethoden optimiert werden. Das spezielle an diesem Gerät ist das Ionenzähl-Multikollektorsystem zum empfindlichen Nachweis sehr geringer Edelgasmengen. Weltweit existiert nur ein einziges weiteres Gerät dieser Art, an der Washington University, St. Louis (USA), wo unter anderem damit die Sonnenwind-Edelgase der Genesis-Mission bestimmt wurden. Die Promotion wurde seit April 2010 am Max-Planck-Institut für Chemie in Zusammenarbeit mit der Universität Heidelberg durchgeführt.

Zwei verschiedene Gruppen von Mikrometeoriten wurden untersucht. Zum einen MMs, gesammelt aus einer geologischen Falle des Miller Butte Bergrückens im Bereich des transantarktischen Gebirges. Diese Mikrometeorite wurden von Luigi Folco, Pierre Rochette und Kollegen in einer PNRA Mission aufgefunden (siehe Rochette et al. (2008)). Die MMs sind recht groß (250 - 1000 µm), teilweise zeigen sie Verwitterung und lagerten dort vermutlich für ca. 1 Ma. Im Oktober 2010 wurden in freundlicher Zusammenarbeit von Luigi Folco, Carole Cordier und Matthias van Ginneken 103 Partikel von insgesamt 51 Mikrometeoriten (MMs) für die Edelgasmessungen zur Verfügung gestellt. Diese MMs setzten sich aus 3 Hauptgruppen zusammen - "Cosmic Spherules - CS" (mehr oder weniger Glaskugeln, die durch vollständiges Aufschmelzen von umgeschmolzenen MMs entstanden sind), "scoriaceous MMs - ScMMs" (teilweise aufgeschmolzene, schlackenartige MMs) und "unmelted MMs - UnMMs" (ungeschmolzene MMs). Die Aufschmelzprozesse sind durch den Eintritt und Durchtritt dieser kleinen extraterrestrischen Partikel durch unsere Erdatmosphäre verursacht.

Die zweite Gruppe von MMs stammt aus dem Schnee des zentralen Bereiches der Antarktis (Dome C (DC) - CONCORDIA Collection (siehe Duprat et al. (2007)) und von Cap Prudhomme (CP) (Maurette et al. (1991)). Diese wurden durch Schmelzen von Schnee extrahiert und gesammelt. Sie sind besonders klein, lagerten nur kurze Zeit (ein paar Jahrzehnte) und sind somit "frisch" und relativ unverwittert. Im November 2010 wurden Proben dieser MMs von Jean Duprat, Cécile Engrand und Michel Maurette (Universität von Paris-Süd, am Campus in Orsay, Frankreich) zur Verfügung gestellt, insgesamt 50 MM Partikel aus 28 verschiedenen MMs. Darunter waren kristalline (Xtal), feinkörnig-umgeschmolzene und kohlige (FgC) sowie teilweise aufgeschmolzene (Sc) Mikrometeorite.

Vor den Messungen an den Mikrometeoriten wurden zunächst Testmessungen mit kleinen Partikeln von größeren Meteoriten durchgeführt.. Die Gase wurden aus den MMs mit einem 30W - CO_2-Laser schrittweise entgast. Meist reichte eine Leistung von ~1 Watt für eine vollständige Entgasung aus. Die extrahierten Edelgase wurden an einer mit Aktivkohle gefüllten Kühlfalle in He+Ne, Ar, Kr und Xe-Fraktionen getrennt, die dann sukzessive in das Massenspektrometer eingelassen und analysiert wurden. Die Probenmessungen wurden durch "Blank"-Messungen und Kalibrationsmessungen ergänzt.

Insgesamt wurden 29 Partikel von 25 verschiedenen TAM MMs und 11 Partikel von insgesamt 10 verschiedenen DC und CP MMs gemessen. Für die meisten Partikel konnten für eine Messung hinreichende Edelgasmengen extrahiert werden. Jedoch zeigten insbesondere die sehr stark aufgeschmolzenen "Cosmic Spherules" und einige der weniger aufgeschmolzenen "scoriaceous MMs" deutliche Anzeichen von Entgasungsprozessen, wahrscheinlich durch die Wechselwirkung mit der Erdatmosphäre. Die MMs von Dome C und Cap Prudhomme waren sehr klein, aber die überwiegende Mehrheit dieser Proben zeigt im Vergleich zu den TAM MMs hohe Edelgas-Konzentrationen.

Gemessene ^{3}He/^{4}HeVerhältnisse lagen zwischen 0.9 x 10^{-4} und 149 x 10^{-4} für die TAM MMs und zwischen 3 x 10^{-4} und 50 x 10^{-4} für die MMs von DC und CP, teilweise allerdings mit großen Unsicherheiten. Ein Teil der TAM UnMMs und die DC MMs zeigten eine Zusammensetzung im Bereich zwischen Sonnenwind (SW) und fraktioniertem Sonnenwind ("FSW"). Der andere (etwas zahlreichere) Teil zeigte deutliche Anzeichen von für kosmogenes Helium.

Auch in Neon zeigten die meisten Un- und ScMMs deutliche Anzeichen von (fraktioniertem) Sonnenwind sowie spallogene Anteile, letzteres insbesondere in den TAM MMs 45c.29, 45b.17 und 45b.08. Hier, nicht überraschend, zeigen insbesondere die CS und ScMMs deutliche Spuren von aufgenommener Erdatmosphäre. Die höchsten gemessenen Konzentrationen für solares ^{20}Ne in den TAM MMs wurden im UnMM X1 gemessen (~3.5 x 10^{-6} cc/g), im Falle der MMs von DC und CP war dies DC 06_09_149 mit ~8.0 x 10^{-5} cc/g. Die DC Werte liegen dabei im Rahmen dessen, was für Dome Fuji MMs von Osawa and Nagao (2002) gefunden wurde. Die Werte für die TAM MMs liegen deutlich niedriger.

Die Tatsache dass die meisten MMs, sowohl TAM als auch DC/CP, ^{40}Ar/^{36}Ar-Verhältnisse deutlich niedriger als in Luft (^{40}Ar/^{36}Ar = 298.56; Lee et al. (2006)) zeigen, deutet darauf hin, dass sie extraterrestrisches primordiales Ar enthalten. Luft-Kontaminationen war zwar nachweisbar, aber außer für ^{40}Ar meist vernachlässigbar. Das niedrigste ^{40}Ar/^{36}Ar-Verhältnis wurde für den TAM-Mikrometeoriten UnMM 45c.33(1) mit 2.0 ± 1.8 gefunden. Der nächstniedrige Wert, mit wesentlich kleinerer Messunsicherheit, ist der des TAM MM 45c.35(3), mit 4.1 ± 0.1. Zusammen mit dem ^{38}Ar/^{36}Ar Verhältnis von 0.185 ± 0.002 weist dies auf einen hohen Anteil der planetaren Komponente "Q(P1)" hin, welche in den höchsten Konzentrationen in kohligen Chondriten gefunden wird. Ähnliches gilt für den kristallinen Dome C MM DC 06_09_149 (^{40}Ar/^{36}Ar = 5.62, ^{38}Ar/^{36}Ar = 0.186).

Krypton in extraterrestrischen Proben zeigt üblicherweise nur geringe Variationen in seiner Isotopenzusammensetzung und reine Kr Auswertungen sind anspruchsvoll. Dennoch zeigten sich insbesondere im Zusammenhang mit den

Ergebnissen für Argon und Xenon Interpretationsmöglichkeiten. Deutlich erkennbar sind Hinweise auf Element- und Isotopenfraktionierung, die durch Prozesse beim Durchgang durch die Erdatmosphäre und Verwitterung auf der Erde verursacht sind. Deutlich sichtbar werden die Effekte in kombinierten Element- oder Isotopenplots von Ar, Kr und Xe. Insbesondere zeigt eine Reihe von MMs korrelierte Isotopenfraktionierungseffekte in Kr und Xe. Die ungeschmolzenen UnMMs hingegen zeigen Edelgaszusammensetzungen die ähnlich zu Q(P1) sind. Einige wenige MMs zeigen einen solaren Einfluss nicht nur bei Helium und Neon, sondern auch bei Ar - insbesondere beim TAM UnMM X1 sowie einer Reihe von DC MMs.

Das Hauptaugenmerk bei den Messungen wurde auf Xenon gelegt. Zum einen bietet das MS "Noblesse" gute Möglichkeiten Xe in geringen Mengen empfindlich zu messen und zum anderen wurde Xe bisher in Mikrometeoriten nur unzureichend gemessen. Die Messungen in dieser Arbeit stellen einen wesentlichen Fortschritt gegenüber den früheren Messungen von Osawa and Nagao (2002) dar. Von den 29 TAM MM Partikeln konnte Xenon für 24 Partikel (wenn auch teilweise und insbesondere bei den leichten Xe Isotopen mit großen Messunsicherheiten) analysiert werden. UnMM 45c.35(3), mit ~1.1 x 10^{-8} cc STP/g, zeigte hierbei die höchste ^{132}Xe Konzentration. Die höchste Konzentration für DC und CP MMs wurde in DC 06_09_189, mit ~1.7 x 10^{-7} cc STP/g gefunden. Insgesamt lag die Xe Konzentration aber sowohl bei den TAM MMs als auch den DC und CP MMs auf ähnlichem Niveau.

Zwei deutlich voneinander verschiedene Gruppierungen sind vorhanden. Eine Gruppe zeigt Xe mit einer Isotopenzusammensetzung ähnlich der der Q(P1)-Komponente. Hierzu gehören meistens die UnMMs. Die andere Gruppe zeigt Xe Verhältnisse ähnlich zu Xe isotopisch fraktioniertem Luft-Xe. Eine MM-Probe ist besonders und deutlich verschieden von allen anderen - 45c.29. Die zwei gemessenen Partikel dieses MMs zeigen in allen Edelgasverhältnissen (unterschiedlich) erhöhte spallogene Anteile. Ebenso enthält dieses MM Spalt-Xenon aus dem Zerfall von ^{244}Pu. Die vermutliche Herkunft (Mutterkörper) dieses MMs konnte bisher sowohl durch die Edelgas- als auch durch petrologische und mineralogische Untersuchungen nicht aufgeklärt werden und benötigt weitere Erforschung.

Insbesondere für die beiden MMs 45c.29 und 45b.17 konnten mit Hilfe des Gehaltes an spallogenem ^{21}Ne zum Teil sehr lange kosmogene Bestrahlungsalter (~9-71Ma) errechnet werden. Über spallogenes ^{38}Ar ergab sich ein Bereich von ~5-186 Ma. Die Mehrzahl der TAM MMs zeigen allerdings kosmische Strahlungsalter von weniger als 1 Ma Jahre. Bei den MMs von DC und CP waren kosmogene Anteile auf Grund der hohen Konzentrationen an solarem Neon und solarem / primordialem Ar nicht nachzuweisen. Daneben muss man berücksichtigen, dass ein Großteil der MMs beim Durchtritt durch die Erdatmosphäre Verluste, insbesondere der leichteren Edelgase He und Ne, erfahren haben kann.

Mikrometeorite lassen sich auf der Erde in großen Zahlen, in verschiedensten mineralogischen Zusammensetzungen und Größen sowie in den verschiedensten Klimazonen auffinden - sicherlich am besten im Bereich von Eis und Schnee. Viele MMs zeigen Alteration, Verwitterung und Interaktion mit der Erdatmosphäre an. Daneben gibt es aber auch manche, die nahezu unverändert sind und das komplette

Spektrum an extraterrestrischen Komponenten zeigen. Die in dieser Arbeit erhaltenen Ergebnisse zeigen, dass die Untersuchung dieser Partikel einen Beitrag leisten kann zum Verständnis der Entstehung der Erdatmosphäre - und damit auch anderer planetarer Atmosphären. Auch können sie dabei helfen, zu verstehen, wie sich Kleinstpartikel im Sonnensystem verhalten.

Abstract

The present study, realized within the framework of the DFG (Deutsche Forschungsgemeinschaft) SPP (Special Priority Program) 1385 "*The First 10 Million Years of the Solar System - a Planetary Materials Approach*", addresses the proposition of analyzing micrometeorites (MMs) (sizes of 50µm - 1mm) on their noble gas content along with their isotopic composition. The experimental studies and the dissertation was performed at the Max-Planck-Institute for Chemistry in Mainz in collaboration with the Heidelberg University since 2010. In particular, the similarities and differences of MMs to larger meteorites were studied. Also of interest was the thermal history of MMs along with changes in their noble gas inventory while passing Earth's atmosphere. In our study we focused on xenon especially in unmelted MMs. This required the operation of a special version of a noble gas mass spectrometer (MS) which in this case was the "Noblesse" from Nu Instruments. Continuous care and optimization of the measurement methods were essential. The specialty of this device is the ion-counting multicollector system for especially high sensitivity and detection of small amounts of noble gases. Worldwide there is only one more device of this type, at Washington University, St. Louis (USA), where, among other things, the solar wind noble gases of the Genesis mission have been determined.

Two different groups of micrometeorites were examined. Firstly MMs collected from a geological trap on top of the Miller Butte ridge, in the area of the Transantarctic Mountains. These micrometeorites were spotted and collected by Luigi Folco, Pierre Rochette and colleagues during a PNRA mission (see Rochette et al. (2008)). The MMs are relatively large (250 - 1000 µm), they sometimes show weathering and were deposited for probably about 1 Ma. In October 2010, with kind cooperation of Luigi Folco, Carole Cordier and Matthias van Ginneken, 103 particles of 51 micrometeorites (MMs) were selected for the noble gas measurements. These MMs consist of the following three main groups - "Cosmic spherules - CS " (more or less glass spherules caused by complete melting of unmelted MMs), "scoriaceous MMs - ScMMs" (partially molten MMs) and "unmelted MMs - UnMMs. The melting processes are caused by the entry and passage of these small extraterrestrial particles through the Earth's atmosphere.

The second group of MMs originated from the snow of the central region of Antarctica (Dome C (DC) - CONCORDIA Collection (see Duprat et al. (2007)) and from Cap Prudhomme (CP) (Maurette et al. (1991)). These particles were extracted and collected by melting snow of the Dome C area and are particularly small. The MMs are deposited only for a short time period (a few decades), thus are "fresh" and relatively unweathered. In November 2010, samples of these MMs were provided with kind support by Jean Duprat, Cécile Engrand and Michel Maurette (University of South-Paris, on the campus in Orsay, France). We were able to acquire a total of 50 MM particles from 28 different MMs. Among them were crystalline (Xtal), fine-grained unmelted and carbonaceous (FgC) and partially molten (Sc) micrometeorites.

Before the first MM measurements were carried out, the measuring facility was tested on reliability and accuracy by using small particles of larger meteorites. We gradually degassed the MMs by using a 30W CO_2-Laser system. For a complete

degassing a power of ~1W was sufficient in most cases. After extraction, the inert gases were partitioned in He + Ne, Ar, Kr and Xe fractions. Furthermore, Ar, Kr and Xe were adsorbed at a cold trap filled with active charcoal. Then the noble gases successively were analyzed using the "Noblesse". The sample measurements were supplemented by "blank" and calibration measurements.

A total of 29 particles of 25 different TAM MMs and 11 particles of a total of 10 different DC and CP MMs were measured.

For most of the particles we were able release sufficient noble gas quantities. However, in particular the very strongly melted "Cosmic spherules " and some of the less melted "scoriaceous MMs" showed clear signs of pre-degassing, probably through the interaction with the Earth's atmosphere. The MMs of Dome C and Cap Prudhomme are very small, but, however, the vast majority of these samples shows high noble gas concentrations compared to the TAM MMs.

Measured ^{3}He/^{4}He ratios were between 0.9 x 10^{-4} and 149 x 10^{-4} for the TAM MMs and between 3 x 10^{-4} and 50 x 10^{-4} for the MMs of DC and CP, although sometimes with accompanied large uncertainties. Part of the TAM UnMMs and the DC MMs showed a composition in the range between solar wind (SW) and fractionated solar wind ("FSW"). The other (slightly more abundant) part showed - beside SW - significant signs of cosmogenic ^{3}He contributions.

Also in neon, most of the Un- and ScMMs clearly showed signs of solar wind and spallogenic contributions, the latter especially within the TAM MMs 45c.29, 45b.17 and 45b.08. Here, not surprisingly, in particular the CS and ScMMs show clear traces of Earth's atmosphere records. The highest measured concentrations for solar ^{20}Ne in the TAM MMs were measured in UnMM X1 (~3.5 x 10^{-6} cc/g), whereas in the case of MMs from DC and CP this was DC 06_09_149 with ~8.0 x 10^{-5} cc/g. The DC values are in the range of what has been found for Dome Fuji MMs measured by Osawa and Nagao (2002). The values for the TAM MMs are significantly lower.

The fact that for most TAM and DC/CP MMs the ^{40}Ar/^{36}Ar ratios are considerable lower than in air (^{40}Ar/^{36}Ar = 298.56; Lee et al. (2006)) suggests that these samples include extraterrestrial primordial Ar. Air contamination was indeed detectable, but except for ^{40}Ar usually negligible. The lowest ^{40}Ar/^{36}Ar of 2.0 ± 1.8 was found for TAM UnMM 45c.33(1). The next lowest value, with a much smaller uncertainty is that of TAM MM 45c.35(3), with 4.1 ± 0.1. In the same context the low ^{38}Ar/^{36}Ar ratio of 0.185 ± 0.002 indicates a high proportion of the planetary component "Q(P1)". This component is detected in higher concentrations in carbonaceous chondrites. The same is true for the crystalline Dome C MM DC 06_09_149 which shows ^{40}Ar/^{36}Ar = 5.62 and ^{38}Ar/^{36}Ar = 0.186.

Krypton in extraterrestrial samples typically shows only small variations in its isotopic composition and pure Kr evaluations are challenging. Nevertheless, for most of the MMs sufficient Kr-amounts were detected and particularly in association with the results for Ar and Xe interpretations are conceivable. It seems that especially isotopic fractionation processes are explainable by using combined elemental and isotopic plots of Ar, Kr and Xe. Here, isotopic fractionation processes are clearly present and often occur due to Earth atmosphere transitions of MMs, extraterrestrial radiation as well as terrestrial weathering. An example is ^{36}Ar/^{132}Xe versus ^{84}Kr/^{132}Xe,

which shows for most of the ScMMs and CS a clear indication of fractionated air. The unmelted UnMMs, however, show noble gas compositions similar to Q (P1). A few MMs indicate a solar influence not only in He and Ne, but also in Ar - especially in the case of TAM UnMM X1 as well as a number of DC MMs .

The main focus of the measurements was on xenon. On the one hand, the MS "Noblesse" gave us the opportunity to measure Xe in small quantities along with high sensitivities. On the other hand, so far, Xe has not been adequately measured within MMs. The results in this work represent a significant improvement compared to previous measurements of Osawa and Nagao (2002). Of the overall 29 TAM MMs we were able to analyze Xe for 24 particles, however, partially and in particular for the light Xe isotopes with large uncertainties. Here, UnMM 45c.35(3) shows the highest concentration of ^{132}Xe with ~1.1 x 10^{-8} cc STP/g. The highest concentration for DC and CP MMs was found in DC 06_09_189, with ~1.7 x 10^{-7} cc STP/g. Overall, however, the Xe concentration was for both, the TAM MMs as well as the DC and CP MMs, at a similar level.

Two distinct groupings are present. One group shows Xe with an isotopic composition similar to that of the Q(P1) component. This is usually true for the UnMMs. The other group shows Xe ratios similar to isotopically fractionated air Xe. A single MM sample is particularly and distinctly different of all others - 45c.29. The two measured particles of this MM show within all noble gas ratios increased, however, variable spallogenic contributions. Also, this MM contains ^{244}Pu fission Xe. The probable origin (parent body) of this MM has so far not been revealed by both the noble gas and by petrological and mineralogical studies and requires further research.

Using the detected spallogenic ^{21}Ne concentrations for the two MMs of 45c.29 and for 45b.17, we were able to calculate rather large CRE-ages of ~9-71 Ma. Cosmogenic ^{38}Ar, on the other hand, revealed a range of ~5-186 Ma. However, the majority of TAM MMs show CRE-ages of less than 1 Ma. The cosmogenic contents in MMs of DC and CP were negligible due to the high levels of solar neon and solar / primordial Ar. In addition, one must consider that the specimens may have lost a large proportion of their original trapped inventory during passage through the Earth's atmosphere, especially concerning the lighter noble gases He and Ne.

On Earth, micrometeorites are explored in large numbers, located in a variety of mineralogical compositions as well as sizes and in different climatic regions - certainly the best region would be those of ice and snow. Many MMs show alteration and weathering effects along with signs for interaction with the Earth's atmosphere. However, there exist some specimens, which are virtually unchanged and show the complete spectrum of extraterrestrial components. The results obtained in this work show that the investigation of these particles may contribute to the understanding of the origin of Earth's atmosphere - and thus also of other planetary atmospheres. Furthermore micrometeorites may also help to understand how tiny particles behave and evolve in the solar system.

List of Figures

List of Tables

Abbreviations

a	years
AGB-stars	asymptotic giant stars
A	ampere
amu	atomic mass unit
Ar	argon
AU	astronomical unit
b.d.l.	below detection limit
BSE mode	Back-scattered electron mode
°C	degree Celsius
C	coulomb
CAIs	calcium-aluminum-rich inclusion
cc STP	cubic centimeter at standard temperature and pressure
CEM	channel electron multiplier
cm	centimeter
cps	counts per second
CRE	cosmic ray exposure age
CS	Cosmic Spherule
CSNSM	Centre de Spectrométrie Nucléaire et de Spectrométrie de Masse
e.g.	for example (exempli gratia)
EMMA	Early Micrometeorite Accretion
EPMA	electron micro probe analyzer
Fig.	figure
FWHM	full width at half maximum
g	gram
Ga	giga years
GCR	galactic cosmic radiation

He	helium
IDPs	interplanetary dust particles
i.e.	that is (id est)
Ka	kilo years
km	kilometer
Kr	krypton
kV	kilovolt
Laser	Light Amplification by Stimulated Emission of Radiation
LDEF	Long Duration Exposure Facility
LSA	Laser and Separation Area
m/z	mass to charge ratio
mA	milliampere
Ma	million years
mbar	millibar
mg	milligram
mm	millimeter
MNA	Museo Nazionale dell'Antartide
MORBs	mid-ocean-ridge basalt
Mohm	milliohm
MPIC	Max-Planck-Institute for Chemistry
MS	mass spectrometer
N	"Noblesse"
n.a.	not available
Ne	neon
NWA	Northwest Africa
OC	ordinary chondrite
OIB	ocean island basalt
PNRA	Programma Nazionale delle Ricerche in Antartide

ppm	parts per million
RGB-stars	red giant branch stars
s	seconds
ScMM	scoriaceous micrometeorite
SCR	solar cosmic radiation
SEM	secondary electron microscopy
SEP	solar energetic particles
SiC	silicon carbide
SIMS	secondary ion mass spectrometry
SPWW	South Pole Water Well
STP	Standard temperature and pressure
SW	solar wind
Tab.	Table
TAM	Transantarctic Mountains
TEM	transmission electron microscopy
TW	Terawatt
UnMM	unmelted micrometeorite
V	volt
Vol. %	volume percent
Xe	xenon
μg	microgram
μm	micrometer
μW	microwatt
Ω	ohm

Acknowledgements

I am indebted and grateful to my supervisor PD Dr. habil. Ulrich Ott for giving me the opportunity to work in this unique noble gas project and for the use of the excellent infrastructure of the cosmochemistry group of the Max-Planck-Institute for Chemistry (MPIC) in Mainz, for his support, long-lasting helpful suggestions and numerous discussions in completion of this research work

Furthermore I am deeply thankful to my supervisor Professor Mario Trieloff of the Heidelberg University, for giving me his advice, support and scientific discussions always appreciated.

My sincere thank you goes to Carole Cordier, Luigi Folco and Matthias van Ginneken from the Museo Nazionale dell'Antartide (MNA), University of Siena, Italy, for providing me with precious Transantarctic Mountain micrometeorite samples and introducing me into the secrets of micrometeorites petrology and the continues support which is greatly appreciated.

Many thanks to Jean Duprat, Cecile Engrand and Michelle Maurette from the Centre de Spectrométrie Nucléaire et de Spectrométrie de Masse (CSNSM), Orsay, France, for providing me with the "fresh" and tiny micrometeorite samples from the Central Antarctic snow and from Cap Prudhomme along with precious knowledge concerning these samples.

I would like to express further deepest thanks to the scientific and technical staff of the cosmochemistry group of the MPIC, Siegfried Herrmann, Christa Sudek and Reinhard Haubold and to the scientific staff of the Institute of Earth Sciences at Heidelberg University for help and encouragement in conducting my work.

Many thanks to Carolyn Crow for her several helpful suggestions, corrections and discussions.

I would like to acknowledge the instant, that this thesis is part of the DFG (Deutsche Forschungsgemeinschaft) project through the SPP (Special Priority Program) 1385 (Project OT 171/5-1).

Further I want to thank Jan Leitner as well as many friends and colleagues for helpful discussions and support.

I want to express my deepest gratitude to my sister Miriam and my brother Oliver for always helping me.

My sincere thanks go to my beloved girlfriend Julia Cartwright, who always stood behind me and gave me encouragement in finalizing this work. Many thanks!

Finally like to dedicate this work to my parents Ingo and Ilse Baecker to whom I owe a lot - I am deeply thankful for everything you ever did for me - thank you!

Contents

Chapter 5 - Micrometeorites from the Transantarctic Mountains (TAM) - Noble gases show indications for multiple populations

Chapter 1 - Motivation

The topic of this thesis is the investigation of noble gases, with special focus on Xenon, in micrometeorites (MMs) recovered at different locations in Antarctica (for details see chapter 4).

As pointed out by Maurette et al. (2000) as well as Osawa and Nagao (2002), micrometeorites - for which the main flux onto Earth peaks at about 220 µm in diameter (Fig.1) (Love and Brownlee (1993)) - may have made an important contribution to the noble gas budget of Earth's atmosphere and the resulting noble gas isotopic composition. Love and Brownlee (1993) derived a total mass influx accreted by Earth of 40 (± 20) 10^6 kg per year based on a study of hypervelocity impact craters on the LDEF (Long Duration Exposure Facility) spacecraft. However, reevaluation by Cremonese et al. (2012) suggests, while the size distribution is similar, lower total mass influx rates of 7.4 (± 1.0) 10^6 kg per year (if the source is mostly asteroidal) or 4.2 (± 0.5) 10^6 (for predominantly cometary matter) (see Fig. 1). The large amount of these small particles combined with a huge variability of mineralogical composition in the MMs makes it worthwhile to study these small particles.

The diversity of MMs and the possible number of different sources for micrometeorites is huge, e.g. MMs from planets, planetoids, asteroids, comets and smaller solar objects from near and far e.g. Genge (1998). To be able to classify micrometeorites it is necessary to study their individual elemental, isotopic and textural compositions (e.g. Genge et al. (2008)); from this one may also be able to establish connection to larger meteorites and their classifications (e.g. Wasson (1974), Bischoff (2001) and Weisberg et al. (2006)).

While the first detailed analyses suggested a dominant connection to CM-chondrite-like material (Kurat et al. (1994); Engrand and Maurette (1998)), this diversity has become more obvious with later investigations. For example, Taylor et al. (2007), Cordier et al. (2010) and Cordier et al. (2012) were able to identify cosmic spherules linked to a vestoid origin. Duprat et al. (2010) identified extremely carbon-rich "ultra-carbonaceous micrometeorites" with large deuterium excesses. Even chondrules have been detected (Genge et al. (2005)). Finally Yada et al. (2008) - maybe not unexpectedly - identified pre-solar grains in MMs. Together, these results provide not only evidence for the extraterrestrial origin of MMs, but also indicate that some compositional parts of MMs must have been formed prior to the solar system.

Little noble gas and petrological research on micrometeorites has been performed before the 1980s. This changed with the development of improved methods of investigation affording higher sensitivity and diagnostical levels. Concerning noble gases, these are rare and in extraterrestrial materials usually are present in a variety of "components". Some are trapped, while others, such as radiogenic and cosmogenic components, are produced in situ (for further information refer to chapter 3.2). Early work on MMs focused mainly on helium and neon with the results showing these to be abundant and showing predominantly solar-wind components, e.g. Amari and Ozima (1985), Amari and Ozima (1988), Olinger (1990), Olinger et al. (1990), Stuart et al. (1999), Wieler (2002b). So far there have been only

a few reports of xenon isotopic measurements on MMs e.g. Osawa et al. (2000) and Osawa and Nagao (2002), however due to large analytical errors the results are not diagnostic. At the MPIC Mainz we have initiated a comprehensive survey about the noble gas content in micrometeorites and hope to fill especially the gap of lacking diagnostic xenon results.

The main goals of my research during my PhD thesis have been:

1) The determination of noble gas contents - helium (He), neon (Ne), argon (Ar), krypton (Kr) and xenon (Xe) - and isotopic compositions in micrometeorites (MMs) - with the focus particularly on Xe.

2) Set up, maintain and improve the measurement procedures of the new high sensitivity mass spectrometer "Noblesse", with multiple ion-counting, from Nu Instruments.

3) Investigate differences and similarities between MMs and their larger relatives - meteorites.

4) Gain information whether / how noble gases in MMs were influenced during passage through the Earth's atmosphere by atmospheric entry heating.
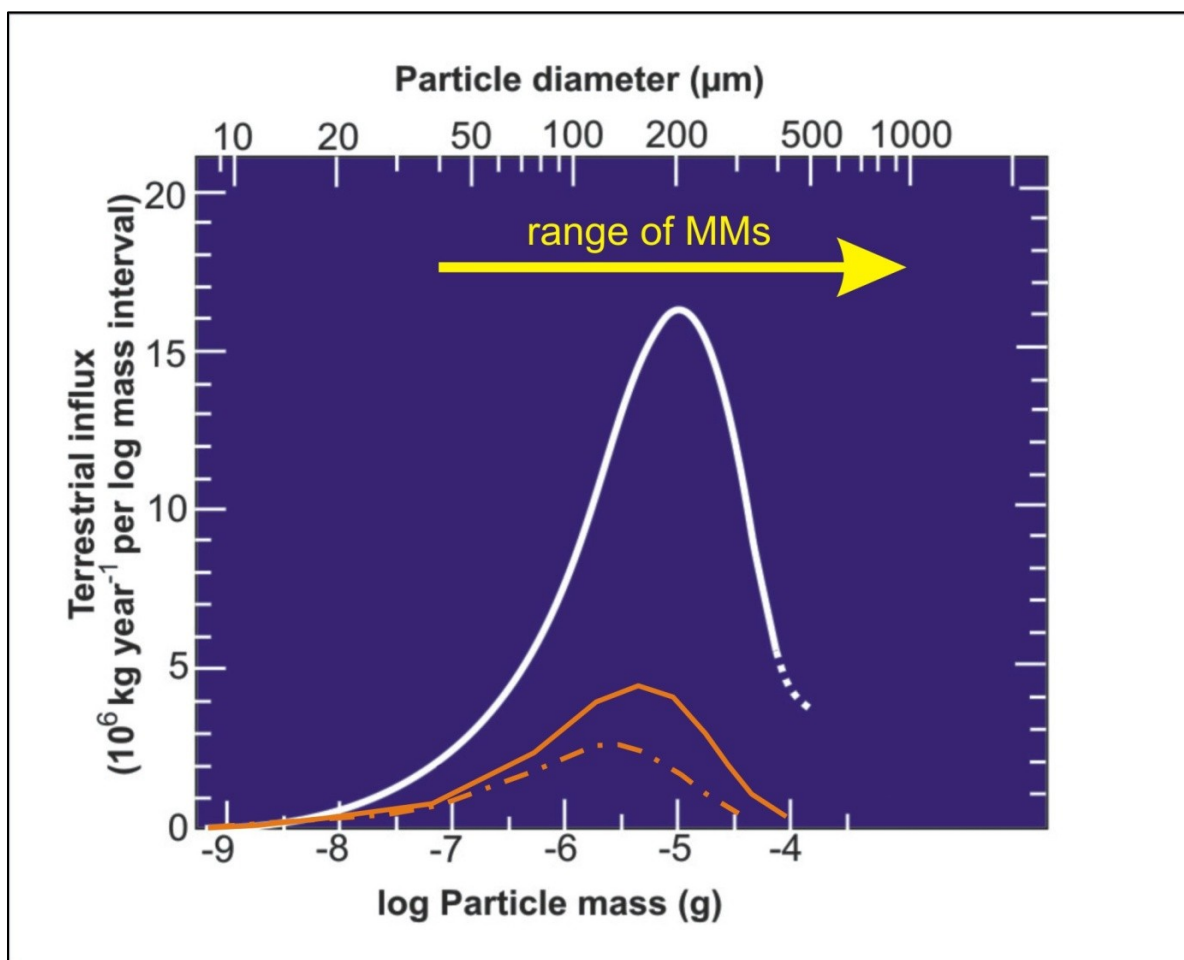
Figure 1. Diagram showing the mass of MMs yearly accreted by the Earth per log mass interval. The white line points out the terrestrial influx estimated by Love and Brownlee (1993). Re-evaluation by Cremonese et al. (2012) suggests similar particle mass distribution but less mass influx per year. The orange line shows their result for the case that the matter influx is primarily of asteroidal origin. The orange dash-dotted line shows the alternative case of cometary matter. After Love and Brownlee (1993) and Cremonese et al. (2012).

Chapter 2 - Introduction

Analyzing meteorites has been a challenge for decades. Various techniques (e.g. wet-chemistry, optical microscopy, thin sections, SEM (secondary electron microscopy), TEM (transmission electron microscopy), electron microprobe, oxygen isotope analyses, noble gas mass spectrometry, ionprobe or SIMS (secondary ion mass spectrometry), and many more, are available and well suited to unravel their mysteries. Since the late 1950s meteorites got in the focus in terms of detailed extraterrestrial matter research. Numerous types and classes were distinguished and examined e.g. Wasson (1974), Bischoff (2001) and Weisberg et al. (2006) - classification of meteorites; Urey and Craig (1953) and Van Schmus and Wood (1967) - subgroups and classification of chondrites; Wiik (1956) and Kallemeyn and Wasson (1981) - differentiation of carbonaceous chondrites; Kallemeyn et al. (1989) - compositions of ordinary chondrites; Wasson and Kimbeblin (1967) and Scott and Wasson (1975) - classification of iron meteorites.

In the 1950s also micrometeorites came into focus as material from which to gain information about how small sized extraterrestrial matter interacts with the Earth's atmosphere (e.g. Whipple (1949), Whipple (1950), Whipple (1951)). According to this and later research, e.g. Fraundorf et al. (1980), parameters like entry-angle, velocity, speed, weight and size of the small particles play a major role during atmospheric entry. Rietmeijer et al. (1986) showed that micrometeorites could be a damaging threat to satellites due to small scale impacts.

Since mid of the 1980s research on MMs has become an essential tool in determining to what extent small particles like MMs and IDPs (interplanetary dust particles) influenced and are still influencing the formation and exchange of solar system matter (planets, planetoids, asteroids and comets). A second question that was addressed was how the accreted matter changed atmospheric compositions and the surfaces through impacting and also to which extent MMs have been involved in the formation of prebiotics and the first organic molecules on Earth (e.g. Brownlee (1985), Maurette et al. (1995) and Maurette et al. (2000)).

Among others the measurement of noble gas components in meteorites is being used to gain information about the formation, origin and composition of the solar system. In the same context it is also of importance to obtain information about the current status of the solar system and its planetary, asteroidial and cometary bodies. Meteoritic material is found on Earth in many different sizes, shapes and compositions (chemical, mineralogical and petrological). Micrometeorites (< 1mm) give the opportunity to expand the knowledge from the study of the larger meteorites, with sizes from ~1mm up to m-sizes. Not only their high abundance and availability makes the MMs interesting. It is also the fact that some of them contain especially fragile, highly primitive material. For example, there is no match among the known macroscopic meteorites to the ultra-carbon-rich MMs found by Duprat et al. (2010). Also, the abundance of pre-solar materials appears to be higher in IDPs than in the most primitive meteorites (e.g. Messenger et al. (2007), Busemann et al. (2009), and Nguyen and Messenger (2011)). Thus, detailed and extended study of the population of small extraterrestrial particles promises to give new, exciting insights into the formation of the early solar system.

2.1 Solar system formation and small particles

In the field of cosmochemistry the formation of the solar system is an important research field. Since most (macroscopic) matter in the solar system formed through certain processes like particle collision, particle condensation and heating / cooling involving small sized grains, it is of importance to link the small particles (e.g. IDPs and MMs) to the big picture.

Most likely our solar system formed out of molecular cloud which suffered a gravitational collapse and with it the formation of our sun (Boss and Goswami (2006)). Clayton (1984) showed how in principle nearly everything in space and with it in our solar system is linked to star formation and nucleosynthesis (Fig. 2). The latest ^{207}Pb–^{206}Pb dating of CAIs (calcium-aluminum-rich inclusions) from the NWA 2364 meteorite (CV3-group) by Bouvier and Wadhwa (2010) suggest a solar system age of 4568.2 million years.

Figure 2. Chart showing the importance of stars and stellar formations in astrophysics and cosmochemistry. The evolution of stars plays an important role in the formation of (our) solar system(s). Without nucleosynthesis and material derived from supernovae a molecular cloud formation and subsequent solar system formation might not be possible. The red dotted line indicates the influence of solar wind on meteorite material and shows that still and in future the solar wind will be implanted on the surface of planetary bodies, planetoids, moons, asteroids, comets and meteoroids. The red dotted lines with a question mark should implicate the importance of meteoritic material in the development of atmospheres and maybe also life in the early Earth history (after Clayton (1984)).

Boss and Goswami (2006) and Montmerle et al. (2006) describe the first part of Solar System evolution as a probably rapid and chaotic event. With time the formation processes slowed down and the Solar System structure became more and

more stable. According to Montmerle et al. (2006) three main stages occurred in the evolution of the solar system:

- *The stellar era* (the first million years - the initial formation of the Sun by accreting material from a circumstellar disk)
- *The disk era* (the first ten million years - the initial formation of planets along with an ongoing disintegration of the circumstellar disk)
- *The "telluric" era* (the first hundred million years - formation of terrestrial-like planets - rocky planet(s) formed with oceans and atmospheres)

Zeilik et al. (1998), among others, discuss the composition of the collapsing nebula and conclude that it must have seen similar to the one our central star has today - mostly hydrogen and a bit of helium. These elements were already exclusively (hydrogen) and mostly (helium) formed when the universe started to exist - during big bang nucleosynthesis, together with a bit of lithium (Fields and Olive (2006)). Heavier elements were present during Solar System formation, accounting for approximately two percent of the solar nebula by mass. Older star cycles ending with supernovae events mostly created these heavier elements through stellar nucleosynthesis (Clayton (1984), Zeilik et al. (1998)).

According to Boss and Goswami (2006) and Montmerle et al. (2006) the masses of the molecular clouds in general range between several solar masses up to more than 10^6 solar masses. Obviously molecular clouds of this size would be able to form million of stars, on the other they normally do not tend to do so (Montmerle et al. (2006)). As this author points out, a possible explanation lies in a gravitational equilibrium which balances gravitation and internal pressure. Presumably due to turbulences in small volumes of the cloud they are eventually able to collapse and form stars (Boss and Goswami (2006) and Montmerle et al. (2006)).

Another important aspect is the possible star formation due to molecular cloud collapse triggered by supernovae shock front events or strong protostellar outflows (see Preibisch and Zinnecker (1999) and Boss and Goswami (2006)). Cameron and Truran (1977) and Boss and Vanhala (2000) explain that short-lived radionuclides (e.g. ^{26}Al), which existed in the early solar nebula, were likely to be formed and injected into the early solar nebula through a supernovae which then triggered a cloud collapse.

Hartquist and Williams (1995) explain how minerals were formed through condensation. First was the formation of high temperature condensates, then successive minerals with lower condensation temperatures formed. Through the ongoing mineralization of the early solar nebula also mineral associations were molded (Hartquist and Williams (1995)).

Montmerle et al. (2006) summarize that after about 1 million years the solar system has a stable configuration and a nearly fully formed central star. They show that the most important time in planet formation is within the *disk era*. Through collision and accretion processes dust particles of submicron size form larger aggregates and somehow in ongoing direct contacts planetesimals of about 10 km in size (Goldreich and Ward (1973)).

The larger the planetesimals became, the higher the gravitational effects between these bodies occurred (Montmerle et al. (2006)). With time the larger planetary bodies grew faster than the smaller ones due to a higher gravitation and a higher collision rate, which is called "runaway growth" (Greenberg et al. (1978) and Chambers (2005)). After millions of years the accretion of material onto the solid cores slowed down. Presumably the outer solar system provided more solid material (water and ice) for the planet formation than the inner solar system did (Chambers (2003)). Hence, the development of larger planetary bodies with a higher gravitation was possible and the formation of the giant gas planets was initiated (Chambers (2003)). For several millions of years gas from the surrounding nebula was accumulated around the planetary bodies and collapsed onto the protoplanets as soon as their masses reached about 20 to 30 Earth masses (M_E) (Montmerle et al. (2006)). However, the systematics of the formation of the giant gas planets is still not fully revealed and understood.

At the stage of the giant gas planet formation, the inner solar system presumably contained planetoid like embryos with sizes from Lunar to Mars (Chambers and Wetherill (1998)). As soon as Jupiter and Saturn reached their final masses, the situation in the inner solar system became much more chaotic (Montmerle et al. (2006)). Several embryonic planetoids and already small differentiated planets collided with each other and formed larger bodies which in the end formed the terrestrial planets and their moons within the inner solar system (Chambers (2003)). Between the inner and the outer solar system, or today between Mars and Jupiter, the main asteroid belt stayed behind. This formation phase continued about 100 million years (Montmerle et al. (2006)). However, also the formation of the terrestrial planets is not fully understood.

Meteorites play an important role in formulating ideas of how the solar system formed. The mineral composition of meteorites makes it possible to obtain knowledge of estimated individual ages and processes leading to planetesimal formation. Among others, CAIs (calcium-aluminum-rich inclusions - components made out of calcium, aluminum and titanium silicates and oxides) containing high temperature mineral phases (condensation temperatures of about and less than 1800 K) and clasts like chondrules (e.g. MacPherson (2003)). According to Amelin et al. (2002) the CAI formation has an age of 4567.2 ± 0.6 million years (measured in CAIs of the CV chondrite Efremovka e.g. Ahrens et al. (1973)) and chondrule formation an age of 4564.7 ± 0.6 million years (measured in chondrules from the CR chondrite Acfer 059 e.g. Endress et al. (1992)). Achondrites were formed presumably through planetary differentiation and mostly have younger ages than chondrites (Montmerle et al. (2006)). In the case of iron meteorites it is not fully revealed whether they are younger and/or older than chondrites. Recent results by Kruijer et al. (2012) suggests that magmatic iron meteorites (IIAB, IIIAB and IVA) were formed during core formation only about 1 to 1.5 Ma after CAI formation. They would in this case have an older age than chondrites.

Since the formation of our solar system, gravitational collision processes played a major role in formation of planetary bodies and planetesimals (see e.g. Chambers (2003)). Following, among others, Anders (1971) and Maurette (2006)

also meteorites and extraterrestrial dust (e.g. MMs, IDPs) are formed through ablation of material from comets and collisions between asteroidal bodies.

Overall, processes during solar system formation and further history led to uncountable small particles, which then were incorporated into planetary material, got destroyed by the sun due to the Poynting-Robertson effect and disappeared from the solar system due to radiation pressure. Most of the small sized particles we analyze today are originated from and were incorporated beforehand in planetary or asteroidean bodies (see also chapter 3.1.2). These dust particles can derive from multiple sources e.g. comets, asteroids, meteoroids, planetoids, moons, planets and multiple distances e.g. Mars-Jupiter main asteroid belt (Krasinsky et al. (2002)), Edgeworth-Kuiper belt (Stern and Colwell (1997)), Oort cloud (Dones et al. (2004)) or probably even to a small extent from all the "empty" spaces in between these extraterrestrial matter accumulating zones.

When a small micro- to millimeter sized object reaches the Earth's atmosphere, it depends - in a simplistic view - on its density, speed, entry-angle and velocity whether and to which degree it gets heated and molten (Love and Brownlee (1994)). Love and Brownlee (1994) presented peak atmospheric temperatures for particles from 2 to 50 µm in diameter and initial speeds from 10 to 25 km/s. Assuming a particle of about 50 µm in diameter and a velocity of 10 km/s, with an entry angle of 45º and a density of 2.0 g/cm^3 the particle would reach a peak temperature of about 980 ºC (Love and Brownlee (1994)). With a velocity of 14 km/s it would already be 1350 ºC (Love and Brownlee (1994)). Taking this model in consideration, it is quite likely that MMs with high velocities and sizes above 50 µm could get fully molten, degassed and form molten droplets, which is different to normal cm to m-sized meteorites. These fully molten droplets are generally called Cosmic Spherules (CS) (see chapter 3.1.4 and e.g. Genge et al. (2008)).

Chapter 3 - State of research

Chapter 3 shall give an overview about various kinds of research that have been performed or are currently being performed, which are related to micrometeorites.

3.1 Micrometeorites (MMs)

Generally micrometeorites are µm-sized (about 30-1000 µm in diameter) extraterrestrial dust particles captured by the Earth (Genge et al. (2008)). Several groups (e.g. Maurette et al. (1991), Taylor et al. (1998), Yada et al. (2005), Duprat et al. (2007), Rochette et al. (2008)) collected MM samples from Antarctica. Although there are places on Earth were MMs have been found (see chapter 3.1.3) it seems that MMs collected from Antarctica and there especially from snow and ice are best preserved against terrestrial contamination and weathering effects (Maurette et al. (2000), Duprat et al. (2007)). It is widely assumed and accepted that MMs derive mostly from asteroids and comets (see Kurat et al. (1994), Maurette (2006), Genge et al. (2008)). Of particular interest in our context is the suggestion by Maurette et al. (2000) that MMs may have possibly made a significant contribution to the volatile inventory of the Earth. Overall the composition of most MMs is similar, but not identical, to CM and CR chondrites, as concluded by Kurat et al. (1994). Duprat et al. (2007) added that MMs in the case of the CONCORDIA collection have similarities to CI chondrites - especially due to their high Fe content.

3.1.1 History

One of the first mentions of the term "micrometeorites" was described by Whipple (1949). However, the first magnetic presumably extraterrestrial spherules were reported in deep-sea sediments by Murray et al. (1891). In 1962/63 some micrometeorite particles could successfully be recovered, using a recoverable sounding rocket, by Soberman et al. (1963), Hemenway et al. (1963) and Soberman and Hemenway (1963). However, the reported particle sizes of up to about 1 µm in Hemenway et al. (1963) suggest that these particles are IDPs (interplanetary dust particles) or fragments of micrometeorites, instead of full sized micrometeorites (50-1000 µm; see e.g. Love and Brownlee (1993)). Marvin and Einaudi (1967) were able to collect cosmic spherules from beach sands. In the beginning of MM research the focus on these small particles was not on mineralogical or petrological properties or noble gases, but on their collection, atmospheric entry velocities, atmospheric interaction and heating (e.g. Fraundorf et al. (1980)). MMs as impactors on lunar rocks and space crafts have been discussed as well e.g. Neukum et al. (1970), Hörz et al. (1971), Nagel et al. (1976), Schramm et al. (1985), Rietmeijer et al. (1986), Schneider (1986).

In the beginning and during the 1980s several research teams began to understand the importance of cosmic dust and micrometeorites in the context to our solar system, and the formation of atmospheres and environments - especially at the time when the Earth atmosphere formed e.g. Brownlee (1979), Fraundorf et al. (1980), Brownlee et al. (1982), Raisbeck and Yiou (1987), Flynn and McKay (1988), Schramm et al. (1989). Brownlee (1985) reviewed the importance of small dust

particles (< 1mm) and pointed out that abundance and friability of this material makes it more than necessary to have a closer look at them. He pointed out that most fragile material is not able to survive passage through the Earth's atmosphere as bigger size and higher mass objects. On the other hand, small friable dust particles are able to survive the atmospheric entry (Brownlee, 1985). Overall Brownlee (1985) clarified that in his opinion the amount, variability and the fast release and evolution of dust from parent bodies gives a better understanding about the distribution of meteoritic matter in the solar system - much better than big meteorites alone could tell.

First noble gas measurements on small μm sized sediment particles and micrometeorites were performed by Olinger (1990) (solar noble gases), Olinger et al. (1990) (Ne only) and Sarda et al. (1991) (He, Ne, Ar, Kr and Xe). Schramm et al. (1989), Beckerling et al. (1992), Presper et al. (1993) and Kurat et al. (1994) focused on the elemental composition, mineralogy and chemistry of micrometeorites. The first large sample set of Antarctic micrometeorites was collected and reported by Maurette et al. (1991), who some years late discussed the relationship of MMs to the formation of Earth's early atmosphere and the generation of the first prebiotic molecules (Maurette et al. (1995)). A systematic research on micrometeorites was started by Genge et al. (1996a). With the possibility of analyzing more and more samples of every small size by using high sensitivity instruments, research on micrometeorites increased further at the end of the 1990s. Stuart et al. (1999) analyzed MMs for their helium content using laser extraction, while Osawa et al. (2000) started the first major noble gas measurements on individual micrometeorites collected from the Dome Fuji Station in Antarctica. Two years later Osawa and Nagao (2002) presented a full range of noble gas results (He to Xe) on numerous Antarctic MMs from the Dome Fuji Station. Dai et al. (2002) analyzed small sized particles (IDPs, MMs and meteorites) on their nano-diamond content. Kehm et al. (2002) initiated combined noble gas and trace element measurements on IDPs, whereas Marty et al. (2002) focused on nitrogen and noble gas isotopes. Besides collections by other groups (e.g. Nakamura et al. (1999), Rochette et al. (2008)) very fresh and unaltered micrometeorites - the CONCORDIA collection, Dome C, Antarctica - could recently be recovered by Duprat et al. (2007) (see chapter 4.1.2). In addition, a huge amount of Antarctic MMs could be collected by Rochette et al. (2008) from the Transantarctic Mountain (TAM) region (see chapter 4.1.1). Maurette (2006) speculated about a connection between micrometeorites, the formation of the Earth's early atmosphere (EMMA - Early Micrometeorite Accretion), climatic effects, the origin of organics to form life on Earth and possible parent bodies. Genge et al. (2008) published a detailed research paper about the classification of micrometeorites (see also chapter 3.1.4). Recent publications reported - to name but a few - oxygen isotopic ratios in cosmic spherules (Suavet et al. (2009)), parent body identification of MMs using oxygen isotopic analysis (Suavet et al. (2010)), cosmic spherules from Vesta-like asteroids (Cordier et al. (2010)), investigations about ultra-carbonaceous Antarctic MMs (Dobrică et al. (2010)), noble gases in L chondrite like MMs recovered from Ordovician rocks (Meier et al. (2010)), HED-like cosmic spherules from TAM (Cordier et al. (2012)), analyses of MMs with chondritic origin from TAM (van Ginneken et al. (2012)) and the effects of atmospheric entry heating on the noble gas and nitrogen content of micrometeorites (Füri et al. (2013)). Particular useful for the current work is

the recent re-assessment of production rates for cosmogenic nuclides in small particles (Trappitsch and Leya (2013)).

3.1.2 Sources in the solar system

There are several possible sources for meteorites and MMs. Processes - which form meteoroids (when fallen and found on Earth: meteorites) in the inner solar system - occur mainly in the asteroid belt between Jupiter and Mars (see e.g. Morbidelli and Gladman (1998), Vokrouhlický and Farinella (2000), Heck et al. (2004)). Ongoing collisions between these bodies and cratering on these bodies form new meteoroids (e.g. Greenberg and Chapman (1983)). In addition, according to Stern and Colwell (1997) also solar system bodies and objects from beyond Neptune's orbit can reach the inner solar system and the Earth's atmosphere - e.g. periodic comets with eccentric orbits and objects from the Kuiper belt (also Edgeworth-Kuiper belt) (refer to Stern and Colwell (1997)). Even objects from the Oort cloud, which has a several hundred times higher distance than the Kuiper belt (Levison et al. (2002)), may enter the inner solar system. Given the fact that MMs are small particles and very abundant it appears likely that they derive from several different parent body sources, however, the main sources should be asteroids and comets (e.g. Genge (1998)). In addition, planets and planetoids are possible sources as well (see e.g. Gounelle et al. (2009), Cordier et al. (2012)). Impacts of meteorites onto surfaces of planets, moons, planetary bodies, asteroids and comets could lead to ejected MM material of various types (e.g. regolithic, crust material or even mantle material), depending on the depth of penetration, which likely is controlled by the size, velocity, density, mass and impact angle of the impactor (e.g. Melosh (1984), Vokrouhlický and Farinella (2000)). However, the mechanisms and parent body sources for MM production are not fully revealed so far. These newly formed MM particles would travel - or to be more precise - be dragged, by gravitational forces and/or the Poynting-Robertson effect (e.g. Robertson (1937), Whipple and Wyatt (1949), Dohnanyi (1978), Klačka (1992)), eventually crossing Earth's orbit. Finally, unless collected by Earth or other planetary bodies, these small MM particles would be dragged further into the inner solar system and in the end fall into the sun.

3.1.3 Sample locations on Earth and in the Earth atmosphere

Collecting micrometeorite samples on Earth is not easy. According to Hemenway et al. (1963) already before the 1960s several attempts (ground-level, mountain-tops, high altitude aircrafts, balloons) had been started to recover MMs from the Earth atmosphere, however, they were plagued by too strong contamination with terrestrial particles and thus were unsuccessful. One of the first successfully accomplished MM sample return missions was reported by Hemenway et al. (1963) who used a recoverable sounding rocket. Since then and especially since beginning of the 1980s the variety of samples which could successfully be collected rose (see chapter 3.1.1 and references therein). Brownlee (1985) explains how MMs are directly collected in Earth's atmosphere by a NASA U2 aircraft. Basically any Earth air- and spacecraft which suffers bombardment can be used as a MM collector (Genge (1998)). Today several places on Earth have been identified as being suitable micrometeorite sampling locations (see Table 1). All these areas are far away from civilization and quite difficult to reach. These are among others: deep-sea sediments, glacier lake deposits, glacier ice and snow (refer to e.g. Harvey and Maurette (1991), Rochette et al. (2008) and references therein, as well as Table 1).

Table 1. Locations of some recent micrometeorite findings with main MM type and references.

Location	Environment	Main type reported (see Fig. 3)	References
Mid-Pacific abyssal	Deep-sea sediments/clay	Cosmic Spherules (CS)	*Blanchard et al. (1980)*
Greenland ice cap	Glacial deposits, "blue lakes"	Unmelted, scoriaceous and melted MMs (CS)	*Maurette et al. (1987)*
Beardmore glacier area, Transantarctic Mountains, Antarctica	Glacial till	Cosmic Spherules (CS)	*Koeberl et al. (1989)*
Cap Prudhomme, Antarctica	Blue ice	Unmelted, scoriaceous and melted MMs (CS)	*Maurette et al. (1991)*
Walcott Névé, Antarctica	Blue ice, glacial deposits	Unmelted, scoriaceous and melted MMs (CS)	*Harvey and Maurette (1991)*
South Pole water well (SPWW), Scott–Amundsen station, Antarctica	Subsurface water well	Mostly Cosmic Spherules (CS), some unmelted and scoriaceous MMs	*Taylor et al. (1998); Taylor et al. (2000)*
Dome Fuji Station, Antarctica	Water tank	Mostly scoriaceous and melted MMs (CS), some unmelted MMs	*Nakamura et al. (1999)*
Yamato Meteroite Ice Field	Blue ice	Unmelted, scoriaceous and melted MMs (CS)	*Yada and Kojima (2000)*
Bare ice region near Syowa Station, Antarctica	Blue ice	Unmelted, scoriaceous and melted MMs (CS	*Iwata and Imae (2002)*
Dome C CONCORDIA Station, Central Antarctica	Snow	Unmelted, scoriaceous and melted MMs (CS)	*Duprat et al. (2007)*
Miller Butte & Frontier Mountain, Transantarctic Mountains, Antarctica	Mountain top; Glacier eroded surface; Autochthonous Glacier deposits	Mostly Cosmic Spherules (CS), some unmelted and scoriaceous MMs	*Rochette et al. (2008)*
Novaya Zemlya glacier	Glacial deposits	Unmelted, scoriaceous and melted MMs (CS)	*Badjukov et al. (2010)*
Central Indian Ocean Basin	Deep-sea sediments	Cosmic Spherules (CS)	*Rudraswami et al. (2011)*

3.1.4 Classification

First of all it is important to point out when and why a small particle can be considered extraterrestrial, i.e. a micrometeorite. As explained in e.g. Genge et al. (2008), a definitive proof for the extraterrestrial parentage is given if the particle shows the presence of reaction products with the cosmic radiation, i.e. cosmogenic noble gas isotopes (see below) or cosmogenic radionuclides (see also Raisbeck and Yiou (1987) and Raisbeck and Yiou (1989)).

Genge et al. (2008) lists some important additional criteria for an extraterrestrial origin that can be used if isotopic analyses are lacking:

i. A partial or full magnetite rim must surround the MM (see Toppani et al. (2001))

ii. Fe-metal with Ni-content should become apparent (Genge et al. (2008))

iii. The composition of the MM should comprise major and minor elements suggesting a chondritic origin (Genge et al. (2008))

iv. If applicable the MM should contain high CaO and Cr_2O_3 olivines combined with FeO-poor olivines which are almost never seen in terrestrial rocks (see Brearley and Jones (1998))

v. If heating occurred to the MM surface it should be consistent with atmospheric entry mechanisms (Genge et al. (2008). However, even using isotopic analyses it might be difficult to distinguish in between these patterns within MMs.

vi. The morphology of the particle could be spherical - however, Genge et al. (2008) point out that several other extraterrestrial and terrestrial sources could be the origin of grains with a spherical shape e.g. impact spherules, meteorite ablation spheres, anthropogenic produced spherules and volcanic glass spherules (see Genge et al. (2008))

One important aspect of MM classification is the extent to which the Earth atmosphere has been interfering with them during their passage through it (see chapter 2). Most of the MMs are rather small (µm-size), but still large, heavy and dense enough to possess a high velocity and kinetic energy while encountering the Earth atmosphere (see e.g. Fraundorf et al. (1980) and Brownlee (1985)). This leads to more or less strong heating and degassing during atmosphere entry. Some MMs in fact seem to acquire terrestrial noble gas patterns which is discussed in chapter 7.

Classifications of different MM types and findings were performed by several authors and groups (e.g. Maurette et al. (1991), Kurat et al. (1994), Taylor et al. (1998), Duprat et al. (2007), Genge et al. (2008)). Generally micrometeorites can be mineralogically divided into several groups, classes and subclasses which are shown in Fig. 3.

In the scheme of Genge et al. (2008) spherical melted droplets forming MMs are called **Cosmic Spherules (CS).** These have been more or less completely molten and heated. Cosmic Spherules bear some relict grains (barred olivine, porphyritic olivine or similar). Others are completely glassy (Genge et al. (2008)). Some MMs have seen already heating on their parent body. Therefore, as Genge et al. (2008) point out, it is not always straightforward to distinguish between those two types of primary and secondary heating. Fig. 3 shows three different types of CS - **S**, **G** and **I** which are suggested by Genge et al. (2008).

- **S-type Cosmic Spherules** are separated in several sub-groups (see Fig. 3) and show different textures which are supposed to go hand in hand with their suffered atmospheric peak temperature. According to Genge et al. (2008) they are the most abundant type analyzed so far. S-type CS are **silicate rich** (S = silicate), and exhibit a chondritic composition. In agreement with this, Taylor et al. (2000) obtained data for about 1600 CS from the South Pole Water Well (SPWW) and the silicate type S accounted for 97 %. A special case are the CAT-spherules which are - similar to the CAIs - rich in Ca, Al and Ti and possess an average Mg/Si ratio of ~1.42 (see Tab. 3a in Taylor et al. (2000)). For a more detailed description see Genge et al. (2008) and references therein.

- **I-type Cosmic Spherules** are **iron rich** (I = iron) with a high amount of FeO, which is mineralogical represented by the iron oxides wüstite ($Fe^{2+}O$) and magnetite ($Fe^{2+}Fe^{3+}_2O_4$), with fewer amounts of other oxides like MgO and SiO_2. Also Ni-rich Fe-metal is observable. For a more detailed description see Genge et al. (2008) and references therein.

- **G-type Cosmic Spherules** are dominated by a **glassy** mesostasis (G = glass) of Si-rich glass and by magnetite dendrites. They are supposed to represent an intermediate type between the iron-rich I-type and the chondritic like S-type. For a more detailed description refer to Genge et al. (2008) and references therein.

According to Genge et al. (2008) the next group is that of the partially melted or **scoriaceous MMs (ScMMs)**. These MMs are characterized for have been less heated and still have a higher portion of relict minerals, grains and matrix left. An important indication for scoriaceous MMs are vacuoles which often can be seen in thin sections. Some important characteristic features are (Genge et al. (2008)):

- ScMMs are on the one hand vesicular and smooth, but on the other hand irregular particles. They are dominated by a mesostasis of fayalitic olivine microphenocrysts within glass (Genge et al. (2008)).

- Scoriaceous MMs often contain relict minerals and relict matrix areas. These relict minerals contain higher amounts of Mg-rich pyroxenes and olivines (Genge et al. (2008)).

- These partial melted particles represent a gradational group between the Cosmic Spherules and the unmelted MMs (Genge et al. (2008))

- Depending on from which kind of unmelted MM (fine-grained or coarse grained - see Fig. 3) the ScMM derives before atmospheric heating occurred; it is called a fine-grained or coarse-grained ScMM (see Genge et al. (2008)).

Due to expected higher noble gas amounts, the **unmelted MMs (UnMMs)** are the most important group for the research performed in this study (see results in chapter 5, 6, 7 and the appendix). Here fine-grained MMs can be found beside coarse grained ones and the much less common refractory and ultra-carbonaceous MMs (see Genge et al. (2008) and Fig. 3).

- Genge et al. (2008) describes unmelted MMs as mostly chondritic particles with an elemental composition near that of the matrices of CI, CM and CR chondrites (see also Kurat et al. (1994), Genge et al. (1997) and Duprat et al. (2007)).

- According to Genge et al. (2008) **fine grained UnMMs (FgMMs)** can be characterized by the presence of micrometer sized mineral particles which sit in a fine-grained and porous groundmass.

- Furthermore fine grained UnMMs are separated in the types C1, C2, and C3 (see Fig. 3 and Table 1 in Genge et al. (2008)).
  - **C1**: Compact and chemically homogenous plus surrounding magnetite (Genge et al. (2008)).
  - **C2**: Compact and chemically heterogeneous plus contain isolated silicates (Genge et al. (2008)).
  - **C3**: Very porous FgMMs containing isolated silicates plus surrounding magnetite (Genge et al. (2008)).

- Following Genge et al. (2008) **coarse-grained UnMMs (CgMMs)** consist of grains with sizes above one micrometer and possess anhydrous silicates (mostly pyroxenes). Visible are also igneous textures containing olivines and pyroxenes, often in a glassy mesostasis.

- Concerning the CgMMs, Genge et al. (2008) distinguishes between chondritic and achondritic types. The chondritic type includes several subtypes which are named porphyritic olivines/pyroxenes, granular olivines/pyroxenes, barred olivines, radiate pyroxenes and Type I CgMMs (reduced, with Mg-rich olivines/pyroxenes containing Fs and Fa <10 mol%) and Type II CgMMs (oxidized, with Fe-rich olivines/pyroxenes containing Fs and Fa >10 mol%). The Type I and Type II systematic for CgMMs is similar to the one used for the characterization of Type I and Type II chondrules (Grossman et al. (1988)). In this context it has to be mentioned that Fs is forsterite (Mg_2SiO_4) and Fa is fayalite (Fe_2SiO_4), which are endmembers in the solid olivine series. The achondritic type shows igneous and differentiated CgMMs – see Fig. 3, Genge et al. (2008) and references therein for further detailed information.

- There are two other classes of UnMMs (Genge et al. (2008)): On the one hand the **refractory MMs** (separated into porous, compact and hydrated), which are dominated by refractory minerals, and on the other hand the **ultracarbonaceous MMs** which are characterized as to possess high amounts of carbon (more than in CI chondrites) (see Nakamura et al. (2005), Dobrică et al. (2012) and Floss et al. (2012)).
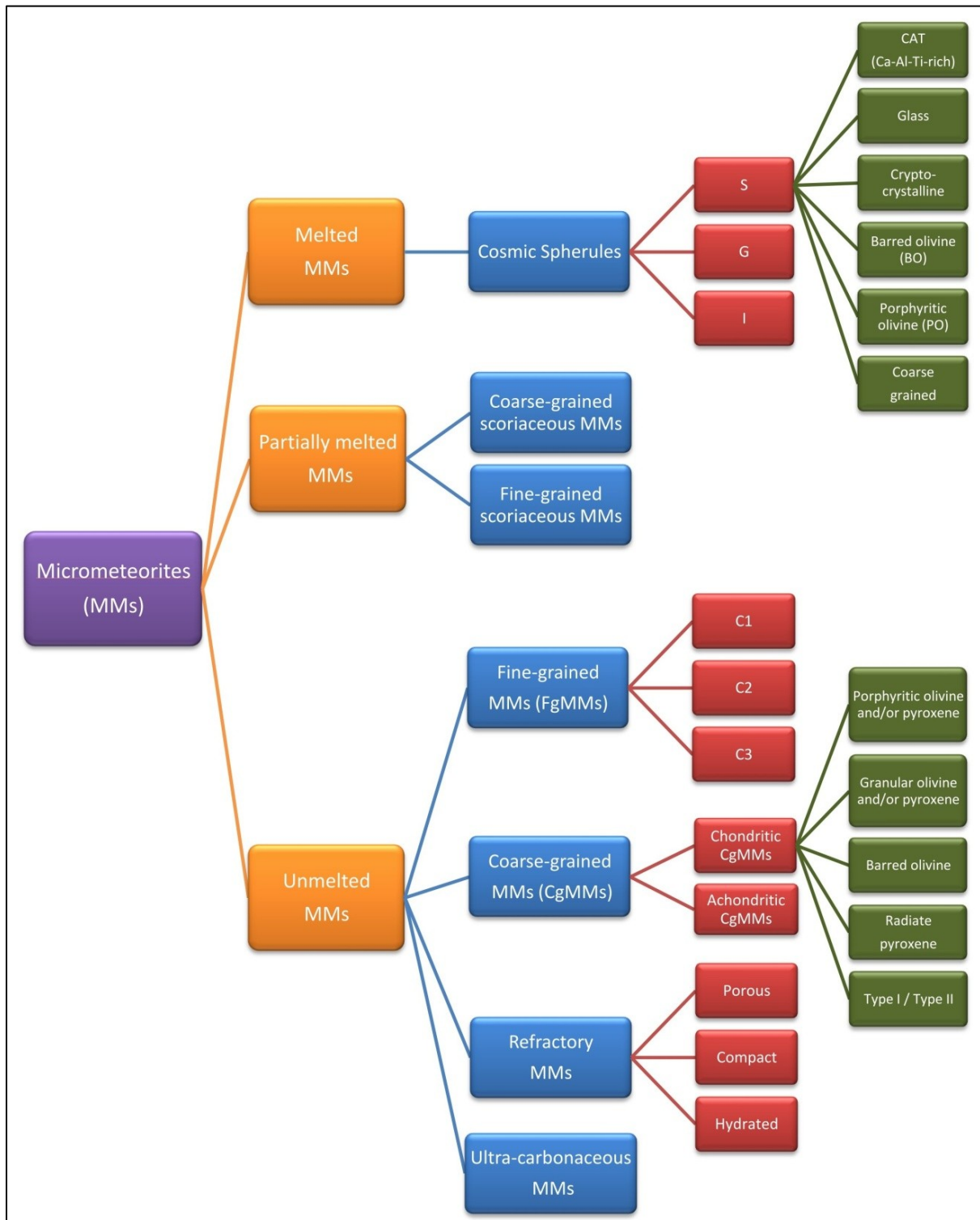
Figure 3. The classification of micrometeorites. Basically there are three different types of micrometeorites - melted MMs (Cosmic Spherules - CS), partially melted MMs (scoriaceous MMs) and unmelted MMs. For explanations see chapter 3.1.4 (after Genge et al. (2008))

3.2 Noble gases

The following two subchapters shall give an overview on noble gases in meteorites and a brief review of noble gas analyses which have already been performed on MM material. It will be clarified which components are supposed to be found and from where they are believed to originate.

3.2.1 Noble gases in meteoritic material - an overview

The noble gases are the elements He (helium), Ne (neon), Ar (argon), Kr (krypton), Xe (xenon) and Rn (radon). Radon is the only noble gas which is radioactive. In the late 19th century William Ramsay and colleagues were able to detect He, later Ar and then Ne, Kr and Xe (Ozima and Podosek (2002)). Rn was discovered by E. Dorn in 1900 (Partington (1957)).

Noble gases are chemically inert in the sense that they have much weaker chemical interactions between each other and with other elements – more or less not more than van-der-Waals forces (e.g. Ozima and Podosek (2002)). They are also rare in the inventories of the Earth and the other terrestrial planets (Ozima and Podosek (2002)). Because of their inertness and resulting little interaction with solid phases they partitioned to a very small extent into and are depleted in any kind of solid mineral phase - on Earth, the terrestrial planets and also the meteorites (Ozima and Podosek (2002)). In the solar system overall noble gases are not rare at all, however. The Sun inhabits most of the matter in the solar system and was able to reserve all volatile elements and with it a huge amount of noble gases (Wieler (2002b)). Solar system abundances of, beside others elements, noble gases can be reviewed in Lodders (2003).

Noble gases in meteorites can be divided into different components – that are either trapped components or in-situ components (see e.g. Ozima and Podosek (2002)).

3.2.1.1 Trapped components (primordial noble gases)

      a. Solar Wind (SW)
      b. Planetary
      c. Presolar
      d. Terrestrial planets

This subchapter shall give an overview about trapped components (also known as primordial noble gases - see Fig. 4), which generally are noble gas components embedded and implanted into meteoritic matter and extraterrestrial bodies (e.g. Swindle (1988)). Table 2 and Table 3 give an overview about the most important trapped components and their associated isotopic compositions in meteoritic matter (see also e.g. Ott (2002)).

Table 2. Isotopic compositions of **He to Kr** in different important trapped components.

Component	$\frac{^3He}{^4He}$ [$* 10^{-4}$]	$\frac{^{20}Ne}{^{22}Ne}$	$\frac{^{21}Ne}{^{22}Ne}$	$\frac{^{36}Ar}{^{38}Ar}$	$\frac{^{86}Kr}{^{84}Kr}$	References
SW	4.645 (8)	13.777 (10)	0.03289 (7)	5.470 (3)	0.3012 (4)	[1, 2, 15]
SW (Fast)	4.478 (11)	13.703 (14)	0.03282 (12)	5.451 (4)	--	[2]
SW (Slow)	4.768 (9)	13.818 (13)	0.03297 (8)	5.479 (3)	--	[2]
"FSW"[#]	2.17 (5) 2.16-2.60	11.2 (2)	0.0295 (5)	4.87 (5) 4.85-5.10	0.3132 (15) 0.3205 (20)	[13, 14]
subsolar*	~2.1	~11.65	--	5.46 (4)	0.3073 (17)	[3, 4]
ureilite*	--	10.70 (25) 10.4 (3)	--	5.26 (6)	0.3091 (12)	[5] [6]
R (Ne-E(L))*	--	< 0.01	< 0.0001	--	--	[7]
G *	--	< 0.1	< 0.0015	--	0.454 - 1.176	[8]
HL*	1.70 (10)	8.500 (57)	0.036 (1)	4.41 (6)	0.3623 (18)	[9, 10]
P3 *	≤ 1.35 (10)	8.910 (57)	0.029 (1)	5.26 (3)	0.3128 (6)	[9, 10]
Q (P1)*	1.23 (2) - 1.59 (4)	10.05 (5) - 10.70 (20)	0.0294 (10)	5.34 (2)	0.3095 (5)	[11, 12]

Uncertainties in the last digits for the SW, "FSW", subsolar, ureilite, HL, P3 and Q (P1) components are given in parentheses.

References: [1] Heber et al. (2009); [2] Heber et al. (2012); [3] Busemann et al. (2001b); [4] Crabb and Anders (1981) in Ott (2002); [5] Göbel et al. (1978) in Ott (2002); [6] Ott et al. (1985) in Ott (2002); [7] Amari et al. (1995) in Ott (2002); [8] Lewis et al. (1994) in Ott (2002); [9] Huss and Lewis (1994a); [10] Huss and Lewis (1994a); re-calculated by Busemann et al. (2000); [11] Busemann et al. (2000); [12] Wieler et al. (1992); [13] Benkert et al. (1993); [14] Wieler and Baur (1994); [15] Meshik et al. (2012).

Table 3. Isotopic compositions of **Xe** in different important trapped components.

Component	$\frac{^{124}Xe}{^{132}Xe}$	$\frac{^{126}Xe}{^{132}Xe}$	$\frac{^{128}Xe}{^{132}Xe}$	$\frac{^{129}Xe}{^{132}Xe}$	$\frac{^{130}Xe}{^{132}Xe}$	$\frac{^{131}Xe}{^{132}Xe}$	$\frac{^{134}Xe}{^{132}Xe}$	$\frac{^{136}Xe}{^{132}Xe}$	Ref.
SW*	0.00492 (7)	0.00417 (9)	0.0842 (3)	1.0401 (10)	0.1649 (4)	0.8263 (13)	0.3692 (7)	0.3003 (6)	[1]
U-Xe*	0.004873	0.004201	0.08411	1.0395	0.1653	0.8243	0.3520	0.2750	[2]
"FSW"	--	--	0.0791 (15)	0.996 (7) 1.038 (4)	0.1513 (20) 0.1570 (14)	0.812 (7) 0.815 (7)	0.3841 (28) 0.3777 (19)	0.3172 (23) 0.3120 (16)	[3]
subsolar*	0.00490 (16)	0.00432 (14)	0.0843 (8)	--	0.1649 (10)	0.8301 (34)	0.3765 (25)	0.3095 (20)	[4]
ureilite*	0.00463 (6)	0.00416 (4)	0.0827 (5)	1.035 (5)	0.1627 (5)	0.8195 (13)	0.3776 (12)	0.3152 (19)	[5]
G*	≡ 0	≡ 0	0.2159 (23)	0.118 (11)	0.4826 (42)	0.1858 (117)	0.0222 (53)	≡ 0.00343	[6]
HL*	0.00833 (9)	0.00564 (8)	0.0905 (6)	1.056 (2)	0.1542 (3)	0.8457 (13)	0.6356 (13)	≡ 0.6991	[7]
P3*	0.00446 (6)	0.00400 (4)	0.0806 (2)	1.042 (4)	0.1589 (2)	0.8247 (10)	0.3767 (10)	≡ 0.3096	[7]
Q (P1)*	0.00455 (2)	0.00406 (2)	0.0822 (2)	1.042 (2)	0.1619 (3)	0.8185 (9)	0.3780 (11)	0.3164 (8)	[8]

Uncertainties in the last digits for the "FSW", subsolar, ureilite, G, HL, P3 and Q (P1) components are given in parentheses.

References: [1] Meshik et al. (2012), [2] Pepin et al. (1995), re-calculated by Ott (2002); [3] Wieler and Baur (1994); [4] Crabb and Anders (1981) in Ott (2002); [5] Göbel et al. (1978) in Ott (2002); [6] Huss and Lewis (1994a) in Ott (2002) (see text and notes at Table 5); [7] Huss and Lewis (1994a); re-calculated by Busemann et al. (2000); [8] Busemann et al. (2000).

* Additional informations to the **component carrier phases** (see also Ott (2002)): **subsolar** - in enstatite; **ureilite** (U) - in diamond & graphite in ureilites; **R** (Ne-E(L)) - in presolar graphites; **G** (Ne-E(H)), Kr-S, Xe-S - in presolar SiC; **HL** - in presolar diamonds; **P3** - in presolar diamonds; **Q** (P1) - in Q carrier phase; **U-Xe** - hypothetical, inferred component.
[#] For detailed information regarding **"FSW"** see Wieler et al. (2007).

a. Solar Wind (SW):

In a steady stream since billions of years the sun implants solar components into the surface of solar system objects. In the past it was assumed that the trapped solar component consisted of two distinct components - SW proper and "SEP" (solar energetic particles) (e.g. Black (1972a), Benkert et al. (1993), Wieler and Baur (1994)). Black (1972a) first suggested the appearance of different Ne components in lunar soils with different energetic levels. Benkert et al. (1993), using closed-system-etching (CSSE), found noble gases (He, Ne, Ar) at larger depth lunar soil, to be isotopically heavier and inferred that they were implanted deeper because of higher energy (SEP). Wieler and Baur (1994) did the same for Kr and Xe.
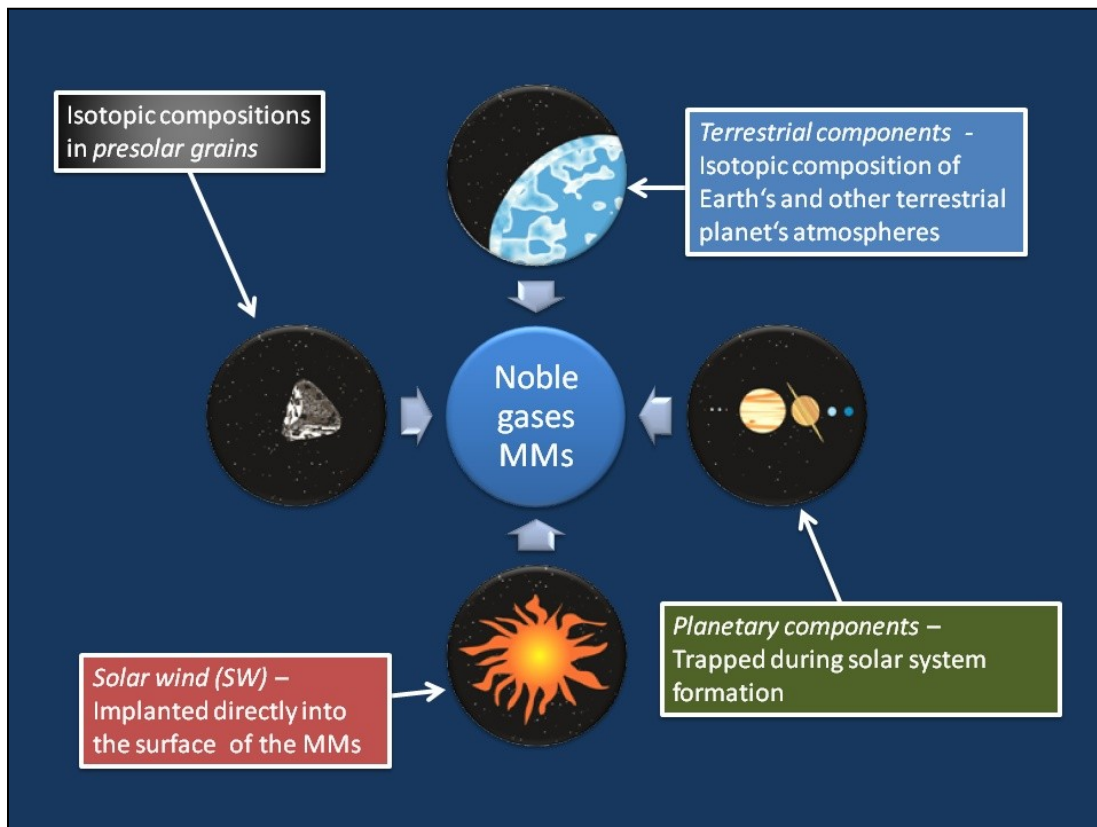
Figure 4. Trapped noble gas components in meteoritic matter (see Ott (2002)).

Results from the analysis of the targets from the Genesis mission showed however that the additional high-energy component is not needed in order to explain the isotopic variations in the implanted particles (Grimberg et al. (2006), Wieler et al. (2007)). Also, as pointed out by, e.g. Wieler et al. (2007), there exist solar energetic particles - also called SEP - which are produced during solar flares which become accelerated to higher energetic level of several MeV (mega electron-volt) per nucleon (e.g. Oetliker et al. (1997)), but their frequency is much too low to account for the implanted noble gas amounts inferred by the Black (1972a) and Benkert et al. (1993) hypothesis. For these reasons, Wieler et al. (2007) suggests to use instead of the term "SEP noble gases" the term "fractionated solar wind noble gases" (FSW) when discussing this "pseudo-component". The latest results of solar wind (SW) measurements from the Genesis mission (Heber et al. (2012)) reveals that the solar wind inhabits a mass dependent fractionation (see Table 2; fast and slow SW) relative to the composition of the Sun.

b. <u>Planetary component:</u>

Noble gases in meteoritic matter that are not of cosmogenic or radiogenic origin have traditionally been called "primordial" (see Gerling and Levskii (1956), Reynolds (1960b), Zähringer and Gentner (1960), König et al. (1961), Stauffer (1961) and Pepin and Signer (1965)). To distinguish those of solar wind origin from the others, the term "planetary" has been introduced shortly after the differences had been recognized (Signer and Suess (1963) and Pepin and Signer (1965)).

For planetary components in meteoritic material one might expect that they are primitive constituents showing the original signature from when the solar system was formed about 4.6 Ga ago (e.g. Pepin (1991)). If we assume that all matter in the solar system formed at the - more or less - same time we might also assume that all matter shows the same noble gas component inventory. But the noble gas inventories of terrestrial planets and of the meteorites show differences among each other and relative to the solar system composition due to the action of fractionation mechanisms, e.g. gravitational escape, degassing and mass-dependent adsorption (Pepin and Porcelli (2002), Pepin (2006)). As to be seen in Fig. 5, some meteoritic noble gases and terrestrial atmospheres do show qualitative similarities. However, the solar composition is completely different (Pepin (1991)).

It is not completely clear how the fractionation mechanisms in meteoritic matter leads to the different patterns of light to heavy noble gas (e.g. Ott (2002)). Expect for SW and the trapping mechanism itself, it is also not completely clarified how some of the other components formed (see e.g. Ott (2002) and references therein). Components which in the first glance appear as unique feature are maybe processed due to mixing and fractionation of multiple sources. An example is the subsolar component in some enstatite chondrites - e.g. Busemann et al. (2001b), Patzer and Schultz (2002) - which seems to occur as a mix of planetary component with a solar wind component. As evident in Fig. 5 all noble gases are depleted in the meteorites and the terrestrial planets, where the depletion of the light noble gases (He, Ne) is much more severe in comparison to the heavier noble gases (Ar, Kr and Xe) (see Pepin (2006)). As Ott (2002) discusses, different kinds of mechanisms may have been responsible for the light noble gas pattern (He, Ne) on the one side and the heavy noble gas inventory (Ar, Kr, Xe) on the other side.

The most important planetary or primordial component seems to be Q (P1) - e.g. Wieler et al. (1992), Busemann et al. (2000), Ott (2002); see also Tables 2 and 3. It is not completely revealed within which mineral phase Q (P1) exactly occurs. Ott (2002) points out that generally the Q (P1) component should have solar nebula origin and hosts most of the Ar, Kr and Xe in ordinary and carbonaceous chondrites. Other components traditionally included as minor components within the planetary gases, like R (Ne-E(L)) - Amari et al. (1995), G (Ne-E(H)) - Lewis et al. (1994), P3 and HL - both Huss and Lewis (1994a) - originate from presolar grains like SiC (silicon carbide), diamond and graphite (see Ott (2002) and references therein as well as the next paragraph). The subsolar component - found in enstatite chondrites (see Crabb and Anders (1981), Tables 2 and 3) - seems to show noble gas patterns intermediate between SW and the planetary (primordial) component.
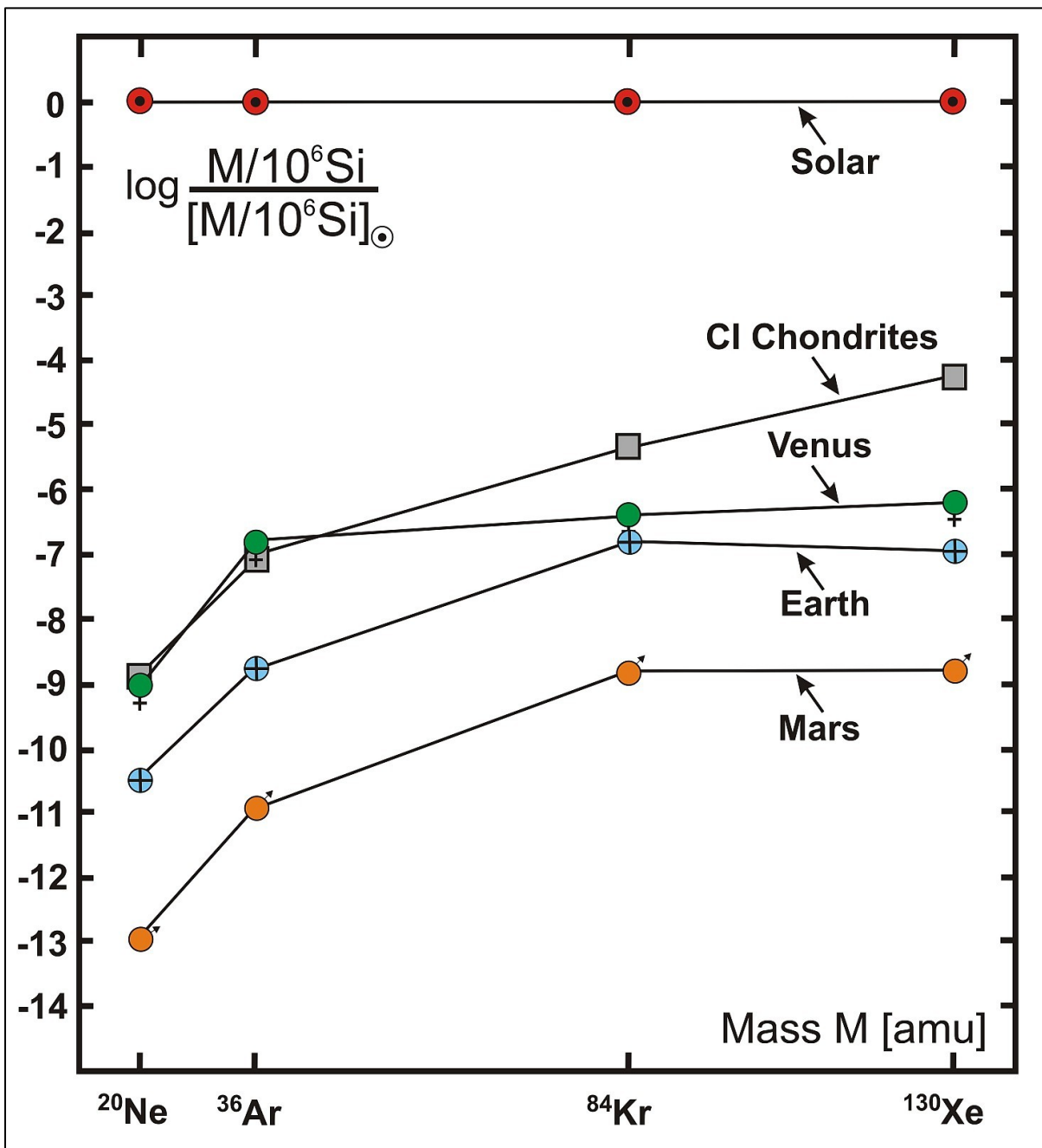
Figure 5 shows different noble gas abundances (^{20}Ne to ^{130}Xe) in the atmospheres of Mars, Earth and Venus and in CI chondrites (primitive material) in comparison to the solar contingent. Units are atoms per 10^6 Si atoms (after Pepin (2006) and references therein).

Pepin (2006) discusses the depletion of noble gas components from solar to the planetary and meteoritic sources. He assumes that this is due to different processes e.g. gravitational escape, outgassing and mass-dependent adsorption mechanisms (see Pepin (2006) and references therein).

c. <u>Presolar component:</u>

Presolar grains represent undestroyed presolar material which was imbedded into meteoritic material (see Hoppe and Zinner (2000), Bernatowicz et al. (2006)). Ott and Hoppe (2007) give - in their Table 1 - an overview about presolar grains which have been observed so far: These are diamond-, SiC-, graphite-, corundum/spinel/hibonite-, silicate-, and silicon nitride-grains. SiC grains in primitive meteorites appear to be completely of presolar origin and mostly condensate out of the wind of AGB (asymptotic giant stars) stars (Ott and Hoppe (2007)). AGB stars are part of the red giant group with higher luminosity, higher temperature and sizes of several solar masses (e.g. Lattanzio and Forestini (1999)). Furthermore Ott and Hoppe (2007) list silicate type pre-solar grains as having the highest abundance of all pre-solar grain types. Most silicate and oxide type presolar grains have their origin from condensation out of the wind of RGB (red giant branch) and presumably AGB stars (Ott and Hoppe (2007)). Presolar graphite grains seem to have a mixed origin. Some should derive from supernovae events, while others must have formed from AGB stars (see Croat et al. (2005), Ott and Hoppe (2007)). The graphite grains often show trapped noble gases with a dominating component of so called Ne-E (Black and Pepin (1969)). This component mostly consists out of ^{22}Ne which formed out of extinct ^{22}Na (Swindle (2002b)). The last group representing presolar grains is known as nanodiamonds. According to Ott and Hoppe (2007) these grains are too small to be investigated individually. Their noble gas signatures include the components Xe-HL and P3 (see Table 2 and 3). Ott and Hoppe (2007) assume that these particles or at least part of their noble gases derive from supernovae events.

d. <u>Terrestrial noble gases:</u>

The terrestrial noble gas inventory has been influenced by the Earth's planetary and atmospheric formation process over the last billions of years. Overall Earth and presumably also other planets in the solar system (e.g. Mars and Venus) show similarities to the planetary component (see Pepin (1991) and b. <u>Planetary component</u>). Also many meteorites do show a similar planetary composition (see Fig. 5).

Table 4 shows the composition and abundance of the major elements and of the noble gases including isotopic abundances in Earth's atmosphere (refer to Ozima and Podosek (2002)); Table 1.2 and 1.3). Noble gas results obtained during research on meteorites show often completely different compositions. This leads to the conclusion that fractionation processes that took place in meteoritic material and on Earth were not the same. Most important, the general view is that Earth´s noble gas inventory - and also the ones of other terrestrial planets - has a secondary origin, (Brown (1952), Ozima and Podosek (2002)) e.g. degassing of solid phases during accretion of the terrestrial planets (see also e.g. Pepin (2006)).

Clear signatures are the depletion of He and (relative) Xe in Earth's atmosphere. For the case of He there is a straightforward explanation, since it is not held by the atmosphere (see e.g. Johnson and Axford (1969); Brinkmann (1970)).

Table 4. shows combined gas data adopted from Table 1.2 and 1.3 in the compilation of Ozima and Podosek (2002) and references therein. The data gives an overview of the elemental composition (dry air) and the noble gas isotopic composition and abundance in Earth's atmosphere- EA.

Gas	Volume fraction	Isotope	Isotope ratios	Atomic abundance [%]
Dry air	1			
N_2	0.78084			
O_2	0.20948			
CO_2	3.10×10^{-4}			
He	5.24×10^{-6}	^{3}He	0.0000014	0.00014
		^{4}He	$\equiv 1$	99.99986
Ne	1.818×10^{-5}	^{20}Ne	9.80	90.5
		^{21}Ne	0.029	0.268
		^{22}Ne	$\equiv 1$	9.23
Ar	9.34×10^{-3}	^{36}Ar	$\equiv 1$	0.3364
		^{38}Ar	0.188	0.0632
		^{40}Ar	295.5	99.6
Kr	1.14×10^{-6}	^{78}Kr	0.0199	0.347
		^{80}Kr	0.1297	2.257
		^{82}Kr	0.6623	11.52
		^{83}Kr	0.6597	11.48
		^{84}Kr	3.276	57.00
		^{86}Kr	$\equiv 1$	17.40
Xe	8.7×10^{-8}	^{124}Xe	0.003537	0.0951
		^{126}Xe	0.003300	0.0887
		^{128}Xe	0.07136	1.919
		^{129}Xe	0.9832	26.44
		^{130}Xe	0.15136	4.070
		^{131}Xe	0.7890	21.22
		^{132}Xe	$\equiv 1$	26.89
		^{134}Xe	0.3879	10.430
		^{136}Xe	0.3294	8.857

The depletion of Xe in Earth's atmosphere is more puzzling and not fully understood (e.g. Ozima and Podosek (2002), Pepin (2006)). Pepin (2006) discusses various mechanisms which may have led to the depletion of different Xe isotopes e.g. fractionation by hydrodynamic escape (see chapter 5.1 and 5.2 in Pepin (2006)). During early time when the Earth was forming, the Sun was more active in the Solar System, conditions were presumably much more energy-rich and therefore loss of noble gases by this process appears possible (Porcelli et al. (2002)). Especially remarkable in this context is that the Xe isotopes are also heavily mass fractionated - the lighter ones (^{124}Xe, ^{126}Xe) are more strongly depleted than the heavier ones (see Pepin (2006)).

Pepin (2006) (like many others before him) also discusses the idea that some Xe could still be captured in Earth's interior as a phase which has not been sampled so far.

3.2.1.2 In situ components (secondary noble gases)

The in-situ components (or secondary noble gases) are formed inside the meteoritic material due to nuclear reactions like radioactive decay and cosmogenic spallation (e.g. Hohenberg et al. (1978)).

a. Radiogenic components

Radiogenic components (daughter isotopes) are formed through the decay of radioactive elements (parent isotopes) (see Table 5). The parent isotopes, like other nuclides, were formed by nucleosynthesis and like the stable ones, were integrated into meteoritic matter at the time of its formation (see e.g. Ozima and Podosek (2002) and Swindle (2002b)). Two of the radioactive parent isotopes in Table 5 (^{129}I and ^{244}Pu) are short-lived extinct nuclides which only survived the first ~100 Ma and first few hundred million years of the formation of the solar system, respectively (see Alexander et al. (1971), Podosek and Swindle (1988) and references therein).

Table 5. Compilation of radiogenic noble gases and their parent isotopes (after Porcelli et al. (2002), and references therein; as well as Ozima and Podosek (2002).

Noble gas daughter isotope	Parent isotope	Half-life	Type of decay
^{40}Ar	^{40}K	1.251 Ga	electron capture decay *
^{129}Xe	^{129}I	15.7 Ma	^{129}I/^{127}I = 1x10^{-4} at 4.56 Ga [1]
^{4}He	^{232}Th	14.01 Ga	^{232}Th $\Rightarrow$ 6α + ^{208}Pb (α-decay)
^{4}He	^{235}U	0.7038 Ga	^{235}U $\Rightarrow$ 7α + ^{207}Pb (α-decay)
^{4}He	^{238}U	4.468 Ga	^{238}U $\Rightarrow$ 8α + ^{206}Pb (α-decay)
$^{131, 132, 134, 136}$Xe	^{238}U	4.468 Ga	spontaneous fission
$^{131, 132, 134, 136}$Xe	^{244}Pu	80 Ma	spontaneous fission; ^{244}Pu/^{238}U = 0.0068 (10) at 4.56 Ga [2]

* The decay of radioactive ^{40}K is resulting in the production of ~90% of ^{40}Ca and only ~10% of ^{40}Ar (see e.g.Ozima and Podosek (2002)).
References: [1] Hohenberg et al. (1967), [2] Hudson et al. (1989)

The most important and commonly used decay systematics for age dating in meteoritic material are:

1) K/Ar (Potassium-Argon) – e.g. Jessberger et al. (1980)
2) Ar/Ar (Argon-Argon) – e.g. Kelley (2002)
3) U/Th/Pb (Uranium-Thorium-Lead) – e.g. Tera and Wasserburg (1972)
4) I/Xe (Iodine-Xenon) – e.g. Reynolds (1960a)
5) Sm/Nd (Samarium-Neodynium) – e.g. Lugmair (1974)
6) Rb/Sr (Rubidium-Strontium) – e.g. Reimold et al. (1981)
7) Lu/Hf (Lutetium-Hafnium) – e.g. Patchett et al. (2004)

b. Cosmogenic components

Cosmogenic components are formed during the process of the spallation of target atom nuclei induced by high energetic cosmic ray particles (e.g. Reedy (1981), Eugster (1988), Graf et al. (1990), Eugster et al. (1993), Ozima and Podosek (2002)). The result is a mix out of cosmogenic noble gas (most important ^{3}He, ^{21}Ne, ^{38}Ar, ^{83}Kr, ^{126}Xe) and other nuclei, which are stable or radioactive, and can be used for determining a cosmic ray exposure (CRE) age - see below (refer to chapter 5.5.2).

Table 6 gives a compilation of commonly observed cosmogenic nuclides (see Eugster et al. (2006)).
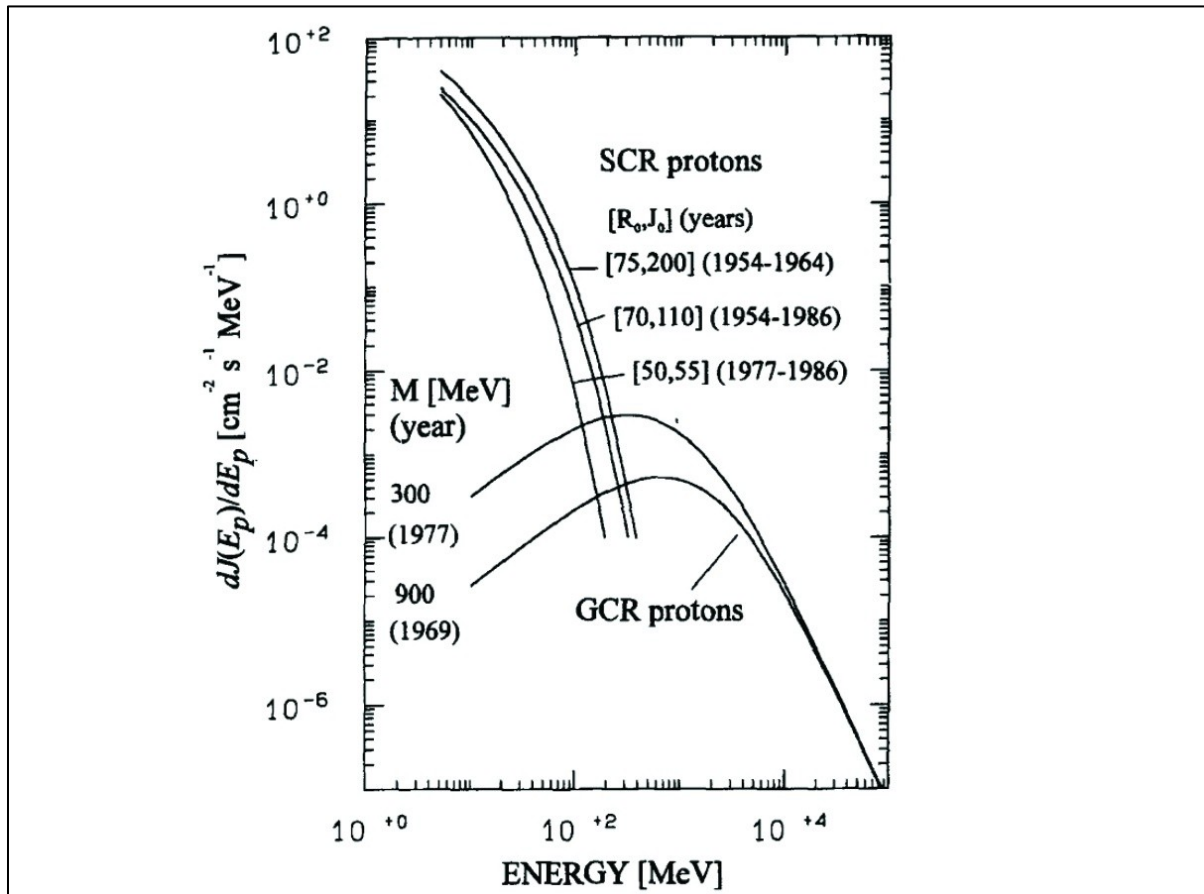
*Figure 6. Spectra of cosmic ray protons (GCR and SCR) at 1 AU adopted from Michel and Neumann (1998). Shown is the **particle flux dJ(E$_p$)/dE$_p$** in [cm^{-2}s^{-1} MeV^1] on the y-axis vs. the **energy [MeV]** on the x-axis. The GCR spectra can be described by the single parameter M [MeV], which describes the modulation of GCR particles through the solar magnetic field while entering the solar system (see Castagnoli and Lal (1980)). Two spectra are shown, one for high solar activity (1969) and one for low solar activity (1977). Average SCR spectra are shown, following Michel and Neumann (1998), for three periods. The spectra are described by two parameters, R$_0$ and J$_0$. R$_0$ is the characteristic rigidity [V], which describes the "hardness" of the spectrum, while J$_0$ is the flux density – the 4π integral flux of protons with energies > 10 MeV in cm^{-2}s^{-1} units (see McGuire and Von Rosenvinge (1984)).*

Different types of energetic particles are observable in interplanetary space (e.g. Ehmann and Kohman (1958); Reedy et al. (1983); Michel and Neumann (1998); Eugster et al. (2006) and references therein). Besides the solar wind (SW) (see chapter 3.2.1.1) it is GCR (galactic cosmic radiation) (see Gleeson and Axford (1968); Simpson (1983); Reedy (1985) and references therein) and SCR (solar cosmic radiation) (see Axford (1965); Fichtel (1971); Reedy and Arnold (1972); Goswami et al. (1988); Shea and Smart (1990) and references therein). The proton spectra of both, GCR and SCR, are shown in Fig. 6.

GCR:

The origin of GCR is discussed over decades (e.g. Dodds et al. (1975); Prantzos (2012)). GCR originate outside of the solar system and are presumably produced through supernova events (e.g. Michel and Neumann (1998) and references therein). However, while extremely high energies of $\geq 10^{15}$ eV are still consistent with a supernova shock wave acceleration mechanism, the original source and the type of acceleration is still not clearly identified (Westphal et al. (1998)). Energies of interest in the context of this work, are however, lower, in the range around 1 GeV per nucleon, where they are most abundant inside the Solar System (Fig. 6).

The GCR are comprised of on average 87% protons and 12% α-particles (Simpson (1983)), and their flux is influenced by solar activity and modulation by the solar magnetic field (Michel and Neumann (1998) and Fig. 6). The GCR flux at 1 AU (*astronomical unit - mean Earth–Sun distance: ~149.6 x 10^6 km; see e.g. Capitaine et al. (2010)*) is ~3 nuclei cm^{-2}s^{-1} and is omnidirectional (4π) (Eugster et al. (2006)).

SCR:

Solar cosmic rays, according to Michel and Neumann (1998) and references therein, are produced during higher solar activity, when the Sun emits energetic particles with about 98% protons and about 2% α-particles (Goswami et al. (1988)) – however, these values can vary and are also linked to the solar cycles. The SCR particles have much less kinetic energy than GCR particles. However, the flux is higher (Fig. 6). Generally the portion of SCR produced cosmogenic nuclides in meteorites is less than what is produced by GCR (e.g. Michel and Neumann (1998); Leya et al. (2000) and references therein).

*Table 6. Compilation of **common** cosmogenic isotopes and **main** target elements found in meteoritic matter (after Eugster et al. (2006)). Especially highlighted (in yellow) are the noble gas isotopes and their main target elements.*

Isotope	Half-life	Main target elements
^{3}H	12.26 a	O, Mg, Si, Fe
^{3}He, ^{4}He	stable	O, Mg, Si, Fe
^{10}Be	1.39 Ma *	O, Mg, Si, Fe
^{14}C	5730 a	O, Mg, Si, Fe
^{20}Ne, ^{21}Ne, ^{22}Ne	stable	Mg, Al, Si, Fe
^{22}Na	2.6 a	Mg, Al, Si, Fe
^{26}Al	717 ka	Si, Al, Fe
^{36}Ar, ^{38}Ar	stable	Fe, Ca, K
^{36}Cl	301 ka	Fe, Ca, K
^{37}Ar	35 d	Fe, Ca, K
^{39}Ar	269 a	Fe, Ca, K
^{40}K	1.251 Ga	Fe, Ni
^{39}K, ^{41}K	stable	Fe, Ni
^{41}Ca	103 ka	Ca, Fe
^{53}Mn	3.74 Ma	Fe, Ni
^{54}Mn	312 d	Fe, Ni
^{59}Ni	76 ka	Ni
^{60}Co	5.27 a	Co, Ni
^{81}Kr	229 ka	Rb, Sr, Y, Zr
^{78}Kr, ^{80}Kr, ^{82}Kr, ^{83}Kr	stable	Rb, Sr, Y, Zr
^{129}I	15.7 Ma	Te, Ba, La, Ce
$^{124-132}$Xe	stable	Te, Ba, La, Ce, (I)
^{150}Sm	stable	Sm
^{156}Gd, ^{158}Gd	stable	Gd

Note: There are several additional cosmogenic isotopes not listed here, which are more rarely measured e.g. ^{7}Be, ^{44}Ti, ^{46}Sc, ^{55}Fe, ^{56}Co and ^{60}Fe (Eugster et al. (2006)).

* The value for ^{10}Be was recently re-evaluated (see Korschinek et al. (2010)).

3.2.1.3 Production rates and age-dating methods

As noted above, the solar wind ions have much less energy than SCR and GCR - only about 1 keV per nucleon, which means that they interact with the surface of an extraterrestrial particle or body (implantation depth ~50 nm, somewhat variable), while not causing nuclear reactions (Eugster et al. (2006)). Due to being a continuous stream, it is still possible for the SW to alter and erode the surface on which it is stopped – especially lighter elements like He and Ne will saturate the material e.g. the lunar regolith is saturated with high SW implantations of Ne and He (e.g. Benkert et al. (1993)). SCR and GCR with their higher energies (Fig. 6) are able to penetrate deeper into the meteoritic matter (see Leya and Masarik (2009) and chapter 3.2.1.2).

Other damages (see Eugster et al. (2006) and references therein) are particle tracks caused during the penetration of heavy SCR and GCR nuclei (which add to the also present tracks caused *in situ* by products of nuclear fission). Eugster et al. (2006) summarizes the three pathways for a cosmic ray nucleus that may occur as a consequence of the collision with target nucleus: **a)** Escape from the body (recoil); **b)** Stop and cause no damage **c)** Stop and cause a nuclear reaction. How often one or the other outcome will result, is depending on particle energy, atomic number, meteoroid size and composition (Eugster et al. (2006)). Because the penetration depths of SCR is generally not more than a few cm, the detectable products from SCR interaction can be remarkably lowered by ablation of extraterrestrial bodies while getting heated up during atmospheric entry (e.g. Garrison et al. (1995)).

As in detail modeled by Leya and Masarik (2009), the high kinetic energy level of GCR makes it possible not only to penetrate deeper, but also to produce during nuclear reactions lower-energy secondary particles, which in turn are still energetic enough to cause nuclear reactions themselves. All in all then a large variety of stable and unstable cosmogenic isotopes are formed (see Table 6). Important in the context of smaller particles like MMs is the fact that the secondary particles become dominant only at depth (compare Fig. 7 and 8 below) and that secondary particle formation can be neglected (see Trappitsch and Leya (2013)). On the other hand, the SCR becomes relatively more important the smaller a particle is because GCR only acts via primary particles (mostly protons - Fig. 7) and that there is less loss of SCR products because there is less ablation during atmospheric entry (Trappitsch and Leya (2013)).

Knowing production rates in meteorites, i.e. the number of product nuclei per unit time (generally given as per Ma), a cosmic ray exposure age for a meteorite can be calculated using cosmogenic nuclides, like ^{10}Be, ^{26}Al, ^{36}Cl and ^{53}Mn (unstable) but also ^{3}He, ^{21}Ne and ^{38}Ar (stable) (e.g. Leya and Masarik (2009)). The production rate of noble gases is generally shown in cm^3 STP/g/Ma (STP = Standard Temperature (273.15 K = 0°C) and Pressure (101.325 Pa = 1013.25 mbar)) - see e.g. Eugster (1988) and also Fig. 8. The predicted production rates in the first 60 cm are not linear as obvious in Fig. 8, which shows the results of modeling by Leya and Masarik (2009). The production rate usually increases in the first centimeters then decreases again. which is primarily due to the successive buildup of a cascade of secondary particles causing nuclear reactions themselves. This phenomenon is generally

described by the term "shielding" (e.g. Eugster et al. (1967)) and is determined by the size of the meteoroid and the position of the sample within it. For practical purposes, the cosmogenic ratio of $(^{22}Ne/^{21}Ne)_c$ is commonly used to describe the effect of shielding (e.g. Reedy (1985)) and to add a correction term to the "nominal" production rate (at "average shielding") that is based on the target element abundances only. The parameter c here indicates that only the cosmogenic part of Ne is used to determine the ratio, i.e. the "shielding factor" for shielding correction.
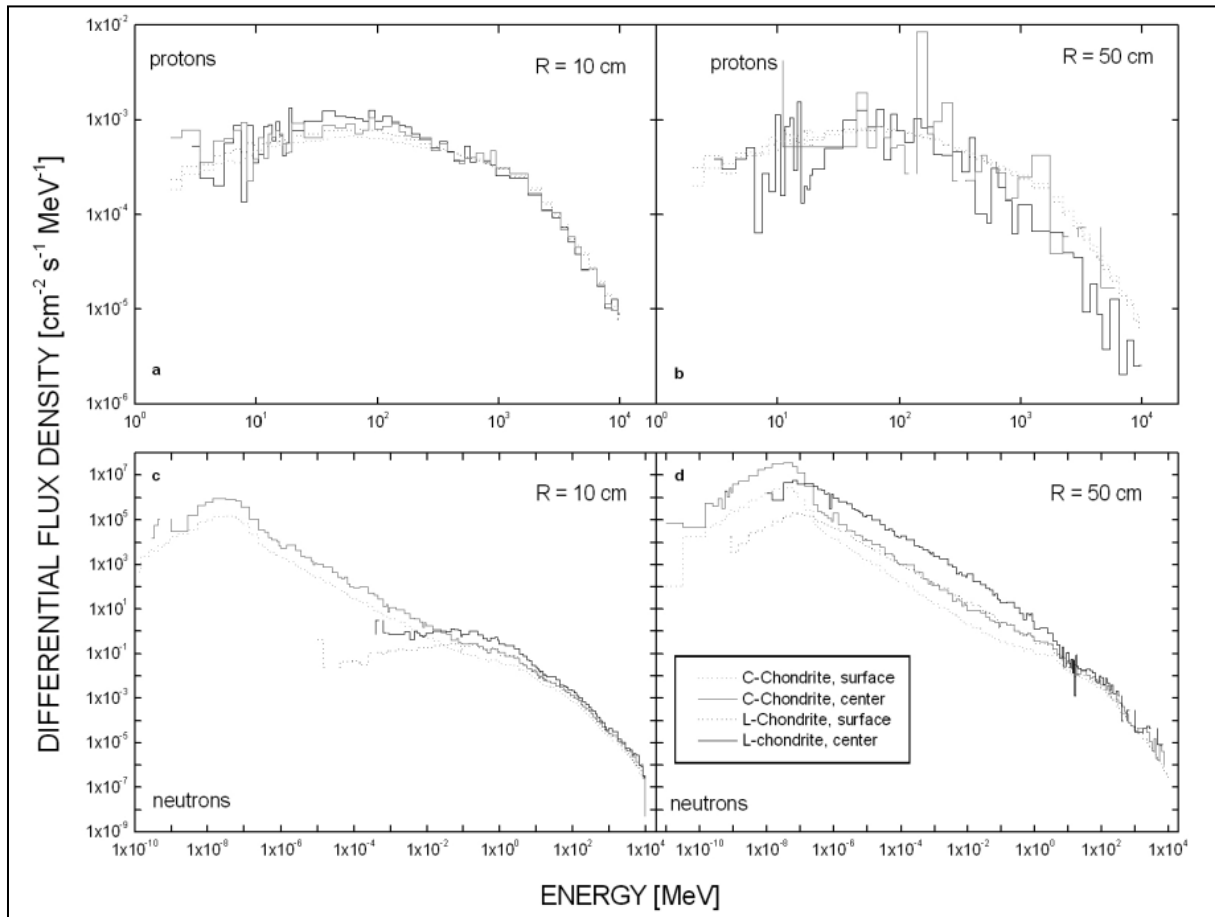
Figure 7. Different spectra showing protons and neutrons at the surface and the center of selected L and C chondrites with sizes of 10 cm and 50 cm, normalized to an dipping flux of primary galactic particles (adopted from Leya and Masarik (2009)). The surface is symbolized with a dotted line, the center with a solid line. The protons are combined in both, primary and secondary. The neutrons are secondary only. In case of the 10 cm chondrites the flux of protons and neutrons at the surface and the center is relatively similar with low variations. The 50 cm chondrites do show high differences between surface and center especially for the neutron flux. This is caused mainly by secondary particle formation due to kinetically high energy GCR which penetrate deeper into the meteoritic material than SCR does (Leya and Masarik (2009)).
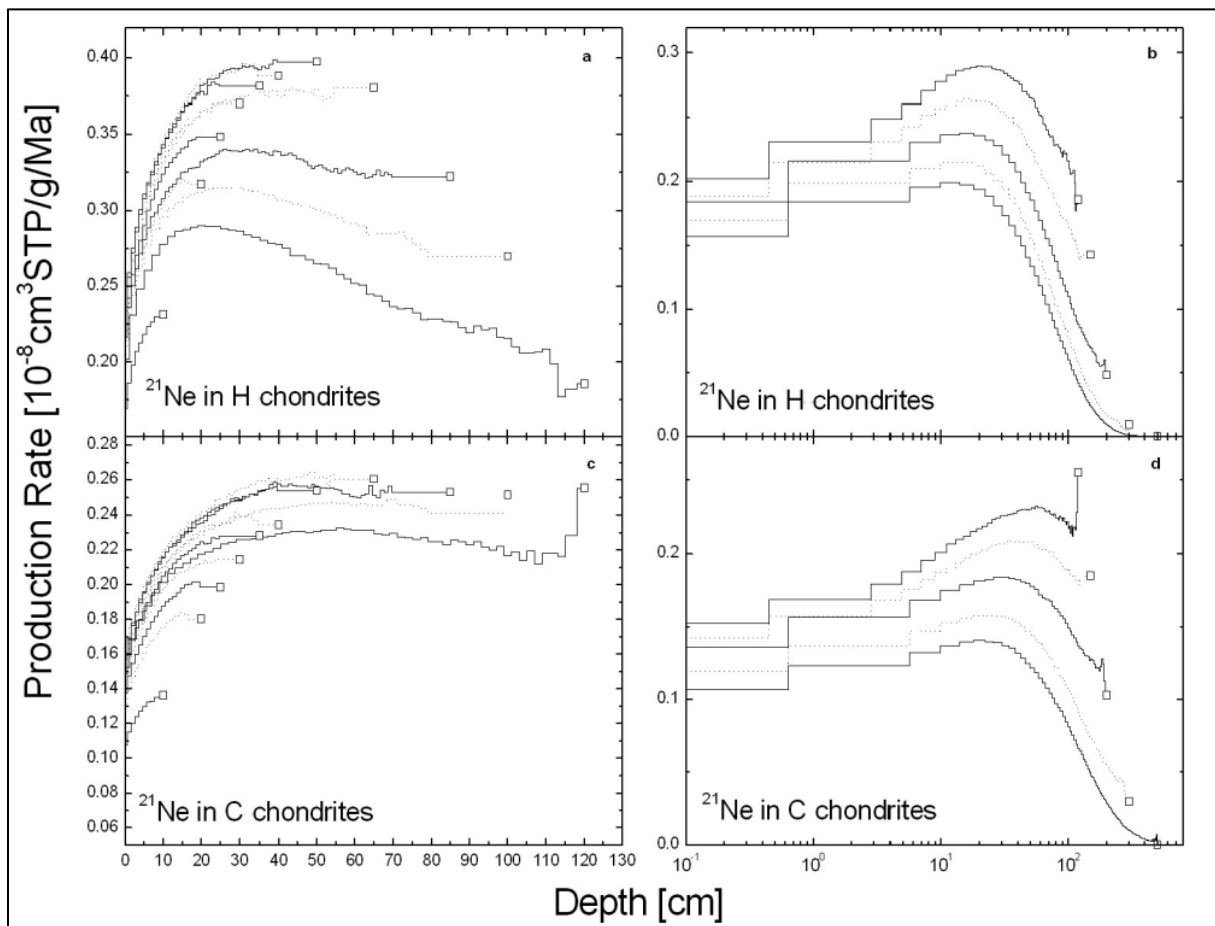
Figure 8. GCR-production rates of ^{21}Ne in H chondrites and C chondrites using a 4 π radiation geometry (adopted from Leya and Masarik (2009)). The left side shows meteorite radii from 10 cm up to 120 cm and the right side from 120 cm to 500 cm. Visible is that the production rate increases in the first centimeters. This is due to the fact that cosmogenic ^{21}Ne is produced by primary and increasing with depth also by secondary particles. After a certain depth of about 20 to 50 cm also the production by secondary particle decreases due to the large shielding (Leya and Masarik (2009)).

Within the noble gas inventory the cosmogenic nuclei most widely used to determine CRE (cosmic ray exposure) ages are ^{3}He, ^{21}Ne and ^{38}Ar (see chapter CRE-ages in the results section). As pointed out by Eugster et al. (2006), several conditions have to be met which are important to calculate a reliable CRE-age using the concentrations of cosmogenic nuclides (see Table 6). These are:

1) Constant flux in time of primary cosmic rays.
2) Constant flux in space of primary cosmic rays.
3) The sample's shape did not change significantly.
4) The chemical composition did not change.
5) Cosmogenic products of former periods of exposure to cosmic rays are known.
6) It has to be ascertained if there exist non-cosmogenic contributions of nuclides of interest.
7) No loss of nuclides of interest occurred other than the one known by radioactive decay rates.

3.2.2 Noble gases in micrometeorites - what has been done so far

Although measuring noble gases in extraterrestrial and terrestrial material is a widely known and applied tool (beside others e.g. Signer and Suess (1963), Göbel et al. (1978), Ott and Begemann (1985), Ott (1988), Swindle (1988), Wieler et al. (1991), Wieler (1998), Ozima and Podosek (2002), Swindle (2002a), Busemann and Eugster (2002), Rai et al. (2003), Mohapatra et al. (2009), Cartwright et al. (2013)) noble gases in MMs have not received as much attention so far.

During his PhD Olinger (1990) measured solar noble gases in individual micrometeorites from Greenland and Antarctica and showed the evidence for the extraterrestrial origin of MMs. Stuart et al. (1999) and Wieler (2002b) showed noble gas results in MMs which focused mostly on He and Ne. Recently Heck et al. (2008) and Meier et al. (2010) published He and Ne noble gas data of L-chondritic Ordovician limestone MMs (chromite grains) with an terrestrial age of roughly 470 Ma. Nakamura and Takaoka (2000), Osawa et al. (2000), Osawa and Nagao (2002) and Marty et al. (2005) published more noble gas results about MMs, though especially Xenon was not detected or not diagnostic due to high errors. However, Sarda et al. (1991) were able to obtain diagnostic results of He to Xe on a single, very large unmelted cosmic dust particle.

The same component mechanism like on larger meteorites (see chapter 3.2.1) should also occur on MMs. However due to the smaller size of the MMs it is very likely that these particles do not survive as long as larger bodies in the solar system. Caused by the Poynting-Robertson effect, small particles are dragged towards the inner solar system and in the falling into the sun. This makes it likely that small particles like MMs to not contain the same amount and the same mixture of trapped and in-situ components as typical for larger meteorites. The small size of less an mm makes it possible that MMs obtain a 4π irradiation of GCR and SCR. But, as discussed already above, unlike in most large meteorites, SCR, not GCR, are likely to produce most of the cosmogenic isotopes in MMs (Trappitsch and Leya (2013)). Also, as considered by these authors recoil of product nuclei, in particular ^{3}He, may influence the inventory found in very small particles.

The classification of micrometeorites reveals a variety of different types (see chapter 3.1.4 and Genge et al. (2008)). Some of these types suffered from heating events while their passage through Earth's atmosphere (see e.g. Fraundorf (1980), Love and Brownlee (1994), Greshake et al. (1998), Toppani et al. (2001) and Füri et al. (2013)), these are commonly scoriaceous MMs and Cosmic Spherules. Due to their small size of only up to a mm in diameter and different to larger meteoroids, MMs are most likely to be severely affected by atmospheric heating processes leading to a change in mineralogy and texture (e.g. Genge et al. (1996a), Genge et al. (1996b)). In the same context the loss of noble gases in MMs is most likely. Especially the lighter noble gases He and Ne will probably be depleted and/or exchanged with Earth atmosphere like composition (e.g. Stuart et al. (1999)). For noble gas measurements larger meteorites are sampled within the core where no atmospheric heating took place. Noble gas results concerning MMs affected by possible atmospheric heating will be discussed in chapter 7.

Chapter 4 - Methodology

This chapter contains a description of how MMs were acquired and selected, how the samples were prepared for the extraction system and for the noble gas measurement. Additionally a detailed description of the improvement of our new high sensitivity mass spectrometer will be given.

4.1 Acquisition and selection of samples

4.1.1 Micrometeorites from the Transantarctic Mountains (TAM)

In October 2010 we acquired micrometeorite samples from the meteorite curator L. Folco at Siena University - Museo Nazionale dell'Antartide (MNA). These micrometeorites were originally collected at Miller Butte (TAM) on Antarctica (see Fig.9) from P. Rochette, L. Folco and colleagues (Rochette et al. (2008)). The TAM MM samples show a high range of different sizes and shapes with only a small terrestrial input (Rochette et al. (2008)). Furthermore, the collection shows a high variety in particle types - e.g. ordinary chondrite like, carbonaceous chondrite like, chondrules, unique particles (Rochette et al. (2008)).

Figure 9. Map showing the Miller Butte micrometeorite traps geographical situation. The small picture on the right gives an overview of Antarctica and some points of interest (e.g. Miller Butte, Dome C) as well as continents and countries near Antarctica. Good to see is the location of Miller Butte in the Transantarctic Mountains and Dome C (CONCORDIA station) in the Central Antarctica snowfield. These two locations are the sources for our micrometeorite sample sets (e.g. Rochette et al. (2008); Duprat et al. (2007)) The big picture in the background shows the location (S 72°42, E160°14) of Miller Butte, where the MMs selected for our noble gas measurements were found (after Google Earth).

Rochette et al. (2008) point out that the sediments, from which the meteoritic material were collected, in majority were deposited in a geological trap due to transport by the Rennick glacier system (see Fig.1 in Rochette et al. (2008)).

Because of large variations in the strength of the wind system, aerial transport contributed only little to the deposition. Among others - e.g. microtectites and terrestrial sediments - the samples were found in decimeter sized pits and have been extracted by the expedition team (see Folco et al. (2008) and Rochette et al. (2008)). The surface where the MMs were collected from has an exposure age of about 1 Ma or more (Rochette et al. (2008)). Nevertheless, as Rochette et al. (2008) explain, the MMs only suffered minor alteration, a fact due to the cold and dry climate at the Miller Butte plateau in Antarctica.

We selected samples from a magnetic fraction and pre-analyzed them with stereo-microscopes and SEM. For further analyses the samples were split into aliquots: one (larger) part stayed in Siena to perform SEM and microprobe analyses and the other (smaller) parts were covered by glass slides and transported to the Max-Planck-Institute for Chemistry in Mainz (MPIC) for noble gas analyses. Detailed information about samples and further investigations are described in chapter 4.3.1.1, chapter 5 and the Appendix.

4.1.2 Micrometeorites from the CONCORDIA collection (Dome C) and from Cap Prudhomme, Antarctica.

In November 2010 other, much smaller types of MMs were selected at CSNSM, University of South Paris, Orsay, France, with the collaboration of C. Engrand and J. Duprat. They had been stored under vacuum conditions and had to be handled in a clean room. Unlike the larger MMs from the Transantarctic Mountains, which could be selected using a magnetic pen, the smaller samples from Dome C (CONCORDIA station) and Cap Prudhomme (Adélie land), Antarctica (Fig. 9) required selection using a very thin brush moistened with distilled water. During the selection, the samples were observed under higher magnification (200 x) due to their small sizes of only 20 to 200 μm in diameter. These were determined under a stereo-microscope using a μm-scale as a reference and then were photographed for future reference. The weight of the samples was calculated using the approximate volume (assuming sphere or cone-head shape) of the MMs and a density of ~2.1 g/cm^3 of CM and CI chondrites reported in Britt and Consolmagno (2003). After selection and size measurement, the samples were deposited between two glass slides. One of the two slides had a cavity in the middle to assure that the samples were not damaged during transport. The glass slides had to be cleaned before the MM samples could be stored in them. In order to do this, they were first washed with a soap solution, then with distilled Milli-Q water (Milli-Q is a registered trademark of the Millipore Corporation, USA), followed by high-level alcohol, and then dried with N$_2$-Air. The samples within the glass slides were transported to the MPIC once the cleaning and MM storage procedure was finished.

Detailed information about samples and further investigations are described in chapter 4.3.1.1, chapter 6 and the Appendix.

4.2 Noble gas extraction and analysis

Noble gases are inert and highly volatile. Because of their rarity in solids, their composition in these is mostly determined by components which are "trapped" and/or produced in-situ (see chapter 3.2 for further information). Because of this sensitivity to "foreign additions", it is of high interest in cosmochemistry to obtain noble gas data from meteoritic samples. Prior to the actual measurements, which are performed by mass spectrometry, the noble gases have to be released from the meteoritic matter to be analyzed. which is usually done by heating them with an oven or with a laser system. While heating, the extracted noble gases are released into a static (i.e. closed system, no pumping), ultra high vacuum system (10^{-8} to 10^{-9} mbar). Nearly all active gases (e.g. H_2, CO_2, N_2, Cl^-), which are released together with the noble gases, are removed through reaction with the surfaces of warm and cold getters (mostly Zr/Al or Zr/Ti). Usually then, in the next step the noble gases Ar, Kr and Xe are adsorbed at a cryogenic cold finger/trap system (e.g. glass, charcoal) which is cooled down to with liquid nitrogen. During this procedure, He and Ne are measured in the mass spectrometer as a further step because they are too volatile and are not adsorbed at the temperature of -196°C. Afterwards the remaining noble gases are released successively from the cold trap by stepwise heating of the charcoal and are pumped into the mass spectrometer for measurements. First Ar, then Kr and at last Xe. For exact mass spectrometric measurements it is of importance to use an exact timeframe since noble gases are rapidly depleted by the high voltage of the ion source in the mass spectrometer, which acts like a weak ion pump. Detailed information regarding the measurement steps for the individual noble gases are described in chapter 4.3.4.

4.2.1 Mass spectrometer

Commonly a mass spectrometer can be described by:

Four parts:

1. Inlet system
2. Ion source
3. Mass analyzer
4. Detector system

Three main processes:

a) Ionization
b) Sorting of ions
c) Detection of ions

In general, mass spectrometry is used for the purpose of separating and detecting atoms by mass within a magnetic sector field. Therefore the atoms have to obtain an electron charge. The kind of ionization which is used depends on the element to be analyzed. For gases commonly the electron collision ionization is used (e.g. Downard

(2004) and Fig.10). Rare gases have to be released from their solid (or, in some cases, liquid) host by heating it (see above). Afterwards these noble gases exist in an atomic/molecular state. It is important to work under static conditions, since the noble gas amounts measured are commonly so low (e.g. in MM samples: Kr, Xe 10^{-13} to 10^{-14} cc STP (~250.000 - 1.5 million atoms) that the pumping system at a mass spectrometer would rapidly vacuum these gases off. Once the gases have been introduced into the ion source, the atoms will be singly- and to some extend doubly-ionized and are accelerated to several keV in the high voltage electric field of the mass spectrometer (Fig.10). In the case of electron collision ionization, the electrons are provided by a heated filament (Downard (2004)). The electrons are charged with energies in the area of 50-100 eV. On their way out of the filament, the electrons follow a path to the anode onto the other side of the chamber (Fig.10 and Downard (2004)). Once the sample gas atoms come in contact with these charged electrons, electrons from the sample gas shell will be expelled and this leads to a formation of positively charged ions (Fig.10 and Downard (2004)). In the case of the mass spectrometer "Noblesse" (for details see chapter 4.3.2) used at the MPIC, electrons which are expelled get collected within a trap while the electron trap current has to be stabilized. Due to the accelerating voltage, the charged electrons are extracted out of the ion source and moved into the magnetic field. There, the ionized components get separated and sorted due to their mass-to-charge ratio (*m/z*) and the Lorentz force (1) (e.g. Duckworth et al. (1986)).

Lorentz-Force: $$\vec{F} = \vec{F}_E + \vec{F}_B = q\,(\vec{E} + \vec{v} \times \vec{B}) \qquad (1)$$

The ion beam gets focused horizontally and vertically during its entry into and exit out of the magnetic field. The separated ions can be deflected on the detector as well as on the collector (Faraday and/or ion multiplier) due to the variation in the magnetic field and can then be quantitatively measured. The detection system is usually coupled with a signal processing unit and a computer system which processes the spectral data stream and the spectral data output (graphical or numerical).
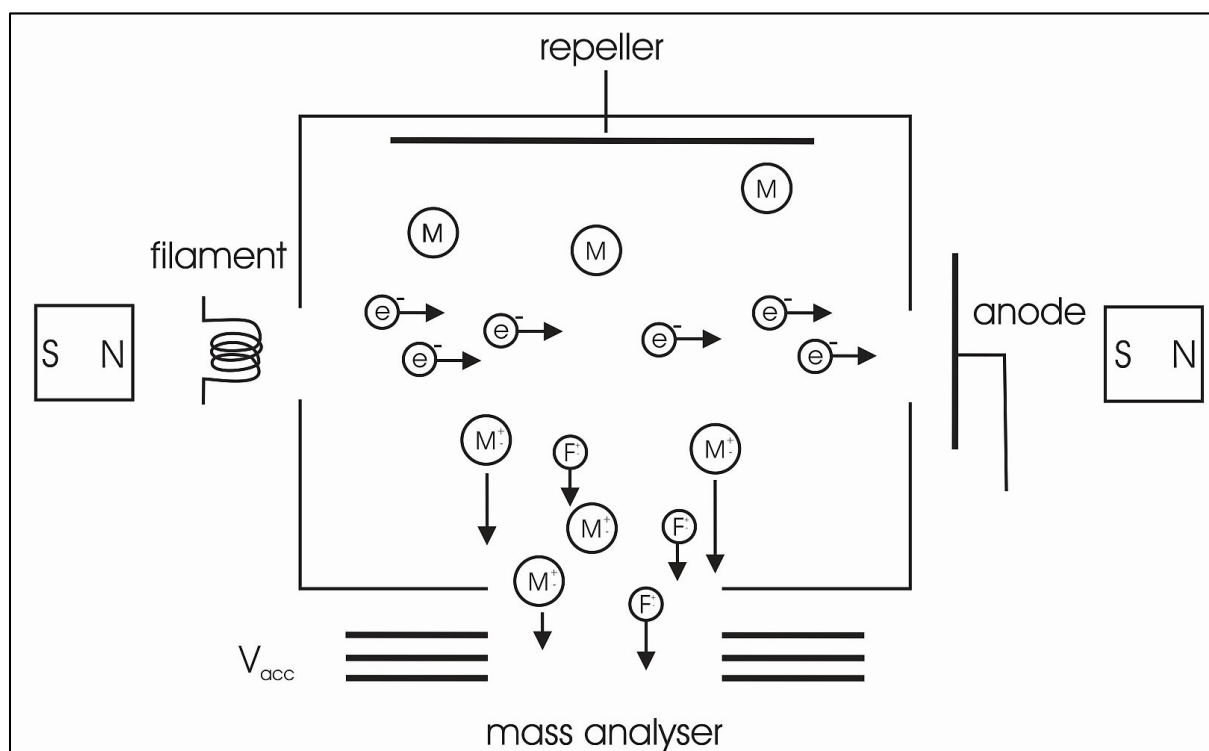
Figure 10. This schematic shows in principle how electrons are used to ionize the gas in the source of a mass spectrometer. The gas was inserted at an earlier stage. The energized electrons (e-) cross the way of the gas isotopes (M, F) from the filament (cathode) to the anode in the ionization chamber. The gas isotopes are directed by a repeller which possesses a positive (+) current. In case of the "Noblesse" (for details see chapter 4.3.2) most of the isotopes in the gas are ionized and exhibit a positive charge (M+ and F+). These newly formed ions are accelerated by a current (Vacc) Afterwards the ions are deviated by a magnetic field and then detected based on m/z (after Downard (2004)).

It is important to have a suitable mass resolution (R) in order to be able to differ between different isotopic peaks or signals (see e.g. Downard (2004)). Equation (2) shows the definition of the mass resolution (R):

$$R = \frac{M}{\Delta M} = \frac{M_1}{M_1 - M_2} \qquad (2)$$

The value R gives the potential resolution capacity of the mass spectrometer. This would mean a mass spectrometer with a mass resolution of 2500 could separate e.g. $^{14}N_2$ (~28.006 amu) and $^{12}C^{16}O$ (~27.995 amu) from each other (amu = atomic mass unit). However, to a certain extent one can assume, the higher the resolution of the machine, the lower the sensitivity becomes. This is due to lower transmission, i.e. the fraction of ions passing through the magnetic field and are finally detected. ΔM displays the smallest mass which is able to be separated by the mass spectrometer. Usually it is not difficult to separate noble gas peaks from each other in a standard mass spectrometer with a resolution below 500. This would be optimal for a higher sensitivity for small noble gas amounts. For Xenon one would need about 130. However, the resolution capacity is of great importance when so called "dirt" or interference masses overlie a portion of a noble gas peak – e.g. ^3He and ^1HD as well as $^1H_3$; ^{20}Ne and $^1H_2{}^{18}O$; ^{22}Ne and ^{40}Ar plus $^{12}C^{16}O_2$; $^1H^{35}Cl$, $^1H^{37}Cl$ and several hydrocarbons interfering with Ar and other noble gases (see chapter 4.3.3).

Commonly used measures of resolution (R) are the 10% valley definition and the 50% peak definition (Downard (2004)). The 10% rule is based on the resolution

of two ion signals at 10% height (Fig. 11). In this definition two neighboring peaks ($\Delta M = 1$) with the same height should not overlap by more than 10% to ensure one is able to separate them. Downard (2004) also discusses the 50% rule, which is known as FWHM (full width at half maximum). The 50% rule is used mostly if two neighbored peaks do not have the same height. In this instance one would get the resolution of the mass spectrometer using ΔM at 50% the height of the peak with mass M (Fig. 11).
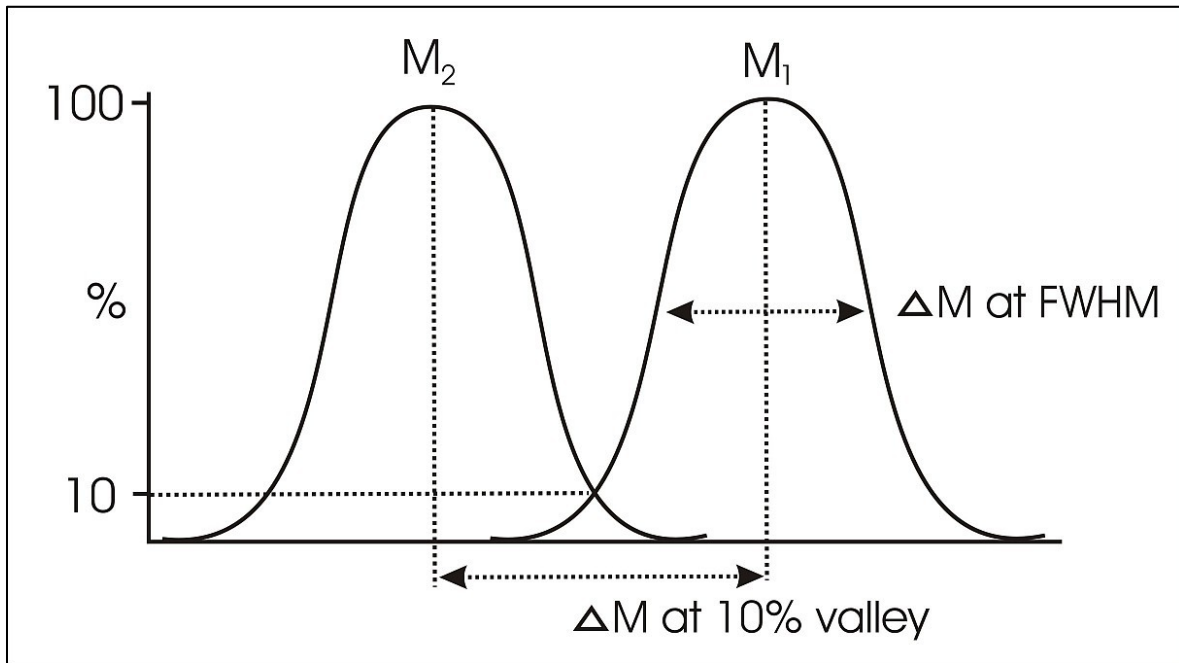
Figure 11. Schematic showing two methods of how to calculate the mass resolution for a mass spectrometer (with certain exceptions). If there are two isotope peaks with the same height one can use the 10 % valley definition. If the two peaks have different heights one usually uses the 50 % peak definition (FWHM - full width at half maximum) - see text for further details (after Downard (2004)).

4.3 Instrumental Setup at MPIC Mainz

Our noble gas measurements were performed on the high sensitivity mass spectrometer "Noblesse" from Nu instruments at the Max-Planck-Institute for Chemistry in Mainz between 2010 and the end of 2012. The whole noble gas analysis system consists of several devices for extraction, cleaning, separation, adsorption, desorption, pumping and measurement. A detailed illustration of the machinery can be seen in Fig. 12 and will be explained in detail in the next few chapters.
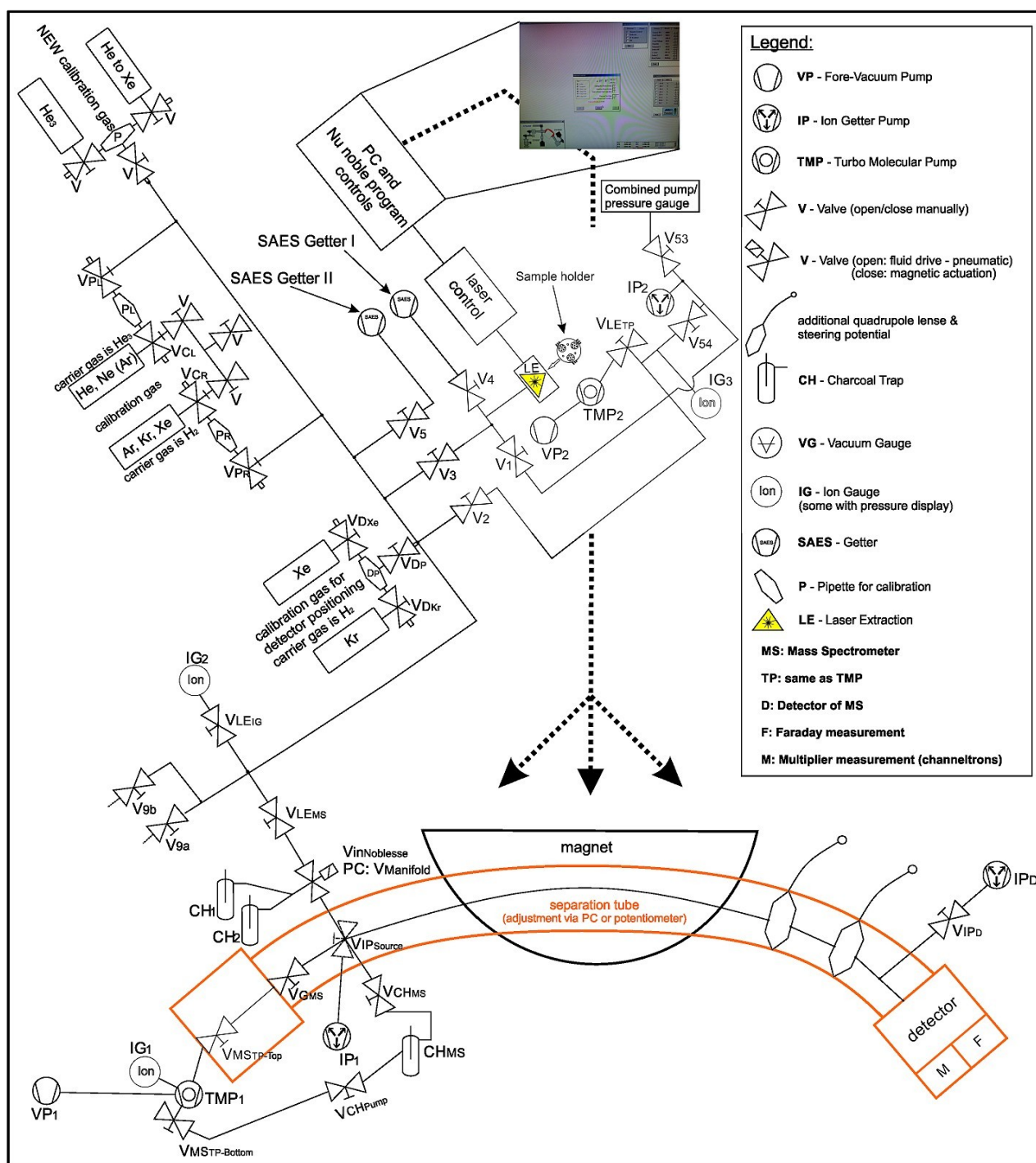
Figure 12. Schematic overview of our laser-extraction and noble gas separation system used with the Nu Instruments mass spectrometer – for enlarged figures refer to chapters 4.3.1 and 4.3.2.

4.3.1 Laser extraction system

This chapter will provide information on how the MM samples were handled and how the sample holder was mounted prior to the gas extraction with the CO_2-laser (see chapter 4.3.1.2). Details about the laser will be provided as well as how the handling of the extraction system, the degassing of the samples, the cleaning and the separation of gases were performed.

4.3.1.1 Sample preparation, mounting and sample holder utilization

Before noble gas analysis, the samples had to be measured for their weight and sizes. A stereo microscope connected to an electronic camera – personal computer combination was used to obtain the sizes electronically. The MMs from Siena, Italy (TAM) (e.g. Rochette et al. (2008) were weighed on the microbalance available at MPIC and, the weights of the samples from Orsay, France (CONCORDIA collection) (e.g. Duprat et al. (2007)) were calculated from the volumetric measurements (see chapter 4.1.2).

The samples from Siena, Italy (TAM) had been partially coated with glue residue so that their surfaces required additional cleaning. The glue originated from the tape used to fix them on glass slides for transportation. To clean the surfaces, each sample was separately stored in a glass container filled with Milli-Q water (Milli-Q is a registered trademark of the Millipore Corporation, USA). Then the glass containers were kept individually in an ultrasonic bath for 10 minutes. This was followed by exchanging the distilled water with an alcohol suspension and repeating the ultrasonic bath. Finally the alcohol suspension was exchanged with distilled water and the samples were again subjected to the ultrasonic cleaning for 10 minutes. In general, the glue on the MMs was successfully removed after one full cleaning cycle. If not, the process was repeated until all the glue was gone. Subsequently the samples were stored in the same glass slide type described for the MM samples from Orsay, France (CONCORDIA collection) in chapter 4.1.1 (see Fig.13).
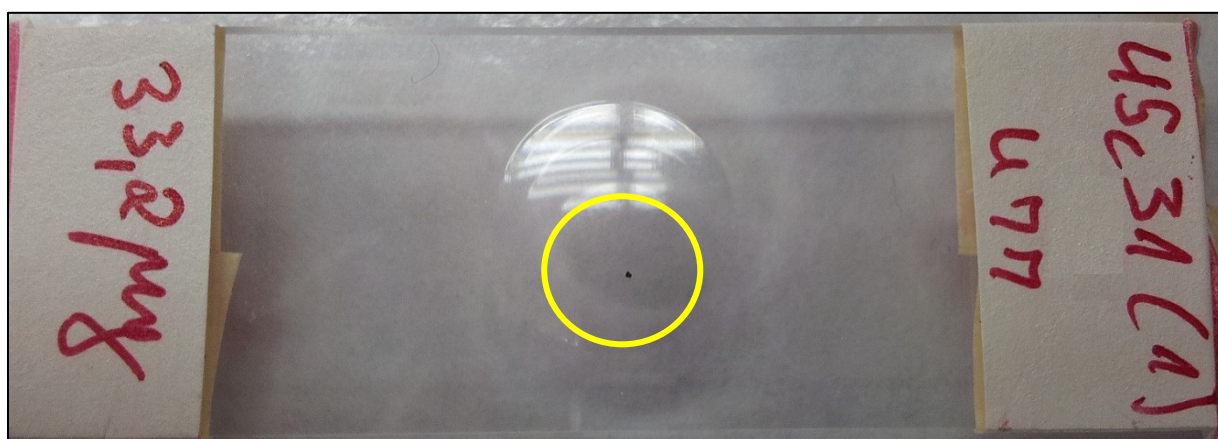
Figure 13. Glass slide showing the TAM MM sample 45c31(1) acquired from MNA, Siena, Italy (weight 33.2 µg) – see yellow circle. After the cleaning process described in the text, all the MM samples were placed in glass slides with cavities to keep them protected against additional contamination.

The first measurements on the "Noblesse" were performed using small fragments of standard samples - Murchison (CM2) (e.g. Fuchs et al. (1973)) and Lakewood (L6) (e.g. Schultz et al. (2005)). This was done to investigate the

separation, calibration and sensitivity capabilities of the extraction and mass spectrometer system (see chapter 4.3.3 and 4.3.4.1). All sample preparation steps described in the next paragraphs were followed prior to measurements.

The measurements of MMs started in early 2011 with the analysis of Cosmic Spherules. It was advantageous to start with Cosmic Spherules because their high abundance in our sample set insured we would not lose our most interesting samples if anything would not work properly. Additionally, the expected low noble gas content made them a good test for the sensitivity level of the "Noblesse". At this stage we were able to select a maximum of 21 samples to put into the sample holder (see Fig. 14). The samples had to have a sufficient distance from each other to guarantee negligible heat interaction from the laser heating (see also chapter 4.3.1.2 and 4.3.3). Laser heating interferences on adjacent samples (pre-degassing) could only occur via heat conduction due to the hot sample holder, less so through the channels enabling released gases tp spread into the system volume, which also connected the samples with each other. The high vacuum in the extraction system would prevent any heat transfer by means of convection.
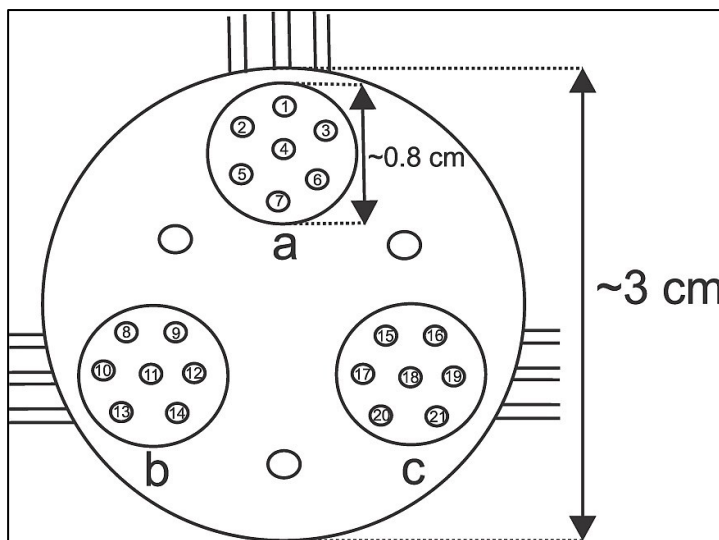
Figure 14. Illustration of the standard Mo sample holder used in the laser extraction system at MPIC Mainz (not true to scale). The smallest circles are the sample cavities (~1.2 mm Ø) which are used to degas samples via laser heating. The slightly larger circles (a-c) symbolize the area where poly crystallline diamond pads is covering the sample cavities to prevent the loss of samples due to transport and laser heating (see text below).

The sample holder (~3 cm in diameter) used in the laser extraction system (see Fig. 15) was made of molybdenum which has a melting point of 2622°C (see page 4-122 in Haynes et al. (2012)). The CO_2 laser would be capable of locally heating the molybdenum (Mo) close to this temperature when at 100% power (see chapter 4.3.1.2). However, the Mo would not melt (see chapter 4.3.3). Before usage, the sample holder was cleaned with 10 minute consecutive ultrasonic baths of acetone, alcohol and distilled water. Thereafter it was placed in an oven at 200°C for 30 minutes for drying, followed by a cooling phase. The specimens were then ready to be stored in the cavities (sizes of ~1.2 mm in diameter) of the sample holder. To avoid contamination the samples were placed using gloves, forceps and aluminum foil in a clean lab environment. The aluminum foil was used as a shuttle (single sided outlet of about 1-2 mm) to put the small samples in their pre-selected cavity without danger of losing them, while the transport was with forceps only. Exact documentation of samples on each sample holder cavity was necessary in order to know which sample would be degassed later. We were able to identify and assign numbers to the individual cavities on the holder consecutively due to its unique channel structure on the surface (Fig. 14 and Fig. 15).

Figure 15. Photo of the molybdenum sample holder used for laser extraction (Fig. 14). 21 samples up to a size of several mm can be placed in the cavities. The samples are degassed at different energy steps of the CO_2-laser, and the released gas can spread along the outlet channels into the vacuum chamber. From there the extracted gases quickly expand into the noble gas separation system. The sample areas are covered with transparent poly crystalline diamond pads to first protect the samples from being lost during transport, but also to prevent that the samples get lost during laser heating. Small meteorite or MM pieces may tend to jump out of the cavities when heated up too rapidly. Poly crystalline diamond was used because it is the only "clean" and hygroscopic transparent medium which can be penetrated by the CO_2 laser due to the laser's special wavelength of 10.6 μm.

After the sample loading procedure was completed, three small transparent poly crystalline diamond pads were placed on top of the sample cavities and were fixated onto the Mo-holder by using Mo-screws (see Fig. 15). An overview of the steps performed follows:

1) All valves of the extraction and separation area are closed before the laser extraction chamber can be opened (Fig. 16). This is done starting with the valves with the biggest distance from the chamber to prevent the system to contaminate with air (Fig. 12).
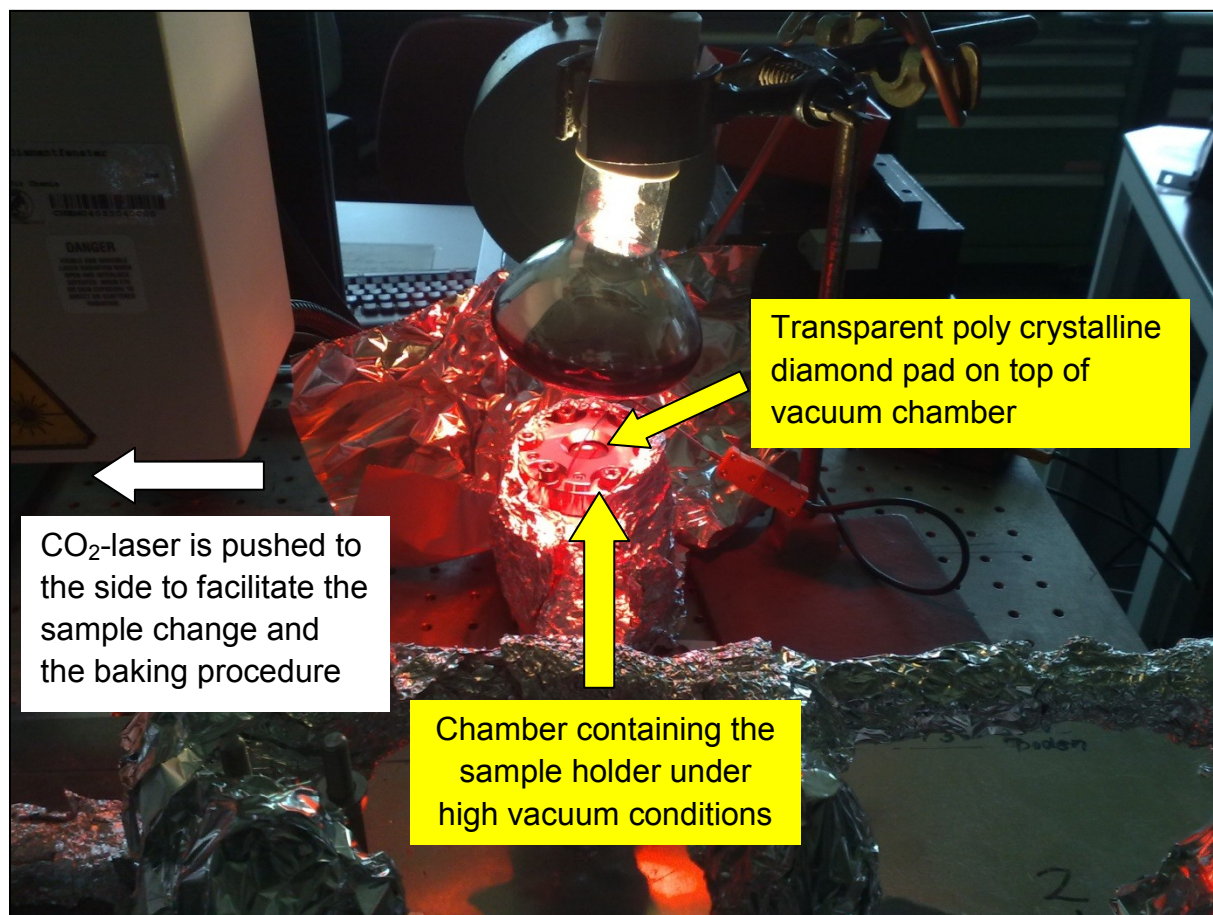
Figure 16. The chamber which contains the sample holder after sample change is visible in the center of the image. It is already surrounded by aluminum foil to keep the heat of the heating tapes inside and on top of the extraction metal tubes. The temperature is measured using a high precision digital thermometer (upper right).

2) The sample holder is mounted in its place in the laser extraction system. For this purpose a chamber is available, containing an socle, which keeps the sample holder in its position after it is installed (Fig. 16).

3) The chamber, containing the sample holder, is covered and tightened on top by a ConFlat flange ("ConFlat" is a registered trademark of Varian Inc., USA) incorporated with a poly crystalline diamond pad. The diamond window is necessary to be able to fire the laser beam onto the samples, since it is the only "clean" and hygroscopic transparent medium which can be penetrated by the CO_2 laser due to the laser's special wavelength of 10.6 μm (see Fig. 16).

4) When all valves are closed, the laser extraction chamber is opened - to prevent contamination, gloves and forceps are used to handle parts. The inside of the chamber may not be touched.

5) The sample holder is placed on its socle within the chamber. Then the chamber is locked with ConFlat flange with diamond window ("ConFlat" is a registered

trademark of Varian Inc., USA) - a new gasket should be used since the older gasket may have been damaged while opening the vacuum system.

6) When the chamber is successfully closed, the laser extraction ion gauges have to be monitored while opening valves $V_{LE_{TP}}$, V2 and V3 (see Fig. 12) consecutively to pump away air with aid of the Fore-Vacuum-Pump and the Turbo-Molecular-Pump. It takes about 20-30 minutes to get the pressure level into the 10^{-2} mbar range after this routine. It needs then a couple of hours to reach a better vacuum of ~10^{-5} mbar.

7) If the pressure is too high (stays on 10^{-1} mbar level), a leak is suspected. This is tested from outside at the assumed leak location with Acetone or He while watching for a change in pressure shown by the ion gauges. If a leak is detected, it has to be fixed, which can be additionally time consuming.

8) As soon as a decent pressure regime is reached (10^{-6} to 10^{-7} mbar), and there are no indications for a leak, the other system valves are opened and the laser extraction system is baked to about 200-220 °C for about two to three days to attain a pressure level of about 10^{-8} to 10^{-9} mbar (after cooling). The sample chamber is heated separately by a red light to about 180 °C (Fig. 16). Afterwards it is enclosed by a black colored metal cave manufactured by the MPIC to guarantee safety while using and activating the laser (Fig. 17).
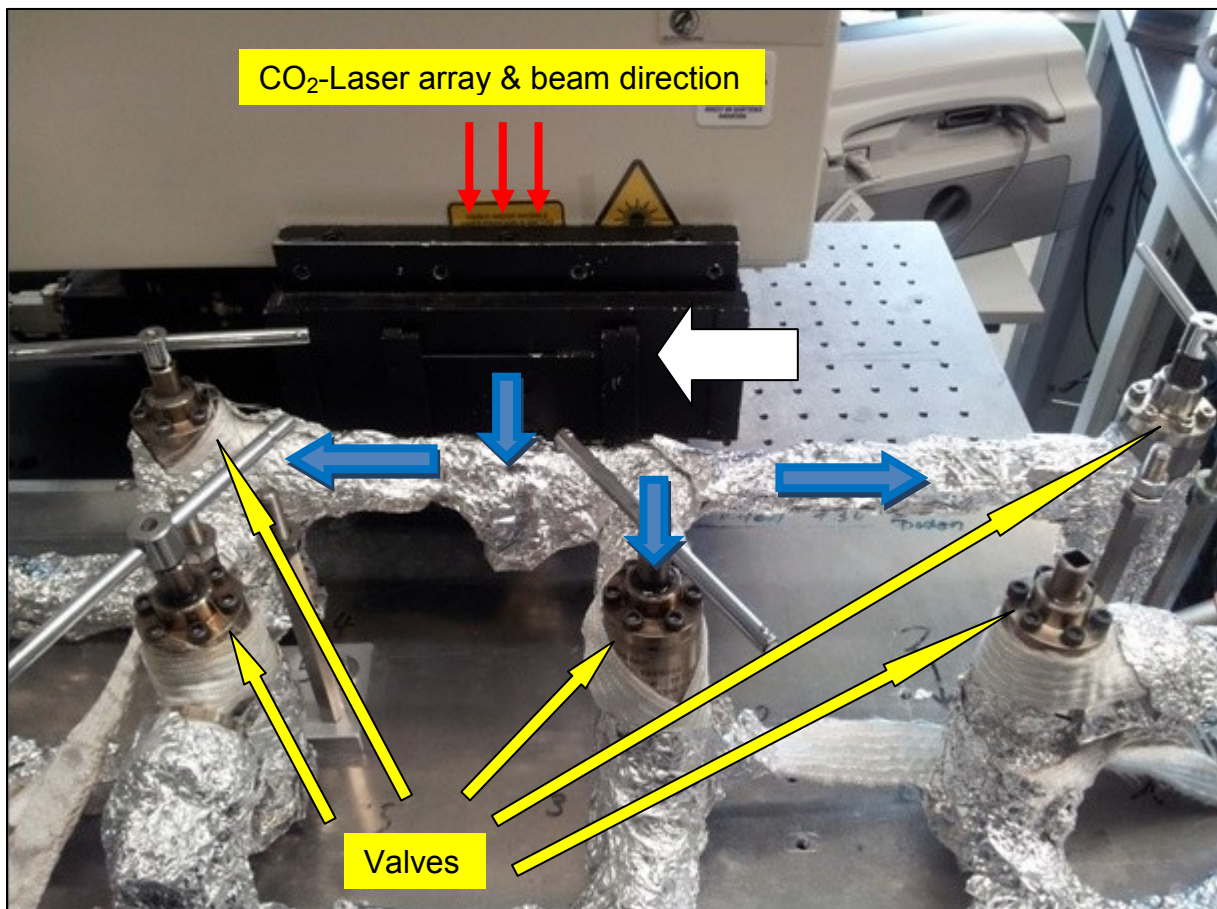
*Figure 17. Completely closed and locked black colored metal chamber (**white arrow**) manufactured by the MPIC, to guarantee safety while using and activating the class 4 laser beam. The direction of the laser beam is indicated by the **red arrows**, and the direction for expansion of the released gases with the **blue arrows**.*

The baking procedure has to be done for the extraction / separation system and the mass spectrometer for the following reasons, if (Fig. 16 and Fig. 18):

1.) Samples were changed and whole or part of the system experienced contamination with air and "dirt" gases.

2.) A leak occurred in the extraction and separation area and the mass spectrometer saw some of the "dirt" gases.

3.) A leak appeared in the mass spectrometer.

4.) The pressure regime of the extraction and separation area and/or the mass spectrometer is not satisfying and one wants to reach a lower blank level and isotopic background.
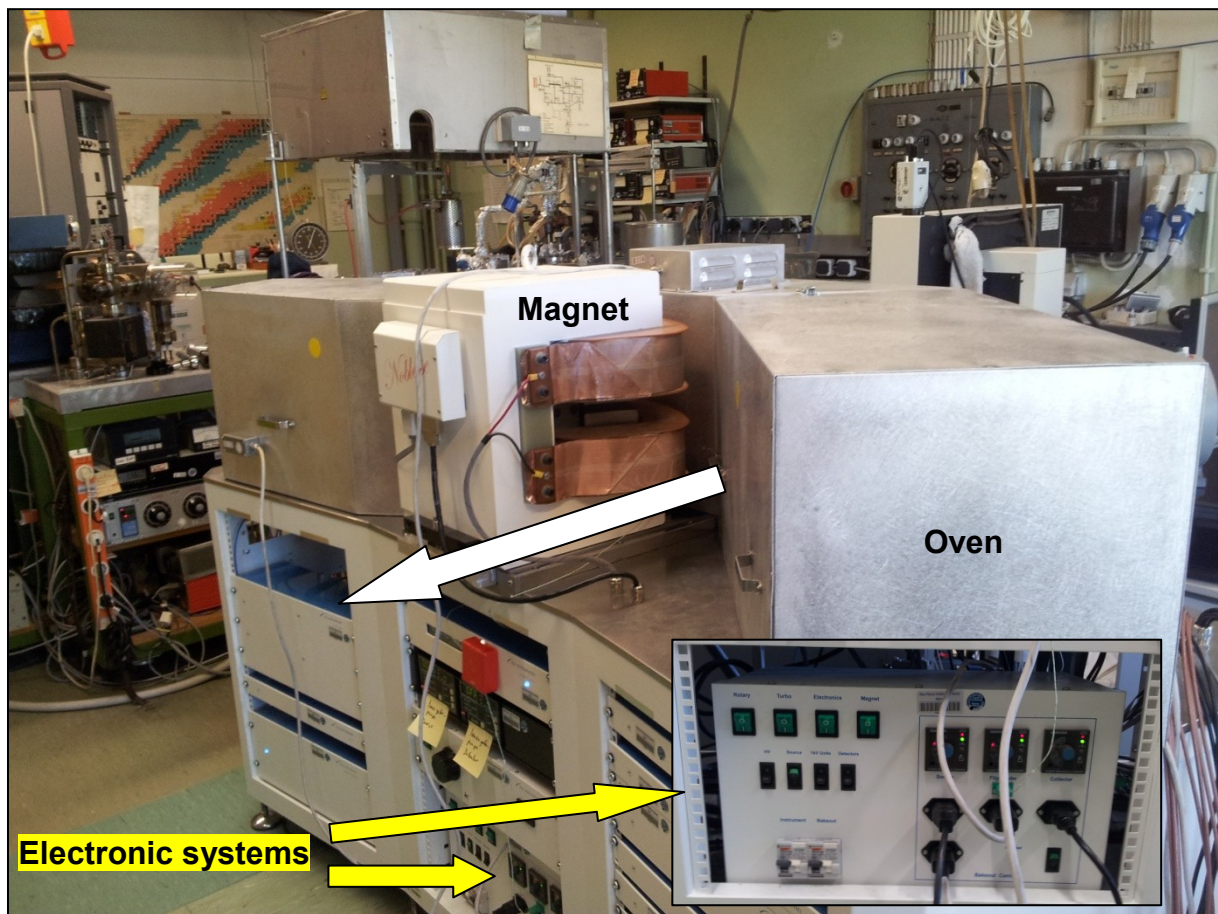
Figure 18. Here the "Noblesse" is made ready for baking. All cable connections are removed and the magnet is moved further to the front (white arrow). Parts of the mass spectrometer which are kept under vacuum conditions are covered by heating boxes (ovens) especially designed for the baking the "Noblesse". The electric cables of these boxes are connected to the baking system which is integrated into the electronic system of the "Noblesse" (yellow arrow).

4.3.1.2 CO$_2$-laser (carbon-dioxide laser) and sample heating

The term "LASER" is a short form for Light Amplification by Stimulated Emission of Radiation (e.g. McGuff et al. (1963)). Basically, a laser is an oscillator and amplifier of optical, monochromatic light through emission of electromagnetic radiation (Kneubühl and Sigrist (2008)). This produces a coherent stream of light which is emitted from the laser system. Lasers can have many different wavelengths (from 0.1 μm to 3 mm), power levels (from 1μW to 1 TW) and beam sizes (< 1mm to 100 m) (Kneubühl and Sigrist (2008)).

Patel (1964) invented the CO$_2$-laser technique which comprises a continuous waves laser (as opposed to more frequently used pulse lasers) and various transition stages of the CO$_2$ (carbon dioxide) molecule in the μm bandwidth (infrared light) range. The advantage of the CO$_2$-laser compared to most other lasers is the high power output and the relatively high degree of efficiency of up to 20% (Kneubühl and Sigrist (2008)). The CO$_2$-laser is a molecular-gas laser and part of the vibration-rotation laser family (Kneubühl and Sigrist (2008)).

To degas the samples, we used a CO$_2$-laser (Model: MIR 10-30 / Class 4) from New Wave Research with a wavelength of 10.6 μm in the mid infrared range (Fig. 19). The laser's highest power output with a water cooling system is about 32 W, and the coolant flow rate has a minimum of 2.0 L\min and maximum of 4.0 L\min. The current is specified with 8A. The MIR 10-30 is a Class 4 laser, which is the highest laser class implying a high energy output. It can cause severe skin and eye damage when directly exposed to the laser. Due to this risk, the laser is aligned on the sample using an optical camera device (Fig. 19 and Fig. 20). The camera is positioned directly on top of the laser's shooting position, which is marked with a crosshair in the PC camera software. The laser position can be adjusted in the x-, y-, and z-position using three small electric motors. Samples from sizes of about 50 μm to several mm placed in the sample holder can be focused with the camera system and can then be degassed with the laser. The focusing of the camera is aligned with the focusing of the laser beam.

Immediately after laser activation, the beam is established through the electric system. Following this, the beam can be directed to the sample area through permeation of poly crystalline windows and lenses made out of germanium, zinc selenite and diamond. Poly crystalline diamond is optimal for our system, not only because the CO$_2$ laser radiation is able to permeate, but also because it provides a high thermal conductivity and is very rigid, "clean" and hygroscopic.

Several mandatory tasks must be completed in order to use and activate the laser system (selected parameters - beam-size, energy output setting and duration of laser-shot - for sample gas extraction are shown in the Appendix with each sample description):

- The whole lower laser area, which is shown above, beside and below the sample chamber has to be closed with at the MPIC manufactured black metal plates. These plates have special contacts which are electrically connected and secured to the PC laser software. The contact circuit must be closed in

order to be able to activate the laser system. The system has been set up in this way for security reasons.

- Water or coolant solution for the cooling circuit has to be switched on.

- The power supply for the CO_2-laser system has to be turned on.

- A light amplifier supplying the optical camera has to be activated.

- The laser PC software supplied by New Wave Research has to be started.

- The laser beam has to be set to continuous wave mode (cw)

- The laser beam size must be selected depending on the sample size; usually in the range of several hundred µm. The beam is then focused onto the sample using the optical camera.

- The laser power output has to be selected. In most cases this is done by starting with a low power setting – see also chapter 4.3.3.
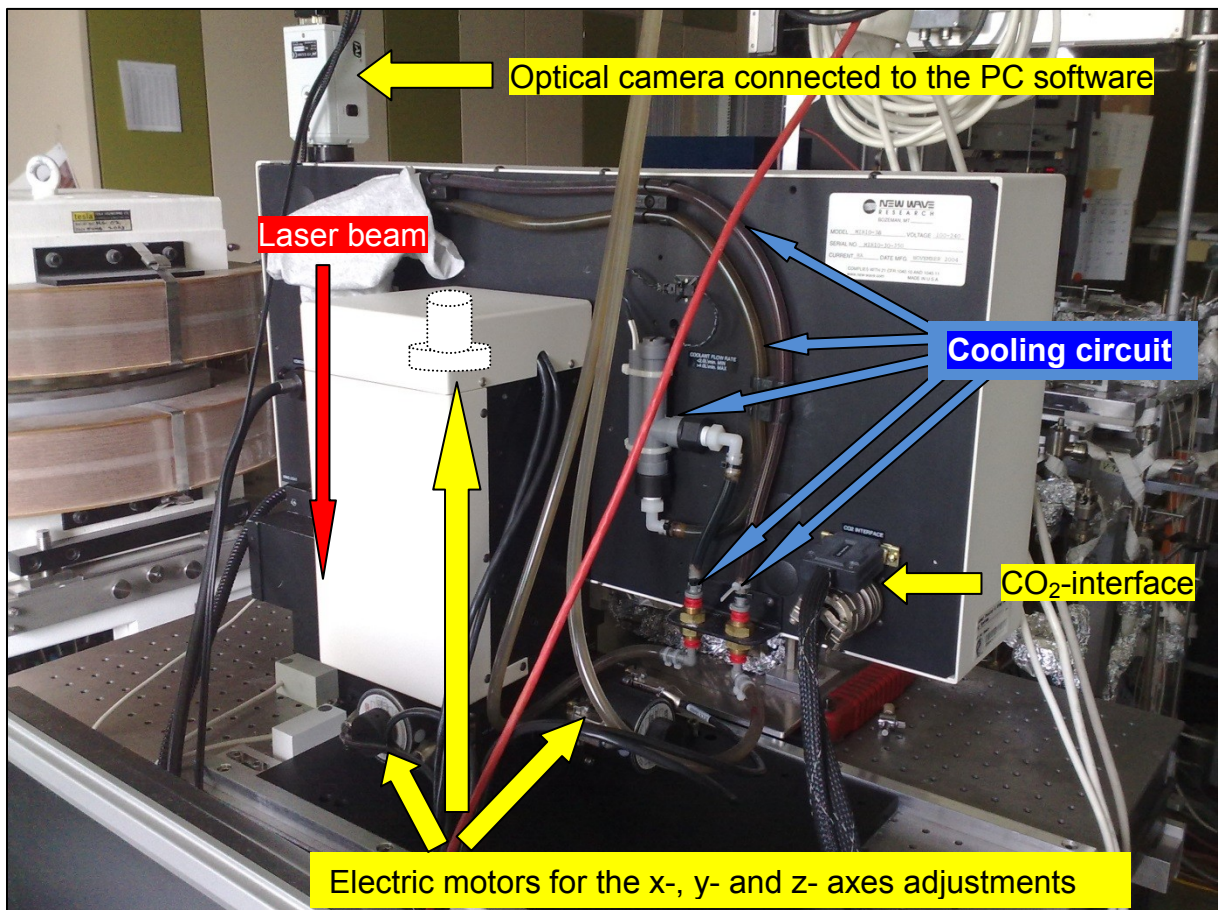
Figure 19. Photo of the CO_2-laser integrated construction (backside) showing several components including – optical camera, cooling parts, electric motors and the CO_2-charge interface. The laser beam is focused by using the optical camera which sits directly on top of the CO_2-laser arrangement.

Figure 20. Picture of the optical camera system used in combination with the CO_2-laser (New Wave Research) in order to focus the laser beam onto the samples with sizes from about 100 µm up to several mm.

As soon as all these above steps are executed and the system is fully functional, the samples can be degassed with the laser. All of these steps were also performed when we measured cold (without laser activation) and hot (with laser activation) blanks (see chapter 4.3.4.3). For calibrations different steps were performed, firstly due to the arrangement of the calibrations gases on the extraction site (Fig. 11) and secondly to the fact that the laser was not necessary to perform calibrations (see chapter 4.3.4.2).

In order to degas the sample, all valves leading to pumps in the extraction system had to be closed (V1 and V3 – see Fig. 12). Valve V4 stayed open to bring the extracted gases in getting in contact with the warm getter (produced by SAES, Italy – Fig. 21) and in initiating the first cleaning step (see next chapter 4.3.1.3). The MM particles were then degassed in three successive heating steps with laser firing durations of 3 x 1 minute each. Usually these three steps included 3 x 1 minute with 3.5% (~0.91 W), followed by 3 x 1 minute with 12% (~5W), at last 3 x 1 minute with 20-100% (~12W-32W) depending on sample and measurement date (late or early in the project) - for details see chapter 4.3.3 and the Appendix. After each heating step (e.g. 3 x 3.5% power output) a complete measurement of He to Xe in the mass spectrometer was performed.

4.3.1.3 Cleaning, calibration and separation area

Overall, system wide various types of pumps (fore-vacuum pump, turbo-molecular pump and ion-getter pump) are available. These pumps are used to clean the system of all types of gases which depends on the state in which the system is. After sample change and system contamination with air, the fore-vacuum pump and the turbo-molecular pump are used to lower the pressure level in the system, to establish a vacuum and to clean the system from most of the gases. The turbo-molecular pump and the ion-getter pumps then are used to pump away spare sample-, blank- or calibration gases as soon as one measurement step is accomplished (He, Ne, Ar, Kr and Xe). The whole system (extraction area and MS) stays in a pumped state except during release of noble gases in the sample-, blank and calibration measurements. Meanwhile several ion gauges help to monitor the system's pressure regime and detect possible air contamination due to leakage.

After the degassing with the CO_2 laser is complete, the inventory of gaseous constituents that are not adsorbed on the metal surfaces of sample holder, sample chamber and extraction tubes are allowed to expand into the cleaning part of the system and equilibrate.

The cleaning area of the extraction system consists out of a warm (getter 1) and a cold (getter 2) Zr-Al getter (Zr 84% and Al 16% - brand name St 101; produced by SAES, Italy; Fig. 21 and Fig. 12; see e.g. Jousten (2008)). The purpose of these non-evaporable getters (NEG) is to clean and separate the extracted sample noble gases from chemically active gases (Jousten (2008)). The different temperature settings of the getters are designed to encompass the different temperature reaction times of the various gases in the sample inventory. The cold getter (~25°C) mainly will adsorb (reversible) H_2, whereas the warm getter (in our case at ~250°C) overall retains chemically other reactive gases (e.g. CO, CO_2, N_2, O_2) (see e.g. Jousten (2008)).

Another part of the extraction line are the multiple noble gas calibration flasks. These metal flasks contain calibration gas and in some cases a carrier gas at reduced pressure (see Fig. 21 and Fig. 12). We used two different flasks for calibration purposes in 2010, one containing He and Ne and the other Ar, Kr and Xe (see Fig. 21). At the beginning of 2011 we changed the system to a single calibration gas flask containing all five noble gases (Fig. 22). At the beginning and during MM noble gas measurements we only used the 2011 calibration gas setup. The cylinders were filled by the MPIC laboratory technician S. Herrmann and were calibrated against the MPIC MAP 215-50 mass spectrometer noble gas standard.

The calibrations gas flasks used in 2010 were filled with a noble gas mix from Messer, Germany.

Flask 1 (He, Ne):

- Volume: 971.9 cc

- Volume pipette: 0.5683 cc (one slug per calibration measurement)

- Composition (in the first slug):
    - ^{3}He: 3.6429 x 10^{-11} cc STP
    - ^{4}He: 5.7601 x 10^{-08} cc STP
    - ^{22}Ne: 1.7167 x 10^{-11} cc STP

Flask 2 (Ar, Kr and Xe):

- Volume: 976.7 cc

- Volume pipette: 0.5665 cc (one slug per calibration measurement)

- Composition (in the first slug):
    - ^{36}Ar: 1.8363 x 10^{-10} cc STP
    - ^{84}Kr: 9.6463 x 10^{-12} cc STP
    - ^{132}Xe: 3.9832 x 10^{-12} cc STP

The calibration gas cylinder used in 2011 and 2012 was filled with a noble gas mix from Air Liquide, France.

Flask (He, Ne, Ar, Kr and Xe):

- Volume: 984.68 cc

- Volume pipette: 0.324 cc (one slug per calibration measurement)

- Composition (in the first slug):
    - ^{3}He: 3.6533 x 10^{-11} cc STP
    - ^{4}He: 7.3426 x 10^{-08} cc STP
    - ^{22}Ne: 2.0719 x 10^{-11} cc STP
    - ^{36}Ar: 2.3404 x 10^{-10} cc STP
    - ^{84}Kr: 8.0740 x 10^{-12} cc STP
    - ^{132}Xe: 4.6185 x 10^{-12} cc STP

The measurement steps described in chapter 4.3.3 were used for both calibrations since He and Ne are not captured at the cold finger (CH-1 and CH-2 – Fig. 23 and Fig. 24). The main differences between the two setups are:

1. With the 2011 arrangement (Fig. 22), it is no longer necessary to perform a two-step introduction of the standard gas in order to measure He to Xe calibration gases as in the 2010 version.

2. The volume of the extraction system changed slightly; therefore a series of new calibrations and blanks had to be performed in order to obtain the right volume factors for new sample measurements.
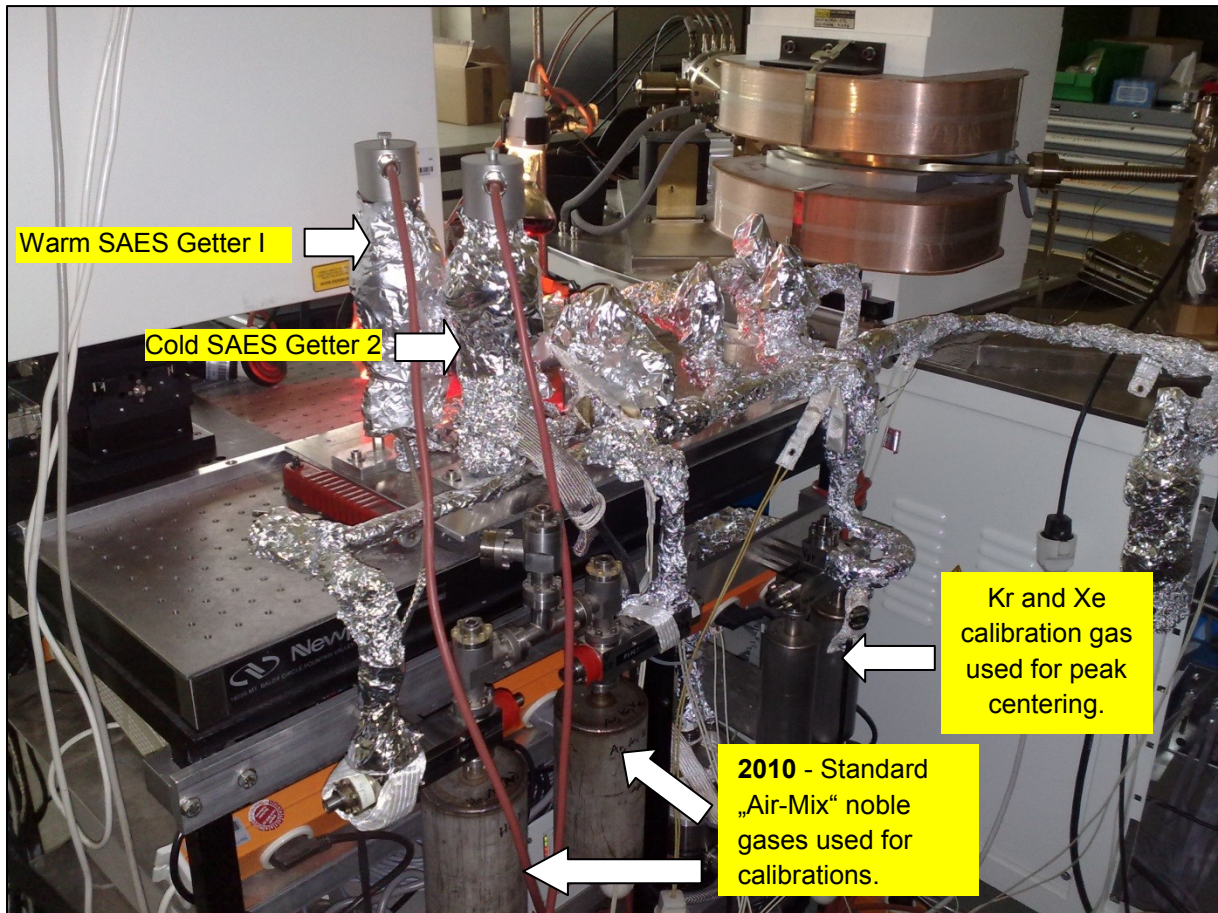
Figure 21. Image of the extraction, cleaning and separation area from 2010. Visible in the upper left corner is the CO₂-laser. On the right, in the background, is a part of the mass spectrometer "Noblesse". As illustrated in this picture, the extraction area is baked after a sample change, apparent from the aluminum foil that surrounds the heating tapes. So far only the 2010 standard calibration flasks are available (lower left corner).
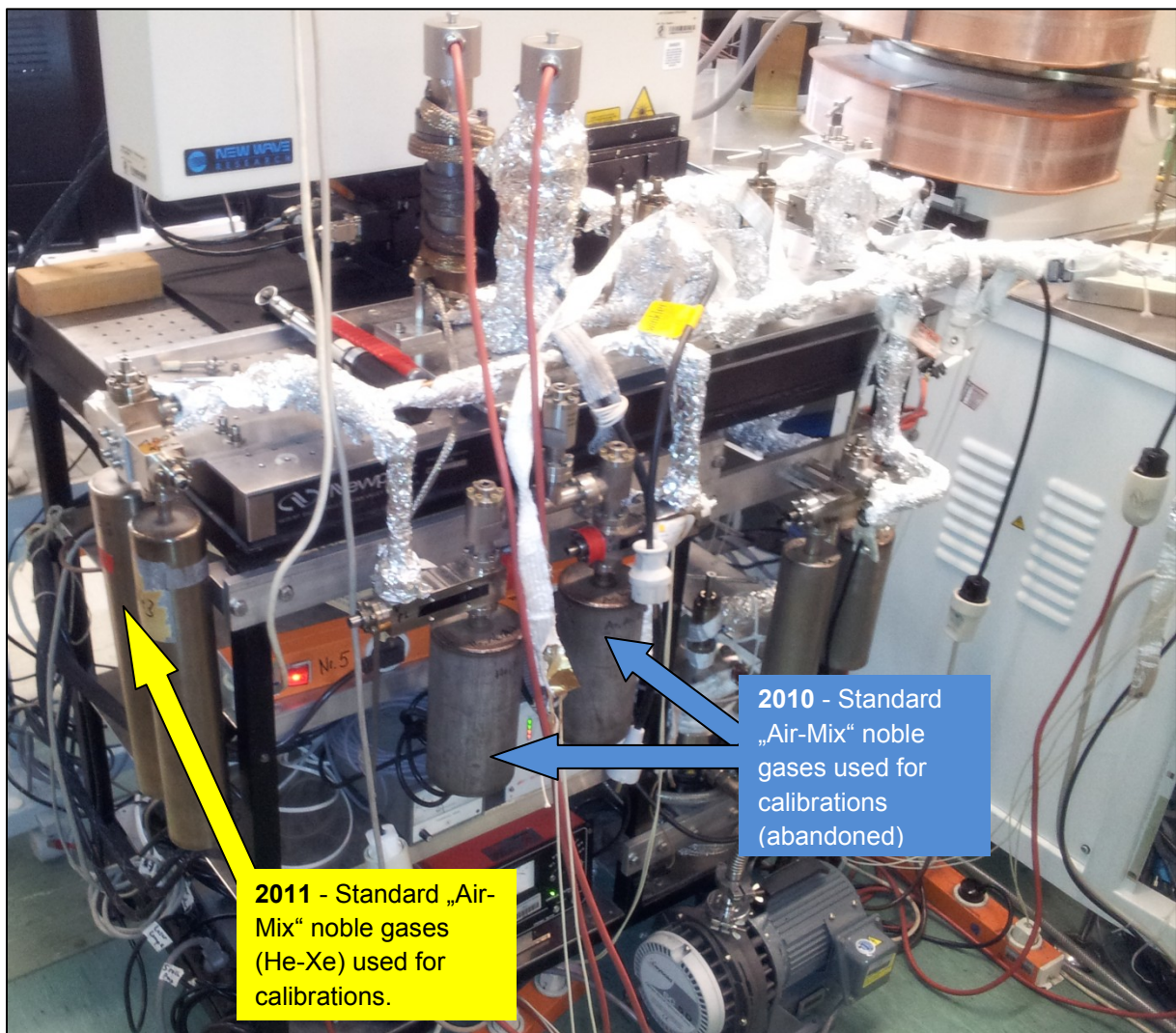
Figure 22. This picture shows the calibration gas flasks modifications made to the extraction system at the beginning 2011 (indicated with yellow arrows). The left of the two flasks contain noble gases from He to Xe. The flask on the right has only ^{3}He and was not used for the MM research. For comparison purposes the older 2010 noble gas standard flasks stayed in their place, but were not used for calibrations measurements anymore (blue arrows).

The third part of the extraction system is the separation arrangement. It consists mainly of two charcoal cold fingers (CH-1 and CH-2, see Fig. 23 and Fig. 12) supported by several valves (see Fig. 12). The valves are used to direct the noble gases through the arrangement depending on the noble gas origin (sample gas, blank gas, calibration gas) and their destination purpose (cleaning, separation, freeze and release at/from cold finger or calibration).

The CH-1 and CH-2 charcoal cold finger have the purpose of adsorbing noble gases at very low temperatures, and then releasing them in a stepwise manner to be measured in the mass spectrometer (see chapter 4.3.4 for the analysis procedure). CH-2 is additionally equipped with a metal cup containing metal Inconel pellets (Inconel is a registered trademark of Special Metals Corporation, USA) - see sketch on the right side in Fig. 23. The Inconel pellets are used for external purposes only. A better temperature constancy is guaranteed, by utilizing the pellets as a thermal inertance buffer, during the noble gas separation and release from the cold fingers. Following Cowan and Tedmon (1973), Inconel metal pellets are made out of an

austenitic (gamma phase iron - γ-Fe) Ni-Cr super alloy and are highly temperature resistant (> 1000°C); see also Dinda et al. (2009). In the past Pb-pellets were used instead. However, due to the lower melt-point of Pb, the charcoal cold fingers could not be kept for a longer duration on a high temperature (> 320°C) for effective cleaning before and/or between use for gas separation. At this juncture one or both cold finger(s) (depending on the project) is/are cooled with liquid N_2 to a minimum temperature of -196°C, so that Ar, Kr and Xe freeze on the cold finger. He and Ne remain in the extraction system as gases due to their high volatility. Another charcoal cold finger is mounted at the mass spectrometer (Fig. 12). Its only purpose is it to adsorb background Ar in the He and Ne fraction (see also chapters 4.3.2 and 4.3.4). For the description of the analyses procedure see chapter 4.3.4.

Charcoal cold finger **(CH-1)**

Charcoal cold finger **(CH-2)** equipped with a metal cup containing temperature-resistant Inconel metal pellets.
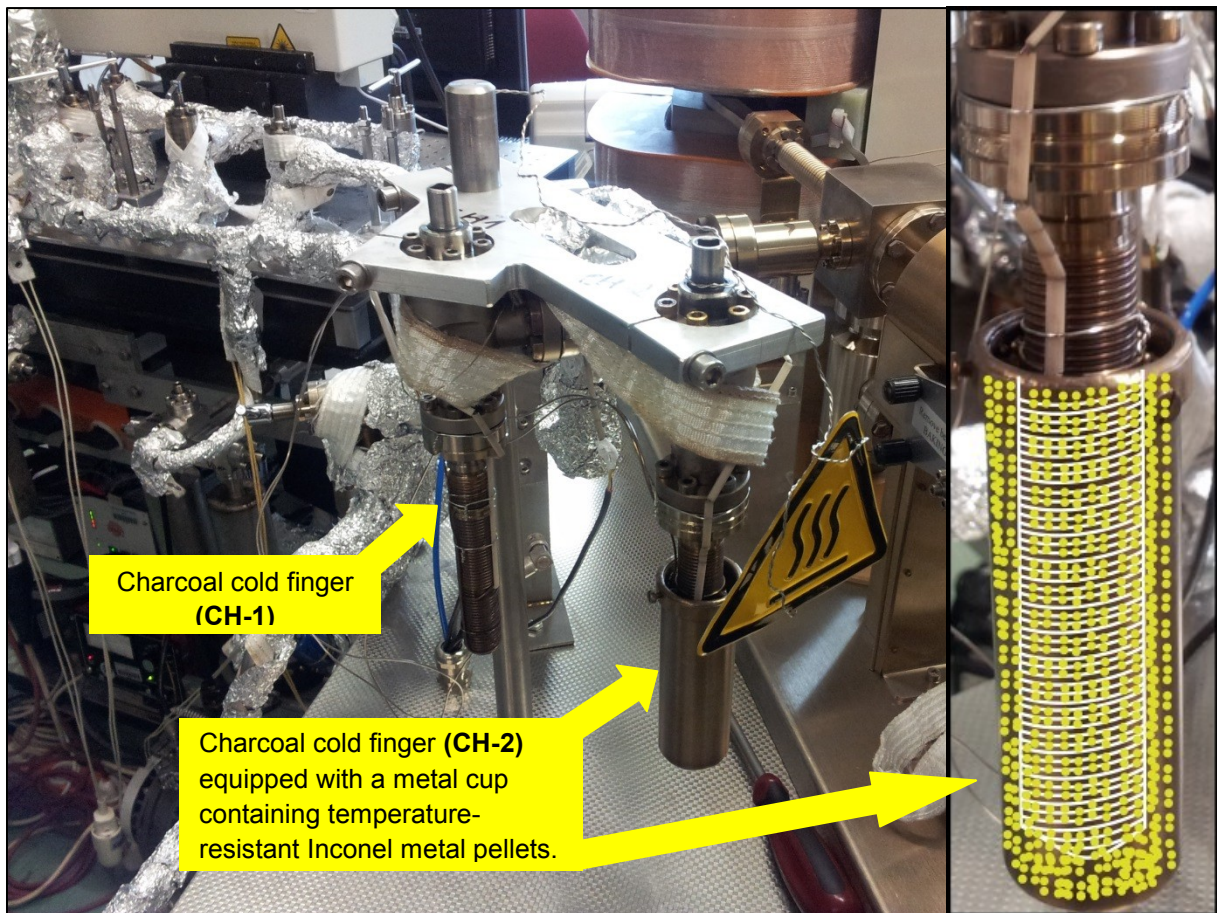
Figure 23. This picture shows the two charcoal cold fingers (CH-1 and CH-2) mounted on the extraction and separation arrangement. CH-2 is additionally equipped with a metal cup containing metal Inconel pellets (Inconel is a registered trademark of the Special Metals Corporation, USA) - see sketch on the right side. The Inconel metal pellets are made out of an austenitic Ni-Cr super alloy and are highly temperature resistant (see e.g. Cowan and Tedmon (1973)).

4.3.2 Nu Instrument noble gas mass spectrometer "Noblesse"

In the laboratory environment, we use a state of the art high-sensitivity noble gas mass spectrometer (MS) from Nu Instruments (Fig. 25) - "Noblesse" - coupled with an extraction system based on a CO_2-laser and separation systems with cold-fingers (see also chapter 4.3.1 and Ott et al. (2010)). The multiple-ion counting detection system leads to high ion detection efficiency. The PhD project focused partly on the aspect of bringing the mass spectrometer into operation and optimizing the procedures for gas extraction, gas handling and ion detection in accordance with the small gas amounts to be expected from MMs.

Information in the following paragraphs of chapter 4.3.2 of general instrument description is, except for other specified references, from the 2003 Nu instrument "Noblesse" manual.

The mass spectrometer "Noblesse" possesses a 75º magnetic sector design with a 240 mm magnet radius. The entrance and exit pole are nonstandard and therefore the dispersion at the collector plane makes it possible to double the magnet radius (480 mm). Because of two additional miniature lens arrays (steering potentials), one is able to alter the dispersion even more. This makes it is possible to perform multi-collector analyses without having to move the collectors themselves in order to measure different elements. The source of the "Noblesse" is a modified Nier design (e.g. Pepin and Signer (1994)) and is optimized for static vacuum (Fig. 24). The process of ionization is induced by a heated tungsten filament which leads into forming an electron beam. The acceleration voltage provided by the electronics, source and filament is up to 8kV. Two ion getter pumps are directly mounted near the source and the collector to maximize pumping effects after measurements. One getter pump is set up immediately behind the source to keep this area clean. Additionally, a fore vacuum pump and a turbo pump are connected to the entire MS system to provide rapid pumping when gas volumes exceed certain limits - e.g. system leaks and gas rich samples. In order to measure high gas volumes the detector and collector area is equipped with a Faraday collector. In the case of low gas amounts, 8 channeltrons are ready to be used in a multicollector mode.

To summarize, the MS array consists of several compartments (see Fig. 25):

- Inlet area (pneumatic and magnetic)

- Ion-source with ionizing filament, ion repeller (small electrode), electron trap, ion accelerator (half plates and zero plate) and beam focusing. (Fig. 24).

- Fore Vacuum-, Turbo- Getter and Ion Getter pump

- Several valves and gauges

- Several digital displays for controlling source, pump and collector activities and values

- Electronic system - connected to a PC via serial interfaces

- Charcoal cold finger

- Magnet and separation tube

- Miniature lens arrays - steering potentials - similar to an electrostatic quadrupole

- Multi-collector array with multiplier (channeltrons) and Faraday detector
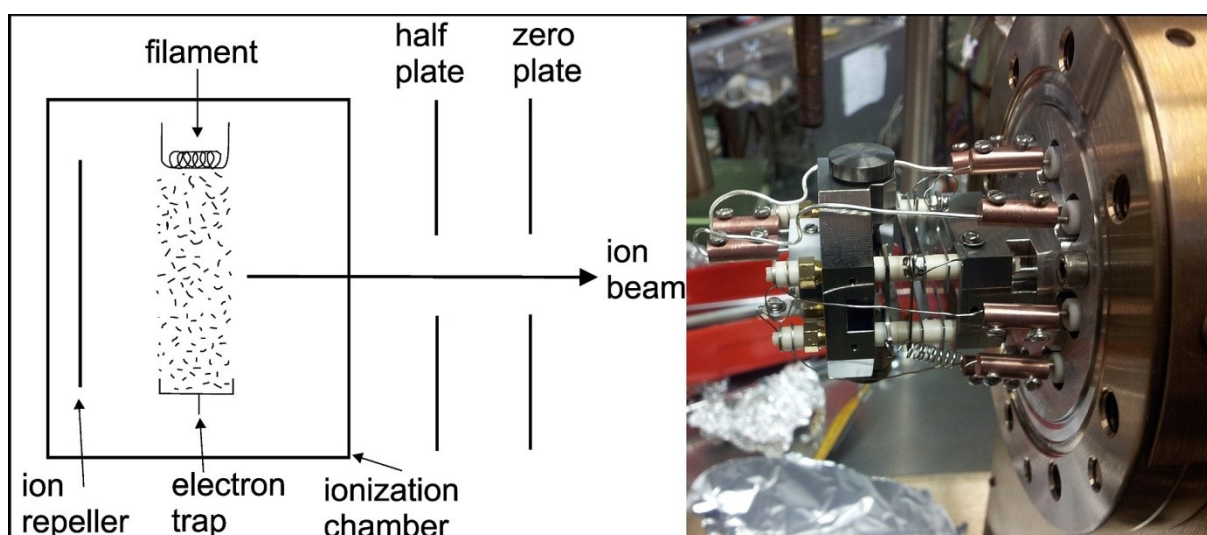
Figure 24. Combined illustration and image of the ion source equipped with the "Noblesse" mass spectrometer. An electron beam, established by a heated tungsten filament, ionizes the rare gas atoms. The majority of electrons sent through the source is picked up on the electron trap. During trap current stabilization, the total emission has to be monitored. The repeller is designed to repel ions out of the source, while the source area is kept at a positive high voltage of 3 to 8 kV. The half and zero plates are used to steer the ions in the beam in the right direction, out of the source chamber. Typical values for filament, emission, trap, repeller and half plates are shown in Fig. 25. (Illustration on the left side after 2003 Nu instruments "Noblesse" manual).
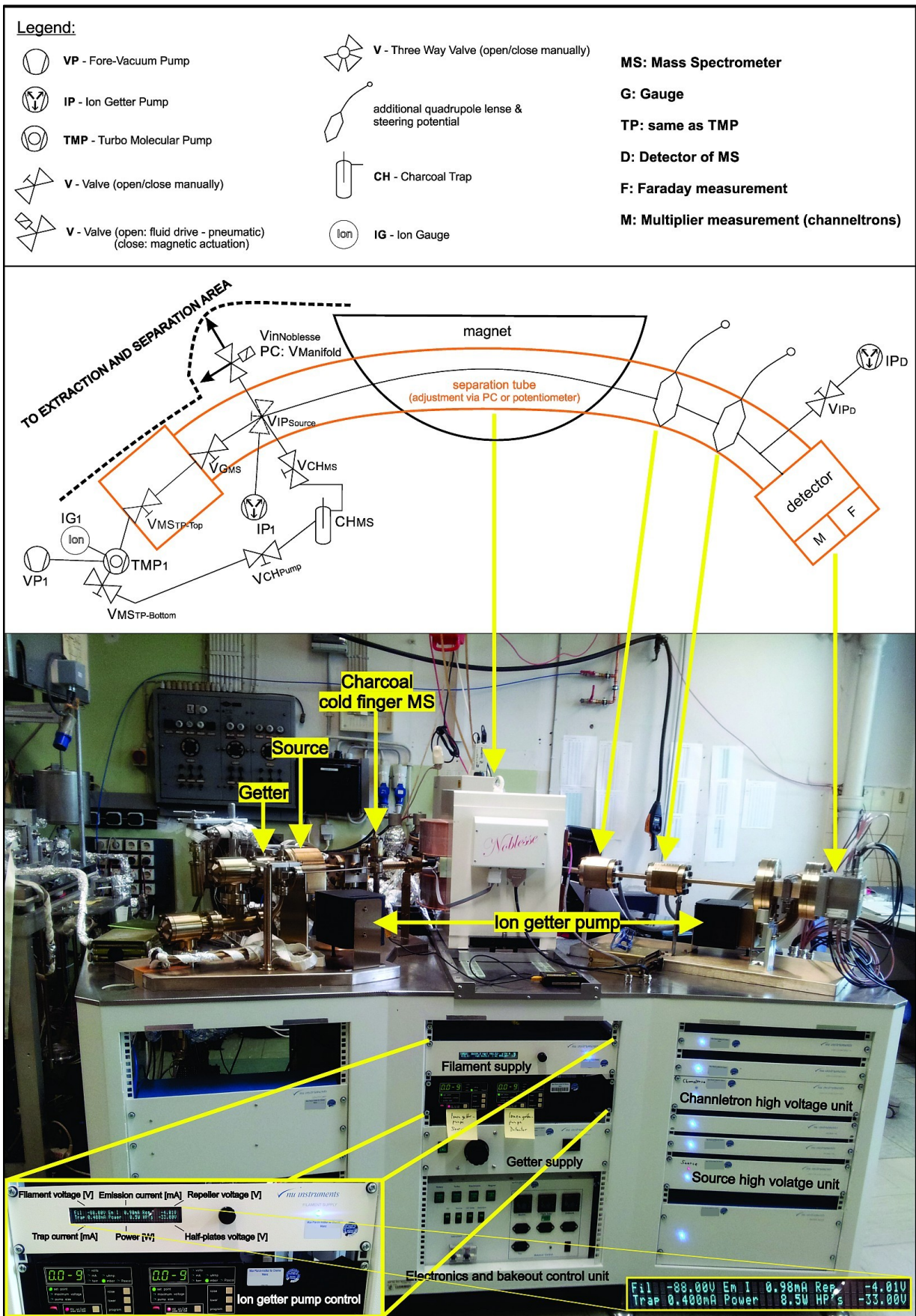
Figure 25. Combined photo and schematic showing the noble gas mass spectrometer "Noblesse" at the MPIC in Mainz. Highlighted are frequently used and important components and units. Exemplary values and units for filament (Fil), emission (Em I), repeller (Rep), trap and half plates (HP´s) are shown in the lower right corner.

Other noble gas mass spectrometers are dedicated to single or double noble gas element detection, hence provide a higher sensitivity for this/these (two) element(s) than the "Noblesse" at MPIC does (see Fig. 26).

Examples are the:

- Noble gas mass spectrometer compressor source build by H. Baur at ETH Zurich, Switzerland, which uses an increased partial pressure induced by a molecular drag pump to achieve a higher sensitivity for He (and Ne) multiplied by about 100 compared to a "conventional" MS (Baur (1999), Burnard et al. (2013)). A possible disadvantage is that due to the high efficiency of the MS, the high pumping rate of the ion source leads to less efficient measurements for heavier ionized noble gas elements (U. Ott, MPIC Mainz, personal communication, 2013).

- Resonance ionization, time-of-flight (TOF) mass spectrometer (RELAX) at the University of Manchester, UK (Gilmour et al. (1994)). Using a combination of a cryogenic sample concentrator, a resonance ionization source and a TOF-MS makes it possible to achieve an increased sensitivity especially for Xe of about 1000 atoms (^{132}Xe) (see Crowther et al. (2008)). However, the instrument is limited to Kr and Xe measurements.

In contrast, it is possible to measure **all** of the noble gases (He to Xe) with high sensitivity using the "Noblesse". This is achieved, besides by using a high-efficiency ion source, by the multi-detection of beams. In a conventional mass spectrometer, usually a single detector mode would be used to measure isotopes. In this case one isotope after another would be measured by changing the magnetic field for each isotope. The disadvantage would be that all atoms introduced in the source would be ionized and pumped, but not detected (e.g. Mellon (1989)). The non detected portion of ions is minimized using multi-detection.

In case of Xe, during the first measurement step all **even**-numbered isotopes from ^{124}Xe to ^{136}Xe are measured simultaneously (Table 7; Step 1 and 1a). For the following second measurement the magnetic field is shifting by one mass unit, resulting in the measurement of the **odd**-numbered isotopes ^{129}Xe and ^{131}Xe (Table 7; Step 2). Results from an exploratory study using a small fragment of the Murchison (CM2) meteorite (e.g. Fuchs et al. (1973)) as an analog are shown in Fig. 26.
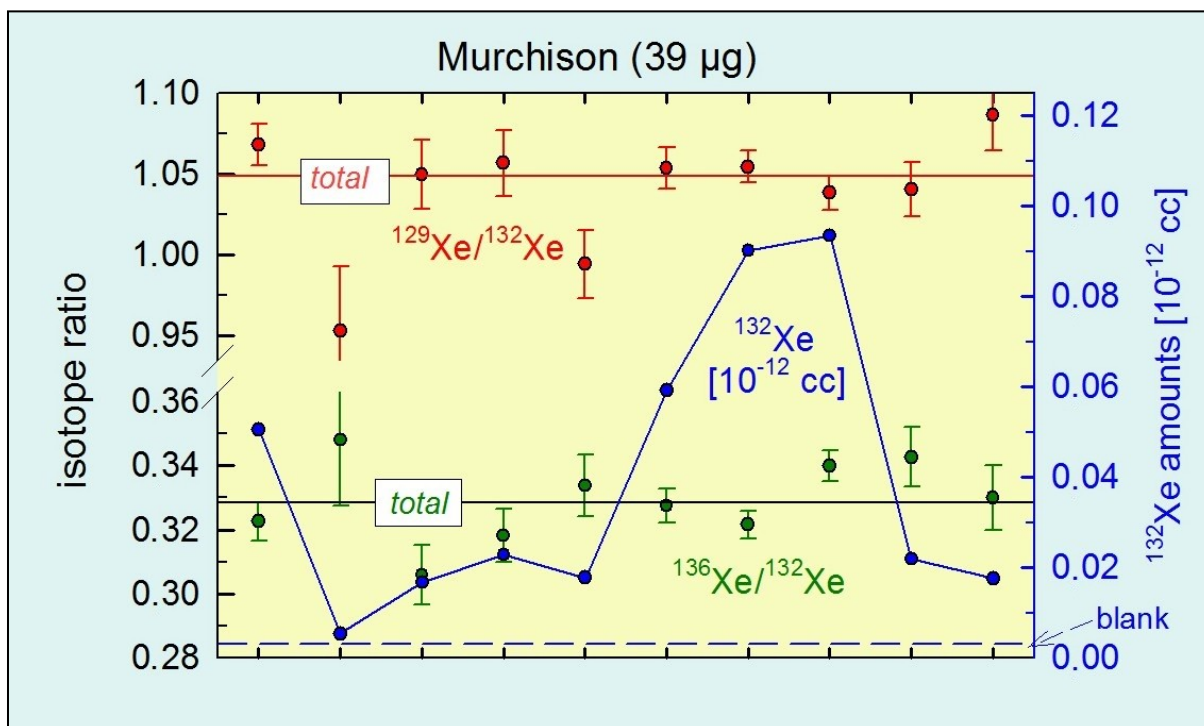
Figure 26. Xe-data obtained for Murchison (CM2) (e.g. Fuchs et al. (1973)) from stepwise analysis. The multi-ion counting of the "Noblesse" provides the possibility of measuring small noble gas amounts with accompanying small diagnostic errors. The blue dashed curve represents the blank level during measurement and shows low amounts of ^{132}Xe in the area of ~3 x 10^{-15} cc STP (~80.000 atoms). Furthermore, for ^{132}Xe amounts of 10^{-13} to 10^{-14} cc STP, the mass spectrometer allows the determination of crucial isotopic ratios (e.g. $^{129}Xe/^{132}Xe$ and $^{136}Xe/^{132}Xe$) with a precision of ~2% to ~3% (red and green line). Murchison is used as an analog since most MMs are thought to resemble meteorites of type CM in composition e.g. Kurat et al. (1994) (unpublished data plot (not blank corrected) made by U. Ott, MPIC, Mainz, for presentation at the 73rd Metsoc poster session in 2010; see also Ott et al. (2010)).

During modification and optimization of the "Noblesse" measurement procedures, a new three step measurement scheme for Xe with an extra channeltron (see Table 7; Step 1a and chapter 4.3.5.1) was implemented, with the aim of achieving an internal calibration of the relative responses of the individual channeltrons. In this new procedure Xe in samples, blanks and calibrations is measured using 20 measurement cycles in the standard procedure (see chapter 4.3.4).

Table 7. "Noblesse" Xe channeltron detector setup for internal calibration.

Channletron-detector	IC 0	IC 1	IC 2	IC 3	IC 4	IC 5	IC 6	IC 7
Step 1	136	134	132	130	128	126	124	
Step 1a		136	134	132	130	128	126	124
Step 2			131	129				

4.3.2.1 Channeltrons

The following paragraph of chapter 4.3.2.1 describing channeltrons, except for other specified references, follows the 2003 Nu instrument "Noblesse" manual.

Channeltrons or channel electron multipliers (CEM) are continuous dynode multipliers, which consist of a thin ceramic or glass vacuum-tube (e.g. Goodrich and Wiley (1962), Richter et al. (1994)). One of the earliest studies performed on an electron multiplier was done by Allen (1947). Following Richter et al. (1994), the inner tube is coated with an emissive high resistance layer (e.g. lead oxide). Single electrons get multiplied into several electrons due to bombardment onto the negatively charged high resistance layer causing secondary emission (Richter et al. (1994)). These newly formed electrons are accelerated down the tube and again form new secondary electrons. This process continuous until the end of the channel and a pulse of 10^6 to 10^8 electrons per incoming ion is reached. Afterwards this pulse will be counted as a single event. Occasionally channeltrons get very warm due to their high resistance of ~ 200 MΩ ("Noblesse": 3-30 MΩ) and high voltage (2-3 kV) when active (Richter et al. (1994)). Therefore these detectors should only be used for the purpose of measuring small gas amounts and be active for a limited amount of time.
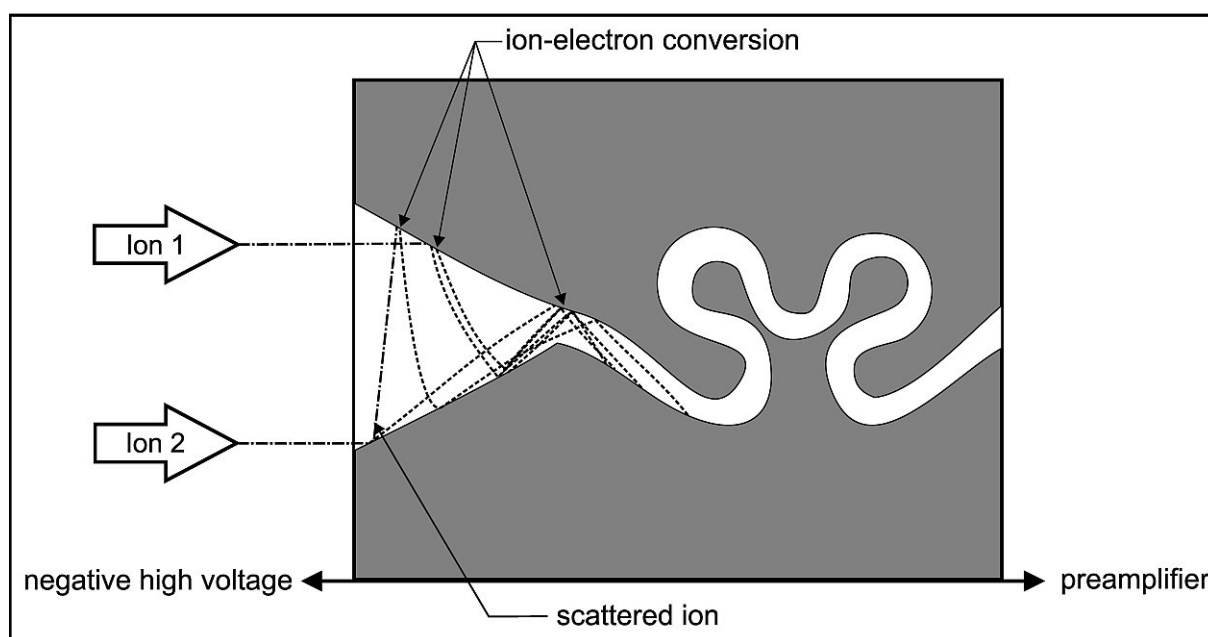
Figure 27. This schematic illustration shows the general mode of operation of a channeltron. Charged particles (ions) arrive at the detector array after going through the source and the magnet area of a mass spectrometer. While hitting the inner tubes emissive and negatively charged resistance layer, the ions get multiplied into several secondary electrons. These conversions continue until the electrons reach the end of the tube. The signal then gets preamplified to be detectable and visible on an analog or digital interpreter (after Richter et al. (1994)).

As also pointed out by Richter et al. (1994), it is essential to know the channeltrons efficiency, stability, dark current and dead time in order to operate them in a useful manner. Furthermore it is important to produce flat top peaks in order to be able to accurately measure and separate peaks that are near to each other in the mass spectrometer (Richter et al. (1994)). The same is important for channeltrons mounted on the "Noblesse" mass spectrometer (Fig. 28), the performance of which is shown in Fig. 29.

Channeltron collector mounted on "Noblesse" at MPIC, Mainz

IC7 | IC5 | IC3 | IC1

Faraday

IC6 | IC4 | IC2 | IC0
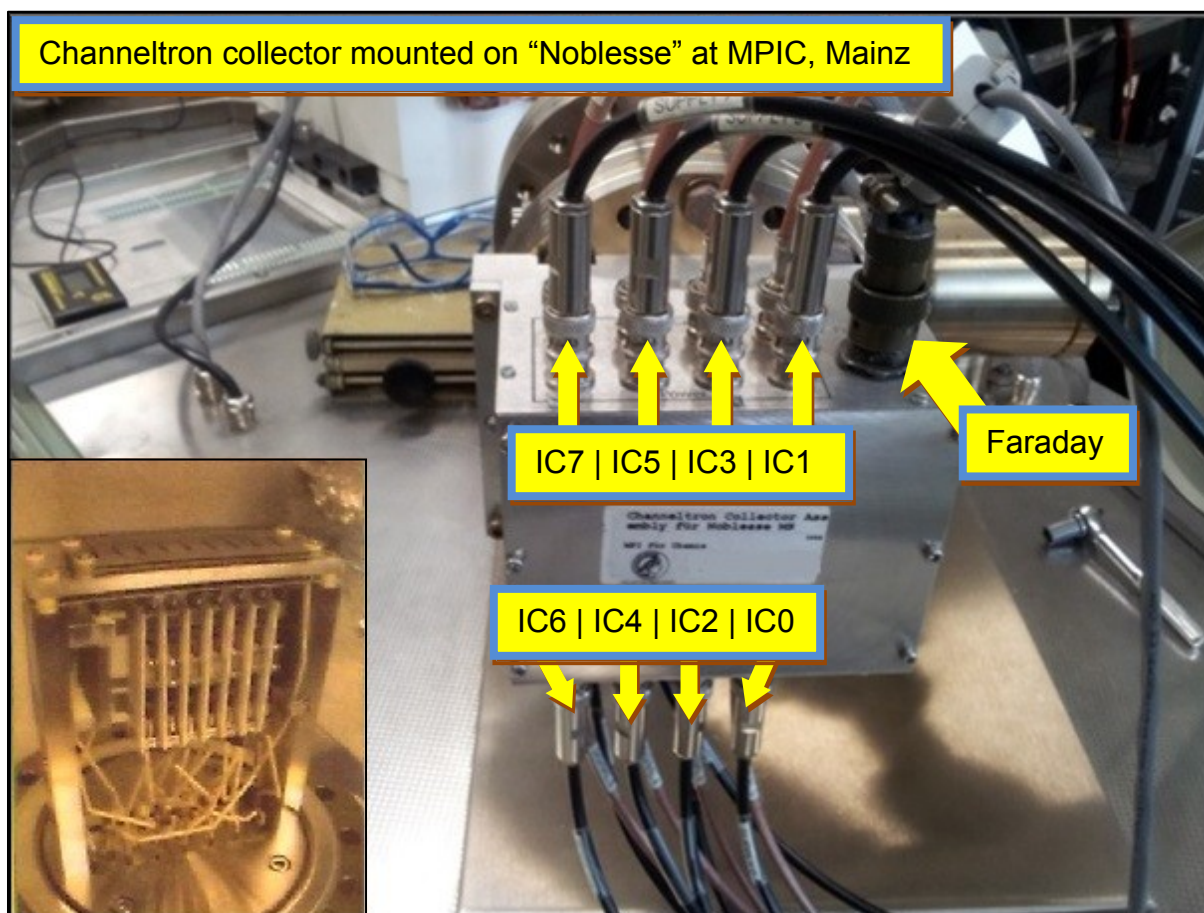
Figure 28. The large picture shows the electronic box, containing the channeltron array (IC0 to IC7) and the Faraday detector, together with the supply and signal wiring mounted on the "Noblesse" mass spectrometer at MPIC in Mainz. The inset picture (lower left) provides an overview of the inner core of the channeltron arrangement. Visible are, the front with slits, the ceramic tubes and the internal wiring (Inset picture with courtesy of U. Ott, MPIC, Mainz).

Generally it is easier to attain flat top peaks while measuring Ar, Kr and Xe rather then He and Ne due to the former's higher *m/z* ratio. A typical channeltron multicollector flat top peak (Xe) for the "Noblesse" is demonstrated in Fig. 29.
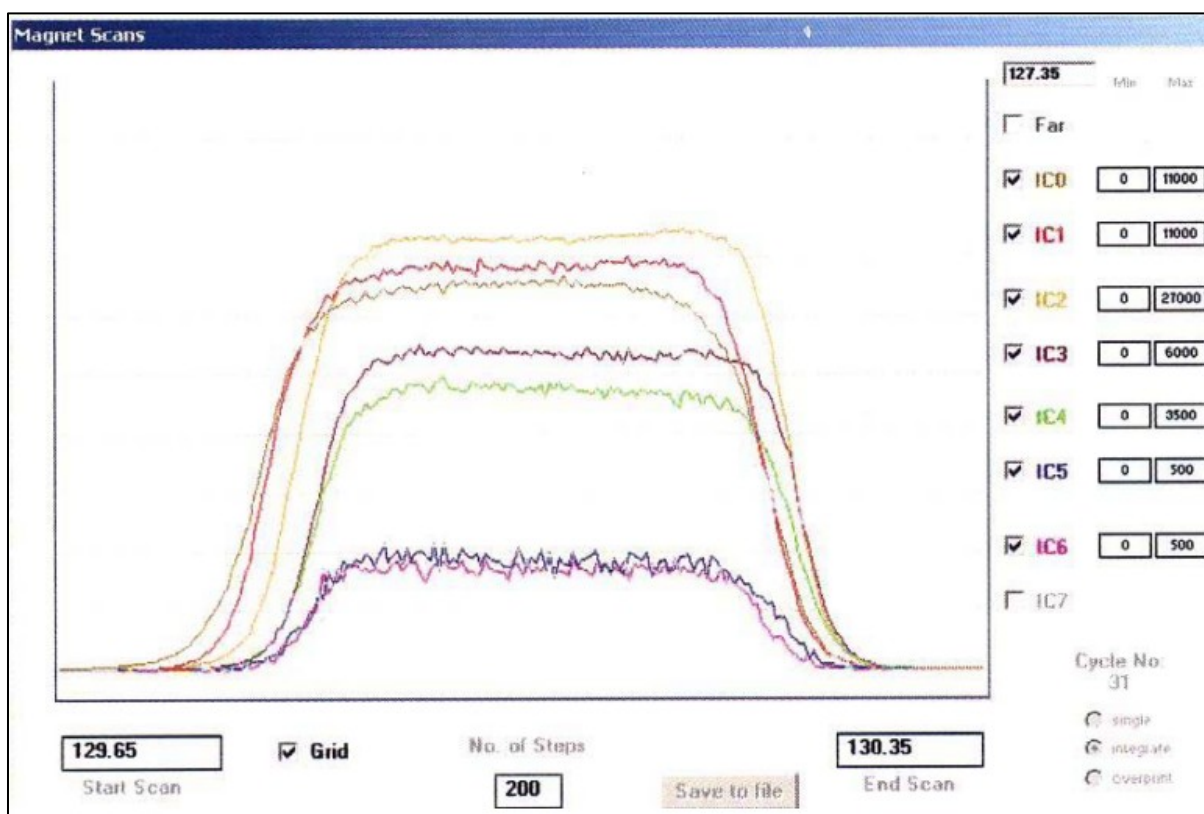
Figure 29. Plot showing a "Noblesse" multi-collector scan for Xe from the standard calibration gas. Also visible are the channeltrons flat top peaks with no change in the count rates along with small changes in the magnetic field. In this example the count rate at the central IC3 is ~3000 cps (^{130}Xe), while that for the largest peak (^{132}Xe on IC2) is ~20000 cps. By setting the magnetic field corresponding to m/z 130 at the central IC3, all other even-numbered Xe isotopes are on the peak plateau of their respective channeltrons and can be measured simultaneously.

Channeltrons are delicate and need constant intercalibration. In this, the level of "cross-talk" is of interest, i.e., for a given signal on one of the channeltrons, how much stray signal is "seen" by neighboring ones, by, e.g. picking the electronic signal up like an "antenna" (Richter et al. (1994)). A check was performed using ^{4}He standard calibration gas in August 2010. After inlet of ^{4}He into the mass spectrometer, each channeltron was successively activated, and the amount of ^{4}He detected was measured. After this, the other channeltrons were successively activated and the observed signal in counts per second [cps] was recorded. The further away the channeltron was from the first one, the less ^{4}He was detected, as expected (in some cases no ^{4}He was detected). Table 8 shows the results. The data show that there is only a small influence (< 1 ‰) on neighboring channeltrons. Even so small that there may be a noticeable influence on the isotopic ratios, if the isotope measured on the neighboring channeltrons is much smaller in abundance. In our data reduction scheme (see below) we have implemented a correction for "cross-talk" based on the results in Table 8, therefore). The result also suggests that apparently channeltron IC3 provides the most reliable results in the multi-detection mode (e.g. for Xe isotopes) since it seems to be least influenced by the "cross-talk" of the other channeltrons (especially IC 2 and IC4). IC0 and IC7 are also potentially suitable for reliable measurements since they obtain "cross-talk" from one neighboring channeltron only.

Table 8. "Cross-talk" survey on the channeltrons of the "Noblesse" in 2010. Results are denoted in counts per second [cps].The yellow marked fields indicate the activated channeltron and its measured overall signal height, whereas the green fields highlight the major "cross-talk" between the activated and neighboring channeltrons. The fields with <5 cps indicate that the measurement is near or at the background of the mass spectrometer.

Channeltron "cross-talk" (green) in [cps]	IC 0	IC1	IC2	IC3	IC4	IC5	IC6	IC7
^{4}He peak set on IC 0	~68000	~600	<5	<5	<5	<5	<5	<5
^{4}He peak set on IC 1	~400	~68000	~300	<5	<5	<5	<5	<5
^{4}He peak set on IC 2	~40	~550	~69000	~200	<10	<5	<5	<5
^{4}He peak set on IC 3	<5	~30	~500	~68000	~200	~100	<5	<5
^{4}He peak set on IC 4	<5	<5	~100	~570	~61000	~200	~20	<5
^{4}He peak set on IC 5	<5	<5	<5	~20	~300	~59000	~80	~20
^{4}He peak set on IC 6	<5	<5	<5	<5	~100	~400	~55000	~120
^{4}He peak set on IC 7	<5	<5	<5	<5	<5	~100	~350	~55000

4.3.3 Improvements on the instrumental setup: gas extraction

In this chapter I will explain how we improved the degassing of samples by the laser, and the measurements by using a different sample holder.

At the beginning of the project, all the measurement and analysis procedures had to be tested and improved. The goal was to optimize the operation of the instrument. This involved performing a large amount of blank and calibration analyses in order to optimize the system and determine how efficiently it worked (see chapters 4.3.4.1 and 4.3.4.2). In the previous chapter it was explained how the sensor/detector array was equipped and how it was maintained and improved. In the next stage of development we used our system on standard samples, including small pieces of the Murchison (CM2) and the Lakewood (L6) meteorite, to extract and measure the noble gases within them. Once complete the data was compared to both, the literature and data produced by our other long used and improved mass spectrometer MAP 215-50.

Two well-characterized meteorites, the carbonaceous chondrite Murchison (CM2) (e.g. Fuchs et al. (1973)) and the ordinary chondrite Lakewood (L6) (e.g. Schultz et al. (2005)), were used to determine the accuracy and reliability of the extraction, separation and measurement system. Murchison was used because it has some similarities to MMs, as already mentioned earlier (see chapter 3.1.4 and Kurat et al. (1994)). Therefore, small pieces (µm-size) of Murchison which were measured on the "Noblesse" were expected to provide information regarding the system's reliability and accuracy when measuring MM type material. Lakewood has a relatively high cosmogenic ^{21}Ne content and was therefore perfect for estimating how much laser power was needed to start degassing major common meteoritic minerals. However, these two meteorites are not fully identical to MMs, so at a later stage in the project we also performed tests using some of the acquired MMs. The test samples chosen were first, very abundant and second, already slightly degassed or fully degassed (i.e. Cosmic Spherules and scoriaceous MMs).

Further we characterized the performance of the extraction system by using metals (Table 9) to determine at which intensity the laser reaches a certain temperature. Commonly, the melting point of elements changes only with extreme transition in pressure (e.g. Tonkov and Ponyatovsky (2005)), hence heating the metals in the sample holder with the laser array, will approximately melt them at their characteristic melting temperature. Additionally, if we know that (idealized) certain minerals like trigonal α-quartz melt at 573°C (1st modification), hexagonal β-quartz at 573-870°C (2nd modification) (e.g. Demange (2012)) and feldspars roughly melt at 1100-1550 °C (e.g. Demange (2012)), but others, like olivines melt at higher temperatures (especially forsterite at 1890°C, e.g. Demange (2012)), the laser intensity can be used to estimate the temperatures during future measurements. However, the more complex the composition of minerals and rocks, the wider the melting point range will be. Nonetheless, this method allows to a certain extent, to determine the optimum temperature at which to extract the noble gases while avoiding getting additional (blank) noble gases from the sample holder.

Still, it is important to keep in mind that it is significantly more difficult to determine the "real" temperature of a sample when using a laser system rather than

in an oven, where essentially a temperature equilibrium is reached. Each material has its specific radiation energy absorption properties and therefore attains its own specific temperature, even for the same laser setting. For example, when lasering a stony sample with a low albedo there is strong energy absorption and the sample reaches a high temperature (ALBEDO *is a reflection coefficient with values between 0 and 1; It is defined as the ratio of incident light versus reflected light from a surface of a body e.g. Russell (1916) and references therein*). Whereas a metal sample with high albedo (e.g. iron or molybdenum) would reflect large portions of the incident energy, resulting in less heating.

Table 9. Laser settings for which the melting points of typical metals were reached using the CO_2-laser extraction system at MPIC in Mainz. The laser´s beam diameter was set to 1000 μm and the mode on continuous wave (cw). All the samples had a similar weights.

Metal or mineral tested	Melt point in °C	Reference	Laser power in [W] needed to melt sample	Percentage laser power needed to melt sample	Duration of laser activity in [s] to melt sample	Melted
Qz (1st mod.)	573	[1]	3.9	10%	8	Yes
Al	660.32	[2]	5.2	12%	9	Yes
Ag	961.78	[2]	15.8	30%	60	Yes
Au	1064.18	[2]	19.7	40%	8	Yes
Cu	1084.62	[2]	20.2	42%	10	Yes
Ni	1455	[2]	22.1	45%	5	Yes
Pt	1768.2	[2]	23.7	50%	2	Yes
Mo	2622	[2]	no melting	no melting	180	No

References: [1] Demange (2012) [2] Haynes et al. (2012)

Generally, radiative equilibrium describes a system where the amount of heat flux, produced by radiation (e.g. by a laser), going into the system and coming out of the system is the same, as well as conduction and convection of heat is insignificant (Modest (2013)). Following Modest (2013), most heat transfers due to conduction and convection show a linear relation to temperature. Furthermore, Modest (2013) explains that usually radiative heat transfers are directly linked in proportion to a temperature change to the fourth power. Results showing the laser energy (in watts) needed to melt the samples versus the characteristic melt temperature (in Kelvin, to the fourth power) are shown in Fig. 30 and Fig. 31. Noticeable in both plots is that Gold (Au), Copper (Cu), Nickel (Ni) and Platinum (Pt) are fitting more or less in a row (symbolized by the dotted straight line). This leads to the assumption that these metals show similar behaviors in energy absorption. Molybdenum (Mo) does not fit and plots below the line which shows that Mo will not melt at the laser energy provided. Silver (Ag) does not plot on the line as well, which maybe can be explained by the preselected laser energy of 15.8 W, which probably is too low to melt the metal within 10 seconds and therefore a longer duration of laser activity was needed to achieve the melting. Quartz (Qz) does not fit on the line due to its energy absorbing capabilities, therefore it melts at a lower laser energy of 3.9 W. Aluminum surprisingly does not fit on the line either, which can be explained by the fact that instead of pure Aluminum, Aluminum-foil was used to perform the test. Aluminum-foil consist out of different other metals and is very thin.
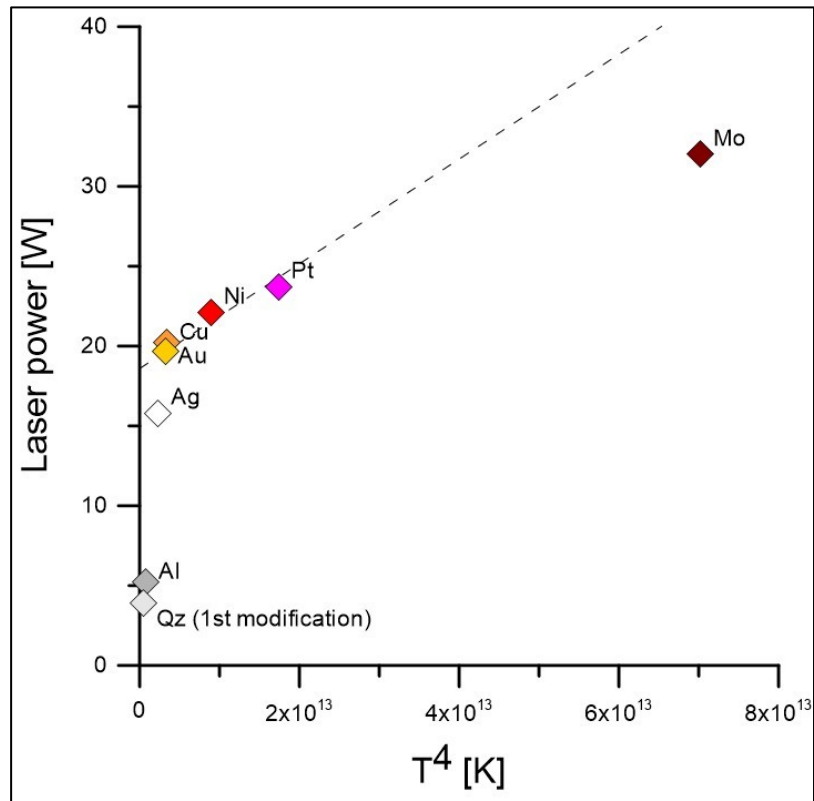
Figure 30. Plot showing the correlation between laser power [W] and temperature (to the power of four), for 7 metals and quartz. Observable is that Au, Cu, Ni and Pt are fitting on a straight line which suggests that these metals have similar energy absorption rates. See text above for more details regarding the results.
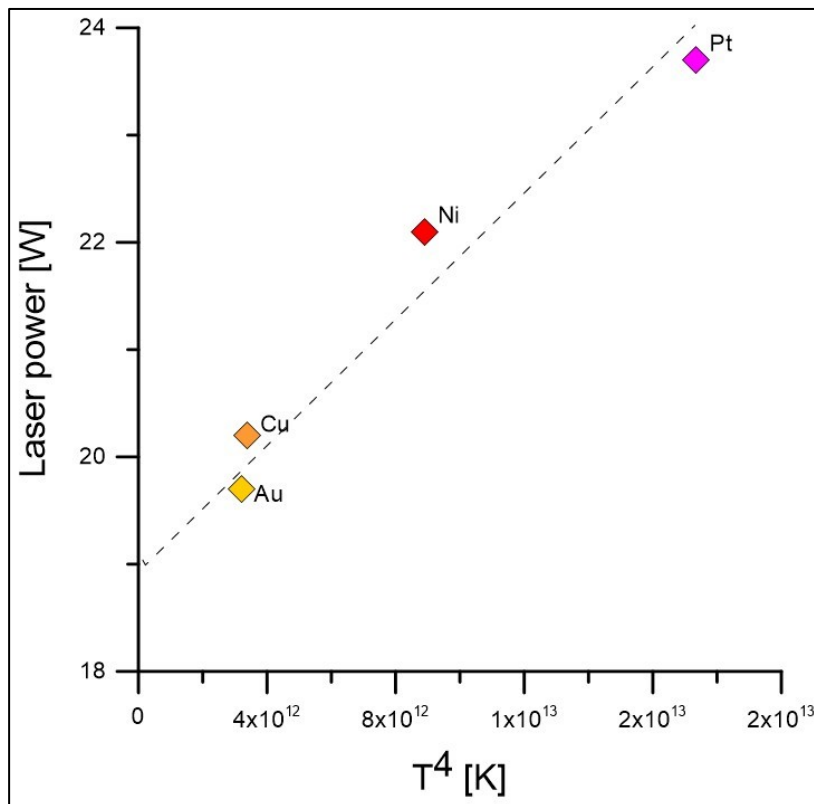
Figure 31. Plot showing the correlation between laser power [W] and temperature to the power of four, for Au, Cu, Ni and Pt. These metals show good energy to temperature correlation (see text above for details).

The sample holder originally used at the beginning of the project was found to be unsuitable for measuring micrometeorites. The sample holes were rather closely spaced in a relatively small area (Fig. 14), which may have resulted in "passive" heating of neighboring sample holes during a sample degassing by the CO_2-laser. Thus we came to the conclusion that it would be better to use less sample holes on the holder and arrange them on top of columns (Fig. 32 and Fig. 33). It was hoped this would help in minimizing the influence on neighboring samples, improve the measuring procedures and lower the blank as much as possible. The new sample holder was realized with generous help of the MPIC mechanical workshop.

Nevertheless, even with the new sample holder, some degassing of neighbored samples still occurred. A further disadvantage was that the vacuum system had to be opened more frequently in order to load new samples, which cost time and increased the danger of acquiring leaks.

Therefore, we went back to the old standard sample holder, and rather than filling all holes with samples, placed only a few as far from each other as possible. Together with a low energy setting of the laser (< 1W), it was possible to limit the release of noble gases to just the samples to be analyzed (see also chapter 4.3.1.2). Nearly no degassing from the sample holder occurred and the blank was very low (see chapter 4.3.4.2 for results and details). An even lower blank might have been achieved by heating the sample holes with the laser before the samples were placed. However, this would have required an extra opening and closing of the extraction system, under high vacuum conditions. Presumably this extra step would have improved the cleanness of the sample holder itself; however, due to the limited duration of the project, it was not possible to implement this procedure.
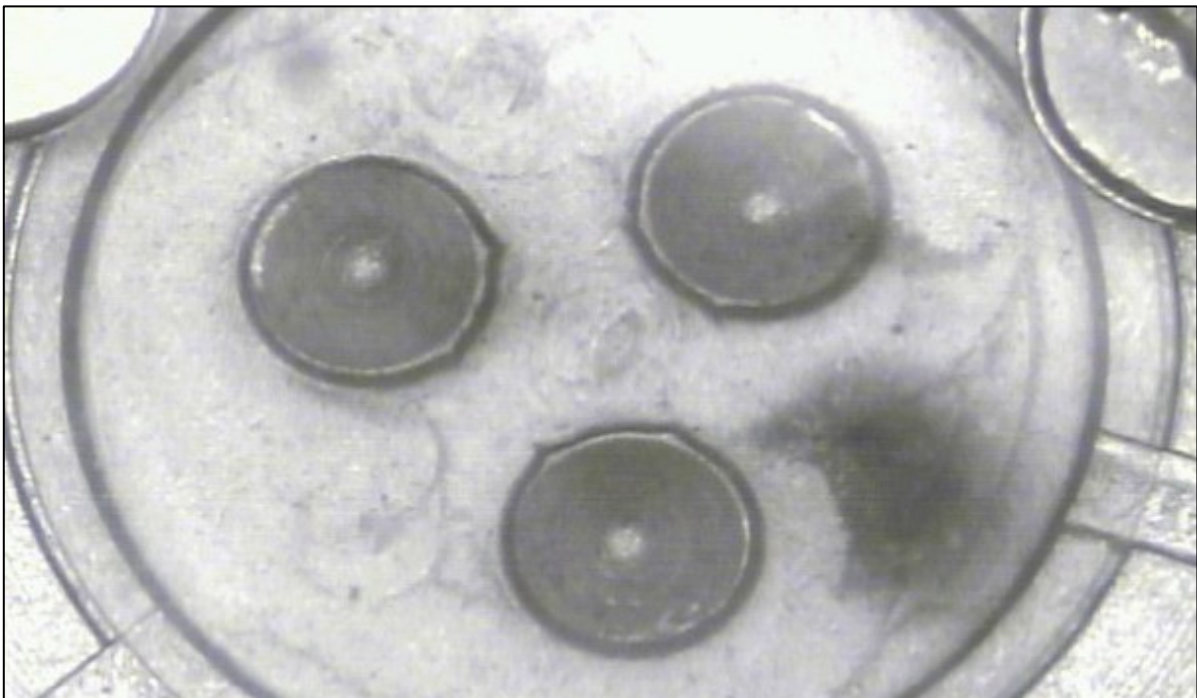
Figure 32. Picture taken through the CO_2-laser's digital camera showing the new sample holder designed and manufactured by the MPIC mechanical workshop in 2011. Less sample holes are used in the attempt to prevent degassing of multiple samples through enhanced temperatures during high laser intensity elsewhere on the sample holder. The sample cavities are as far away from each other as possible and are arranged on top of columns.
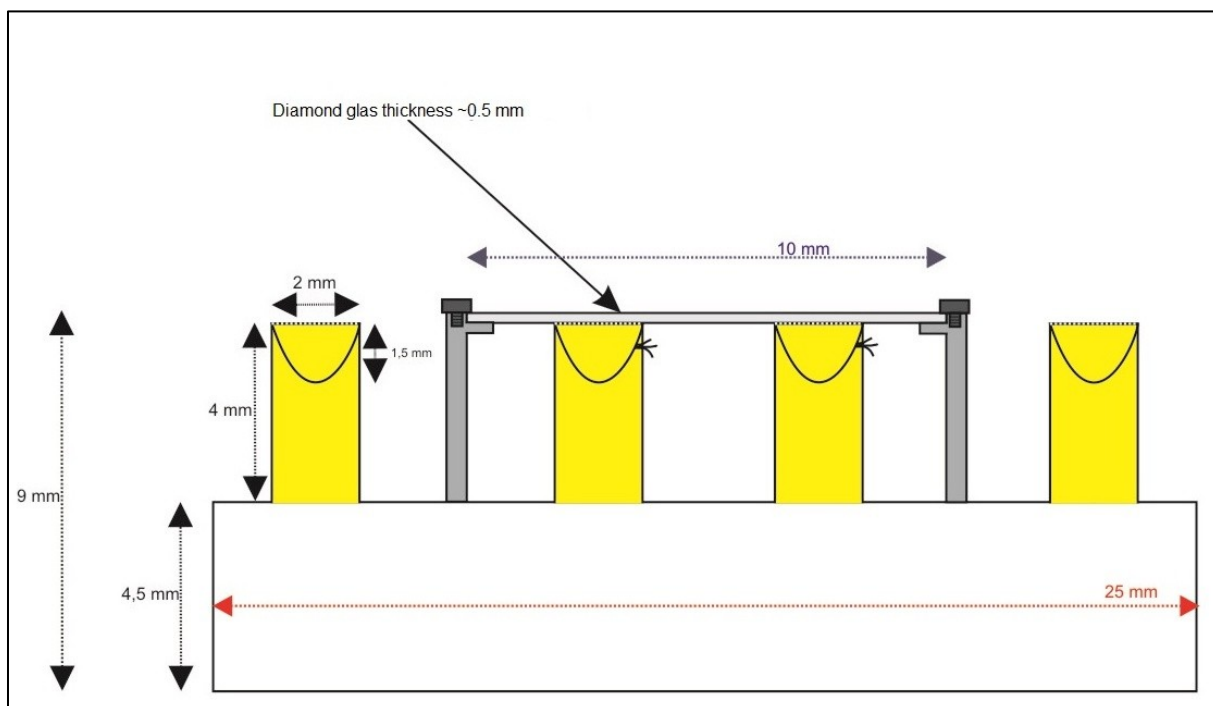
Figure 33. Schematic illustrating the new sample holder for the laser extraction system manufactured by and constructed with help of the MPIC mechanical workshop in 2011 (illustration not to scale). The final sample holder was of a slightly different design (see Fig. 32).

4.3.4 Analysis procedure

This chapter describes the analysis procedures for samples, blanks and calibrations. Overall the procedures were similar for all three types of measurement, those for samples and blanks essentially identical. For the calibrations the laser was not used and the steps were slightly different. Most the volume, into which the gases to be analyzed equilibrated, was the same in all cases. This is essential in order to get correct results.

Before any samples, blanks or calibrations could be measured some pre-preparation steps had to be performed. In the morning or at the beginning of a new measurement the temperature of charcoal cold fingers (CH-1, CH-2 and CH-MS) which had been at about 300 to 320°C during standby was lowered to about 30°C before starting. The pressure readings of the ion gauges and turbo pumps at the extraction system (between 1.9×10^{-9} to 4.0×10^{-9} mbar in a long used, well pumped system) and the mass spectrometer were checked before continuing. While the charcoal cold fingers were cooling down, the rise of the ^{40}Ar signal for the mass spectrometer in static mode was checked by scanning the mass range m/z = 39.8 - 40.2 m/z for the channeltron IC3. Normally it was in the range 500 to 4000 counts/min (~1.4×10^{-13} to ~1.1×10^{-12} cc STP/min). After this the rate of rise was checked for the whole system volume (MS plus laser extraction and noble gas separation area), where the values typically were about 2500 to 20000 counts/min (~6.7×10^{-13} to ~5.4×10^{-12} cc STP/min). Directly after measurements of calibrations and gas-rich samples, these values were somewhat higher due to system memory (especially for Ar, Kr and Xe).

After completion of the ^{40}Ar-rise check, if the result was satisfactory, occasionally the interference masses (dynamic underground) of Ne and Ar were measured in:

1) The mass spectrometer (pumped with the turbo pump - TP) and in

2) A system wide pumped status (with TP)

for Neon: MS 18 (^{1}H$_2$^{18}O), MS 40 (^{40}Ar), MS 44 (^{12}C^{16}O$_2$) (Ne-tuning)

for Argon: ^{35}Cl, ^{37}Cl, MS 39 (mostly hydrocarbons) (Ar-tuning)

The so obtained values were used in correcting the analysis data for isobaric interferences, e.g. the ratio of doubly charged to singly charged ^{12}C^{16}O$_2$ (m/z = 22 to m/z = 44; the contribution of Ne at m/z = 22 was assumed to be negligible in the pumped system).

It was necessary to measure the whole isotopic underground of the MS after a system leak, contamination with air, sample change, charcoal exchange or if the filament was broken and had to be exchanged. Here also, the whole underground measurement procedure was performed once for the mass spectrometer alone, and individually for the whole extraction, separation and MS system.

The whole underground measurement procedure involved the masses:

for Helium: 2, 3, 4 (He-tuning)

for Neon: 16, 18, 20, 21, 22, 28, 40 and 44 (Ne-tuning)

for Argon: 28, 35, 36, 37, 38, 39, 40 and 44 (Ar-tuning)

The measurement of the interference masses is an important tool, since it provides information about the state of the system and it indicates if the measurement of the noble gases may be influenced by a high background. As noted above, the measurement of the interference masses is also especially important for reducing and correcting collected data.

After all basic preparations had been performed, valves 1 (V1) and valve 3 (V3) were closed to ensure that later none of the gas to be analyzed was pumped by the ion gauges, ion getter pump or the turbo molecular pump (Fig. 12). The CO_2 laser was then put online (only for blank and sample measurements). It was focused onto the sample, or on an area on which the laser supposed to fire on, using the digital camera. At the beginning of the project, we started with higher laser energy power levels of up to 32W to degas the samples (refer to chapter 4.3.3.1 - standard samples). Later we went to very low output energies of about 0.9 to 5W. Normally the laser activation duration for samples and sample-holder was 60s for three activations in a row. With every laser step the energy power level was raised slightly (see results in the Appendix).

Before the next step, we waited approximately 10 minutes, in order to let the gas react with the warm SAES getter I. The same waiting time was used for calibrations. During this period the charcoal cold fingers CH-1 or CH-2 (depending on which one would be used for separation) and CH-MS were cooled with liquid Nitrogen to -197°C. In order to perform a stepwise release of the noble gases (Ar, Kr, Xe) it is imperative that the charcoal cold finger used for separation is surrounded by a metal cup filled with metal pellets (Pb or Inconel) – see chapter 4.3.1.3. This has the effect to increase the thermal inertia resulting in a more constant and homogeneous temperature. The valves on top of the cold fingers were closed during initial cooling - first to prevent a system contamination due to a possible leak in charcoal finger itself, and second to prevent that calibration or extracted sample/blank noble gases were already adsorbed before the interaction with the warm/cold getter was completed. We then closed all valves to the mass spectrometer (V2, $V_{inNoblesse}$), and proceeded by opening V3 and V5 to deliver the noble gases and the other "dirt" gases to the cold SAES getter II. The released gases interacted with the cold getter (7 min.). During the initial cold finger cooling phase previously described, it was important to maintain a constant level of liquid N_2 at the charcoal cold fingers.

After the pre-cleaning period of the noble gases was accomplished, the valve V_{LEMS} and cold finger valves (CH-1 or CH-2) were opened. The gases were exposed to the charcoal cold fingers for 25 minutes allowing Ar to Xe to sublimate. Ne and He did not sublimate during this process. Meanwhile, the "Noblesse" mass spectrometer

software was set up for the measurements. This was accomplished by performing the following steps:

- o Turn on HT (High Voltage MS)

- o Close ion getter- and turbo pumps

- o Load Ar-Tuning

- o Measure MS background with the Faraday cup in mV (mostly ^{40}Ar):

  - ▪ The "Noblesse" Faraday cup offers an electrical resistance of 1 x 10^{11} Ω (Ohm).

    Because of (3)

    $$I = \frac{V}{R} \qquad (3)$$

    With I (current) [A] (ampere), V (voltage) [V] (volt) and R (resistance) [Ω] (ohm)

    1 mV measured with the Faraday cup corresponds to 1 x 10^{-14} A, equivalent to 62414 cps for a counting efficiency of a channeltron of 100%..

  - ▪ This number may vary due to uncertainties in the electrical resistance and variation in the counting efficiency of the mass spectrometer, i.e. not at 100% efficiency.

  - ▪ If one intended to measure unknown background with the delicate channeltrons in cps (IC0 to IC7), it is important to pretest with the Faraday (mV) cup to make sure the signals are low enough. The maximum corresponding voltage for use with ICs was chosen as 1.5 to 2.5 mV, corresponding to about 100.000 to 150.000 cps.

- o Turn off HT. It is turned on again just before the measurement starts to ensure that the system is not pumped unnecessarily and that a defined moment t_0 is set for extrapolation purposes.

After ~15 of 25 minutes the valves to the mass spectrometer's turbo and ion getter pumps are closed (V_{MSTP}, V_{CHPump}, $V_{IPSource}$, $V_{IPDetector}$). Then V_{CHMS} is opened. This is intended to reduce background at the Ne masses, before the measurement start by absorption of the "dirt" gases (especially non sample/calibration ^{40}Ar) to the charcoal CH-MS, so that the background reaches low and stable values. The CH-MS has only a cleaning function.

The valves of CH-1 or CH-2 are closed after 25 minutes of noble gases sublimation. At this point Ar, Kr and Xe are fixed to the charcoal cold finger while He and Ne, which are still present as free gases in the extraction system, can be expanded into the MS for counting.

Generally the noble gas inlet duration is about 4 minutes. The following tables give a detailed overview of the measurement steps for each noble gas:

Helium (He) and Neon (Ne) measurement:

*Table 10. Overview of the important steps and routines performed for **Helium and Neon** measurements on the "Noblesse" mass spectrometer. In the "order" column, the abbreviations LSA (Laser and Separation Area) and N ("Noblesse") are used to clarify the area in which the step was performed. For identification of valves (e.g. V-IP$_D$) refer to Fig. 12. Note also that nominal mass values always refer to measurement on IC3 (center of the detector arrangement). See **Appendix F** for specific measurement steps.*

Order	Task	Description
1 (N)	He & Ne inlet – open V$_{inNoblesse}$	He and Ne were released into the mass spectrometer for about 4 minutes (high voltage (HT) MS off, pump valves closed)
2 (N)	Sublimate remaining ^{40}Ar to the CH-MS	The gas was exposed to the cold fingers for another 5 minutes to sublimate the remaining "dirt" ^{40}Ar onto the CH-MS
3 (N)	Load He-Tuning file and pre-check peaks	Usually there was enough time to perform a short manual peak centering on the He-peaks before the main measurement started, due to the slow depletion rate of He and Ne in the mass spectrometer. ^{3}He and HD / H$_3$ (HD=Deuterium) were mostly measured on channeltron IC3. Depending on the amount of He, the much more abundant ^{4}He was measured using the Faraday cup or IC3. The peaks for ^{3}He and HD / H$_3$ are located very close to each other and are not fully resolved by the Noblesse. Therefore a constant recalibration for these two peaks was necessary prior to each measurement in order to prevent obtaining wrong results due to peak drift. This is true especially for blank measurements (see Fig. 34). *Figure 34. Basic chart showing possible peak drift during ^{3}He and HD / H$_3$ measurement.*
4 (N)	He measurement routine	As soon as He was ready for measurement, the He tuning file had to be loaded. The peaks were determined using the "edit scan" function in the "Noblesse" operating system. ^{4}He was at nominal *m/z* 3.76-3.84 on Faraday and *m/z* 3.97-4.01 on channeltron IC3. ^{3}He and HD/H$_3$ at *m/z* 2.990-3.015 on IC3. Peak scales were then adjusted in the

		"Noblesse" software. If the Faraday was activated, the peak heights were shown in mV; if the channeltrons were used, they were shown in cps.
5 (N)	Measurement of He	Step 1: Measurement of ^{4}He; Step 2: Measurement of ^{3}He and HD / H$_3$. See **Appendix F** for specific measurement steps.
6 (N)	Save acquired data to file and laboratory notebook.	As soon as the measurement was finished the acquired He data was saved in data files. In addition to the saved data file, the most important results were recorded in the laboratory notebook.
7 (N)	Show result plot	To verify that all the measured He data was correct, it was important to review the data using the option "show result plot" in the "Noblesse" PC program. The result plot would show a more or less horizontal straight line due to good statistics if the data were in optimal condition.
8 (LSA)	Open V2 for 1 min.	Valve V2 had to be opened in order to pump down He and Ne from the laser extraction and separation area using the turbo-molecular-pump. V3 and V5 were closed as a precondition and to provide the right volume for the next measurement step: Argon
9 (LSA)	**During Ne measurement:** **Important pre-steps for the following argon analysis**	Close valve of CH-1 or CH-2 (whichever is in use for noble gas separation). Switch Temperature on CH-1 or CH-2 from **-197°C to -165°C**. Always keep the liquid N$_2$ flasks filled up. Keep V2 open in order to pump the LSA. Wait **exactly 25 minutes** from the time the temperature reaches -165°C; this is critical for Ar (and accompanying small amount of Kr) to be reproducibly released from the charcoal cold finger. It is important that at this point no liquid N$_2$ gets into the cup with the Inconel metal pellets (see Fig. 23). If this happened, the freezing effect would be too strong and the temperature would be lowered again. This would result in readsorption of already released Ar-, Kr- and Xe- isotopes.
10 (N)	**Overall tasks performed for He, Ne, Ar, Kr and Xe.**	**Basically the same steps were performed for Ne, Ar, Kr and Xe as were for He:** Gas inlet for 4 min. (open V$_{inNoblesse}$), load tuning file, pre-check peaks, switch on channeltrons and HT, select measurement routine and cycle amount (15 cycles for He, Ne, Ar; 5 cycles for Ar interference masses; 10 cycles for Kr and Xe standard calibration gas; 20 cycles for Kr and Xe), start measurement, fill up or refill liquid N$_2$ flasks, look at result plot when measurement is finished, save data file and record important data to the laboratory notebook.

11 (N)	Measurement of Ne	The tuning file for Neon was loaded, the Faraday was switched off and additionally IC3, IC0 and IC6 were activated in order to measure multiple isotopes at the same time (^{20}Ne, ^{21}Ne, ^{22}Ne, $^{1}H_2^{18}O$ (*m/z* 18), CO_2 (*m/z* 44) and ^{40}Ar – see Fig. 35). See **Appendix F** for specific measurement steps. Later ^{20}Ne had to be corrected for $^{1}H_2^{18}O$ and $^{40}Ar^{++}$ interference and ^{22}Ne for CO_2^{++} interference, which is explained in chapter 4.3.5.1.
		Figure 35. Sketch of typically measured peaks and their relative positions during Ne measurement on the "Noblesse".
12 (N)	Open V-IP$_D$, V-MS-TP$_{Top}$ then close VCH$_{MS}$, open V-CH$_{Pump}$	After the Ne measurement was finished, the MS was pumped with the ion getter and the turbo molecular pump. The temperature of CH-MS was raised to 300°C in order to release and pump down the previously captured "dirt" gases. All pump valves were closed again after completing the cleaning process. CH-MS was kept on 300°C, with the valve to the mass spectrometer closed.
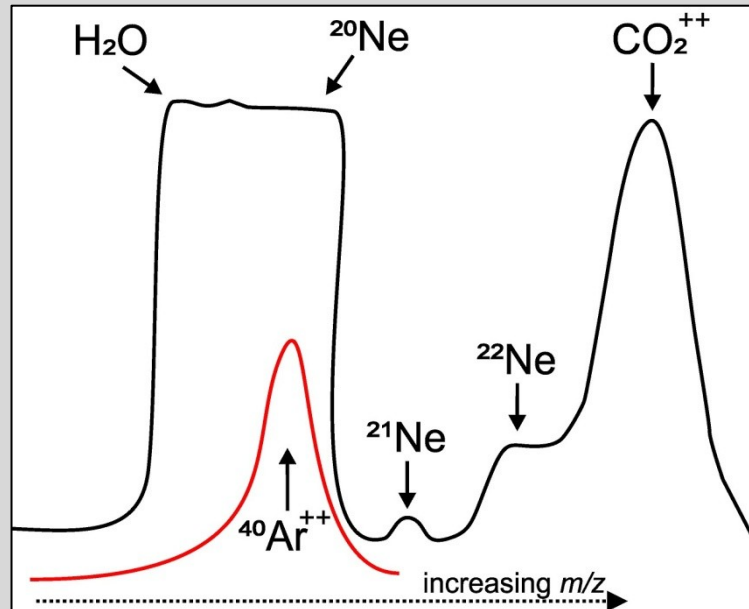
Argon (Ar) measurement:

*Table 11. Overview of the important steps and routines performed for **Argon** measurements on the "Noblesse" mass spectrometer. In the "order" column, the abbreviations LSA (Laser and Separation Area) and N ("Noblesse") are used to clarify the area in which the step was performed. For identification of valves (e.g. V-IP$_D$) refer to Fig. 12. See **Appendix F** for specific measurement steps.*

Order	Task	Description
1 (LSA)	Release Ar from the charcoal cold finger	V2 was closed and the valve to CH-1 or CH-2 (whichever was in use for noble gas separation) was opened. This releases the Ar gases into the provided LSA area.
2 (N)	Measurement of Ar	Generally the same steps as described in number 10 of Ne and He measurement were performed for Ar analyses (see above).
		Usually the most abundant isotope in blanks, sample and calibration measurements was ^{40}Ar. Therefore it was normally measured using the Faraday cup (in mV). Sometimes, especially when calibrations and gas-rich samples were analyzed, also ^{36}Ar also had to be measured using the Faraday cup (see Fig. 36). As an upper limit for channeltron measurements we chose about 100.000 to 150.000 cps, which correspondes to ~1.5 to 2.5 mV on the Faraday detector. The amount of ^{36}Ar therefore had to be checked prior the actual data taken. ^{38}Ar was usually measured on channeltron IC3. See **Appendix F** for specific measurement steps.
		Figure 36 Sketch of typically measured peaks and their positions during Ar measurement on the "Noblesse" (Far = Faraday; IC3 = channeltron)
		V5 was then opened in order to prepare for the next measurement step: Krypton
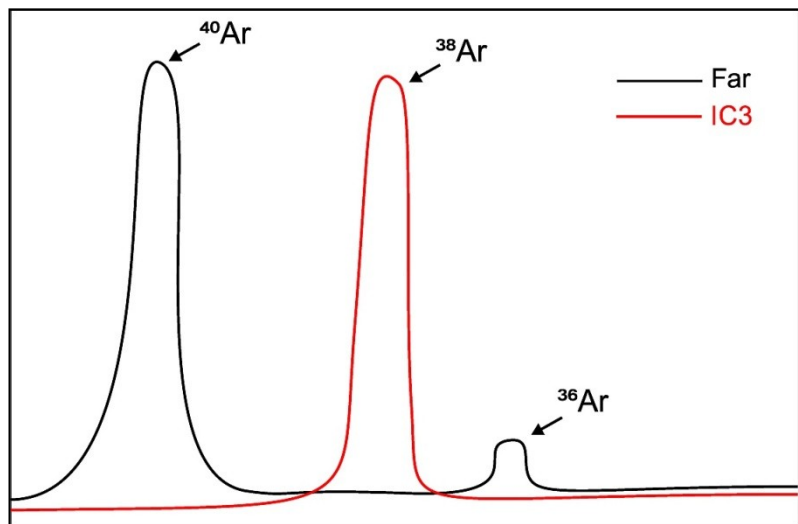
3 (LSA)	**During Ar measurement:** **Important pre-steps regarding the Krypton analysis**	Pump down Ar from the LSA including CH-1 or CH-2 (whichever was in use for noble gas separation).
		Close valve to CH-1 or CH-2. Switch Temperature on CH-1 or CH-2 from **-165°C to -135°C**.
		Always keep the liquid N_2 flasks filled up.
		Keep V2 open in order to pump the LSA.
		Wait **exactly 25 minutes** from the time the temperature reached -135°C; this is critical for Kr to be released reproducibly from the charcoal cold finger.
3 (LSA)	During Ar detection: Inlet of Kr standard calibration gas.	Evacuate gas sampling pipette for 1 min. (open V-DP).
		Close V-DP and then open V DKr for 1 min.
		Close V2, and then close V DKr.
		Open the gas sampling pipette for 2 min – then close it again. The Kr standard calibration gas will now expand and react for 5 min. with the cold getter in order to reduce the level of "dirt" gases.
4 (N)	Measurement of Ar interference masses (^{35}Cl, ^{37}Cl, m/z 39)	After Ar was measured and the data was successfully obtained and stored, the Ar interference reference masses (^{35}Cl, ^{37}Cl and m/z 39 (hydrocarbons) were measured on IC3, in order to perform corrections (see chapter 4.3.5.1). See **Appendix F** for specific measurement steps.
		Figure 37. Sketch of typically measured peaks and their positions during Ar interference masses measurement on the "Noblesse".
5 (N)	Manual peak measurement of ^{84}Kr and ^{132}Xe	In order to determine how much Kr and Xe was present in the Ar fraction, the peaks were measured manually and the results were recorded in the laboratory notebook. These values were important in determining how good the separation of Ar, Kr and Xe at the cold finger was. Once this was finished and all the previously obtained data were saved, the remaining gases in the MS were pumped down by the ion getter and turbo molecular pump.

Krypton (Kr) and Xenon (Xe) measurements:

*Table 12. Overview of the important steps and routines performed for **Krypton and Xenon** measurements on the "Noblesse" mass spectrometer. In the "order" column, the abbreviations LSA (Laser and Separation Area) and N ("Noblesse") are used to clarify the area in which the step was performed. For identification of valves (e.g. V-IP$_D$) refer to Fig. 11. See **Appendix F** for specific measurement steps.*

Order	Task	Description
1 (N)	**Step 1 - Kr:** Measurement of Kr standard calibration gas	The same steps were performed as described in number 10 of Ne and He measurement (see above). Generally Kr and Xe measurements were performed using exactly the same scheme. See **Appendix F** for specific measurement steps.
		The purpose of measuring the Kr standard calibration gas is to provide Kr peak information to the "Noblesse" system. This is important if Kr has a low abundance in the blank or sample gas, because the automated peak centering would not properly work in such cases. Once the measurement was accomplished and all the obtained data was saved, the remaining gases in the MS were pumped down by the ion getter and turbo molecular pump for about 1 min.
2 (LSA)	**Step 2 - Kr:** Release Kr from the charcoal cold finger	During the measurement of the Kr standard calibration gas, V2 was opened and gases from the LSA were pumped down.
		Then V$_{LEMS}$ was closed and the valve to CH-1 or CH-2 (whichever was in use for noble gas separation) was opened. The released Kr gas was then released into the smaller LSA area. The volume used for expansion of Kr is smaller compared to the one in case of the He/Ne and Ar fractions resulting in higher sensitivity. In any case, always the same volume is used for blanks, calibrations and samples.
3 (N)	**Step 3 - Kr:** Measurement of Kr	Generally the same steps were performed as described in number 10 of Ne and He measurement (see above). See **Appendix F** for specific measurement steps.
		Very often Kr in blanks and sample measurements showed only low gas amounts. As explained above, the system then used the previous peak position data from the Kr standard calibration gas to locate peaks in the Kr from samples or blanks. The different Kr isotopes were usually measured on eight channeltrons (IC0-IC7, see Appendix F). This is done in order to save time, which is important because the gas is depleted by the pumping action of high voltage provided by the MS source.

4 (LSA)	**During Kr measurement:** **Important pre-steps regarding the Xenon analysis**	Pump down Kr from the LSA including CH-1 or CH-2 (whichever was in use for noble gas separation). Close valve to CH-1 or CH-2. Switch Temperature on CH-1 or CH-2 from **-135°C to +170°C**. The use of liquid N_2 flask can be taken off. Keep V2 open in order to pump the LSA. Wait **25 minutes** from the time the temperature reaches +170°C. Xe was then released from the charcoal cold finger.
5 (LSA)	<u>During Kr detection:</u> Inlet of Xe standard calibration gas	Evacuate gas sampling pipette for 1 min. (open V-DP). Close V-DP and then open V DKr for 1 min. Close V2, and then close V DKr. Open the gas sampling pipette for 2 min – then close it again. The Xe standard calibration gas will now expand and react for 5 min. with the cold getter.
4 (N)	**Step 4 - Kr:** Manual peak measurement of ^{40}Ar and ^{132}Xe in Kr fraction.	In order to determine how much Ar and Xe was in the Kr fraction, the ^{40}Ar and ^{132}Xe peaks were measured manually and the results were recorded in the laboratory notebook. Once this was finished and all the previous obtained data were saved, the remaining gases in the MS were pumped down by the ion getter and turbo molecular pump. These values were important in determining how good the separation of Ar, Kr and Xe at the cold finger was.
5 (N)	**Step 1 - Xe:** Measurement of Xe standard calibration gas	The Xe calibration standard was measured in exactly the same way as the Kr calibration standard. See **Appendix F** for specific measurement steps. However, these steps are performed after the real Kr measurement is accomplished (Step 2-4 - Kr).
6 (LSA)	**Step 2 - Xe:** Release Xe from the charcoal cold finger	See explanations for krypton; every step for xenon was performed in exactly the same way as for krypton.
7 (N)	**Step 3 - Xe:** Measurement of Xe	Exactly the same steps performed as for the Kr fraction. Very often the abundances of Xe in blanks and sample measurements were very low. As explained above, in these cases the system took the peak position data determined from the Xe standard calibration gas. The different Xe isotopes were usually measured on eight channeltrons (IC0-IC7, see Appendix F). This is done in order to save time and Xe is depleted by the pumping action of the high voltage provided by the MS source. See **Appendix F** for specific measurement steps.

| 8 (N) | **Step 4 - Xe:** Manual peak measurement of ^{40}Ar and ^{84}Kr in Xe fraction. | In order to determine the amount of Ar and Kr in the Xe fraction, the peaks were measured manually and the results were recorded in the laboratory notebook. These values were important in determining how good the separation of Ar, Kr and Xe at the cold finger was. |
| 9 (N) and (LSA) | Set the measurement system into stand-by or restart mode. | Once all measurements were finished, the remaining gases in the MS, the laser extraction and separation area were pumped down using ion getter and turbo molecular pumps. CH-1 and CH-2 were heated up to 320°C and the valves to CH-1, CH-2, V_{LEMS}, V2, V3, V5, V4, V1 and V54 were opened in order to fully pump the system for restart or overnight status. Usually the valves to the turbo molecular pumps were closed overnight and the valves to the ion getter pumps stayed open. The detector array (ICs and Faraday) was turned off and the MS high voltage stayed on. The baseline detection was set on *m/z* 1.1 to 1.3. |

4.3.4.1 Noble gas calibrations

Performing noble gas calibrations was, beside blank measurements, the most important step in obtaining exact concentrations of noble gas measured from MMs. Beside these, calibration gases were also used to run several tests to check the mass spectrometer's resolution, sensitivity and peak separation abilities. In 2010 we used two different calibration gas containers for the "Noblesse": an "Air" flask for He and Ne measurements and a "Mix" flask for Ar, Kr and Xe measurements. At the beginning of MM measurements, these containers were exchanged for a single "Mix" flask from Air Liquide containing all the noble gases (see chapter 3.2.1.1, Table 4 and chapter 4.3.1.3, Fig. 21 and Fig. 22). The signal of each measured noble gas isotope was compared to its calibration gas companion, so it was therefore important to know precisely the calibration gas composition. Generally a defined calibration gas "slug" was taken out of noble gas container (volume = 984.68 cc) using a pipette system, the volume of which was 0.324 cc (see chapter 4.3.1.3). The calibration gas elemental composition of the single "Mix" gas container in 2011 and 2012 was as follows: He 51.30 Vol.%, Ne 0.157 Vol.%, Ar 48.52 Vol. %, Kr 0.0099 Vol. % and for Xe 0.012 Vol. %; with an error of about 2%.

For the in 2011-2012 used single "Mix" gas container the amounts and associated ratios for the noble gas isotopes are listed in Table 13 counting for **"slug" #1**. These amounts get reduced with every "slug" by the corrsponding volume ratio of 0.324 cc (volume pipette) / 984.68 cc (volume flask).

Table 13. Noble gas amounts and ratios for ***"slug" #1*** *used within the "Mix" calibration gas flask for measurements on the "Noblesse" MS in 2011 and 2012.*

Isotope	Amount of gas [cc STP]	Isotopes	Ratios
^{3}He	3.653E-11	^{3}He/^{4}He	4.976E-04
^{4}He	7.343E-08	^{4}He/^{3}He	2.010E+03
^{22}Ne	2.072E-11	^{4}He/^{22}Ne	3.544E+03
^{36}Ar	2.340E-10	^{22}Ne/^{36}Ar	8.853E-02
^{84}Kr	8.074E-12	^{36}Ar/^{84}Kr	2.899E+01
^{132}Xe	4.619E-12	^{84}Kr/^{132}Xe	1.748E+00

The calibration gas used for Kr and Xe peak centering was supplied from two separated Kr and Xe flasks (see chapter 4.3.1.3, Fig 21 and Fig. 22). Before actual Kr and Xe measurements could be made, a "slug" of Kr and later Xe was taken using a pipette system. This was especially important for sample measurements due to very low Kr and Xe gas amounts and their associated difficult peak centering (see chapter 4.3.4 for further information). Amounts of Kr and Xe in the calibration gas containers for **"slug" #1** are listed in Table 14. These amounts get reduced with every "slug" by the corrsponding volume ratio of 0.311 cc (volume pipette) / 500 cc (volume for each flask).

Table 14. Noble gas amounts taken from the Kr and Xe calibration gas flasks for ***"slug" #1*** *used for peak centering measurements on the "Noblesse".*

Isotope	Amount of gas [cc STP]	Isotope	Amount of gas [cc STP]
^{84}Kr	8.598E-12	^{132}Xe	4.145E-12

Noble gas sensitivities - determined for the channeltrons [cc STP/cps] and the Faraday detector [cc STP/V] - from calibrations are shown in Fig. 38 for all the noble gases He-Xe. Overall a total of 62 calibration measurements were performed between the beginning of 2011 and the end of 2012. However, some are not included in Fig. 38, because no useful results were obtained, due to events like leaks, charcoal separation problems and peak adjustment problems. The average calibration values and variations over time are shown in Table 15.

The Channeltrons are delicate detectors and their performance can deteriorate with time, in particular after having "seen" large signals (which is the reason we tried to keep signals on the Channeltrons below a maximum of 100,000 cps). Another important factor is the depletion of isotopes due to the high voltage in the MS source. Ar, Kr and especially Xe are well ionized and therefore are depleted much faster than the lighter isotopes He and Ne. Thus, it was very important to start the measurement of Ar and especially Kr and Xe soon after inlet into the MS and activation of the high voltage. Then, during data reduction, it was important to extrapolate to the turn-on instant of the high voltage.

For Kr and Xe we used a smaller volume for expansion in the laser extraction area, due to their expected low amounts in blank and sample measurements. Hence, one will get a different volume factor compared to He, Ne and Ar. Fig. 38 illustrates the high stability of the system. However, as the scatter shows, small variations in the system configuration can lead to overall count rate changes. A major change of about 23% occurred after the exchange of the filaments in 2011 and 2012 (see Table 15), which is a result of a slightly different performance of the ion source.
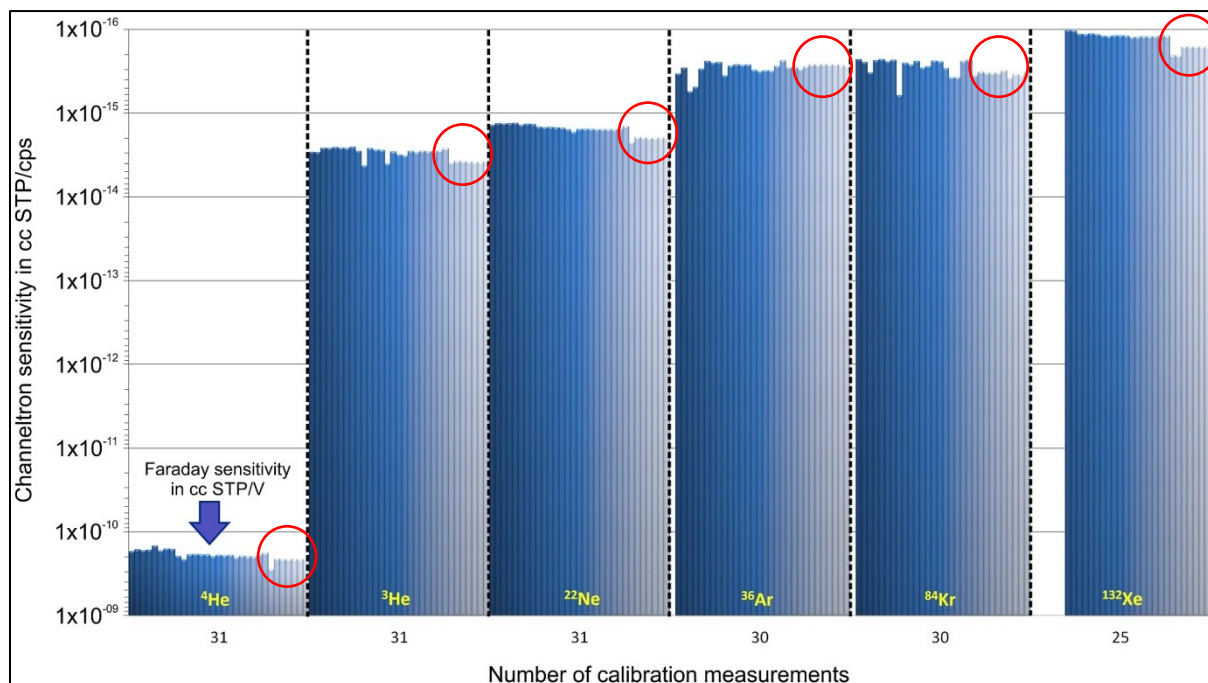
Figure 38. Presented in logarithmic scale are sensitivities determined in selected calibration measurements using the channeltrons – 31 calibrations for He and Ne, 30 for Ar and Kr and 25 for Xe. Overall 62 calibration measurements were performed between 2011 and 2012. However, not all are shown here because of failed calibrations due to incidents like leaks, noble gas separation problems, filament failure and pump failure. The red circles indicate effect of the filament exchange in August 2012.

Xenon is measured with the highest sensitivity (^{132}Xe with ~1.03 x 10^{-16} cc STP/cps). However, after the second filament exchange in August 2012 (red circle in Fig. 38), the overall count rate decreased for all the noble gases on both the channeltrons and the Faraday, due to a different performance of the ion source.

Table 15. Noble gas results showing the average sensitivities in [cc STP/cps] and [cc STP/V] as well as the standard deviations of the sensitivities over time in [%] for "good" calibrations measured with the "Noblesse" from 2011 to 2012 (overall). Additionally presented are the average sensitivities and deviations of the calibration measurements after filament exchanges (filament 1,2 and 3).

Isotope	No. of calibrations	Average sensitivity in cc STP/cps 2011-2012 (**Overall**)	Standard deviations 2011-2012 (**Overall**)
^{4}He	31	1.93 x 10^{-10} cc STP/V	± 12.7 %
^{3}He	31	3.11 x 10^{-15}	± 16.9 %
^{22}Ne	31	1.59 x 10^{-15}	± 15.1 %
^{36}Ar	30	2.69 x 10^{-16}	± 22.6 %
^{84}Kr	30	3.01 x 10^{-16}	± 25.6 %
^{132}Xe	25	1.33 x 10^{-16}	± 21.0 %

Isotope	No. of calibrations	Average sensitivity in cc STP/cps Jan-Jul 2011 (**Filament 1**)	Standard deviations Jan-Jul 2011 (**Filament 1**)
^{4}He	8	1.64 x 10^{-10} cc STP/V	± 4.3 %
^{3}He	8	2.68 x 10^{-15}	± 5.8 %
^{22}Ne	8	1.35 x 10^{-15}	± 1.8 %
^{36}Ar	8	3.38 x 10^{-16}	± 33 %
^{84}Kr	7	2.49 x 10^{-16}	± 13.6 %
^{132}Xe	2	1.03 x 10^{-16}	± 0.5 %

Isotope	No. of calibrations	Average sensitivity in cc STP/cps Aug-Jun 2011/12 (**Filament 2**)	Standard deviations Aug-Jun 2011/12 (**Filament 2**)
^{4}He	16	1.94 x 10^{-10} cc STP/V	± 4.3 %
^{3}He	16	3.03 x 10^{-15}	± 15.6 %
^{22}Ne	16	1.53 x 10^{-15}	± 3.9 %
^{36}Ar	16	2.86 x 10^{-16}	± 10.3 %
^{84}Kr	16	3.08 x 10^{-16}	± 31.1 %
^{132}Xe	16	1.19 x 10^{-16}	± 3.0 %

Isotope	No. of calibrations	Average sensitivity in cc STP/cps Aug-Oct 2012 (**Filament 3**)	Standard deviations Aug-Oct 2012 (**Filament 3**)
^{4}He	7	2.23 x 10^{-10} cc STP/V	± 11.6 %
^{3}He	7	3.81 x 10^{-15}	± 1.7 %
^{22}Ne	7	2.00 x 10^{-15}	± 4.8 %
^{36}Ar	6	2.64 x 10^{-16}	± 1.7 %
^{84}Kr	7	3.37 x 10^{-16}	± 6.2 %
^{132}Xe	7	1.74 x 10^{-16}	± 12.1 %

4.3.4.2 Blanks

Like stable calibrations, low and reproducible blanks are essential for obtaining reliable data from sample measurements. It is important to get the blank level of the extraction, cleaning and separation area, as well as the MS, as low as possible in order to measure noble gases from very low gas releases. From the beginning of 2011 to the end of 2012, 46 blanks were measured along with sample and calibration measurements. After events like contamination with air due to leaks, charcoal exchange, filament exchange, the array had to be cleaned using the baking system (see chapter 4.3.1.1). Usually after baking the instrument, blanks were first measured in a "cold" mode (without heating the sample holder) then in a "hot" mode (with heating of the sample holder). Blank levels can vary in accordance with the heating procedure and due to events such as exchange of a broken filament, charcoal exchange, recovery from leaks or in rare cases, slight inadvertent sample degassing.

Blank levels for isotopes from He to Xe are shown in Fig. 39 to Fig. 42 (not corrected for interferences - see chapter 4.3.5). The measurements were performed as explained in chapter 4.3.4. The blank level was low and almost constant over time for all the noble gases, except in the circumstances mentioned earlier. After the second filament exchange, the tuning files for all noble gas isotopes were updated. The different performance of the ion source after filament exchange is visible in the isotope detection of He to Xe seen in Fig. 39 to 42. The most significant blank improvement over time was obtained for Ne. However, the results shown in the Ne plot (Fig. 40) are not corrected for interferences e.g. ^{20}Ne still includes contributions of $^{1}H_2^{18}O$ and $^{40}Ar^{++}$ (see chapter 4.3.5). It is very likely that contributions of the interference masses improved over time rather than Ne itself. Conversely, due to low gas amounts in blanks, He, Kr and Xe varied the most. However, the detection limits could be improved for all the noble gases except for Ar. Table 16 shows isotopic values and ratios for Ne and Ar for 31 blanks selected for data reduction from 2011 to 2012 (not corrected for interferences). The data is subdivided into cold blanks (laser active) and hot blanks (laser not active). The ratios for Ne are (except twice) below the ones for Earth atmosphere (Eberhardt et al. (1965)). Interestingly, the Ar ratios show a slightly different pattern in six cases, where the ratios of $^{38}Ar/^{36}Ar$ are above air (Lee et al. (2006)) and $^{40}Ar/^{36}Ar$ are below air. This may indicate slight inadvertent degassing of sample material during blank measurements or measurement of blanks short after sample exchange and calibrations, which means still a slight contamination with air and interference masses (see chapter 4.3.5). Often the detection of Ne and Ar in blanks was low (see Fig. 40 and 41) and for ^{21}Ne as well as ^{38}Ar near the average sensitivity of the "Noblesse" (see Table 15). This might also influenced the ratio results in one or the other way. Overall the blank results were, more or less, stable over time. Earlier research from Ott et al. (2010) revealed a level of ~3 x 10^{-15} cc STP for ^{132}Xe blank measurements. Our blank measurements showed the highest level for ^{132}Xe of ~1.4 x 10^{-14} cc STP, with an average of ~1.2 x 10^{-14} cc STP from 2011 to 2012. The lowest amount detected of ^{132}Xe in blanks was ~5.9 x 10^{-16} cc STP. In the period from August 2012 to November 2012 the blank level of ^{132}Xe was stable at ~1.4 x 10^{-15} cc STP (see Fig. 42). The isotopic ratios in blanks for Kr and Xe show similarities to air (Basford et al. (1973)) at least for

^{83}Kr/^{84}Kr and ^{86}Kr/^{84}Kr, as well as for ^{129}Xe/^{132}Xe to ^{136}Xe/^{132}Xe. However, it was difficult to determine values and ratios for Kr and Xe in blanks - especially for the lower Kr and Xe *m/z* isotopes, due to their very low abundance and detection of about 5 - 150 counts per second. Overall the Kr and Xe selection of blank amounts and ratios for the data correction was made, in taking several blanks into account, which were measured over a longer time period (mostly some months).

Table 16. Results of 31 blank measurements (cold and hot) selected for data reduction. Except in two cases, the Ne ratios show values below or near air (Eberhardt et al. (1965)). The same picture is given for the Ar ratios. Except in six times where ^{38}Ar/^{36}Ar is plotting above air (Lee et al. (2006)) and ^{40}Ar/^{36}Ar is plotting below air, indicating some kind of contamination due to sample change, leaks or slight inadvertent degassing of sample material. Overall the blank results seem to be stable over time.

Date	Laser Power (W)	^{20}Ne/^{22}Ne	+-	^{21}Ne/^{22}Ne	+-	^{38}Ar/^{36}Ar	+-	^{40}Ar/^{36}Ar	+-
24.02.11	0 (cold)	6.13	0.15	0.013	0.003	0.593	0.030	49.4	4.2
23.08.11	0 (cold)	2.25	0.05	0.008	0.001	0.197	0.001	9.4	0.0
11.01.12	0 (cold)	3.91	0.15	0.010	0.003	0.164	0.001	219.0	0.7
09.02.12	0 (cold)	5.05	0.17	0.009	0.002	0.202	0.003	235.2	1.5
16.04.12	0 (cold)	9.86	0.44	0.023	0.004	0.195	0.004	227.7	1.7
13.09.12	0 (cold)	3.05	0.15	0.008	0.003	0.195	0.003	240.7	1.7
10.02.11	30	5.33	0.13	0.010	0.002	0.190	0.004	248.0	2.1
23.02.11	31	6.94	0.15	0.024	0.003	0.338	0.005	223.9	73.7
08.04.11	21	5.22	0.15	0.104	0.006	0.194	0.004	247.3	3.2
03.05.11	15	6.24	0.19	0.011	0.003	0.190	0.002	142.1	1.0
21.06.11	15	4.92	0.19	0.009	0.003	0.183	0.002	226.4	1.0
11.07.11	15	5.24	0.25	0.006	0.002	0.178	0.003	242.2	1.3
18.07.11	3x15	4.12	0.13	0.019	0.005	0.178	0.002	262.1	1.0
23.08.11	15	2.11	0.05	0.009	0.002	0.173	0.002	257.2	1.2
21.10.11	15	4.49	0.15	0.013	0.003	0.185	0.004	269.0	3.7
02.11.11	15	7.97	0.19	0.024	0.003	0.184	0.001	283.8	1.0
13.01.12	6.6	9.83	0.19	0.028	0.003	0.192	0.004	279.8	4.1
20.01.12	6.6	5.92	0.24	0.013	0.003	0.183	0.003	268.3	4.0
10.02.12	5	6.46	0.22	0.017	0.003	0.185	0.002	279.4	1.9
21.02.12	5	7.14	0.37	0.015	0.004	0.194	0.002	289.0	2.4
27.03.12	5	8.41	0.27	0.018	0.004	0.178	0.003	275.7	4.5
17.04.12	5	8.03	0.26	0.023	0.004	0.182	0.003	254.5	1.5
24.04.12	3x0.91	7.43	0.38	0.018	0.004	0.175	0.003	275.5	3.0
06.06.12	3x0.91	7.70	0.50	0.013	0.005	0.181	0.003	279.8	4.6
14.06.12	3x0.91	7.46	0.39	0.020	0.005	0.175	0.002	283.2	1.7
14.09.12	3x0.91	4.07	0.12	0.015	0.003	0.593	0.030	49.4	4.2
24.09.12	3x0.91	4.94	0.19	0.012	0.004	0.197	0.001	9.4	0.0
01.10.12	3x0.91	5.15	0.23	0.021	0.004	0.164	0.001	219.0	0.7
15.10.12	3x0.91	5.72	0.26	0.014	0.005	0.202	0.003	235.2	1.5
22.10.12	3x5	5.61	0.26	0.017	0.006	0.195	0.004	227.7	1.7
26.10.12	3x0.91-30	6.05	0.33	0.010	0.004	0.195	0.003	240.7	1.7
EA	[1], [2]	9.80		0.029		0.1885	0.0003	298.6	0.3

EA (Earth atmosphere): [1] Eberhardt et al. (1965) [2] Lee et al. (2006)
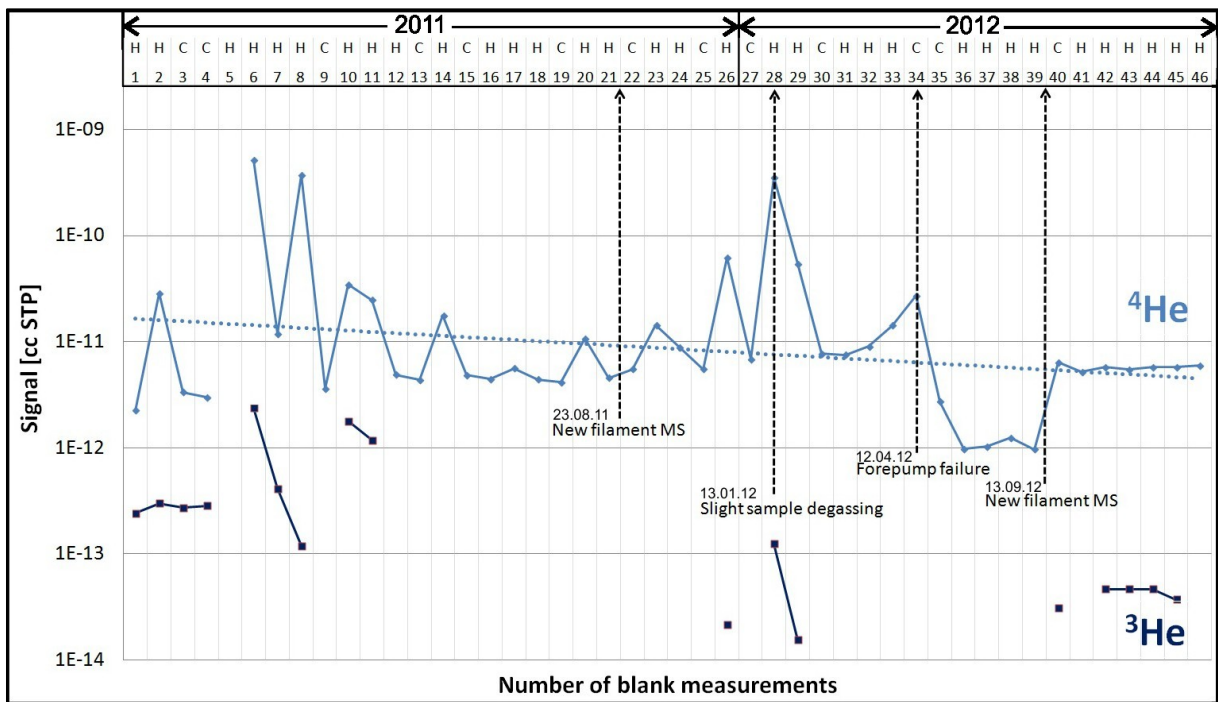
Figure 39. Results from 46 **He** blank measurements between 2011 and 2012 (logarithmic scale) - not corrected for interferences. C = "cold" blank; H = "hot" blank. ^{4}He shows a slightly improved detection trend to lower blanks, which is illustrated by a best fit-line. ^{3}He was often not detectable due to its low abundance. Events that caused higher blank levels are e.g. slight degassing of neighboring samples, exchange of MS filaments, variation of interference masses and pump failures. A further reason for blank level variations is the incorporation of both, blanks measured with (H) and without (C) laser heating of the sample holder, to simulate different sample heating scenarios.
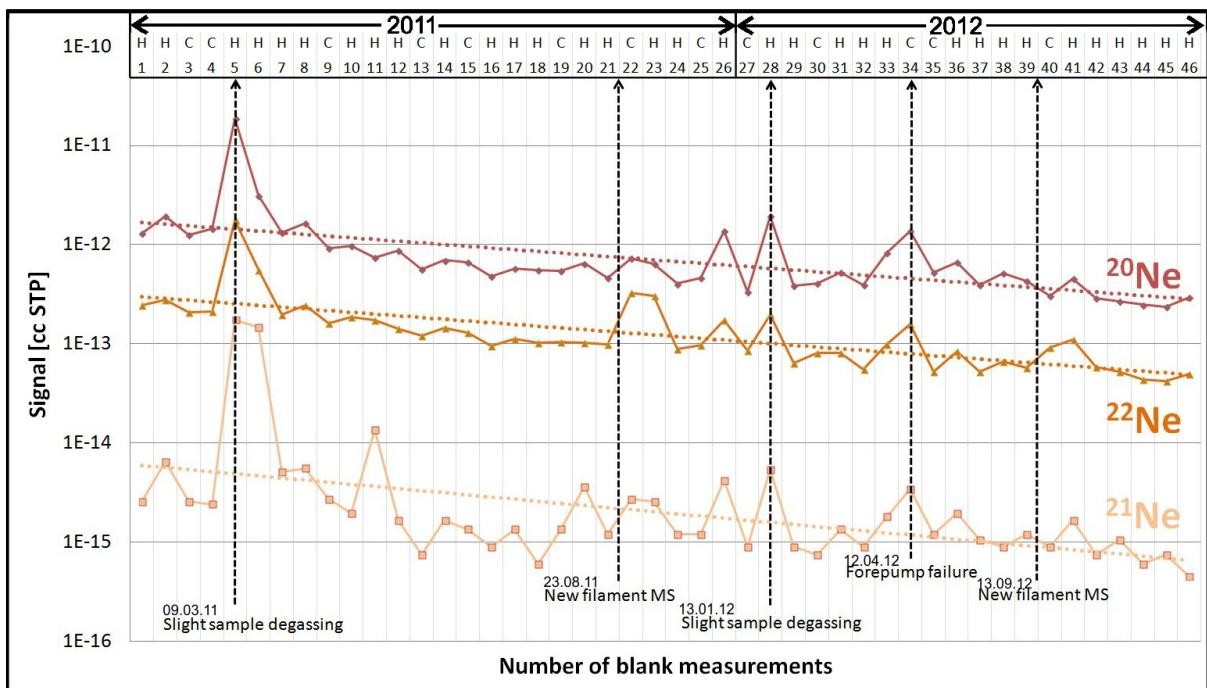
Figure 40. Results from 46 **Ne** blank measurements between 2011 and 2012 (logarithmic scale) - not corrected for interferences. C = "cold" blank; H = "hot" blank. For all Ne isotopes the trend is to lower blanks, as illustrated by the best-fit lines. Events that caused higher blank levels are e.g. slight degassing of neighboring samples, exchange of MS filaments, variation of interference masses and pump failures. A further reason for blank level variations is the incorporation of both, blanks measured with (H) and without (C) laser heating of the sample holder, to simulate different sample heating scenarios.
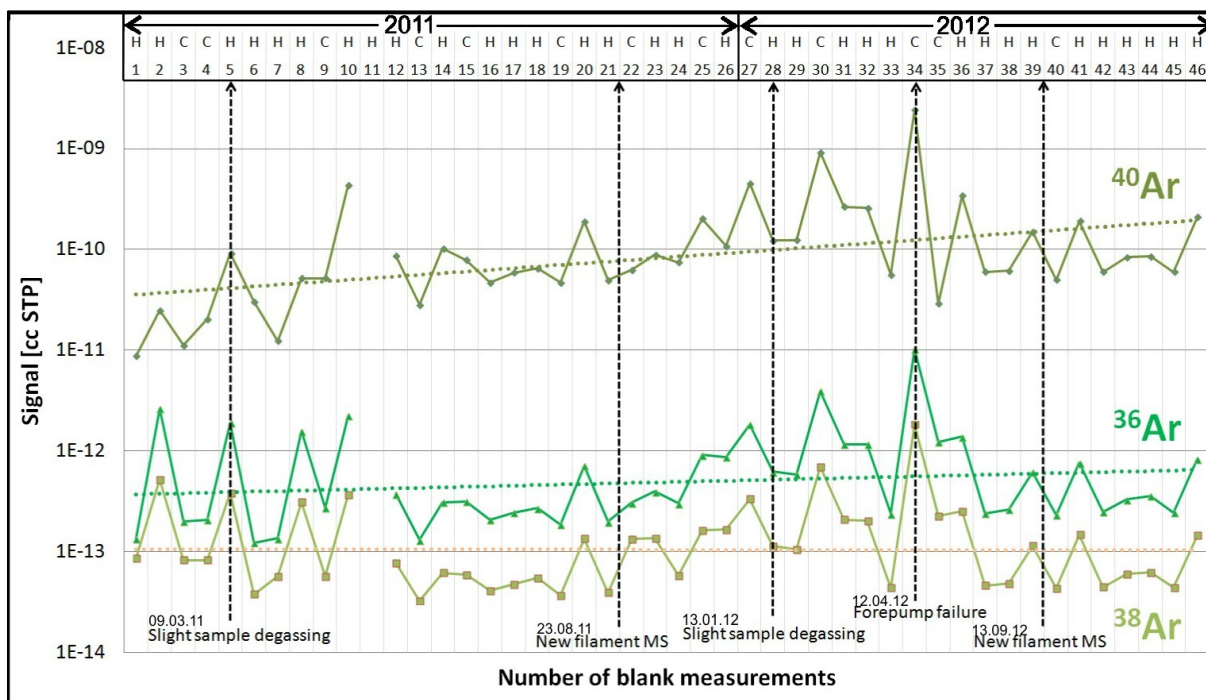
*Figure 41. Results from 46 **Ar** blank measurements between 2011 and 2012 (logarithmic scale) - not corrected for interferences. C = "cold" blank; H = "hot" blank. ^{36}Ar and especially ^{40}Ar show a trend to slightly higher blanks, as illustrated by the best-fit lines. ^{38}Ar stayed more or less at a constant blank level. The increase in Ar blank levels may be due to events like exchange of MS filaments, variation of interference masses and a pump failure. Also leaks which sometimes occurred can be a reason for the higher blank levels. A further reason for these variations is the incorporation of blanks measured with (H) and without (C) laser heating of the sample holder to simulate different sample heating scenarios.*
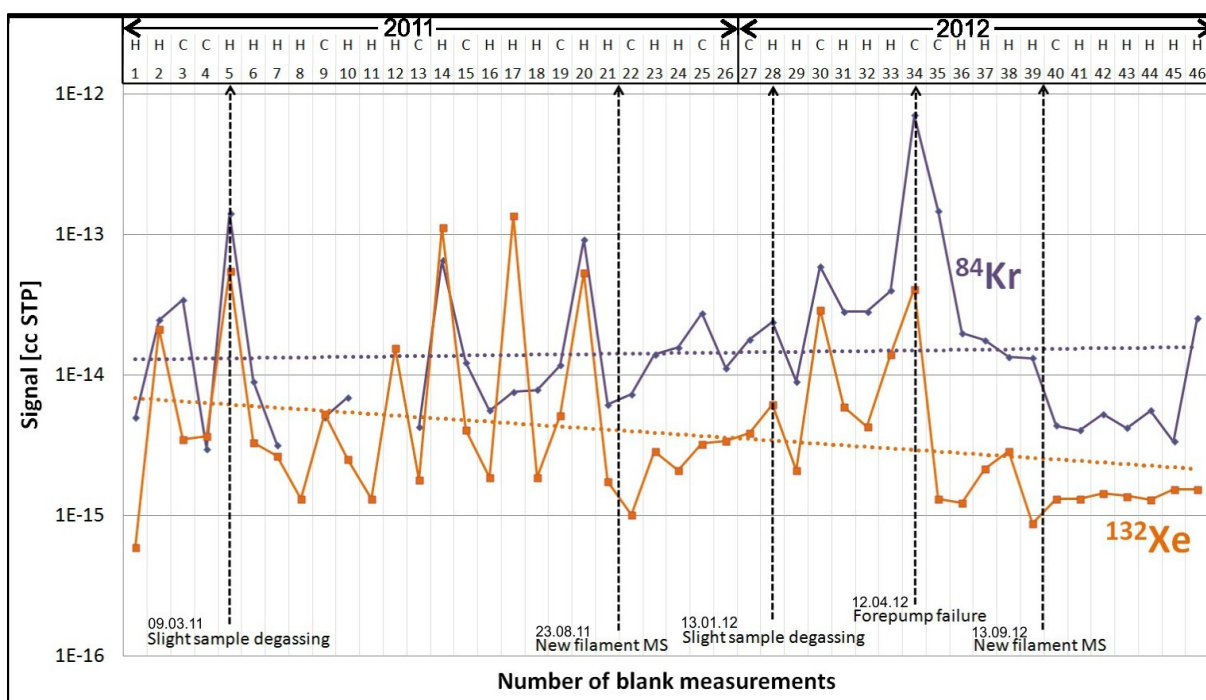
*Figure 42. Results from 46 **Kr and Xe** blank measurements between 2011 and 2012 (logarithmic scale) - not corrected for interferences. C = "cold" blank; H = "hot" blank. ^{132}Xe shows a clear improvement over time, which is illustrated by the best-fit line. ^{84}Kr did not change very much. Ocassionally high values occured presumably due to serious events like exchange of MS filaments and a pump failure. Also, leaks which sometimes occurred may have been a reason for a higher blank. A further reason for these variations is the incorporation of blanks measured with (H) and without (C) laser heating of the sample holder to simulate different sample heating scenarios.*

4.3.5 Data reduction, correction and concentration calculation

The raw noble gas data were extracted from the "Noblesse" software and inserted into data reduction Excel spreadsheets made and provided by PD Dr. U. Ott, MPIC Mainz, Germany.

As explained in chapter 4.3.4, the following reference (pilot) masses had to be measured in order to correct the sample data for interferences (Table 17).

He: HD / H_3 (only important for ^{3}He measurement as explained in chapter 4.3.4)

Ne: H_2O (m/z = 18), $^{40}Ar^+$ (m/z = 40) and CO_2^+ (m/z = 44)

Ar: ^{35}Cl (m/z = 35), ^{37}Cl (m/z = 37) and hydrocarbons (m/z = 39)

Kr: C_6H_6 (benzene; m/z = 78.1)

In the cases of Ne and Ar, the correction for interference masses is of particular importance. For example, the signal at mass m/z = 22 derives not only from ^{22}Ne, but also contains a contribution from doubly charged CO_2^{++}. For correction singly charged CO_2^+ at m/z = 44 was measured, and the Ne data accordingly corrected based on the independently determined ratio of doubly to singly charged CO_2 (0.7 ± 0.3%). Similarly, corrections for doubly charged $^{40}Ar^{++}$ and $^1H_2^{18}O$ were applied at m/z = 20, to obtain the true ^{20}Ne signal. In fact, in a very good high vacuum MS it is common that $^1H_2^{18}O$, $^{40}Ar^{++}$ and CO_2^{++} are primarily responsible for the small observed "virtual" ^{20}Ne and ^{22}Ne peaks in several blank measurements (see chapter 4.3.4.2). It is possible to correct "real" sample Ne by using interference mass values obtained from these measurements.

Concerning Ar measurements, the reference masses ^{35}Cl (m/z = 35), ^{37}Cl (m/z = 37) and (as representative for hydrocarbons) m/z = 39 were collected. ^{35}Cl served as a measure for the HCl interference at ^{36}Ar and ^{38}Ar (^{37}Cl was measured for consistency only), while the measured signal at m/z = 39 was used as a measure for hydrocarbon interferences influencing ^{36}Ar and ^{38}Ar. The measured Ar data was corrected for the interfering masses in a similar way as described for Ne. Correction factors used for this work are shown in Table 17.

Table 17. Correction factors obtained from interference masses used in this work for Ne and Ar measured with the "Noblesse". Uncertainties in the last digits are given in parenthesis.

Nobel gas isotope	Corresponding masses	Interference isotopes	Correction factor [%]
^{20}Ne	m/z = 20	$^1H_2^{18}O/^1H_2^{16}O$	0.20 (1)
^{20}Ne	m/z = 20	$^{40}Ar^{++}/^{40}Ar^+$	5.0-8.6 (3.0)
^{22}Ne	m/z = 22	CO_2^{++}/ CO_2^+.	0.7-0.9 (3)
^{36}Ar	m/z = 36	^{35}Cl (HCl), ^{37}Cl	1.6 (6)
^{38}Ar	m/z = 38	^{35}Cl (HCl), ^{37}Cl	0.5 (2)
^{36}Ar	m/z = 36	*Hydrocarbons (m/z = 39)*	10.0 (10.0)
^{38}Ar	m/z = 38	*Hydrocarbons (m/z = 39)*	3.0 (3.0)

For our measurements and results - i.e., blanks, calibrations and samples - the correction factors for ^{22}Ne typically would correspond to values from 2.1 x 10^{-15} cc STP to 4.8 x 10^{-13} cc STP. For ^{20}Ne they would correspond to values between 1.5 x 10^{-15} cc STP and a maximum of 1.1 x 10^{-12} cc STP. In the case of Ar they would correspond to values from 6.7 x 10^{-16} cc STP to 8.9 x 10^{-14} cc STP for ^{36}Ar and from 2.7 x 10^{-16} cc STP to 2.5 x 10^{-14} cc STP for ^{38}Ar. However, in most cases the amount of interference isotopes which have to be corrected, would roughly correspond to the amount of sample, blank or calibration gases. Most of the time the amount of interference isotopes was stable and only changed due to serious events like vacuum seepage and pump failures.

During Kr measurements, the mass 78.1 was measured in order to correct ^{78}Kr and subsequently the ^{78}Kr/^{84}Kr ratio. However, the measurement of both turned out not to be very reliable, so no data for ^{78}Kr will be reported.

The Xe measurement and data reduction for the "Noblesse" are a special case and are explained separately in chapter 4.3.5.1 (see further down).

Overall the data reduction for He to Xe was similar and is explained as follows:

1. The obtained raw data (cps and ratios of sample, blank, calibration and interference mass measurements) was copied from the "Noblesse" software into the Excel spreadsheet for He, Ne, Ar, Kr or Xe. The "Noblesse" software provided the possibility to extrapolate the data on the time zero - manually or automatically. Therefore one was able to select between linear, expo (exponential) and in rare cases the arithmetic mean. In most cases the automatic selection of the "Noblesse" software worked just fine. In cases of low Xe gas amounts we selected exponential for the straight counts/second (cps) ^{132}Xe results to optimize the yield; i.e. ^{132}Xe = ~100 cps (linear) would give us ^{132}Xe = ~103 cps with the exponential extrapolation option.

2. In a further step the obtained sample data is corrected for the crosstalk of the Channeltrons (see chapter 4.3.2.1). For calibrations no such correction is done, hence, the effects of the crosstalk are part of the calibration factors, i.e., if the sample´s noble gases show the same compositon like in Earth´s athmosphere, no correction is performed. If the isotopic composition of the samples is different, we correct for the discrepancy (up or down). In this case it depends on the frequency of the neighboring isotopes of being higher or lower than air, in relation to the affected isotope.

3. Sample names, the weight of the sample, the date of the sample degassing and measurement and the power of the laser were noted down.

4. After examination of all blank results, a reliable "realistic" blank was selected for correction, with appropriate generous uncertainties assigned both in abundances and isotope ratios.

5. The calibration gas results were corrected for blank and interference masses in the same way in a different Excel-spreadsheet followed by choosing the particular CAL (calibration) - Nr. factor (cc STP) from which the calibration gas amount was calculated as follows:

$$\left(\frac{1 - (\text{Vol. CAL gas pipette})}{(\text{Vol. CAL gas pipette} + \text{Vol. CAL gas cylinder})}\right)^{(\text{CAL-Nr.} - 1)} * \text{Noble gas amount of "Mix"} [cc\ STP] \quad (4)$$

In regard to the "Noblesse" and the used calibration flasks this would imply:

^{3}He:

$$\left(\frac{1 - 0.324\ \text{cc}}{(0.324\ \text{cc} + 984.68\ \text{cc})}\right)^{(\text{CAL-Nr.} - 1)} * 3.65329 * 10^{-11}\ \text{cc STP} \quad (5)$$

^{4}He:

$$\left(\frac{1 - 0.324\ \text{cc}}{(0.324\ \text{cc} + 984.68\ \text{cc})}\right)^{(\text{CAL-Nr.} - 1)} * 7.34255 * 10^{-8}\ \text{cc STP} \quad (6)$$

Ne:

$$\left(\frac{1 - 0.324\ \text{cc}}{(0.324\ \text{cc} + 984.68\ \text{cc})}\right)^{(\text{CAL-Nr.} - 1)} * 2.07186 * 10^{-11}\ \text{cc STP} \quad (7)$$

Ar:

$$\left(\frac{1 - 0.324\ \text{cc}}{(0.324\ \text{cc} + 984.68\ \text{cc})}\right)^{(\text{CAL-Nr.} - 1)} * 2.3404 * 10^{-10}\ \text{cc STP} \quad (8)$$

Kr:

$$\left(\frac{1 - 0.324\ \text{cc}}{(0.324\ \text{cc} + 984.68\ \text{cc})}\right)^{(\text{CAL-Nr.} - 1)} * 8.074 * 10^{-12}\ \text{cc STP} \quad (9)$$

Xe:

$$\left(\frac{1 - 0.324\ \text{cc}}{(0.324\ \text{cc} + 984.68\ \text{cc})}\right)^{(\text{CAL-Nr.} - 1)} * 4.6185 * 10^{-12}\ \text{cc STP} \quad (10)$$

Where CAL-Nr. is the number of the "slug" used. A "slug" is amount of calibration gas taken out of the "Mix" flask via the pipette system and depends on the volume ratio of the pipette (0.324 cm^3) relative to that of the flask (984.68 cm^3). The numerical values at the end of the equation correspond to the gas amount that was present in the first slug directly after filling the flask, and had been determined via pressure and volume ratio measurements during filling of the flask (see chapter 4.3.4.1).

The sensitivity factor (cc STP/cps for channeltron measurements, cc STP/mV for Faraday measurements) is then calculated by dividing the amount of the calibration gas by the by the measured signal. Due to the stability of the system, the sensitivity factor did not vary much (see chapter 4.3.4.1). Similarly discrimination factors were determined by dividing the "true" isotope ratios (air values except for He) by the measured ratios for the calibration.

6. Average "realistic" sensitivity factors and discrimination correction factors are selected, with proper generous uncertainties assigned, for correction of sample data.

7. Sample data are first corrected for blanks and interference masses in the same way as the calibration data (see above). Following this, the noble gas abundance (cc STP) is being determined using the sensitivity factor calculated from the calibration measurements, and the isotopic ratios by applying the discrimination correction.

8. Using the weight of the sample, the concentrations in cc STP/g are calculated.

9. The entire calculation and correction procedure is repeated for each heating and degassing step of the sample.

10. From the obtained noble gas results, the abundances of the trapped and cosmogenic components are calculated. For cosmogenic results and discussion see chapter 5.4.7.

4.3.5.1 Xenon - internal and external calibration calculations and results

The Xenon data was generally obtained using the data reduction process explained in the previous chapter. In addition to this procedure, Xe was analyzed using different Excel spreadsheets for so-called "external a", "external b" and "internal" data reduction. These spreadsheets were developed and provided by PD Dr. U. Ott, MPIC Mainz, Germany.

The "external a" and "external b" spreadsheets use the conventional approach, as also applied for the other gases, of obtaining the applied correction factors (including the response of the individual channeltrons) for isotope discrimination offline, i.e. from the calibration measurements. The "internal" scheme, on the other hand, tries to get the correction factors for the channeltrons "online", i.e. during the sample measurement itself.

As explained in chapter 4.3.2 the "Noblesse" measurement scheme for Xe was improved using a new three-step measurement scheme for Xe **plus** an internal calibration with an extra channeltron (see Table 18). In this new scheme every Xe isotope was measured twice on different channeltrons, except for ^{131}Xe and ^{129}Xe. This gave us the possibility of calculating comparison factors between channeltrons.

Table 18. "Noblesse" Xe channeltron detector setup for internal calibration.

Channeltron-detector	IC 0	IC 1	IC 2	IC 3	IC 4	IC 5	IC 6	IC 7
Step 1	136	134	132	130	128	126	124	
Step 1a		136	134	132	130	128	126	124
Step 2			131	129				

To illustrate how the comparison factors were determined, take the case of ^{132}Xe. This isotope was measured on both IC2 and IC3 and the resulting signals were "132a" from IC2 and "132b" from IC3. Usually IC2 detected slightly more cps than IC3 for ^{132}Xe, which resulted in a comparison factor of about 0.87. In the same way relative sensitivity factors were determined also for the other detector pairs (Table 19). The "external a" and "external b" values were based on the output from the "Noblesse" software (see Appendix F and Table 19). For the internal correction the overall factors relative to IC2 and to IC3 were determined. Since only factors for adjacent channeltrons could be determined, these are mostly a product of several factors, e.g. the relative factor between channeltrons 3 and 1 is the product of the factors between 3 and 2 and between 2 and 1. Corrections based on these factors were then applied to the step 1 data (=a, relative to IC2, where ^{132}Xe measured) and to the step 1a data (=b, relative to IC3). Final results from the ratios were then obtained from a weighted mean of the two individual "internally-corrected" results. The steps of the calculation shown in Table 19 (see also Appendix F) were performed within the Excel-spreadsheets for calculating these ratios and results. The advantage of this approach, it was hoped, was that the relative detection efficiencies of the channeltrons were determined during the measurement itself, and thus not influenced by fluctuations. Special cases were the odd isotopes 129 and 131, since these were measured only once each in step 2. ^{129}Xe/^{132}Xe uses ^{132}Xe measured in step 1a, while ^{132}Xe/^{132}Xe uses ^{132}Xe measured in step 1, since in this way each

isotope pair is measured with the same detector (see Table 18 and Appendix F) and no correction for relative detection efficiency is required.

Table 19. "Noblesse" Xe configuration and analysis steps for internal data reduction.

Step 1 & Step 2 (External a)	Step 1a & Step 2 (External b)	Factors formed (ICs)		Final results (Internal)
132a(cps)	132-b(cps)	3/2	132-b/132a	136/132
136a/132a	136-b/132-b	1/0	136-b/136a	134/132
134a/132a	134-b/132-b	2/1	134-b/134a	131/132
131/132a	130-b/132-b	4/3	130-b/130a	130/132
130a/132a	129/132-b	5/4	128-b/128a	129/132
128a/132a	128-b/132-b	6/5	126-b/126a	128/132
126a/132a	126-b/132-b	7/6	124-b/124a	126/132
124a/132a	124-b/132-b			124/132

The following Xe data is provided in delta notation (δ) [‰]. The formula for Xe follows the formula for carbon isotopes, which are measured relative to the reference standard V-PDB (Vienna Pee Dee Belemnite) and are calibrated using the reference standard NBS. For Xe ratios, the following equation was used, here exemplarily for ^{129}Xe:

$$\boldsymbol{\delta\ ^{129}Xe}[‰] = \left(\frac{(\frac{^{129}Xe_{sample}}{^{132}Xe_{sample}})}{(\frac{^{129}Xe_{standard\,(Air,SW)}}{^{132}Xe_{standard\,(Air,SW)}})} - 1 \right) \times 1000 \qquad (11)$$

Fig. 43 shows Xe isotopes in per mil-deviations [δ] from air Xe composition (Basford et al. (1973)) for 25 selected calibration measurements. The Xe isotopes are normalized to ^{132}Xe. Further results will be explained and discussed in more detail in chapter 5.4.5. The results in Fig. 43 illustrate the ability of the three different analysis corrections (external a, b or internal) to fit the data with stable results and small errors (for the whole data set see Appendix). Due to the often expected low Xe gas amounts in samples, it is reasonable to expect benefits for these isotopes regarding the different internal and external assessments. When comparing the graphs in Fig. 43, it is clear that for ^{128}Xe to ^{136}Xe, the internal calibration provides the most stable and best fit because the measured ratios are near the known air Xe ratios. ^{124}Xe/^{132}Xe and ^{126}Xe/^{132}Xe show wider ratio variations with larger errors due to low gas amounts and because the channeltron setup requires application of several of the determines internal calibration factors - four factors in case of ^{124}Xe/^{132}Xe, including such based on the relative signals of low-abundant ^{126}Xe and ^{124}Xe, which results in large uncertainties for these. For this reason and because even if the raw measurements for ^{124}Xe and ^{126}Xe are very large due to their low abundance, these

isotopes will not be further considered. Otherwise, the Xe-data reported in the results and discussion chapter are based on the internal calibration data.
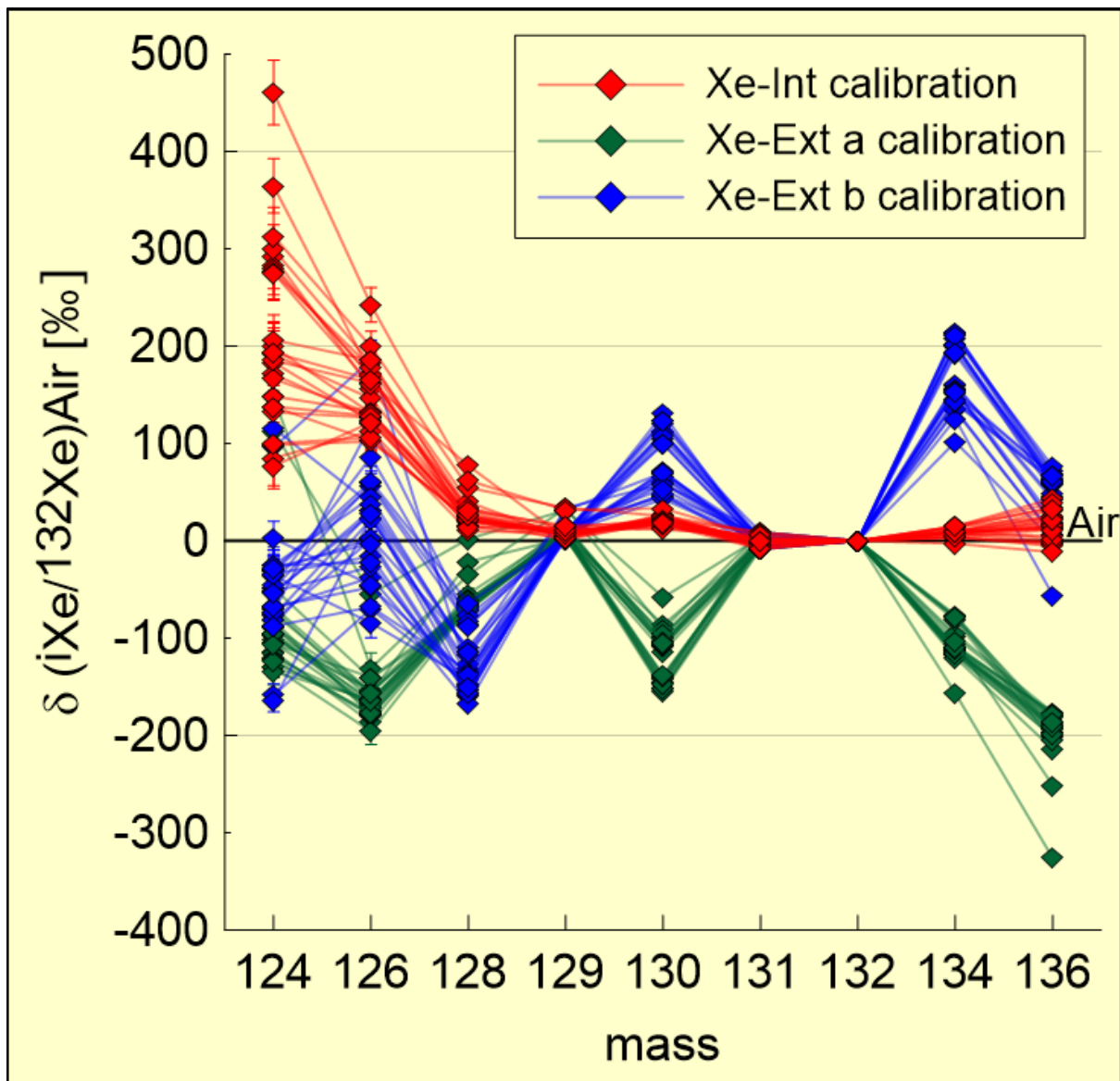
Figure 43. Plot of Xe isotopes shown in per mil-deviations from air Xe composition (Basford et al. (1973)). The plot illustrates the results of 25 selected calibrations analyzed using three differnet calibration calculations - internal (int), external a (ext a) and external b (ext b). The external calibration results were provided by the "Noblesse" software; the internal calibration was made by PD Dr. U. Ott, MPIC Mainz and is based on calculations between the external a and b results (see text above for further explanations).

Chapter 5 - Micrometeorites from the Transantarctic Mountains (TAM) - Noble gases show indications for multiple populations

In this chapter I will describe which MM samples from the Transantarctic Mountains were selected and how the noble gases specifically for these samples were extracted and measured. After this the results will be discussed and conclusions will be given. The complete data set is given in the Appendix. Major contributions to the mineralogy and petrology of the MM samples were provided by our colleagues from the University of Siena / MNA - C. Cordier, L. Folco and M. van Ginneken (chapter 5.3 and Appendix).

5.1 Introduction

During the Italian PNRA (*Programma Nazionale delle Ricerche in Antartide)* missions in 2003 and 2006, the scientists P. Rochette, L. Folco and colleagues were able to collect thousands of micrometeorites in different geological traps on top of Frontier Mountain and Miller Butte (and others), Victoria Land, Antarctica (see chapter 4.1.1. Fig. 44 and Fig. 45). All the sample sites were located near the Rennick glacier system which deposited sediments through transport in geological traps and pitfalls (Rochette et al. (2008)).
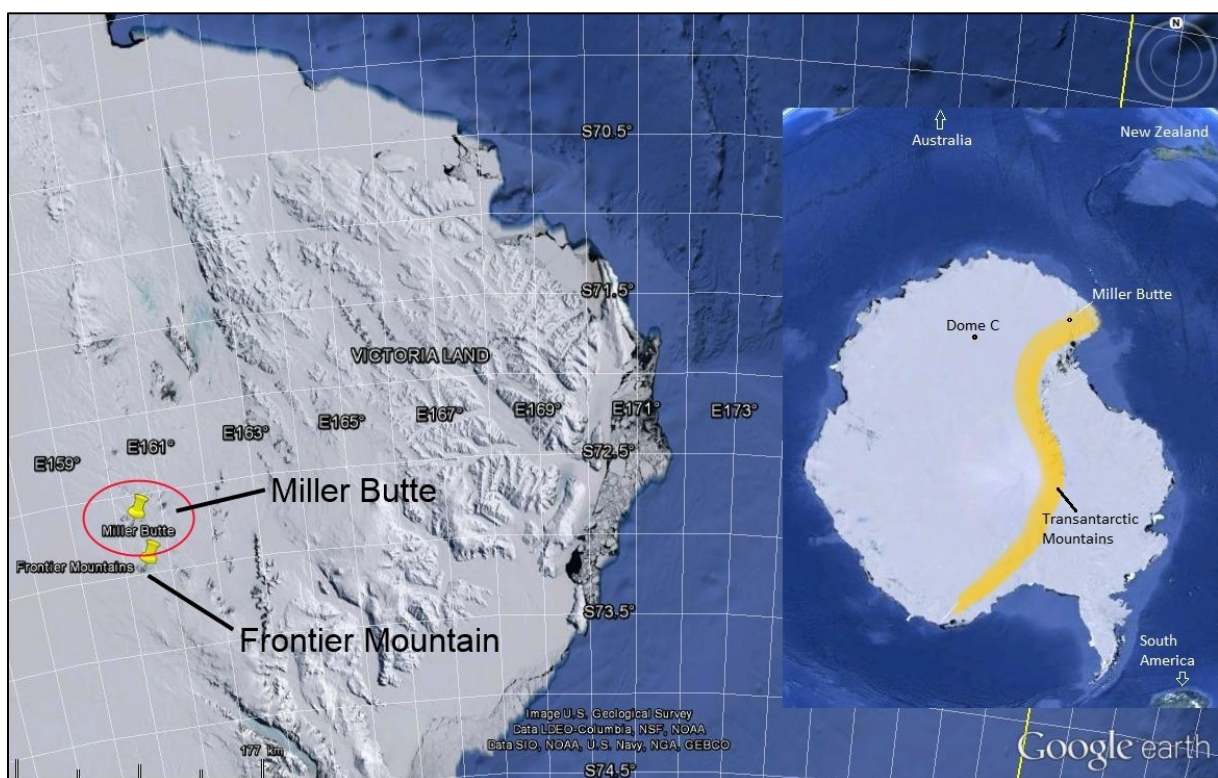
Figure 44. Map showing the MM sample location Miller Butte in the Transantarctic Mountains, Victoria Land, Antarctica (S 72°42, E160°14) (see Rochette et al. (2008)). For orientation in the small picture on the right some locations and continents near Antarctica have been added (after Google Earth).

Bastian Baecker | Chapter 5 - Micrometeorites from the Transantarctic Mountains (TAM) - Noble gases show indications for multiple populations

91

Figure 45. Image showing a geological trap (intersection joints) for sediments and MMs on top of Miller Butte, TAM, Antarctica (S 72°42, E160°14) on a glacial, polished and granitic surface. The altitude of the trap is at about 2600 m. (Image credit L. Folco, MNA, Siena University, Italy).

5.2 Mineralogy and petrology

This chapter is meant to provide basic information about the acquired samples and will give an overview about the MMs selected for noble gas measurements. More detailed mineralogical and petrological information for the measured MM samples can be found in the Appendix. Some of this information was obtained during my stay in Siena, Italy (see chapter 4.1). Others are from petrological work of C. Cordier, L. Folco and M. van Ginneken (2010 at MNA, Siena) and especially from detailed petrological work of C. Cordier in 2011 and 2012 (see Appendix).

5.2.1 Sample set micrometeorites - Miller Butte - Victoria Land - TAM

Our sample set from Miller Butte (51 MMs) comprised 26 Cosmic Spherules (CS), 11 scoriaceous MMs (Sc) and 14 unmelted MMs (Un) (see Fig. 46 and chapter 3.1.4 for the classification of MMs) which had been split into aliquots. One part stayed in Siena for petrological analyses, the other part was transported to the MPIC in Mainz for noble gas measurements. The original MM samples had sizes of about 350 to 1350 µm in diameter, were weighed at MNA, Siena, Italy, and originated from the MM sample pool which had been magnetically extracted from other sediments (see Rochette et al. (2008)). They had been discovered on top of Miller Butte, a mountain complex near Frontier Mountain in the TAM area, Victoria Land, Antarctica (Rochette et al. (2008). Depending on the trap the samples from which they had been selected,

Bastian Baecker | Chapter 5 - Micrometeorites from the Transantarctic Mountains (TAM) - Noble gases show indications for multiple populations

92

they were named 45b or 45c. Table 20 provides information about all the acquired MM samples from Miller Butte.

Table 20. Roster of 103 particles from 51 different MM samples acquired in 2010 at MNA, Siena University, with the aid of L. Folco, C. Cordier and M. van Ginneken. The 51 samples comprise 26 CS, 11 ScMMs and 14 UnMMs and had been obtained from Miller Butte, TAM, Antarctica by P. Rochette, L. Folco and colleagues (see Rochette et al. (2008)). Samples measured for noble gases are marked in yellow. For abbreviations see chapter 3.1.4. Detailed petrographical description are given in the Appendix.

Sample	Particle number	Noble gas measurement date	Weight (µg)	Diameter (µm)	Class	Type / Subtype
45b.02	whole sample	Not measured	654.6 ± 0.1	775 x 686	CS	n.a.
45b.03	whole sample	Not measured	934.5 ± 0.1	977 x 868	CS	n.a.
45b.05	1	Not measured	24.4 ± 0.2	376 x 235	CS	BO
45b.05	2	Not measured	15.2 ± 0.2	314 x 227	CS	BO
45b.05	3	Not measured	17.9 ± 0.2	319 x 249	CS	BO
45b.05	4	Not measured	12.7 ± 0.2	417 x 382	CS	BO
45b.05	5	Not measured	5.6 ± 0.2	202 x 171	CS	BO
45b.07	1	Not measured	155.5 ± 0.1	551 x 606	CS	PO
45b.07	2	Not measured	9.5 ± 0.1	393 x 293	CS	PO
45b.08	1	10/24/11-10/27/11	119.3 ± 0.1	654 x 374	ScMM	Cg
45b.08	2	Not measured	27.2 ± 0.1	346 x 265	ScMM	Cg
45b.09	1	07/18/11	126.9 ± 0.1	626 x 557	UnMM	Fg
45b.09	2	Not measured	21.9 ± 0.1	397 x 283	UnMM	Fg
45b.10	1	Not measured	67.8 ± 0.1	523 x 324	UnMM	Cg
45b.10	2	10/17/12+10/18/12	95.5 ± 0.1	494 x 418	UnMM	Cg
45b.11	1	Not measured	22.8 ± 0.1	315 x 230	ScMM	PO
45b.11	2	Not measured	21.0 ± 0.1	278 x 377	ScMM	PO
45b.12	whole sample	Not measured	107.0 ± 0.1	612 x 349	ScMM	Cg
45b.13	1	07/20/11+07/21/11	137.6 ± 0.1	547 x 455	ScMM	PO
45b.13	2	Not measured	10.4 ± 0.1	174 x 125	ScMM	PO
45b.14	1	10/03/12+10/04/12	56.5 ± 0.1	514 x 432	ScMM	Cg
45b.14	2	Not measured	18.2 ± 0.1	356 x 244	ScMM	Cg
45b.15	1	09/17/12+09/18/12	30.3 ± 0.1	422 x 300	ScMM	PO
45b.15	2	Not measured	9.7 ± 0.1	364 x 161	ScMM	PO
45b.16	whole sample	06/18/12+06/19/12	138.3 ± 0.1	572 x 463	UnMM	Cg
45b.17	1	06/20/12	56.2 ± 0.1	416 x 283	UnMM	Cg
45b.17	2	Not measured	9.8 ± 0.2	446 x 131	UnMM	Cg
45b.18	1	11/11/11+11/17/11	5.3 ± 0.1	253 x 235	UnMM	Fg
45b.18	2	Not measured	4.9 ± 0.1	167 x 185	UnMM	Fg
45b.19	1	01/19/12	55.9 ± 0.1	450 x 292	CS	BO
45b.19	2	Not measured	11.8 ± 0.1	255 x 160	CS	BO
45b.20	1	Not measured	35.7 ± 0.1	505 x 504	ScMM	Fg
45b.20	2	09/25/12+09/26/12	77.3 ± 0.1	613 x 482	ScMM	Fg
45b.21	whole sample	01/18/12+01/19/12	24.8 ± 0.1	571 x 212	UnMM	Fg
45b.22	1	Not measured	9.3 ± 0.1	238 x 178	ScMM	PO
45b.22	2	05/04/11	9.2 ± 0.1	268 x 191	ScMM	PO
45b.22	3	Not measured	26.7 ± 0.1	387 x 177	ScMM	PO
45b.23	whole sample	Not measured	32.0 ± 0.2	508 x 278	CS	PO
45c.02	whole sample	Not measured	175.6 ± 0.1	505 x 503	CS	n.a.
45c.03	whole sample	Not measured	439.5 ± 0.2	719 x 627	CS	n.a.
45c.04	whole sample	Not measured	364.0 ± 0.2	644 x 606	CS	V
45c.05	1	Not measured	58.5 ± 0.1	576 x 352	CS	BO
45c.05	2	Not measured	54.8 ± 0.2	445 x 340	CS	BO
45c.06	whole sample	Not measured	422.1 ± 0.2	678 x 711	CS	n.a.
45c.07	1	Not measured	27.4 ± 0.1	533 x 327	CS	CC
45c.07	2	Not measured	7.7 ± 0.2	279 x 235	CS	CC

Bastian Baecker | Chapter 5 - Micrometeorites from the Transantarctic Mountains (TAM) - Noble gases show indications for multiple populations

93

Sample	Particle number	Noble gas measurement date	Weight (µg)	Diameter (µm)	Class	Type / Subtype
45c.07	3	Not measured	8.7 ± 0.1	254 x 162	CS	CC
45c.07	4	Not measured	5.3 ± 0.1	214 x 172	CS	CC
45c.07	5	Not measured	4.2 ± 0.1	236 x 165	CS	CC
45c.09	whole sample	Not measured	37.3 ± 0.2	418 x 316	CS	PO
45c.10	1	Not measured	26.4 ± 0.1	429 x 289	CS	PO
45c.10	2	Not measured	160.6 ± 0.1	347 x 248	CS	PO
45c.11	1	Not measured	11.9 ± 0.1	353 x 195	CS	CC
45c.11	2	Not measured	8.6 ± 0.2	296 x 241	CS	CC
45c.11	3	Not measured	7.3 ± 0.2	322 x 268	CS	CC
45c.12	whole sample	Not measured	39.0 ± 0.1	358 x 357	CS	PO
45c.13	1	Not measured	66.3 ± 0.1	568 x 459	CS	PO
45c.13	2	Not measured	17.1 ± 0.1	354 x 253	CS	PO
45c.13	3	Not measured	27.6 ± 0.1	459 x 180	CS	PO
45c.14	whole sample	Not measured	16.3 ± 0.1	264 x 237	CS	PO
45c.15	1	Not measured	26.0 ± 0.1	388 x 202	CS	PO
45c.15	2	Not measured	31.5 ± 0.2	480 x 340	CS	PO
45c.15	3	Not measured	5.4 ± 0.1	175 x 134	CS	PO
45c.15	4	Not measured	9.9 ± 0.1	292 x 187	CS	PO
45c.15	5	Not measured	7.1 ± 0.2	338 x 183	CS	PO
45c.15	6	Not measured	4.2 ± 0.1	232 x 151	CS	PO
45c.16	1	Not measured	149.6 ± 0.1	561 x 532	CS	PO
45c.16	2	05/02/11	105.1 ± 0.1	465 x 324	CS	PO
45c.17	whole sample	03/31/11	126.3 ± 0.2	630 x 476	CS	PO
45c.18	whole sample	Not measured	184.6 ± 0.2	413 x 413	CS	I
45c.19	whole sample	Not measured	423.4 ± 0.1	655 x 633	CS	n.a.
45c.20	whole sample	Not measured	81.6 ± 0.2	473 x 350	CS	n.a.
45c.21	whole sample	04/28/11	337.9 ± 0.2	720 x 556	CS	n.a.
45c.24	whole sample	09/27/12+10/02/12	34.0 ± 0.2	489 x 330	UnMM	Fg
45c.25	1	Not measured	30.2 ± 0.1	404 x 284	ScMM	PO
45c.25	2	04/19/12+04/20/12	142.3 ± 0.1	580 x 528	ScMM	PO
45c.27	1	Not measured	30.1 ± 0.1	462 x 303	ScMM	PO
45c.27	2	06/09/11+06/14/11	38.0 ± 0.1	521 x 337	ScMM	PO
45c.27	3	Not measured	22.7 ± 0.1	357 x 289	ScMM	PO
45c.28	whole sample	Not measured	18.6 ± 0.1	383 x 356	CS	CC
45c.29	1	09/18/12+09/19/12	22.1 ± 0.2	337 x 255	UnMM	Cg
45c.29	2	06/12/12+06/13/12	24.2 ± 0.2	305 x 187	UnMM	Cg
45c.29	3	Not measured	7.0 ± 0.1	232 x 167	UnMM	Cg
45c.29	4	Not measured	1.5 ± 0.1	77 x 43	UnMM	Cg
45c.31	1	02/22/12+02/23/12	33.2 ± 0.3	460 x 372	ScMM	PO
45c.31	2	Not measured	6.5 ± 0.1	291 x 200	ScMM	PO
45c.31	3	Not measured	6.1 ± 0.1	250 x 201	ScMM	PO
45c.33	1	06/08/12+06/11/12	58.7 ± 0.2	512 x 379	UnMM	Fg
45c.33	2	Not measured	11.1 ± 0.2	268 x 253	UnMM	Fg
45c.33	3	Not measured	n.a.	n.a.	UnMM	Fg
45c.34	1	10/08/12+10/16/12	34.1 ± 0.1	428 x 318	UnMM	Fg
45c.34	2	Not measured	6.9 ± 0.1	238 x 223	UnMM	Fg
X1 (45c.35)	1	11/03/11+11/04/11	35.0 ± 0.1	427 x 315	UnMM	Cg
45c.35	2	02/13/12+02/14/12	5.4 ± 0.1	152 x 135	UnMM	Cg
45c.35	3	09/02/11+09/05/11+ 09/06/11	29.0 ± 0.1	428 x 245	UnMM	Cg
45c.35	4	Not measured	3.5 ± 0.1	215 x 116	UnMM	Cg
45c.35	5	Not measured	n.a.	n.a.	UnMM	Cg
45c.37	1	Not measured	15.4 ± 0.1	439 x 159	UnMM	Fg
45c.37	2	02/14/12+02/15/12	28.5 ± 0.1	498 x 379	UnMM	Fg
45c.37	3	02/16/12	13.1 ± 0.1	322 x 205	UnMM	Fg
20c-349	1	Not measured	12.6 ± 0.1	309 x 147	UnMM	Aggregate
20c-350	2	Not measured	1.8 ± 0.1	101 x 78	UnMM	Aggregate
20c-350	3	Not measured	0.6 ± 0.1	83 x 63	UnMM	Aggregate

Bastian Baecker | Chapter 5 - Micrometeorites from the Transantarctic Mountains (TAM) - Noble gases show indications for multiple populations

94

It is important to point out that some samples could not be definitely assigned to a group. Some of these showed patterns similar to Cosmic Spherules; others were more like scoriaceous MMs or even contained areas with an unmelted MM texture. Particles selected for noble gas extraction are marked in yellow and are listed with the date of measurement (Table 20).
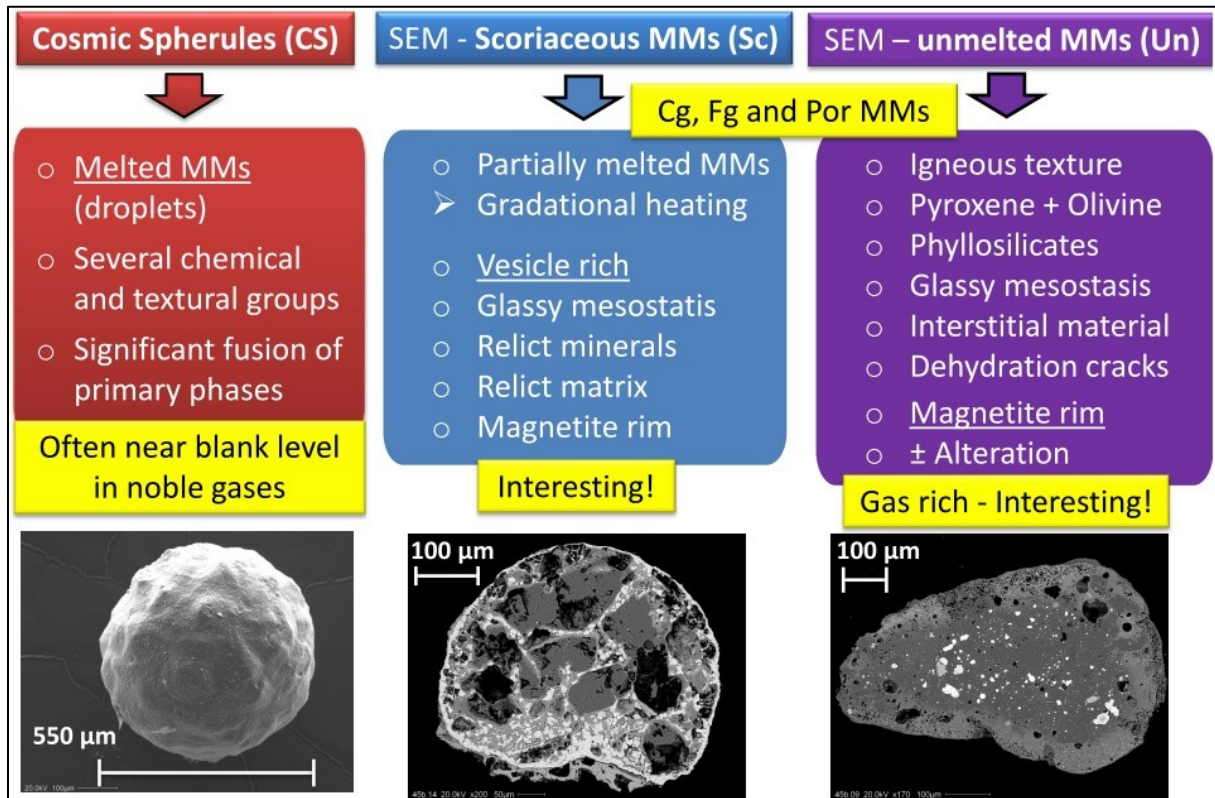
Figure 46. Chart showing a basic description of the mineralogical and petrological classification of MMs - see also and chapter 3.1.4 (after Genge et al. (2008)).

Bastian Baecker | Chapter 5 - Micrometeorites from the Transantarctic Mountains (TAM) - Noble gases show indications for multiple populations

95

5.3 Addendum to the experimental procedure - TAM MM samples

The main experimental procedure has been explained in chapter 4. Here, some important additions and remarks will be given. Cosmic Spherules were selected for the first noble gas measurements. This was because of their large size and expected low gas amounts. This allowed, on the one hand, to test how well the gas extraction, separation and the sensitivity of the mass spectrometer worked. On the other hand we would not risk losing precious samples during this exploratory stage. After this we turned to scoriaceous MMs, and, after we were satisfied with the performance of the system we started the measurements of unmelted MM particles. As can be seen in Table 20, most of the MMs were not measured in whole but only an aliquot was used for noble gas analysis. The reason was that the samples had been cut at MNA, Siena, Italy, into several (mostly 2) pieces, to allow additional investigations by our Italian and French colleagues.

5.4 Noble gas results and discussion

We obtained noble gas results for 29 particles of overall 25 MMs from the Transantarctic Mountains / Miller Butte area (see Table 20 and Appendix). These samples comprised 16 unmelted MMs, 9 scoriaceous MMs, and 4 Cosmic Spherules. Up to four laser power steps were used for degassing the particles, (see Appendix), but generally one to two steps were sufficient. The results (totals) are presented in the following chapters and tables. The complete data set including individual extraction steps is given in the Appendix. All results shown in this chapter are corrected for blank and interferences (see Appendix), and, in case of Xe, the internal calibration approach (see chapter 4.3.5.1) has been used.

Bastian Baecker | Chapter 5 - Micrometeorites from the Transantarctic Mountains (TAM) - Noble gases show indications for multiple populations

96

5.4.1 Helium (He)

Overall the TAM MMs show low amounts of ^{3}He, while the concentration of ^{4}He varies significantly (see Table 21). The ^{3}He concentrations are in the range (where detectable) of 5 x 10^{-12} cc STP/g to 6 x 10^{-8} cc STP/g, ^{4}He concentrations vary between 3.7 x 10^{-8} cc STP/g and 1.2 x 10^{-5} cc STP/g. This is much less than found by Osawa and Nagao (2002) who measured overall ^{4}He concentrations between 10^{-6} cc STP/g and 10^{-3} cc STP/g in MMs collected at the Dome Fuji station in Antarctica. A possible reason for some difference could be the higher masses and sizes of the MMs from the TAM, which may have experienced a different thermal history during transition through Earth´s atmosphere than the smaller Dome Fuji MMs. Also, as evident in Table 21, most of our unmelted MMs and two scoriaceous MMs show ratios of ^{3}He/^{4}He larger than SW (^{3}He/^{4}He = 4.645 x 10^{-4}; Heber et al. (2012)). This is clear evidence for a contribution from spallation He which is characterized by very high ^{3}He/^{4}He (~0.2; e.g. Wieler (2002a)). This is opposite to the situation found for most MMs by Osawa and Nagao (2002) and Stuart et al. (1999) as well as about 50% of the IDPs by Pepin et al. (2000), where ^{3}He/^{4}He is below the solar ratio along with higher ^{4}He concentrations (see Fig. 47). Note that the relative contribution from spallation He may become enhanced during atmospheric entry heating (see e.g. Love and Brownlee (1991), Füri et al. (2013)) and terrestrial weathering (e.g. Osawa (2012)), since it is not so easily lost as implanted solar wind He. On the other hand, in small particles < 100 μm in size like the IDPs, a significant fraction of spallation He is immediately lost during production due to recoil (Trappitsch and Leya (2013)), which may partly explain the lower abundance in IDPs compared to our TAM micrometeorites.

In Fig. 47 the complete data set for ^{3}He/^{4}He in 10^{-4} units is plotted versus ^{4}He in cc STP/g, showing the He noble gas results of 16 UnMMs, 9 ScMMs and 3 CS. The highest ^{3}He concentration of 5.9 x 10^{-8} cc STP/g is found within the unmelted MM 45c.29 (1).The maximum ^{3}He/^{4}He of 149 x 10^{-4} is larger than any ratio given for AMMs by Osawa and Nagao (2002) and also larger than any ratio in the IDP data set of Pepin et al. (2000), only exeeded by one exceptional enigmatic IDP (with ^{3}He/^{4}He = 200 x 10^{-4}) analyzed by Nier and Schlutter (1993). In all, the 45c.29 micrometeorite is different from the other micrometeorites in the measured TAM collection and will be discussed in more detail in chapter 5.4.8.

A group of 4 UnMMs and 2 ScMMs are plotting in the zone between SW and "FSW" (^{3}He/^{4}He = 2.17 x 10^{-4}; Benkert et al. (1993)). "FSW" is "implantation-fractionated SW-Ne" (Wieler et al. (2007)) and has taken the place of former "SEP" (solar energetic particles) suggested by Benkert et al. (1993) - see also chapter 3.2.1.1 (solar wind). They may be characterized by a mixture between SW and "FSW", similarly as bulk He in lunar soil minerals and bulk solar-wind rich meteorites (Benkert et al. (1993); Black (1972a); Black (1972b)). This will become clearer in the discussion of the Ne isotopes below (see chapters 5.4.2, 5.4.7 and 6.4.2, 6.4.7).

The results for the measured Cosmic Spherules and 2 scoriaceous MMs show even lower ^{3}He/^{4}He ratios, on the level of planetary *trapped* components such as HL, P3 (Huss and Lewis (1994a)) - see Fig. 47. P3 and HL are carried by pre-solar nanodiamond and dominate trapped He and Ne in primitive meteorites (e.g. Ott

Bastian Baecker | Chapter 5 - Micrometeorites from the Transantarctic Mountains (TAM) - Noble gases show indications for multiple populations

97

(2002)), like Murchison (Fuchs et al. (1973)). While the thermally labile P3 component is an unlikely presence, the results may indicate the presence of the HL component and thus presolar diamond in these MMs.

*Table 21. **He** results for 29 different TAM MM samples. Given are the totals, calculated from the individual measurement steps as indicated, for details see Appendix. Uncertainties in the last digits are given in parenthesis. Values marked with $^\$$ are 2σ upper limits. For comparison also the compositions of SW, "FSW", Q (P1), HL and P3 are given.*

Sample	Particle no.	Step(s) used	^{4}He (10^{-12} cc STP)	^{3}He (10^{-12} cc STP)	^{4}He (10^{-8} cc STP/g)	^{3}He (10^{-8} cc STP/g)	^{3}He/^{4}He (10^{-4})
45b.08 (Sc)	1	all	225 (11)	0.094 (18)	189 (9)	0.079 (15)	4.20 (81)
45b.09 (Un)	1	1	29.8 (2.2)	-	23.5 (1.7)	-	-
45b.10 (Un)	2	1	15.7 (4.3)	0.063 (7)	16.4 (4.5)	0.066 (7)	40.4 (11.9)
45b.13 (Sc)	1	1	8.51 (1.68)	0.0007 (3)	6.19 (1.22	0.0005 (2)	0.88 (41)
45b.14 (Sc)	1	n.a.	-	-	-	-	-
45b.15 (Sc)	1	1	64.7 (5.1)	0.010 (3)	214 (17)	0.033 (9)	1.54 (43)
45b.16 (Un)	w.s.	2	9.01 (1.93)	0.084 (15)	6.51 (1.40)	0.061 (11)	93.3 (25.8)
45b.17 (Un)	1	all	615 (28)	1.47 (6)	1095 (49)	2.61 (11)	23.8 (1.5)
45b.18 (Un)	1	1	17.8 (5.7)	0.021 (14)	335 (107)	0.402 (261)	12.0 (8.7)
45b.19 (CS)	1	all	488 (10)	0.059 (15)	873 (17)	0.106 (27)	1.21 (31)
45b.20 (Sc)	2	1	35.5 (4.3)	0.066 (10)	46.0 (5.6)	0.085 (13)	18.5 (3.5)
45b.21 (Un)	w.s.	all	1159 (33)	0.333 (48)	4675 (135)	1.34 (19)	2.87 (42)
45b.22 (Sc)	2	1	< 7 $^\$$	-	< 79 $^\$$	-	-
45c.16 (CS)	2	1	3.84 (2.53)	0.0007 (3)	3.65 (2.41)	0.0006 (3)	1.77 (1.43)
45c.17 (CS)	w.s.	1	19.1 (3.4)	0.0036 (11)	15.1 (2.7)	0.0029 (8)	1.90 (65)
45c.21 (CS)	w.s.	n.a.	-	-	-	-	-
45c.24 (Un)	w.s.	1	160 (5)	0.099 (6)	469 (15)	0.292 (18)	6.22 (44)
45c.25 (Sc)	2	1	32.3 (4.0)	0.057 (15)	22.7 (2.8)	0.040 (10)	17.5 (5.0)
45c.27 (Sc)	2	1	< 5 $^\$$	< 0.001 $^\$$	< 12 $^\$$	< 0.002 $^\$$	-
45c.29 (Un)	1	all	87.3 (7.0)	1.30 (2)	395 (32)	5.90 (11)	149.4 (12.3)
45c.29 (Un)	2	1	1064 (45)	0.639 (28)	4396 (190)	2.64 (12)	6.01 (36)
45c.31 (Sc)	1	all	310 (10)	0.126 (23)	933 (29)	0.379 (69)	4.06 (75)
45c.33 (Un)	1	all	3633 (149)	1.29 (5)	6189 (253)	2.20 (9)	3.55 (21)
45c.34 (Un)	1	all	83.0 (6.2)	0.140 (9)	244 (18)	0.410 (26)	16.8 (1.7)
X1 (Un)	1	1	1339 (23)	0.601 (13)	3827 (67)	1.72 (4)	4.49 (13)
45c.35 (Un)	2	1	64.7 (5.9)	0.095 (16)	1198 (112)	1.76 (30)	14.7 (2.9)
45c.35 (Un)	3	1+2	3600 (50)	0.972 (42)	12412 (177)	3.35 (15)	2.70 (12)
45c.37 (Un)	2	1	135 (6)	0.031 (16)	474 (22)	0.109 (56)	2.30 (1.19)
45c.37 (Un)	3	1	44.5 (5.9)	< 0.037 $^\$$	340 (45)	< 0.286 $^\$$	-

Component	References						^{3}He/^{4}He (10^{-4})
SW	[1]						4.645 (8)
"FSW"	[2]						2.17 (5)
Q (P1)	[3]						1.23 (2)
HL	[4]						1.70 (10)
P3	[4]						1.35 (10)

References: [1] Heber et al. (2012); [2] Benkert et al. (1993); [3] Busemann et al. (2000); [4] Huss and Lewis (1994a); Note: w.s. = whole sample, n.a. = not detectable (below blank level). For detailed information regarding "FSW" see Wieler et al. (2007).

Bastian Baecker | Chapter 5 - Micrometeorites from the Transantarctic Mountains (TAM) - Noble gases show indications for multiple populations

98

Figure 47. The ratio $^3He / ^4He$ in 10^{-4} units is plotted vs. ^4He in cc STP/g. Besides our AMM data, also data for the CM2 meteorite Murchison (obtained at MPIC in 2011), data of other AMM noble gas measurements from Stuart et al. (1999) and Osawa and Nagao (2002) as well as noble gas data of IDPs is plotted (Pepin et al. (2000)). Plotted for comparison are the $^3He / ^4He$ ratios of SW (Heber et al. (2012)), "FSW" (Benkert et al. (1993) and Wieler et al. (2007)), HL and P3 (both Huss and Lewis (1994a)). Spallation He is characterized by much higher $^3He / ^4He$ (~0.2; e.g. Wieler (2002a)) than observed here.

Bastian Baecker | Chapter 5 - Micrometeorites from the Transantarctic Mountains (TAM) - Noble gases show indications for multiple populations

99

5.4.2 Neon (Ne)

Amounts and concentrations of ^{22}Ne along with ^{20}Ne/^{22}Ne and ^{21}Ne/^{22}Ne ratios for each TAM MM are presented in Table 22 and the Appendix. Overall, data for 16 UnMMs, 9 ScMMs and 4 CS is given. The concentrations of ^{22}Ne vary between 2×10^{-10} cc STP/g for the scoriaceous sample 45c.25(2) and 3.5×10^{-7} cc STP/g for the unmelted MM X1. The ratio ^{20}Ne/^{22}Ne ranges from 5.30 (45c.29(1) - UnMM) to 12.34 (45c.17 - CS) and the ratio ^{21}Ne/^{22}Ne from 0.024 (45c.24(1) - UnMM) to 0.571 (45c.29(1) - UnMM). The unmelted and most of the scoriaceous samples show cosmogenic and solar contributions, whereas one scoriaceous and three of the four CS plot close to air (EA; ^{20}Ne/^{22}Ne = 9.8 and ^{21}Ne/^{22}Ne = 0.029; Eberhardt et al. (1965)), with only a hint of other components. The other CS is not plotting near air but shows large uncertainties.

Fig. 48 and Fig. 49 are three isotope plots of ^{20}Ne/^{22}Ne and ^{21}Ne/^{22}Ne showing the results for the MMs mentioned above, AMM data from Osawa and Nagao (2002) as well as data for Murchison which was measured at the MPIC in 2011. Also plotted for comparison are SW (13.777, 0.03289; Heber et al. (2012)), Ne-B (12.5, 0.0335; Black and Pepin (1969)), "FSW" (11.2, 0.0295; Benkert et al. (1993) and Wieler et al. (2007)), Q(P1) (10.67, 0.0294; Busemann et al. (2000)), Earth atmosphere (EA) (Eberhardt et al. (1965)), P3 (8.91, 0.029) and HL (8.5, 0.036) (both Huss and Lewis (1994a)), Ne-G (~0; Lewis et al. (1994)) as well as GCR (0.83, 0.80-0.95; Garrison et al. (1995)) and the composition of SCR (0.89-1.97, 0.55-0.67). The latter has been calculated from Mg, Al, Si at 0.5-10 g/cm^2 using elemental production rates from Reedy (1992) and using the composition of CM chondrites (Wasson and Kallemeyn (1988)). 5 MMs (4 unmelted and 1 scoriaceous) are markedly shifted in the direction of spallation. In particular, the "special" unmelted MM 45c.29(1) (marked as purple star) shows the highest ^{21}Ne$_{cos}$ contribution of ^{21}Ne$_{cos}$ = 1.6×10^{-7} cc STP/g (see chapter 5.4.7). This concentration is higher than the highest one detected in the MMs measured by Osawa and Nagao (2002) (1.3×10^{-7} cc STP/g). The other part of the "special" MM (45c.29(2)) is less shifted in the direction of spallation, with ratios of ^{20}Ne/^{22}Ne = 8.26 and ^{21}Ne/^{22}Ne = 0.340, showing contributions of trapped (solar) components. The majority of the MMs is plotting between SW (solar wind) and EA (Earth atmosphere) (Fig. 49), where of these 3 unmelted (e.g. 45b.09(1)) and 3 scoriaceous MMs show small cosmogenic contributions. The noble gas abundances and concentrations in CS are low and mostly indistinguishable from air.

Bastian Baecker | Chapter 5 - Micrometeorites from the Transantarctic Mountains (TAM) - Noble gases show indications for multiple populations

100

*Table 22. **Ne** results for 29 different TAM MM samples. Given are the totals, calculated from the individual measurement steps as indicated, for details see Appendix. Uncertainties in the last digits are given in parenthesis. Values marked with [$] are 2σ upper limits. For comparison also the compositions of SW, "FSW", Q (P1), EA and HL are given.*

Sample	Particle no.	Step(s) used	22Ne (10^-12 cc STP)	22Ne (10^-8 cc STP/g)	20Ne/22Ne	21Ne/22Ne
45b.08 (Sc)	1	2+3	1.98 (5)	1.66 (4)	5.35 (9)	0.548 (12)
45b.09 (Un)	1	1	7.95 (13)	6.27 (10)	10.48 (16)	0.129 (1)
45b.10 (Un)	2	1	0.12 (2)	0.13 (2)	7.44 (1.02)	0.292 (41)
45b.13 (Sc)	1	1	3.45 (6)	2.50 (4)	12.12 (19)	0.033 (1)
45b.14 (Sc)	1	1	< 0.06 [$]	< 0.11 [$]	-	-
45b.15 (Sc)	1	1	0.10 (3)	0.33 (11)	9.64 (1.60)	0.031 (8)
45b.16 (Un)	w.s.	all	16.26 (80)	11.76 (58)	11.27 (9)	0.039 (1)
45b.17 (Un)	1	all	6.54 (35)	11.64 (62)	7.11 (6)	0.398 (5)
45b.18 (Un)	1	1	0.36 (3)	6.80 (63)	11.86 (57)	0.041 (3)
45b.19 (CS)	1	all	0.19 (7)	0.34 (13)	10.58 (2.36)	0.030 (8)
45b.20 (Sc)	2	1	0.37 (3)	0.48 (3)	11.24 (52)	0.066 (5)
45b.21 (Un)	w.s.	all	1.50 (12)	6.05 (47)	11.22 (50)	0.029 (2)
45b.22 (Sc)	2	1	0.40 (3)	4.39 (34)	11.16 (49)	0.074 (5)
45c.16 (CS)	2	1	0.10 (4)	0.10 (4)	10.41 (2.54)	0.041 (10)
45c.17 (CS)	w.s.	1	0.07 (4)	0.05 (3)	12.34 (3.01)	0.044 (23)
45c.21 (CS)	w.s.	1	0.30 (3)	0.09 (1)	9.88 (62)	0.035 (4)
45c.24 (Un)	w.s.	1	0.33 (2)	0.97 (7)	11.48 (58)	0.024 (4)
45c.25 (Sc)	2	1	0.03 (3)	0.02 (2)	-	-
45c.27 (Sc)	2	1	0.23 (1)	0.62 (4)	10.35 (34)	0.063 (5)
45c.29 (Un)	1	1+2	6.42 (10)	29.06 (54)	5.30 (13)	0.571 (7)
45c.29 (Un)	2	1	4.04 (6)	16.68 (28)	8.26 (8)	0.340 (5)
45c.31 (Sc)	1	all	4.59 (6)	13.82 (18)	11.85 (11)	0.038 (1)
45c.33 (Un)	1	all	7.89 (11)	13.43 (19)	11.46 (9)	0.042 (1)
45c.34 (Un)	1	1	0.12 (2)	0.36 (7)	10.84 (1.38)	0.033 (7)
X1 (Un)	1	all	12.12 (17)	34.63 (49)	10.13 (21)	0.050 (1)
45c.35 (Un)	2	1	0.45 (4)	8.38 (67)	10.58 (57)	0.100 (7)
45c.35 (Un)	3	2	3.08 (7)	10.61 (26)	11.07 (21)	0.043 (1)
45c.37 (Un)	2	all	0.20 (5)	0.71 (17)	10.79 (1.66)	0.038 (7)
45c.37 (Un)	3	1	< 0.10 [$]	< 0.78 [$]	-	-

Component	References			20Ne/22Ne	21Ne/22Ne
SW	[1]			13.777 (10)	0.03289 (7)
"FSW"	[2]			11.2 (2)	0.0295 (5)
Q (P1)	[3]			10.67 (2)	0.0294 (10)
EA	[4]			9.80	0.029
HL	[5]			8.50 (6)	0.036 (1)

References: [1] Heber et al. (2012)*, [2]* Benkert et al. (1993) *[3]* Busemann et al. (2000)*, [4]* Eberhardt et al. (1965), *[5]* Huss and Lewis (1994a)*; <u>Note</u>: w.s. = whole sample, For detailed information regarding* **"FSW"** *see Wieler et al. (2007).*

Bastian Baecker | Chapter 5 - Micrometeorites from the Transantarctic Mountains (TAM) - Noble gases show indications for multiple populations

101
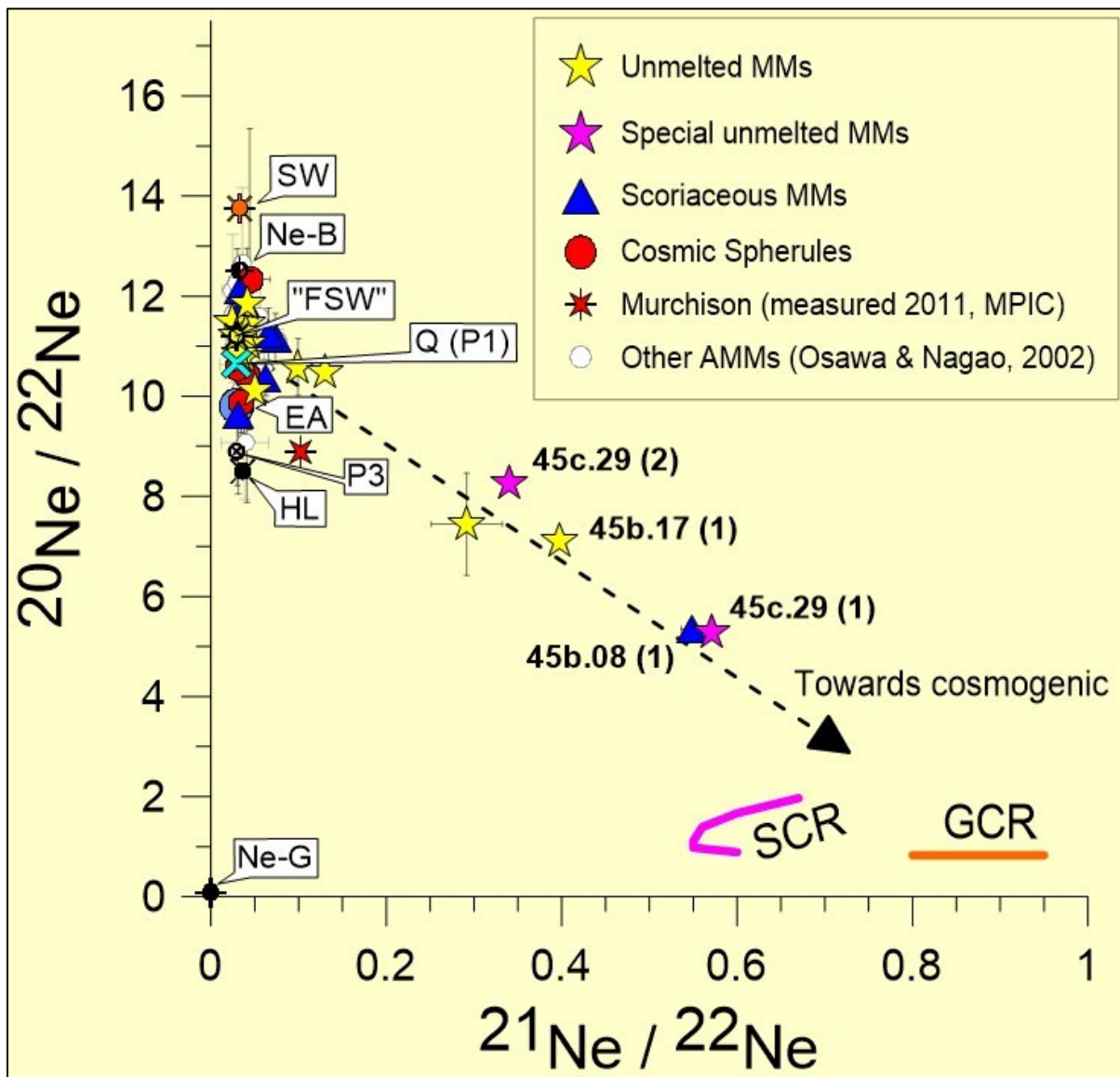
Figure 48. Three isotope plot of $^{20}Ne / ^{22}Ne$ vs. $^{21}Ne / ^{22}Ne$ for our data, for Murchison (measured at the MPIC in 2011) and AMM data from Osawa and Nagao (2002). Also plotted for comparison are SW (Heber et al. (2012)), Ne-B (Black and Pepin (1969)), "FSW" (Benkert et al. (1993) and Wieler et al. (2007)), Q (P1) (Busemann et al. (2000)), Earth atmosphere (EA) (Eberhardt et al. (1965)), P3 (Huss and Lewis (1994a)), HL (Huss and Lewis (1994a)), Ne-G (Lewis et al. (1994)), GCR (Garrison et al. (1995)) and the compositions of SCR - calculated from, Mg, Al, Si at 0.50-10.0 g/cm^2 (Reedy (1992)) using CM chondrite composition (Wasson and Kallemeyn (1988)).

Bastian Baecker | Chapter 5 - Micrometeorites from the Transantarctic Mountains (TAM) - Noble gases show indications for multiple populations

102
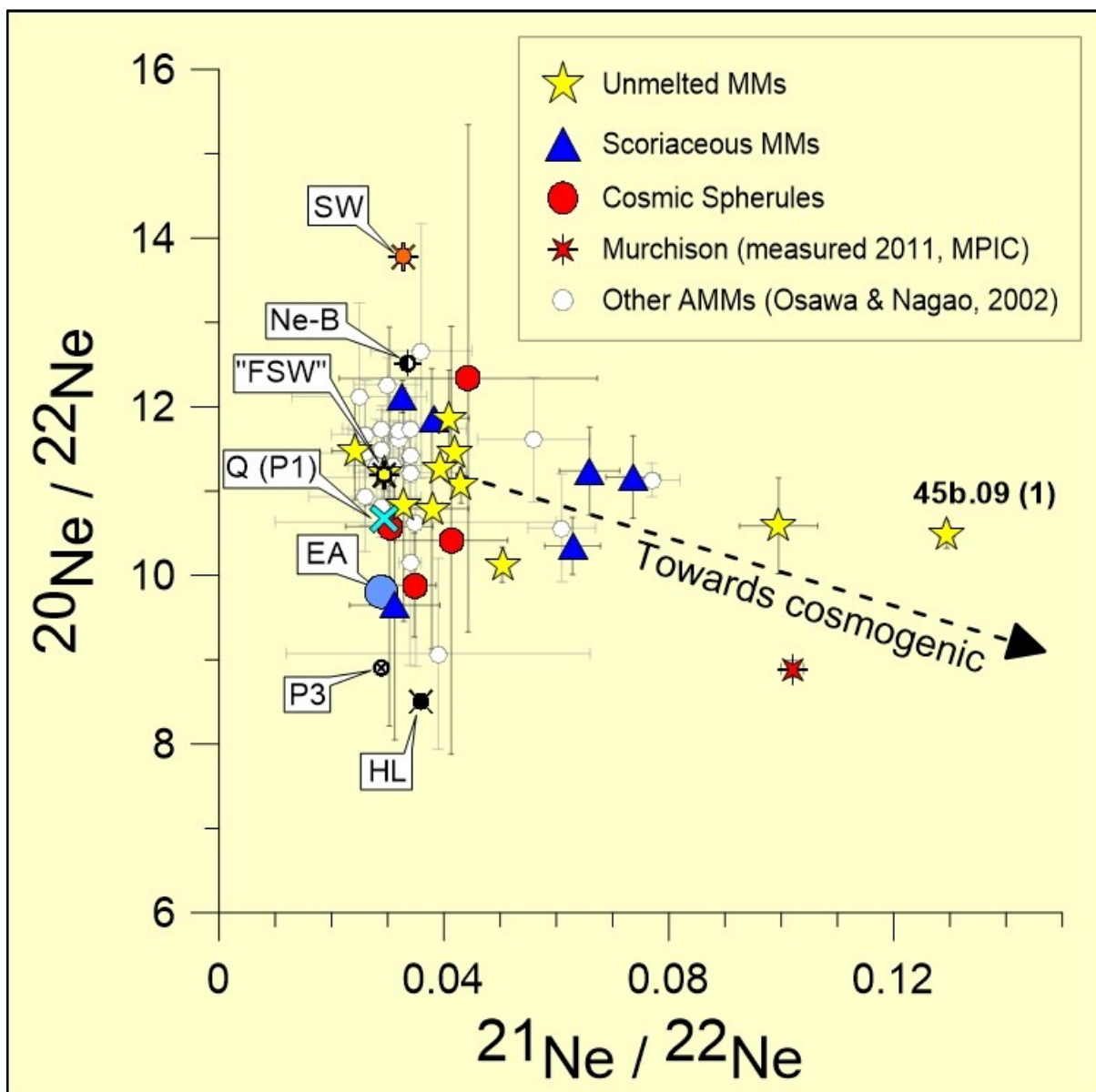
Figure 49. Three isotope plot of ^{20}Ne / ^{22}Ne vs. ^{21}Ne / ^{22}Ne, upper left of Fig. 48 enlarged. For details see Fig. 48.

Bastian Baecker | Chapter 5 - Micrometeorites from the Transantarctic Mountains (TAM) - Noble gases show indications for multiple populations

103

5.4.3 Argon (Ar)

Table 23, Fig. 50 and Fig. 51 show the results of this study. For further detailed results see Appendix. With the exception of 4 MMs with mostly large uncertainties (1 unmelted, 2 scoriaceous and 1 CS), all of the MMs plot below EA ($^{40}Ar/^{36}Ar$ = 298.56; Lee et al. (2006)). In $^{40}Ar/^{36}Ar$, the measured values range from 1.95 (in the unmelted MM 45c.33(1)) up to 349 (in the scoriaceous MM 45c.25(2)), whereas for $^{38}Ar/^{36}Ar$ the results vary from slightly below EA ($^{38}Ar/^{36}Ar$ = 0.1885; Lee et al. (2006)) to the high value of ~0.35 (UnMM 45c.29(2)).

As shown in Fig. 50, especially the two measured particles of 45c.29 are plotting in the direction of spallation. This is different from the results for the other TAM MMs and also different from the results reported by Osawa and Nagao (2002). Generally though, our measured unmelted MMs plot in similar regions as most of the AMMs measured by Osawa and Nagao (2002), i.e. near Q-phase Ar (Q(P1)); Busemann et al. (2000)), SW (Heber et al. (2012)) and "FSW" (Benkert et al. (1993)) with probably varying contributions of EA (Earth atmosphere, Lee et al. (2006)) - see also Fig. 51.

Our results do not support predicitions in some previous research (e.g. Rochette et al. (2008), Dobrică et al. (2011)) that large MMs should show a relationship to ordinary chondrites. In this case, one would mostly expect low ^{36}Ar abundances along with high $^{40}Ar/^{36}Ar$ ratios (see Schultz and Franke (2004)), in contrast to our findings. The only way out would be significant presence of trapped solar wind ^{36}Ar. Indeed, most of the MMs having low $^{40}Ar/^{36}Ar$ ratios and contain larger trapped ^{36}Ar contributions also show high solar wind ^{20}Ne concentrations. This is especially true for the two MMs with the lowest $^{40}Ar/^{36}Ar$ ratio of 1.95 (45c.33(1)) and 4.09 (45c.35(3)), which also show high $^{20}Ne/^{22}Ne$ ratios of 11.46 and 11.07 respectively (see Table 22), indicating higher solar wind contributions. These two samples show $^{20}Ne/^{36}Ar$ ratios of 3.5 (45c.33(1)) and 0.8 (45c.35(3)), however, distinctly lower than solar wind (42: Table 4 in Heber et al. (2012)).

One of the few exceptions is 45c.37(2) which shows no measurable solar wind derived ^{20}Ne along with a relatively low $^{40}Ar/^{36}Ar$ ratios of 45.9. For this MM it seems reasonable to assume that planetary ^{36}Ar is present. The same seems to be true for 45c.29(1) and 45c.29(2), which both show lower $^{40}Ar/^{36}Ar$ ratios of 50 and 108, lower $^{20}Ne/^{22}Ne$ ratios of 5.3 and 8.3 (indicating significant spallogenic Ne) along with large trapped ^{36}Ar concentrations of 5.4 x 10^{-7} cc STP/g and 4.0 x 10^{-7} cc STP/g, respectively. However, in the case of MMs it is important to always keep in mind the possible thermal history, which might lead to fractionated isotopic results. Elemental compositions along with possible linked meteorite classes for our MMs are discussed in further detail in chapter 5.4.6.

Concerning ^{38}Ar measured in TAM MMs, most is trapped ^{38}Ar with, in most cases, only small amounts of cosmogenic ^{38}Ar (see chapter 5.4.7). Exceptions are 45b.17(1) and both samples of 45c.29, which show clearly the presence of cosmogenic Ar, as indicated by $^{38}Ar/^{36}Ar$ distinctly higher than even "FSW" (Fig. 50 and 51).

Bastian Baecker | Chapter 5 - Micrometeorites from the Transantarctic Mountains (TAM) - Noble gases show indications for multiple populations

104

This is somewhat different to the earlier MM data by Osawa and Nagao (2002), who do not report any cosmogenic ^{38}Ar at all and who found less variation in the abundance of trapped Ar.

The lowest ^{40}Ar concentration was obtained for CS 45c.16 with 8×10^{-7} cc STP/g, the highest for 45c.37 (3) with 7×10^{-4} cc STP/g. The other TAM MMs show ^{40}Ar concentrations between 1.2×10^{-6} cc STP/g and 5.3×10^{-5} cc STP/g which is, in most cases, similar to the results obtained by Osawa and Nagao (2002) who found ^{40}Ar concentrations between 2×10^{-6} cc STP/g and 4×10^{-5} cc STP/g.
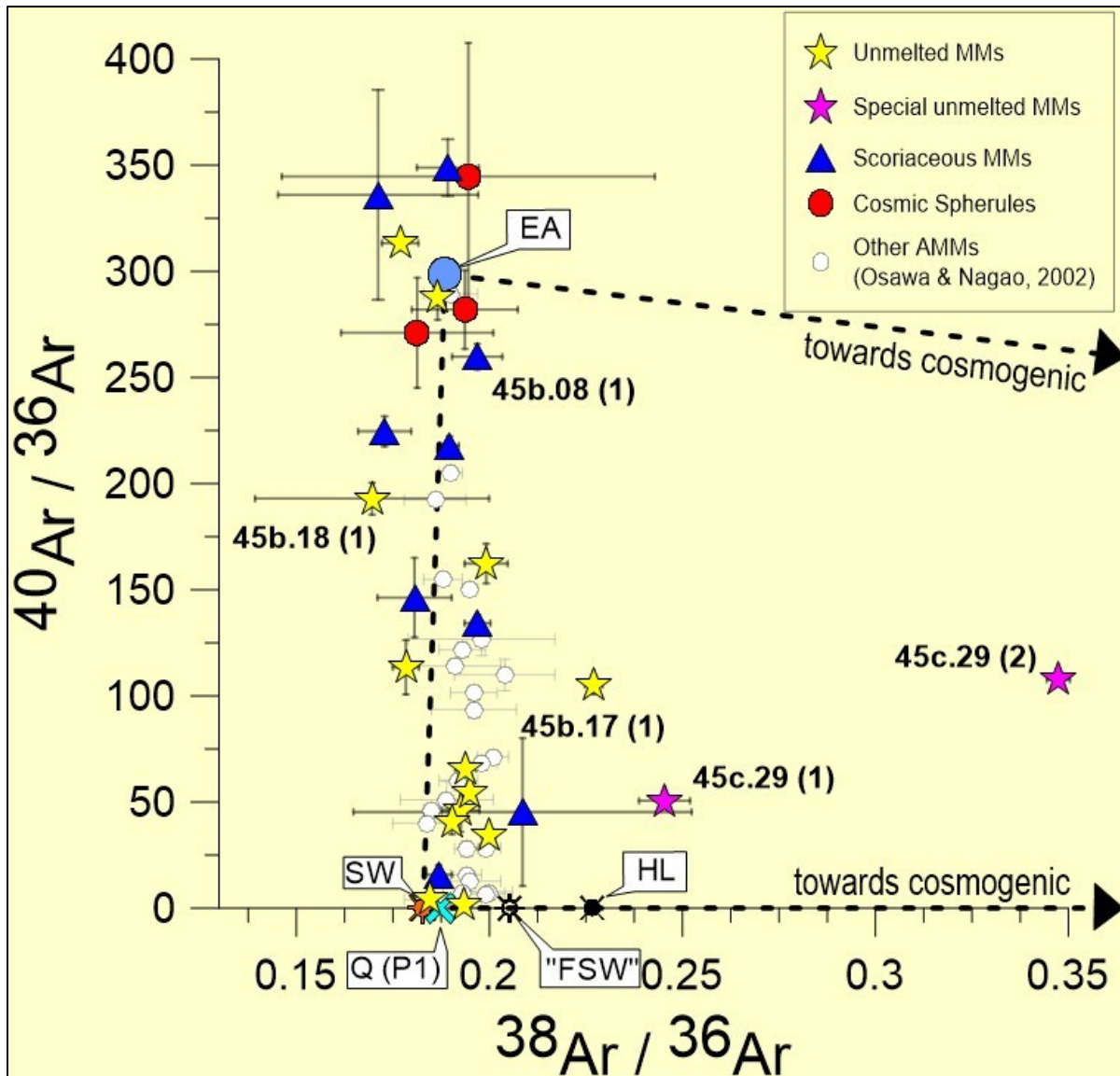
Figure 50. Three isotope plot of ^{40}Ar / ^{36}Ar vs. ^{38}Ar / ^{36}Ar for our data and AMM data from Osawa and Nagao (2002). Also plotted for comparison are SW (Heber et al. (2012)), "FSW" (Wieler (2002b)) and Wieler et al. (2007)), Q (P1) (Busemann et al. (2000)), Earth atmosphere (EA) (Lee et al. (2006)), and HL (Huss and Lewis (1994a)). Except four samples (most of them with large errors), the TAM MMs plot below Earth atmosphere. Most of the unmelted MMs plot in a region indicating a mixture of components, whereas others are plotting directly near SW and Q (P1). The dotted lines indicating a triangle between EA, SW and cosmogenic Ar (Alaerts et al. (1979) in Busemann et al. (2000)). The samples which plot right of the line EA-SW must have cosmogenic contributions, those which plot above the line EA-cosmogenic contain radiogenic ^{40}Ar.

Bastian Baecker | Chapter 5 - Micrometeorites from the Transantarctic Mountains (TAM) - Noble gases show indications for multiple populations

105

*Table 23. **Ar** results for 29 different TAM MM samples. Listed are the totals, calculated from the indicated measurement steps. Detailed results are contained in the Appendix. Uncertainties in the last digits are given in parentheses. Values marked with [$] are 2σ upper limits. For comparison the compositions of SW, Q (P1), EA and HL are shown at the bottom.*

Sample	Particle no.	Step(s) used	^{36}Ar (10^{-12} cc STP)	^{36}Ar (10^{-8} cc STP/g)	^{40}Ar (10^{-8} cc STP/g)	^{38}Ar/^{36}Ar	^{40}Ar/^{36}Ar
45b.08 (Sc)	1	all	3.55 (20)	2.98 (17)	774 (42)	0.1969 (65)	260 (6)
45b.09 (Un)	1	1	6.12 (26)	4.82 (20)	316 (21)	0.1940 (26)	65.5 (2.5)
45b.10 (Un)	2	1	11.7 (3)	12.2 (3)	3839 (87)	0.1769 (47)	313 (3)
45b.13 (Sc)	1	all	25.8 (1.0)	18.7 (8)	4082 (183)	0.1898 (24)	218 (4)
45b.14 (Sc)	1	1	0.211 (132)	0.373 (233)	143 (56)	0.1712 (259)	336 (49)
45b.15 (Sc)	1	1	6.84 (19)	22.6 (6)	387 (104)	0.1869 (35)	15.7 (4.5)
45b.16 (Un)	w.s.	all	19.1 (5)	13.8 (3)	500 (57)	0.1999 (19)	34.1 (3.7)
45b.17 (Un)	1	all	5.51 (25)	9.81 (44)	1082 (66)	0.2271 (23)	105 (4)
45b.18 (Un)	1	1	0.674 (43)	12.7 (8)	2454 (118)	0.1696 (303)	193 (8)
45b.19 (CS)	1	all	0.734 (310)	1.31 (56)	356 (143)	0.1813 (197)	271 (26)
45b.20 (Sc)	2	1	0.647 (132)	0.837 (171)	135 (41)	0.1806 (96)	146 (19)
45b.21 (Un)	w.s.	all	15.0 (5)	60.4 (1.9)	2434 (455)	0.1903 (15)	40.3 (5.5)
45b.22 (Sc)	2	1	0.270 (171)	2.94 (1.85)	-	0.2086 (438)	-
45c.16 (CS)	2	1	0.244 (170)	0.232 (162)	79.9 (37.4)	0.1946 (483)	345 (63)
45c.17 (CS)	w.s.	1	1.05 (25)	0.832 (196)	235 (49)	0.1937 (137)	282 (18)
45c.21 (CS)	w.s.	n.a.	-	-	-	-	-
45c.24 (Un)	w.s.	1	8.03 (20)	23.6 (6)	< 218 [$]	-	-
45c.25 (Sc)	2	all	3.33 (50)	2.34 (35)	828 (106)	0.1893 (80)	349 (13)
45c.27 (Sc)	2	1	0.594 (89)	1.56 (24)	351 (55)	0.1729 (69)	225 (7)
45c.29 (Un)	1	1+2	12.0 (3)	54.2 (1.3)	2848 (210)	0.2454 (66)	50.5 (3.3)
45c.29 (Un)	2	1	9.66 (38)	39.9 (1.6)	4575 (155)	0.3474 (30)	108 (3)
45c.31 (Sc)	1	all	8.60 (50)	25.9 (1.5)	2240 (119)	0.1969 (34)	134 (4)
45c.33 (Un)	1	1	20.9 (1.5)	35.7 (2.6)	120 (52)	0.1935 (20)	1.95 (1.84)
45c.34 (Un)	1	all	4.99 (20)	14.6 (6)	440 (104)	0.1784 (34)	113 (13)
X1 (Un)	1	all	17.2 (3)	49.1 (9)	2657 (104)	0.1948 (16)	54.1 (0.8)
45c.35 (Un)	2	1	1.68 (16)	31.1 (3.0)	5261 (704)	0.1992 (56)	162 (9)
45c.35 (Un)	3	2+3	45.0 (8)	155 (3)	634 (163)	0.1845 (15)	4.09 (0.85)
45c.37 (Un)	2	all	5.74 (50)	20.1 (1.7)	1010 (446)	0.1925 (49)	45.9 (10.0)
45c.37 (Un)	3	all	33.0 (1.0)	252 (8)	72538 (2415)	0.1866 (12)	287 (10)

Component	References					^{38}Ar/^{36}Ar	^{40}Ar/^{36}Ar
SW	[1]					0.183 (1)	-
"FSW"	[2]					0.205 (2)	-
Q (P1)	[3]					0.187 (1)	-
EA	[4]					0.1885 (3)	298.56 (31)
HL	[5]					0.227 (3)	-

References: [1] Heber et al. (2012), [2] Wieler (2002b), [3] Busemann et al. (2000), [4] Lee et al. (2006), [5] Huss and Lewis (1994a);
*Note: w.s. = whole sample, n.a. = not detectable (below blank level); For detailed information regarding **"FSW"** see Wieler et al. (2007).*

Bastian Baecker | Chapter 5 - Micrometeorites from the Transantarctic Mountains (TAM) - Noble gases show indications for multiple populations

106

Figure 51. Three isotope plot of ^{40}Ar / ^{36}Ar vs. ^{38}Ar / ^{36}Ar, right side of Fig. 50 enlarged. For details see Fig. 50.

Bastian Baecker | Chapter 5 - Micrometeorites from the Transantarctic Mountains (TAM) - Noble gases show indications for multiple populations

107

5.4.4 Krypton (Kr)

The results of our measurements are listed Table 24 and the Appendix. Overall the concentrations of ^{84}Kr in the TAM MMs are relatively low (lowest in ScMM 45b.14(1): 1.7 x 10^{-10} cc STP/g; highest in UnMM 45c.37(3): 2.4 x 10^{-8} cc STP/g) and generally lower than ^{84}Kr concentrations in AMMs reported by Osawa and Nagao (2002) of 8.9 x 10^{-10} cc STP/g to 1.4 x 10^{-7} cc STP/g. Two Cosmic Spherules (CS) and one scoriaceous MM do not show any Kr concentrations above blank level. The isotopic ratios listed in Table 24 do not show immediately obvious correlations. The ^{80}Kr/^{84}Kr ratio varies between 0.032 (ScMM 45b.08(1)) and 0.055 (ScMM 45b.14(1)), whereas most of the sample show ratio values between 0.032 and 0.048. Results for ^{82}Kr/^{84}Kr are more interesting, since it seems that much more variations are visible. The lowest ratio is given by the ScMM 45b.08(1) with 0.180, whereas the highest ratio is obtained for 45b.14 with 0.245, though the uncertainty of ± 0.030 is quite high. Obvious is that about half of the samples show ^{82}Kr/^{84}Kr ratios near or above SW (Meshik et al. (2012)), Q(P1) (Busemann et al. (2000)) and EA (Basford et al. (1973)). For the other half, ratios significantly below SW, Q(P1) and EA were measured. As discussed in more detail in case of Xe, isotopic fractionation leading to a relative depletion of the lighter isotopes appears to have taken place for several samples. In addition a variable mixture of several trapped components may be present, in particular the ones with the lower ^{82}Kr/^{84}Kr ratios may show contributions of the component HL (Huss and Lewis (1994a)). However, the remaining Kr ratios do not show HL contributions (see also Fig. 52 and Fig. 53). The situation is similar in case of ^{83}Kr/^{84}Kr, also suggesting a variable mixture of several trapped components. Here the lowest ratio is that measured for UnMM X1 with 0.182 and the highest for ScMM 45b.20(2) with 0.209 As evident from Table 24, again two main groups are determinable. Considering ^{86}Kr/^{84}Kr, ScMM 45b.08(1) shows the highest ratio with 0.333, the lowest is given by the UnMM 45b.18(1) with 0.236, though with a large uncertainty of ± 0.041. The next lowest one would be those of ScMM 45b.14(1) (0.280), but here again the uncertainty is large with ± 0.039. The lowest ^{86}Kr/^{84}Kr ratio measured with a relatively small uncertainty is the one of UnMM 45c.34(1) with 0.292 (±0.012). Most of the samples again show results near SW, Q(P1) and EA but away from the HL component (see Table 24). The situation is shown in a ^{86}Kr/^{84}Kr vs. ^{83}Kr/^{84}Kr plot in Fig. 52 and a ^{86}Kr/^{84}Kr vs. ^{82}Kr/^{84}Kr plot in Fig. 53: all of the samples plot near Earth atmosphere (EA) the "planetary" Q(P1) component and SW. A trend is not immediately visible, also due to the relatively large errors. A different correlation can be made if one compares the overall results for amounts, concentrations and ratios of Kr (Table 24) and Xe (Table 25). It seems that similar mechanisms influenced the heavier noble gases in the same way, since the values within each sample differ in the same way in Kr and Xe. This will be shown in more detail in chapter 5.4.5. Cosmogenic Kr is nearly not detectable in our measurements for MMs from TAM, which probably is due to higher amounts of trapped Kr and which is characteristic for primitive chondrites (for results see chapter 5.4.7)

Bastian Baecker | Chapter 5 - Micrometeorites from the Transantarctic Mountains (TAM) - Noble gases show indications for multiple populations

108

Table 24. **Kr** results for 29 different TAM MM samples. Reported are the totals, based on the individual measurement steps as indicated - for details see the Appendix. Uncertainties in the last digits are given in parentheses. For comparison also the compositions of SW, Q(P1), EA and HL are given.

Sample	Particle no.	Step(s) used	^{84}Kr (10^{-12} cc STP)	^{84}Kr (10^{-8} cc STP/g)	^{80}Kr/^{84}Kr	^{82}Kr/^{84}Kr	^{83}Kr/^{84}Kr	^{86}Kr/^{84}Kr
45b.08 (Sc)	1	all	0.431 (39)	0.362 (33)	0.032 (1)	0.180 (3)	0.190 (2)	0.333 (4)
45b.09 (Un)	1	1	0.235 (10)	0.185 (8)	0.034 (1)	0.185 (3)	0.199 (3)	0.329 (4)
45b.10 (Un)	2	1	0.409 (18)	0.429 (19)	0.035 (1)	0.188 (7)	0.196 (6)	0.299 (9)
45b.13 (Sc)	1	all	1.469 (63)	1.068 (46)	0.036 (1)	0.190 (1)	0.196 (1)	0.326 (2)
45b.14 (Sc)	1	1	0.009 (3)	0.017 (6)	0.055 (11)	0.245 (30)	0.193 (24)	0.280 (39)
45b.15 (Sc)	1	1	0.146 (11)	0.482 (37)	0.042 (2)	0.201 (12)	0.197 (10)	0.306 (16)
45b.16 (Un)	whole sample	all	0.086 (11)	0.062 (8)	0.045 (3)	0.189 (10)	0.201 (8)	0.293 (11)
45b.17 (Un)	1	all	0.146 (11)	0.261 (20)	0.032 (2)	0.182 (5)	0.189 (5)	0.322 (7)
45b.18 (Un)	1	1	0.010 (5)	0.181 (94)	0.047 (12)	0.220 (36)	0.198 (26)	0.236 (41)
45b.19 (CS)	1	all	0.037 (5)	0.066 (10)	0.045 (4)	0.221 (11)	0.205 (10)	0.322 (13)
45b.20 (Sc)	2	1	0.064 (6)	0.082 (8)	0.047 (4)	0.210 (14)	0.209 (12)	0.321 (19)
45b.21 (Un)	whole sample	all	0.146 (11)	0.587 (42)	0.038 (2)	0.201 (5)	0.198 (4)	0.308 (6)
45b.22 (Sc)	2	n.a.	-	-	-	-	-	-
45c.16 (CS)	2	n.a.	-	-	-	-	-	-
45c.17 (CS)	whole sample	1	0.075 (10)	0.060 (8)	0.034 (5)	0.195 (6)	0.207 (5)	0.296 (7)
45c.21 (CS)	whole sample	n.a.	-	-	-	-	-	-
45c.24 (Un)	whole sample	1	0.105 (9)	0.309 (25)	0.043 (3)	0.218 (13)	0.201 (10)	0.325 (17)
45c.25 (Sc)	2	all	0.258 (20)	0.182 (14)	0.039 (1)	0.200 (4)	0.204 (4)	0.303 (5)
45c.27 (Sc)	2	1	0.031 (2)	0.081 (6)	0.035 (4)	0.182 (9)	0.199 (9)	0.298 (12)
45c.29 (Un)	1	1+2	0.159 (6)	0.720 (30)	0.043 (2)	0.197 (9)	0.201 (7)	0.332 (14)
45c.29 (Un)	2	1	0.228 (16)	0.940 (65)	0.044 (2)	0.182 (4)	0.195 (4)	0.318 (6)
45c.31 (Sc)	1	all	0.071 (16)	0.215 (47)	0.037 (3)	0.191 (10)	0.189 (9)	0.303 (14)
45c.33 (Un)	1	1	0.360 (21)	0.613 (36)	0.038 (1)	0.194 (3)	0.204 (3)	0.316 (6)
45c.34 (Un)	1	all	0.068 (6)	0.198 (19)	0.045 (3)	0.205 (9)	0.188 (8)	0.292 (12)
X1 (Un)	1	all	0.038 (8)	0.110 (22)	0.037 (5)	0.215 (13)	0.182 (11)	0.296 (15)
45c.35 (Un)	2	1	0.076 (9)	1.405 (164)	0.039 (2)	0.193 (7)	0.192 (7)	0.330 (10)
45c.35 (Un)	3	2+3	0.203 (16)	0.700 (55)	0.035 (3)	0.205 (4)	0.207 (3)	0.317 (4)
45c.37 (Un)	2	all	0.067 (17)	0.235 (61)	0.040 (3)	0.210 (12)	0.199 (12)	0.316 (18)
45c.37 (Un)	3	all	0.319 (78)	2.438 (592)	0.038 (2)	0.197 (7)	0.206 (9)	0.309 (15)

Component	References			^{80}Kr/^{84}Kr	^{82}Kr/^{84}Kr	^{83}Kr/^{84}Kr	^{86}Kr/^{84}Kr
SW	[1]			0.0412 (2)	0.2054 (2)	0.2034 (2)	0.3012 (4)
Q (P1)	[2]			0.03937 (7)	0.2018 (2)	0.2018 (2)	0.3095 (5)
EA	[3]			0.039599 (20)	0.20217 (4)	0.2014 (2)	0.3052 (3)
HL	[4]			0.0305 (10)	≡ 0.1590	0.1989 (10)	0.3623 (18)

References: [1] Meshik et al. (2012), [2] Busemann et al. (2000), [3] Basford et al. (1973), [4] Huss and Lewis (1994a); re-calculated by Busemann et al. (2000); Note: n.a. = not detectable (below blank level).

Bastian Baecker | Chapter 5 - Micrometeorites from the Transantarctic Mountains (TAM) - Noble gases show indications for multiple populations

109

Figure 52. Three isotope plot of ^{86}Kr / ^{84}Kr vs. ^{83}Kr / ^{84}Kr for our data. Also plotted for comparison are SW (Meshik et al. (2012)), Q (P1) (Busemann et al. (2000)), Earth atmosphere (EA) (Basford et al. (1973)) and HL (Huss and Lewis (1994a); recalculated by Busemann et al. (2000)).

Bastian Baecker | Chapter 5 - Micrometeorites from the Transantarctic Mountains (TAM) - Noble gases show indications for multiple populations

110
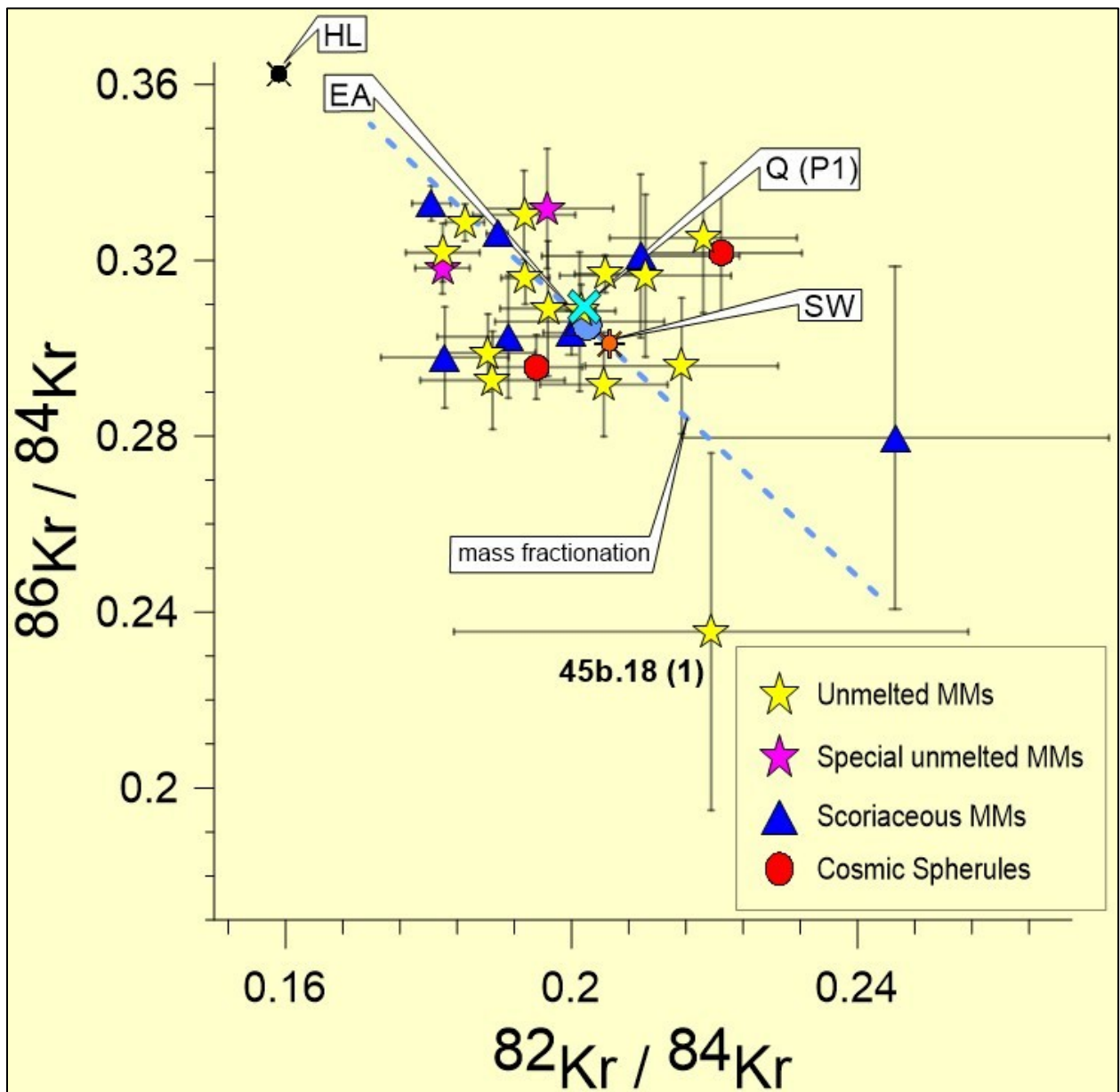
Figure 53. Three isotope plot of ^{86}Kr / ^{84}Kr vs. ^{82}Kr / ^{84}Kr for our data. Also plotted for comparison are SW (Meshik et al. (2012)), Q (P1) (Busemann et al. (2000)), Earth atmosphere (EA) (Basford et al. (1973)) and HL (Huss and Lewis (1994a); recalculated by Busemann et al. (2000)).

Bastian Baecker | Chapter 5 - Micrometeorites from the Transantarctic Mountains (TAM) - Noble gases show indications for multiple populations

111

5.4.5 Xenon (Xe)

As discussed in chapter 4.3.5.1, three different schemes of data reduction for the isotopic composition were tested on the Xe calibration gas results - "internal", "ext a" and "ext b", with the "internal" approach yielding the best reproducibility. Therefore, this method was also used for the samples in order to calculate the isotopic ratios. As explained in chapter 4.3.5.1, the count rates for ^{124}Xe and ^{126}Xe had very large errors due to their low abundance and therefore these isotopes will not be further considered. Our results for Xe in TAM MMs are shown in Table 25, Figs. 54 to 64 and the Appendix.

In the same way as Kr (see above), Xe shows relatively large variations along with low amounts and concentrations. Overall it seems that the MMs from "45b" seem to contain less of both Kr and Xe than the MMs "45c". This is only a general trend and not necessary true for each single MM. Further below (Fig. 62 to Fig. 64) it will be shown that similar fractionation processes influenced the Kr and Xe inventory of the TAM MMs in the same way. The highest concentration of ^{132}Xe was found for the UnMM 45c.35(3) with 1.1 x 10^{-8} cc STP/g, the lowest for ScMM 45b.14(1) with 1.1 x 10^{-10} cc STP/g (see Table 25). For 5 samples, no Xe amounts above blank level were detected (3 CS, 1 ScMM and 1 UnMM). Most of the samples show concentrations in the range of ~1 x 10^{-9} cc STP/g to ~5 x 10^{-9} cc STP/g which is consistent with, though slightly lower than, the results reported by Osawa and Nagao (2002), whose samples ranged from a minimum of 1 x 10^{-9} cc STP/g up to 2.1 x 10^{-8} cc STP/g. Sarda et al. (1991) measured a ^{132}Xe concentration of overall (3 steps) ~3.7 x 10^{-9} cc STP/g, within a single, large MM.

Our results for ^{129}Xe/^{132}Xe presented in Fig. 53 show a clearly improved precision compared to the earlier measurements of Osawa and Nagao (2002). Consequently, despite similarities in the overall results for Kr and Xe, the results for Xe provide significantly more information regarding the presence of important components like SW, Q(P1), EA and HL (see Table 25). Also, as evident in Figs. 53 to 56, correlations become more distinctive in the comparison of samples to each other. Furthermore, ratios like ^{129}Xe/^{132}Xe (indicating the presence of radiogenic Xe from the extinct ^{129}I isotope) and ^{136}Xe/^{132}Xe (indicating presence of ^{244}Pu fission Xe and/or Xe-HL) allow to infer the possible primitiveness of the MMs. This is especially true, among others, for the UnMM 45c.29 (1) and (2). This "special" sample will be discussed in chapter 5.4.8.

Not counting ScMM 45b.14(1) with its very large error, ^{128}Xe/^{132}Xe ranges from 0.058 (UnMM 45b.10(2)) to 0.085 (UnMM 45c.35(3)), with most of the samples between about 0.060 and 0.080 - i.e. mostly in the range between EA, SW and Q(P1), but with several values also below EA. The data appear to fall into two groups, a fact that will be discussed further below. ^{129}Xe/^{132}Xe shows values between 0.890 (ScMM 45b.08(1)) and 1.060 (UnMM 45c.29(2)) - here again, mostly between EA, SW and Q(P1) and some also below EA. For ^{130}Xe/^{132}Xe, again not counting ScMM 45b.14(1) because of the large error, values range from 0.141 (UnMM 45c.29(1) and UnMM X1) to 0.166 (UnMM 45c.37(2) and (3)), where most are between ~0.145 and ~0.160. Here the "45b" MM group is mostly showing ratios near or below EA and also below HL. The "45c" MM group also shows some results in this

Bastian Baecker | Chapter 5 - Micrometeorites from the Transantarctic Mountains (TAM) - Noble gases show indications for multiple populations

112

range (e.g. UnMM X1, UnMM 45c.29(1) and (2), ScMM 45c.25(2)), but most of the MMs are located near SW and the "planetary" Q(P1) component. The ^{131}Xe/^{132}Xe ratio shows variations between 0.729 (UnMM 45c.35(2), with large error) and 0.828 (UnMM 45c.33(1)), which shows once more that various components and fractionation processes influenced the Xe composition of the TAM MMs, probably led by EA, SW, Q(P1) and HL. It appears noteworthy, though that most of the MMs in this ratio are closer to EA than to SW and Q(P1), with values below ~0.800. The ratios ^{134}Xe/^{132}Xe and ^{136}Xe/^{132}Xe show a similar behavior to each other. ^{134}Xe/^{132}Xe shows ratios between 0.363 (CS 45b.19) and 0.418 (ScMM 45c.27), whereas the values for ^{136}Xe/^{132}Xe vary between 0.312 (Sc 45b.14(1)) and 0.396 (UnMM 45c.29(2)). In both cases about 90% of the MMs have ratios higher than SW and Q(P1) and about 80% show values near or above EA, possibly influenced by the HL component (^{134}Xe/^{132}Xe = ~0.636, ^{136}Xe/^{132}Xe = ~0.699; both Huss and Lewis (1994a)).

Bastian Baecker | Chapter 5 - Micrometeorites from the Transantarctic Mountains (TAM) - Noble gases show indications for multiple populations

113
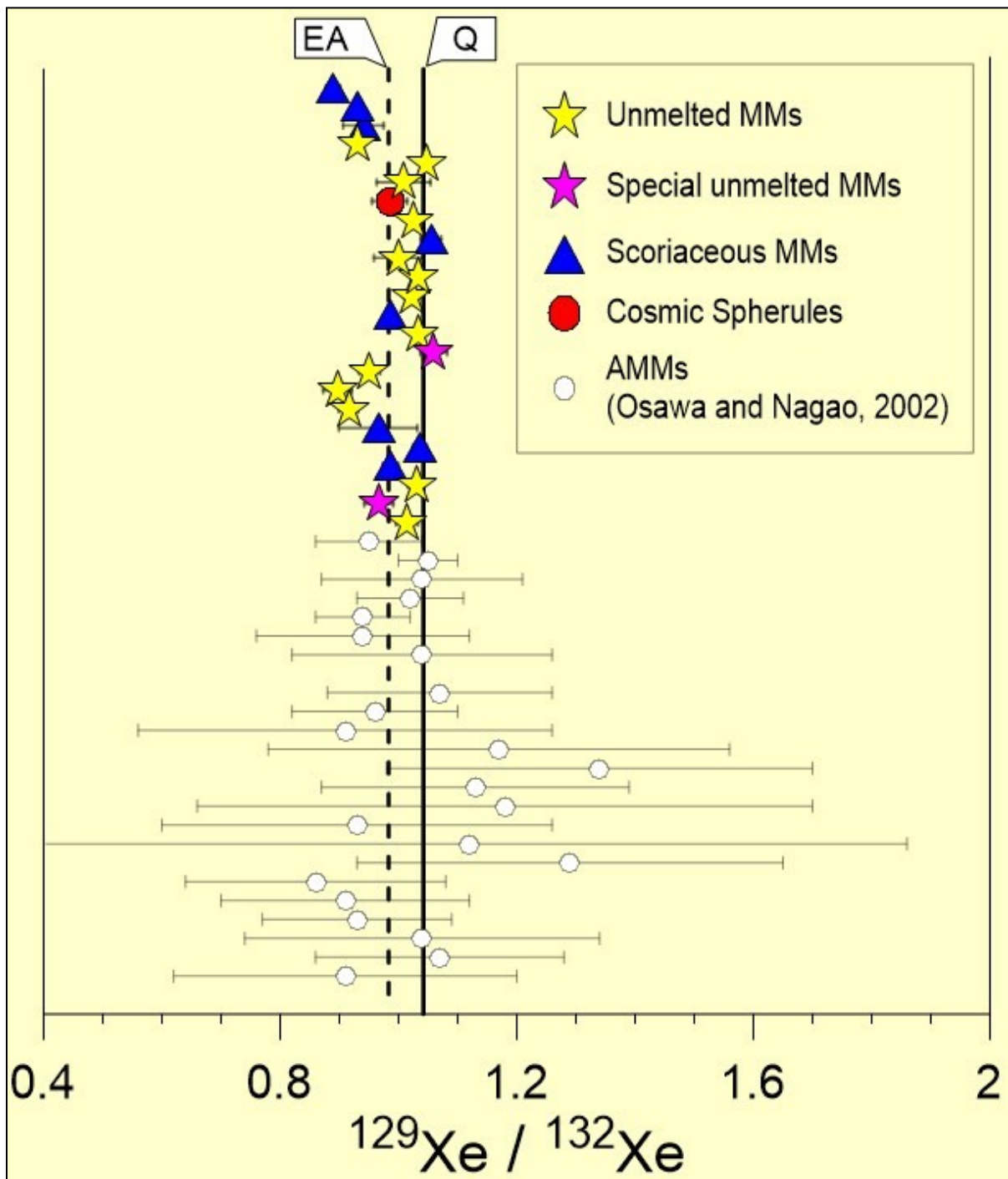
Figure 54. $^{129}Xe/^{132}Xe$ plot showing our data and data from Osawa and Nagao (2002). The solid line shows roughly the ratio of carbonaceous chondrites matrix, while the dashed line shows the composition of air Xe. All of our samples have small $^{129}Xe / ^{132}Xe$ and analytical uncertainties are significantly smaller than the results of Osawa and Nagao (2002) (after Osawa and Nagao (2002), with our data added in color).

Bastian Baecker | Chapter 5 - Micrometeorites from the Transantarctic Mountains (TAM) - Noble gases show indications for multiple populations

114

*Table 25. **Xe** results for 29 different TAM MM samples. Listed are totals based on selected measurement steps as indicated - for details see Appendix. The listed results are based on the "internal calibration" ("int") data reduction approach. Uncertainties in the last digits are in parenthesis. For comparison also the compositions of SW, Q(P1), EA and HL are given.*

Sample	Particle no.	Step(s) used	^{132}Xe (10^{-12} cc STP)	^{132}Xe (10^{-8} cc STP/g)	^{128}Xe/^{132}Xe (INT)	^{129}Xe/^{132}Xe (INT)	^{130}Xe/^{132}Xe (INT)	^{131}Xe/^{132}Xe (INT)	^{134}Xe/^{132}Xe (INT)	^{136}Xe/^{132}Xe (INT)
45b.08 (Sc)	1	2	0.080 (4)	0.067 (3)	0.063 (2)	0.890 (12)	0.145 (2)	0.751 (9)	0.407 (6)	0.372 (8)
45b.09 (Un)	1	1	0.103 (8)	0.081 (6)	0.069 (1)	0.932 (10)	0.150 (2)	0.769 (8)	0.401 (4)	0.356 (5)
45b.10 (Un)	2	1	0.037 (1)	0.039 (1)	0.058 (4)	0.916 (17)	0.145 (4)	0.804 (18)	0.404 (10)	0.362 (12)
45b.13 (Sc)	1	all	0.405 (31)	0.294 (22)	0.067 (1)	0.930 (7)	0.148 (1)	0.764 (5)	0.397 (2)	0.349 (3)
45b.14 (Sc)	1	1	0.006 (1)	0.011 (1)	0.049 (20)	0.966 (66)	0.116 (17)	0.781 (58)	0.370 (31)	0.312 (37)
45b.15 (Sc)	1	1	0.232 (3)	0.767 (11)	0.080 (2)	1.036 (11)	0.158 (2)	0.796 (10)	0.383 (4)	0.330 (5)
45b.16 (Un)	w.s.	all	0.045 (3)	0.033 (2)	0.079 (4)	0.951 (18)	0.156 (4)	0.774 (16)	0.386 (9)	0.335 (10)
45b.17 (Un)	1	all	0.027 (1)	0.048 (2)	0.063 (4)	0.897 (24)	0.143 (4)	0.777 (17)	0.392 (11)	0.348 (12)
45b.18 (Un)	1	n.a.	-	-	-	-	-	-	-	-
45b.19 (CS)	1	all	0.017 (2)	0.030 (3)	0.071 (6)	0.985 (30)	0.146 (6)	0.758 (24)	0.363 (15)	0.317 (16)
45b.20 (Sc)	2	1	0.081 (1)	0.105 (2)	0.078 (3)	0.987 (13)	0.157 (3)	0.768 (11)	0.387 (6)	0.341 (8)
45b.21 (Un)	w.s.	all	0.180 (4)	0.725 (17)	0.080 (2)	1.025 (9)	0.160 (2)	0.809 (7)	0.381 (4)	0.329 (5)
45b.22 (Sc)	2	n.a.	-	-	-	-	-	-	-	-
45c.16 (CS)	2	n.a.	-	-	-	-	-	-	-	-
45c.17 (CS)	w.s.	n.a.	-	-	-	-	-	-	-	-
45c.21 (CS)	w.s.	n.a.	-	-	-	-	-	-	-	-
45c.24 (Un)	w.s.	1	0.190 (3)	0.560 (9)	0.079 (2)	1.030 (14)	0.158 (2)	0.814 (10)	0.384 (5)	0.325 (6)
45c.25 (Sc)	2	all	0.277 (16)	0.194 (11)	0.071 (2)	0.987 (8)	0.151 (1)	0.784 (6)	0.387 (3)	0.330 (5)
45c.27 (Sc)	2	1	0.0078 (5)	0.020 (1)	0.075 (6)	0.941 (34)	0.153 (8)	0.793 (37)	0.418 (17)	0.328 (21)
45c.29 (Un)	1	1+2	0.037 (5)	0.169 (21)	0.070 (6)	0.967 (25)	0.141 (5)	0.783 (22)	0.398 (12)	0.365 (14)
45c.29 (Un)	2	1	0.031 (1)	0.129 (6)	0.065 (4)	1.060 (23)	0.146 (4)	0.798 (16)	0.414 (11)	0.396 (13)
45c.31 (Sc)	1	all	0.058 (4)	0.175 (12)	0.078 (4)	1.055 (17)	0.155 (3)	0.782 (14)	0.395 (8)	0.347 (9)
45c.33 (Un)	1	all	0.344 (4)	0.587 (7)	0.081 (1)	1.034 (7)	0.163 (1)	0.828 (6)	0.388 (3)	0.331 (4)
45c.34 (Un)	1	all	0.070 (1)	0.206 (4)	0.082 (3)	1.014 (19)	0.161 (3)	0.816 (14)	0.389 (8)	0.324 (9)
X1 (Un)	1	1	0.010 (1)	0.028 (2)	0.072 (9)	1.009 (45)	0.141 (8)	0.775 (33)	0.374 (19)	0.357 (24)
45c.35 (Un)	2	1	0.012 (2)	0.214 (44)	0.070 (11)	1.000 (42)	0.166 (9)	0.729 (38)	0.366 (23)	0.317 (25)
45c.35 (Un)	3	all	0.320 (11)	1.103 (38)	0.085 (1)	1.047 (6)	0.166 (1)	0.818 (4)	0.378 (3)	0.325 (4)
45c.37 (Un)	2	all	0.105 (4)	0.367 (13)	0.079 (3)	1.032 (11)	0.159 (2)	0.822 (11)	0.380 (5)	0.327 (6)
45c.37 (Un)	3	all	0.079 (4)	0.605 (27)	0.080 (3)	1.022 (13)	0.158 (3)	0.798 (12)	0.384 (7)	0.323 (8)

Component	References			^{128}Xe/^{132}Xe	^{129}Xe/^{132}Xe	^{130}Xe/^{132}Xe	^{131}Xe/^{132}Xe	^{134}Xe/^{132}Xe	^{136}Xe/^{132}Xe
SW	[1]			0.0842 (3)	1.0401 (10)	0.1649 (4)	0.8263 (13)	0.3692 (7)	0.3003 (6)
Q (P1)	[2]			0.0822 (2)	1.042 (2)	0.1619 (3)	0.8185 (9)	0.3780 (11)	0.3164 (8)
EA	[3]			0.07136 (9)	0.9832 (12)	0.15136 (12)	0.7890 (11)	0.3879 (6)	0.3294 (4)
HL	[4]			0.0905 (6)	1.056 (2)	0.1542 (3)	0.8457 (13)	0.6356 (13)	≡ 0.6991

References: [1] Meshik et al. (2012), [2] Busemann et al. (2000), [3] Basford et al. (1973), [4] Huss and Lewis (1994a); re-calculated by Busemann et al. (2000); Note: w.s. = whole sample, n.a. = not detectable (below blank level).

Bastian Baecker | Chapter 5 - Micrometeorites from the Transantarctic Mountains (TAM) - Noble gases show indications for multiple populations

115

The following plots allow to have a closer look at the obtained Xe data.

Fig. 55 shows data in per mil-deviations [δ] from solar wind Xe composition (Meshik et al. (2012)) of 4 selected unmelted TAM MMs, 45b.21, 45c.35(3), 45c.37(2) and (3). Shown for comparison are also data for Murchison (measured at the MPIC in 2011), the "planetary" Q-Xe component (Busemann et al. (2000)) and Air-Xe (EA; Basford et al. (1973)). These 4 unmelted MMs are representative for the group of MMs showing similarities to primitive meteorites like Murchison and to Q-Xe, i.e., they are dominated by trapped planetary xenon. Although most of these MMs show overall the same pattern, there are slight differences, i.e., especially within the lighter Xe isotopes.
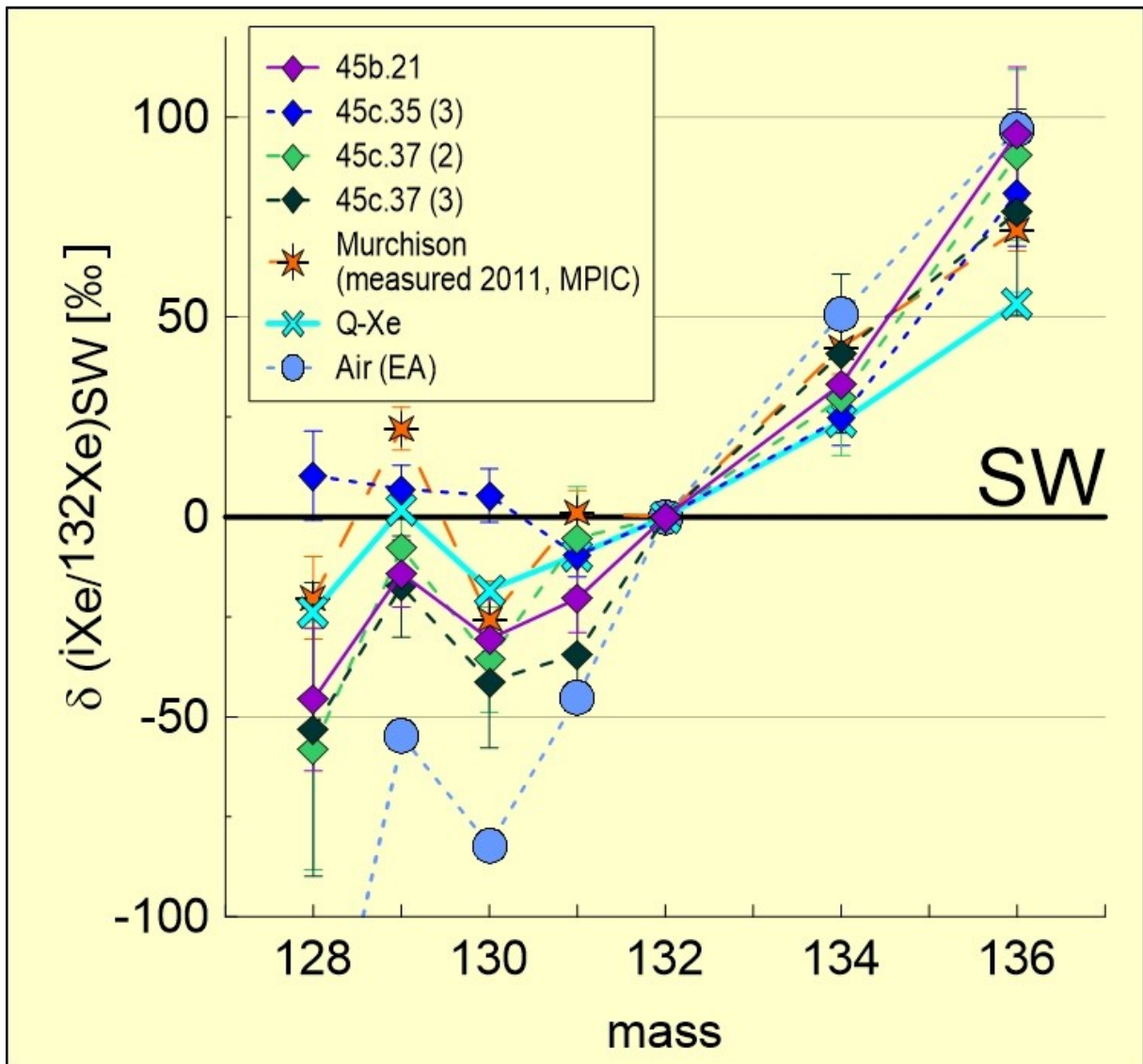
Figure 55. Plot of Xe isotopes shown in per mil-deviations [δ] from solar wind Xenon composition. SW – solar wind (Meshik et al. (2012)). Plotted are Xe-data for selected TAM-MMs along with, for comparison, Murchison (measured at the MPIC in 2011), Q (P1) (Busemann et al. (2000)) and Earth atmosphere (EA) (Basford et al. (1973)).

While 45c.35(3) is showing a "unique" pattern in all of the lighter Xe isotopes and is plotting above SW and above Q-Xe, the other three MMs in Fig. 55, plot for the light isotopes below SW and Q-Xe and have a similar curve progression. In contrast, for the heavy Xe isotopes, all of the MMs plot above SW, between Q-Xe and Air-Xe.

Bastian Baecker | Chapter 5 - Micrometeorites from the Transantarctic Mountains (TAM) - Noble gases show indications for multiple populations

116

Overall it seems that 45b.21, 45c.37(2) and 45c.37(3) show a mixture of Q-Xe and air. Here again, maybe especially the lighter Xe isotopes are affected by fractionation processes that occurred in space and/or on Earth.

A closer look is provided by Fig. 56, which is a delta isotope plot of ^{130}Xe/^{132}Xe versus ^{136}Xe/^{132}Xe in per mil-deviations [δ] from Air-Xe (EA) composition (Basford et al. (1973)). Presented are 17 unmelted MMs, 5 scoriaceous MMs and 1 Cosmic Spherule. Not included are MMs where Xe was below blank level (see Appendix for detailed results).
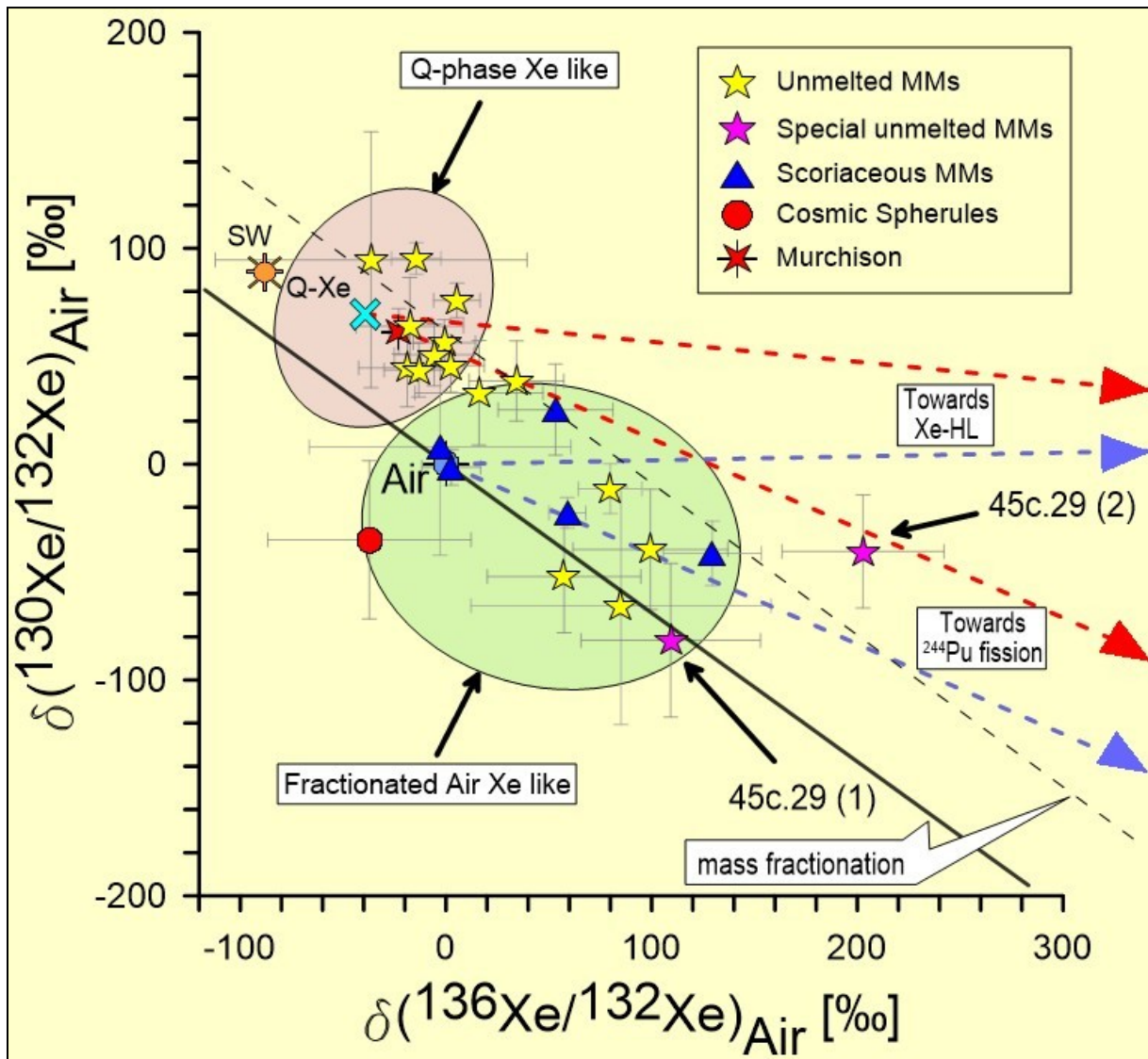
Figure 56. Delta isotope plot of ^{130}Xe / ^{132}Xe vs. ^{136}Xe / ^{132}Xe for the TAM-MM samples in per mil-deviations [δ] from Earth atmosphere Xenon composition. Earth atmosphere (Air) (Basford et al. (1973)). Also plotted for comparison are Murchison (measured at the MPIC in 2011), SW (Meshik et al. (2012)), Q (P1) (Busemann et al. (2000)), HL (Huss and Lewis (1994b)) and ^{244}Pu fission (Ozima and Podosek (2002).

The majority of the UnMMs with small uncertainties plot in the range of Q-Xe. Some admixture of SW is possible. 2 unmelted MMs and 1 scoriaceous MM plot in between SW, Q-Xe and Air-Xe which indicates a similarity to the unmelted MMs described before but indicates the additional presence of some Air-Xe. 2 scoriaceous MMs and 1 Cosmic Spherule plot near or below Earth atmosphere (Air) showing the

Bastian Baecker | Chapter 5 - Micrometeorites from the Transantarctic Mountains (TAM) - Noble gases show indications for multiple populations

117

thermal history of these particles. Additionally, 5 unmelted and 2 scoriaceous MMs plot in the general range of Air-Xe too, but in detail show a different mass-fractionation-like "heavy" composition, characterized by lower than air $^{130}Xe/^{132}Xe$ and higher than air $^{136}Xe/^{132}Xe$.
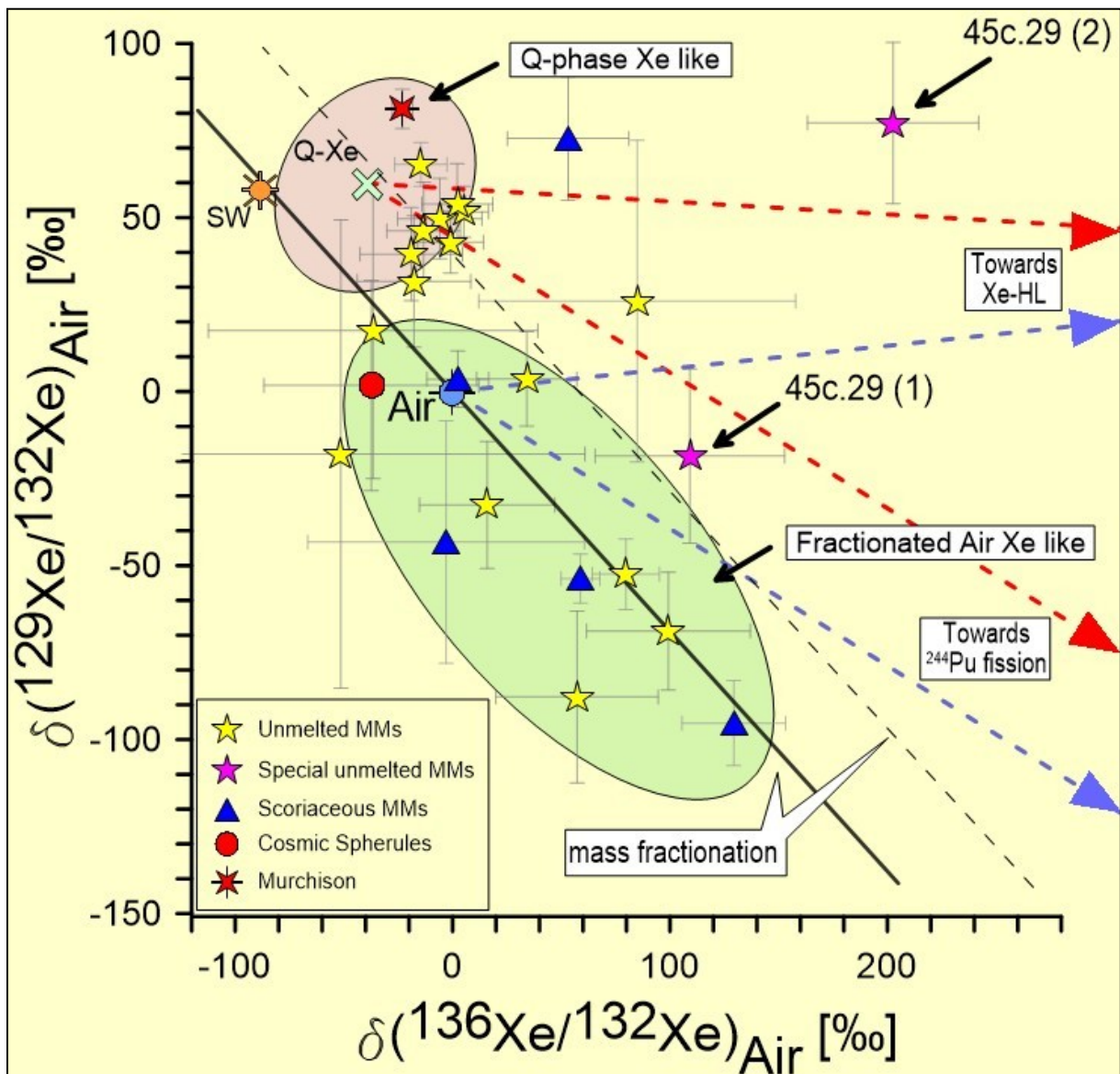
Figure 57. Delta isotope plot of ^{129}Xe / ^{132}Xe vs. ^{136}Xe / ^{132}Xe for the TAM-MM samples in per mil-deviations [δ] from Earth atmosphere Xenon composition. Earth atmosphere (Air) (Basford et al. (1973)). Also plotted for comparison are Murchison (measured at the MPIC in 2011), SW (Meshik et al. (2012)), Q (P1) (Busemann et al. (2000)), HL (Huss and Lewis (1994b)) and ^{244}Pu fission (Ozima and Podosek (2002)).

Fig. 57 is a similar delta isotope plot of $^{129}Xe/^{132}Xe$ versus $^{136}Xe/^{132}Xe$ in per mil-deviations [δ] from Air-Xe (EA) composition (Basford et al. (1973)).

Again, as in Fig.56, the majority of the unmelted MMs plot in the area of Q-Xe. Additionally 7 different unmelted MMs plot in an area consistent with mass-fractionated air Xe. The same is the case for the single Cosmic Spherule and 4 scoriaceous MMs. Last but not least, 1 more ScMM and 3 more UnMMs plot in the directions of either Xe-HL or ^{244}Pu fission. If one compares Fig. 56 and Fig. 57, most of the MMs plot consistently in similar regions, i.e., the UnMMs plot near Q-Xe, whereas most of the ScMMs and the CS plot near air Xe. However, especially the

Bastian Baecker | Chapter 5 - Micrometeorites from the Transantarctic Mountains (TAM) - Noble gases show indications for multiple populations

118

two particles from sample 45c.29 seem to be different from the rest and do not plot in both figures in the same direction (see the following text).

As already noted in case of Ne and Ar, the unmelted MM 45c.29, which was divided into several particles for additional measurements (see chapter 4.3.1.1), is a "special" MM. For Xe this is evidenced by Fig. 56 to 59 as well as the data shown in Table 25 and the Appendix. In Fig. 56 one of the particles from this MM (45c.29(1)) plots on the Air-Xe mass fractionation line. The other particle (45c.29(2)) plots distinctly in the direction of ^{244}Pu, consistent with a mixture of Q-Xe and ^{244}Pu fission Xe. The situation is different in Fig. 57, where the same particles plot above the respective mass fractionation / mixing lines. The most straightforward explanation is the additional presence of radiogenic ^{129}Xe in this MM. The results are discussed in further detail in chapter 5.4.8.
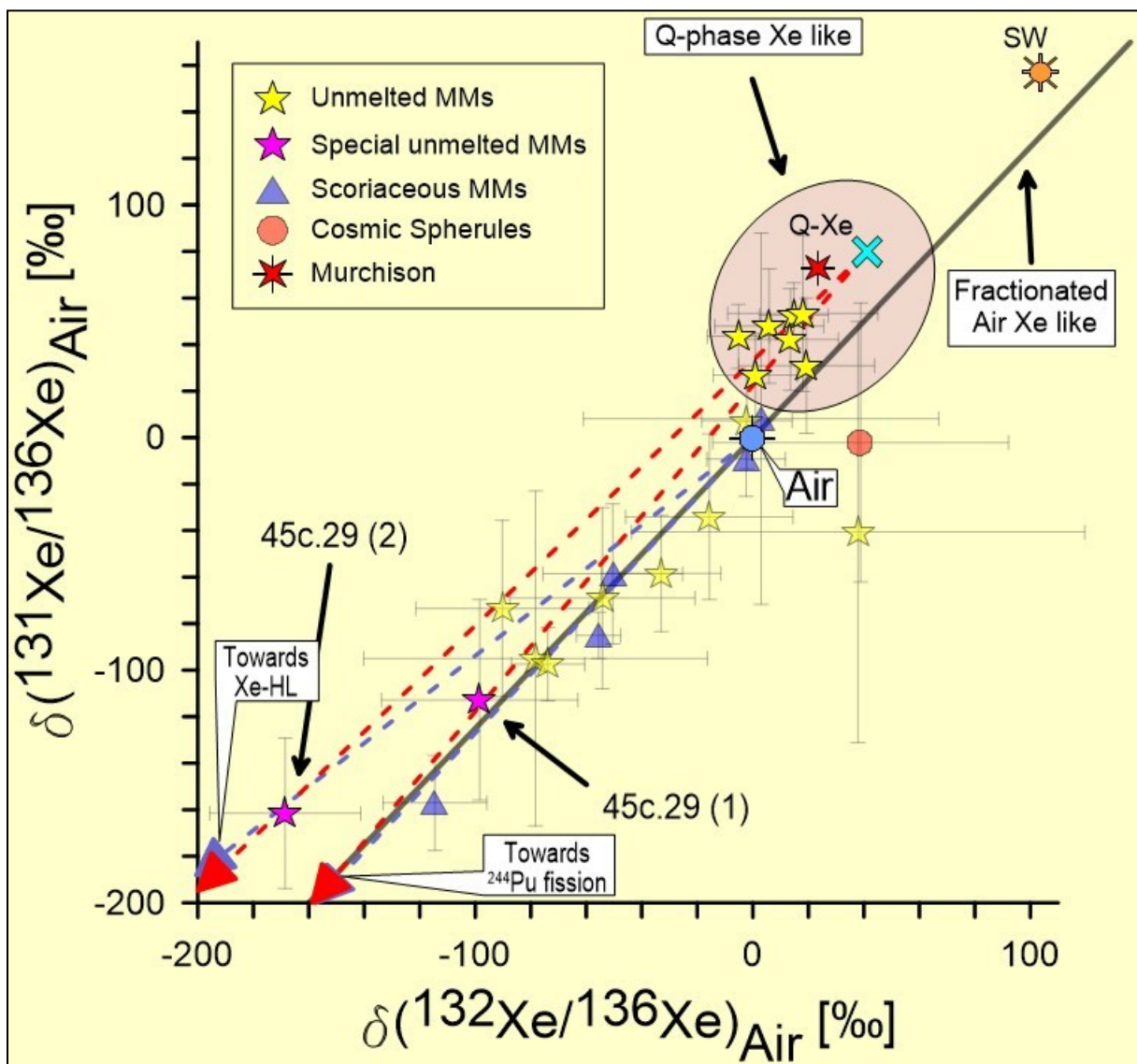
Figure 58. Delta isotope plot of ^{131}Xe / ^{136}Xe vs. ^{132}Xe / ^{136}Xe for the TAM-MM samples in per mil-deviations [δ] from Earth atmosphere Xenon composition. Earth atmosphere (Air) (Basford et al. (1973)). Also plotted for comparison are Murchison (measured at the MPIC in 2011), SW (Meshik et al. (2012)), Q (P1) (Busemann et al. (2000)), HL (Huss and Lewis (1994b)) and ^{244}Pu fission (Ozima and Podosek (2002)).

Bastian Baecker | Chapter 5 - Micrometeorites from the Transantarctic Mountains (TAM) - Noble gases show indications for multiple populations

119

Considering additional delta isotope plots of $^{131}Xe/^{136}Xe$ versus $^{132}Xe/^{136}Xe$ and of $^{130}Xe/^{136}Xe$ versus $^{132}Xe/^{136}Xe$ in per mil-deviations [δ] from Air-Xe (EA) composition (Basford et al. (1973)), these conclusions seem to be confirmed (see Fig. 58 and Fig. 59). Those UnMMs and ScMMs additionally plotting in the direction of Xe-HL and ^{244}Pu fission are influenced by fractionation with Earth atmosphere. This is indicated by the "Air" fractionation line and will be shown in more detail further below (see also Fig. 62 to Fig. 64). Also, with these additional plots it becomes obvious that the UnMMs plotting in Fig. 56 and 57 near Q-Xe and SW are more clearly influenced by the planetary trapped component Q-Xe than by solar wind.
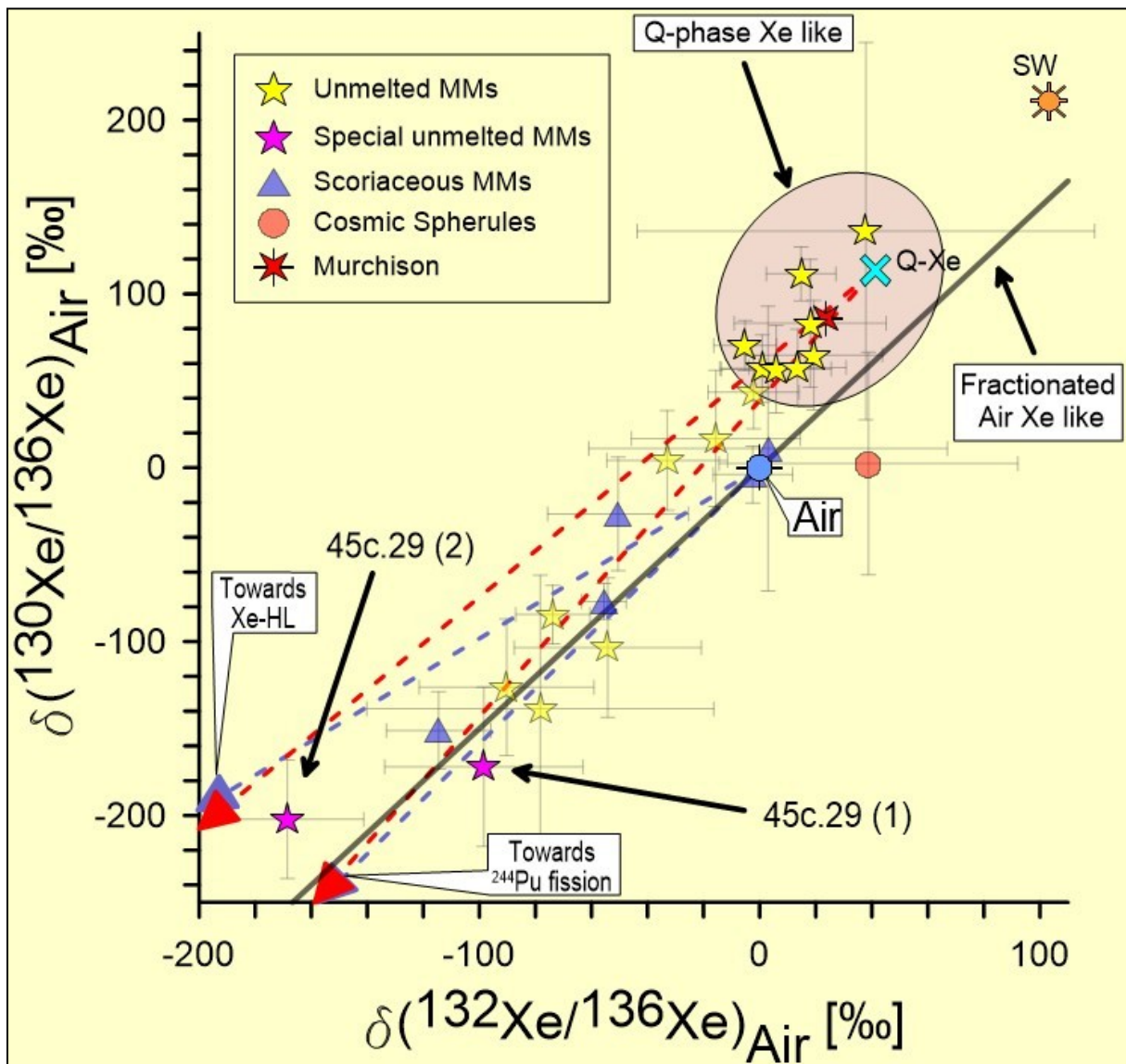
Figure 59. Delta isotope plot of $^{130}Xe / ^{136}Xe$ vs. $^{132}Xe / ^{136}Xe$ for the TAM-MM samples in per mil-deviations [δ] from Earth atmosphere Xenon composition. Earth atmosphere (Air) (Basford et al. (1973)). Also plotted for comparison are Murchison (measured at the MPIC in 2011), SW (Meshik et al. (2012)), Q (P1) (Busemann et al. (2000)), HL (Huss and Lewis (1994b)) and ^{244}Pu fission (Ozima and Podosek (2002)).

Two more delta isotope plots of $^{130}Xe/^{132}Xe$ versus $^{131}Xe/^{132}Xe$ and of $^{128}Xe/^{132}Xe$ versus $^{131}Xe/^{132}Xe$ in per mil-deviations [δ] from Air-Xe (EA) composition (Basford et al. (1973)) are shown in Fig. 60 and Fig. 61. This allows to focus on fractionation processes rather than on the presence of Xe-HL and ^{244}Pu fission Xe.

Bastian Baecker | Chapter 5 - Micrometeorites from the Transantarctic Mountains (TAM) - Noble gases show indications for multiple populations

120

Clearly, two distinct groups are visible. One group of only unmelted TAM MMs is plotting near Q-Xe and SW and the other group is plotting near Earth athmosphere indicating fractionated air-Xe.
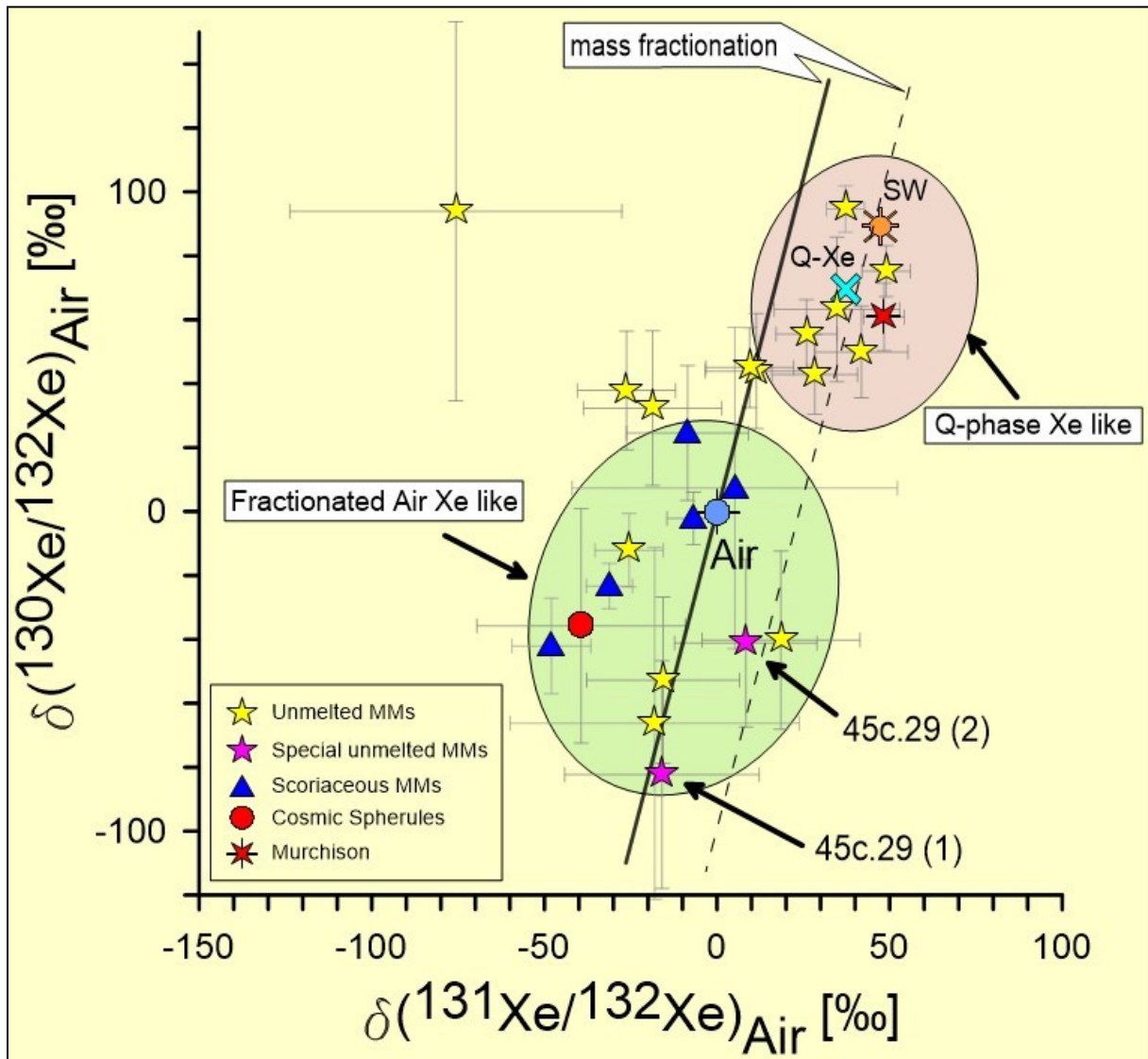
Figure 60. Delta isotope plot of ^{130}Xe / ^{132}Xe vs. ^{131}Xe / ^{132}Xe for the TAM-MM samples in per mil-deviations [δ] from Earth atmosphere Xenon composition. Earth atmosphere (Air) (Basford et al. (1973)). Also plotted for comparison are Murchison (measured at the MPIC in 2011), SW (Meshik et al. (2012)) and Q (P1) (Busemann et al. (2000)).

Bastian Baecker | Chapter 5 - Micrometeorites from the Transantarctic Mountains (TAM) - Noble gases show indications for multiple populations

121
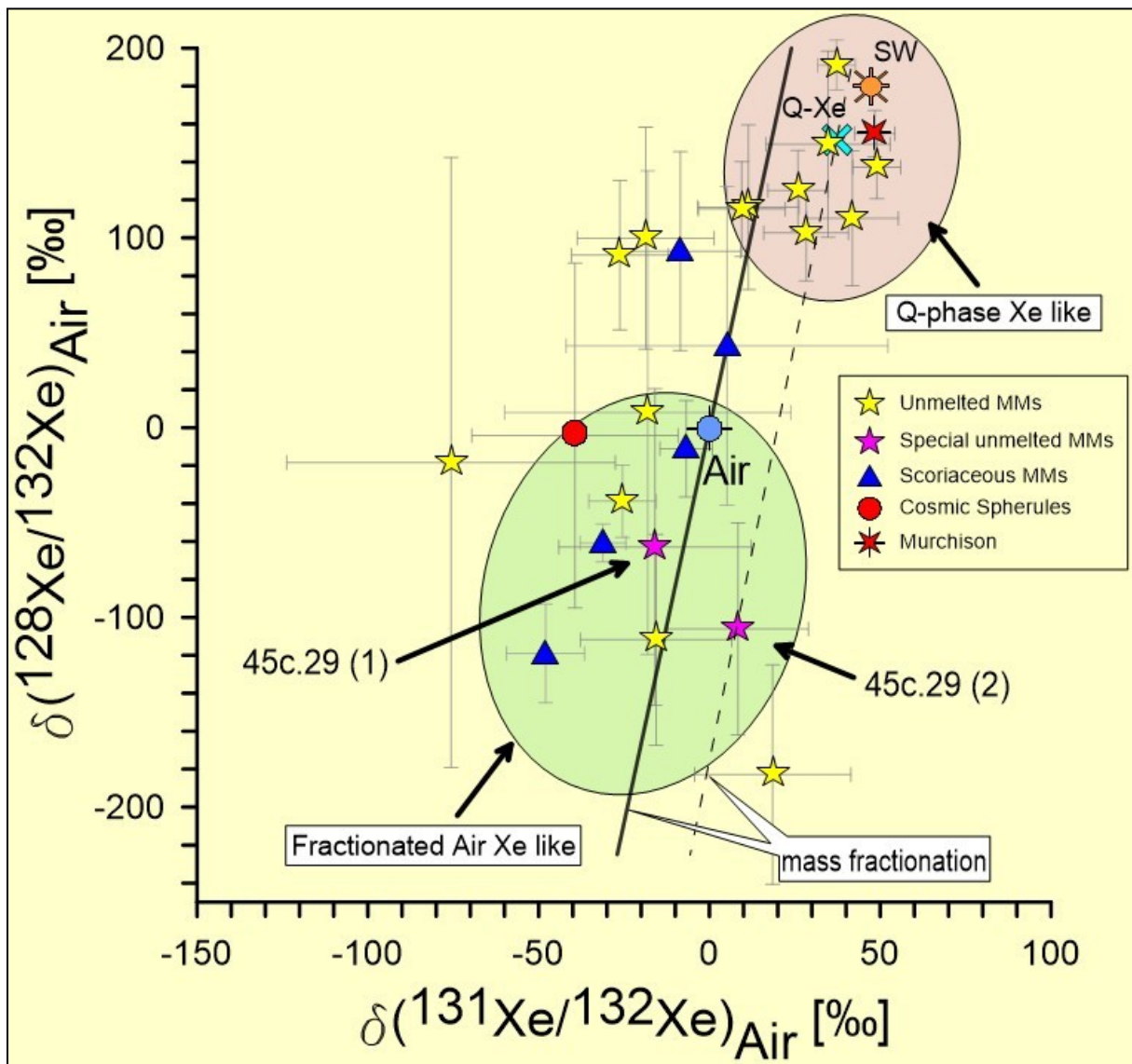
Figure 61. Delta isotope plot of ^{128}Xe / ^{132}Xe vs. ^{131}Xe / ^{132}Xe for the TAM-MM samples in per mil-deviations [δ] from Earth atmosphere Xenon composition. Earth atmosphere (Air) (Basford et al. (1973)). Also plotted for comparison are Murchison (measured at the MPIC in 2011), SW (Meshik et al. (2012)) and Q (P1) (Busemann et al. (2000)).

Having shown that Xe in some TAM MMs is characterized by planetary components and radiogenic Xe, it is of interest to have a closer look on the fractionation processes resulting in trapped mass fractionated atmospheric Xe. To do this, a combined view of delta plots for Kr, Xe and a combination of Kr and Xe is useful. Fig. 62 is a delta isotope plot of $^{129}Xe/^{132}Xe$ versus $^{136}Xe/^{132}Xe$ in per mil-deviations [δ] from Air-Xe (EA) composition (Basford et al. (1973)), where only those TAM MMs are shown that plot near or on the air fractionation line. These are 2 ScMMs and 4 UnMMs of the "45b" group and 2 ScMMs from the "45c" group. Obviously, the "45b" group seems to contain more MMs which are influenced by fractionated atmospheric Xe.

The case for Kr is shown in Fig. 63, which shows $^{80}Kr/^{84}Kr$ vs. $^{82}Kr/^{84}Kr$ in per mil-deviations [δ] from Air-Xe (EA) composition (Basford et al. (1973)). Here, slightly more TAM MMs plot on or near the Earth atmosphere fractionation line than in Fig. 62. Overall these are 2 ScMMs and 4 UnMMs of the "45b" group and 3 ScMMs and 3

Bastian Baecker | Chapter 5 - Micrometeorites from the Transantarctic Mountains (TAM) - Noble gases show indications for multiple populations

122

UnMMs of the "45c" group. It seems that the MMs of group "45b" plot distinctly nearer to the fractionation line than the "45c" samples.
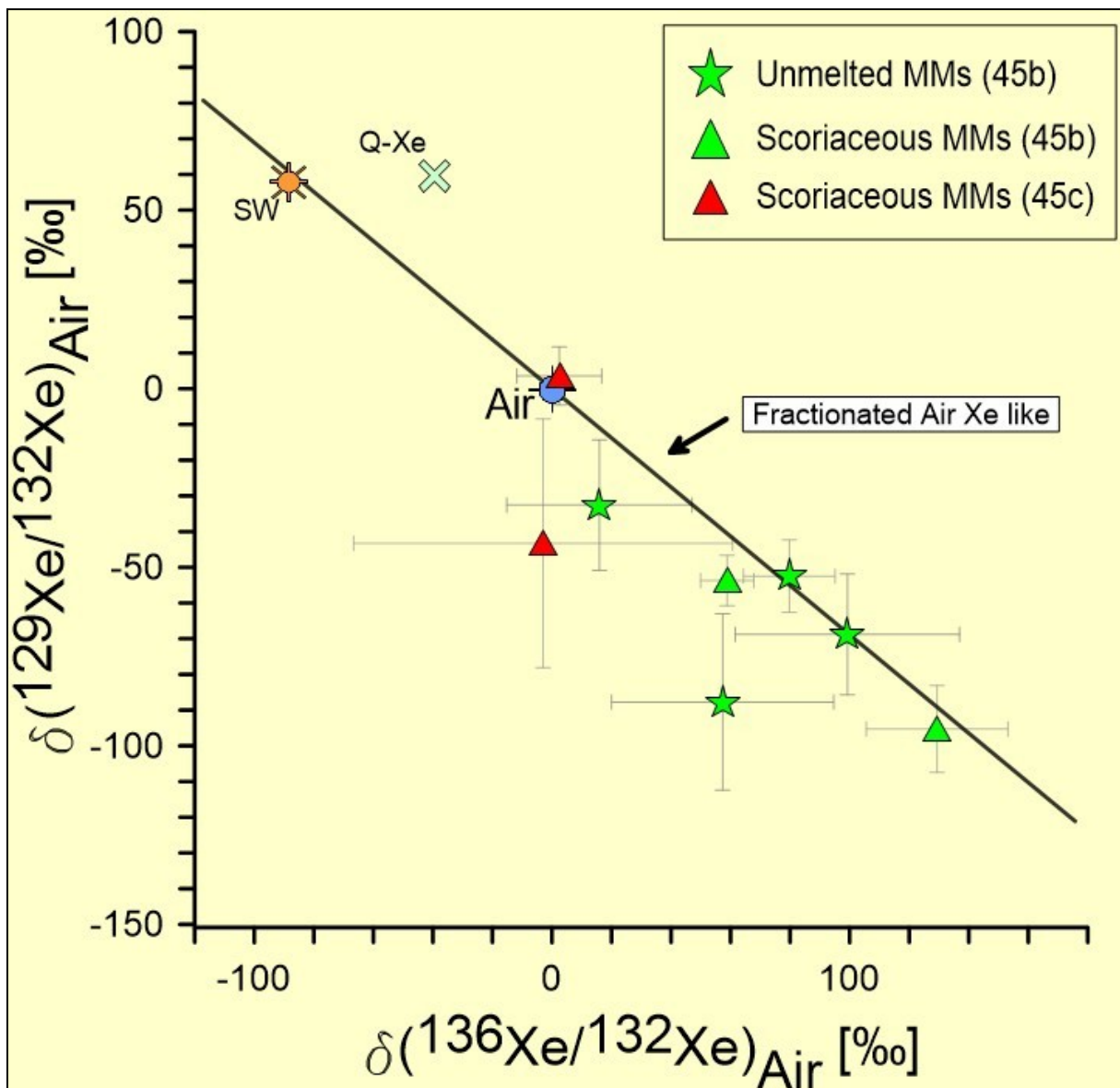
Figure 62. Delta isotope plot of ^{129}Xe / ^{132}Xe vs. ^{136}Xe / ^{132}Xe for the TAM-MM samples in per mil-deviations [δ] from Earth atmosphere Xenon composition. Earth atmosphere (Air) (Basford et al. (1973)). Also plotted for comparison are SW (Meshik et al. (2012)) and Q (P1) (Busemann et al. (2000)).

Yet, it is maybe of less fortune to assess air fractionation processes taking both plots and the data in Fig. 62 and 63 into consideration as a separate issue. This is why two additional delta isotope plots of $^{82}Kr/^{84}Kr$ vs. $^{129}Xe/^{132}Xe$ and $^{80}Kr/^{84}Kr$ vs. $^{136}Xe/^{132}Xe$ in per mil-deviations [δ] from Air-Xe (EA) composition (Basford et al. (1973)), should assist to link certain fractionation processes occurring in Kr and Xe simultaneously (see Fig. 64 and 65).

In both figures, certain ScMMs and UnMMs of group"45b" and "45c" plot on or near the Earth atmosphere fractionation line. In Fig. 64 these are 2 ScMMs and 4 UnMMs of the "45b" group and 2 ScMMs of the "45c" group. This seems to be consitent with the data shown for Xe in Fig. 62. In Fig. 63, however, more ScMMs and UnMMs of group "45c" plot on or near the Earth atmosphere fractionation line.

Bastian Baecker | Chapter 5 - Micrometeorites from the Transantarctic Mountains (TAM) - Noble gases show indications for multiple populations

123

These are the same 2 ScMMs and 4 UnMMs of group "45b", but more than in Fig. 62 (3 ScMMs and 3 UnMMs) of the "45c" group. While the uncertainties for Kr are larger than for Xe, the trend is the same.
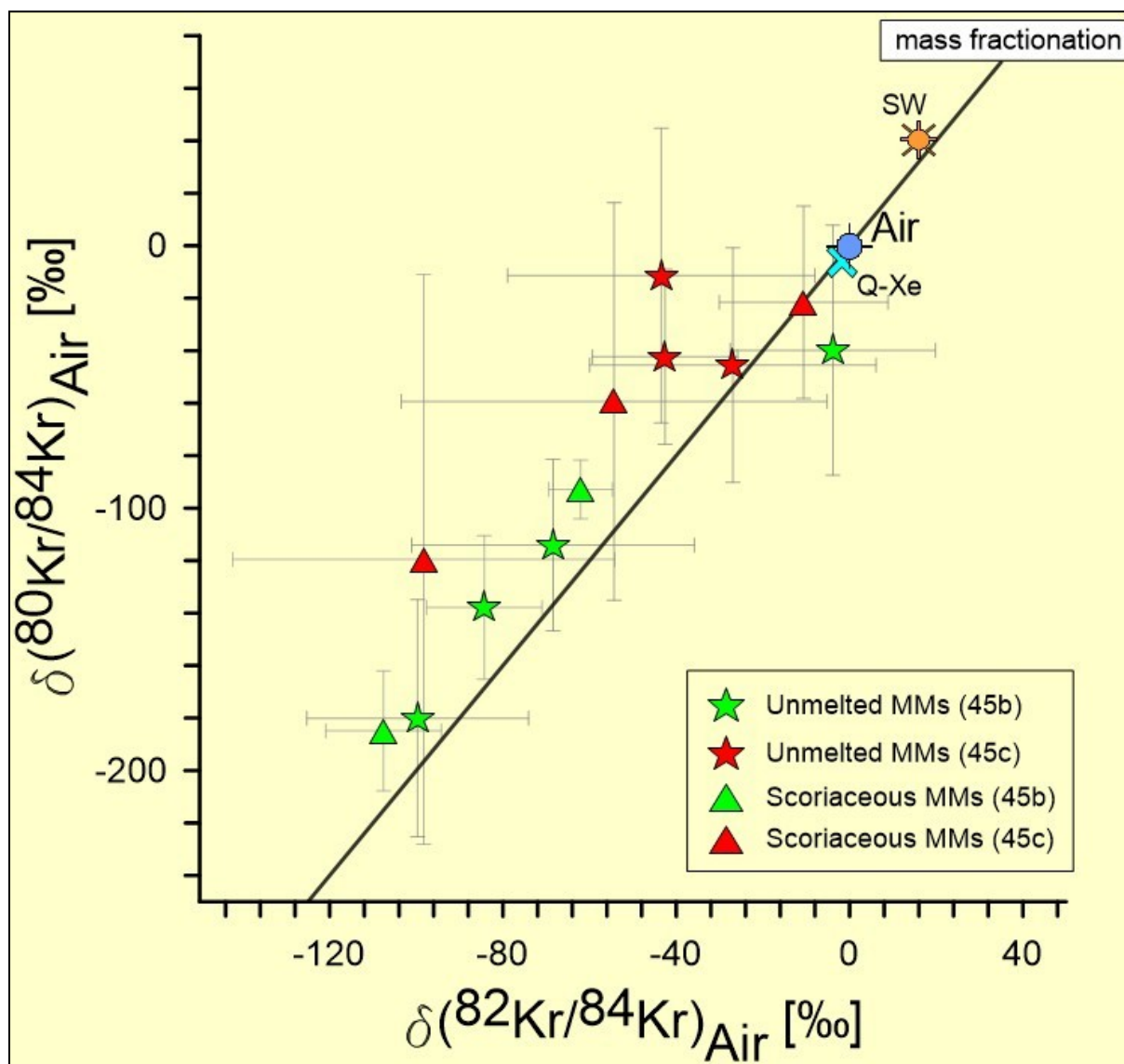
Figure 63. Delta isotope plot of ^{80}Kr / ^{84}Kr vs. ^{82}Kr / ^{84}Kr for the TAM-MM samples in per mil-deviations [δ] from Earth atmosphere Xenon composition. Earth atmosphere (Air) (Basford et al. (1973)). Also plotted for comparison are SW (Meshik et al. (2012)) and Q (P1) (Busemann et al. (2000)).

Finally, Figs. 64 and 65 compare the effects in Kr and Xe for these MM samples by plotting $^{82}Kr/^{84}Kr$ vs. $^{129}Xe/^{132}Xe$ and $^{80}Kr/^{84}Kr$ vs. $^{136}Xe/^{132}Xe$, respectively. These figures clearly show that the data points fall along the solid lines, which are fractionation lines, if the relative effects in Kr and Xe scale with ΔM/M, which is what is expected for mass fractionation.

As mentioned above and in the previous chapters, the MMs from TAM show three main information patterns:

First, within the noble gases inventory of many MMs mass fractionation processes are clearly present.

Second, except for $^{134}Xe/^{132}Xe$ and $^{136}Xe/^{132}Xe$, the Xe isotope ratios show distinctive differences between the "45b" and the "45c" MM groups. This could be

Bastian Baecker | Chapter 5 - Micrometeorites from the Transantarctic Mountains (TAM) - Noble gases show indications for multiple populations

124

explained in principle with fractionation processes that occurred on Earth during the deposition of the MMs. While I am not aware of any reported evidence for isotopic fractionation during Xe loss due to weathering, it remains a distinct though remote possibility that such a process fractionated MMs from the "45b" group by weathering while deposited e.g. in water in the last 1Ma (see Rochette et al. (2008)).

Third, two main groups of samples seem to be present. One seems to be influenced by the terrestrial atmosphere (EA), possibly during heating while penetrating Earth atmosphere - this group mainly consists of scoriaceous MMs but also some unmelted MMs. The second group (mainly unmelted MMs) was able to retain its SW and "planetary" (Q(P1)) information and shows results near these components (see Table 25 and Fig. 54 to Fig. 64).
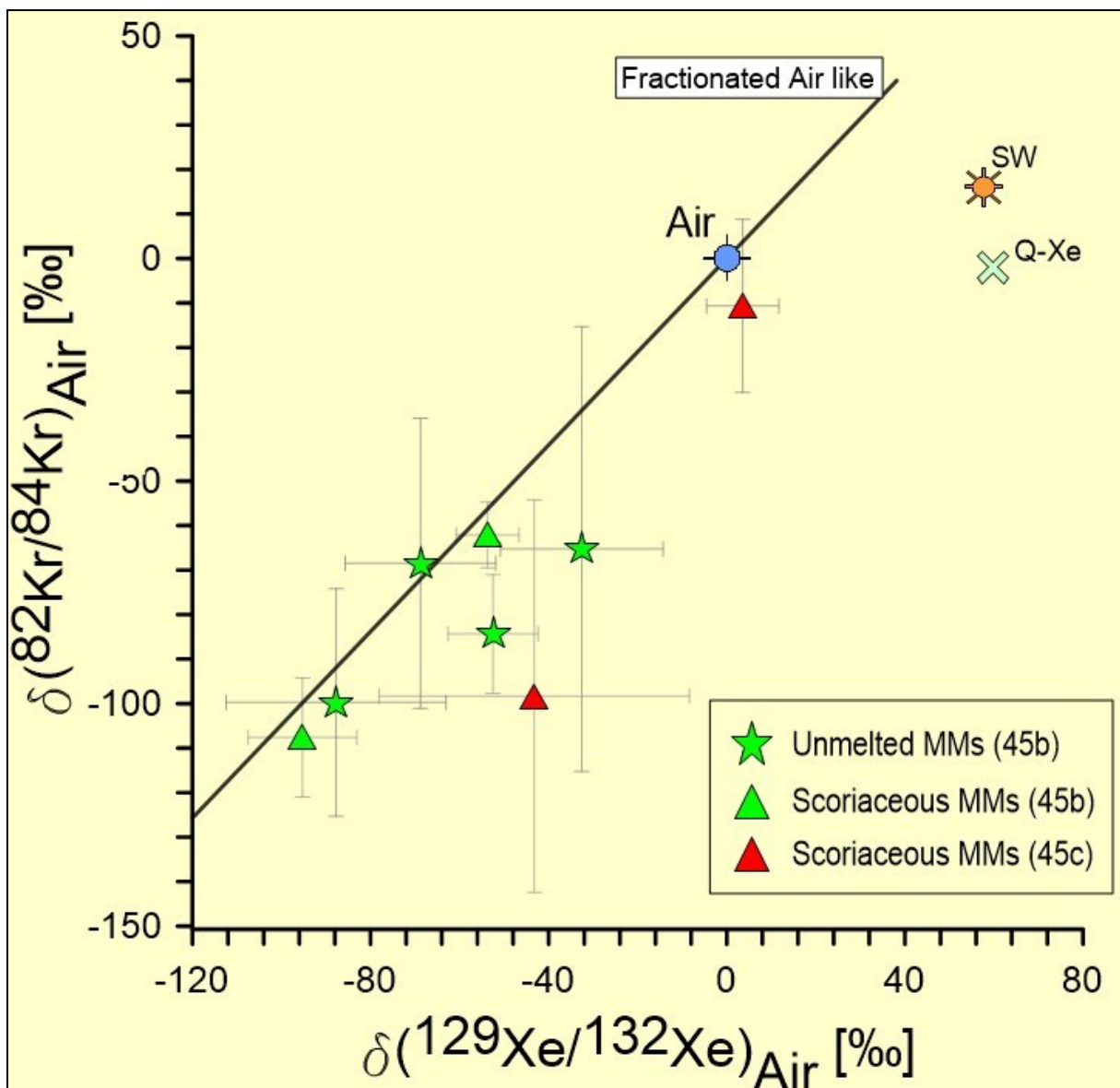
Figure 64. Delta isotope plot of ^{82}Kr / ^{84}Kr vs. ^{129}Xe / ^{132}Xe for the TAM-MM samples in per mil-deviations [δ] from Earth atmosphere Xenon composition. Earth atmosphere (Air) (Basford et al. (1973)). Also plotted for comparison are SW (Meshik et al. (2012)) and Q (P1) (Busemann et al. (2000)).

Also, especially the UnMMs of the "45c" group show similarities in $^{129}Xe/^{132}Xe$ (Table 25) to the matrix of carbonaceous chondrites like Murchison (1.037 (2); e.g. Wieler et

Bastian Baecker | Chapter 5 - Micrometeorites from the Transantarctic Mountains (TAM) - Noble gases show indications for multiple populations

125

al. (1992)). The remaining MMs mostly plot below this result. The results reported in Table A1 in Osawa and Nagao (2002) are in a similar range, though with larger uncertainties. Note, however that the highest ratio these authors measured is 1.67 (39). Sarda et al. (1991), measured values of ~0.98 to ~1.06 in a single, large MM.
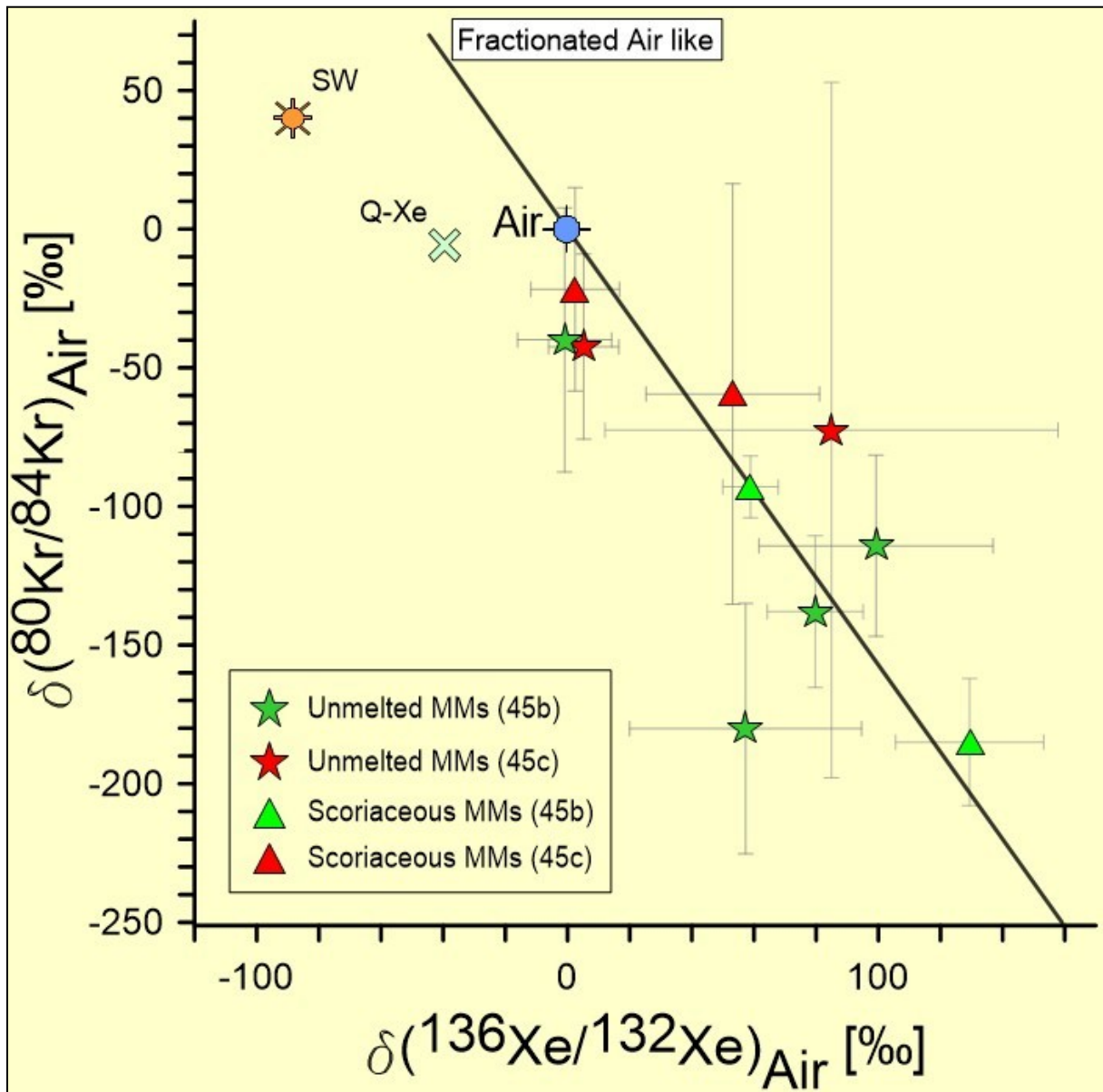
Figure 65. Delta isotope plot of ^{80}Kr / ^{84}Kr vs. ^{136}Xe / ^{132}Xe for the TAM-MM samples in per mil-deviations [δ] from Earth atmosphere Xenon composition. Earth atmosphere (Air) (Basford et al. (1973)). Also plotted for comparison are SW (Meshik et al. (2012)) and Q (P1) (Busemann et al. (2000)).

Bastian Baecker | Chapter 5 - Micrometeorites from the Transantarctic Mountains (TAM) - Noble gases show indications for multiple populations

126

5.4.6 Elemental abundance ratios

Results for elemental abundance ratios are shown in Table 26, as well as in Fig. 66 to Fig. 69 and in the Appendix for measured unmelted, scoriaceous MMs and Cosmic Spherules from TAM. Fig. 66 shows the $^{36}Ar/^{132}Xe$ ratio plotted versus the isotopic composition of $^{38}Ar/^{36}Ar$ for data obtained for the TAM MMs, along with data from Osawa and Nagao (2002), as well as the components SW (Vogel et al. (2011)), EA (Ozima and Podosek (2002)), Q(P1) (Busemann et al. (2000)), P3 and HL (both Huss and Lewis (1994a)).
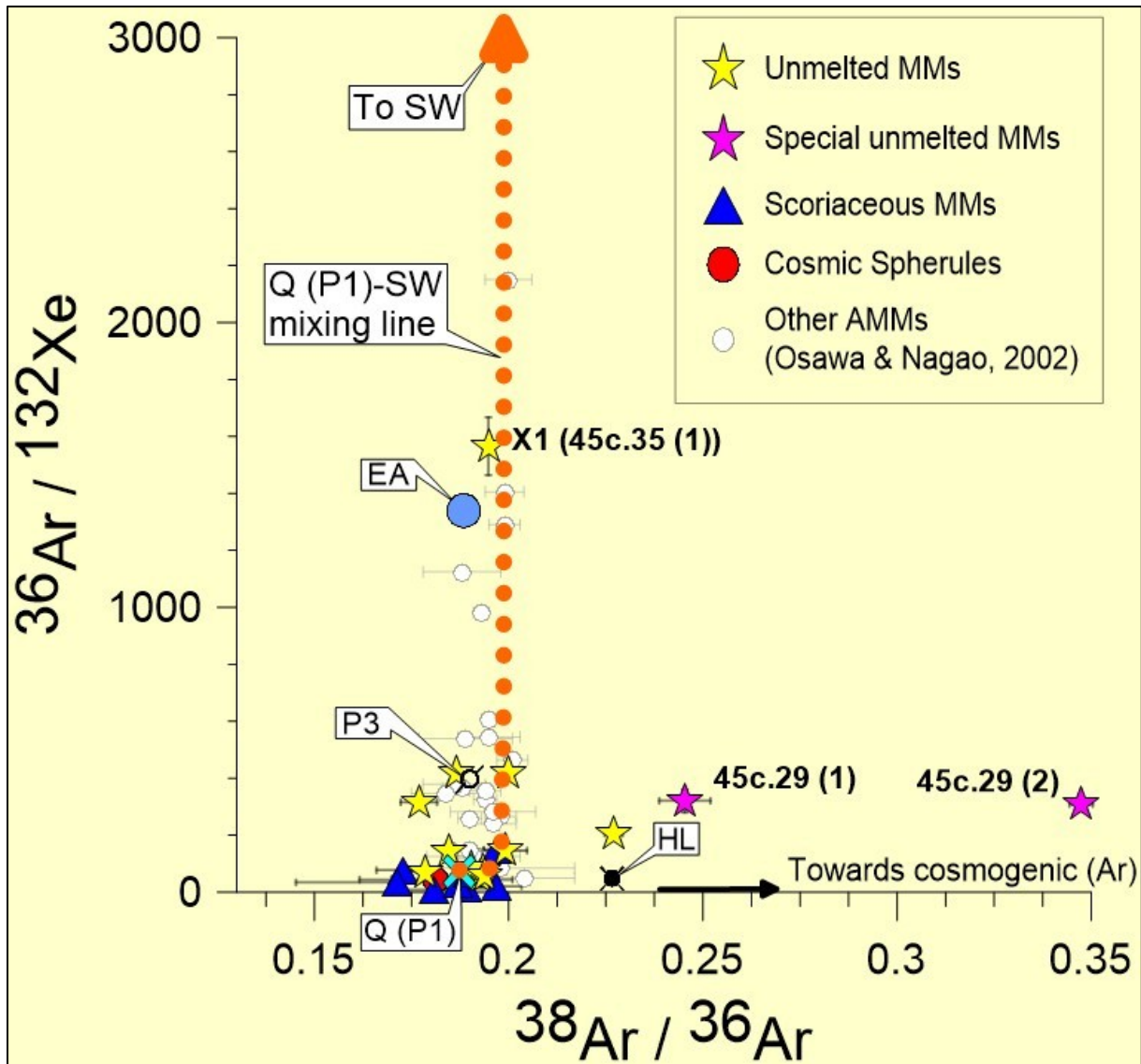
Figure 66. Isotope plot of $^{36}Ar / ^{132}Xe$ vs. $^{38}Ar / ^{36}Ar$ for our samples and data from Osawa and Nagao (2002). Also plotted for comparison are "to SW" (Vogel et al. (2011)), EA (Ozima and Podosek (2002)), Q (P1) (Busemann et al. (2000)), P3 and HL (Huss and Lewis (1994a)).

Most of the measured samples plot near or around the Q(P1) component, indicating a primordial pattern containing trapped Ar. In Fig. 66 only one sample (UnMM X1) shows evidence for a mixture of SW and Q(P1), however, in most (unmelted) samples SW is much more abundant when taking ^{20}Ne besides ^{36}Ar in consideration (see Table 22 and 23 and Fig. 69). Also, a contribution of Earth atmosphere (EA) is possible, though not supported by results shown in Table 26, in

Bastian Baecker | Chapter 5 - Micrometeorites from the Transantarctic Mountains (TAM) - Noble gases show indications for multiple populations

127

Fig. 67 and in Fig. 68 but well determined for Xe in some MMs (see previous chapter). The data given by Osawa and Nagao (2002) are similar: their results comprise several MM samples showing a Q(P1) influence along with a possible Air-SW mixture. Three of our UnMMs plot in the direction of cosmogenic ^{38}Ar. Especially the "special" UnMM particles 45c.29(1) and 45c.29(2) seem to contain large amounts of cosmogenic Ar (see chapter 5.4.7).

Table 26. Elemental abundance ratios for 29 different TAM MM samples. Listed are totals, calculated from the indicated measurement steps - for details see Appendix. Uncertainties in the last digits are given in parentheses. For comparison also the compositions of SW, Q(P1) and EA are listed.

Sample	Particle no.	Step(s) used	^{36}Ar/^{132}Xe	^{84}Kr/^{132}Xe
45b.08 (Sc)	1	2	19.9 (1.9)	4.73 (52)
45b.09 (Un)	1	1	59.2 (5.2)	2.28 (20)
45b.10 (Un)	2	1	315 (11)	11.0 (6)
45b.13 (Sc)	1	all	63.6 (5.5)	3.63 (32)
45b.14 (Sc)	1	1	33.6 (21.4)	1.50 (58)
45b.15 (Sc)	1	all	29.4 (9)	0.63 (5)
45b.16 (Un)	whole sample	all	420 (28)	1.88 (27)
45b.17 (Un)	1	all	205 (14)	5.44 (50)
45b.18 (Un)	1	n.a.	-	-
45b.19 (CS)	1	all	43.2 (18.9)	2.16 (40)
45b.20 (Sc)	2	1	7.98 (1.64)	0.79 (7)
45b.21 (Un)	whole sample	all	83.4 (3.3)	0.81 (6)
45b.22 (Sc)	2	n.a.	-	-
45c.16 (CS)	2	n.a.	-	-
45c.17 (CS)	whole sample	n.a.	-	-
45c.21 (CS)	whole sample	n.a.	-	-
45c.24 (Un)	whole sample	1	42.2 (1.2)	0.55 (5)
45c.25 (Sc)	2	all	12.0 (1.9)	0.93 (9)
45c.27 (Sc)	2	1	76.5 (12.4)	3.98 (38)
45c.29 (Un)	1	all	320 (41)	4.25 (56)
45c.29 (Un)	2	1	308 (18)	7.27 (59)
45c.31 (Sc)	1	all	148 (13)	1.23 (28)
45c.33 (Un)	1	all	75.6 (4.6)	1.05 (6)
45c.34 (Un)	1	all	70.8 (3.2)	0.96 (9)
X1 (Un)	1	1	1565 (101)	3.16 (64)
45c.35 (Un)	2	1	145 (33)	6.57 (1.54)
45c.35 (Un)	3	all	141 (5)	0.64 (5)
45c.37 (Un)	2	all	54.9 (5.1)	0.64 (17)
45c.37 (Un)	3	all	416 (23)	4.03 (99)
Component	**References**		^{36}Ar/^{132}Xe	^{84}Kr/^{132}Xe
SW	[1]		23360 (1800)	9.84 (76)
Q (P1)	[2]		76 (7)	0.81 (5)
EA	[3]		1343	27.78

References: *[1] Vogel et al. (2011), [2] Busemann et al. (2000), [3] calculated from Table 1.2 and 1.3 in Ozima and Podosek (2002)),*
Note: *w.s. = whole sample, n.a. = not detectable (below blank level).*

Bastian Baecker | Chapter 5 - Micrometeorites from the Transantarctic Mountains (TAM) - Noble gases show indications for multiple populations

128

Fig. 67 and Fig. 68 are element ratio plots of ^{36}Ar / ^{132}Xe vs. ^{84}Kr / ^{132}Xe for our data, for Murchison (measured at MPIC 2011) and data from Osawa and Nagao (2002), featuring also SW (Vogel et al. (2011)), EA and EA (dissolved in water) (Ozima and Podosek (2002)), Q (P1) (Busemann et al. (2000)) and "subsolar" (Crabb and Anders (1981) in Ott (2002)). Ratios of ^{36}Ar/^{132}Xe show the lowest values within the ScMM 45b.20(2) (7.98), the highest within the UnMM X1 (1565), whereas ^{84}Kr/^{132}Xe ratios shown in Table 26 vary between 0.55 (UnMM 45c.24) and 11.0 (UnMM 45b.10(2)). Osawa and Nagao (2002) reported values for ^{36}Ar/^{132}Xe in the range 49 to 2150 and for ^{84}Kr/^{132}Xe from 0.73 to 10.44.
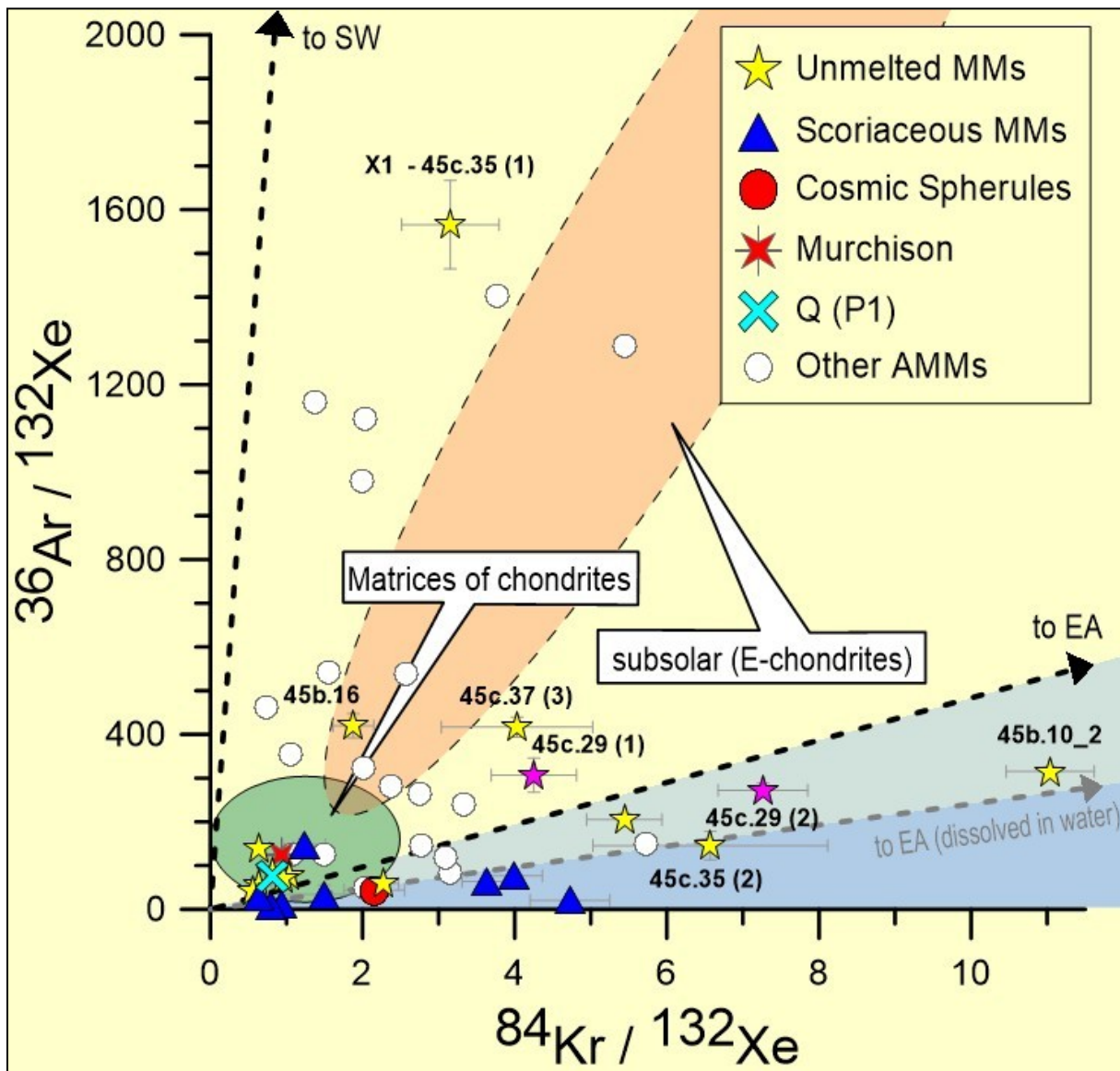
Figure 67. Elemental ratio plot of ^{36}Ar / ^{132}Xe vs. ^{84}Kr / ^{132}Xe for our data, for Murchison (measured at MPIC 2011) and data from Osawa and Nagao (2002), featuring also SW (Vogel et al. (2011)), EA and EA (dissolved in water) (Ozima and Podosek (2002)), Q (P1) (Busemann et al. (2000)) and "subsolar" (Crabb and Anders (1981) in Ott (2002)).

Overall, if one compares our results with those from Osawa and Nagao (2002), the range is similar. The main difference can be found in the combination of lower overall ratios for 6 of our UnMMs and 5 of our ScMMs, indicating a larger contribution of the "planetary" Q(P1) component in these samples. Only two of the MMs reported

Bastian Baecker | Chapter 5 - Micrometeorites from the Transantarctic Mountains (TAM) - Noble gases show indications for multiple populations

129

by Osawa and Nagao (2002) are plotting within the "matrices of chondrites" (Figs. 67 and 68) region.

Those (mostly unmelted) MMs (45b.15(1), 45b.20(2), 45b.21, 45c.24(1), 45c.33(1), 45c.34(1), 45c.35(2), 45c.35(3), 45c.37(2)) with observed low $^{36}Ar/^{132}Xe$ and low $^{84}Kr/^{132}Xe$ ratios are also the ones containing Xe (see previous chapter, Table 25 and the Appendix) with an isotopic composition close to "planetary" Q(P1), which is typically found in bulk CM chondrites like Murchison. The element plots in Fig. 67 and 68 emphasize these results.
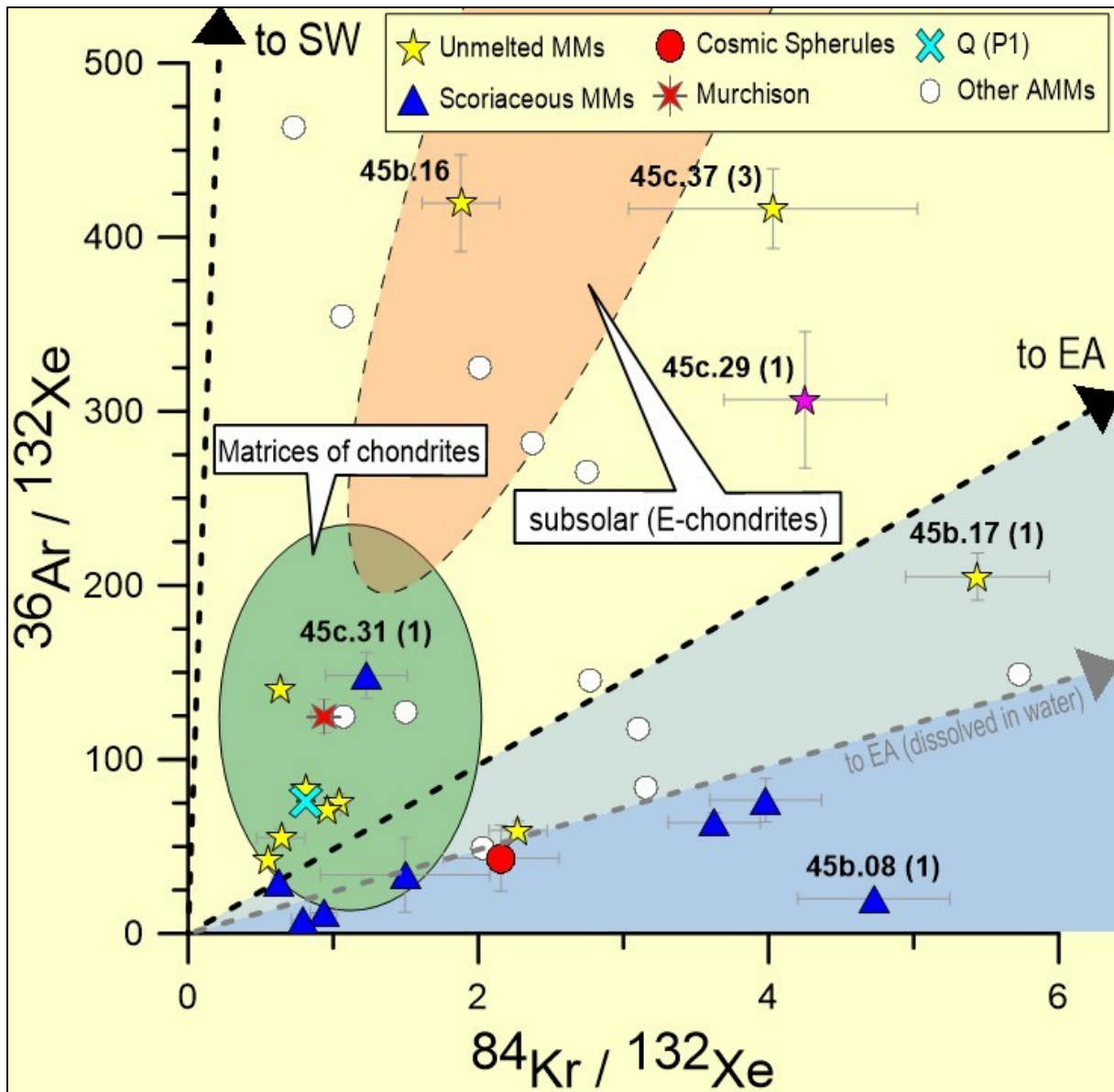
Figure 68. Elemental ratio plot of $^{36}Ar / ^{132}Xe$ vs. $^{84}Kr / ^{132}Xe$, lower right side of Fig. 67 enlarged. For details see Fig. 67.

Visible in Figs. 67 and 68 are also, again three major groupings. As noted above, one group plots directly near the Q(P1) component showing low $^{36}Ar/^{132}Xe$ and low $^{84}Kr/^{132}Xe$ values; these are 6 unmelted MMs and 3 scoriaceous MMs (see Fig. 67 and Fig. 68). The second group shows even lower $^{36}Ar/^{132}Xe$, but highly variable $^{84}Kr/^{132}Xe$ ratios, indicating that these MMs are influenced by fractionated Earth atmosphere. This is true for 5 unmelted MMs, 6 scoriaceous MMs and one

Bastian Baecker | Chapter 5 - Micrometeorites from the Transantarctic Mountains (TAM) - Noble gases show indications for multiple populations

130

Cosmic Spherule. The UnMM 45c.35(2), 6 scoriaceous MMs and the Cosmic Spherule plot even lower near or below the EA (dissolved in water) fractionation line, indicating that these particles were likely influenced by aqueous weathering on Earth or even further fractionated like the desert chondrites studied by Scherer et al. (1994). The third group shows higher $^{36}Ar/^{132}Xe$ ratios along with higher $^{84}Kr/^{132}Xe$ ratios, indicating that samples are enriched in Ar and Kr in relation to Xe and Q-gas, similar to the "subsolar" component found in enstatite chondrites (E-chondrites) (see Crabb and Anders (1981) and Busemann et al. (2001b)). Another possibility is former presence of solar wind proper, from which the lighter noble gases have been lost preferentially. (see Fig. 69).
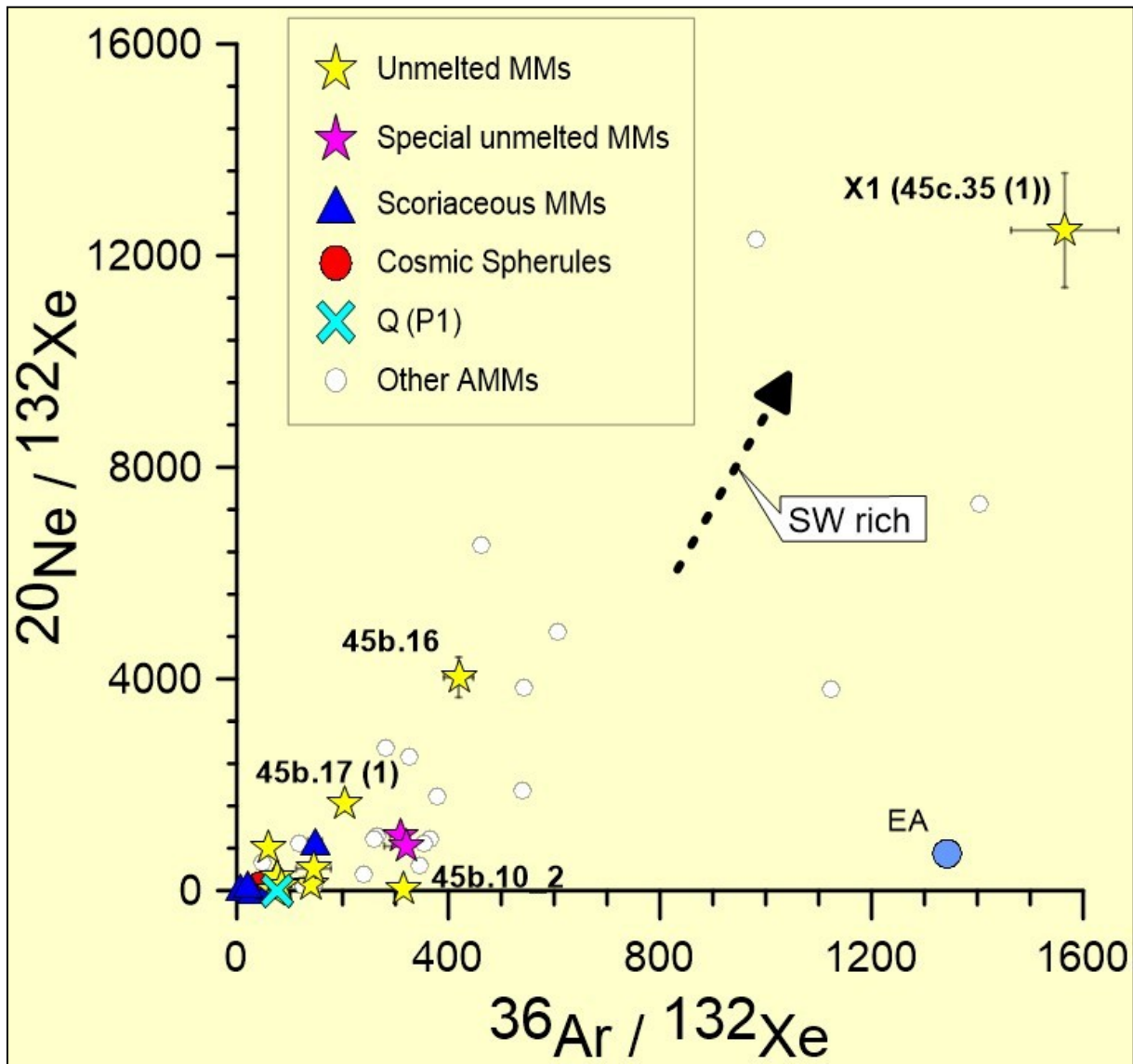
Figure 69. Elemental ratio plot of $^{20}Ne / ^{132}Xe$ vs. $^{36}Ar / ^{132}Xe$ for our data and data from Osawa and Nagao (2002), featuring also EA (Ozima and Podosek (2002)) and Q (P1) (Busemann et al. (2000)).

Fig. 69 is element ratio plot of $^{20}Ne/^{132}Xe$ vs. $^{36}Ar/^{132}Xe$ for our data and data from Osawa and Nagao (2002), featuring also EA (Ozima and Podosek (2002)) and Q (P1) (Busemann et al. (2000)). Most of the MMs show low ratios of $^{20}Ne/^{132}Xe$ and $^{36}Ar/^{132}Xe$, only UnMM 45.17(1), UnMM 45b.16 and in particular X1 show an elemental composition shifted towards SW. In general, MMs from Osawa and Nagao

Bastian Baecker | Chapter 5 - Micrometeorites from the Transantarctic Mountains (TAM) - Noble gases show indications for multiple populations

131

(2002) seem to contain larger SW contributions in this kind of representation. As described in previous chapters, in most cases the noble gas inventory of most of the TAM MMs was rather similar to the one found by Osawa and Nagao (2002). It is conceivable however that due to the overall smaller size of the MMs of Osawa and Nagao (2002), the thermal history of their particles was different from the one the TAM MMs experienced, which may have led to a different degree of loss of SW trapped gases. This is in agreement with data obtained for the MMs of the CONCORDIA collection (Duprat et al. (2007)) which seem to be, in general, SW rich along with smaller sizes (see chapter 6). Overall it seems that most of the MMs containing SW are shifted to the right from a simple mixing of Q and SW, indicating that these samples may have preferentially lost the lighter gases, i.e. trapped ^{20}Ne, due to possible thermal processes, alteration and/or weathering.

Fig. 70 is an elemental plot presenting trapped ^{36}Ar and ^{84}Kr concentrations versus trapped ^{132}Xe concentrations, for our data and data of typical ordinary and carbonaceous chondrites (Marti (1967)), along with AMM data from Osawa and Nagao (2002)). The area of carbonaceous chondrites is shown in a more red tone, the area of ordinary chondrites in a more green one. The individual single colored field shows are labeled by a number indicating the class of the meteorite. Symbols for the chondrite types are explained in the box on the upper left, symbols for MMs in the two boxes on the lower right side of Fig. 70. In case of the TAM MMs (especially for those dominated by the Q(P1) component), the symbols are filled with colors for the comparison of trapped ^{36}Ar with trapped ^{132}Xe, whereas the symbols for comparison of trapped ^{84}Kr with ^{132}Xe are empty.

Three features are obvious. Overall, all of the AMMs (TAM and MMs from Osawa and Nagao (2002)) plot not lower than type 5 (H, L, LL) chondrites. The unmelted MMs from TAM, as well as the MMs from Osawa and Nagao (2002) exhibit larger noble gas concentrations in both Ar, Kr and Xe, resembling carbonaceous chondrites and type 3 (H, L, LL) ordinary chondrites. ScMMs and the CS plot in a similar - though not the same - range, when Kr is considered, but except for some, not in the Ar plot, a sign of the fractionated nature of their noble gases. In assessing these differences and in particular with regard to the comparison with macro-meteorites, it is useful to keep in mind that the larger meteorites in their inner portions are not affected by atmospheric entry heating. This, nevertheless, still allows to perform a comparison between our measured MMs and the MMs from Osawa and Nagao (2002). Generally it seems that the MMs from Osawa and Nagao (2002) with a smaller weight (between 0.5 µg and 6.0 µg) retained the "lighter" Ar and in some case also the "heavier" Kr and Xe better than the more heavy MMs from TAM (weights between 9.2 and 337 µg). Especially the ScMMs and the CS seem to have lost a large fraction of trapped ^{36}Ar. As already mentioned earlier, this is especially interesting in connection with our measured AMMs from Dome C (Duprat et al. (2007)), which plot in a similar area like the AMMs from Osawa and Nagao (2002) and are of light weight as well (see Table 30 and chapter 6.4.6).

Bastian Baecker | Chapter 5 - Micrometeorites from the Transantarctic Mountains (TAM) - Noble gases show indications for multiple populations

132
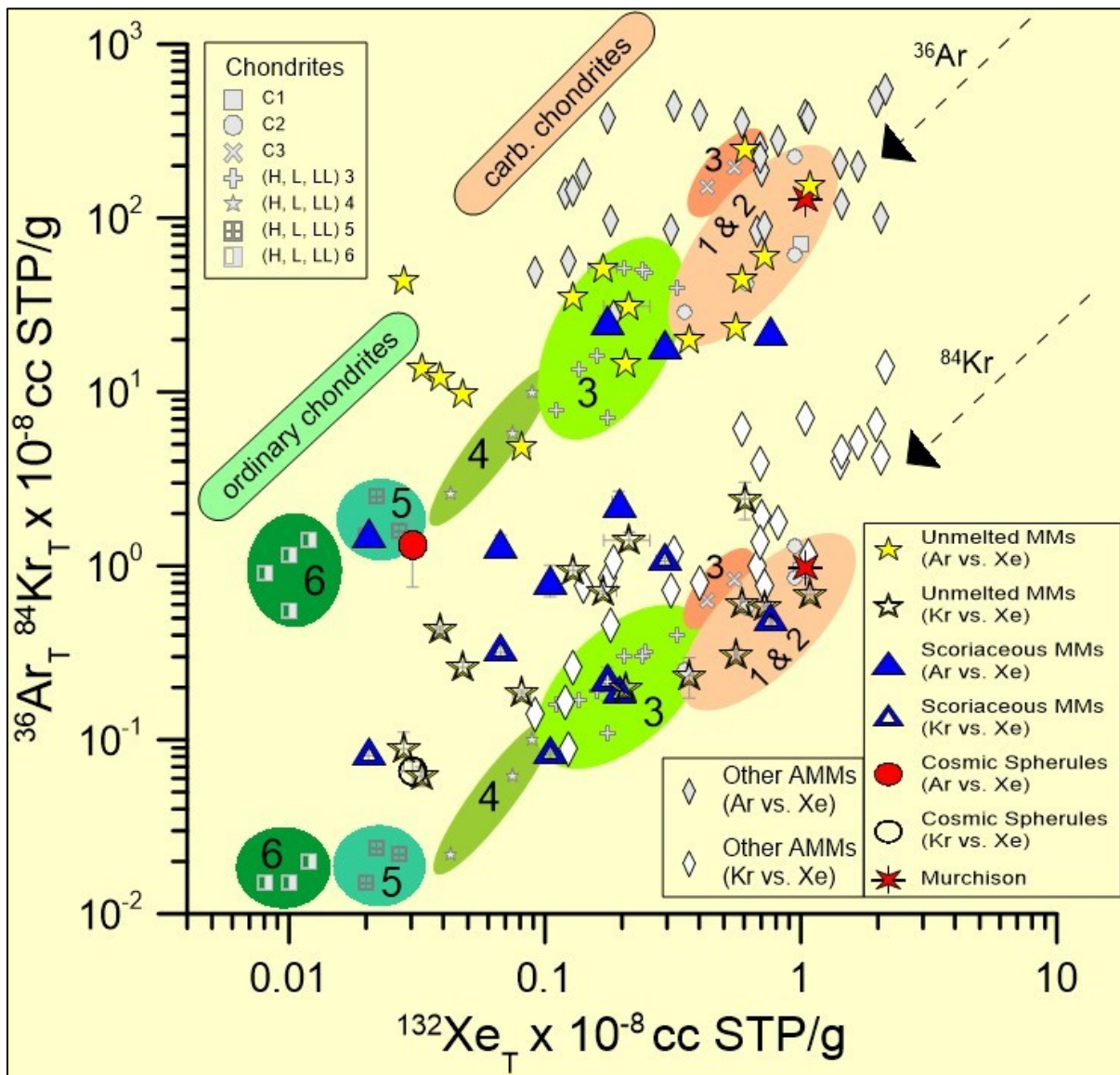
Figure 70. Plot of Ar, Kr and Xe, showing the measured concentrations of trapped ^{36}Ar and ^{84}Kr vs. ^{132}Xe in units of 10^{-8} cc STP/g, for our data, for Murchison (measured at MPIC 2011) and data from Osawa and Nagao (2002) as well as Marti (1967).

Bastian Baecker | Chapter 5 - Micrometeorites from the Transantarctic Mountains (TAM) - Noble gases show indications for multiple populations

133

5.4.7 Cosmogenic concentrations and CRE-Ages

Cosmogenic ^{21}Ne and ^{38}Ar concentrations and ^{21}Ne/^{38}Ar ratios are given in Table 27. 18 MMs show measurable cosmogenic ^{21}Ne contributions, 10 MMs only show upper limits and for 1 MM the overall cosmogenic contributions are below blank level. The cosmogenic concentrations for ^{21}Ne and ^{38}Ar are calculated by using an Excel spreadsheet provided by U. Ott (MPIC Mainz, Germany).

Cosmogenic ^{21}Ne concentrations are generally calculated in 5 iterations for each measurement step by, basically, multiplying the results of the ^{21}Ne/^{22}Ne ratio with the measured concentrations of ^{22}Ne and multiplying it again with results of measured trapped and total concentrations of ^{21}Ne as follows:

$$^{21}Ne_{cos} = ((^{21}Ne / {}^{22}Ne)_{meas} \times {}^{22}Ne_{meas} \times (1 - ({}^{21}Ne_{trapped} / {}^{21}Ne_{total}))) \qquad (12)$$

The ^{21}Ne$_{trapped}$/^{21}Ne$_{total}$ is obtained via the (estimated) (^{20}Ne/^{21}Ne)$_{trapped}$ ratio. The trapped ^{20}Ne/^{21}Ne ratio on the other hand is estimated by dividing three times iteratively, starting from an assumed value, until a close match between the (new) assumed (expected) and resulting ratio is achieved. Finally the ^{21}Ne$_{trapped}$/^{21}Ne$_{total}$ ratio was calculated as follows:

$$((^{20}Ne / {}^{21}Ne)_{meas} - ({}^{20}Ne / {}^{21}Ne_{cos}) / (({}^{20}Ne / {}^{21}Ne_{trapped}) - ({}^{20}Ne / {}^{21}Ne_{cos})) \quad (13)$$

Cosmogenic ^{38}Ar concentrations are calculated by multiplying the results of the calculated ^{38}Ar$_{trapped}$/^{38}Ar$_{total}$ ratio obtained from the ^{36}Ar/^{38}Ar ratio with the measured ^{38}Ar concentrations as follows:

$$(^{38}Ar \times (1 - ({}^{38}Ar_{trapped} / {}^{38}Ar_{total}))) \qquad (14)$$

The ^{38}Ar$_{trapped}$/^{38}Ar$_{total}$ ratio itself is calculated similar to the one for Ne explained above, as follows:

$$((^{36}Ar / {}^{38}Ar)_{meas} - ({}^{36}Ar / {}^{38}Ar_{cos})) / (({}^{36}Ar / {}^{38}Ar_{trapped}) - ({}^{36}Ar / {}^{38}Ar_{cos})) \qquad (15)$$

Choosing the proper (^{36}Ar/^{38}Ar)$_{trapped}$ ratio for this calculation is not straightforward, also compared to the case of Ne. Unlike the latter, which is a three-isotope system, Ar is for practical purposes a two-isotope system (^{36}Ar and ^{38}Ar) only since ^{40}Ar can vary independently due to radiogenic contributions. For our choice of trapped ^{36}Ar/^{38}Ar the calculated cosmogenic ^{38}Ar abundances (Table 27) are essentially upper limits only (see below).

Some MMs show combined high amounts of trapped and cosmogenic Ne (e.g. ScMM 45c.31(1) and UnMM 45c.33(1)). For these we used a somewhat different approach and calculated the relative concentrations assuming that the trapped Ne is of a mixture of SW (solar wind) and "FSW" ("fractionated solar wind noble gases"; e.g. Wieler et al. (2007) - see also chapter 3.2.1.1). Taking this into consideration, we

Bastian Baecker | Chapter 5 - Micrometeorites from the Transantarctic Mountains (TAM) - Noble gases show indications for multiple populations

134

calculated the "expected" trapped $^{21}Ne/^{22}Ne$ using the obtained $^{20}Ne/^{22}Ne$ value for the trapped component. For these "extreme" cases, for this calculation the cosmogenic contributions to ^{22}Ne and ^{20}Ne were considered negligible. This makes sense in the case of the gas rich MMs, since a mixture of components like SW and "FSW" is also found for e.g. meteoritic and moon (regolith) material (e.g. Benkert et al. (1993)). If the trapped Ne-HL component (Huss and Lewis (1994a)) is also present, with a distinctly higher $^{21}Ne/^{22}Ne$ than SW/"FSW", one may overestimate in this approach the amounts and concentrations of $^{21}Ne_{cos}$. However, the effect should be negligible and SW/"FSW" dominant if trapped $^{20}Ne/^{22}Ne$ is >10.5 as is the case for most of our samples (compare Figs. 48, 49 and Table 22)

In the case of the TAM MMs the exact procedure for calculating cosmogenic ^{21}Ne is affecting the results only minor. However, it is more important for the MMs from Dome C (CONCORDIA Collection) which are discussed in chapter 6.4.7.

The thus obtained $^{21}Ne_{cos}$ concentrations are in the range from 5 x 10^{-12} cc STP/g (CS 45c.21, with large errors) to ~1.6 x 10^{-7} cc STP/g (UnMM 45c.29(1)). The UnMMs show generally the highest concentrations, between ~0.1 to 1 x 10^{-8} cc STP/g. The results of 4.4 x 10^{-8} cc STP/g, 5.3 x 10^{-8} cc STP/g and 16.1 x 10^{-8} cc STP/g for the three UnMMs 45b.17, 45c.29(2) and 45c.29(1), respectively, are exceptional within our sample set and comparable to the highest concentrations reported by Osawa and Nagao (2002). These authors reported for two particles $^{21}Ne_{cos}$ concentrations of 13 x 10^{-8} cc STP/g and 8.6 x 10^{-8} cc STP/g, only slightly lower than of what we measured for the UnMM 45c.29(1). Olinger et al. (1990) were able to obtain $^{21}Ne_{cos}$ concentrations for Greenland particles between ~0.3 x 10^{-8} cc STP/g and ~5 x 10^{-8} cc STP/g, but with relatively large uncertainties (12-67%); they also had some samples showing only upper limits. Their results are similar to the results for most of our ScMMs and UnMMs, but overall higher than the cosmogenic ^{21}Ne contributions we measured in the whole sample set of TAM MMs.

As noted above, in case of cosmogenic Ar, the concentrations listed in Table 27 are essentially upper limits only. This is because the amounts of cosmogenic ^{38}Ar relative to trapped ^{38}Ar are small, so the choice of trapped $^{36}Ar/^{38}Ar$ is critical. The choice is also not straightforward. For our calculations we used a value of 5.31, close to Q and Earth atmosphere, but an argument can be made that in many cases the ratio is lower due to the presence of "FSW"-Ar with a ratio of 4.87 (see Wieler (2002b) and Wieler et al. (2007)) – note that also for Ne in most cases with SW present, the trapped ratios are closer to "FSW"-Ne than to unfractionated SW-Ne.

Even with our choice, only 12 MMs showed noticeable contributions of cosmogenic Ar. Four MMs showed only upper limits, whereas for 13 MMs there was no measurable $^{38}Ar_{cos}$. Where "detectable", the results for $^{38}Ar_{cos}$ are in the range of 5 x 10^{-10} cc STP/g to ~7 x 10^{-8} cc STP/g, with about 50% of the TAM MMs showing no or only upper limit contributions. The highest $^{38}Ar_{cos}$ were detected for three UnMMs (45b.17, 45c.29(1) and 45c.29(2)) with 0.43 x 10^{-8} cc STP/g, 3.5 x 10^{-8} cc STP/g and 7.2 x 10^{-8} cc STP/g, respectively. These are the only ones with $^{38}Ar/^{36}Ar$ significantly higher than in any possibly present trapped component, thus these numbers depend also little on the assumptions about the latter. Not surprisingly, the same particles contain also the highest concentrations of $^{21}Ne_{cos}$.

Bastian Baecker | Chapter 5 - Micrometeorites from the Transantarctic Mountains (TAM) - Noble gases show indications for multiple populations

135

Additionally, as mentioned earlier, no signatures of cosmogenic contributions were detectable in Kr and Xe in the MM samples from the TAM. This is due to the relatively high amounts of trapped Kr and Xe relative to the cosmogenic part, like it is typical for primitive chondrites (e.g. Eugster (1988)) and also, of course, due to the limited accuracy of our Kr and Xe measurements for these small samples.

The *nominal* calculated ^{21}Ne/^{38}Ar ratios for 10 TAM MMs are in the range of 0.74 to 21.36. Some of our measured samples show low ^{21}Ne/^{38}Ar ratios between 0.44 and 1.84, which may indicate an achondritic parentage (high Ca relative to Mg). However, most of these low ratios have relatively large errors, due to low gas amounts of ^{21}Ne$_{cos}$ and/or ^{38}Ar$_{cos}$ and, as noted above, cosmogenic ^{38}Ar abundances are upper limits, so cosmogenic ^{21}Ne/^{38}Ar ratios are lower limits (see Table 27). It is conceivable also that significant losses of cosmogenic ^{38}Ar occurred during passage through the atmosphere (cf. Füri et al. (2013)), with losses somewhat less than for ^{21}Ne$_{cos}$, thus also lowering the cosmogenic Ne/Ar ratio. One MM, however, shows a low cosmogenic ^{21}Ne/^{38}Ar ratio with a low analytical uncertainty along with only little influence of the choice of trapped Ar composition - this is unique: UnMM 45c.29(2), with (^{21}Ne/^{38}Ar) = 0.74(4). A second particle of the same UnMM 45c.29 - named UnMM 45c.29(1) - gave different results, however (also with a low analytical and low systematic uncertainty): a much higher (^{21}Ne/^{38}Ar)$_{cos}$ ratio of 4.60 (47), along with a three times higher concentration of ^{21}Ne$_{cos}$ than for 45c.29(2), but with only about half the concentration of ^{38}Ar$_{cos}$ (see Table 27), a clear sign of inhomogenous chemical composition. This "special" UnMM is discussed in further detail in chapter 5.4.8.

Using the measured cosmogenic concentrations, one is able to calculate the cosmogenic exposure ages (CRE) of the MMs using the elemental composition in combination with production rates. A general overview about production rates along with age-dating methods is given in chapter 3.2.1.3. Given the systematic uncertainties in cosmogenic ^{38}Ar, we use this isotope only for the clearly resolved 45b.17 and the special sample 45c.29.

For our micrometeorites we used cosmogenic production rates for SCR (solar cosmic rays) and GCR (galactic cosmic rays) - see Table 28. The SCR production rates (at 1 AU distance from the Sun) were calculated using an Excel spreadsheet especially prepared for MMs along with selected different chemical compositions provided by R. Trappitsch and I. Leya (University of Bern, Switzerland) (see also Trappitsch and Leya (2013) and http://noblegas.unibe.ch (access 12/15/2013)). In case of the GCR (galactic cosmic rays) we used the elemental production rates for irradiation at the surface of a large body in 2π geometry, converted to 4π by multiplying with a factor 2: in case of ^{21}Ne$_{cos}$ we used the rates of Leya et al. (2001) and for ^{38}Ar$_{cos}$ those of Leya et al. (2001) (Fe, Ni) and Hohenberg et al. (1978) (Ca). These rates were used within an Excel spreadsheet provided by U. Ott (MPIC Mainz, Germany), to calculate specific GCR production rates for single MMs with an assumed elemental composition.

A problem with this calculation is that we, so far, do not have direct information about the bulk elemental composition of the specific sample used for noble gas analysis. We only have a general idea about the meteorite class from the

Bastian Baecker | Chapter 5 - Micrometeorites from the Transantarctic Mountains (TAM) - Noble gases show indications for multiple populations

136

mineralogical and petrological analysis (where available) made and provided by C. Cordier (2010 at MNA, University of Siena, Italy - now at ISTerre, University of Grenoble, France - see Appendix D) - see Tables 29 and 30. In our calculation we are using the mean composition of the respective general class (for literature sources see Table 28). CRE ages and the distances from where the MM started their voyage were calculated following Trappitsch and Leya (2013), using their spreadsheet, which takes into account as input SCR and GCR production rates at 1 AU, as well as the sizes and weights of the MMs. The spreadsheet combines the effects of SCR and GCR irradiation as a function of the Sun, recoil losses of cosmogenic products as well as the spiraling in of the MMs due to the Poynting-Robertson effect. Here the SCR production rate is considered to decrease with $1/r^2$ (where r is the distance from the Sun) and the GCR production rate to be the same within the relevant part of the Solar system.

The Poynting-Robertson effect is non-gravitational and is affecting small particles orbiting around the Sun by dragging them in spirals slowly towards the central star (see e.g. Wyatt and Whipple (1950), Klačka (1993) and Kimura et al. (2002)). The following formula from Wyatt and Whipple (1950) and modified by Trappitsch and Leya (2013) is used to calculate the time which particles in circular orbits - due to the Poynting-Robertson effect - need to travel in spiral from the starting point of their voyage to 1 AU:

$$T_{PR} = 7.0 \times 10^6 \times s \times \rho \times (a^2 - 1) \text{ years} \qquad (16)$$

with s = grain radius (cm); ρ = density (g/cm^3) and a = starting position (AU) of particle to 1 AU

Generally, we used calculated densities of each TAM MM **particle** (from the Trappitsch and Leya (2013) Excel spreadsheet mentioned earlier - see formula below) along with (mean geometric) sizes of the **whole** TAM MMs, to calculate the overall weights of each **whole** TAM MM sample. This was necessary, since the gross weight was not obtained during sample selection at MNA, Siena University, Italy and finally to be able to include the "full" Poynting-Roberston effect into our CRE calculations.

The density for each MM, on the other hand, was calculated using the calculated volume and the weight of each TAM MM **particle** as follows (from the Trappitsch and Leya (2013) Excel spreadsheet mentioned earlier):

$$\text{density MM } [\tfrac{g}{cm^3}] = ((\frac{\text{weight MM [µg]} \times 0.000001}{\text{volume MM [cm}^3]})) \qquad (17)$$

The volume used in equation (17) was calculated for each TAM MM particle using the mean geometric size of each particle within the following formula (from the Trappitsch and Leya (2013) Excel spreadsheet mentioned earlier):

$$\text{vol. MM } [cm^3] = ((\frac{\text{mean geometric size MM [µm]}}{2}) \times 0.0001)^3 \times 4 \times (\frac{3.1415}{3}) \qquad (18)$$

Bastian Baecker | Chapter 5 - Micrometeorites from the Transantarctic Mountains (TAM) - Noble gases show indications for multiple populations

137

Table 27. Concentrations of cosmogenic ^{21}Ne, ^{38}Ar and ^{21}Ne/^{38}Ar ratios for the TAM MM samples. Totals, based on the sum of individual measurement = steps as indicated - for more details see Appendix. Uncertainties in the last digits are given in parenthesis. Values with $^{\$}$ are 2σ upper limits. Where no values for cosmogenic ^{38}Ar are given, they could not be determined because of too large concentrations of trapped Ar. Note that in general cosmogenic ^{38}Ar concentrations are upper limits only and cosmogenic ^{21}Ne/^{38}Ar ratios are lower limits only (errors in parentheses do not include systematic uncertainties; see text for discussion).

Sample	Particle no.	Weight (µg)	Step(s) used	^{21}Ne$_{cos}$	^{38}Ar$_{cos}$ *	^{21}Ne$_{cos}$/^{38}Ar$_{cos}$ #
				(10^{-8} cc STP/g)		
45b.08 (Sc)	1	119.3 (1)	2+3	0.886 (28)	0.050 (11)	17.67 (3.90)
45b.09 (Un)	1	126.9 (1)	1	0.641 (18)	0.030 (18)	21.36 (12.90)
45b.10 (Un)	2	95.5 (1)	1	0.035 (8)	-	-
45b.13 (Sc)	1	137.6 (1)	1	0.005 (2)	-	-
45b.14 (Sc)	1	56.5 (1)	2	< 0.142 $^{\$}$	-	-
45b.15 (Sc)	1	30.3 (1)	1	< 0.018 $^{\$}$	-	-
45b.16 (Un)	whole sample	138.3 (1)	2	0.109 (10)	0.162 (41)	0.67 (18)
45b.17 (Un)	1	56.2 (1)	all	4.41 (25)	0.431 (38)	10.24 (1.07)
45b.18 (Un)	1	5.3 (1)	1	0.072 (27)	-	-
45b.19 (CS)	1	55.9 (1)	all	< 0.012 $^{\$}$	-	-
45b.20 (Sc)	2	77.3 (1)	1	0.018 (3)	-	-
45b.21 (Un)	whole sample	24.8 (1)	1	< 0.134 $^{\$}$	0.113 (105)	-
45b.22 (Sc)	2	9.2 (1)	1	0.194 (24)	< 0.348 $^{\$}$	-
45c.16 (CS)	2	105.1 (1)	1	< 0.004 $^{\$}$	< 0.026 $^{\$}$	-
45c.17 (CS)	whole sample	126.3 (2)	1	< 0.003 $^{\$}$	< 0.031 $^{\$}$	-
45c.21 (CS)	whole sample	337.9 (2)	1	0.0005 (5)	-	-
45c.24 (Un)	whole sample	34.0 (2)	1	-	-	-
45c.25 (Sc)	2	142.3 (1)	1	< 0.005 $^{\$}$	< 0.019 $^{\$}$	-
45c.27 (Sc)	2	38.0 (1)	1	0.020 (3)	-	-
45c.29 (Un)	1	22.1 (2)	1+2	16.14 (38)	3.51 (35)	4.60 (47)
45c.29 (Un)	2	24.2 (2)	1	5.32 (13)	7.23 (33)	0.74 (4)
45c.31 (Sc)	1	33.2 (3)	all	0.108 (13)	0.249 (106)	0.44 (19)
45c.33 (Un)	1	58.7 (2)	all	0.161 (11)	0.204 (116)	0.78 (44)
45c.34 (Un)	1	34.1 (1)	1	< 0.011 $^{\$}$	-	-
X1 (Un)	1	35.0 (1)	1	0.710 (75)	0.386 (133)	1.84 (67)
45c.35 (Un)	2	5.4 (1)	1	0.608 (71)	0.379 (205)	1.60 (89)
45c.35 (Un)	3	29.0 (1)	2	0.138 (29)	-	-
45c.37 (Un)	2	28.5 (1)	1	< 0.016 $^{\$}$	0.078 (52)	-
45c.37 (Un)	3	13.1 (1)	1	< 0.042 $^{\$}$	-	-

* = upper limits; # lower limits.

Bastian Baecker | Chapter 5 - Micrometeorites from the Transantarctic Mountains (TAM) - Noble gases show indications for multiple populations

138

As mentioned above, the highest cosmogenic ^{21}Ne and ^{38}Ar concentrations were obtained for the "special" UnMM 45c.29. Both particles of this MM show high contributions. UnMM 45c.29(1) with 16.14 x 10^{-8} cc STP/g of ^{21}Ne$_{cos}$ and (nominally) 3.51 x 10^{-8} cc STP/g of ^{38}Ar$_{cos}$, corresponding to a ^{21}Ne/^{38}Ar ratio of 4.60. Interestingly, although both particles are from the same MM, UnMM 45c.29(2) shows lower ^{21}Ne$_{cos}$ (5.32 x 10^{-8} cc STP/g) and higher ^{38}Ar$_{cos}$ contributions than UnMM 45c.29(1), which results in a ^{21}Ne/^{38}Ar ratio of 0.74. This "special" MM will be discussed in more detail in chapter 5.4.8.

Another MM with high cosmogenic contributions is UnMM 45b.17(1). This MM shows ^{21}Ne$_{cos}$ with 4.41 x 10^{-8} cc STP/g and a nominal (upper limit) ^{38}Ar$_{cos}$ of 0.431 x 10^{-8} cc STP/g. The ratio of ^{21}Ne/^{38}Ar is 10.24. This would be higher than in the most ordinary (~6.8; Eugster (1988)) and carbonaceous (~6.5; Eugster (1988)) chondrites and similar to values found for diogenites (~11.6; Eugster and Michel (1995)).

In general and especially in the case of MMs, it is important to discuss the probability of loss of lighter noble gases (e.g. ^{21}Ne$_{cos}$) compared to heavier ones (e.g. ^{38}Ar$_{cos}$) and with it the effect on the measured ratios. It is very likely, especially in the case of Cosmic Spherules and scoriaceous MMs that a loss of (lighter) noble gases occurs. In that context, Füri et al. (2013) report on an experiment using pulse heating of pieces of Orgueil (CI) meteorite (e.g. Nagy et al. (1961)) for simulation of the passage of micrometeorites through the Earth's atmosphere. These authors conclude that there is a high probability for a ^{21}Ne$_{cos}$ loss of ≥ 90% for mean MMs. Such a high loss is difficult to reconcile with the results of our MM measurements. Most of the unmelted MMs do show sufficient cosmogenic Ne amounts to calculate CRE ages that range from 0.1 to several Ma (see Table 29). This leads to the assumption that at least the unmelted MMs retained major parts of their cosmogenic Ne. Moreover, they contain even larger amounts of solar wind neon, which would be much more readily lost.

The calculated CRE-ages (in Ma) along with departure distances of the particles (in AU) calculated using the Trappitsch and Leya (2013) procedure are shown in Table 29 and Table 30. Based on the mineralogical and petrological analysis (where available) made and provided by C. Cordier (2010 at MNA, University of Siena, Italy - now at ISTerre, University of Grenoble, France), for most of our measured MMs a chondritic composition in the direction of ordinary chondrites with low or high Fe contents was used in defining the production rates. One MM appeared to be of carbonaceous chondrite origin (UnMM 45b.18(1)) and for the two 45c.29 particles the conclusion is uncertain, one piece looking more chondritic, the other more achondritic, as judged from the cosmogenic ^{21}Ne/^{38}Ar ratio (see also discussion in next chapter).

Bastian Baecker | Chapter 5 - Micrometeorites from the Transantarctic Mountains (TAM) - Noble gases show indications for multiple populations

139

*Table 28. SCR and GCR production rates for MMs with different elemental compositions along with an assumed 4π irradiation at 1AU. **SCR** production rates calculated using an Excel spreadsheet provided by R. Trappitsch and I. Leya (University of Bern, Switzerland) - see also Trappitsch and Leya (2013) and http://noblegas.unibe.ch (access 15/12/2013). **GCR** production rates for $^{21}Ne_{cos}$ calculated using an Excel spreadsheet provided by U. Ott (MPIC Mainz, Germany) using production rates from Leya et al. (2001) for the lunar surface converted to a 4π irradiation. **GCR** production rates for $^{38}Ar_{cos}$ calculated using an Excel file provided by U. Ott (MPIC Mainz, Germany) using production rates for Fe and Ni from Leya et al. (2001) and for Ca from Hohenberg et al. (1978) for the lunar surface converted to a 4π irradiation.*

Cosmogenic nuclide	Assumed meteoritic composition	Elemental production rates at 1 AU (in 10^{-8} cc STP/g/Ma)		References for meteoritic compositions used to calculate the production rates
		SCR	GCR	
$^{21}Ne_{cos}$	OC (L)	1.489	0.273	Wasson and Kallemeyn (1988)
	OC (H)	1.390	0.256	Wasson and Kallemeyn (1988)
	CC (CI)	0.967	0.173	Palme and Jones (2003); Wasson and Kallemeyn (1988)
	EUC	0.814	0.198	Mittlefehldt et al. (1998)
	ANG	0.909	0.213	Mittlefehldt et al. (1998)
$^{38}Ar_{cos}$	OC (L)	0.230	0.035	Wasson and Kallemeyn (1988)
	OC (H)	0.220	0.040	Wasson and Kallemeyn (1988)
	CC (CI)	0.164	0.027	Palme and Jones (2003); Wasson and Kallemeyn (1988)
	EUC	1.253	0.102	Mittlefehldt et al. (1998)
	ANG	1.995	0.155	Mittlefehldt et al. (1998)

<u>Note:</u> *SCR was calculated using a rigidity spectrum with $J_0 = 100$ cm^{-2} s^{-1} and $R_0 = 125$ MV. ; OC = ordinary chondrite; CC = carbonaceous chondrite, EUC = Eucrite; ANG = Angrite.*

Based on ^{21}Ne, most of the MMs show calculated CRE-ages from below 0.01 to about 0.8 Ma and started their travel at between 1 AU and 1.96 AU. Three MMs seem to be different. UnMM 45b.17(1) has a CRE-age of 8.5 Ma and a travel distance of 4.3 AU. Even older ages and longer distances are indicated for the two 45c.29 particles. Depending on the assumed chemical composition, the calculated CRE-ages are between about 46 Ma and 71 Ma and the travel started at about 9-12 AU for 45c.29(1). The corresponding CRE-ages of the second particle 45c.29(2) are about 11-19 Ma and travel started at about 4.6-6 AU. Probably the truth lies somewhat in-between the results of those both particles.

For reasons given above (systematic uncertainties resulting in generally upper limits to cosmogenic Ar only), we list ^{38}Ar CRE ages and travel distances only for the UnMM 45b.17 and for the "special" UnMM 45c.29 (little affected by the systematic uncertainties). The resulting CRE-ages are 4.7 for 45b.17, for 45c.29 they are between 5.7 and 83 Ma (45c.29(1)) and between 21 and 186 Ma (45c.29(2)), depending on their mineralogical parentage (Table 30).

Bastian Baecker | Chapter 5 - Micrometeorites from the Transantarctic Mountains (TAM) - Noble gases show indications for multiple populations

140

Table 29. Cosmic ray exposure ages using $^{21}Ne_{cos}$ for the TAM MMs (where available) along with orbital distance using production rates from Table 28. Mean meteoritic elemental compositions have been assumed based on the mineralogical and petrological pre-analysis (where available) made and provided by C. Cordier (2010 at MNA, University of Siena, Italy - now at ISTerre, University of Grenoble, France - see Appendix D). For the "special" MM 45c.29 results for both achondritic and chondritic compositions are given.

Sample	Weight (µg) of whole sample (calculated) [%]	Size (µm) of whole sample [§]	Assumed composition	$^{21}Ne_{cos}$ (10^{-8} cc STP/g)	CRE [#] SCR + GCR (Ma)	Starting position (AU)
45b.08 (1) (Sc)	273.5	677	OC (L)	0.886 (28)	0.81 (3)	1.74 (3)
45b.09 (1) (Un)	248.4	740	OC (L)	0.641 (18)	0.58 (2)	1.70 (2)
45b.10 (2) (Un)	243.7	624	OC (L)	0.035 (8)	0.02 (1)	1.02 (1)
45b.13 (1) (Sc)	343.1	679	OC (L)	0.005 (2)	< 0.01	< 1.00
45b.16 (Un)	138.3	518	OC (L)	0.109 (10)	0.07 (1)	1.08 (1)
45b.17 (1) (Un)	223.6	555	OC (L)	4.41 (25)	8.5 (7)	4.28 (16)
45b.18 (1) (Un)	64.4	560	CC (CI)	0.072 (27)	0.08 (4)	1.24 (10)
45b.20 (2) (Sc)	166.6	707	OC (L)	0.018 (3)	~0.01	<1.02
45b.22 (2) (Sc)	65.4	443	OC (L)	0.194 (24)	0.14 (2)	1.26 (3)
45c.21 (CS)	337.9	638	OC (L)	0.0005 (5)	< 0.01	< 1.00
45c.27 (2) (Sc)	177.9	717	OC (L)	0.020 (3)	0.01 (1)	1.02 (1)
45c.29 (1) (Un)	335.7	647	OC (L)	16.14 (38)	46.0 (1.3)	9.31 (12)
			EUC		70.7 (2.0)	11.52 (15)
			ANG		64.8 (1.8)	11.03 (14)
45c.29 (2) (Un)	335.7	647	OC (L)	5.32 (13)	10.6 (4)	4.55 (7)
			EUC		19.0 (5)	6.02 (7)
			ANG		17.0 (5)	5.71 (8)
45c.31 (1) (Sc)	352.8	915	OC (L)	0.108 (13)	0.07 (1)	1.11 (1)
45c.33 (1) (Un)	305.5	774	OC (L)	0.161 (11)	0.10 (1)	1.13 (1)
X1 (45c.35(1)) (Un)	55.6	371	OC (H)	0.710 (75)	0.78 (12)	1.96 (11)
45c.35 (2) (Un)	55.6	371	OC (H)	0.608 (71)	0.62 (10)	1.81 (10)
45c.35 (3) (Un)	55.6	371	OC (H)	0.138 (29)	0.09 (2)	1.15 (3)

<u>Note:</u> [%]*Weights were calculated using assumed densities (see text and formulas above)* [§]*Sizes of MMs are geometric mean of major and minor axis;* [#] *CRE-ages calculated assuming 4π irradiation with GCR and SCR; OC = ordinary chondrite; CC = carbonaceous chondrite, EUC = Eucrite; ANG = Angrite.*

Bastian Baecker | Chapter 5 - Micrometeorites from the Transantarctic Mountains (TAM) - Noble gases show indications for multiple populations

141

Osawa and Nagao (2002) were able to obtain CRE-ages using $^{21}Ne_{cos}$ results for three MMs from Dome Fuji (out of 27, for the others no cosmogenic Ne could be obtained) as well. These three samples contain cosmogenic ^{21}Ne concentrations of 8.6×10^{-8} to 1.3×10^{-7} cc STP/g, which are overall higher than the ones measured for the TAM MMs (except the 45c.29 particles and 45b.17(1)) - see Table 29 and 30. Using these authors "Model 1" - which calculates CRE-ages using $^{21}Ne_{cos}$ production by GCR and SCR and assuming that the SCR has a stronger impact (square of heliocentric distance) while approching the Sun - agrees in the broadest sense with the model of Trappitsch and Leya (2013). Osawa and Nagao (2002) calculated CRE-ages of 24 to 159 Ma with travel distances of 16 to 42 AU for the three MMs using the cosmogenic Ne concentrations mentioned above. Trappitsch and Leya (2013) calculated similar "real" ages of 37 to 233 Ma and travel distances of 23 to 34 AU for the same particles.

Table 30. Cosmic ray exposure ages using $^{38}Ar_{cos}$ for the TAM MMs 45b.17 and 45c.29 along with orbital distance using production rates from Table 28. Results for both assumed achondritic and chondritic compositions are given.

Sample	Weight (µg) of <u>whole</u> sample (calculated) [%]	Size (µm) of <u>whole</u> sample [§]	Assumed composition	$^{38}Ar_{cos}$ (10^{-8} cc STP/g)	CRE [#] SCR + GCR (Ma)	Starting position (AU)
45b.17 (1) (Un)	223.6	555	OC (L)	0.431 (38)	4.7 (6)	3.27 (21)
45c.29 (1) (Un)	335.7	647	OC (L)	3.51 (35)	82.6 (9.6)	12.4 (7)
			EUC		13.1 (2.2)	5.03 (43)
			ANG		5.7 (1.0)	3.41 (29)
45c.29 (2) (Un)	335.7	647	OC (L)	7.23 (33)	186 (9)	18.6 (0.5)
			EUC		42.0 (2.7)	8.91 (29)
			ANG		21.2 (1.7)	6.35 (24)

<u>Note:</u> [%]*Weights were calculated using assumed densities (see text and formulas above)* [§]*Sizes of MMs are geometric mean of major and minor axis;* [#] *CRE-ages calculated assuming 4π irradiation with GCR and SCR; OC = ordinary chondrite; CC = carbonaceous chondrite, EUC = Eucrite; ANG = Angrite.*

Bastian Baecker | Chapter 5 - Micrometeorites from the Transantarctic Mountains (TAM) - Noble gases show indications for multiple populations

142

5.4.8 Evidences for an achondritic parentage of MM 45c.29?

As already described in the previous chapter, the unmelted MM 45c.29 is different from all the other TAM MMs measured. Table 31 shows a summary of significant noble gases measured for the two particles of this MM. It was possible to obtain noble gas results for all isotopes, with relatively small errors. In the case of helium especially 45c.29(1) plots in the direction of spallation (see Fig. 47). He data in Table 31 shows a low ^{3}He/^{4}He ratio for 45c.29(2) of only ~6 x 10^{-4}. When comparing the results for both particles, it is obvious that ^{4}He is making the main difference in terms of the ^{3}He/^{4}He ratio (^{3}He factor 2; ^{4}He factor 10). The ^{4}He excess in particle 45c.29(2) may have a radiogenic origin (U, Th, Pu) which would correlate with the results obtained for Xe (excess of heavy isotopes of fission origin). This is supported by the fact that solar ^{20}Ne is rather similar in both particles, indicating that the difference in excess ^{4}He is not of solar wind origin. The Ne plot (Fig. 48) shows cosmogenic contributions for both particles, as well, though here again, the effect in 45c.29(1) is somewhat more pronounced. For Ar we have a similar picture (see Fig. 50). In this case 45c.29(2) has the larger cosmogenic contributions (see previous chapter). For Kr in general it is difficult to find strong trends (Figs. 52 and 53). Xe on the other hand provides plenty of information regarding components.

*Table 31. **He, Ne, Ar, Kr and Xe** results UnMM 45c.29(1) and (2). Given are the totals, calculated from the individual measurement steps as indicated, for details see Appendix. Uncertainties in the last digits are given in parenthesis.*

Sample	Particle no.	^{4}He	^{3}He	^{4}He	^{3}He	^{3}He/^{4}He
		(10^{-12} cc STP)		(10^{-8} cc STP/g)		(10^{-4})
45c.29 (Un)	1	87.3 (7.0)	1.30 (2)	395 (32)	5.90 (11)	149.4 (12.3)
45c.29 (Un)	2	1064 (45)	0.639 (28)	4396 (190)	2.64 (12)	6.01 (36)

Sample	Particle no.	^{22}Ne	^{22}Ne	^{20}Ne/^{22}Ne	^{21}Ne/^{22}Ne
		(10^{-12} cc STP)	(10^{-8} cc STP/g)		
45c.29 (Un)	1	6.42 (10)	29.06 (54)	5.30 (13)	0.571 (7)
45c.29 (Un)	2	4.04 (6)	16.68 (28)	8.26 (8)	0.340 (5)

Sample	Particle no.	^{36}Ar	^{36}Ar	^{40}Ar	^{38}Ar/^{36}Ar	^{40}Ar/^{36}Ar
		(10^{-12} cc STP)	(10^{-8} cc STP/g)	(10^{-8} cc STP/g)		
45c.29 (Un)	1	12.0 (3)	54.2 (1.3)	2848 (210)	0.2454 (66)	50.5 (3.3)
45c.29 (Un)	2	9.66 (38)	39.9 (1.6)	4575 (155)	0.3474 (30)	108 (3)

Sample	Particle no.	^{84}Kr	^{84}Kr	^{80}Kr	^{82}Kr	^{83}Kr	^{86}Kr
		(10^{-12} cc STP)	(10^{-8} cc STP/g)	$\equiv$ ^{84}Kr			
45c.29 (Un)	1	0.159 (6)	0.720 (30)	0.043 (2)	0.197 (9)	0.201 (7)	0.332 (14)
45c.29 (Un)	2	0.228 (16)	0.940 (65)	0.044 (2)	0.182 (4)	0.195 (4)	0.318 (6)

Sample	Part. no.	^{132}Xe-INT	^{132}Xe-INT	^{128}Xe	^{129}Xe	^{130}Xe	^{131}Xe	^{134}Xe	^{136}Xe
		(10^{-12} cc STP)	(10^{-8} cc STP/g)			$\equiv$ ^{132}Xe (INT)			
45c.29 (Un)	1	0.037 (5)	0.169 (21)	0.070 (6)	0.967 (25)	0.141 (5)	0.783 (22)	0.398 (12)	0.365 (14)
45c.29 (Un)	2	0.031 (1)	0.129 (6)	0.065 (4)	1.060 (23)	0.146 (4)	0.798 (16)	0.414 (11)	0.396 (13)

Bastian Baecker | Chapter 5 - Micrometeorites from the Transantarctic Mountains (TAM) - Noble gases show indications for multiple populations

143

As evident from Fig. 56, where $\delta(^{130}Xe/^{132}Xe)_{Air}$ is plotted vs. $\delta(^{136}Xe/^{132}Xe)_{Air}$, both particles (more or less) plot in the direction of ^{244}Pu fission. At least 45c.29(1) seems to have also obtained a small fraction of Earth atmosphere like Xe. A different picture is visible in Fig. 57 ($\delta(^{129}Xe/^{132}Xe)_{Air}$ vs. $\delta(^{136}Xe/^{132}Xe)_{Air}$), here 45c.29(1) does not show any contributions from air like Xe and plots clearly in the direction of ^{244}Pu. 45c.29(2), however, seems to plot in the direction of Xe-HL (primordial Xe released out of nano-diamonds). This may be more of a coincidence and is more likely to also reflect the presence of radiogenic ^{129}Xe (see also above and Fig. 71 below). In Fig. 58 and Fig. 59. which show $\delta(^{131}Xe/^{136}Xe)_{Air}$ plotted vs. $\delta(^{132}Xe/^{136}Xe)_{Air}$ and $\delta(^{130}Xe/^{136}Xe)_{Air}$ plotted vs. $\delta(^{132}Xe/^{136}Xe)_{Air}$ again, both particles, 45c.29(1) and (2) are plotting distinctly in the direction of ^{244}Pu fission and / or Xe-HL, though here once more 45c.29(1) is showing Xe Earth atmosphere contributions. Obviously, the situation is complicated, so it is not straightforward to come to an overall conclusion. Contributions acquired during transition of Earth atmosphere seem to be low and the particles apparently retained most of their original noble gas composition. A possible explanation is an achondritic parentage, as discussed in detail below.

Fig. 71 is a plot of Xe isotopes shown in per mil-deviations [δ] from solar wind xenon composition (Meshik et al. (2012)), along with Xe data for the two measured particles 45c.29 (1) and (2) as well as data for an angrite (Sahara 99555; Busemann and Eugster (2002)), an eucrite (Millbillillie; Busemann and Eugster (2002)), Earth Atmosphere (EA; Basford et al. (1973)) and the primordial Q-Xe component (Busemann et al. (2000)). The isotopic data for the eucrite and the angrite shown in this figure have been corrected for cosmogenic contributions based on the measured $^{126}Xe/^{130}Xe$ ratio and the spallation systematics derived from the angrite Angra dos Reis (Hohenberg et al. (1981)). UnMM 45c.29(1) and especially 45c.29(2) seem to be similar to eucrites and angrites in that the heavy Xe isotopes are enhanced due to the presence of fission Xe. However, unlike for the angrite and eucrite, there is no strong deficit in $^{129}Xe/^{132}Xe$ in Fig. 71, so the particles, unlike eucrites/angrites apparently also contain radiogenic ^{129}Xe. Obviously UnMM 45c.29 is not as volatile-depleted as the angrites and the eucrites. The fission component seen in the heavy Xe isotopes is from ^{244}Pu, as clearly obvious in Fig. 72 and Fig. 73, which are three isotope plots of $^{132}Xe/^{130}Xe$ vs. $^{136}Xe/^{130}Xe$ and $^{134}Xe/^{130}Xe$ vs. $^{136}Xe/^{130}Xe$. In particular, this is clearly demonstrated in this plot also for 45c.29(2), which in some of the plots discussed earlier (Figs. 58 and 59) appeared to possibly contain Xe-HL as the component rich in the heavy isotopes. The other 2 ScMMs and 4 UnMMs plotting in the direction of ^{244}Pu fission do not contain high amounts of radiogenic Xe, here rather mass fractionation is the reason for their characteristics in Xe - as mentioned already in the Xe chapter 5.4.5.

Coming to the other noble gases, both particles 45c.29(1) and 45c.29(2) show slightly to remarkably high $^{38}Ar/^{36}Ar$ ratios of 0.245 and 0.348, respectively, which is an indication for a high cosmogenic to trapped noble gas ratio. Remarkable is in particular the low $^{21}Ne_{cos}/^{38}Ar_{cos}$ ratio of 0.74 (4) of 45c.29(2), which, similar as the Xe isotopes discussed above, points to the possibility of achondritic parentage. This is because the result indicates that especially 45c.29(2) must have a high Ca to Mg ratio, which are the most important target elements for cosmogenic Ar and Ne,

Bastian Baecker | Chapter 5 - Micrometeorites from the Transantarctic Mountains (TAM) - Noble gases show indications for multiple populations

144

respectively (with Fe also contributing significantly to Ar for a chondritic Fe/Ca ratio). Again, as mentioned earlier, also partial degassing of especially $^{21}Ne_{cos}$ might be another - less likely - possibility to lower the Ne/Ar ratios.
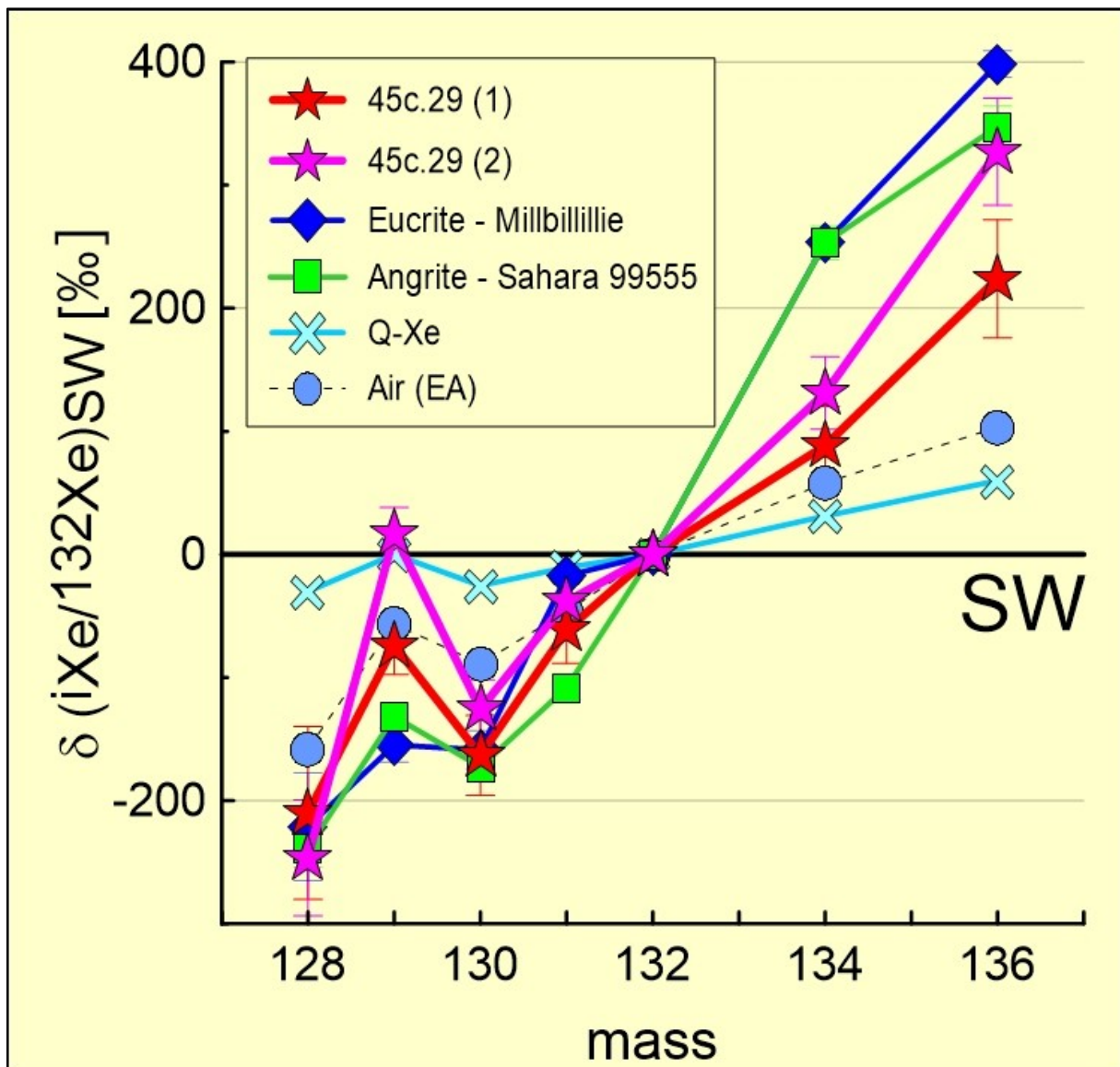
Figure 71. Isotope plot of Xe showing our data in the "special" unmelted MM 45c.29 (1) and 45c.29 (2) compared to EA (Basford et al. (1973)), Q-Xe (Busemann et al. (2000)), an eucrite, Millbillillie (Busemann and Eugster (2002)) and an angrite, Sahara 99555 (Busemann and Eugster (2002)). Isotopes shown in per mil-deviations from SW Xe (Meshik et al. (2012)) composition. The eucrite and angrite isotopic data have been corrected for cosmogenic contributions via $^{126}Xe/$ ^{130}Xe and the spallation systematics derived from the angrite Angra dos Reis by Hohenberg et al. (1981).

Bastian Baecker | Chapter 5 - Micrometeorites from the Transantarctic Mountains (TAM) - Noble gases show indications for multiple populations

145
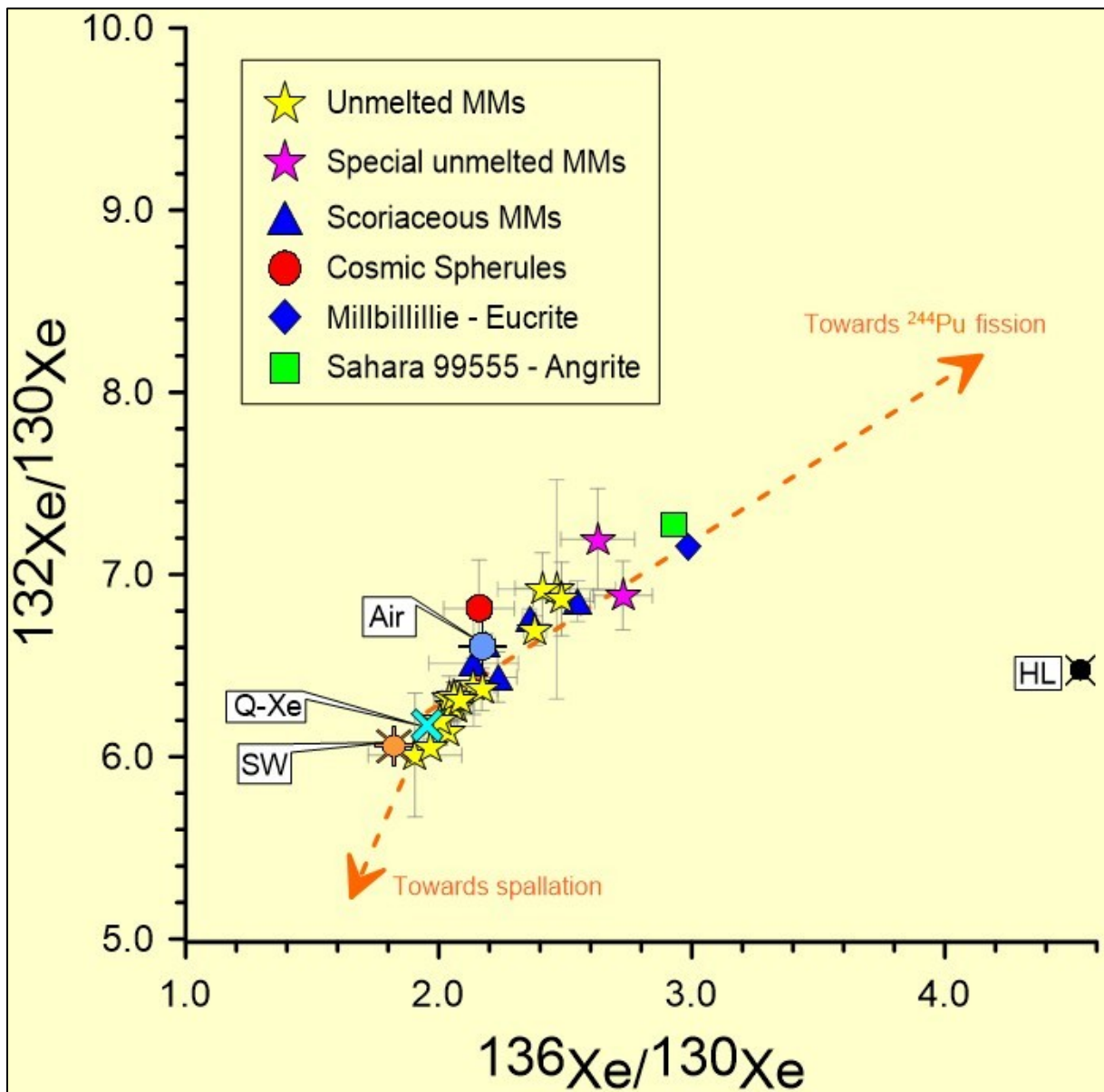
Figure 72. Three isotope plot of ^{132}Xe / ^{130}Xe vs. ^{136}Xe / ^{130}Xe showing data of our TAM-MM samples. Also plotted for comparison are SW (Meshik et al. (2012)), Q(P1) (Q-Xe) (Busemann et al. (2000)), EA (Air) (Basford et al. (1973)), an eucrite, Millbillillie (Busemann and Eugster (2002)) and an angrite, Sahara 99555 (Busemann and Eugster (2002)). The orange dashed lines are mixing lines representing on the one hand ^{244}Pu fission (Ozima and Podosek (2002)) and on the other spallation Xe (Hohenberg et al. (1981)).

Table 32 shows a roster of $^{21}Ne_{cos}/^{38}Ar_{cos}$ for different chondrite and achondrite groups (typical values), compared to 45c.29(2). None of these is below 1. 45c.29(1), on the other hand, shows a ratio of 4.60 (47) which is similar, but still not identical, to typical values for chondrites.

In our assessment of CRE ages (chapter 5.4.7) both samples show high CRE-ages for all choices of compositions, both from $^{21}Ne_{cos}$ (~46-71 Ma, 45c.29(1) and 11-19 Ma, 45c.29(2)) and from $^{38}Ar_{cos}$ (~5.7-83 Ma, 45c.29(1) and 21-186 Ma, 45c.29(2)), (see Table 29 and Table 30). Furthermore, both, C. Cordier and L. Folco report in personal communication (2014) that UnMM 45c.29 shows a heterogeneous and complex mineralogical and petrological composition with no direct and easy evidence of its parentage. Impact and shock related mechanism may have changed

Bastian Baecker | Chapter 5 - Micrometeorites from the Transantarctic Mountains (TAM) - Noble gases show indications for multiple populations

146

the original composition (petrology/mineralogy and/or noble gas inventory) of this MM (C. Cordier, pers. comm., 2014).
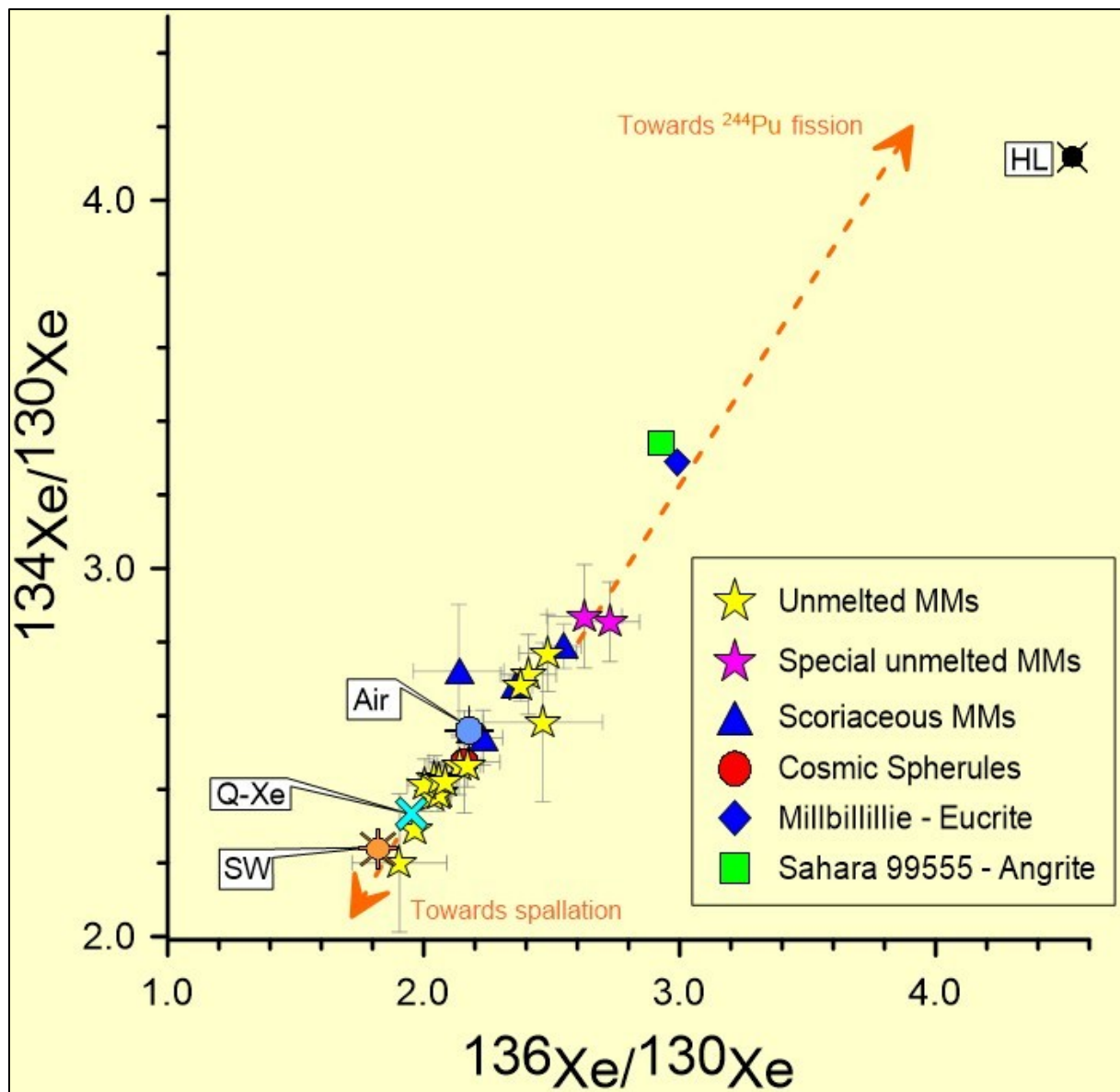
Figure 73. Three isotope plot of ^{134}Xe / ^{130}Xe vs. ^{136}Xe / ^{130}Xe showing data of our TAM-MM samples. Also plotted for comparison are SW (Meshik et al. (2012)), Q(P1) (Q-Xe) (Busemann et al. (2000)), EA (Air) (Basford et al. (1973)), an eucrite, Millbillillie (Busemann and Eugster (2002)) and an angrite, Sahara 99555 (Busemann and Eugster (2002)). The orange dashed lines are mixing lines representing on the one hand ^{244}Pu fission (Ozima and Podosek (2002)) and on the other spallation Xe (Hohenberg et al. (1981)).

Bastian Baecker | Chapter 5 - Micrometeorites from the Transantarctic Mountains (TAM) - Noble gases show indications for multiple populations

147

Table 32. Comparison of cosmogenic $^{21}Ne/^{38}Ar$ ratios (calculated for GCR) typically measured in different achondrite groups to our unmelted MM 45c29(2). The differences between SCR and GCR are small (compare Table 28).

Sample	$^{21}Ne_{cos}/^{38}Ar_{cos}$	Reference
Un 45c29	0.74 (± 0.04)	This work
Angrites	~1.05	Compilation Schultz and Franke (2004)
Eucrites	1.3	Eugster and Michel (1995)
Howardites	2.8	Eugster and Michel (1995)
Mesosiderites (silicates)	5.1	Albrecht et al. (2000)
Acapulcoites	5.2	Weigel et al. (1999)
Lodranites	6.5	Weigel et al. (1999)
Carbonaceous chondrites	6.5	Eugster (1988)
Ordinary chondrites	6.8	Eugster (1988)
Diogenites	11.6	Eugster and Michel (1995)

Another possibility for explaining the unusual cosmogenic Ne and Ar results is that - provided 45c.29 is of primitive (maybe C3) origin - the particle 45c.29(2) may resemble a large CAI fragment, i.e. high temperature inclusion, which was separated from the other parts of the MM while cutting at MNA, Siena University, Italy. Using, e.g. the mean chemical composition of refractory inclusions from C3V chondrites given by Sylvester et al. (1993) to calculate the SCR and GCR elemental production rates (see Table 33 and chapter 5.4.7), the resulting $^{21}Ne_{cos}/^{38}Ar_{cos}$ ratios are 0.23 for SCR and 0.65 for GCR irradiation. Both results are below 1, similar as observed for 45c.29(2) (Table 32). The observed presence of ^{244}Pu fission Xe would also be consistent with observations on CAIs (e.g. Drozd et al. (1977); Göbel et al. (1982)).

*Table 33. SCR and GCR production rates for 45c.29(2) with CAI elemental composition along with an assumed 4π irradiation at 1AU. **SCR** production rates calculated using an Excel spreadsheet provided by R. Trappitsch and I. Leya (University of Bern, Switzerland) - see also Trappitsch and Leya (2013) and http://noblegas.unibe.ch (access 15/12/2013). **GCR** production rates calculated using an Excel spreadsheet provided by U. Ott (MPIC Mainz, Germany) using production rates from Hohenberg et al. (1978)) for the lunar surface converted to a 4π irradiation.*

Cosmogenic nuclide	Assumed meteoritic composition	Elemental production rates at 1 AU (in 10^{-8} cc STP/g/Ma)		References for the CAI composition used to calculate the production rates
		SCR	**GCR**	
$^{21}Ne_{cos}$	CAI	0.913	0.180	Sylvester et al. (1993)
$^{38}Ar_{cos}$	CAI	3.850	0.275	Sylvester et al. (1993)

<u>Note:</u> *SCR was calculated using a rigidity spectrum with $J_0 = 100$ cm^{-2} s^{-1} and $R_0 = 125$ MV. ; CAI = Calcium-Aluminum-rich inclusion*

Our results suggest that this particle has a complex history with no direct or unique conclusion concerning its parentage. Noble gases leave room for interpretation in the chondritic and or achondritic direction. In case of an achondrite source, the noble gas data suggests that it may represent a hitherto unknown unique type of achondrite. The sample shows, besides the cosmogenic contributions, the influence of solar wind, indicating that this MM collected SW as a single particle in space. However, given its size, UnMM 45c.29 would have survived only about 3-4 Ma due to the Poynting-Robertson effect (e.g. Wyatt and Whipple (1950), Kimura et

Bastian Baecker | Chapter 5 - Micrometeorites from the Transantarctic Mountains (TAM) - Noble gases show indications for multiple populations

148

al. (2002)) in the inner solar system (travel from 2.5 AU to 1 AU). Therefore, the possibility needs to be considered that this MM was part of a larger meteoroid/planetoid/moon **or** the regolith of an asteroid for some tens of Ma. If the MM was part of an meteoroid it must have split off some time before Earth atmosphere entry in order to obtain the SW signature. This is evident of the magnetite rim by which this MM is surrounded. The cosmogenic contributions would have been implanted mostly while part of the precursor meteoroid. If the MM was part of an asteroid, planetoid or moon, it may have been separated due to e.g. an impact, at a larger distance to Earth. It is possible, in this case that the MM obtained SW already while in the regolith of the parent body, in addition to SW implanted during its journey to Earth. Again, only a maximum travel time of ~3-4 Ma is possible. In any case, more research has to be performed on this unusual MM to unravel its history. It is foreseen that in the near future a more detailed petrographic analysis from C. Cordier and L. Folco will be available, including oxygen isotope analysis.

5.5 Summary and Conclusions

The TAM MM collection includes a variety of different sample sets (Rochette et al. (2008)). The numerous number of large MMs and the suitability for multi-analytical approach shows the importance of this collection. The comprehensive noble gas analysis (He-Xe) for 29 particles of 25 TAM MMs on the one hand confirms results obtained in earlier MM research (e.g. Olinger et al. (1990), Sarda et al. (1991), Osawa et al. (2000), Osawa and Nagao (2002)), showing first that MMs are extraterrestrial and contain several different components (SW, "FSW", Q(P1) and SCR, GCR). In addition, they show that a population of MMs has acquired isotopically fractionated Earth atmosphere, most likely during transition through the Earth's atmosphere (see also chapter 7). MMs may have made and may still make important contributions to the (early) Earth's noble gas inventory.

In this work we focused on ScMMs and UnMMs due to expected higher gas amounts. Some UnMMs have a clear relationship to carbonaceous chondrites and phase-Q. Also, the noble gas results indicate the probability of multiple populations and sources for TAM MMs.

UnMM 45c.29 seems to resemble on the one hand a primitive (achondrite) source, contains ^{244}Pu fission xenon and appears similar, but not identical, in this respect to angrites and eucrites. On the other hand this MM shows a mineralogically complex history and possibly was altered due to shock and impact on the parent body (C. Cordier and L. Folco; personal communication, 2014).

The high sensitivity noble gas mass spectrometer "Noblesse" made it possible to especially measure Xe in TAM MMs, with mostly low uncertainties. The CRE-ages suggest that most MMs travelled only short distances until reaching Earth's atmosphere and also lost noble gases during transition through the atmosphere, reflecting the thermal history of especially Cosmic Spherules and scoriaceous MMs. In future work the analyzed noble gases will be combined with petrographic data and oxygen isotopic analyses performed by C. Cordier and L. Folco.

Bastian Baecker | Chapter 5 - Micrometeorites from the Transantarctic Mountains (TAM) - Noble gases show indications for multiple populations

149

Chapter 6 - Micrometeorites from the CONCORDIA collection (Dome C) and from Cap Prudhomme, Antarctica – Noble gases show the possibility for a single population

This chapter provides basic mineralogical information, remarks concerning the measurement methodology for the specific samples here, followed by presentation of noble gas results and discussions as well as conclusions regarding the MM samples collected from the ultraclean snow the CONCORDIA station at Dome C, central Antarctica. For the complete data compilation see the Appendix. Our colleagues J. Duprat, C. Engrand and M. Maurette from CSNSM, University of South Paris, Orsay, provided us with MMs from the CONCORDIA collection (Duprat et al. (2007) and from Cap Prudhomme (e.g. Maurette et al. (1991)) and contributed by giving mineralogical information and SEM images of the samples (see chapter 6.2 and Appendix).

6.1 Introduction

In January 2000 and January 2002 micrometeorites with sizes of 30 to 1000 µm were collected by J. Duprat, C. Engrand and colleagues from snow near the CONCORDIA station at Dome C (see Fig. 44, inset picture). The station is located at S 75º, E 123º (see Duprat et al. (2007)). Using snow melting, the samples were extracted and filtered out of snow layers formed in the 1970's to 1980's, and then stored at the CONCORDIA station (Duprat et al. (2007)). The samples from Cap Prudhomme (Adélie land) had been extracted earlier from ice which was recovered during expeditions in 1994 (Maurette (2006)).

6.2 Mineralogy and petrology

Chapter 6.2 gives basic information about all acquired samples and an overview of the MMs selected for noble gas measurements. Further mineralogical and petrological information regarding the measured MM samples can be found in the Appendix. Some of the information provided is from the detailed petrological work of J. Duprat, C. Engrand and colleagues at CSNSM, Orsay.

6.2.1 Sample set micrometeorites - CONCORDIA collection (Dome C) and from Cap Prudhomme

Overall we acquired 28 different MM samples from the CONCORDIA collection and from Cap Prudhomme. The MMs from the CONCORDIA collection comprised of 18 particles from 11 different samples of crystalline (Xtal) and fine grained (FgC) origin. Ten of these were selected for our noble gas study. The 32 MM particles from the Cap Prudhomme sample set included 17 Xtal-MMs, with the remainder FgC- and Sc MMs. We measured only one scoriaceous MM from this collection. Table 34 provides information about all the acquired Dome C / Cap Prudhomme MM samples. An illustration of the general shape and form of selected Dome C MMs is shown in Fig. 74. Duprat et al. (2007) describe them as rich in Fe-sulfides. Overall the fine

Bastian Baecker | Chapter 6 - Micrometeorites from the CONCORDIA collection (Dome C) and from Cap Prudhomme, Antarctica – Noble gases show the possibility for a single population

150

grained matrix shows elemental abundances characteristic for undepleted primitive CI carbonaceous chondrites. As pointed out by Duprat et al. (2007), the MMs from Dome C snow have been little affected by terrestrial weathering. This contrasts with the samples from Cap Prudhomme (Adélie land), which show much higher terrestrial weathering effects (C. Engrand; personal communication, 2010; see also Duprat et al. (2007)).
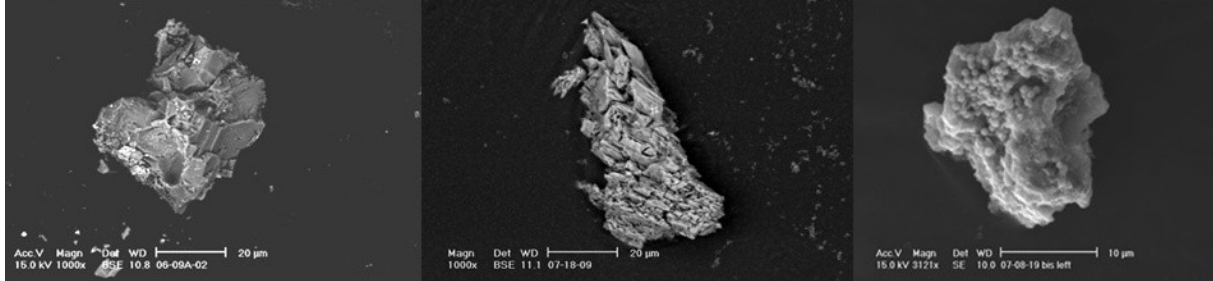
Figure 74. Micrographs of MMs from Dome C. On the left and in the middle Xtal unmelted MMs; on the right a FgC unmelted MM (image credit J. Duprat and C. Engrand, CSNSM, Orsay, France).

The respective sample name of each Dome C sample consists of the following combination: DC (Dome C) 06 (2006) 09 (number of the nylon net where particles were selected from) 247 (number of sample) PL (particle) 07_107C (number of particle) 7 (position). The Cap Prudhomme samples have a similar code system CP (Cap Prudhomme) 9-1-1994 (date) PL (particle) 10-109D (number of particle) 9 (position).

Bastian Baecker | Chapter 6 - Micrometeorites from the CONCORDIA collection (Dome C) and from Cap Prudhomme, Antarctica – Noble gases show the possibility for a single population

151

Table 34. Roster of 50 particles from 28 different MM samples acquired in 2010 at CSNSM, University of South Paris, Orsay, with the aid of J. Duprat, C. Engrand and M.Maurette. The 28 samples comprise 6 Xtal and 5 FgC MMs from the CONCORDIA collection (Dome C) and 7 Xtal, 9 FgC and 1 Sc MMs from Cap Prudhomme. The MMs were collected at Dome C and Cap Prudhomme, Antarctica by J. Duprat, C. Engrand, M. Maurette and colleagues (see Duprat et al. (2007) and Maurette (2006)). Samples measured for noble gases are marked in yellow. For abbreviations see chapter 3.1.4. Petrographical description and SEM images are in the Appendix.

Sample	Particle number	Noble gas measurement date	Weight (μg) (calculated)	Diameter (μm)	Class
DC 06_07_213	PL 09_20 7 (1)	04/23/12	~1.1	97 x 91	Xtal
DC 06_07_213	PL 09_20 7 (2)	Not measured	~0.3	92 x 63	Xtal
DC 06_08_01	PL06_09A 1	04/25/12+04/26/12	~1.4	110 x 92	Xtal
DC 06_08_40	PL06_09D 3 (1)	Not measured	~0.4	98 x 59	Xtal
DC 06_08_40	PL06_09D 3 (2)	Not measured	~0.1	50 x 25	Xtal
DC 06_08_40	PL06_09D 3 (3)	Not measured	~0.1	63 x 48	Xtal
DC 06_08_40	PL06_09D 3 (4)	Not measured	~0.1	44 x 31	Xtal
DC 06_09_11	PL07_01A 11	04/26/12	~1.3	137 x 111	FgC/Sc
DC 06_09_50	PL07_02B 2	04/18/12+04/19/12	~3.3	141 x 134	FgC
DC 06_09_57	PL07_02B 9 (1)	10/24/12	~0.15	74 x 36	FgC
DC 06_09_57	PL07_02B 9 (2)	10/25/12	~0.05	19 x 18	FgC
DC 06_09_63	PL07_02C 3	01/16/12+01/17/12	~3.3	198 x 141	FgC/Xtal
DC 06_09_141	PL07_04C 9 (1)	10/24/12	~0.7	84 x 79	Xtal
DC 06_09_141	PL07_04C 9 (2)	Not measured	~0.4	93 x 64	Xtal
DC 06_09_149	PL07_05A 5 (1)	10/23/12	~0.3	85 x 60	Xtal
DC 06_09_149	PL07_05A 5 (2)	Not measured	~0.1	49 x 39	Xtal
DC 06_09_189	PL07_06A 9	10/18/12	~1.0	93 x 92	FgC/Sc
DC 06_09_247	PL07_07C 7	Not measured	~4.0	208 x 149	Xtal
CP 9-1-1994	PL 10-109-A 2	Not measured	1.5 ± 0.1	162 x 147	Xtal
CP 9-1-1994	PL 10-109-A 9 (1)	Not measured	15.0 ± 0.1	255 x 232	Xtal
CP 9-1-1994	PL 10-109-A 9 (2)	Not measured	n.a.	171 x 147	Xtal
CP 9-1-1994	PL 10-109-B 6 (1)	Not measured	11.2 ± 0.1	268 x 194	Xtal
CP 9-1-1994	PL 10-109-B 6 (2)	Not measured	3.6 ± 0.1	211 x 141	Xtal
CP 9-1-1994	PL 10-109-B 3 (1)	Not measured	2.3 ± 0.1	267 x 149	FgC
CP 9-1-1994	PL 10-109-B 3 (2)	Not measured	n.a.	137 x 106	FgC
CP 9-1-1994	PL 10-109-D 3 (1)	Not measured	6.9 ± 0.1	214 x 193	Xtal
CP 9-1-1994	PL 10-109-D 3 (2)	Not measured	4.1 ± 0.1	195 x 150	Xtal
CP 9-1-1994	PL 10-109-D 3 (3)	Not measured	2.0 ± 0.1	143 x 97	Xtal
CP 9-1-1994	PL 10-109-D 5 (1)	Not measured	8.2 ± 0.1	224 x 196	Xtal
CP 9-1-1994	PL 10-109-D 5 (2)	Not measured	7.2 ± 0.1	215 x 179	Xtal
CP 9-1-1994	PL 10-109-D 2	Not measured	1.8 ± 0.1	160 x 124	FgC
CP 9-1-1994	PL 10-109-D 6 (1)	Not measured	n.a.	147 x 73	FgC
CP 9-1-1994	PL 10-109-D 6 (2)	Not measured	1.4 ± 0.1	127 x 105	FgC
CP 9-1-1994	PL 10-109-D 6 (3)	Not measured	n.a.	n.a.	FgC
CP 9-1-1994	PL 10-109-D 7	Not measured	2.2 ± 0.1	190 x 163	Xtal
CP 9-1-1994	PL 10-109-D 8	Not measured	4.0 ± 0.1	169 x 143	FgC/Sc
CP 9-1-1994	PL 10-109-D 9	11/07/11+11/08/11	6.2 ± 0.1	252 x 188	Sc
CP 9-1-1994	PL 10-109-D 11 (1)	Not measured	3.1 ± 0.1	211 x 171	Xtal
CP 9-1-1994	PL 10-109-D 11 (2)	Not measured	n.a.	n.a.	Xtal
CP 9-1-1994	PL 10-109-C 4 (1)	Not measured	1.3 ± 0.1	197 x 117	FgC/Sc
CP 9-1-1994	PL 10-109-C 4 (2)	Not measured	1.0 ± 0.1	149 x 144	FgC/Sc
CP 9-1-1994	PL 10-109-C 4 (3)	Not measured	0.7 ± 0.1	114 x 89	FgC/Sc
CP 9-1-1994	PL 10-109-C 4 (4)	Not measured	n.a.	n.a.	FgC/Sc
CP 9-1-1994	PL 10-109-C 5 (1)	Not measured	3.5 ± 0.1	165 x 126	FgC
CP 9-1-1994	PL 10-109-C 5 (2)	Not measured	n.a.	159 x 119	FgC
CP 9-1-1994	PL 10-109-C 7 (1)	Not measured	1.9 ± 0.1	153 x 109	FgC
CP 9-1-1994	PL 10-109-C 8 (1)	Not measured	2.1 ± 0.1	176 x 112	FgC/Sc
CP 9-1-1994	PL 10-109-C 8 (2)	Not measured	n.a.	141 x 106	FgC/Sc
CP 9-1-1994	PL 10-109-C 9 (1)	Not measured	1.1 ± 0.1	145 x 135	FgC
CP 9-1-1994	PL 10-109-C 9 (2)	Not measured	n.a.	108 x 84	FgC

Bastian Baecker | Chapter 6 - Micrometeorites from the CONCORDIA collection (Dome C) and from Cap Prudhomme, Antarctica – Noble gases show the possibility for a single population

152

6.3 Addendum to the experimental procedure - CONCORDIA collection (Dome C) and from Cap Prudhomme

The main experimental procedure is explained in chapter 4. However, some important additions and remarks will be given here. AMMs from the CONCORDIA collection and from Cap Prudhomme were measured on the "Noblesse" some months after the first TAM MMs (see chapter 5). This was, to make sure that one had enough experience with the laser extraction and separation, as well as the operation of the "Noblesse" for measuring these small sized MMs. As shown in Table 34, we started by measuring samples with larger sizes first, then successively measuring smaller MMs, as soon as we reached a satisfying measurement and detection level. As can be seen in Table 34, the MMs were not selected and measured as a whole but as sample aliquots. In contrast to the MMs from TAM, the weights of the MMs from the CONCORDIA Collection (Dome C) were not measured using a microbalance (see chapter 4.1.2), but rather calculated from the observed size. This was, because the sample "freshness" should be preserved, avoiding contamination with terrestrial air, by keeping the samples covered with glass slides as long as possible. In addition, some of the Dome C MMs had sizes smaller than 50 µm which made it difficult weighing them, not only because of the correspondingly low weight, but also because they had to be moved with a thin brush under binocular microscope. MMs from Cap Prudhomme were handled similar to the TAM MMs. These samples were mostly large enough to place them on the microbalance by using "normal" eye-sight and they presumably had already "seen" contamination by terrestrial air in Antarctica by being deposited in water and sediments (see Maurette et al. (1991))

6.4 Noble gas results and discussion

We obtained noble gas results for 11 particles of overall 10 MMs from the CONCORDIA Collection (DC) and from Cap Prudhomme (CP) (see Table 34 and the Appendix). These particles comprised 4 crystalline (Xtal) MMs, 1 fine-grained carbonaceous, crystalline (FgC/Xtal) MM, 3 fine-grained carbonaceous (FgC) MMs, 2 fine-grained carbonaceous, scoriaceous (FgC/Sc) MMs and 1 scoriaceous MM. In most cases, it was sufficient to use a single laser power step to fully degas the particles, (see Appendix). In rare cases a second step was necessary . The results (totals) are presented in the following chapters and tables. The complete data set including individual extraction steps is given in the Appendix. All results shown in this chapter are corrected for blank and interferences (see Appendix), and, in case of Xe, the internal calibration approach (see chapter 4.3.5.1) has been used.

Bastian Baecker | Chapter 6 - Micrometeorites from the CONCORDIA collection (Dome C) and from Cap Prudhomme, Antarctica – Noble gases show the possibility for a single population

153

6.4.1 Helium (He)

Unlike the TAM MMs (see chapter 5.4.1) the MMs from Dome C and Cap Prudhomme show relatively high ^{3}He concentrations in the range of 1.2 x 10^{-8} cc STP/g to 156 x 10^{-8} cc STP/g (Table 35). Two samples show only upper limits. The errors obtained for our concentrations are high, mostly due to the large uncertainties of the (in most cases calculated) weight of the samples. The lowest DC and CP MM ^{3}He concentrations are in the range of the highest concentrations of the TAM MMs (~2 to ~5 x 10^{-8} cc STP/g), whereas the highest DC and CP MM concentrations are similar to the highest ones measured for AMMs by Osawa and Nagao (2002) of ~28 to ~250 x 10^{-8} cc STP/g. The results indicate that the MMs from the CONCORDIA Collection were able to retain ^{3}He much more efficient than the larger TAM MMs. This presumably is due to their small size and "freshness", indicating a more moderate thermal history and low weathering effects on Earth. ^{4}He is found in even larger concentrations of about 1.4 x 10^{-6} cc STP/g up to about 4.8 x 10^{-3} cc STP/g, which is about 10x higher than those found for TAM MMs, but in a similar range compared to AMMs measured by Osawa and Nagao (2002) (1 x 10^{-6} to 9.7 x 10^{-3} cc STP/g). Fig. 75 shows ^{3}He/^{4}He plotted versus ^{4}He for our measured MMs from DomeC and Cap Prudhomme and for Murchison (measured at the MPIC in 2011), along with AMM data from Stuart et al. (1999) and Osawa and Nagao (2002), as well as IDP data from Pepin et al. (2000). For comparison, also the isotope ratios for SW (Heber et al. (2012)), "FSW" (Benkert et al. (1993) and Wieler et al. (2007)) and HL and P3 (both Huss and Lewis (1994a)) are indicated by the dashed lines. Overall it seems that the FgC-type MMs contain more He than the other types, i.e. Xtal and Sc (see Table 35). However, it is also evident in Fig. 75 that Xtal-type MMs show higher ^{3}He/^{4}He ratios, whereas FgC-types plot near the SW isotopic composition. But even though the MMs from Dome C are of small size, they still do not show ^{4}He concentrations that are comparable to those in the IDPs measured by Pepin et al. (2000).

Bastian Baecker | Chapter 6 - Micrometeorites from the CONCORDIA collection (Dome C) and from Cap Prudhomme, Antarctica – Noble gases show the possibility for a single population

154

*Table 35. **He** results for 11 MMs from the CONCORDIA collection (Dome C) and from Cap Prudhomme. Given are the totals, calculated from the individual measurement steps as indicated, for details see Appendix. Uncertainties in the last digits are given in parenthesis. Values marked with $ are 2σ upper limits. For comparison also the compositions of SW, "FSW", Q (P1), HL and P3 are given.*

Sample	Particle no.	Step(s) used	^{4}He	^{3}He	^{4}He	^{3}He	^{3}He/^{4}He
			(10^{-12} cc STP)		(10^{-8} cc STP/g)		(10^{-4})
DC 06_07_213 (Xtal)	PL 09_20 7 (1)	all	16.2 (3.9)	0.013 (3)	1517 (392)	1.22 (30)	8.04 (2.66)
DC 06_08_01 (Xtal)	PL06_09A 1	1	19.5 (3.9)	0.028 (3)	1424 (304)	2.01 (27)	14.1 (3.3)
DC 06_09_11 (FgC/Sc)	PL07_01A 11	all	86.7 (4.2)	0.028 (6)	6714 (614)	2.13 (49)	3.18 (0.70)
DC 06_09_50 (FgC)	PL07_02B 2	1	12150 (188)	3.63 (15)	368171 (12533)	109.9 (5.7)	2.98 (0.13)
DC 06_09_57 (FgC)	PL07_02B 9 (1)	all	< 10 $	< 0.005 $	< 6411 $	< 3.62 $	-
DC 06_09_57 (FgC)	PL07_02B 9 (2)	all	< 1 $	0.070 (29)	< 1829 $	139.7 (57.7)	-
DC 06_09_63 (FgC/Xtal)	PL07_02C 3	all	3152 (43)	1.37 (18)	95526 (3169)	41.6 (5.6)	4.36 (0.58)
DC 06_09_141 (Xtal)	PL07_04C 9 (1)	all	8.69 (4.26)	0.044 (7)	1241 (634)	6.22 (1.38)	50.1 (26.0)
DC 06_09_149 (Xtal)	PL07_05A 5 (1)	all	47.9 (4.3)	0.121 (7)	15973 (5517)	40.4 (13.7)	25.3 (2.7)
DC 06_09_189 (FgC/Sc)	PL07_06A 9	all	4799 (68)	1.56 (3)	479919 (48472)	156.3 (15.9)	3.26 (0.08)
CP 9-1-1994 (Sc)	PL 10-109D 9	1	8.86 (5.67)	< 0.032 $	143 (92)	< 0.522 $	-

Component	References						^{3}He/^{4}He
							(10^{-4})
SW	[1]						4.645 (8)
"FSW"	[2]						2.17 (5)
Q (P1)	[3]						1.23 (2)
HL	[4]						1.70 (10)
P3	[4]						1.35 (10)

*References: [1] Heber et al. (2012); [2] Benkert et al. (1993); [3] Busemann et al. (2000); [4] Huss and Lewis (1994a); Note: For detailed information regarding **"FSW"** see Wieler et al. (2007).*

Bastian Baecker | Chapter 6 - Micrometeorites from the CONCORDIA collection (Dome C) and from Cap Prudhomme, Antarctica – Noble gases show the possibility for a single population

155

Figure 75. The ratio ^{3}He / ^{4}He in 10^{-4} units is plotted vs. ^{4}He in cc STP/g. Besides our AMM data, also data for the CM2 meteorite Murchison (obtained at MPIC in 2011), data of other AMM noble gas measurements from Stuart et al. (1999) and Osawa and Nagao (2002) as well as noble gas data for IDPs by Pepin et al. (2000) are shown. Plotted for comparison are the ^{3}He / ^{4}He ratios of SW (Heber et al. (2012)), "FSW" (Benkert et al. (1993) and Wieler et al. (2007)), HL and P3 (both Huss and Lewis (1994a)). Spallation He is characterized by much higher ^{3}He / ^{4}He (~0.2; e.g. Wieler (2002a)) than observed here.

Bastian Baecker | Chapter 6 - Micrometeorites from the CONCORDIA collection (Dome C) and from Cap Prudhomme, Antarctica – Noble gases show the possibility for a single population

156

6.4.2 Neon (Ne)

Unlike the MMs from TAM (see chapter 5.4.2), the measured ratios for the different DC and CP MMs show only little variation, possibly indicating a single population. However, the concentrations vary quite significantly (see Table 36 and the Appendix). Fig. 76 is a three isotope plot of Ne showing $^{20}Ne/^{22}Ne$ versus $^{21}Ne/^{22}Ne$ for our data, for Murchison (measured at the MPIC in 2011) and AMM data from Osawa and Nagao (2002). Also plotted for comparison are SW (Heber et al. (2012)), Ne-B (Black and Pepin (1969)), "FSW" (Benkert et al. (1993) and Wieler et al. (2007)), Q (P1) (Busemann et al. (2000)), Earth atmosphere (EA) (Eberhardt et al. (1965)), P3 (Huss and Lewis (1994a)), HL (Huss and Lewis (1994a)) and data for lunar ilmenites and pyroxenes. All of the measured samples have high $^{20}Ne/^{22}Ne$ ratios, in the range of 11.17 (DC 06_07_213) to 12.27 (DC 06_09_50), indicating abundant solar-type ^{20}Ne. The arithmetic mean is ~11.6, showing that probably the samples experienced fractionation similar to "FSW" (see Wieler et al. (2007)). Xtal DC 06_09_149 shows the highest ^{20}Ne concentration of 8 x 10^{-5} cc STP/g, which is more than 20 times higher than the highest concentration found in the TAM MMs (see Table 22). Compared to the results of Osawa and Nagao (2002), the ^{20}Ne concentrations show a similar range and also the isotopic compositions are similar (see Fig. 76). The same holds in comparison with lunar ilmenites and pyroxenes (Benkert et al. (1993)), as well as gas rich-meteorites (e.g. Wieler (2002b); Black (1972b)). Cosmogenic contributions within the DC and CP MMs are low ($^{21}Ne/^{22}Ne$ is between 0.025, with a large error, and 0.033) with 3 MMs plotting closer to air, while the remaining samples plot nearer to SW (see Table 36). Naturally, any derived CRE-ages must be highly uncertain, since trapped SW is so dominant that $^{21}Ne_{cos}$ is barely detectable (see chapter 6.4.7 for details).

Bastian Baecker | Chapter 6 - Micrometeorites from the CONCORDIA collection (Dome C) and from Cap Prudhomme, Antarctica – Noble gases show the possibility for a single population

157

*Table 36. **Ne** results for 11 different CONCORDIA collection (Dome C) and Cap Prudhomme MM samples. Given are the totals, calculated from the individual measurement steps as indicated - for details see Appendix. Uncertainties in the last digits are given in parentheses. Values with $^\$$ are 2σ upper limits. For comparison also the isotopic compositions of SW, "FSW", Q(P1), EA and HL are listed.*

Sample	Particle no.	Step(s) used	^{22}Ne (10^{-12} cc STP)	^{22}Ne (10^{-8} cc STP/g)	^{20}Ne/^{22}Ne	^{21}Ne/^{22}Ne
DC 06_07_213 (Xtal)	PL 09_20 7 (1)	all	0.83 (3)	77.58 (7.76)	11.17 (29)	0.028 (2)
DC 06_08_01 (Xtal)	PL06_09A 1	1	3.22 (5)	234.9 (17.6)	11.43 (12)	0.032 (1)
DC 06_09_11 (FgC/Sc)	PL07_01A 11	all	0.52 (3)	40.62 (3.82)	11.71 (45)	0.033 (2)
DC 06_09_50 (FgC)	PL07_02B 2	1	3.89 (6)	117.8 (4.0)	12.27 (11)	0.032 (1)
DC 06_09_57 (FgC)	PL07_02B 9 (1)	all	< 0.07 $^\$$	< 46.91 $^\$$	-	-
DC 06_09_57 (FgC)	PL07_02B 9 (2)	all	< 0.01 $^\$$	< 12.60 $^\$$	-	-
DC 06_09_63 (FgC/Xtal)	PL07_02C 3	1	1.76 (10)	53.22 (3.56)	11.88 (41)	0.031 (2)
DC 06_09_141 (Xtal)	PL07_04C 9 (1)	all	0.22 (2)	31.66 (5.69)	11.14 (85)	0.025 (4)
DC 06_09_149 (Xtal)	PL07_05A 5 (1)	all	2.06 (4)	688.0 (229.7)	11.65 (14)	0.032 (1)
DC 06_09_189 (FgC/Sc)	PL07_06A 9	all	3.09 (5)	309.1 (31.4)	11.89 (11)	0.032 (1)
CP 9-1-1994 (Sc)	PL 10-109D 9	1	0.18 (3)	2.89 (0.52)	11.94 (97)	0.028 (5)

Component	References				^{20}Ne/^{22}Ne	^{21}Ne/^{22}Ne
SW	[1]				13.777 (10)	0.03289 (7)
"FSW"	[2]				11.2 (2)	0.0295 (5)
Q (P1)	[3]				10.67 (2)	0.0294 (10)
EA	[4]				9.80	0.029
HL	[5]				8.50 (6)	0.036 (1)

References: [1] Heber et al. (2012)*, [2]* Benkert et al. (1993) *[3]* Busemann et al. (2000)*, [4] Eberhardt et al. (1965), [5]* Huss and Lewis (1994a)*; Note: For detailed information regarding **"FSW"** see Wieler et al. (2007).*

Bastian Baecker | Chapter 6 - Micrometeorites from the CONCORDIA collection (Dome C) and from Cap Prudhomme, Antarctica – Noble gases show the possibility for a single population

158

Figure 76. Three isotope plot of ^{20}Ne / ^{22}Ne vs. ^{21}Ne / ^{22}Ne for our data, for Murchison (measured at the MPIC in 2011) and AMM data from Osawa and Nagao (2002). Also plotted for comparison are SW (Heber et al. (2012)), Ne-B (Black and Pepin (1969)), "FSW" (Benkert et al. (1993) and Wieler et al. (2007)), Q (P1) (Busemann et al. (2000)), Earth atmosphere (EA) (Eberhardt et al. (1965)), P3 (Huss and Lewis (1994a)), HL (Huss and Lewis (1994a)) and data for lunar ilmenites and pyroxenes (Benkert et al. (1993)), as well as cometary matter (Marty et al. (2008))).

Bastian Baecker | Chapter 6 - Micrometeorites from the CONCORDIA collection (Dome C) and from Cap Prudhomme, Antarctica – Noble gases show the possibility for a single population

159

6.4.3 Argon (Ar)

Argon results for 11 different Dome C and Cap Prudhomme micrometeorites are listed in Table 37 and plotted in a three isotope plot of ^{40}Ar / ^{36}Ar versus ^{38}Ar / ^{36}Ar for our data, selected TAM MM data (see chapter 5.4.3) and AMM data published by Osawa and Nagao (2002) (Fig. 77). For comparison also SW (Heber et al. (2012)), "FSW" (Benkert et al. (1993)) and Wieler et al. (2007)), Q (P1) (Busemann et al. (2000)), Earth atmosphere (EA) (Lee et al. (2006)), and HL (Huss and Lewis (1994a) are given (for values see Table 37).

All of the measured MMs show $^{40}Ar/^{36}Ar$ ratios distinctly lower than air ($^{40}Ar/^{36}Ar$ = 298.56; Lee et al. (2006)), indicative for a dominant extra-terrestrial component. The values range from a low of 5.6 (DC 06_09_149 (Xtal)) up to 237 (DC 06_09_57 (FgC)), whereas for $^{38}Ar/^{36}Ar$ the results vary between a puzzling (see below) 0.15 (DC 06_09_57 (FgC)) and 0.205 (DC 06_08_01 (Xtal)). As already explained for the TAM MMs (chapter 5.4.3), probably most of the ^{38}Ar is trapped along with only small cosmogenic contributions.

The MMs DC 06_09_149, DC 06_08_01, DC 06_09_50 and CP PL10-109D9 plot close to the SW and Q(P1) compositions (Fig. 77), whereas the remaining MMs plot in the direction of air and/or radiogenic Ar. As obvious in Fig. 77 and similar as in the case of Ne (Fig. 76), none of the samples show large discernible cosmogenic contributions (see chapter 6.4.7 for details). Overall ratio variations are in the range of the MMs measured by Osawa and Nagao (2002). ^{36}Ar ranges between about 2 x 10^{-7} cc STP/g (CP PL10-109D9) and 6 x 10^{-5} cc STP/g (DC 06-09-57(2)), whereas ^{40}Ar concentrations vary between 1 x 10^{-5} cc STP/g (CP PL10-109D9) and 1.2 x 10^{-3} cc STP/g (DC 06-09-57(2)). Clearly visible are the differences in amounts and concentrations between the DC samples and the (single) CP sample. The latter clearly shows the lowest Ar concentrations of all MMs. DC 06-09-57(2) shows the highest ^{36}Ar concentration we have found (~ 6 x 10^{-5} cc STP/g), which is about 10 times higher than the maximum observed by Osawa and Nagao (2002). This MM is puzzling, in particular the remarkably low $^{38}Ar/^{36}Ar$ ratio of ~0.15, which is difficult to explain. A possibility is that this MM acquired an unusually large amount of fractionated air argon. The low (relative to air) $^{40}Ar/^{36}Ar$ ratio, which deviates from the air ratio by ~32%, within uncertainties twice the ~20% deviation in $^{38}Ar/^{36}Ar$, may point in this direction. Interestingly, the Xe (although not the Kr) data, within their large uncertainties, seem to indicate a similar trend of large fractionation favoring the light isotopes. In any case, overall the ^{36}Ar and ^{40}Ar concentrations are in a similar range compared to data from Osawa and Nagao (2002). Compared to the data for the TAM MMs (Table 23), especially the concentrations of ^{36}Ar, but also in some cases the ^{40}Ar concentrations, are about 10 to 100 times higher.

Bastian Baecker | Chapter 6 - Micrometeorites from the CONCORDIA collection (Dome C) and from Cap Prudhomme, Antarctica – Noble gases show the possibility for a single population

160

*Table 37. **Ar** results for 11 different CONCORDIA collection (Dome C) and Cap Prudhomme MM samples. Given are the totals, calculated from the individual measurement steps as indicated - for details see Appendix. Uncertainties in the last digits are given in parentheses. For comparison also the isotopic compositions of SW, Q(P1), EA and HL are listed.*

Sample	Particle no.	Step(s) used	^{36}Ar (10^{-12} cc STP)	^{36}Ar (10^{-8} cc STP/g)	^{40}Ar (10^{-8} cc STP/g)	^{38}Ar/^{36}Ar	^{40}Ar/^{36}Ar
DC 06_07_213 (Xtal)	PL09_20 7 (1)	all	2.79 (34)	261 (40)	54040 (8428)	0.1841 (33)	202 (5)
DC 06_08_01 (Xtal)	PL06_09 A 1	1	2.61 (32)	190 (27)	4746 (2450)	0.2051 (38)	19.7 (10.8)
DC 06_09_11 (FgC/Sc)	PL07_01 A 11	all	2.14 (27)	165 (25)	18834 (3583)	0.1906 (41)	107 (9)
DC 06_09_50 (FgC)	PL07_02 B 2	all	19.7 (2.1)	596 (67)	18625 (3903)	0.1935 (23)	30.4 (2.6)
DC 06_09_57 (FgC)	PL07_02 B 9 (1)	all	0.299 (132)	199 (159)	53906 (41647)	0.1726 (189)	237 (34)
DC 06_09_57 (FgC)	PL07_02 B 9 (2)	all	2.98 (1.20)	5958 (2400)	1236210 (499179)	0.1495 (39)	204 (4)
DC 06_09_63 (FgC/Xtal)	PL07_02 C 3	all	10.8 (4)	327 (16)	55669 (3843)	0.1830 (20)	170 (6)
DC 06_09_141 (Xtal)	PL07_04 C 9 (1)	all	0.512 (132)	73,2 (21.6)	11782 (4816)	0.1731 (116)	142 (23)
DC 06_09_149 (Xtal)	PL07_05 A 5 (1)	all	8.64 (21)	2881 (963)	19511 (12370)	0.1863 (36)	5.62 (3.76)
DC 06_09_189 (FgC/Sc)	PL07_06 A 9	all	14.6 (3)	1458 (149)	318697 (32722)	0.1848 (36)	218 (2)
CP 9-1-1994 (Sc)	PL 10-109D 9	1	1.16 (5)	18.7 (0.8)	977 (87)	0.1719 (177)	52.1 (3.2)

Component	References					^{38}Ar/^{36}Ar	^{40}Ar/^{36}Ar
SW	[1]					0.183 (1)	-
"FSW"	[2]					0.205 (2)	-
Q (P1)	[3]					0.187 (1)	-
EA	[4]					0.1885 (3)	298.56 (31)
HL	[5]					0.227 (3)	-

References: [1] Heber et al. (2012), [2] Wieler (2002b), [3] Busemann et al. (2000), [4] Lee et al. (2006) [5] Huss and Lewis (1994a); Note: n.a. = not detectable (below blank level); For detailed information regarding "FSW" see Wieler et al. (2007).

Bastian Baecker | Chapter 6 - Micrometeorites from the CONCORDIA collection (Dome C) and from Cap Prudhomme, Antarctica – Noble gases show the possibility for a single population

161
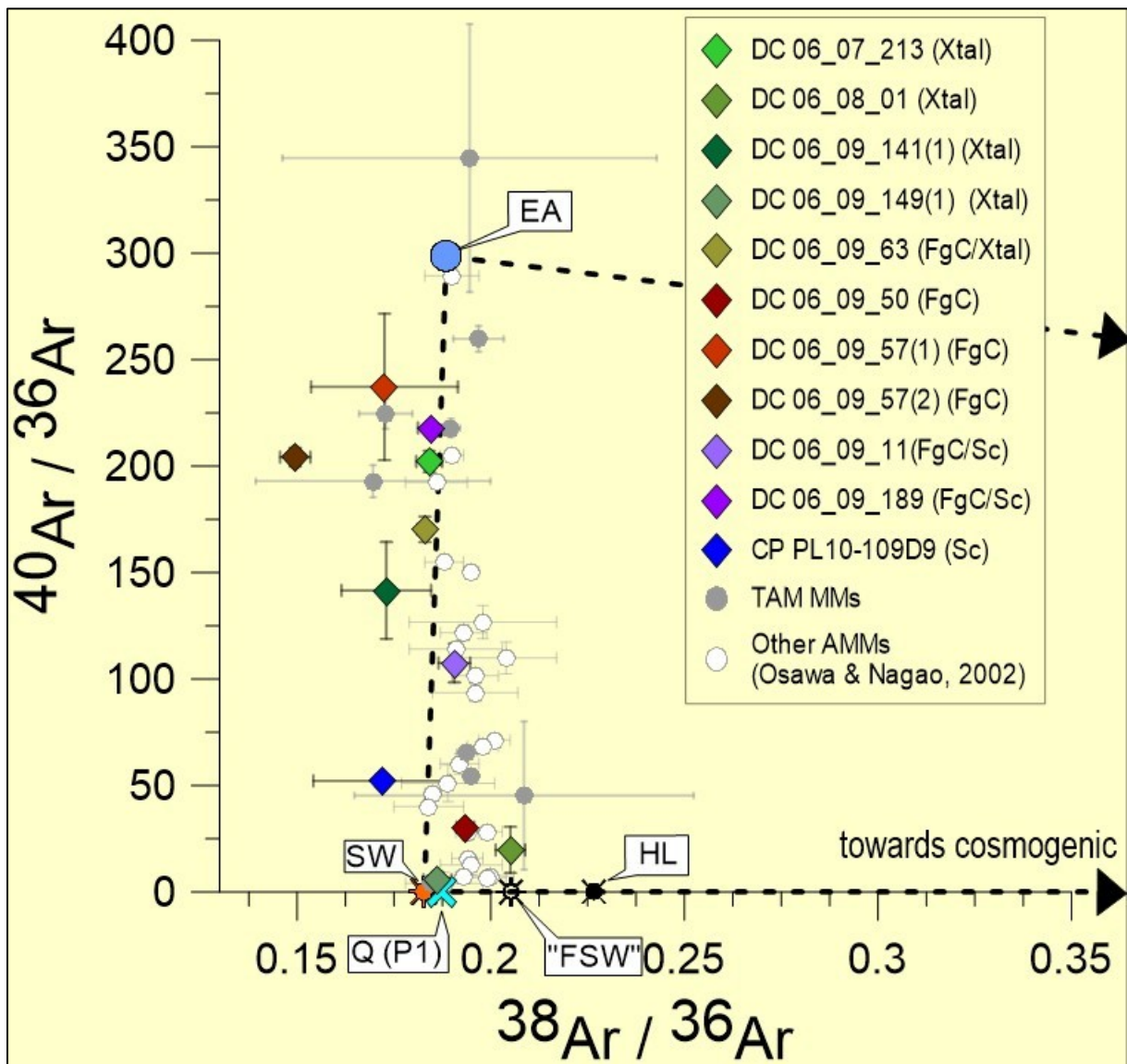
Figure 77. Three isotope plot of $^{40}Ar / ^{36}Ar$ vs. $^{38}Ar / ^{36}Ar$ for our data, selected TAM MM data (see chapter 5.4.3) and AMM data from Osawa and Nagao (2002). Also plotted for comparison are SW (Heber et al. (2012)), "FSW" (Wieler (2002b)) and Wieler et al. (2007)), Q (P1) (Busemann et al. (2000)), Earth atmosphere (EA) (Lee et al. (2006)), and HL (Huss and Lewis (1994a)). All of the Dome C and Cap Prudhomme MMs plot below Earth atmosphere. Most of the MMs plot in a region indicating mixed components, whereas others are plotting directly near to SW and Q (P1). The dotted lines indicating a triangle between EA, SW and cosmogenic Ar (Alaerts et al. (1979) in Busemann et al. (2000)). The samples which plot right of the line EA-SW must have cosmogenic contributions, those which plot above the line EA-cosmogenic contain radiogenic ^{40}Ar.

Bastian Baecker | Chapter 6 - Micrometeorites from the CONCORDIA collection (Dome C) and from Cap Prudhomme, Antarctica – Noble gases show the possibility for a single population

162

6.4.4 Krypton (Kr)

Results of Kr measurements for MMs from DC and CP are listed in Table 38 and the Appendix. Fig. 78 is a three isotope plot of $^{86}Kr/^{84}Kr$ versus $^{83}Kr/^{84}Kr$ for our data and selected TAM MM data (see chapter 5.4.4). Also plotted for comparison are SW (Meshik et al. (2012)), Q (P1) (Busemann et al. (2000)), Earth atmosphere (EA) (Basford et al. (1973)) and HL (Huss and Lewis (1994a); recalculated by Busemann et al. (2000)). As documented in Table 38, the samples show varying ^{84}Kr concentrations ranging from 0.9×10^{-8} cc STP/g (DC 06_09_11 (FgC/Sc)) up to 7×10^{-7} cc STP/g (DC 06_09_189 (FgC/Sc)). Here again, similar to Ar and Xe (see below), DC 06_09_57(2) (FgC) is especially gas rich (4.1×10^{-7} cc STP/g). These concentrations are about 10 to 20 times higher than those for TAM MMs, but similar to those reported by Osawa and Nagao (2002) (8.9×10^{-10} cc STP/g to 1.4×10^{-7} cc STP/g). For two samples only upper limits for ^{84}Kr could be established and for the CP MM no Kr data were obtained. No real trend is apparent in the isotopic compositions (Fig. 78). Similar as in the case of the TAM MMs (chapter 5.4.4) the Kr sample gas probably comprises several components (EA, SW, Q(P1)). Taken at face value, the variations within the Kr ratios seem to be stronger compared to the TAM MMs (compare Table 24 and Table 38), with the exception of $^{86}Kr/^{84}Kr$. Four of our MM samples (DC 06_08_01 (Xtal); DC 06_09_57(2) (FgC); DC 06_09_141 (Xtal) and DC 06_09_149 (Xtal)) show $^{80}Kr/^{84}Kr$ ratios (0.043 to 0.062) above SW (~0.041; Meshik et al. (2012)). The case of $^{82}Kr/^{84}Kr$ is similar, where additionally, DC 06_09_11 (FgC/Sc) shows a ratio of 0.274, far above SW (~0.205; Meshik et al. (2012)). However, all of these ratios show large uncertainties, and so the large scatter and sometimes high values may simply reflect statistical uncertainties when such small Kr gas amounts are measured. Cosmogenic contributions in any case are low (see Appendix).

Bastian Baecker | Chapter 6 - Micrometeorites from the CONCORDIA collection (Dome C) and from Cap Prudhomme, Antarctica – Noble gases show the possibility for a single population

163

*Table 38. **Kr** results for 11 different CONCORDIA collection (Dome C) and Cap Prudhomme MM samples. Given are the totals, calculated from the individual measurement steps as indicated - for details see Appendix. Uncertainties in the last digits are given in parentheses. Values with $ are 2σ upper limits. For comparison also the isotopic compositions of SW, Q(P1), EA and HL are listed.*

Sample	Particle no.	Step(s) used	^{84}Kr (10^{-12} cc STP)	^{84}Kr (10^{-8} cc STP/g)	^{80}Kr/^{84}Kr	^{82}Kr/^{84}Kr	^{83}Kr/^{84}Kr	^{86}Kr/^{84}Kr
DC 06_07_213 (Xtal)	PL 09_20 7 (1)	all	0.027 (6)	2.536 (607)	0.035 (5)	0.198 (17)	0.201 (12)	0.331 (20)
DC 06_08_01 (Xtal)	PL06_09A 1	1	0.016 (6)	1.151 (439)	0.043 (8)	0.226 (27)	0.186 (18)	0.310 (27)
DC 06_09_11 (FgC/Sc)	PL07_01A 11	all	0.012 (6)	0.910 (461)	0.038 (11)	0.274 (36)	0.209 (26)	0.312 (37)
DC 06_09_50 (FgC)	PL07_02B 2	1	0.039 (6)	1.172 (188)	0.038 (4)	0.209 (12)	0.200 (9)	0.288 (13)
DC 06_09_57 (FgC)	PL07_02B 9 (1)	all	< 0.013 $	< 8.356 $	-	-	-	-
DC 06_09_57 (FgC)	PL07_02B 9 (2)	all	0.021 (10)	41.25 (19.47)	0.053 (7)	0.215 (23)	0.201 (18)	0.323 (30)
DC 06_09_63 (FgC/Xtal)	PL07_02C 3	all	0.069 (8)	2.079 (239)	0.045 (3)	0.215 (8)	0.206 (7)	0.287 (10)
DC 06_09_141 (Xtal)	PL07_04C 9 (1)	all	< 0.010 $	< 1.486 $	-	-	-	-
DC 06_09_149 (Xtal)	PL07_05A 5 (1)	all	0.009 (5)	3.133 (2.002)	0.062 (13)	0.250 (38)	0.219 (27)	0.333 (44)
DC 06_09_189 (FgC/Sc)	PL07_06A 9	all	0.716 (32)	71.58 (7.84)	0.038 (1)	0.195 (7)	0.196 (6)	0.293 (8)
CP 9-1-1994 (Sc)	PL 10-109D 9	n.a.	-	-	-	-	-	-

Component	References				^{80}Kr/^{84}Kr	^{82}Kr/^{84}Kr	^{83}Kr/^{84}Kr	^{86}Kr/^{84}Kr
SW	[1]				0.0412 (2)	0.2054 (2)	0.2034 (2)	0.3012 (4)
Q (P1)	[2]				0.03937 (7)	0.2018 (2)	0.2018 (2)	0.3095 (5)
EA	[3]				0.039599 (20)	0.20217 (4)	0.2014 (2)	0.3052 (3)
HL	[4]				0.0305 (10)	≡ 0.1590	0.1989 (10)	0.3623 (18)

References: [1] Meshik et al. (2012) [2] Busemann et al. (2000) [3] Basford et al. (1973) [4] Huss and Lewis (1994a); re-calculated by Busemann et al. (2000); <u>Note:</u> n.a. = not detectable (below blank level).

Bastian Baecker | Chapter 6 - Micrometeorites from the CONCORDIA collection (Dome C) and from Cap Prudhomme, Antarctica – Noble gases show the possibility for a single population

164

Figure 78. Three isotope plot of ^{86}Kr / ^{84}Kr vs. ^{83}Kr / ^{84}Kr for our data and selected TAM MM data (see chapter 5.4.4). Also plotted for comparison are SW (Meshik et al. (2012)), Q (P1) (Busemann et al. (2000)), Earth atmosphere (EA) (Basford et al. (1973)) and HL (Huss and Lewis (1994a); recalculated by Busemann et al. (2000)).

Bastian Baecker | Chapter 6 - Micrometeorites from the CONCORDIA collection (Dome C) and from Cap Prudhomme, Antarctica – Noble gases show the possibility for a single population

165

6.4.5 Xenon (Xe)

As discussed in chapter 4.3.5.1 three different schemes of data reduction were tested on the Xe calibration gas results - "internal", "ext a" and "ext b", with the "internal" approach yielding the best reproducibility. Therefore, this method was also used for the samples in order to calculate the isotopic ratios. As explained in chapter 4.3.5.1, the statistical uncertainties for ^{124}Xe and ^{126}Xe are very large due to their low abundance and therefore these isotopes will not be further considered.

We obtained Xe data for 11 different CONCORDIA collection (Dome C) and Cap Prudhomme MMs. The results are shown in Table 39, Figs. 79 to 81 and the Appendix. Due to the small size of the DC MMs and the probably large weathering effects on the CP MM resulting in low Xe amounts, the results show generally larger analytical errors than the measurements of the TAM MMs. For two samples (DC 06_09_141 (Xtal) and DC 06_09_57(1) (FgC)) only upper limits were obtained. However, the highest concentration of ^{132}Xe (for the DC samples between 8.5 x 10^{-9} cc STP/g and 1.7 x 10^{-7} cc STP/g; see Table 39) is 8 to 170 times larger than those in MMs from TAM (1 to 5 x 10^{-9} cc STP/g) and those reported by Osawa and Nagao (2002) (1 x 10^{-9} cc STP/g to 2.1 x 10^{-8} cc STP/g). Sarda et al. (1991) measured a ^{132}Xe concentration of overall ~3.7 x 10^{-9} cc STP/g (3 steps), within a single, large MM.

As mentioned in the Ar and Kr chapters, DC 06_09_189 and DC 06_09_57(2) show by far the highest gas concentrations. Generally, Xtal MMs are very similar to each other, as are the FgC MMs. However, if one compares Xtal with FgC MMs there is a slight hint for a systematic difference in the isotope ratios. Xtal MMs show often lower nominal abundances of the lighter isotopes, while for the heavier isotopes it is the opposite (larger ratios in the Xtal MMs than in the FgC MMs; (see Table 39)). This may indicate that Xtal MMs contain larger contributions of SW and / or Q(P1), whereas FgC MMs possibly are influenced by air, HL or ^{244}Pu fission. The ^{128}Xe/^{132}Xe ratios ranges from 0.041 (DC 06_08_01 (Xtal)) to 0.102 (DC 06_09_57(2) (FgC)), but, however, all ratios are similar within the uncertainties. Except for DC 06_07_213 (Xtal) and DC 06_08_01 (Xtal), which are lower than EA (Basford et al. (1973)), most of the ratios lie between the values for EA, SW and Q(P1). ^{129}Xe/^{132}Xe shows values between 0.911 (DC 06_09_149 (Xtal)) and 1.200 (DC 06_09_57 (FgC)) - here again, mostly between EA, SW and Q(P1) and in a few cases below EA. On the other hand, the gas-rich sample DC 06_09_57(2) (FgC) has higher ^{128}Xe/^{132}Xe and ^{129}Xe/^{132}Xe ratios than SW, Q(P1) and HL, though with large uncertainties. For ^{130}Xe/^{132}Xe the results show a variation from 0.124 (DC 06_09_149 (Xtal)) to 0.167 (DC 06_09_63 (FgC/Xtal), whereas most of the samples have ratios between ~0.140 to ~0.166. The ^{131}Xe/^{132}Xe ratio is in the range of 0.632 (DC 06_08_01 (Xtal)) and 0.898 (DC 06_09_149 (Xtal)). ^{134}Xe/^{132}Xe shows ratios between 0.362 (CP 9-1-1994 (Sc)) and 0.431 (DC 06_08_01 (Xtal)), whereas the values for ^{136}Xe/^{132}Xe vary between 0.159 (DC 06_09_57(2) (FgC)) and 0.513 (DC 06_09_149 (Xtal)).

It is important to emphasize that nearly all ratios show large uncertainties and a critical inspection may come to the conclusion that within uncertainties the ratios for

Bastian Baecker | Chapter 6 - Micrometeorites from the CONCORDIA collection (Dome C) and from Cap Prudhomme, Antarctica – Noble gases show the possibility for a single population

166

the various samples are indistinguishable from both, each other and the various major trapped components (Q, EA, SW) that may be expected to be present – if looked at each isotope ratio in isolation. The situation becomes different, however, if various isotopic ratios are considered in context, as demonstrated below in Figs. 79 and 80. Moreover, with respect to the gas-rich sample DC 06_09_57 (2) it is intriguing that the trend for enrichment of the light vs. the heavy isotopes is the same as seen in the enigmatic composition of its argon (see chapter 6.4.3).

Bastian Baecker | Chapter 6 - Micrometeorites from the CONCORDIA collection (Dome C) and from Cap Prudhomme, Antarctica – Noble gases show the possibility for a single population

167

*Table 39. **Xe** results for 11 different CONCORDIA collection (Dome C) and Cap Prudhomme MM samples. Listed are totals based on selected measurement steps as indicated - for details see Appendix. The listed results are based on the "internal calibration" ("int") data reduction approach. Uncertainties in the last digits are in parenthesis. Values with $ are 2σ upper limits. For comparison also the compositions of SW, Q(P1), EA and HL are given.*

Sample	Particle no.	Step(s) used	^{132}Xe (10^{-12} cc STP)	^{132}Xe (10^{-8} cc STP/g)	$^{128}Xe/^{132}Xe$ (INT)	$^{129}Xe/^{132}Xe$ (INT)	$^{130}Xe/^{132}Xe$ (INT)	$^{131}Xe/^{132}Xe$ (INT)	$^{134}Xe/^{132}Xe$ (INT)	$^{136}Xe/^{132}Xe$ (INT)
DC 06_07_213 (Xtal)	PL 09_20 7 (1)	all	0.009 (2)	0.848 (194)	0.060 (11)	0.947 (47)	0.135 (8)	0.841 (46)	0.412 (24)	0.394 (30)
DC 06_08_01 (Xtal)	PL06_09A 1	1	0.004 (2)	0.284 (135)	0.041 (23)	0.921 (78)	0.137 (16)	0.632 (75)	0.431 (48)	0.342 (49)
DC 06_09_11 (FgC/Sc)	PL07_01A 11	all	0.010 (2)	0.781 (160)	0.083 (10)	1.033 (44)	0.166 (9)	0.783 (40)	0.370 (21)	0.333 (24)
DC 06_09_50 (FgC)	PL07_02B 2	1	0.029 (2)	0.870 (79)	0.072 (5)	0.995 (23)	0.162 (4)	0.784 (19)	0.397 (11)	0.349 (13)
DC 06_09_57 (FgC)	PL07_02B 9 (1)	1	< 0.002 $	< 1.120 (2σ)	-	-	-	-	-	-
DC 06_09_57 (FgC)	PL07_02B 9 (2)	all	0.002 (1)	3.92 (2.27)	0.102 (64)	1.200 (139)	0.135 (48)	0.746 (157)	0.312 (78)	0.159 (91)
DC 06_09_63 (FgC/Xtal)	PL07_02C 3	all	0.018 (3)	0.543 (79)	0.084 (8)	0.980 (31)	0.167 (6)	0.777 (29)	0.368 (16)	0.334 (18)
DC 06_09_141 (Xtal)	PL07_04C 9 (1)	n.a.	-	-	-	-	-	-	-	-
DC 06_09_149 (Xtal)	PL07_05A 5 (1)	all	0.001 (1)	0.353 (296)	-	0.911 (210)	0.124 (86)	0.898 (254)	0.384 (134)	0.513 (182)
DC 06_09_189 (FgC/Sc)	PL07_06A 9	all	0.173 (3)	17.27 (1.75)	0.073 (2)	0.991 (14)	0.153 (2)	0.782 (9)	0.386 (5)	0.318 (5)
CP 9-1-1994 (Sc)	PL 10-109D 9	1	0.009 (1)	0.145 (10)	0.077 (10)	1.035 (46)	0.158 (9)	0.869 (41)	0.362 (24)	0.299 (29)

Component	References				$^{128}Xe/^{132}Xe$	$^{129}Xe/^{132}Xe$	$^{130}Xe/^{132}Xe$	$^{131}Xe/^{132}Xe$	$^{134}Xe/^{132}Xe$	$^{136}Xe/^{132}Xe$
SW	[1]				0.0842 (3)	1.0401 (10)	0.1649 (4)	0.8263 (13)	0.3692 (7)	0.3003 (6)
Q (P1)	[2]				0.0822 (2)	1.042 (2)	0.1619 (3)	0.8185 (9)	0.3780 (11)	0.3164 (8)
EA	[3]				0.07136 (9)	0.9832 (12)	0.15136 (12)	0.7890 (11)	0.3879 (6)	0.3294 (4)
HL	[4]				0.0905 (6)	1.056 (2)	0.1542 (3)	0.8457 (13)	0.6356 (13)	≡ 0.6991

References: [1] Meshik et al. (2012), [2] Busemann et al. (2000), [3] Basford et al. (1973), [4] Huss and Lewis (1994a); re-calculated by Busemann et al. (2000); Note: n.a. = not detectable (below blank level).

Bastian Baecker | Chapter 6 - Micrometeorites from the CONCORDIA collection (Dome C) and from Cap Prudhomme, Antarctica – Noble gases show the possibility for a single population

168

Figures 79 and 80 are delta isotope plots of ^{130}Xe/^{132}Xe versus ^{136}Xe/^{132}Xe and ^{129}Xe/^{132}Xe versus ^{136}Xe/^{132}Xe, respectively showing per mil-deviations [δ] from Earth atmosphere Xenon composition (Basford et al. (1973)). Also plotted in both figures for comparison are Murchison (measured at the MPIC in 2011), SW (Meshik et al. (2012)). Q (P1) (Busemann et al. (2000)), and trends towards HL (Huss and Lewis (1994b)) and ^{244}Pu fission (Ozima and Podosek (2002). Both figures show similar results.
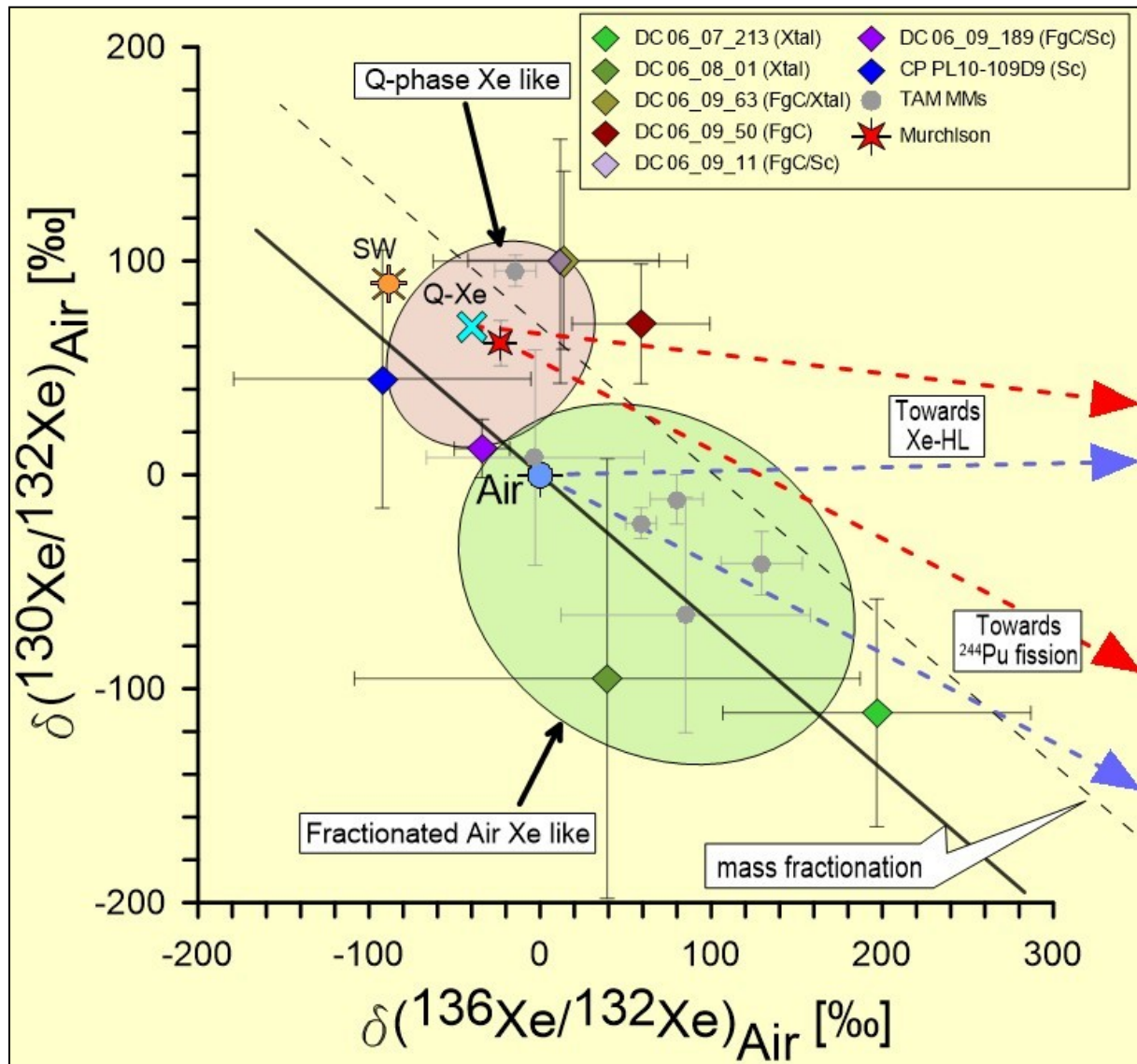
Figure 79. Delta isotope plot of ^{130}Xe / ^{132}Xe vs. ^{136}Xe / ^{132}Xe for the Dome C and Cap Prudhomme MM samples in per mil-deviations [δ] from Earth atmosphere Xenon composition. Earth atmosphere (Air) (Basford et al. (1973)). Also plotted for comparison are selected TAM MM results (see chapter 5.4.5), Murchison (measured at the MPIC in 2011), SW (Meshik et al. (2012)). Q (P1) (Busemann et al. (2000)), HL (Huss and Lewis (1994b)) and ^{244}Pu fission (Ozima and Podosek (2002). The MMs DC 06_09_57(2) (FgC) and DC 06_09_149 (Xtal) are offscale (see Table 39).

DC 06_09_50 (FgC), DC 06_09_189 (FgC/Sc) and CP PL 10-109D9 (Sc) plot close to the Q composition (Busemann et al. (2000)), but may have been affected by mass fractionation and Xe-HL (Huss and Lewis (1994b)). DC 06_07_213 (Xtal) and DC 06_08_01 (Xtal) appear to have lost their original trapped Xe, similar to some

Bastian Baecker | Chapter 6 - Micrometeorites from the CONCORDIA collection (Dome C) and from Cap Prudhomme, Antarctica – Noble gases show the possibility for a single population

169

TAM MMs (see chapter 5.4.5), and acquired mass fractionated air Xe instead. Also Xe-HL (in primitive diamonds; Huss and Lewis (1994b)) could be a reason for the relative depletion of ^{129}Xe, ^{130}Xe and enrichment in heavier Xe isotopes in some MMs. As shown in Fig. 79, in a plot of ^{130}Xe/^{132}Xe versus ^{136}Xe/^{132}Xe, despite their rather larger errors, DC 06_09_11 (FgC/Sc) and DC 06_09_63 (FgC/Xtal) appear to contain Xe resembling in its isotopic composition Xe from primitive meteorites. However, as evident from Fig. 80, only for DC 06_09_11 (FgC/Sc) this seems to be true. Here, DC 06_09_63 (FgC/Xtal) is plotting near Earth atmosphere (Air).
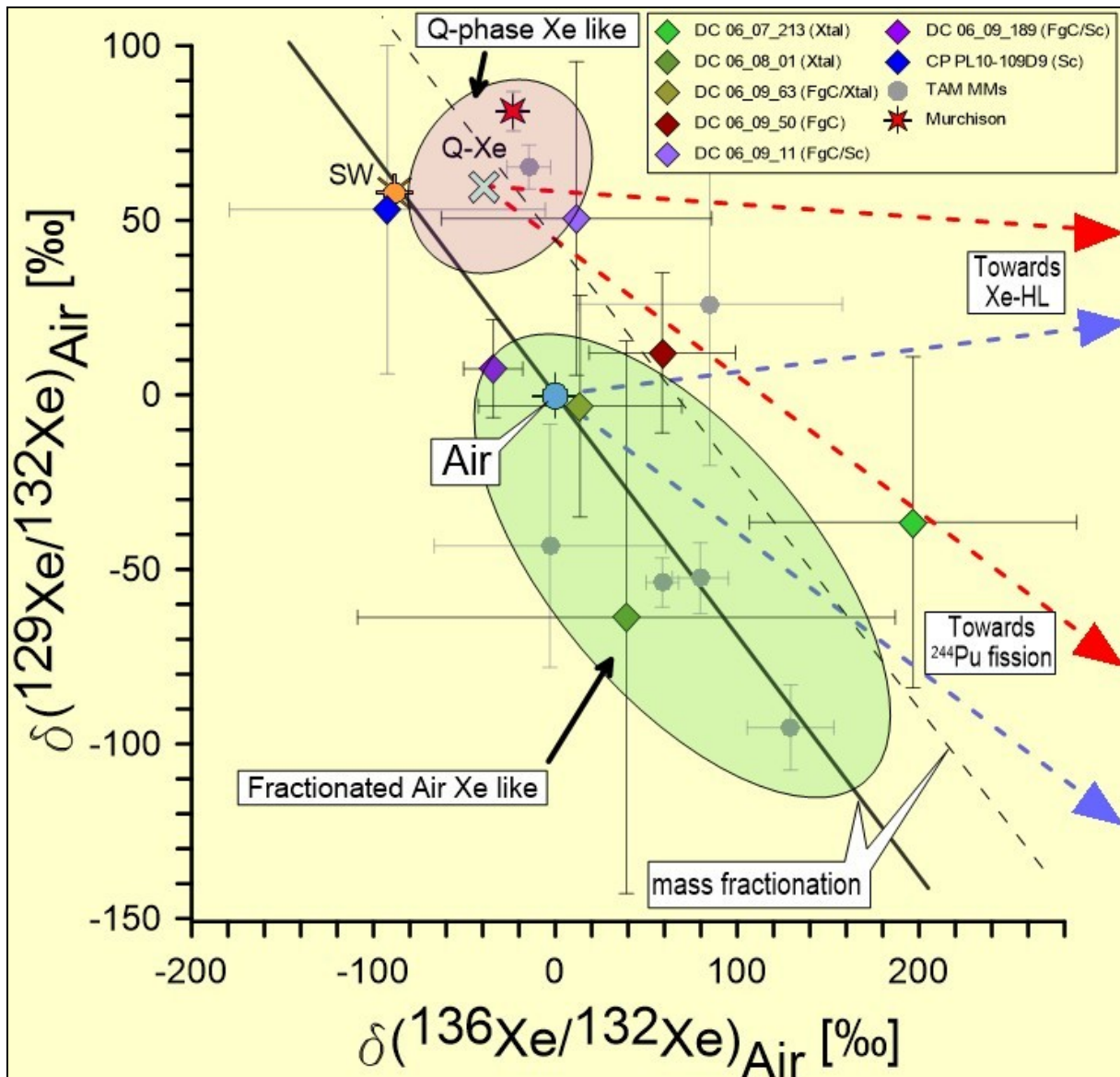
Figure 80. Delta isotope plot of ^{129}Xe / ^{132}Xe vs. ^{136}Xe / ^{132}Xe for the Dome C and Cap Prudhomme MM samples in per mil-deviations [δ] from Earth atmosphere Xenon composition. Earth atmosphere (Air) (Basford et al. (1973)). Also plotted for comparison are selected TAM MM results (see chapter 5.4.5), Murchison (measured at the MPIC in 2011), SW (Meshik et al. (2012)). Q (P1) (Busemann et al. (2000)), HL (Huss and Lewis (1994b)) and ^{244}Pu fission (Ozima and Podosek (2002). The MMs DC 06_09_57(2) (FgC) and DC 06_09_149 (Xtal) are offscale (see Table 39).

Fig. 81 compares the overall Xe isotopic data of our Dome C and Cap Prudhomme MMs compared to SW (Meshik et al. (2012)), Q-Xe (Busemann et al. (2000)) and TAM MM data (chapter 5.4.5). As mentioned above, generally it seems

Bastian Baecker | Chapter 6 - Micrometeorites from the CONCORDIA collection (Dome C) and from Cap Prudhomme, Antarctica – Noble gases show the possibility for a single population

170

that Xtal and FgC MMs show only little variations within their respective mineralogical group. However, when comparing the "typical" (average) Xtal MM with the "typical" FgC MM, there appears to be a systematic difference. The FgC type MMs (more or less) are shifted relative to air into the direction of SW and the planetary component Q (P1), indicating a similarity to primitive meteorites. The Xtal MMs on the other hand show strong variations within the lighter Xe isotopes, but seem to be generally enriched in the heavier Xe isotopes, indicating strong mass fractionation and/or possibly [244]Pu fission influence. However, as evident from Fig. 81, also various TAM MMs do show similar isotopic variations (compare group 1 and group 2).
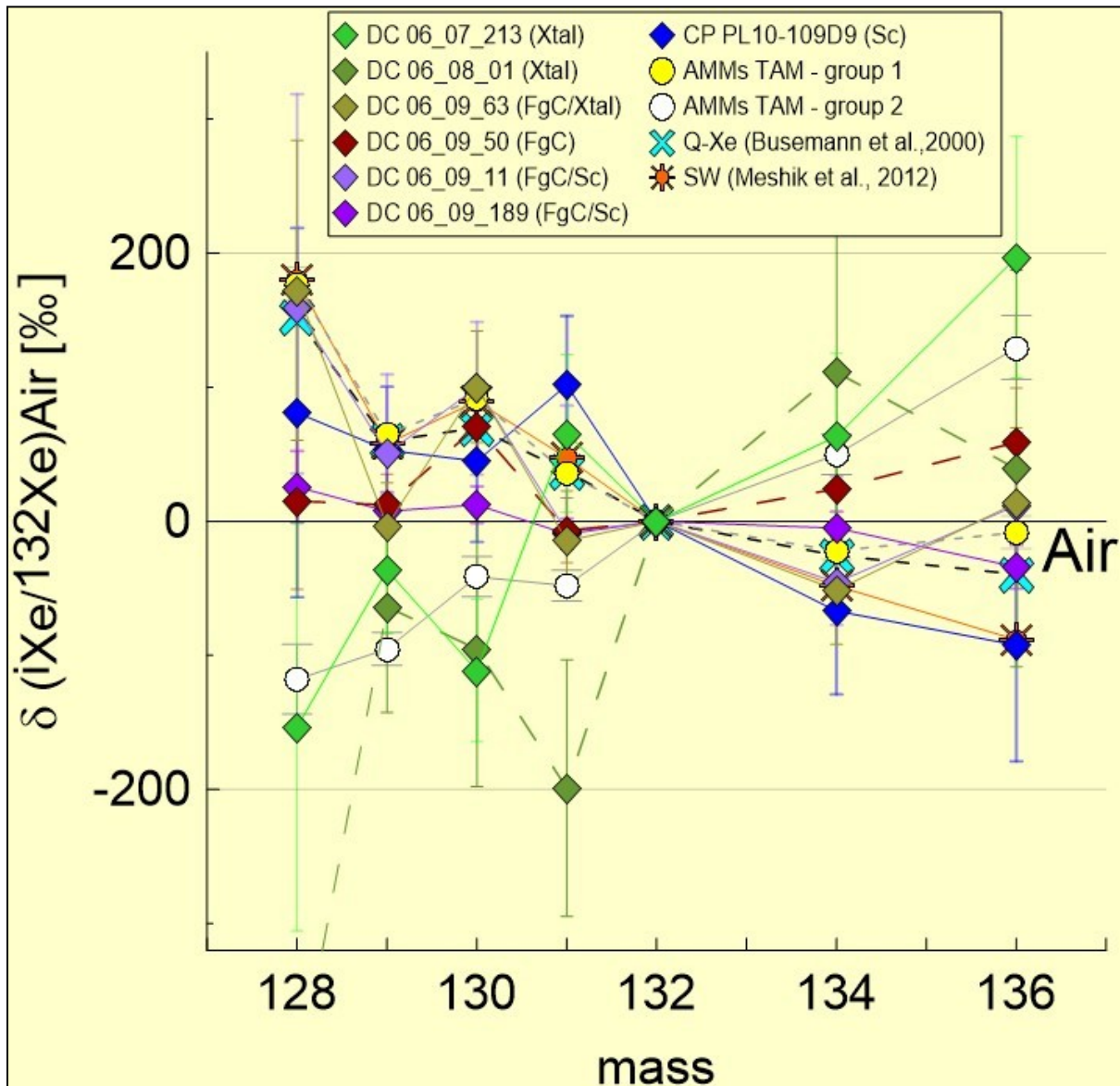
Figure 81. Isotope plot of Xe showing our data in Dome C and Cap Prudhomme MMs compared to SW (Meshik et al. (2012)), Q-Xe (Busemann et al. (2000)) and selected TAM MM results (see chapter 5.4.5). Isotopes shown in per mil-deviations from air Xe (Basford et al. (1973)) composition.

Bastian Baecker | Chapter 6 - Micrometeorites from the CONCORDIA collection (Dome C) and from Cap Prudhomme, Antarctica – Noble gases show the possibility for a single population

171

6.4.6 Elemental abundance ratios

Elemental abundance ratios for the measured MMs from the CONCORDIA collection (Dome C) and from Cap Prudhomme are shown in Table 40, as well as in Figs. 82 to 84 and in the Appendix. Fig. 82 shows the isotopic ratio of $^{38}Ar/^{36}Ar$ plotted against the $^{36}Ar/^{132}Xe$ ratio for the DC and CP MMs, along with selected TAM MM data (see chapter 5.4.6), data from Osawa and Nagao (2002), as well as the components SW (Vogel et al. (2011)), EA (Ozima and Podosek (2002)), Q(P1) (Busemann et al. (2000)), P3 and HL (both Huss and Lewis (1994a)).
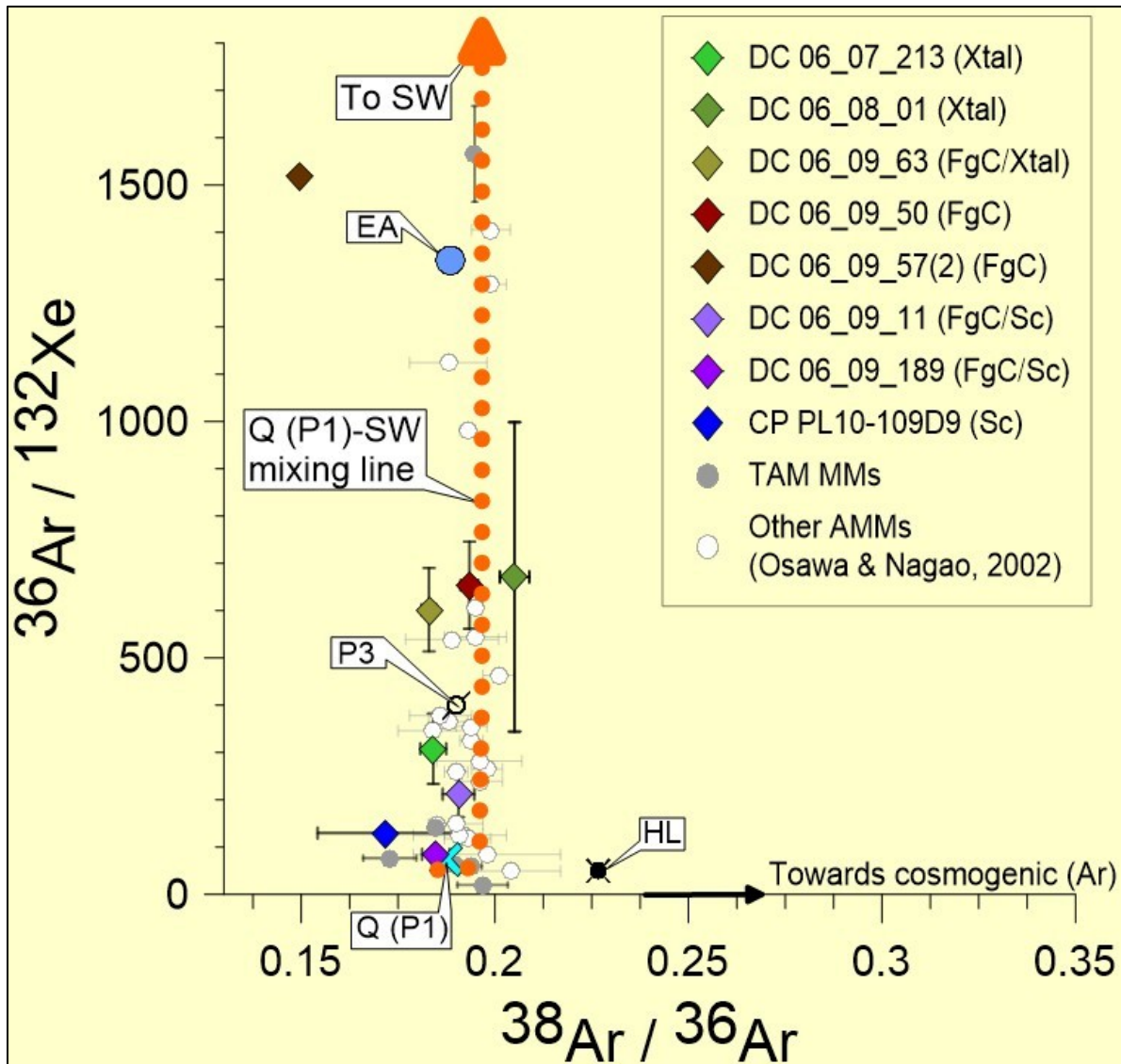
Figure 82. Isotope plot of ^{36}Ar / ^{132}Xe vs. ^{38}Ar / ^{36}Ar for our Dome C / Cap Prudhomme samples, selected TAM MM data (see chapter 5.4.6 and the Appendix) and data from Osawa and Nagao (2002). Also plotted for comparison are SW (Vogel et al. (2011)), EA (Ozima and Podosek (2002)), Q (P1) (Busemann et al. (2000)), P3 and HL (both Huss and Lewis (1994a)). The MM DC 06_09_149 is offscale at $^{36}Ar/^{132}Xe$ = 8152 (± 6258).

Unlike the TAM MMs (see Fig. 66), which in most cases plot near Q (P1) in this type of plot, the samples from DC and CP plot at higher $^{36}Ar/^{132}Xe$, in the direction of EA and SW, similar to the data of Osawa and Nagao (2002), indicating mixing of different components. The possible grouping of Xtal and FgC MMs for Ar,

Bastian Baecker | Chapter 6 - Micrometeorites from the CONCORDIA collection (Dome C) and from Cap Prudhomme, Antarctica – Noble gases show the possibility for a single population

172

Kr and Xe data, mentioned in previous chapters, is only barely visible. The gas rich sample DC 06_09_57(2) (FgC) plots in an unexpected area, above Earth atmosphere in the direction of SW, but with a low $^{38}Ar/^{36}Ar$ ratio (concerning the latter see discussion in chapter 6.4.3).

Table 40. Elemental abundance ratios for 11 different particles of CONCORDIA collection (Dome C) and Cap Prudhomme MMs. Listed are totals, calculated from the indicated measurement steps - for details see Appendix. Uncertainties in the last digits are given in parentheses. For comparison also the compositions of SW, Q(P1) and EA are listed.

Sample	Particle no.	Step(s) used	$^{36}Ar/^{132}Xe$	$^{84}Kr/^{132}Xe$
DC 06_07_213 (Xtal)	PL 09_20 7 (1)	all	308 (74)	2.99 (91)
DC 06_08_01 (Xtal)	PL06_09A 1	1	671 (327)	4.06 (2.45)
DC 06_09_11 (FgC/Sc)	PL07_01A 11	all	212 (48)	1.17 (62)
DC 06_09_50 (FgC)	PL07_02B 2	1	654 (92)	1.35 (24)
DC 06_09_57 (FgC)	PL07_02B 9 (1)	n.a.	-	-
DC 06_09_57 (FgC)	PL07_02B 9 (2)	all	1518 (1069)	10.5 (7.8)
DC 06_09_63 (FgC/Xtal)	PL07_02C 3	all	602 (88)	3.83 (69)
DC 06_09_141 (Xtal)	PL07_04C 9 (1)	n.a.	-	-
DC 06_09_149 (Xtal)	PL07_05A 5 (1)	all	8152 (6258)	8.86 (8.34)
DC 06_09_189 (FgC/Sc)	PL07_06A 9	all	84.4 (2.2)	4.14 (20)
CP 9-1-1994 (Sc)	PL 10-109D 9	1	129 (10)	-
Component	**References**		$^{36}Ar/^{132}Xe$	$^{84}Kr/^{132}Xe$
SW	[1]		23360 (1800)	9.84 (76)
Q (P1)	[2]		76 (7)	0.81 (5)
EA	[3]		1343	27.78

References: [1] Vogel et al. (2011), [2] Busemann et al. (2000), [3] calculated from Table 1.2 and 1.3 in Ozima and Podosek (2002), Note: n.a. = not detectable (below blank level).

Fig. 83 is an elemental ratio plot of $^{36}Ar / ^{132}Xe$ vs. $^{84}Kr / ^{132}Xe$ for our DC / CP data, for Murchison (measured at MPIC 2011), data of selected TAM MMs (see chapter 5.4.6) and data from Osawa and Nagao (2002), featuring also SW (Vogel et al. (2011)), EA and EA dissolved in water (Ozima and Podosek (2002)), Q (P1) (Busemann et al. (2000)) and "subsolar" (Crabb and Anders (1981) in Ott (2002)). The ratio of $^{36}Ar/^{132}Xe$ shows the lowest value for DC 06_09_189 (FgC/Sc) (84.9), which is almost 10 times higher than the minimum for MMs from TAM. The highest values are those for DC 06_09_149 (Xtal) with 8152 and DC 06_09_57(2) (FgC) with 1518, both with very large uncertainties (see Table 40). $^{84}Kr/^{132}Xe$ ratios shown in Table 40 vary between 1.17 (DC 06_09_11 (FgC/Sc)) and 10.5 (DC 06_09_57(2) (FgC)), a similar range as for TAM MMs. Osawa and Nagao (2002) reported values for $^{36}Ar/^{132}Xe$ between 49 and 2150, for $^{84}Kr/^{132}Xe$ in the range of 0.73 to 10.44, similar to our DC/CP samples. Compared to the TAM MMs (6 UnMMs and 5 ScMMs), the DC MMs appear to show lower contributions of the "planetary" Q(P1) relative to other trapped components, which is reflected in the higher overall ratios.

Bastian Baecker | Chapter 6 - Micrometeorites from the CONCORDIA collection (Dome C) and from Cap Prudhomme, Antarctica – Noble gases show the possibility for a single population

173
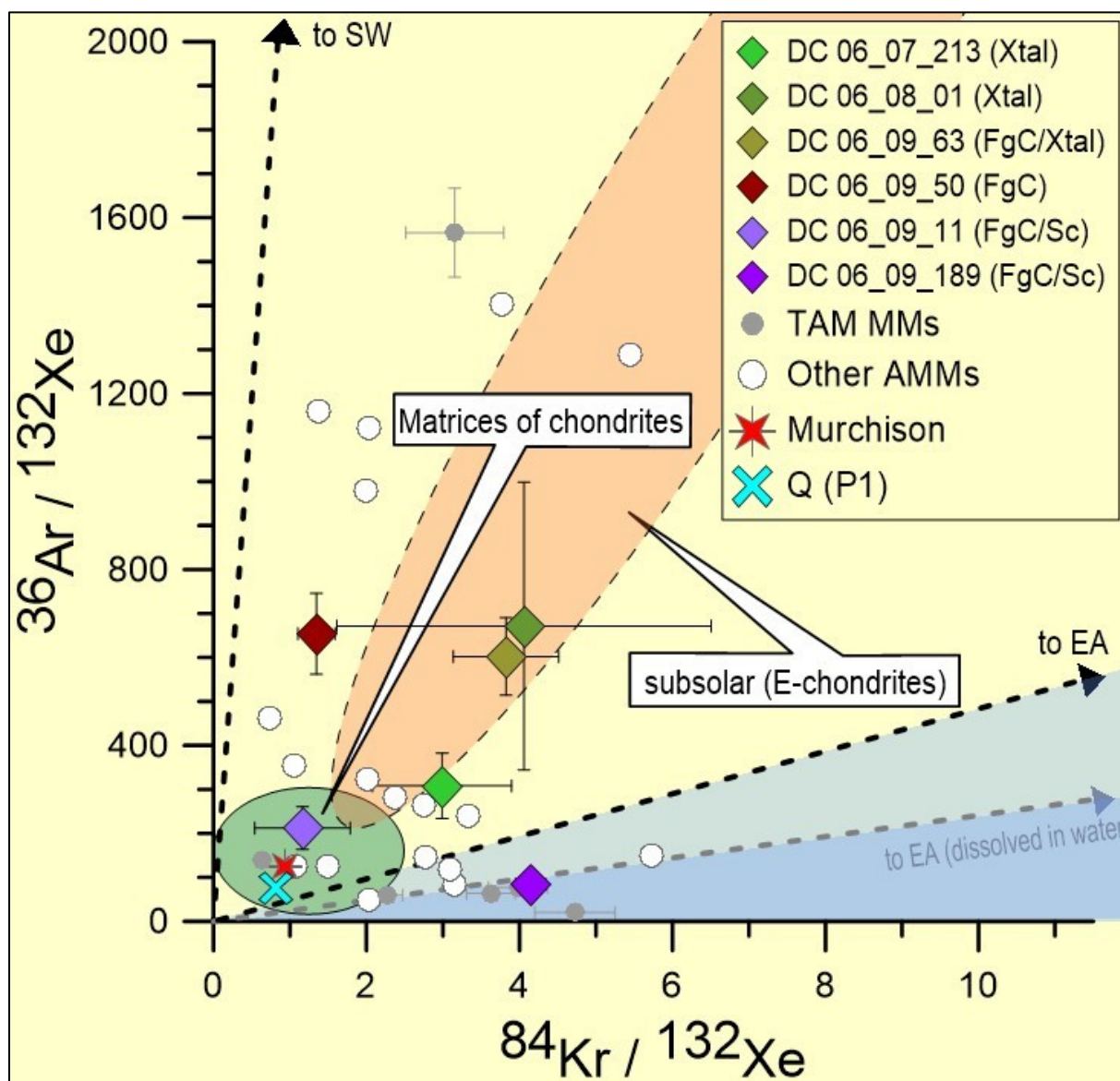
Figure 83. Elemental ratio plot of $^{36}Ar / ^{132}Xe$ vs. $^{84}Kr / ^{132}Xe$ for our data, for Murchison (measured at MPIC 2011), data of selected TAM MMs (see chapter 5.4.6 and the Appendix) and data from Osawa and Nagao (2002), featuring also SW (Vogel et al. (2011)), EA and EA (dissolved in water) (Ozima and Podosek (2002)), Q (P1) (Busemann et al. (2000)) and "subsolar" (Crabb and Anders (1981) in Ott (2002)). Beside MMs with unavailable data, two MMs (DC 06_09_57 (FgC) and DC 06_09_149 (Xtal)) are not plotted due to large uncertainties (see Table 40).

Three Xtal MMs plot in the direction of the subsolar component found in enstatite chondrites (see Crabb and Anders (1981)), but SW contributions (contributing more to Ar than to Kr and more to Kr than to Xe) are more likely. Only 1 MM (DC 06_09_189 (FgC/Sc)) shows a low, Q-like, $^{36}Ar/^{132}Xe$ ratio of 84, but $^{84}Kr/^{132}Xe$ is high at 4.1, indicating that this MM may have been influenced by fractionated Earth atmosphere, not unlikely, given its thermal history as a possibly scoriaceous micrometeorite.

Fig. 84 shows trapped ^{36}Ar and ^{84}Kr concentrations plotted against trapped ^{132}Xe concentrations, for our data, data of selected TAM MMs (see chapter 5.4.6) and data of typical ordinary and carbonaceous chondrites (Marti (1967)), along with AMM data from Osawa and Nagao (2002).

Bastian Baecker | Chapter 6 - Micrometeorites from the CONCORDIA collection (Dome C) and from Cap Prudhomme, Antarctica – Noble gases show the possibility for a single population

174
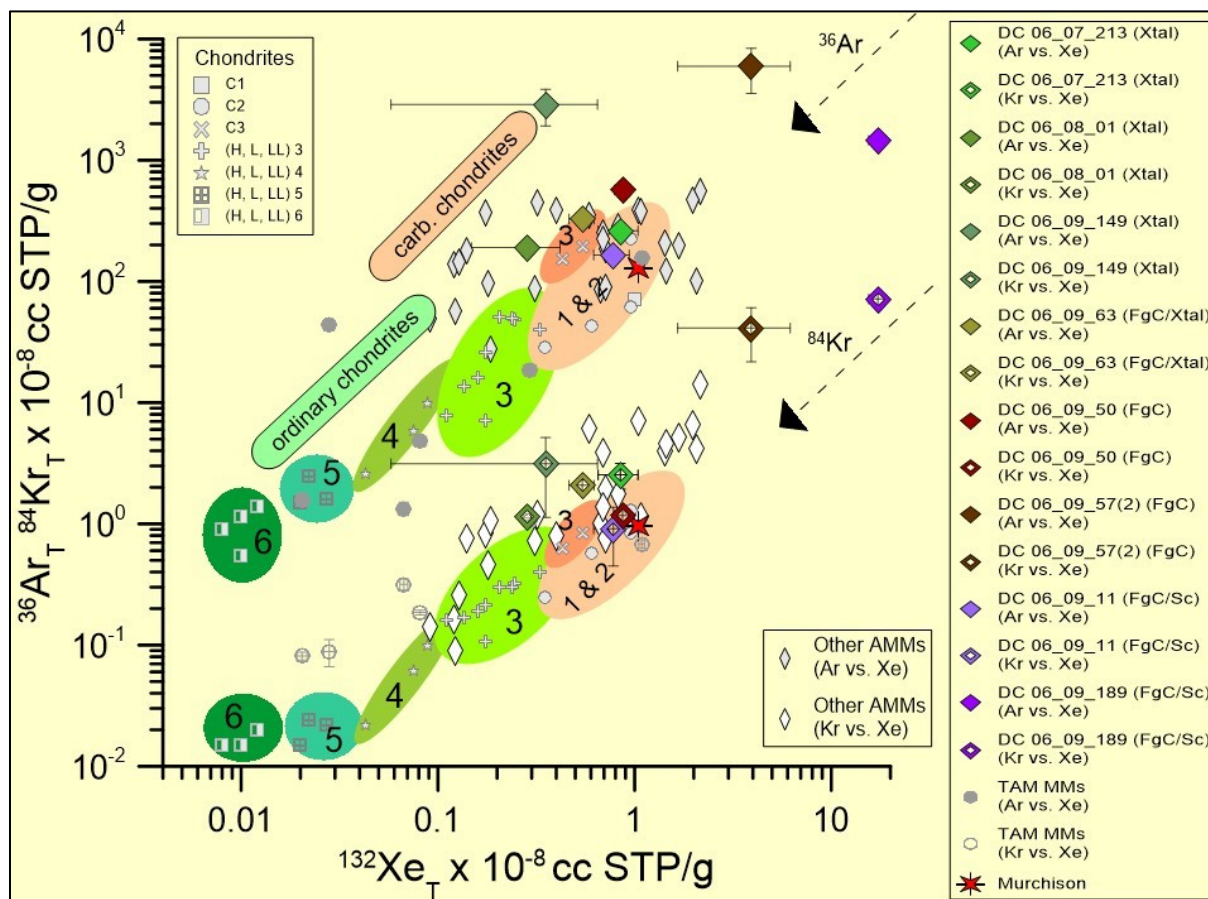
Figure 84. Concentrations of ^{36}Ar and ^{84}Kr vs. ^{132}Xe in units of 10^{-8} cc STP/g are plotted, for our DC/CP data, selected TAM data (see chapter 5.4.6 and the Appendix), for Murchison (measured at MPIC 2011) and data from Osawa and Nagao (2002) as well as data from Marti (1967).

The area of carbonaceous chondrites is held in a more red tone, the area of ordinary chondrites in a greener one. The numbers in the colored fields show the respective meteorite classes. Symbols for chondrites are shown in the box in the upper left, symbols for MMs in the two boxes on the right side. In case of the DC MMs, the symbols are filled with colors for the comparison of trapped ^{36}Ar with trapped ^{132}Xe, whereas the symbols for comparison of trapped ^{84}Kr with ^{132}Xe are empty. All 8 DC samples with Ar, Kr and Xe available, plot in or near the carbonaceous chondrite region. Ar and Kr are higher than even in the carbonaceous and ordinary chondrites measured by Marti (1967) – maybe due to SW Ar (high $^{36}Ar/^{132}Xe$ & high $^{84}Kr/^{132}Xe$) and air contamination in Kr (high $^{84}Kr/^{132}Xe$) - note that the meteorite data largely reflect the abundance in them of the "planetary" Q (P1) component. As discussed in the individual chapters for Ar, Kr and Xe the DC MMs and the MMs from Osawa and Nagao (2002) seem to be characterized by larger concentrations in Ar, Kr and Xe than the TAM MMs, resembling carbonaceous chondrites. By far the largest trapped ^{132}Xe concentrations are seen in DC 06_09_57 (2) (FgC) and DC 06_09_189 (FgC/Sc). Also, once more, as in the Ar, Kr and Xe sections it seems that Xtal MMs and FgC MMs form two separate groups, with FgC MMs showing the highest gas noble gas concentrations, but with Xtal MMs apparently more similar to each other.

Bastian Baecker | Chapter 6 - Micrometeorites from the CONCORDIA collection (Dome C) and from Cap Prudhomme, Antarctica – Noble gases show the possibility for a single population

175

6.4.7 Cosmogenic concentrations and CRE-Ages

Results for cosmogenic ^{21}Ne as well as nominal ^{38}Ar concentrations and ^{21}Ne/^{38}Ar ratios are given in Table 41. For detailed explanations regarding the calculation of cosmogenic ^{21}Ne and ^{38}Ar concentrations along with CRE-ages see chapter 5.4.7.

Only 4 DC MMs (out of 10) show detectable cosmogenic ^{21}Ne contributions, due to the large amounts of trapped neon. 2 MMs from DC as well as the CP MM show upper limits only and for 4 MMs from DC the overall cosmogenic contributions were below blank level. In all cases measured ^{20}Ne/^{22}Ne was >11, hence, as in the case of the TAM MMs with dominating SW / "FSW", we calculated the relative concentrations assuming that trapped Ne is of a mixture of SW (solar wind) and "FSW" ("fractionated solar wind noble gases"; e.g. Wieler et al. (2007) - see also chapter 3.2.1.1). Taking this in consideration, we calculated the expected ^{21}Ne/^{22}Ne using the obtained ^{20}Ne/^{22}Ne value for the trapped component, making use of the fact that in such "extreme" cases, the cosmogenic contributions to ^{22}Ne and ^{20}Ne are negligible. See chapter 5.4.7 for further discussion of the approach.

The ^{21}Ne$_{cos}$ concentrations are, where available, in the range of ~0.1 (DC 06_09_50 (FgC)) to ~0.5 x 10^{-8} (DC 06_08_01 (Xtal)) cc STP/g, naturally with large uncertainties. These concentrations are at the lower end of what was measured for TAM MMs (Table 27) and lower than in the 3 (out of 27) MMs in which cosmogenic ^{21}Ne was detected by Osawa and Nagao (2002).

In the case of cosmogenic ^{38}Ar and as already explained for the TAM MMs in chapter 5.4.7, the concentrations listed in Table 41 are essentially upper limits only. Consequentially, ^{21}Ne$_{cos}$/^{38}Ar$_{cos}$ ratios in Table 41 are lower limits. Even so only two DC MMs showed positive nominal (upper limit) cosmogenic contributions. Additional 2 MMs showed only upper limits for the nominal (i.e. for our choice of trapped composition) abundance, whereas for different 7 MMs no measurable ^{38}Ar$_{cos}$ was available at all. The nominal values for ^{38}Ar$_{cos}$ in the two positive DC MMs (DC 06_09_50 (FgC); DC 06_08_01 (Xtal)) are 3.17 x 10^{-8} cc STP/g and 3.60 x 10^{-8} cc STP/g. Note that the results could be further compromised by isotopic fractionation effects.

The nominal cosmogenic ^{21}Ne/^{38}Ar ratios for the 2 DC MMs are 0.03 and 0.15. Unlike the case of the TAM MMs, the chemical composition of the DC MMs can confidently be assumed carbonaceous chondrite-like, so, if real, the low (^{21}Ne/^{38}Ar)$_{cos}$ ratio must be due to a secondary effect. This is unlikely to be weathering on Earth of these rather fresh material, so significant loss during atmospheric entry heating must in fact be considered seriously (see discussion in chapter 5.4.7 and Füri et al. (2013)). Arguing against this, on the other hand, the fact that in at least four of the DC MMs, with ^{3}He/^{4}He ratios higher than SW, clear evidence was found for the presence of cosmogenic ^{3}He (DC 06_07_213, DC 06_08_01, DC 06_09_141 and DC 07_09_149). Systematic uncertainties in deriving cosmogenic abundances in samples with extremely dominant trapped Ne and Ar are thus the most important problem. In fact, none of the DC/CP MMs has a ^{38}Ar/^{36}Ar ratio higher than the "FSW"

Bastian Baecker | Chapter 6 - Micrometeorites from the CONCORDIA collection (Dome C) and from Cap Prudhomme, Antarctica – Noble gases show the possibility for a single population

176

value (see Table 37), and thus, considered conservatively, for all the cosmogenic Ar abundance is compatible with zero.

Taking the calculated cosmogenic concentrations at face value, one is able to calculate the cosmogenic exposure ages (CRE) using the elemental composition in combination with production rates. For details of the approach see chapter 5.4.7. In case of the mineralogy, we are assuming a carbonaceous chondrite (CI) composition for the DC MMs, as suggested by Duprat et al. (2007), which results in the production rates (at 1 AU) given in Table 28 (chapter 5.4.7). The resulting CRE-ages (in Ma) along with starting positions (in AU) of the four particles with positive $^{21}Ne_{cos}$ are shown in Table 42. The results suggest CRE-ages between about 0.1 to 1.6 Ma and travel starting from about 1.4 AU to 4.5 AU. However, the uncertainties are large.

For the reasons given in chapter 5.4.7 and above (systematic uncertainties resulting in generally upper limits to cosmogenic Ar only), we do not list CRE ages and travel distances for the CONCORDIA Collection (Dome C) MMs and the single Cap Prudhomme MM based on ^{38}Ar.

Table 41. Concentrations of cosmogenic ^{21}Ne, ^{38}Ar and $^{21}Ne/^{38}Ar$ ratios for the Dome C and Cap Prudhomme MM samples. Totals, based on the sum of individual measurement steps as indicated - for more details see Appendix. Uncertainties in the last digits are given in parenthesis. Values with $^\$$ are 2σ upper limits. Where no values for cosmogenic ^{38}Ar are given, they could not be determined because of too large concentrations of trapped Ar. Note that in general cosmogenic ^{38}Ar concentrations are upper limits only and cosmogenic $^{21}Ne/^{38}Ar$ ratios are lower limits only (errors in parentheses do not include systematic uncertainties; see text in chapter 5.4.7 for discussion).

Sample	Particle no.	Weight (μg) (calculated)	Step(s) used	$^{21}Ne_{cos}$	$^{38}Ar_{cos}$*	$^{21}Ne_{cos}/^{38}Ar_{cos}$#
				(10^{-8} cc STP/g)		
DC 06_07_213 (Xtal)	PL 09_20 7 (1)	~1.1	all	-	-	-
DC 06_08_01 (Xtal)	PL06_09A 1	~1.4	1	0.523 (201)	3.60 (1.03)	0.15 (7)
DC 06_09_11 (FgC/Sc)	PL07_01A 11	~1.3	all	0.125 (111)	< 2.11 $^\$$	-
DC 06_09_50 (FgC)	PL07_02B 2	~3.3	1	0.094 (94)	3.17 (1.87)	0.03 (3)
DC 06_09_57 (FgC)	PL07_02B 9 (1)	~0.15	all	-	-	-
DC 06_09_57 (FgC)	PL07_02B 9 (2)	~0.05	all	-	-	-
DC 06_09_63 (FgC/Xtal)	PL07_02C 3	~3.3	1	< 0.252 $^\$$	< 1.38 $^\$$	-
DC 06_09_141 (Xtal)	PL07_04C 9 (1)	~0.7	all	-	-	-
DC 06_09_149 (Xtal)	PL07_05A 5 (1)	~0.3	all	< 3.536 $^\$$	-	-
DC 06_09_189 (FgC/Sc)	PL07_06A 9	~1.0	all	0.480 (358)	-	-
CP 9-1-1994 (Sc)	PL 10-109D 9	6.2 (1)	1	< 0.044 $^\$$	-	-

* = upper limits; # = lower limits

Bastian Baecker | Chapter 6 - Micrometeorites from the CONCORDIA collection (Dome C) and from Cap Prudhomme, Antarctica – Noble gases show the possibility for a single population

177

Table 42. Cosmic ray exposure ages using $^{21}Ne_{cos}$ for the CONCORDIA Collection MMs (where available) along with starting position using production rates from Table 28 (chapter 5.4.7). Mean CI meteoritic composition is assumed (see Duprat et al. (2007)).

Sample	Weight (µg) of <u>whole</u> sample (calculated) [%]	Size (µm) of <u>whole</u> sample[§]	Assumed composition	$^{21}Ne_{cos}$ (10^{-8} cc STP/g)	CRE [#] SCR+GCR (Ma)	Starting position (AU)
DC 06_08_01 (Xtal)	~1.4	101	CC (CI)	0.523 (201)	1.6 (1.0)	4.22 (1.10)
DC 06_09_11 (FgC/Sc)	~1.3	124	CC (CI)	0.125 (111)	0.2 (2)	2.21 (1.10)
DC 06_09_50 (FgC)	~3.3	138	CC (CI)	0.094 (94)	0.1 (1)	1.39 (39)
DC 06_09_189 (FgC/Sc)	~1.0	93	CC (CI)	0.480 (358)	1.5 (1.3)	4.48 (2.66)

<u>Note:</u> [%]*Weights were calculated using assumed volumes and densities (see chapter 4.1.2)* [§]*Sizes of MM particles are mean of major and minor axis (see Table 33);* [#] *CRE-ages calculated assuming 4π irradiation with GCR and SCR; CC = carbonaceous chondrite.*

6.5 Summary and Conclusions

Overall, the MMs from the DC / CP MM collection are rather similar to each other, showing high concentrations of SW (evident in He, Ne and Ar) along with evidence for fractionation processes influencing the noble gas inventory. Nevertheless, there seem to be slight differences between FgC and Xtal MMs. The small size and low weight of these MMs made it challenging to measure them in a very precise manner. Still, the comprehensive noble gas analysis (He-Xe) for 11 particles of 10 DC and CP MMs clearly reveals higher gas concentrations than found for the TAM MMs (see chapter 5) and, at least for a few MMs, also higher than in earlier research (e.g. Olinger et al. (1990), Sarda et al. (1991), Osawa et al. (2000), Osawa and Nagao (2002)). These small particles probably have travelled or have been delivered to Earth over a rather short distance only, with a possible regolith history. This is indicated by the high SW abundances and the low cosmogenic contributions. Some DC and CP MMs may have also received fractionated air gases (especially the Xtal MMs), during transition through the Earth's atmosphere (see chapter 7) and/or during their preservation in the snow/ice near Dome C. Overall these MMs seem to be "fresher" then the MMs from TAM (see chapter 5). This is not surprising, since they were recovered by scientists after being deposited for decades only (see Duprat et al. (2007)), not for ~1 Ma as the TAM MMs (see Rochette et al. (2008)).

Bastian Baecker | Chapter 6 - Micrometeorites from the CONCORDIA collection (Dome C) and from Cap Prudhomme, Antarctica – Noble gases show the possibility for a single population

178

Chapter 7 - Air contamination and noble gas loss in micrometeorites during atmospheric entry onto Earth

7.1 Introduction

Several previous studies (e.g. Greshake et al. (1998), Stuart et al. (1999), Genge et al. (2000), Osawa and Nagao (2002), Cordier et al. (2011), Rudraswami et al. (2012), Marrocchi and Marty (2013) and Füri et al. (2013)) showed that mineralogical differentiation, air contamination and noble gas loss in MMs is occurring through various mechanisms, i.e., fractionation processes on the parent body, loss and/or exchange of isotopes through thermal events during Earth atmosphere transition, fractionation processes during deposition in water and sediments on Earth, weathering of MM samples while exposed to the environment in geological traps. This chapter shall give an overview about the possible significance of air contamination and noble gas loss in the measured MMs from TAM, as well as from DC and CP.

7.2 Noble gas results and discussion

Noble gas results indicating possible air contamination and/or noble gas loss for our measured MMs are shown in Figs. 85 to 89 (for detailed results see Appendix). Fig. 85 and Fig. 86 show the $^{36}Ar/^{132}Xe$ ratio plotted versus the isotopic composition of $^{40}Ar/^{36}Ar$, whereas the Figs. 87 and 88 show ratios of $^{84}Kr/^{132}Xe$ vs. $^{40}Ar/^{36}Ar$ for data obtained for the TAM MMs and DC / CP MMs, along with data from Osawa and Nagao (2002), as well as the components SW (Vogel et al. (2011)), EA (Ozima and Podosek (2002)), EFA (elementally fractionated air) (Mohapatra et al. (2002)) and Q(P1) (Busemann et al. (2000)).

For TAM MMs: In case of $^{36}Ar/^{132}Xe$ as well as $^{84}Kr/^{132}Xe$, most of the MMs plot near the Q(P1) composition, which is an indication for primordial noble gases. On the other hand, 2 UnMMs, 5 ScMMs and the single Cosmic Spherule plot near the composition of "elementally fractionated air - EFA" which has been suggested by Mohapatra et al. (2002). This low temperature component explains to a great extent the influence of terrestrial weathering, i.e. dry desert weathering along with carbonate formation (see Mohapatra et al. (2009), on the inventory of especially the heavy noble gases Kr and Xe (enrichment). Here the main fractionation is caused by additional noble gas adsorption (Mohapatra et al. (2009)) rather than noble gas loss due to e.g. heating during Earth atmosphere transition. In this connection, Xe is favored over Kr and Kr is favored over Ar, which results in low ratios of $^{36}Ar/^{132}Xe$ (~25) as well as $^{84}Kr/^{132}Xe$ (~1) (for both see Mohapatra et al. (2009)) compared to air (1343 and 27.8, respectively; Ozima and Podosek (2002)). The plots in Figs. 85 and 87 suggest that at least for the 8 TAM MMs mentioned above, weathering along with fractionation due to adsorption and solution of noble gases in water may play an important part (Ozima and Podosek (2002)). The impact of Antarctic "cold desert" weathering on the noble gas inventory of meteorites was addressed in further reserach, e.g. Schwenzer et al. (2007).

Bastian Baecker | Chapter 7 - Air contamination and noble gas loss in micrometeorites during atmospheric entry onto Earth

179

As for the $^{40}Ar/^{36}Ar$ ratio, especially the scoriaceous MMs and the single Cosmic Spherule are plotting in the direction of air-Ar indicating air contamination; while overall also many plot close to the Q-air mixing line. This is not a surprising result, since we presume a strong thermal history for these types of MMs.

As already mentioned in chapter 5.4.6, the MMs measured by Osawa and Nagao (2002) show beside possible air contamination also SW influence, a fact indicated by high $^{36}Xe/^{132}Xe$ ratios. In our case, only the UnMM X1 (45c.35(1)) shows evidence for significant SW contributions to Ar. The UnMMs 45c.37(3) and 45c.10(2) seem to have acquired a mix of air-Ar and probably "FSW"/SW-Ar.
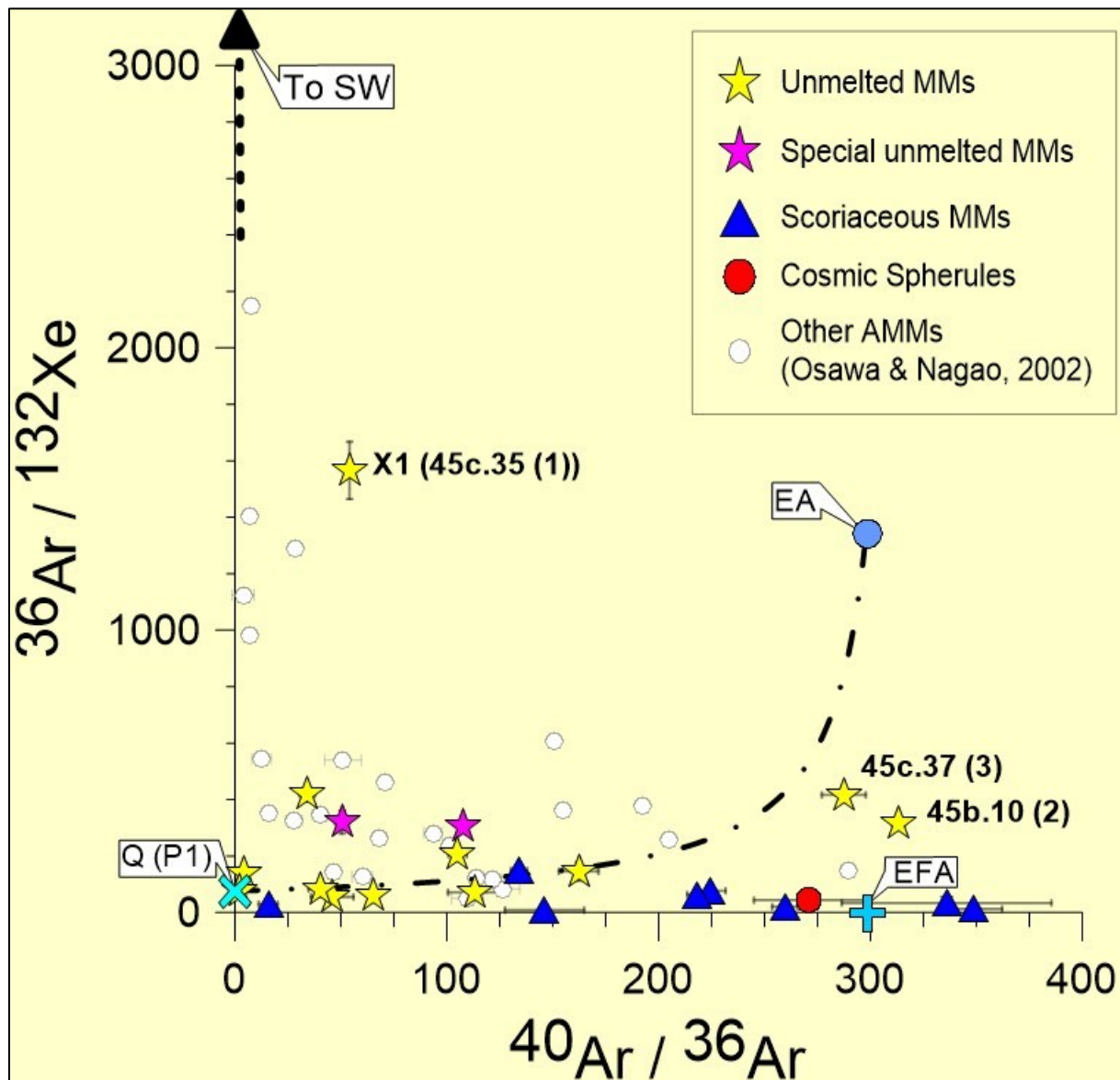
Figure 85. Isotope plot of $^{36}Ar / ^{132}Xe$ vs. $^{40}Ar / ^{36}Ar$ for the TAM MM samples and data from Osawa and Nagao (2002). Also plotted for comparison are "to SW" (Vogel et al. (2011)), EA (Ozima and Podosek (2002)), EFA (elementally fractionated air) (Mohapatra et al. (2002)) and Q (P1) (Busemann et al. (2000)). The dashed line is the mixing curve for mixing between Q and (unfractionated) air.

Bastian Baecker | Chapter 7 - Air contamination and noble gas loss in micrometeorites during atmospheric entry onto Earth

180
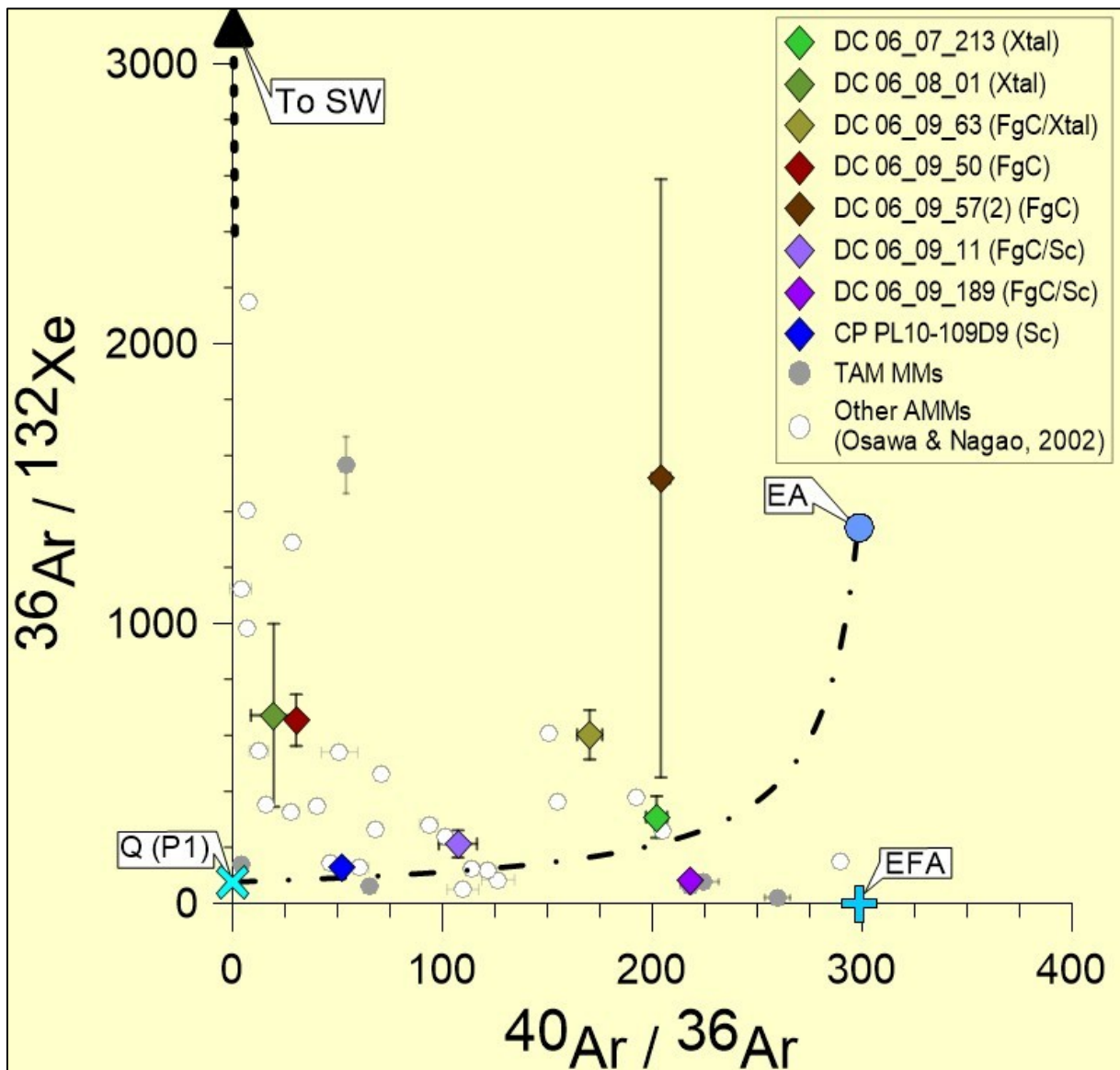
Figure 86. Isotope plot of $^{36}Ar / ^{132}Xe$ vs. $^{40}Ar / ^{36}Ar$ for our Dome C and Cap Prudhomme MMs and data from Osawa and Nagao (2002), as well as selected TAM MM data. Also plotted for comparison are "to SW" (Vogel et al. (2011)), EA (Ozima and Podosek (2002)), EFA (elementally fractionated air) (Mohapatra et al. (2002)) and Q (P1) (Busemann et al. (2000)). The dashed line is the mixing curve for mixing between Q and (unfractionated) air.

For DC / CP MMs: As indicated in Fig. 86 and 88, most of the DC/CP MMs show air contamination mixed to various degrees with Q. The $^{36}Ar/^{132}Xe$, as well as the $^{84}Kr/^{132}Xe$ ratio shows that the MMs of DC and CP contain a less strong primordial pattern than the MMs from TAM but probably a larger "FSW"/SW contribution. This is not surprising given their significantly higher He and Ne abundances (see chapter 6). Here, the previously mentioned "EFA" component (Mohapatra et al. (2002)) seems to be of less importance, which may again reflects the "freshness" of these samples. The also earlier mentioned grouping of Xtal vs. FgC MMs is recognizable only in parts in this representation. Overall it seems that the MMs from DC and CP show more similarities with the MMs measured by Osawa and Nagao (2002) than the TAM MMs (compare also chapters 5 and 6).

Bastian Baecker | Chapter 7 - Air contamination and noble gas loss in micrometeorites during atmospheric entry onto Earth

181

Of course, some of the high $^{40}Ar/^{36}Ar$ ratios could also be due to the presence of radiogenic ^{40}Ar. It is telling, though, that the ratio never clearly exceed the ratio in air.
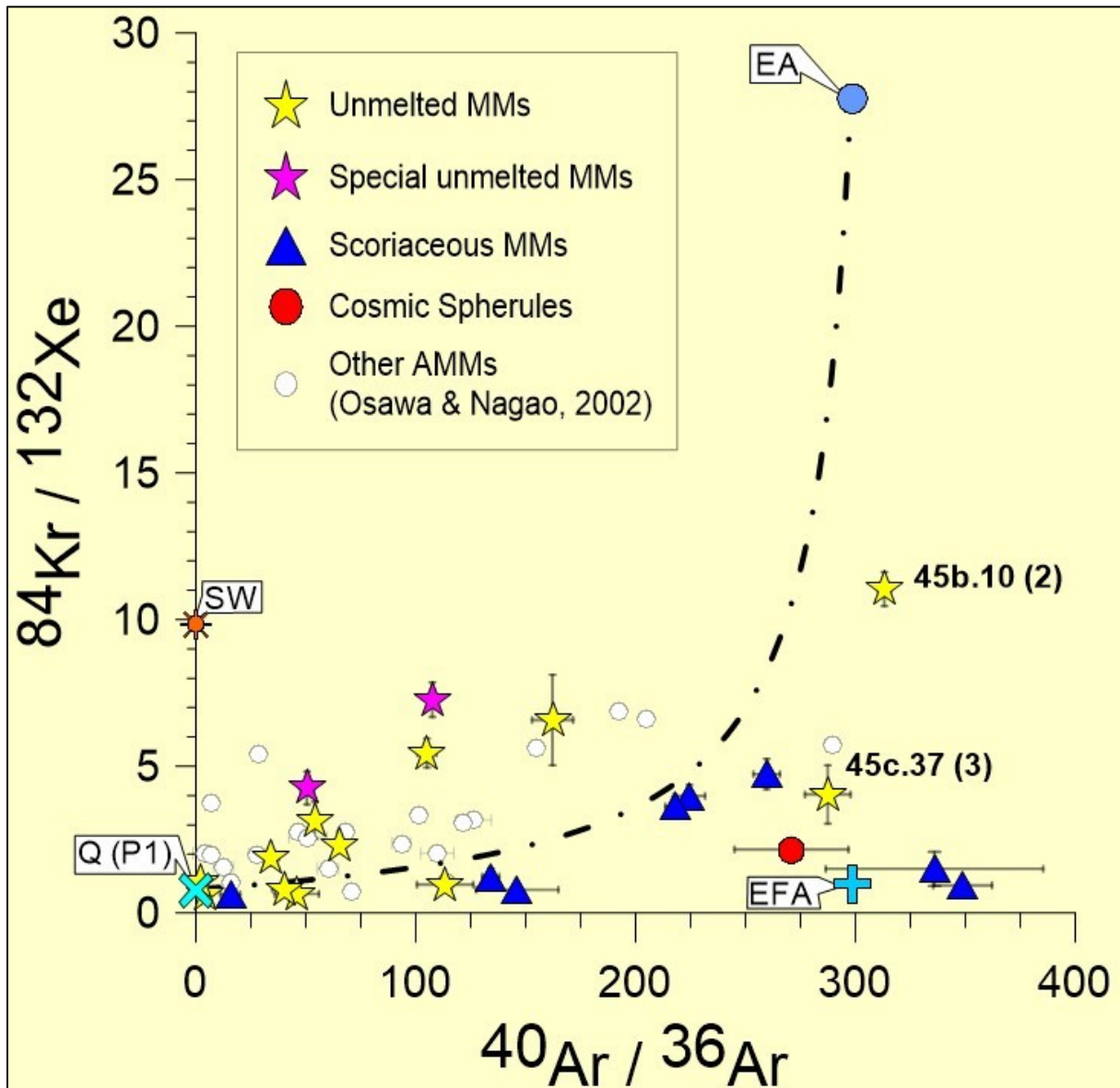
Figure 87. Isotope plot of $^{84}Kr / ^{132}Xe$ vs. $^{40}Ar / ^{36}Ar$ for the TAM MM samples and data from Osawa and Nagao (2002). Also plotted for comparison are SW (Vogel et al. (2011)), EA (Ozima and Podosek (2002)), EFA (elementally fractionated air) (Mohapatra et al. (2002)) and Q (P1) (Busemann et al. (2000)). The dashed line is the mixing curve for mixing between Q and (unfractionated) air.

Fig. 89 is a isotope plot of Xe in per mil-deviations from air Xe composition (Basford et al. (1973)) and compares overall, Xe isotopic data of selected TAM, DC and CP MMs (see chapters 5, 6 and the Appendix) to SW (Meshik et al. (2012)) and Q-Xe (Busemann et al. (2000)). The MM data shown were obtained by calculating as the weighted mean of values of selected MMs in the two groups below, as follows, since these are immediately recognizable.

Bastian Baecker | Chapter 7 - Air contamination and noble gas loss in micrometeorites during atmospheric entry onto Earth

182
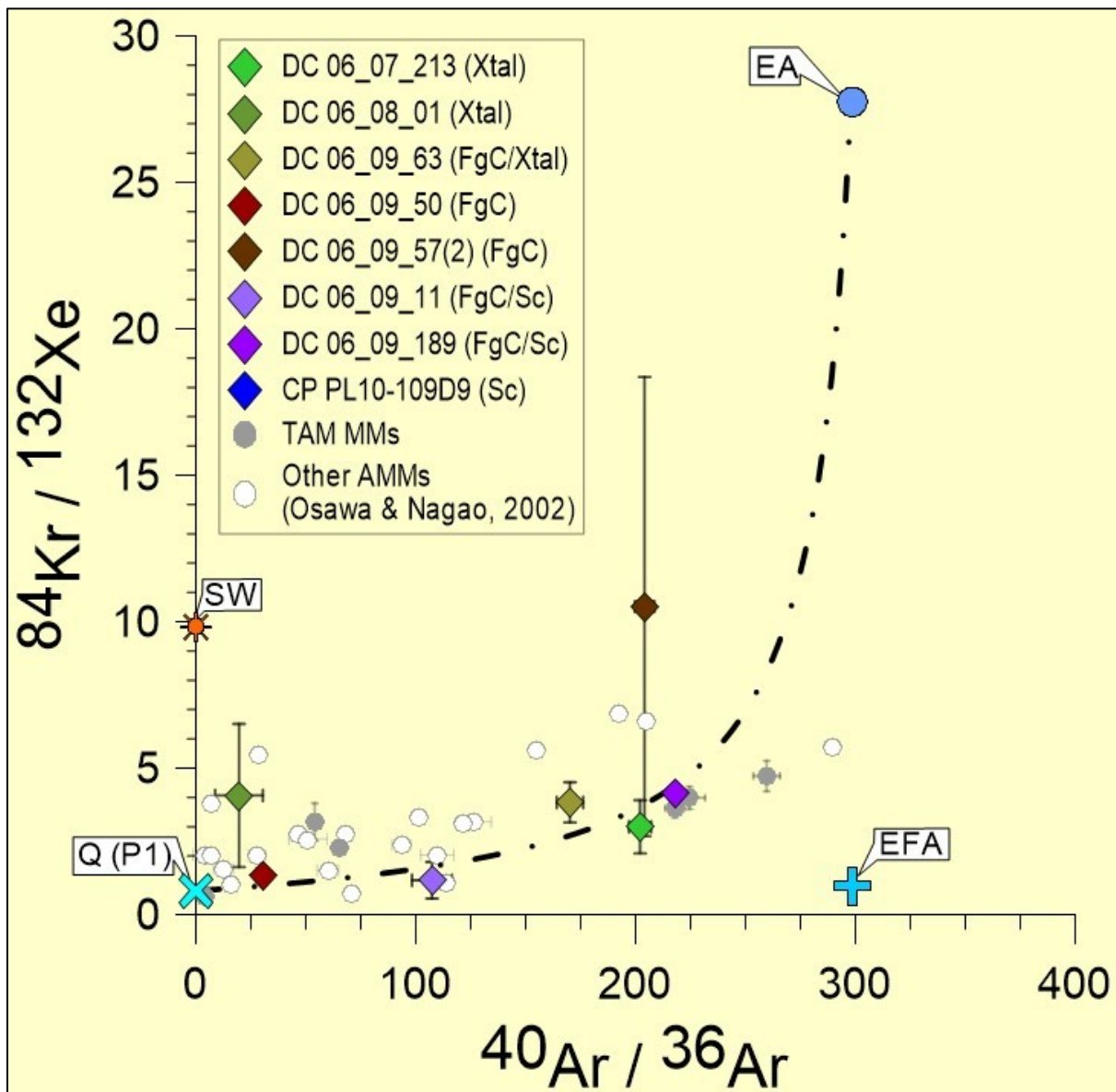
Figure 88. Isotope plot of ^{84}Kr / ^{132}Xe vs. ^{40}Ar / ^{36}Ar for our Dome C and Cap Prudhomme MMs and data from Osawa and Nagao (2002), as well as selected TAM MM data. Also plotted for comparison are SW (Vogel et al. (2011)), EA (Ozima and Podosek (2002)), EFA (elementally fractionated air) (Mohapatra et al. (2002)) and Q (P1) (Busemann et al. (2000)). The dashed line is the mixing curve for mixing between Q and (unfractionated) air.

One group is enriched in the lighter Xe isotopes, along with depleted heavier Xe isotopes compared to air, similar to the planetary Q-phase Xe, indicating trapped planetary components. This group consists of the following MMs: 45b.14(1), 45b.15(1), 45b.20(2), 45b.21, 45c.24, 45c.29(2), 45c.34(1), 45c.35(2), 45c.35(3), 45c.37(2), 45c.37(3), CP PL10-109D9 and DC 06_09_189. The other group seems to be of opposite character and shows a loss of original trapped Xe and acquired instead mass fractionated air Xe. This group includes the following MMs: 45b.08(1), 45b.09(1), 45b.10(2), 45b.13(1), 45b.17(1), 45c.29(1), DC 06_07_213 and DC 06_08_01.

Bastian Baecker | Chapter 7 - Air contamination and noble gas loss in micrometeorites during atmospheric entry onto Earth

183
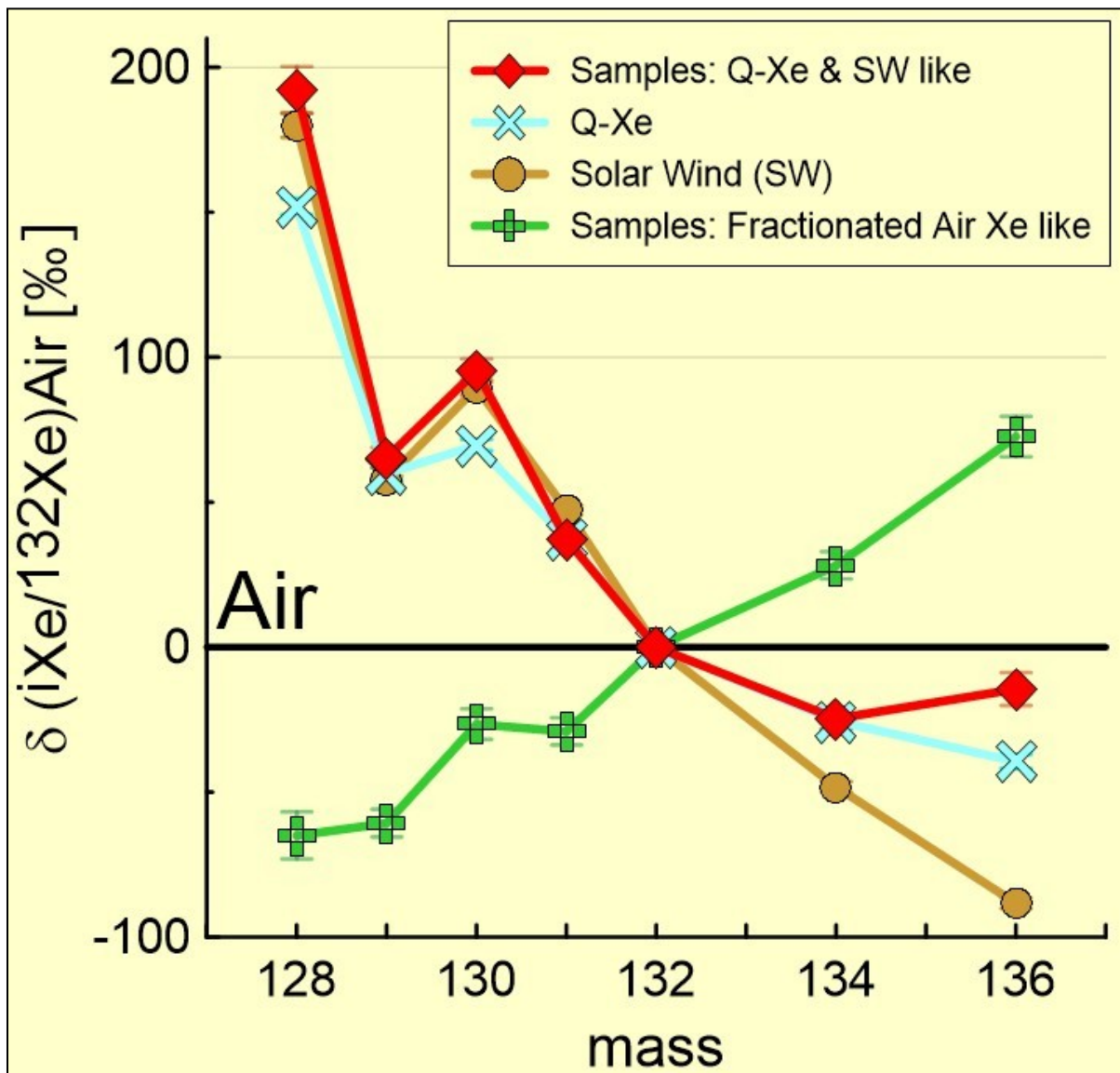
Figure 89. Isotope plot of Xe showing the weighted mean of selected overall TAM, DC and CP MM data (for details see text) of two groups compared to SW (Meshik et al. (2012)) and Q-Xe (Busemann et al. (2000)). Shown are per mil-deviations from the air Xe (Basford et al. (1973)) composition.

7.3 Summary and Conclusions

Overall the graphs show only indications for air contamination, although it seems to be clearly present. Air contamination is difficult to estimate, since the presence of a mix of different components was already proven in the earlier chapters and also the thermal history is not completely revealed. Nevertheless, variations within $^{40}Ar/^{36}Ar$ are larger for TAM MMs than for most DC/CP MMs. This is probably due to the different size distribution of these samples. Following most of the studies mentioned above, size and time of deposition of MMs (besides mineralogy, entry angle and speed) play an important role for the thermal history and for weathering effects on Earth. However, the results shown in this chapter as well as in chapters 5 and 6 also support the idea that some of the MMs were able to retain larger amounts of their original noble gas inventory. Mostly scoriaceous MMs and Cosmic Spherules, but, however, also some unmelted MMs, do show severe depletions and air contamination effects reflecting their thermal history.

Bastian Baecker | Chapter 7 - Air contamination and noble gas loss in micrometeorites during atmospheric entry onto Earth

184

Appendix

A. Additional remarks for reading an interpreting the tables

- **total*** = results can differ in the last digit due to rounding.

- Total results including 2σ values which are shown in some steps.

- Uncertainties are given with the symbol **±**

- **#** = an additional step was performed which is not shown here due to He-Xe results below detection limit.

- **$** = only corrected for blank values in cc STP.

- For Xe INT, EXTa and EXTb explanations see chapter 4.3.5.1.

- Data labelled as "*not corrected for blank*" are basically corrected for isobaric interferences

B. Noble gas data for measured micrometeorites - corrected for blank and isobaric interferences

Data tables for He to Xe - isotopic analysis for all measured micrometeorites.

Table X1. Noble gas data He to Xe for sample 45b.08_1 (corrected for blank)

Sample	45b.08_1			
Size [µm]	654 x 374			
Weight [µg]	119.3 ± 0.1			
Date of measurement	24/10/11	25/10/11	26/10/11	24/-27/10/11#
Laser-Power	3 x 0.13 W	3 x 0.91 W	3 x 5 W	
Laser-Beam	250 µm	600 µm	600 µm	
Step(s)	1	2	3	total*
^{4}He [in 10^{-8} cc/g]	18.2	165.2	5.1	188.5
±	4.7	5.7	4.7	8.8
^{4}He [in 10^{-12} cc]	21.7	197.1	6.0	224.9
±	5.7	6.8	5.6	10.5
^{3}He [in 10^{-12} cc/g]	-	338.0	452.9	790.9
±	-	115.1	92.4	147.6
^{3}He [in 10^{-16} cc]	-	403.3	540.3	943.5
±	-	137.3	110.2	176.1
^{3}He/^{4}He	-	0.00020	0.00893	0.00042
±	-	0.00007	0.00853	0.00008
^{22}Ne [in 10^{-8} cc/g]	-	0.09	1.57	1.66
±	-	0.03	0.04	0.04
^{22}Ne [in 10^{-12} cc]	-	0.11	1.88	1.98
±	-	0.03	0.04	0.05
^{20}Ne/^{22}Ne	-	7.44	5.23	5.35
±	-	0.91	0.07	0.09
^{21}Ne/^{22}Ne	-	0.372	0.558	0.548
±	-	0.050	0.012	0.012
^{21}Ne$_{cos}$ [in 10^{-8} cc/g]	-	0.031	0.855	0.886
±	-	0.010	0.026	0.028
^{21}Ne$_{cos}$ [in 10^{-12} cc]	-	0.037	1.020	1.057
±	-	0.012	0.031	0.034
^{20}Ne$_{trap}$ [in 10^{-8} cc/g]	-	0.64	7.51	8.15
±	-	0.21	0.48	0.52
^{20}Ne$_{trap}$ [in 10^{-12} cc]	-	0.76	8.96	9.72
±	-	0.25	0.57	0.63
^{36}Ar [in 10^{-8} cc/g]	0.75	1.34	0.89	2.98
±	0.04	0.12	0.11	0.17
^{36}Ar [in 10^{-12} cc]	0.89	1.60	1.06	3.55
±	0.05	0.14	0.14	0.20
^{38}Ar/^{36}Ar	0.163	0.195	0.228	0.197
±	0.023	0.004	0.007	0.007
^{40}Ar/^{36}Ar	265.7	328.1	151.6	259.7
±	8.3	8.9	12.5	6.0
^{40}Ar [in 10^{-8} cc/g]	199.2	439.6	134.9	773.7
±	6.3	30.2	28.6	42.0
^{40}Ar [in 10^{-12} cc]	237.6	524.5	160.9	923.0
±	7.5	36.0	34.1	50.1
^{38}Ar$_{cos}$ [in 10^{-8} cc/g]	-	0.010	0.041	0.050
±	-	0.007	0.008	0.011
^{38}Ar$_{cos}$ [in 10^{-12} cc]	-	0.012	0.048	0.060
±	-	0.009	0.010	0.013
^{84}Kr [in 10^{-8} cc/g]	0.0231	0.3179	0.0206	0.3616
±	0.0044	0.0323	0.0043	0.0329
^{84}Kr [in 10^{-12} cc]	0.0275	0.3793	0.0245	0.4313
±	0.0053	0.0385	0.0051	0.0392
^{80}Kr/^{84}Kr	0.039	0.032	0.033	0.032
±	0.005	0.001	0.004	0.001
^{82}Kr/^{84}Kr	0.185	0.180	0.186	0.180
±	0.013	0.003	0.014	0.003
^{83}Kr/^{84}Kr	0.198	0.190	0.182	0.190
±	0.013	0.003	0.013	0.002
^{86}Kr/^{84}Kr	0.304	0.336	0.321	0.333
±	0.020	0.004	0.017	0.004
^{83}Kr$_{cos}$ [in 10^{-8} cc/g]	-	-	-	-
±	-	-	-	-
^{83}Kr$_{cos}$ [in 10^{-12} cc]	-	-	-	-
±	-	-	-	-

Date of measurement	24/10/11	25/10/11	26/10/11	24-27/10/11#
Laser-Power	3 x 0.13 W	3 x 0.91 W	3 x 5 W	
Laser-Beam	250 µm	600 µm	600 µm	
Step(s)	1	2	3	total*
^{132}Xe - INT [in 10^{-8} cc/g]	-	0.0673	-	-
±	-	0.0030	-	-
^{132}Xe - INT [in 10^{-12} cc]	-	0.0802	-	-
±	-	0.0036	-	-
^{128}Xe/^{132}Xe - INT	-	0.063	-	-
±	-	0.002	-	-
^{129}Xe/^{132}Xe - INT	-	0.890	-	-
±	-	0.012	-	-
^{130}Xe/^{132}Xe - INT	-	0.145	-	-
±	-	0.002	-	-
^{131}Xe/^{132}Xe - INT	-	0.751	-	-
±	-	0.009	-	-
^{134}Xe/^{132}Xe - INT	-	0.407	-	-
±	-	0.006	-	-
^{136}Xe/^{132}Xe - INT	-	0.372	-	-
±	-	0.008	-	-
^{132}Xe - EXTa [in 10^{-8} cc/g]	-	0.0671	-	-
±	-	0.0019	-	-
^{132}Xe - EXTa [in 10^{-12} cc]	-	0.0801	-	-
±	-	0.0023	-	-
^{128}Xe/^{132}Xe - EXTa	-	0.062	-	-
±	-	0.002	-	-
^{129}Xe/^{132}Xe - EXTa	-	0.889	-	-
±	-	0.012	-	-
^{130}Xe/^{132}Xe - EXTa	-	0.144	-	-
±	-	0.003	-	-
^{131}Xe/^{132}Xe - EXTa	-	0.751	-	-
±	-	0.009	-	-
^{134}Xe/^{132}Xe - EXTa	-	0.406	-	-
±	-	0.006	-	-
^{136}Xe/^{132}Xe - EXTa	-	0.361	-	-
±	-	0.006	-	-
^{132}Xe - EXTb [in 10^{-8} cc/g]	-	0.0670	-	-
±	-	0.0021	-	-
^{132}Xe - EXTb [in 10^{-12} cc]	-	0.0799	-	-
±	-	0.0025	-	-
^{128}Xe/^{132}Xe - EXTb	-	0.062	-	-
±	-	0.002	-	-
^{129}Xe/^{132}Xe - EXTb	-	0.889	-	-
±	-	0.013	-	-
^{130}Xe/^{132}Xe - EXTb	-	0.143	-	-
±	-	0.003	-	-
^{131}Xe/^{132}Xe - EXTb	-	0.751	-	-
±	-	0.002	-	-
^{134}Xe/^{132}Xe - EXTb	-	0.411	-	-
±	-	0.005	-	-
^{136}Xe/^{132}Xe - EXTb	-	0.373	-	-
±	-	0.005	-	-
^{21}Ne$_{cos}$/^{38}Ar$_{cos}$	-	3.23	21.11	17.67
±	-	2.66	4.30	3.90
^{36}Ar/^{132}Xe$_{(Int)}$	-	19.92	-	-
±	-	1.94	-	-
^{84}Kr/^{132}Xe$_{(Int)}$	-	4.73	-	-
±	-	0.52	-	-

Table X2. Noble gas data He to Xe for sample 45b.09_1 (corrected for blank)

Sample	45b.09_1						
Size [µm]	626 x 557						
Weight [µg]	126.9 ± 0.1						
Date of measurement	18/07/11	18/07/11	18/07/11	**Date of measurement**	18/07/11	18/07/11	18/07/11
Laser-Power	4 x 5 W	3 x 15 W		**Laser-Power**	4 x 5 W	3 x 15 W	
Laser-Beam	600 µm	600 µm		**Laser-Beam**	600 µm	600 µm	
Step(s)	1	2	total*	**Step(s)**	1	2	total*
^{4}He [in 10^{-8} cc/g]	23.5	-	-	^{132}Xe - INT [in 10^{-8} cc/g]	0.0815	-	-
±	1.7	-	-	±	0.0062	-	-
^{4}He [in 10^{-12} cc]	29.8	-	-	^{132}Xe - INT [in 10^{-12} cc]	0.1034	-	-
±	2.2	-	-	±	0.0079	-	-
^{3}He [in 10^{-12} cc/g]	-	-	-	^{128}Xe/^{132}Xe - INT	0.069	-	-
±	-	-	-	±	0.001	-	-
^{3}He [in 10^{-16} cc]	-	-	-	^{129}Xe/^{132}Xe - INT	0.932	-	-
±	-	-	-	±	0.010	-	-
^{3}He/^{4}He	-	-	-	^{130}Xe/^{132}Xe - INT	0.150	-	-
±	-	-	-	±	0.002	-	-
^{22}Ne [in 10^{-8} cc/g]	6.267	0.010	6.277	^{131}Xe/^{132}Xe - INT	0.769	-	-
±	0.104	0.009	0.105	±	0.008	-	-
^{22}Ne [in 10^{-12} cc]	7.952	0.013	7.966	^{134}Xe/^{132}Xe - INT	0.401	-	-
±	0.132	0.012	0.133	±	0.004	-	-
^{20}Ne/^{22}Ne	10.48	-	-	^{136}Xe/^{132}Xe - INT	0.356	-	-
±	0.16	-	-	±	0.005	-	-
^{21}Ne/^{22}Ne	0.129	0.121	0.129	^{132}Xe - EXTa [in 10^{-8} cc/g]	0.0797	-	-
±	0.001	0.063	0.001	±	0.0233	-	-
^{21}Ne$_{cos}$ [in 10^{-8} cc/g]	0.641	-	-	^{132}Xe - EXTa [in 10^{-12} cc]	0.1011	-	-
±	0.018	-	-	±	0.0295	-	-
^{21}Ne$_{cos}$ [in 10^{-12} cc]	0.814	-	-	^{128}Xe/^{132}Xe - EXTa	0.067	-	-
±	0.023	-	-	±	0.001	-	-
^{20}Ne$_{trap}$ [in 10^{-8} cc/g]	65.2	-	-	^{129}Xe/^{132}Xe - EXTa	0.933	-	-
±	3.9	-	-	±	0.009	-	-
^{20}Ne$_{trap}$ [in 10^{-12} cc]	82.7	-	-	^{130}Xe/^{132}Xe - EXTa	0.147	-	-
±	4.9	-	-	±	0.002	-	-
^{36}Ar [in 10^{-8} cc/g]	4.82	-	-	^{131}Xe/^{132}Xe - EXTa	0.775	-	-
±	0.20	-	-	±	0.008	-	-
^{36}Ar [in 10^{-12} cc]	6.12	-	-	^{134}Xe/^{132}Xe - EXTa	0.402	-	-
±	0.26	-	-	±	0.004	-	-
^{38}Ar/^{36}Ar	0.194	-	-	^{136}Xe/^{132}Xe - EXTa	0.355	-	-
±	0.003	-	-	±	0.004	-	-
^{40}Ar/^{36}Ar	65.5	-	-	^{132}Xe - EXTb [in 10^{-8} cc/g]	0.0790	-	-
±	2.5	-	-	±	0.0233	-	-
^{40}Ar [in 10^{-8} cc/g]	315.9	-	-	^{132}Xe - EXTb [in 10^{-12} cc]	0.1002	-	-
±	20.5	-	-	±	0.0296	-	-
^{40}Ar [in 10^{-12} cc]	400.9	-	-	^{128}Xe/^{132}Xe - EXTb	0.067	-	-
±	26.0	-	-	±	0.001	-	-
^{38}Ar$_{cos}$ [in 10^{-8} cc/g]	0.030	-	-	^{129}Xe/^{132}Xe - EXTb	0.934	-	-
±	0.018	-	-	±	0.009	-	-
^{38}Ar$_{cos}$ [in 10^{-12} cc]	0.038	-	-	^{130}Xe/^{132}Xe - EXTb	0.147	-	-
±	0.023	-	-	±	0.002	-	-
^{84}Kr [in 10^{-8} cc/g]	0.1854	-	-	^{131}Xe/^{132}Xe - EXTb	0.775	-	-
±	0.0081	-	-	±	0.002	-	-
^{84}Kr [in 10^{-12} cc]	0.2353	-	-	^{134}Xe/^{132}Xe - EXTb	0.406	-	-
±	0.0103	-	-	±	0.004	-	-
^{80}Kr/^{84}Kr	0.034	-	-	^{136}Xe/^{132}Xe - EXTb	0.362	-	-
±	0.001	-	-	±	0.004	-	-
^{82}Kr/^{84}Kr	0.185	-	-	^{21}Ne$_{cos}$/^{38}Ar$_{cos}$	21.36	-	-
±	0.003	-	-	±	12.90	-	-
^{83}Kr/^{84}Kr	0.199	-	-	^{36}Ar/^{132}Xe $_{(Int)}$	59.19	-	-
±	0.003	-	-	±	5.18	-	-
^{86}Kr/^{84}Kr	0.329	-	-	^{84}Kr/^{132}Xe $_{(Int)}$	2.28	-	-
±	0.004	-	-	±	0.20	-	-
^{83}Kr$_{cos}$ [in 10^{-8} cc/g]	-	-	-				
±	-	-	-				
^{83}Kr$_{cos}$ [in 10^{-12} cc]	-	-	-				
±	-	-	-				

Table X3. Noble gas data He to Xe for sample 45b.10_2 (corrected for blank)

Sample	45b.10_2		
Size [µm]	494 x 418		
Weight [µg]	95.5 ± 0.1		
Date of measurement	17/10/12	18/10/12	17+18/10/12
Laser-Power	3 x 0.91 W	2 x 15 W 1 x 5 - 20 W	
Laser-Beam	360 µm	360 µm	
Step(s)	1	2	total*
^{4}He [in 10^{-8} cc/g]	16.4	-	-
±	4.5	-	-
^{4}He [in 10^{-12} cc]	15.7	-	-
±	4.3	-	-
^{3}He [in 10^{-12} cc/g]	662.1	-	-
±	74.6	-	-
^{3}He [in 10^{-16} cc]	632.3	-	-
±	71.2	-	-
^{3}He/^{4}He	0.0040	-	-
±	0.0012	-	-
^{22}Ne [in 10^{-8} cc/g]	0.131	-	-
±	0.025	-	-
^{22}Ne [in 10^{-12} cc]	0.125	-	-
±	0.024	-	-
^{20}Ne/^{22}Ne	7.44	-	-
±	1.02	-	-
^{21}Ne/^{22}Ne	0.292	-	-
±	0.041	-	-
^{21}Ne$_{cos}$ [in 10^{-8} cc/g]	0.035	-	-
±	0.008	-	-
^{21}Ne$_{cos}$ [in 10^{-12} cc]	0.034	-	-
±	0.008	-	-
^{20}Ne$_{trap}$ [in 10^{-8} cc/g]	0.9	-	-
±	0.2	-	-
^{20}Ne$_{trap}$ [in 10^{-12} cc]	0.9	-	-
±	0.2	-	-
^{36}Ar [in 10^{-8} cc/g]	12.22	< 0.32 (2σ)	-
±	0.27	-	-
^{36}Ar [in 10^{-12} cc]	11.67	< 0.31 (2σ)	-
±	0.26	-	-
^{38}Ar/^{36}Ar	0.177	-	-
±	0.005	-	-
^{40}Ar/^{36}Ar	313.2	-	-
±	3.1	-	-
^{40}Ar [in 10^{-8} cc/g]	3838.9	< 93.38 (2σ)	-
±	87.5	-	-
^{40}Ar [in 10^{-12} cc]	3666.1	< 89.18 (2σ)	-
±	83.5	-	-
^{38}Ar$_{cos}$ [in 10^{-8} cc/g]	-	-	-
±	-	-	-
^{38}Ar$_{cos}$ [in 10^{-12} cc]	-	-	-
±	-	-	-
^{84}Kr [in 10^{-8} cc/g]	0.4286	< 0.010 (2σ)	-
±	0.0194	-	-
^{84}Kr [in 10^{-12} cc]	0.4094	< 0.009 (2σ)	-
±	0.0185	-	-
^{80}Kr/^{84}Kr	0.035	-	-
±	0.001	-	-
^{82}Kr/^{84}Kr	0.188	-	-
±	0.007	-	-
^{83}Kr/^{84}Kr	0.196	-	-
±	0.006	-	-
^{86}Kr/^{84}Kr	0.299	-	-
±	0.009	-	-
^{83}Kr$_{cos}$ [in 10^{-8} cc/g]	-	-	-
±	-	-	-
^{83}Kr$_{cos}$ [in 10^{-12} cc]	-	-	-
±	-	-	-

Date of measurement	17/10/12	18/10/12	17+18/10/12
Laser-Power	3 x 0.91 W	2 x 15 W 1 x 5 - 20 W	
Laser-Beam	360 µm	360 µm	
Step(s)	1	2	total*
^{132}Xe - INT [in 10^{-8} cc/g]	0.0388	-	-
±	0.0010	-	-
^{132}Xe - INT [in 10^{-12} cc]	0.0371	-	-
±	0.0010	-	-
^{128}Xe/^{132}Xe - INT	0.058	-	-
±	0.004	-	-
^{129}Xe/^{132}Xe - INT	0.916	-	-
±	0.017	-	-
^{130}Xe/^{132}Xe - INT	0.145	-	-
±	0.004	-	-
^{131}Xe/^{132}Xe - INT	0.804	-	-
±	0.018	-	-
^{134}Xe/^{132}Xe - INT	0.404	-	-
±	0.010	-	-
^{136}Xe/^{132}Xe - INT	0.362	-	-
±	0.012	-	-
^{132}Xe - EXTa [in 10^{-8} cc/g]	0.0388	-	-
±	0.0010	-	-
^{132}Xe - EXTa [in 10^{-12} cc]	0.0371	-	-
±	0.0010	-	-
^{128}Xe/^{132}Xe - EXTa	0.061	-	-
±	0.003	-	-
^{129}Xe/^{132}Xe - EXTa	0.915	-	-
±	0.017	-	-
^{130}Xe/^{132}Xe - EXTa	0.142	-	-
±	0.005	-	-
^{131}Xe/^{132}Xe - EXTa	0.803	-	-
±	0.018	-	-
^{134}Xe/^{132}Xe - EXTa	0.388	-	-
±	0.009	-	-
^{136}Xe/^{132}Xe - EXTa	0.338	-	-
±	0.009	-	-
^{132}Xe - EXTb [in 10^{-8} cc/g]	0.0383	-	-
±	0.0012	-	-
^{132}Xe - EXTb [in 10^{-12} cc]	0.0366	-	-
±	0.0012	-	-
^{128}Xe/^{132}Xe - EXTb	0.071	-	-
±	0.003	-	-
^{129}Xe/^{132}Xe - EXTb	0.916	-	-
±	0.017	-	-
^{130}Xe/^{132}Xe - EXTb	0.155	-	-
±	0.005	-	-
^{131}Xe/^{132}Xe - EXTb	0.804	-	-
±	0.006	-	-
^{134}Xe/^{132}Xe - EXTb	0.413	-	-
±	0.009	-	-
^{136}Xe/^{132}Xe - EXTb	0.355	-	-
±	0.008	-	-
^{21}Ne$_{cos}$/^{38}Ar$_{cos}$	-	-	-
±	-	-	-
^{36}Ar/^{132}Xe $_{(Int)}$	314.82	-	-
±	10.94	-	-
^{84}Kr/^{132}Xe $_{(Int)}$	11.04	-	-
±	0.58	-	-

Table X4. Noble gas data He to Xe for sample 45b.13_1 (corrected for blank)

Sample	45b.13_1		
Size [µm]	547 x 455		
Weight [µg]	137.6 ± 0.1		
Date of measurement	20/07/11	21/07/11	20+21/07/12
Laser-Power	3 x 5 W	3 x 15 W	
Laser-Beam	600 µm	600 µm	
Step(s)	1	2	total*
^{4}He [in 10^{-8} cc/g]	6.2	-	-
±	1.2	-	-
^{4}He [in 10^{-12} cc]	8.5	-	-
±	1.7	-	-
^{3}He [in 10^{-12} cc/g]	5.4	-	-
±	2.3	-	-
^{3}He [in 10^{-16} cc]	7.5	-	-
±	3.2	-	-
^{3}He/^{4}He	0.00009	-	-
±	0.00004	-	-
^{22}Ne [in 10^{-8} cc/g]	2.505	< 0.02 (2σ)	-
±	0.043	-	-
^{22}Ne [in 10^{-12} cc]	3.447	< 0.02 (2σ)	-
±	0.059	-	-
^{20}Ne/^{22}Ne	12.12	-	-
±	0.19	-	-
^{21}Ne/^{22}Ne	0.033	-	-
±	0.001	-	-
^{21}Ne$_{cos}$ [in 10^{-8} cc/g]	0.005	-	-
±	0.002	-	-
^{21}Ne$_{cos}$ [in 10^{-12} cc]	0.007	-	-
±	0.003	-	-
^{20}Ne$_{trap}$ [in 10^{-8} cc/g]	30.4	-	-
±	1.8	-	-
^{20}Ne$_{trap}$ [in 10^{-12} cc]	41.8	-	-
±	2.5	-	-
^{36}Ar [in 10^{-8} cc/g]	18.38	0.35	18.73
±	0.75	0.06	0.75
^{36}Ar [in 10^{-12} cc]	25.29	0.49	25.78
±	1.03	0.08	1.03
^{38}Ar/^{36}Ar	0.190	0.172	0.190
±	0.002	0.009	0.002
^{40}Ar/^{36}Ar	217.1	260.6	217.9
±	4.5	10.2	4.4
^{40}Ar [in 10^{-8} cc/g]	3989.5	92.0	4081.5
±	182.1	14.1	182.7
^{40}Ar [in 10^{-12} cc]	5489.5	126.6	5616.2
±	250.6	19.4	251.3
^{38}Ar$_{cos}$ [in 10^{-8} cc/g]	-	-	-
±	-	-	-
^{38}Ar$_{cos}$ [in 10^{-12} cc]	-	-	-
±	-	-	-
^{84}Kr [in 10^{-8} cc/g]	1.0616	0.0062	1.0678
±	0.0459	0.0011	0.0459
^{84}Kr [in 10^{-12} cc]	1.4607	0.0086	1.4693
±	0.0631	0.0015	0.0631
^{80}Kr/^{84}Kr	0.036	0.040	0.036
±	0.000	0.011	0.000
^{82}Kr/^{84}Kr	0.190	0.187	0.190
±	0.001	0.021	0.001
^{83}Kr/^{84}Kr	0.196	0.206	0.196
±	0.001	0.025	0.001
^{86}Kr/^{84}Kr	0.326	0.319	0.326
±	0.002	0.027	0.002
^{83}Kr$_{cos}$ [in 10^{-8} cc/g]	-	-	-
±	-	-	-
^{83}Kr$_{cos}$ [in 10^{-12} cc]	-	-	-
±	-	-	-

Date of measurement	20/07/11	21/07/11	20+21/07/12
Laser-Power	3 x 5 W	3 x 15 W	
Laser-Beam	600 µm	600 µm	
Step(s)	1	2	total*
^{132}Xe - INT [in 10^{-8} cc/g]	0.2940	0.0004	0.2944
±	0.0224	0.0003	0.0224
^{132}Xe - INT [in 10^{-12} cc]	0.4046	0.0005	0.4051
±	0.0309	0.0004	0.0309
^{128}Xe/^{132}Xe - INT	0.067	0.143	0.067
±	0.001	0.070	0.001
^{129}Xe/^{132}Xe - INT	0.930	0.995	0.930
±	0.007	0.372	0.007
^{130}Xe/^{132}Xe - INT	0.148	0.145	0.148
±	0.001	0.084	0.001
^{131}Xe/^{132}Xe - INT	0.764	0.404	0.764
±	0.005	0.280	0.005
^{134}Xe/^{132}Xe - INT	0.397	0.568	0.397
±	0.002	0.164	0.002
^{136}Xe/^{132}Xe - INT	0.349	0.532	0.349
±	0.003	0.254	0.003
^{132}Xe - EXTa [in 10^{-8} cc/g]	0.2876	0.0004	0.2880
±	0.0140	0.0003	0.0140
^{132}Xe - EXTa [in 10^{-12} cc]	0.3957	0.0005	0.3962
±	0.0193	0.0004	0.0193
^{128}Xe/^{132}Xe - EXTa	0.066	0.116	0.066
±	0.001	0.054	0.001
^{129}Xe/^{132}Xe - EXTa	0.931	0.996	0.931
±	0.006	0.351	0.006
^{130}Xe/^{132}Xe - EXTa	0.147	0.083	0.147
±	0.001	0.097	0.001
^{131}Xe/^{132}Xe - EXTa	0.771	0.407	0.770
±	0.005	0.282	0.005
^{134}Xe/^{132}Xe - EXTa	0.399	0.368	0.399
±	0.002	0.136	0.002
^{136}Xe/^{132}Xe - EXTa	0.356	0.312	0.356
±	0.002	0.124	0.002
^{132}Xe - EXTb [in 10^{-8} cc/g]	0.2869	< 0.001 (2σ)	-
±	0.0121	-	-
^{132}Xe - EXTb [in 10^{-12} cc]	0.3948	< 0.001 (2σ)	-
±	0.0167	-	-
^{128}Xe/^{132}Xe - EXTb	0.066	-	-
±	0.001	-	-
^{129}Xe/^{132}Xe - EXTb	0.932	-	-
±	0.006	-	-
^{130}Xe/^{132}Xe - EXTb	0.147	-	-
±	0.001	-	-
^{131}Xe/^{132}Xe - EXTb	0.771	-	-
±	0.002	-	-
^{134}Xe/^{132}Xe - EXTb	0.399	-	-
±	0.003	-	-
^{136}Xe/^{132}Xe - EXTb	0.354	-	-
±	0.002	-	-
^{21}Ne$_{cos}$ /^{38}Ar$_{cos}$	-	-	-
±	-	-	-
^{36}Ar/^{132}Xe $_{(Int)}$	62.51	942.33	63.63
±	5.41	795.09	5.48
^{84}Kr/^{132}Xe $_{(Int)}$	3.61	16.62	3.63
±	0.32	14.07	0.32

Table X5. Noble gas data He to Xe for sample 45b.14_1 (corrected for blank)

Sample	45b.14_1						
Size [μm]	494 x 418						
Weight [μg]	56.5 ± 0.1						
Date of measurement	03/10/12	04/10/12	03+04/10/12	**Date of measurement**	03/10/12	04/10/12	03+04/10/12
Laser-Power	3 x 0.91 W	2 x 5 W 1 x 5 - 27 W		**Laser-Power**	3 x 0.91 W	2 x 5 W 1 x 5 - 27 W	
Laser-Beam	600 μm	600 μm		**Laser-Beam**	600 μm	600 μm	
Step(s)	1	2	total*	**Step(s)**	1	2	total*
^{4}He [in 10^{-8} cc/g]	-	-	-	^{132}Xe - INT [in 10^{-8} cc/g]	0.0111	-	-
±	-	-	-	±	0.0015	-	-
^{4}He [in 10^{-12} cc]	-	-	-	^{132}Xe - INT [in 10^{-12} cc]	0.0063	-	-
±	-	-	-	±	0.0008	-	-
^{3}He [in 10^{-12} cc/g]	-	-	-	^{128}Xe/^{132}Xe - INT	0.049	-	-
±	-	-	-	±	0.020	-	-
^{3}He [in 10^{-16} cc]	-	-	-	^{129}Xe/^{132}Xe - INT	0.966	-	-
±	-	-	-	±	0.066	-	-
^{3}He/^{4}He	-	-	-	^{130}Xe/^{132}Xe - INT	0.116	-	-
±	-	-	-	±	0.017	-	-
^{22}Ne [in 10^{-8} cc/g]	< 0.11 (2σ)	< 0.09 (2σ)	-	^{131}Xe/^{132}Xe - INT	0.781	-	-
±	-	-	-	±	0.058	-	-
^{22}Ne [in 10^{-12} cc]	< 0.06 (2σ)	< 0.05 (2σ)	-	^{134}Xe/^{132}Xe - INT	0.370	-	-
±	-	-	-	±	0.031	-	-
^{20}Ne/^{22}Ne	-	-	-	^{136}Xe/^{132}Xe - INT	0.312	-	-
±	-	-	-	±	0.037	-	-
^{21}Ne/^{22}Ne	-	-	-	^{132}Xe - EXTa [in 10^{-8} cc/g]	0.0111	-	-
±	-	-	-	±	0.0015	-	-
^{21}Ne$_{cos}$ [in 10^{-8} cc/g]	-	< 0.142 (2σ)	-	^{132}Xe - EXTa [in 10^{-12} cc]	0.0063	-	-
±	-	-	-	±	0.0008	-	-
^{21}Ne$_{cos}$ [in 10^{-12} cc]	-	< 0.080 (2σ)	-	^{128}Xe/^{132}Xe - EXTa	0.058	-	-
±	-	-	-	±	0.012	-	-
^{20}Ne$_{trap}$ [in 10^{-8} cc/g]	< 1.4 (2σ)	-	-	^{129}Xe/^{132}Xe - EXTa	0.966	-	-
±	-	-	-	±	0.067	-	-
^{20}Ne$_{trap}$ [in 10^{-12} cc]	< 0.8 (2σ)	-	-	^{130}Xe/^{132}Xe - EXTa	0.113	-	-
±	-	-	-	±	0.017	-	-
^{36}Ar [in 10^{-8} cc/g]	0.37	-	-	^{131}Xe/^{132}Xe - EXTa	0.785	-	-
±	0.23	-	-	±	0.058	-	-
^{36}Ar [in 10^{-12} cc]	0.21	-	-	^{134}Xe/^{132}Xe - EXTa	0.379	-	-
±	0.13	-	-	±	0.027	-	-
^{38}Ar/^{36}Ar	0.171	-	-	^{136}Xe/^{132}Xe - EXTa	0.335	-	-
±	0.026	-	-	±	0.025	-	-
^{40}Ar/^{36}Ar	336.0	-	-	^{132}Xe - EXTb [in 10^{-8} cc/g]	0.0113	-	-
±	49.5	-	-	±	0.0011	-	-
^{40}Ar [in 10^{-8} cc/g]	143.0	-	-	^{132}Xe - EXTb [in 10^{-12} cc]	0.0064	-	-
±	55.9	-	-	±	0.0006	-	-
^{40}Ar [in 10^{-12} cc]	80.8	-	-	^{128}Xe/^{132}Xe - EXTb	0.072	-	-
±	31.6	-	-	±	0.011	-	-
^{38}Ar$_{cos}$ [in 10^{-8} cc/g]	-	-	-	^{129}Xe/^{132}Xe - EXTb	0.966	-	-
±	-	-	-	±	0.067	-	-
^{38}Ar$_{cos}$ [in 10^{-12} cc]	-	-	-	^{130}Xe/^{132}Xe - EXTb	0.139	-	-
±	-	-	-	±	0.013	-	-
^{84}Kr [in 10^{-8} cc/g]	0.0166	-	-	^{131}Xe/^{132}Xe - EXTb	0.789	-	-
±	0.0061	-	-	±	0.029	-	-
^{84}Kr [in 10^{-12} cc]	0.0094	-	-	^{134}Xe/^{132}Xe - EXTb	0.373	-	-
±	0.0034	-	-	±	0.031	-	-
^{80}Kr/^{84}Kr	0.055	-	-	^{136}Xe/^{132}Xe - EXTb	0.329	-	-
±	0.011	-	-	±	0.024	-	-
^{82}Kr/^{84}Kr	0.245	-	-	^{21}Ne$_{cos}$/^{38}Ar$_{cos}$	-	-	-
±	0.030	-	-	±	-	-	-
^{83}Kr/^{84}Kr	0.193	-	-	^{36}Ar/^{132}Xe $_{(Int)}$	33.57	-	-
±	0.024	-	-	±	21.42	-	-
^{86}Kr/^{84}Kr	0.280	-	-	^{84}Kr/^{132}Xe $_{(Int)}$	1.50	-	-
±	0.039	-	-	±	0.58	-	-
^{83}Kr$_{cos}$ [in 10^{-8} cc/g]	-	-	-				
±	-	-	-				
^{83}Kr$_{cos}$ [in 10^{-12} cc]	-	-	-				
±	-	-	-				

Table X6. Noble gas data He to Xe for sample 45b.15_1 (corrected for blank)

Sample	45b.15_1		
Size [µm]	422 x 300		
Weight [µg]	30.3 ± 0.1		
Date of measurement	17/09/12	18/09/12	17+18/09/12
Laser-Power	3 x 0.91 W	3 x 5 W	
Laser-Beam	600-360 µm	360 µm	
Step(s)	1	2	total*
^{4}He [in 10^{-8} cc/g]	213.6	-	-
±	16.8	-	-
^{4}He [in 10^{-12} cc]	64.7	-	-
±	5.1	-	-
^{3}He [in 10^{-12} cc/g]	328.4	-	-
±	87.1	-	-
^{3}He [in 10^{-16} cc]	99.5	-	-
±	26.4	-	-
^{3}He/^{4}He	0.00015	-	-
±	0.00004	-	-
^{22}Ne [in 10^{-8} cc/g]	0.333	< 0.31 (2σ)	-
±	0.107	-	-
^{22}Ne [in 10^{-12} cc]	0.101	< 0.09 (2σ)	-
±	0.033	-	-
^{20}Ne/^{22}Ne	9.64	-	-
±	1.60	-	-
^{21}Ne/^{22}Ne	0.031	-	-
±	0.008	-	-
^{21}Ne$_{cos}$ [in 10^{-8} cc/g]	< 0.018 (2σ)	< 0.009 (2σ)	-
±	-	-	-
^{21}Ne$_{cos}$ [in 10^{-12} cc]	< 0.006 (2σ)	< 0.003 (2σ)	-
±	-	-	-
^{20}Ne$_{trap}$ [in 10^{-8} cc/g]	3.2	< 3.3 (2σ)	-
±	1.2	-	-
^{20}Ne$_{trap}$ [in 10^{-12} cc]	1.0	< 1.0 (2σ)	-
±	0.4	-	-
^{36}Ar [in 10^{-8} cc/g]	22.56	-	-
±	0.62	-	-
^{36}Ar [in 10^{-12} cc]	6.84	-	-
±	0.19	-	-
^{38}Ar/^{36}Ar	0.187	-	-
±	0.003	-	-
^{40}Ar/^{36}Ar	15.7	-	-
±	4.5	-	-
^{40}Ar [in 10^{-8} cc/g]	386.9	-	-
±	104.4	-	-
^{40}Ar [in 10^{-12} cc]	117.2	-	-
±	31.6	-	-
^{38}Ar$_{cos}$ [in 10^{-8} cc/g]	-	-	-
±	-	-	-
^{38}Ar$_{cos}$ [in 10^{-12} cc]	-	-	-
±	-	-	-
^{84}Kr [in 10^{-8} cc/g]	0.4824	-	-
±	0.0374	-	-
^{84}Kr [in 10^{-12} cc]	0.1462	-	-
±	0.0113	-	-
^{80}Kr/^{84}Kr	0.042	-	-
±	0.002	-	-
^{82}Kr/^{84}Kr	0.201	-	-
±	0.012	-	-
^{83}Kr/^{84}Kr	0.197	-	-
±	0.010	-	-
^{86}Kr/^{84}Kr	0.306	-	-
±	0.016	-	-
^{83}Kr$_{cos}$ [in 10^{-8} cc/g]	-	-	-
±	-	-	-
^{83}Kr$_{cos}$ [in 10^{-12} cc]	-	-	-
±	-	-	-

Date of measurement	17/09/12	18/09/12	17+18/09/12
Laser-Power	3 x 0.91 W	3 x 5 W	
Laser-Beam	600-360 µm	360 µm	
Step(s)	1	2	total*
^{132}Xe - INT [in 10^{-8} cc/g]	0.7666	$	-
±	0.0111	$	-
^{132}Xe - INT [in 10^{-12} cc]	0.2323	0.0018	0.2323
±	0.0033	0.0008	0.0033
^{128}Xe/^{132}Xe - INT	0.080	0.161	0.080
±	0.002	0.071	0.002
^{129}Xe/^{132}Xe - INT	1.036	0.920	1.036
±	0.011	0.141	0.011
^{130}Xe/^{132}Xe - INT	0.158	0.209	0.158
±	0.002	0.055	0.002
^{131}Xe/^{132}Xe - INT	0.796	0.913	0.796
±	0.010	0.157	0.010
^{134}Xe/^{132}Xe - INT	0.383	0.433	0.383
±	0.004	0.078	0.004
^{136}Xe/^{132}Xe - INT	0.330	0.410	0.330
±	0.005	0.105	0.005
^{132}Xe - EXTa [in 10^{-8} cc/g]	0.8666	0.0069	0.8735
±	0.0955	0.0031	0.0955
^{132}Xe - EXTa [in 10^{-12} cc]	0.2626	0.0021	0.2647
±	0.0289	0.0009	0.0289
^{128}Xe/^{132}Xe - EXTa	0.078	0.080	0.078
±	0.002	0.032	0.002
^{129}Xe/^{132}Xe - EXTa	1.027	0.911	1.026
±	0.014	0.150	0.014
^{130}Xe/^{132}Xe - EXTa	0.155	0.189	0.155
±	0.003	0.052	0.003
^{131}Xe/^{132}Xe - EXTa	0.795	0.911	0.796
±	0.010	0.157	0.010
^{134}Xe/^{132}Xe - EXTa	0.376	0.287	0.375
±	0.006	0.067	0.006
^{136}Xe/^{132}Xe - EXTa	0.325	0.279	0.324
±	0.013	0.057	0.013
^{132}Xe - EXTb [in 10^{-8} cc/g]	0.8024	0.0065	0.8089
±	0.1031	0.0021	0.1031
^{132}Xe - EXTb [in 10^{-12} cc]	0.2431	0.0020	0.2451
±	0.0312	0.0006	0.0312
^{128}Xe/^{132}Xe - EXTb	0.076	0.115	0.077
±	0.003	0.031	0.003
^{129}Xe/^{132}Xe - EXTb	1.028	0.913	1.027
±	0.014	0.149	0.014
^{130}Xe/^{132}Xe - EXTb	0.159	0.121	0.158
±	0.003	0.037	0.003
^{131}Xe/^{132}Xe - EXTb	0.795	0.921	0.796
±	0.004	0.098	0.004
^{134}Xe/^{132}Xe - EXTb	0.393	0.487	0.394
±	0.006	0.084	0.006
^{136}Xe/^{132}Xe - EXTb	0.334	0.336	0.334
±	0.011	0.063	0.011
^{21}Ne$_{cos}$/^{38}Ar$_{cos}$	-	-	-
±	-	-	-
^{36}Ar/^{132}Xe $_{(Int)}$	29.43	-	-
±	0.90	-	-
^{84}Kr/^{132}Xe $_{(Int)}$	0.63	-	-
±	0.05	-	-

Table X7. Noble gas data He to Xe for sample 45b.16_1 (corrected for blank)

Sample				45b.16			
Size [μm]				572 x 463			
Weight [μg]				138.3 ± 0.1			
Date of measurement	18/06/12	19/06/12	18+19/06/12	**Date of measurement**	18/06/12	19/06/12	18+19/06/12
Laser-Power	3 x 0.91 W	3 x 5 - 8 W		**Laser-Power**	3 x 0.91 W	3 x 5 - 8 W	
Laser-Beam	600-360 μm	360 μm		**Laser-Beam**	600-360 μm	360 μm	
Step(s)	1	2	total*	**Step(s)**	1	2	total*
^{4}He [in 10^{-8} cc/g]	23.5	6.5	30.0	^{132}Xe - INT [in 10^{-8} cc/g]	0.0284	0.0045	0.0329
±	1.7	1.4	2.2	±	0.0010	0.0018	0.0020
^{4}He [in 10^{-12} cc]	32.5	9.0	41.5	^{132}Xe - INT [in 10^{-12} cc]	0.0392	0.0062	0.0455
±	2.4	1.9	3.1	±	0.0014	0.0024	0.0028
^{3}He [in 10^{-12} cc/g]	< 299 (2σ)	608.0	-	^{128}Xe/^{132}Xe - INT	0.074	0.108	0.079
±	-	106.2	-	±	0.003	0.022	0.004
^{3}He [in 10^{-16} cc]	< 414 (2σ)	840.9	-	^{129}Xe/^{132}Xe - INT	0.927	1.104	0.951
±	-	146.8	-	±	0.017	0.076	0.018
^{3}He/^{4}He	-	0.00933	-	^{130}Xe/^{132}Xe - INT	0.153	0.176	0.156
±		0.00258	-	±	0.004	0.015	0.004
^{22}Ne [in 10^{-8} cc/g]	0.934	10.821	11.755	^{131}Xe/^{132}Xe - INT	0.763	0.844	0.774
±	0.054	0.579	0.581	±	0.016	0.060	0.016
^{22}Ne [in 10^{-12} cc]	1.292	14.965	16.257	^{134}Xe/^{132}Xe - INT	0.389	0.370	0.386
±	0.074	0.800	0.804	±	0.008	0.038	0.009
^{20}Ne/^{22}Ne	11.40	11.26	11.27	^{136}Xe/^{132}Xe - INT	0.336	0.325	0.335
±	0.20	0.09	0.09	±	0.010	0.041	0.010
^{21}Ne/^{22}Ne	0.035	0.040	0.039	^{132}Xe - EXTa [in 10^{-8} cc/g]	0.0282	0.0049	0.0331
±	0.001	0.001	0.001	±	0.0012	0.0013	0.0018
^{21}Ne$_{cos}$ [in 10^{-8} cc/g]	0.005	0.109	0.114	^{132}Xe - EXTa [in 10^{-12} cc]	0.0390	0.0068	0.0458
±	0.001	0.010	0.010	±	0.0016	0.0018	0.0024
^{21}Ne$_{cos}$ [in 10^{-12} cc]	0.007	0.151	0.158	^{128}Xe/^{132}Xe - EXTa	0.067	0.096	0.072
±	0.002	0.014	0.014	±	0.003	0.021	0.004
^{20}Ne$_{trap}$ [in 10^{-8} cc/g]	10.6	121.81	132.45	^{129}Xe/^{132}Xe - EXTa	0.924	1.085	0.948
±	0.9	9.41	9.45	±	0.018	0.075	0.019
^{20}Ne$_{trap}$ [in 10^{-12} cc]	14.7	168.46	183.18	^{130}Xe/^{132}Xe - EXTa	0.152	0.161	0.153
±	1.2	13.02	13.07	±	0.004	0.014	0.004
^{36}Ar [in 10^{-8} cc/g]	1.23	12.57	13.79	^{131}Xe/^{132}Xe - EXTa	0.764	0.841	0.775
±	0.10	0.31	0.33	±	0.016	0.055	0.016
^{36}Ar [in 10^{-12} cc]	1.70	17.38	19.08	^{134}Xe/^{132}Xe - EXTa	0.389	0.347	0.383
±	0.14	0.43	0.45	±	0.008	0.027	0.008
^{38}Ar/^{36}Ar	0.200	0.200	0.200	^{136}Xe/^{132}Xe - EXTa	0.327	0.276	0.319
±	0.006	0.002	0.002	±	0.008	0.025	0.007
^{40}Ar/^{36}Ar	87.5	28.9	34.1	^{132}Xe - EXTb [in 10^{-8} cc/g]	0.0287	0.0061	0.0348
±	12.4	3.8	3.7	±	0.0009	0.0011	0.0014
^{40}Ar [in 10^{-8} cc/g]	128.7	371.5	500.2	^{132}Xe - EXTb [in 10^{-12} cc]	0.0398	0.0084	0.0481
±	21.7	52.9	57.2	±	0.0012	0.0015	0.0019
^{40}Ar [in 10^{-12} cc]	178.0	513.8	691.8	^{128}Xe/^{132}Xe - EXTb	0.066	0.076	0.068
±	30.0	73.2	79.1	±	0.003	0.007	0.003
^{38}Ar$_{cos}$ [in 10^{-8} cc/g]	0.016	0.162	0.179	^{129}Xe/^{132}Xe - EXTb	0.921	1.036	0.941
±	0.008	0.041	0.042	±	0.017	0.048	0.016
^{38}Ar$_{cos}$ [in 10^{-12} cc]	0.023	0.224	0.247	^{130}Xe/^{132}Xe - EXTb	0.139	0.147	0.140
±	0.011	0.056	0.057	±	0.004	0.013	0.004
^{84}Kr [in 10^{-8} cc/g]	0.0304	0.0315	0.0618	^{131}Xe/^{132}Xe - EXTb	0.762	0.817	0.772
±	0.0050	0.0061	0.0079	±	0.005	0.021	0.006
^{84}Kr [in 10^{-12} cc]	0.0420	0.0435	0.0855	^{134}Xe/^{132}Xe - EXTb	0.393	0.390	0.392
±	0.0070	0.0085	0.0110	±	0.007	0.022	0.007
^{80}Kr/^{84}Kr	0.043	0.047	0.045	^{136}Xe/^{132}Xe - EXTb	0.341	0.331	0.340
±	0.004	0.005	0.003	±	0.007	0.018	0.006
^{82}Kr/^{84}Kr	0.172	0.206	0.189	^{21}Ne$_{cos}$/^{38}Ar$_{cos}$	0.32	0.67	0.64
±	0.013	0.015	0.010	±	0.18	0.18	0.16
^{83}Kr/^{84}Kr	0.184	0.217	0.201	^{36}Ar/^{132}Xe$_{(Int)}$	43.22	2785.46	419.57
±	0.011	0.012	0.008	±	3.97	1084.77	27.77
^{86}Kr/^{84}Kr	0.304	0.282	0.293	^{84}Kr/^{132}Xe$_{(Int)}$	1.07	6.97	1.88
±	0.015	0.017	0.011	±	0.18	3.03	0.27
^{83}Kr$_{cos}$ [in 10^{-8} cc/g]	-	0.0005	-				
±	-	0.0004	-				
^{83}Kr$_{cos}$ [in 10^{-12} cc]	-	0.0007	-				
±	-	0.0006	-				

Table X8. Noble gas data He to Xe for sample 45b.17_1 (corrected for blank)

Sample	45b.17_1		
Size [µm]	416 x 283		
Weight [µg]	56.2 ± 0.1		
Date of measurement	20/06/12	Date of measurement	20/06/12
Laser-Power	3 x 0.91 W	Laser-Power	3 x 0.91 W
Laser-Beam	600 µm	Laser-Beam	600 µm
Step(s)	1	Step(s)	1
^{4}He [in 10^{-8} cc/g]	1094.6	^{132}Xe - INT [in 10^{-8} cc/g]	0.0479
±	49.0	±	0.0023
^{4}He [in 10^{-12} cc]	615.1	^{132}Xe - INT [in 10^{-12} cc]	0.0269
±	27.5	±	0.0013
^{3}He [in 10^{-12} cc/g]	26075.2	^{128}Xe/^{132}Xe - INT	0.063
±	1131.3	±	0.004
^{3}He [in 10^{-16} cc]	14654.3	^{129}Xe/^{132}Xe - INT	0.897
±	635.2	±	0.024
^{3}He/^{4}He	0.00238	^{130}Xe/^{132}Xe - INT	0.143
±	0.00015	±	0.004
^{22}Ne [in 10^{-8} cc/g]	11.643	^{131}Xe/^{132}Xe - INT	0.777
±	0.624	±	0.017
^{22}Ne [in 10^{-12} cc]	6.543	^{134}Xe/^{132}Xe - INT	0.392
±	0.350	±	0.011
^{20}Ne/^{22}Ne	7.11	^{136}Xe/^{132}Xe - INT	0.348
±	0.06	±	0.012
^{21}Ne/^{22}Ne	0.398	^{132}Xe - EXTa [in 10^{-8} cc/g]	0.0476
±	0.005	±	0.0025
^{21}Ne$_{cos}$ [in 10^{-8} cc/g]	4.412	^{132}Xe - EXTa [in 10^{-12} cc]	0.0267
±	0.245	±	0.0014
^{21}Ne$_{cos}$ [in 10^{-12} cc]	2.479	^{128}Xe/^{132}Xe - EXTa	0.065
±	0.137	±	0.004
^{20}Ne$_{trap}$ [in 10^{-8} cc/g]	79.2	^{129}Xe/^{132}Xe - EXTa	0.893
±	6.2	±	0.026
^{20}Ne$_{trap}$ [in 10^{-12} cc]	44.5	^{130}Xe/^{132}Xe - EXTa	0.140
±	3.5	±	0.005
^{36}Ar [in 10^{-8} cc/g]	9.81	^{131}Xe/^{132}Xe - EXTa	0.777
±	0.44	±	0.018
^{36}Ar [in 10^{-12} cc]	5.51	^{134}Xe/^{132}Xe - EXTa	0.404
±	0.25	±	0.010
^{38}Ar/^{36}Ar	0.227	^{136}Xe/^{132}Xe - EXTa	0.343
±	0.002	±	0.008
^{40}Ar/^{36}Ar	105.1	^{132}Xe - EXTb [in 10^{-8} cc/g]	0.0482
±	4.4	±	0.0018
^{40}Ar [in 10^{-8} cc/g]	1082.2	^{132}Xe - EXTb [in 10^{-12} cc]	0.0271
±	66.1	±	0.0010
^{40}Ar [in 10^{-12} cc]	608.2	^{128}Xe/^{132}Xe - EXTb	0.066
±	37.1	±	0.004
^{38}Ar$_{cos}$ [in 10^{-8} cc/g]	0.431	^{129}Xe/^{132}Xe - EXTb	0.890
±	0.038	±	0.024
^{38}Ar$_{cos}$ [in 10^{-12} cc]	0.242	^{130}Xe/^{132}Xe - EXTb	0.146
±	0.022	±	0.005
^{84}Kr [in 10^{-8} cc/g]	0.2605	^{131}Xe/^{132}Xe - EXTb	0.774
±	0.0200	±	0.006
^{84}Kr [in 10^{-12} cc]	0.1464	^{134}Xe/^{132}Xe - EXTb	0.401
±	0.0112	±	0.010
^{80}Kr/^{84}Kr	0.032	^{136}Xe/^{132}Xe - EXTb	0.371
±	0.002	±	0.009
^{82}Kr/^{84}Kr	0.182	^{21}Ne$_{cos}$/^{38}Ar$_{cos}$	10.24
±	0.005	±	1.07
^{83}Kr/^{84}Kr	0.189	^{36}Ar/^{132}Xe $_{(Int)}$	204.87
±	0.005	±	13.55
^{86}Kr/^{84}Kr	0.322	^{84}Kr/^{132}Xe $_{(Int)}$	5.44
±	0.007	±	0.50
^{83}Kr$_{cos}$ [in 10^{-8} cc/g]	-		
±	-		
^{83}Kr$_{cos}$ [in 10^{-12} cc]	-		
±	-		

Table X9. Noble gas data He to Xe for sample 45b.18_1 (corrected for blank)

Sample				45b.18_1			
Size [µm]				253 x 235			
Weight [µg]				5.3 ± 0.1			
Date of measurement	11/11/11	17/11/11	11+17/11/11	**Date of measurement**	11/11/11	17/11/11	11+17/11/11
Laser-Power	3 x 0.91 W	3 x 5 W		**Laser-Power**	3 x 0.91 W	3 x 5 W	
Laser-Beam	250 µm	200 µm		**Laser-Beam**	250 µm	200 µm	
Step(s)	1	2	total*	**Step(s)**	1	2	total*
^{4}He [in 10^{-8} cc/g]	335.1	-	-	^{132}Xe - INT [in 10^{-8} cc/g]	-	-	-
±	107.4	-	-	±	-	-	-
^{4}He [in 10^{-12} cc]	17.8	-	-	^{132}Xe - INT [in 10^{-12} cc]	-	-	-
±	5.7	-	-	±	-	-	-
^{3}He [in 10^{-12} cc/g]	4022.8	-	-	^{128}Xe/^{132}Xe - INT	-	-	-
±	2606.1	-	-	±	-	-	-
^{3}He [in 10^{-16} cc]	213.2	-	-	^{129}Xe/^{132}Xe - INT	-	-	-
±	138.1	-	-	±	-	-	-
^{3}He/^{4}He	0.00120	-	-	^{130}Xe/^{132}Xe - INT	-	-	-
±	0.00087	-	-	±	-	-	-
^{22}Ne [in 10^{-8} cc/g]	6.796	< 1.37 (2σ)	-	^{131}Xe/^{132}Xe - INT	-	-	-
±	0.630	-	-	±	-	-	-
^{22}Ne [in 10^{-12} cc]	0.360	< 0.07 (2σ)	-	^{134}Xe/^{132}Xe - INT	-	-	-
±	0.033	-	-	±	-	-	-
^{20}Ne/^{22}Ne	11.86	-	-	^{136}Xe/^{132}Xe - INT	-	-	-
±	0.57	-	-	±	-	-	-
^{21}Ne/^{22}Ne	0.041	-	-	^{132}Xe - EXTa [in 10^{-8} cc/g]	-	-	-
±	0.003	-	-	±	-	-	-
^{21}Ne$_{cos}$ [in 10^{-8} cc/g]	0.043	< 0.035 (2σ)	-	^{132}Xe - EXTa [in 10^{-12} cc]	-	-	-
±	0.028	-	-	±	-	-	-
^{21}Ne$_{cos}$ [in 10^{-12} cc]	0.002	< 0.002 (2σ)	-	^{128}Xe/^{132}Xe - EXTa	-	-	-
±	0.001	-	-	±	-	-	-
^{20}Ne$_{trap}$ [in 10^{-8} cc/g]	80.5	< 15.3 (2σ)	-	^{129}Xe/^{132}Xe - EXTa	-	-	-
±	9.5	-	-	±	-	-	-
^{20}Ne$_{trap}$ [in 10^{-12} cc]	4.3	< 0.8 (2σ)	-	^{130}Xe/^{132}Xe - EXTa	-	-	-
±	0.5	-	-	±	-	-	-
^{36}Ar [in 10^{-8} cc/g]	12.73	-	-	^{131}Xe/^{132}Xe - EXTa	-	-	-
±	0.85	-	-	±	-	-	-
^{36}Ar [in 10^{-12} cc]	0.67	-	-	^{134}Xe/^{132}Xe - EXTa	-	-	-
±	0.04	-	-	±	-	-	-
^{38}Ar/^{36}Ar	0.170	-	-	^{136}Xe/^{132}Xe - EXTa	-	-	-
±	0.030	-	-	±	-	-	-
^{40}Ar/^{36}Ar	192.9	-	-	^{132}Xe - EXTb [in 10^{-8} cc/g]	-	-	-
±	7.5	-	-	±	-	-	-
^{40}Ar [in 10^{-8} cc/g]	2454.3	-	-	^{132}Xe - EXTb [in 10^{-12} cc]	-	-	-
±	117.8	-	-	±	-	-	-
^{40}Ar [in 10^{-12} cc]	130.1	-	-	^{128}Xe/^{132}Xe - EXTb	-	-	-
±	5.7	-	-	±	-	-	-
^{38}Ar$_{cos}$ [in 10^{-8} cc/g]	-	-	-	^{129}Xe/^{132}Xe - EXTb	-	-	-
±	-	-	-	±	-	-	-
^{38}Ar$_{cos}$ [in 10^{-12} cc]	-	-	-	^{130}Xe/^{132}Xe - EXTb	-	-	-
±	-	-	-	±	-	-	-
^{84}Kr [in 10^{-8} cc/g]	0.1807	-	-	^{131}Xe/^{132}Xe - EXTb	-	-	-
±	0.0943	-	-	±	-	-	-
^{84}Kr [in 10^{-12} cc]	0.0096	-	-	^{134}Xe/^{132}Xe - EXTb	-	-	-
±	0.0050	-	-	±	-	-	-
^{80}Kr/^{84}Kr	0.047	-	-	^{136}Xe/^{132}Xe - EXTb	-	-	-
±	0.012	-	-	±	-	-	-
^{82}Kr/^{84}Kr	0.220	-	-	^{21}Ne$_{cos}$/^{38}Ar$_{cos}$	-	-	-
±	0.036	-	-	±	-	-	-
^{83}Kr/^{84}Kr	0.198	-	-	^{36}Ar/^{132}Xe $_{(Int)}$	-	-	-
±	0.026	-	-	±	-	-	-
^{86}Kr/^{84}Kr	0.236	-	-	^{84}Kr/^{132}Xe $_{(Int)}$	-	-	-
±	0.041	-	-	±	-	-	-
^{83}Kr$_{cos}$ [in 10^{-8} cc/g]	-	-	-				
±	-	-	-				
^{83}Kr$_{cos}$ [in 10^{-12} cc]	-	-	-				
±	-	-	-				

Table X10. Noble gas data He to Xe for sample 45b.19_1 (corrected for blank)

Sample		45b.19_1	
Size [µm]		450 x 292	
Weight [µg]		55.9 ± 0.1	
Date of measurement	19/01/12	Date of measurement	19/01/12
Laser-Power	3 x 0.91 W	Laser-Power	3 x 0.91 W
Laser-Beam	250 µm	Laser-Beam	250 µm
Step(s)	1	Step(s)	1
^{4}He [in 10^{-8} cc/g]	873.0	^{132}Xe - INT [in 10^{-8} cc/g]	0.0304
±	17.4	±	0.0033
^{4}He [in 10^{-12} cc]	488.0	^{132}Xe - INT [in 10^{-12} cc]	0.0170
±	9.7	±	0.0019
^{3}He [in 10^{-12} cc/g]	1058.9	^{128}Xe/^{132}Xe - INT	0.071
±	271.7	±	0.006
^{3}He [in 10^{-16} cc]	591.9	^{129}Xe/^{132}Xe - INT	0.985
±	151.9	±	0.030
^{3}He/^{4}He	0.00012	^{130}Xe/^{132}Xe - INT	0.146
±	0.00003	±	0.006
^{22}Ne [in 10^{-8} cc/g]	0.335	^{131}Xe/^{132}Xe - INT	0.758
±	0.133	±	0.024
^{22}Ne [in 10^{-12} cc]	0.187	^{134}Xe/^{132}Xe - INT	0.363
±	0.074	±	0.015
^{20}Ne/^{22}Ne	10.58	^{136}Xe/^{132}Xe - INT	0.317
±	2.36	±	0.016
^{21}Ne/^{22}Ne	0.030	^{132}Xe - EXTa [in 10^{-8} cc/g]	0.0302
±	0.008	±	0.0094
^{21}Ne$_{cos}$ [in 10^{-8} cc/g]	0.012	^{132}Xe - EXTa [in 10^{-12} cc]	0.0169
±	0.000	±	0.0053
^{21}Ne$_{cos}$ [in 10^{-12} cc]	0.007	^{128}Xe/^{132}Xe - EXTa	0.069
±	0.000	±	0.006
^{20}Ne$_{trap}$ [in 10^{-8} cc/g]	3.5	^{129}Xe/^{132}Xe - EXTa	0.978
±	1.6	±	0.032
^{20}Ne$_{trap}$ [in 10^{-12} cc]	1.9	^{130}Xe/^{132}Xe - EXTa	0.143
±	0.9	±	0.007
^{36}Ar [in 10^{-8} cc/g]	1.31	^{131}Xe/^{132}Xe - EXTa	0.761
±	0.56	±	0.023
^{36}Ar [in 10^{-12} cc]	0.73	^{134}Xe/^{132}Xe - EXTa	0.369
±	0.31	±	0.012
^{38}Ar/^{36}Ar	0.181	^{136}Xe/^{132}Xe - EXTa	0.322
±	0.020	±	0.011
^{40}Ar/^{36}Ar	271.0	^{132}Xe - EXTb [in 10^{-8} cc/g]	0.0284
±	25.9	±	0.0047
^{40}Ar [in 10^{-8} cc/g]	355.6	^{132}Xe - EXTb [in 10^{-12} cc]	0.0159
±	142.7	±	0.0026
^{40}Ar [in 10^{-12} cc]	198.8	^{128}Xe/^{132}Xe - EXTb	0.071
±	79.8	±	0.005
^{38}Ar$_{cos}$ [in 10^{-8} cc/g]	-	^{129}Xe/^{132}Xe - EXTb	0.976
±	-	±	0.036
^{38}Ar$_{cos}$ [in 10^{-12} cc]	-	^{130}Xe/^{132}Xe - EXTb	0.144
±	-	±	0.007
^{84}Kr [in 10^{-8} cc/g]	0.0656	^{131}Xe/^{132}Xe - EXTb	0.759
±	0.0098	±	0.012
^{84}Kr [in 10^{-12} cc]	0.0366	^{134}Xe/^{132}Xe - EXTb	0.367
±	0.0055	±	0.014
^{80}Kr/^{84}Kr	0.045	^{136}Xe/^{132}Xe - EXTb	0.331
±	0.004	±	0.013
^{82}Kr/^{84}Kr	0.221	^{21}Ne$_{cos}$/^{38}Ar$_{cos}$	-
±	0.011	±	-
^{83}Kr/^{84}Kr	0.205	^{36}Ar/^{132}Xe $_{(Int)}$	43.20
±	0.010	±	18.88
^{86}Kr/^{84}Kr	0.322	^{84}Kr/^{132}Xe $_{(Int)}$	2.16
±	0.013	±	0.40
^{83}Kr$_{cos}$ [in 10^{-8} cc/g]	-		
±	-		
^{83}Kr$_{cos}$ [in 10^{-12} cc]	-		
±	-		

Table X11. Noble gas data He to Xe for sample 45b.20_2 (corrected for blank)

Sample	45b.20_2						
Size [µm]	613 x 482						
Weight [µg]	77.3 ± 0.1						
Date of measurement	25/09/12	26/09/12	25+26/09/12	Date of measurement	25/09/12	26/09/12	25+26/09/12
Laser-Power	1 x 0.91 - 11 W 2 x 3.3 W	2 x 5 W 1 x 11 - 33 W		Laser-Power	1 x 0.91 - 11 W 2 x 3.3 W	2 x 5 W 1 x 11 - 33 W	
Laser-Beam	600 - 250 µm	250 µm		Laser-Beam	600 - 250 µm	250 µm	
Step(s)	1	2	total*	Step(s)	1	2	total*
^{4}He [in 10^{-8} cc/g]	46.0	-	-	^{132}Xe - INT [in 10^{-8} cc/g]	0.1049	-	-
±	5.6	-	-	±	0.0019	-	-
^{4}He [in 10^{-12} cc]	35.5	-	-	^{132}Xe - INT [in 10^{-12} cc]	0.0811	-	-
±	4.3	-	-	±	0.0014	-	-
^{3}He [in 10^{-12} cc/g]	850.4	597.3	1447.7	^{128}Xe/^{132}Xe - INT	0.078	-	-
±	125.0	138.8	186.8	±	0.003	-	-
^{3}He [in 10^{-16} cc]	657.3	461.7	1119.0	^{129}Xe/^{132}Xe - INT	0.987	-	-
±	96.6	107.3	144.4	±	0.013	-	-
^{3}He/^{4}He	0.00185	-	-	^{130}Xe/^{132}Xe - INT	0.157	-	-
±	0.00035	-	-	±	0.003	-	-
^{22}Ne [in 10^{-8} cc/g]	0.484	< 0.06 (2σ)	-	^{131}Xe/^{132}Xe - INT	0.768	-	-
±	0.033	-	-	±	0.011	-	-
^{22}Ne [in 10^{-12} cc]	0.374	< 0.05 (2σ)	-	^{134}Xe/^{132}Xe - INT	0.387	-	-
±	0.026	-	-	±	0.006	-	-
^{20}Ne/^{22}Ne	11.24	-	-	^{136}Xe/^{132}Xe - INT	0.341	-	-
±	0.52	-	-	±	0.008	-	-
^{21}Ne/^{22}Ne	0.066	-	-	^{132}Xe - EXTa [in 10^{-8} cc/g]	0.1049	-	-
±	0.005	-	-	±	0.0019	-	-
^{21}Ne$_{cos}$ [in 10^{-8} cc/g]	0.018	-	-	^{132}Xe - EXTa [in 10^{-12} cc]	0.0811	-	-
±	0.003	-	-	±	0.0014	-	-
^{21}Ne$_{cos}$ [in 10^{-12} cc]	0.014	-	-	^{128}Xe/^{132}Xe - EXTa	0.074	-	-
±	0.003	-	-	±	0.002	-	-
^{20}Ne$_{trap}$ [in 10^{-8} cc/g]	5.4	< 1.2 (2σ)	-	^{129}Xe/^{132}Xe - EXTa	0.989	-	-
±	0.5	-	-	±	0.014	-	-
^{20}Ne$_{trap}$ [in 10^{-12} cc]	4.2	< 0.9 (2σ)	-	^{130}Xe/^{132}Xe - EXTa	0.154	-	-
±	0.4	-	-	±	0.003	-	-
^{36}Ar [in 10^{-8} cc/g]	0.84	-	-	^{131}Xe/^{132}Xe - EXTa	0.773	-	-
±	0.17	-	-	±	0.011	-	-
^{36}Ar [in 10^{-12} cc]	0.65	-	-	^{134}Xe/^{132}Xe - EXTa	0.374	-	-
±	0.13	-	-	±	0.005	-	-
^{38}Ar/^{36}Ar	0.181	-	-	^{136}Xe/^{132}Xe - EXTa	0.323	-	-
±	0.010	-	-	±	0.006	-	-
^{40}Ar/^{36}Ar	146.2	-	-	^{132}Xe - EXTb [in 10^{-8} cc/g]	0.1038	-	-
±	18.7	-	-	±	0.0114	-	-
^{40}Ar [in 10^{-8} cc/g]	135.2	-	-	^{132}Xe - EXTb [in 10^{-12} cc]	0.0802	-	-
±	40.9	-	-	±	0.0088	-	-
^{40}Ar [in 10^{-12} cc]	104.5	-	-	^{128}Xe/^{132}Xe - EXTb	0.069	-	-
±	31.6	-	-	±	0.002	-	-
^{38}Ar$_{cos}$ [in 10^{-8} cc/g]	-	-	-	^{129}Xe/^{132}Xe - EXTb	0.987	-	-
±	-	-	-	±	0.014	-	-
^{38}Ar$_{cos}$ [in 10^{-12} cc]	-	-	-	^{130}Xe/^{132}Xe - EXTb	0.153	-	-
±	-	-	-	±	0.003	-	-
^{84}Kr [in 10^{-8} cc/g]	0.0825	-	-	^{131}Xe/^{132}Xe - EXTb	0.769	-	-
±	0.0076	-	-	±	0.004	-	-
^{84}Kr [in 10^{-12} cc]	0.0638	-	-	^{134}Xe/^{132}Xe - EXTb	0.394	-	-
±	0.0059	-	-	±	0.006	-	-
^{80}Kr/^{84}Kr	0.047	-	-	^{136}Xe/^{132}Xe - EXTb	0.336	-	-
±	0.004	-	-	±	0.005	-	-
^{82}Kr/^{84}Kr	0.210	-	-	^{21}Ne$_{cos}$/^{38}Ar$_{cos}$	-	-	-
±	0.014	-	-	±	-	-	-
^{83}Kr/^{84}Kr	0.209	-	-	^{36}Ar/^{132}Xe $_{(Int)}$	7.98	-	-
±	0.012	-	-	±	1.64	-	-
^{86}Kr/^{84}Kr	0.321	-	-	^{84}Kr/^{132}Xe $_{(Int)}$	0.79	-	-
±	0.019	-	-	±	0.07	-	-
^{83}Kr$_{cos}$ [in 10^{-8} cc/g]	-	-	-				
±	-	-	-				
^{83}Kr$_{cos}$ [in 10^{-12} cc]	-	-	-				
±	-	-	-				

Table X12. Noble gas data He to Xe for sample 45b.21 (corrected for blank)

Sample				45b.21			
Size [µm]				571 x 212			
Weight [µg]				24.8 ± 0.1			
Date of measurement	18/01/12	19/01/12	18+19/01/12	Date of measurement	18/01/12	19/01/12	18+19/01/12
Laser-Power	3 x 0.91 W	3 x 5 W		Laser-Power	3 x 0.91 W	3 x 5 W	
Laser-Beam	250 µm	250 µm		Laser-Beam	250 µm	250 µm	
Step(s)	1	2	total*	Step(s)	1	2	total*
^{4}He [in 10^{-8} cc/g]	4457.5	217.9	4675.4	^{132}Xe - INT [in 10^{-8} cc/g]	0.4746	0.2501	0.7247
±	109.2	78.7	134.6	±	0.0142	0.0098	0.0173
^{4}He [in 10^{-12} cc]	1105.5	54.0	1159.5	^{132}Xe - INT [in 10^{-12} cc]	0.1177	0.0620	0.1797
±	26.7	19.5	33.1	±	0.0035	0.0024	0.0042
^{3}He [in 10^{-12} cc/g]	12327.6	1091.1	13418.7	^{128}Xe/^{132}Xe - INT	0.077	0.086	0.080
±	1780.0	722.7	1921.2	±	0.002	0.003	0.002
^{3}He [in 10^{-16} cc]	3057.2	270.6	3327.8	^{129}Xe/^{132}Xe - INT	1.019	1.038	1.025
±	441.3	179.2	476.3	±	0.011	0.015	0.009
^{3}He/^{4}He	0.00028	0.00050	0.00029	^{130}Xe/^{132}Xe - INT	0.158	0.164	0.160
±	0.00004	0.00038	0.00004	±	0.002	0.003	0.002
^{22}Ne [in 10^{-8} cc/g]	5.492	0.562	6.053	^{131}Xe/^{132}Xe - INT	0.806	0.817	0.809
±	0.376	0.290	0.475	±	0.009	0.012	0.007
^{22}Ne [in 10^{-12} cc]	1.362	0.139	1.501	^{134}Xe/^{132}Xe - INT	0.384	0.376	0.381
±	0.093	0.072	0.118	±	0.005	0.007	0.004
^{20}Ne/^{22}Ne	11.24	11.05	11.22	^{136}Xe/^{132}Xe - INT	0.333	0.321	0.329
±	0.44	3.27	0.50	±	0.006	0.008	0.005
^{21}Ne/^{22}Ne	0.029	0.034	0.029	^{132}Xe - EXTa [in 10^{-8} cc/g]	0.4746	0.2501	0.7247
±	0.002	0.011	0.002	±	0.1386	0.0733	0.1568
^{21}Ne$_{cos}$ [in 10^{-8} cc/g]	< 0.134 (2σ)	< 0.020 (2σ)	-	^{132}Xe - EXTa [in 10^{-12} cc]	0.1177	0.0620	0.1797
±	-	-	-	±	0.0344	0.0182	0.0389
^{21}Ne$_{cos}$ [in 10^{-12} cc]	< 0.033 (2σ)	< 0.005 (2σ)	-	^{128}Xe/^{132}Xe - EXTa	0.076	0.084	0.079
±	-	-	-	±	0.002	0.002	0.001
^{20}Ne$_{trap}$ [in 10^{-8} cc/g]	61.3	6.16	67.45	^{129}Xe/^{132}Xe - EXTa	1.018	1.036	1.024
±	5.9	3.68	6.96	±	0.011	0.016	0.009
^{20}Ne$_{trap}$ [in 10^{-12} cc]	15.2	1.53	16.73	^{130}Xe/^{132}Xe - EXTa	0.157	0.164	0.160
±	1.5	0.91	1.73	±	0.003	0.003	0.002
^{36}Ar [in 10^{-8} cc/g]	32.54	27.89	60.42	^{131}Xe/^{132}Xe - EXTa	0.805	0.817	0.809
±	1.36	1.33	1.91	±	0.008	0.012	0.007
^{36}Ar [in 10^{-12} cc]	8.07	6.92	14.99	^{134}Xe/^{132}Xe - EXTa	0.375	0.374	0.375
±	0.34	0.33	0.47	±	0.004	0.006	0.004
^{38}Ar/^{36}Ar	0.192	0.189	0.190	^{136}Xe/^{132}Xe - EXTa	0.318	0.325	0.320
±	0.002	0.002	0.001	±	0.004	0.006	0.003
^{40}Ar/^{36}Ar	22.2	61.4	40.3	^{132}Xe - EXTb [in 10^{-8} cc/g]	0.4712	0.2470	0.7182
±	7.9	7.6	5.5	±	0.0654	0.0346	0.0740
^{40}Ar [in 10^{-8} cc/g]	721.1	1712.8	2433.9	^{132}Xe - EXTb [in 10^{-12} cc]	0.1169	0.0612	0.1781
±	321.5	322.6	455.4	±	0.0162	0.0086	0.0183
^{40}Ar [in 10^{-12} cc]	178.8	424.8	603.6	^{128}Xe/^{132}Xe - EXTb	0.076	0.079	0.077
±	79.7	80.0	112.9	±	0.002	0.002	0.001
^{38}Ar$_{cos}$ [in 10^{-8} cc/g]	0.113	< 0.201 (2σ)	-	^{129}Xe/^{132}Xe - EXTb	1.018	1.037	1.024
±	0.105	-	-	±	0.012	0.017	0.010
^{38}Ar$_{cos}$ [in 10^{-12} cc]	0.028	< 0.050 (2σ)	-	^{130}Xe/^{132}Xe - EXTb	0.156	0.163	0.158
±	0.026	-	-	±	0.002	0.004	0.002
^{84}Kr [in 10^{-8} cc/g]	0.3511	0.2357	0.5868	^{131}Xe/^{132}Xe - EXTb	0.806	0.818	0.810
±	0.0333	0.0263	0.0425	±	0.004	0.005	0.003
^{84}Kr [in 10^{-12} cc]	0.0871	0.0585	0.1455	^{134}Xe/^{132}Xe - EXTb	0.385	0.377	0.382
±	0.0083	0.0065	0.0105	±	0.005	0.006	0.004
^{80}Kr/^{84}Kr	0.038	0.038	0.038	^{136}Xe/^{132}Xe - EXTb	0.326	0.321	0.324
±	0.002	0.003	0.002	±	0.004	0.006	0.003
^{82}Kr/^{84}Kr	0.202	0.201	0.201	^{21}Ne$_{cos}$/^{38}Ar$_{cos}$	-	-	-
±	0.006	0.008	0.005	±	-	-	-
^{83}Kr/^{84}Kr	0.194	0.203	0.198	^{36}Ar/^{132}Xe $_{(Int)}$	68.56	111.51	83.38
±	0.006	0.007	0.004	±	3.51	6.87	3.26
^{86}Kr/^{84}Kr	0.313	0.302	0.308	^{84}Kr/^{132}Xe $_{(Int)}$	0.74	0.94	0.81
±	0.007	0.010	0.006	±	0.07	0.11	0.06
^{83}Kr$_{cos}$ [in 10^{-8} cc/g]	-	-	-				
±	-	-	-				
^{83}Kr$_{cos}$ [in 10^{-12} cc]	-	-	-				
±	-	-	-				

Table X13. Noble gas data He to Xe for sample 45b.22_2 (corrected for blank)

Sample	45b.22_2						
Size [μm]	268 x 191						
Weight [μg]	9.2 ± 0.2						
Date of measurement	04/05/11	04/05/11	04/05/11	**Date of measurement**	04/05/11	04/05/11	04/05/11
Laser-Power	3 x 5 W	3 x 15 W		**Laser-Power**	3 x 5 W	3 x 15 W	
Laser-Beam	1000 μm	1000 μm		**Laser-Beam**	1000 μm	1000 μm	
Step(s)	1	2	total*	**Step(s)**	1	2	total*
^{4}He [in 10^{-8} cc/g]	< 79 (2σ)	-	-	^{132}Xe - INT [in 10^{-8} cc/g]	-	-	-
±	-	-	-	±	-	-	-
^{4}He [in 10^{-12} cc]	< 7 (2σ)	-	-	^{132}Xe - INT [in 10^{-12} cc]	-	-	-
±	-	-	-	±	-	-	-
^{3}He [in 10^{-12} cc/g]	-	-	-	^{128}Xe/^{132}Xe - INT	-	-	-
±	-	-	-	±	-	-	-
^{3}He [in 10^{-16} cc]	-	-	-	^{129}Xe/^{132}Xe - INT	-	-	-
±	-	-	-	±	-	-	-
^{3}He/^{4}He	-	-	-	^{130}Xe/^{132}Xe - INT	-	-	-
±	-	-	-	±	-	-	-
^{22}Ne [in 10^{-8} cc/g]	4.391	< 0.66 (2σ)	-	^{131}Xe/^{132}Xe - INT	-	-	-
±	0.338	-	-	±	-	-	-
^{22}Ne [in 10^{-12} cc]	0.404	< 0.06 (2σ)	-	^{134}Xe/^{132}Xe - INT	-	-	-
±	0.030	-	-	±	-	-	-
^{20}Ne/^{22}Ne	11.16	-	-	^{136}Xe/^{132}Xe - INT	-	-	-
±	0.49	-	-	±	-	-	-
^{21}Ne/^{22}Ne	0.074	-	-	^{132}Xe - EXTa [in 10^{-8} cc/g]	-	-	-
±	0.005	-	-	±	-	-	-
^{21}Ne$_{cos}$ [in 10^{-8} cc/g]	0.194	< 0.313 (2σ)	-	^{132}Xe - EXTa [in 10^{-12} cc]	-	-	-
±	0.024	-	-	±	-	-	-
^{21}Ne$_{cos}$ [in 10^{-12} cc]	0.018	< 0.029 (2σ)	-	^{128}Xe/^{132}Xe - EXTa	-	-	-
±	0.002	-	-	±	-	-	-
^{20}Ne$_{trap}$ [in 10^{-8} cc/g]	48.8	-	-	^{129}Xe/^{132}Xe - EXTa	-	-	-
±	5.1	-	-	±	-	-	-
^{20}Ne$_{trap}$ [in 10^{-12} cc]	4.5	-	-	^{130}Xe/^{132}Xe - EXTa	-	-	-
±	0.5	-	-	±	-	-	-
^{36}Ar [in 10^{-8} cc/g]	2.94	-	-	^{131}Xe/^{132}Xe - EXTa	-	-	-
±	1.85	-	-	±	-	-	-
^{36}Ar [in 10^{-12} cc]	0.27	-	-	^{134}Xe/^{132}Xe - EXTa	-	-	-
±	0.17	-	-	±	-	-	-
^{38}Ar/^{36}Ar	0.209	-	-	^{136}Xe/^{132}Xe - EXTa	-	-	-
±	0.044	-	-	±	-	-	-
^{40}Ar/^{36}Ar	-	-	-	^{132}Xe - EXTb [in 10^{-8} cc/g]	-	-	-
±	-	-	-	±	-	-	-
^{40}Ar [in 10^{-8} cc/g]	-	-	-	^{132}Xe - EXTb [in 10^{-12} cc]	-	-	-
±	-	-	-	±	-	-	-
^{40}Ar [in 10^{-12} cc]	-	-	-	^{128}Xe/^{132}Xe - EXTb	-	-	-
±	-	-	-	±	-	-	-
^{38}Ar$_{cos}$ [in 10^{-8} cc/g]	< 0.348 (2σ)	< 1.677 (2σ)	-	^{129}Xe/^{132}Xe - EXTb	-	-	-
±	-	-	-	±	-	-	-
^{38}Ar$_{cos}$ [in 10^{-12} cc]	< 0.032 (2σ)	< 0.154 (2σ)	-	^{130}Xe/^{132}Xe - EXTb	-	-	-
±	-	-	-	±	-	-	-
^{84}Kr [in 10^{-8} cc/g]	-	-	-	^{131}Xe/^{132}Xe - EXTb	-	-	-
±	-	-	-	±	-	-	-
^{84}Kr [in 10^{-12} cc]	-	-	-	^{134}Xe/^{132}Xe - EXTb	-	-	-
±	-	-	-	±	-	-	-
^{80}Kr/^{84}Kr	-	-	-	^{136}Xe/^{132}Xe - EXTb	-	-	-
±	-	-	-	±	-	-	-
^{82}Kr/^{84}Kr	-	-	-	^{21}Ne$_{cos}$/^{38}Ar$_{cos}$	-	-	-
±	-	-	-	±	-	-	-
^{83}Kr/^{84}Kr	-	-	-	^{36}Ar/^{132}Xe $_{(Int)}$	-	-	-
±	-	-	-	±	-	-	-
^{86}Kr/^{84}Kr	-	-	-	^{84}Kr/^{132}Xe $_{(Int)}$	-	-	-
±	-	-	-	±	-	-	-
^{83}Kr$_{cos}$ [in 10^{-8} cc/g]	-	-	-				
±	-	-	-				
^{83}Kr$_{cos}$ [in 10^{-12} cc]	-	-	-				
±	-	-	-				

Table X14. Noble gas data He to Xe for sample 45c.16_2 (corrected for blank)

Sample	45c.16_2						
Size [μm]	465 x 324						
Weight [μg]	105.1 ± 0.2						
Date of measurement	02/05/11	02/05/11	02/05/11	**Date of measurement**	02/05/11	02/05/11	02/05/11
Laser-Power	3 x 5 W	3 x 15 W		**Laser-Power**	3 x 5 W	3 x 15 W	
Laser-Beam	1000 μm	1000 μm		**Laser-Beam**	1000 μm	1000 μm	
Step(s)	1	2	total*	**Step(s)**	1	2	total*
^{4}He [in 10^{-8} cc/g]	3.7	-	-	^{132}Xe - INT [in 10^{-8} cc/g]	-	-	-
±	2.4	-	-	±	-	-	-
^{4}He [in 10^{-12} cc]	3.8	-	-	^{132}Xe - INT [in 10^{-12} cc]	-	-	-
±	2.5	-	-	±	-	-	-
^{3}He [in 10^{-12} cc/g]	6.5	< 9 (2σ)	-	^{128}Xe/^{132}Xe - INT	-	-	-
±	3.0	-	-	±	-	-	-
^{3}He [in 10^{-16} cc]	6.8	< 10 (2σ)	-	^{129}Xe/^{132}Xe - INT	-	-	-
±	3.2	-	-	±	-	-	-
^{3}He/^{4}He	0.00018	-	-	^{130}Xe/^{132}Xe - INT	-	-	-
±	0.00014	-	-	±	-	-	-
^{22}Ne [in 10^{-8} cc/g]	0.098	-	-	^{131}Xe/^{132}Xe - INT	-	-	-
±	0.042	-	-	±	-	-	-
^{22}Ne [in 10^{-12} cc]	0.103	-	-	^{134}Xe/^{132}Xe - INT	-	-	-
±	0.044	-	-	±	-	-	-
^{20}Ne/^{22}Ne	10.41	-	-	^{136}Xe/^{132}Xe - INT	-	-	-
±	2.54	-	-	±	-	-	-
^{21}Ne/^{22}Ne	0.041	-	-	^{132}Xe - EXTa [in 10^{-8} cc/g]	-	-	-
±	0.010	-	-	±	-	-	-
^{21}Ne$_{cos}$ [in 10^{-8} cc/g]	< 0.004 (2σ)	< 0.012 (2σ)	-	^{132}Xe - EXTa [in 10^{-12} cc]	-	-	-
±	-	-	-	±	-	-	-
^{21}Ne$_{cos}$ [in 10^{-12} cc]	< 0.004 (2σ)	< 0.013 (2σ)	-	^{128}Xe/^{132}Xe - EXTa	-	-	-
±	-	-	-	±	-	-	-
^{20}Ne$_{trap}$ [in 10^{-8} cc/g]	1.0	-	-	^{129}Xe/^{132}Xe - EXTa	-	-	-
±	0.5	-	-	±	-	-	-
^{20}Ne$_{trap}$ [in 10^{-12} cc]	1.1	-	-	^{130}Xe/^{132}Xe - EXTa	-	-	-
±	0.5	-	-	±	-	-	-
^{36}Ar [in 10^{-8} cc/g]	0.23	-	-	^{131}Xe/^{132}Xe - EXTa	-	-	-
±	0.16	-	-	±	-	-	-
^{36}Ar [in 10^{-12} cc]	0.24	-	-	^{134}Xe/^{132}Xe - EXTa	-	-	-
±	0.17	-	-	±	-	-	-
^{38}Ar/^{36}Ar	0.195	-	-	^{136}Xe/^{132}Xe - EXTa	-	-	-
±	0.048	-	-	±	-	-	-
^{40}Ar/^{36}Ar	344.6	-	-	^{132}Xe - EXTb [in 10^{-8} cc/g]	-	-	-
±	62.9	-	-	±	-	-	-
^{40}Ar [in 10^{-8} cc/g]	79.9	2.4	82.3	^{132}Xe - EXTb [in 10^{-12} cc]	-	-	-
±	37.4	37.3	52.8	±	-	-	-
^{40}Ar [in 10^{-12} cc]	84.0	2.5	86.5	^{128}Xe/^{132}Xe - EXTb	-	-	-
±	39.3	39.2	55.5	±	-	-	-
^{38}Ar$_{cos}$ [in 10^{-8} cc/g]	< 0.026 (2σ)	< 0.957 (2σ)	-	^{129}Xe/^{132}Xe - EXTb	-	-	-
±	-	-	-	±	-	-	-
^{38}Ar$_{cos}$ [in 10^{-12} cc]	< 0.028 (2σ)	< 1.006 (2σ)	-	^{130}Xe/^{132}Xe - EXTb	-	-	-
±	-	-	-	±	-	-	-
^{84}Kr [in 10^{-8} cc/g]	-	-	-	^{131}Xe/^{132}Xe - EXTb	-	-	-
±	-	-	-	±	-	-	-
^{84}Kr [in 10^{-12} cc]	-	-	-	^{134}Xe/^{132}Xe - EXTb	-	-	-
±	-	-	-	±	-	-	-
^{80}Kr/^{84}Kr	-	-	-	^{136}Xe/^{132}Xe - EXTb	-	-	-
±	-	-	-	±	-	-	-
^{82}Kr/^{84}Kr	-	-	-	^{21}Ne$_{cos}$/^{38}Ar$_{cos}$	-	-	-
±	-	-	-	±	-	-	-
^{83}Kr/^{84}Kr	-	-	-	^{36}Ar/^{132}Xe $_{(Int)}$	-	-	-
±	-	-	-	±	-	-	-
^{86}Kr/^{84}Kr	-	-	-	^{84}Kr/^{132}Xe $_{(Int)}$	-	-	-
±	-	-	-	±	-	-	-
^{83}Kr$_{cos}$ [in 10^{-8} cc/g]	-	-	-				
±	-	-	-				
^{83}Kr$_{cos}$ [in 10^{-12} cc]	-	-	-				
±	-	-	-				

Table X15. Noble gas data He to Xe for sample 45c.17 (corrected for blank)

Sample				45c.17			
Size [µm]				630 x 476			
Weight [µg]				126.3 ± 0.2			
Date of measurement	31/03/11	31/03/11	31/03/11	**Date of measurement**	31/03/11	31/03/11	31/03/11
Laser-Power	3 x 5 W	3 x 15 W		**Laser-Power**	3 x 5 W	3 x 15 W	
Laser-Beam	1000 µm	1000 µm		**Laser-Beam**	1000 µm	1000 µm	
Step(s)	1	2	total*	**Step(s)**	1	2	total*
^{4}He [in 10^{-8} cc/g]	15.1	-	-	^{132}Xe - INT [in 10^{-8} cc/g]	-	-	-
±	2.7	-	-	±	-	-	-
^{4}He [in 10^{-12} cc]	19.1	-	-	^{132}Xe - INT [in 10^{-12} cc]	-	-	-
±	3.4	-	-	±	-	-	-
^{3}He [in 10^{-12} cc/g]	28.8	< 11 (2σ)		^{128}Xe/^{132}Xe - INT	-	-	-
±	8.4	-		±	-	-	-
^{3}He [in 10^{-16} cc]	36.4	< 14 (2σ)		^{129}Xe/^{132}Xe - INT	-	-	-
±	10.6	-		±	-	-	-
^{3}He/^{4}He	0.00019	-	-	^{130}Xe/^{132}Xe - INT	-	-	-
±	0.00006	-	-	±	-	-	-
^{22}Ne [in 10^{-8} cc/g]	0.054	< 0.07 (2σ)		^{131}Xe/^{132}Xe - INT	-	-	-
±	0.033	-		±	-	-	-
^{22}Ne [in 10^{-12} cc]	0.069	< 0.09 (2σ)		^{134}Xe/^{132}Xe - INT	-	-	-
±	0.042	-		±	-	-	-
^{20}Ne/^{22}Ne	12.34	-	-	^{136}Xe/^{132}Xe - INT	-	-	-
±	3.01	-	-	±	-	-	-
^{21}Ne/^{22}Ne	0.044	-	-	^{132}Xe - EXTa [in 10^{-8} cc/g]	-	-	-
±	0.023	-	-	±	-	-	-
^{21}Ne$_{cos}$ [in 10^{-8} cc/g]	< 0.003 (2σ)	-	-	^{132}Xe - EXTa [in 10^{-12} cc]	-	-	-
±	-	-	-	±	-	-	-
^{21}Ne$_{cos}$ [in 10^{-12} cc]	< 0.004 (2σ)	-	-	^{128}Xe/^{132}Xe - EXTa	-	-	-
±	-	-	-	±	-	-	-
^{20}Ne$_{trap}$ [in 10^{-8} cc/g]	0.7	-	-	^{129}Xe/^{132}Xe - EXTa	-	-	-
±	0.4	-	-	±	-	-	-
^{20}Ne$_{trap}$ [in 10^{-12} cc]	0.8	-	-	^{130}Xe/^{132}Xe - EXTa	-	-	-
±	0.6	-	-	±	-	-	-
^{36}Ar [in 10^{-8} cc/g]	0.83	< 0.33 (2σ)	-	^{131}Xe/^{132}Xe - EXTa	-	-	-
±	0.20	-	-	±	-	-	-
^{36}Ar [in 10^{-12} cc]	1.05	< 0.42 (2σ)	-	^{134}Xe/^{132}Xe - EXTa	-	-	-
±	0.25	-	-	±	-	-	-
^{38}Ar/^{36}Ar	0.194	-	-	^{136}Xe/^{132}Xe - EXTa	-	-	-
±	0.014	-	-	±	-	-	-
^{40}Ar/^{36}Ar	281.9	-	-	^{132}Xe - EXTb [in 10^{-8} cc/g]	-	-	-
±	18.5	-	-	±	-	-	-
^{40}Ar [in 10^{-8} cc/g]	234.5	-	-	^{132}Xe - EXTb [in 10^{-12} cc]	-	-	-
±	48.8	-	-	±	-	-	-
^{40}Ar [in 10^{-12} cc]	296.2	-	-	^{128}Xe/^{132}Xe - EXTb	-	-	-
±	61.7	-	-	±	-	-	-
^{38}Ar$_{cos}$ [in 10^{-8} cc/g]	< 0.031 (2σ)	-	-	^{129}Xe/^{132}Xe - EXTb	-	-	-
±	-	-	-	±	-	-	-
^{38}Ar$_{cos}$ [in 10^{-12} cc]	< 0.039 (2σ)	-	-	^{130}Xe/^{132}Xe - EXTb	-	-	-
±	-	-	-	±	-	-	-
^{84}Kr [in 10^{-8} cc/g]	0.0596	-	-	^{131}Xe/^{132}Xe - EXTb	-	-	-
±	0.0083	-	-	±	-	-	-
^{84}Kr [in 10^{-12} cc]	0.0753	-	-	^{134}Xe/^{132}Xe - EXTb	-	-	-
±	0.0105	-	-	±	-	-	-
^{80}Kr/^{84}Kr	0.034	-	-	^{136}Xe/^{132}Xe - EXTb	-	-	-
±	0.005	-	-	±	-	-	-
^{82}Kr/^{84}Kr	0.195	-	-	^{21}Ne$_{cos}$/^{38}Ar$_{cos}$	-	-	-
±	0.006	-	-	±	-	-	-
^{83}Kr/^{84}Kr	0.207	-	-	^{36}Ar/^{132}Xe $_{(Int)}$	-	-	-
±	0.005	-	-	±	-	-	-
^{86}Kr/^{84}Kr	0.296	-	-	^{84}Kr/^{132}Xe $_{(Int)}$	-	-	-
±	0.007	-	-	±	-	-	-
^{83}Kr$_{cos}$ [in 10^{-8} cc/g]	< 0.0011 (2σ)	-					
±	-	-					
^{83}Kr$_{cos}$ [in 10^{-12} cc]	< 0.0014 (2σ)	-					
±	-	-	-				

Table X16. Noble gas data He to Xe for sample 45c.21 (corrected for blank)

Sample	45c.21		
Size [µm]	720 x 556		
Weight [µg]	337.9 ± 0.2		

Date of measurement	28/04/11	28/04/11	28/04/11
Laser-Power	3 x 5 W	3 x 15 W	
Laser-Beam	1000 µm	1000 µm	
Step(s)	1	2	total*
^{4}He [in 10^{-8} cc/g]	-	-	-
±	-	-	-
^{4}He [in 10^{-12} cc]	-	-	-
±	-	-	-
^{3}He [in 10^{-12} cc/g]	-	-	-
±	-	-	-
^{3}He [in 10^{-16} cc]	-	-	-
±	-	-	-
^{3}He/^{4}He	-	-	-
±	-	-	-
^{22}Ne [in 10^{-8} cc/g]	0.090	-	-
±	0.008	-	-
^{22}Ne [in 10^{-12} cc]	0.305	-	-
±	0.027	-	-
^{20}Ne/^{22}Ne	9.88	-	-
±	0.62	-	-
^{21}Ne/^{22}Ne	0.035	-	-
±	0.004	-	-
^{21}Ne$_{cos}$ [in 10^{-8} cc/g]	0.001	-	-
±	0.000	-	-
^{21}Ne$_{cos}$ [in 10^{-12} cc]	0.002	-	-
±	0.002	-	-
^{20}Ne$_{trap}$ [in 10^{-8} cc/g]	0.9	-	-
±	0.1	-	-
^{20}Ne$_{trap}$ [in 10^{-12} cc]	3.0	-	-
±	0.4	-	-
^{36}Ar [in 10^{-8} cc/g]	-	-	-
±	-	-	-
^{36}Ar [in 10^{-12} cc]	-	-	-
±	-	-	-
^{38}Ar/^{36}Ar	-	-	-
±	-	-	-
^{40}Ar/^{36}Ar	-	-	-
±	-	-	-
^{40}Ar [in 10^{-8} cc/g]	< 25.40 (2σ)	-	-
±	-	-	-
^{40}Ar [in 10^{-12} cc]	< 85.86 (2σ)	-	-
±	-	-	-
^{38}Ar$_{cos}$ [in 10^{-8} cc/g]	-	-	-
±	-	-	-
^{38}Ar$_{cos}$ [in 10^{-12} cc]	-	-	-
±	-	-	-
^{84}Kr [in 10^{-8} cc/g]	-	-	-
±	-	-	-
^{84}Kr [in 10^{-12} cc]	-	-	-
±	-	-	-
^{80}Kr/^{84}Kr	-	-	-
±	-	-	-
^{82}Kr/^{84}Kr	-	-	-
±	-	-	-
^{83}Kr/^{84}Kr	-	-	-
±	-	-	-
^{86}Kr/^{84}Kr	-	-	-
±	-	-	-
^{83}Kr$_{cos}$ [in 10^{-8} cc/g]	-	-	-
±	-	-	-
^{83}Kr$_{cos}$ [in 10^{-12} cc]	-	-	-
±	-	-	-

Date of measurement	28/04/11	28/04/11	28/04/11
Laser-Power	3 x 5 W	3 x 15 W	
Laser-Beam	1000 µm	1000 µm	
Step(s)	1	2	total*
^{132}Xe - INT [in 10^{-8} cc/g]	-	-	-
±	-	-	-
^{132}Xe - INT [in 10^{-12} cc]	-	-	-
±	-	-	-
^{128}Xe/^{132}Xe - INT	-	-	-
±	-	-	-
^{129}Xe/^{132}Xe - INT	-	-	-
±	-	-	-
^{130}Xe/^{132}Xe - INT	-	-	-
±	-	-	-
^{131}Xe/^{132}Xe - INT	-	-	-
±	-	-	-
^{134}Xe/^{132}Xe - INT	-	-	-
±	-	-	-
^{136}Xe/^{132}Xe - INT	-	-	-
±	-	-	-
^{132}Xe - EXTa [in 10^{-8} cc/g]	-	-	-
±	-	-	-
^{132}Xe - EXTa [in 10^{-12} cc]	-	-	-
±	-	-	-
^{128}Xe/^{132}Xe - EXTa	-	-	-
±	-	-	-
^{129}Xe/^{132}Xe - EXTa	-	-	-
±	-	-	-
^{130}Xe/^{132}Xe - EXTa	-	-	-
±	-	-	-
^{131}Xe/^{132}Xe - EXTa	-	-	-
±	-	-	-
^{134}Xe/^{132}Xe - EXTa	-	-	-
±	-	-	-
^{136}Xe/^{132}Xe - EXTa	-	-	-
±	-	-	-
^{132}Xe - EXTb [in 10^{-8} cc/g]	-	-	-
±	-	-	-
^{132}Xe - EXTb [in 10^{-12} cc]	-	-	-
±	-	-	-
^{128}Xe/^{132}Xe - EXTb	-	-	-
±	-	-	-
^{129}Xe/^{132}Xe - EXTb	-	-	-
±	-	-	-
^{130}Xe/^{132}Xe - EXTb	-	-	-
±	-	-	-
^{131}Xe/^{132}Xe - EXTb	-	-	-
±	-	-	-
^{134}Xe/^{132}Xe - EXTb	-	-	-
±	-	-	-
^{136}Xe/^{132}Xe - EXTb	-	-	-
±	-	-	-
^{21}Ne$_{cos}$/^{38}Ar$_{cos}$	-	-	-
±	-	-	-
^{36}Ar/^{132}Xe $_{(Int)}$	-	-	-
±	-	-	-
^{84}Kr/^{132}Xe $_{(Int)}$	-	-	-
±	-	-	-

Table X17. Noble gas data He to Xe for sample 45c.24 (corrected for blank)

Sample	45c.24		
Size [µm]	489 x 330		
Weight [µg]	34.0 ± 0.1		
Date of measurement	27/09/12	02/10/12	27.09 / 02.10.12
Laser-Power	3 x 0.91 W	2 x 5W 1 x 9.8W	
Laser-Beam	600-250 µm	250 µm	
Step(s)	1	2	total*
^{4}He [in 10^{-8} cc/g]	469.3	-	-
±	14.9	-	-
^{4}He [in 10^{-12} cc]	159.5	-	-
±	5.1	-	-
^{3}He [in 10^{-12} cc/g]	2920.1	1007.0	3927.1
±	183.3	261.0	318.9
^{3}He [in 10^{-16} cc]	992.8	342.4	1335.2
±	62.3	88.7	108.4
^{3}He/^{4}He	0.00062	-	-
±	0.00004	-	-
^{22}Ne [in 10^{-8} cc/g]	0.970	< 0.20 (2σ)	-
±	0.073	-	-
^{22}Ne [in 10^{-12} cc]	0.330	< 0.07 (2σ)	-
±	0.025	-	-
^{20}Ne/^{22}Ne	11.48	-	-
±	0.58	-	-
^{21}Ne/^{22}Ne	0.024	-	-
±	0.004	-	-
^{21}Ne$_{cos}$ [in 10^{-8} cc/g]	-	-	-
±	-	-	-
^{21}Ne$_{cos}$ [in 10^{-12} cc]	-	-	-
±	-	-	-
^{20}Ne$_{trap}$ [in 10^{-8} cc/g]	11.1	< 1.5 (2σ)	-
±	1.2	-	-
^{20}Ne$_{trap}$ [in 10^{-12} cc]	3.8	< 0.5 (2σ)	-
±	0.4	-	-
^{36}Ar [in 10^{-8} cc/g]	23.62	< 0.86 (2σ)	-
±	0.60	-	-
^{36}Ar [in 10^{-12} cc]	8.03	< 0.29 (2σ)	-
±	0.20	-	-
^{38}Ar/^{36}Ar	-	-	-
±	-	-	-
^{40}Ar/^{36}Ar	-	-	-
±	-	-	-
^{40}Ar [in 10^{-8} cc/g]	< 218.81 (2σ)	-	-
±	-	-	-
^{40}Ar [in 10^{-12} cc]	< 74.39 (2σ)	-	-
±	-	-	-
^{38}Ar$_{cos}$ [in 10^{-8} cc/g]	-	-	-
±	-	-	-
^{38}Ar$_{cos}$ [in 10^{-12} cc]	-	-	-
±	-	-	-
^{84}Kr [in 10^{-8} cc/g]	0.3093	< 0.026 (2σ)	-
±	0.0250	-	-
^{84}Kr [in 10^{-12} cc]	0.1052	< 0.009 (2σ)	-
±	0.0085	-	-
^{80}Kr/^{84}Kr	0.043	-	-
±	0.003	-	-
^{82}Kr/^{84}Kr	0.218	-	-
±	0.013	-	-
^{83}Kr/^{84}Kr	0.201	-	-
±	0.010	-	-
^{86}Kr/^{84}Kr	0.325	-	-
±	0.017	-	-
^{83}Kr$_{cos}$ [in 10^{-8} cc/g]	-	-	-
±	-	-	-
^{83}Kr$_{cos}$ [in 10^{-12} cc]	-	-	-
±	-	-	-

Date of measurement	27/09/12	02/10/12	27.09 / 02.10.12
Laser-Power	3 x 0.91 W	2 x 5W 1 x 9.8W	
Laser-Beam	600-250 µm	250 µm	
Step(s)	1	2	total*
^{132}Xe - INT [in 10^{-8} cc/g]	0.5596	0.0033	0.5629
±	0.0087	0.0024	0.0090
^{132}Xe - INT [in 10^{-12} cc]	0.1903	0.0011	0.1914
±	0.0029	0.0008	0.0030
^{128}Xe/^{132}Xe - INT	0.079	-	-
±	0.002	-	-
^{129}Xe/^{132}Xe - INT	1.030	0.828	1.029
±	0.014	0.191	0.014
^{130}Xe/^{132}Xe - INT	0.158	0.119	0.158
±	0.002	0.080	0.002
^{131}Xe/^{132}Xe - INT	0.814	0.415	0.811
±	0.010	0.234	0.010
^{134}Xe/^{132}Xe - INT	0.384	0.369	0.383
±	0.005	0.129	0.005
^{136}Xe/^{132}Xe - INT	0.325	0.368	0.325
±	0.006	0.163	0.006
^{132}Xe - EXTa [in 10^{-8} cc/g]	0.5631	0.0033	0.5664
±	0.0087	0.0024	0.0090
^{132}Xe - EXTa [in 10^{-12} cc]	0.1914	0.0011	0.1926
±	0.0029	0.0008	0.0030
^{128}Xe/^{132}Xe - EXTa	0.081	-	-
±	0.001	-	-
^{129}Xe/^{132}Xe - EXTa	1.030	0.841	1.029
±	0.011	0.211	0.011
^{130}Xe/^{132}Xe - EXTa	0.157	0.073	0.157
±	0.002	0.073	0.002
^{131}Xe/^{132}Xe - EXTa	0.816	0.381	0.813
±	0.009	0.278	0.009
^{134}Xe/^{132}Xe - EXTa	0.373	0.276	0.372
±	0.004	0.129	0.004
^{136}Xe/^{132}Xe - EXTa	0.315	0.172	0.314
±	0.004	0.078	0.004
^{132}Xe - EXTb [in 10^{-8} cc/g]	0.5610	0.0030	0.5640
±	0.0163	0.0016	0.0164
^{132}Xe - EXTb [in 10^{-12} cc]	0.1907	0.0010	0.1918
±	0.0055	0.0006	0.0056
^{128}Xe/^{132}Xe - EXTb	0.082	-	-
±	0.001	-	-
^{129}Xe/^{132}Xe - EXTb	1.030	0.824	1.029
±	0.011	0.224	0.011
^{130}Xe/^{132}Xe - EXTb	0.162	0.142	0.162
±	0.002	0.056	0.002
^{131}Xe/^{132}Xe - EXTb	0.815	0.423	0.813
±	0.004	0.176	0.004
^{134}Xe/^{132}Xe - EXTb	0.383	0.471	0.384
±	0.004	0.144	0.004
^{136}Xe/^{132}Xe - EXTb	0.316	0.394	0.317
±	0.003	0.100	0.003
^{21}Ne$_{cos}$/^{38}Ar$_{cos}$	-	-	-
±	-	-	-
^{36}Ar/^{132}Xe (Int)	42.21	-	-
±	1.24	-	-
^{84}Kr/^{132}Xe (Int)	0.55	-	-
±	0.05	-	-

Table X18. Noble gas data He to Xe for sample 45c.25_2 (corrected for blank)

Sample				45c.25_2			
Size [µm]				580 x 528			
Weight [µg]				142.3 ± 0.1			
Date of measurement	19/04/12	20/04/12	19+20/04/12	**Date of measurement**	19/04/12	20/04/12	19+20/04/12
Laser-Power	3 x 0.91 W	3 x 5 W		**Laser-Power**	3 x 0.91 W	3 x 5 W	
Laser-Beam	600 µm	600 µm		**Laser-Beam**	600 µm	600 µm	
Step(s)	1	2	total*	**Step(s)**	1	2	total*
^{4}He [in 10^{-8} cc/g]	22.7	-	-	^{132}Xe - INT [in 10^{-8} cc/g]	0.1898	0.0047	0.1945
±	2.8	-	-	±	0.0111	0.0017	0.0112
^{4}He [in 10^{-12} cc]	32.3	-	-	^{132}Xe - INT [in 10^{-12} cc]	0.2701	0.0066	0.2768
±	4.0	-	-	±	0.0158	0.0025	0.0160
^{3}He [in 10^{-12} cc/g]	397.4	< 21 (2σ)	-	^{128}Xe/^{132}Xe - INT	0.071	0.045	0.071
±	103.2	-	-	±	0.002	0.019	0.002
^{3}He [in 10^{-16} cc]	565.6	< 29 (2σ)	-	^{129}Xe/^{132}Xe - INT	0.989	0.875	0.987
±	146.9	-	-	±	0.008	0.068	0.008
^{3}He/^{4}He	0.00175	-	-	^{130}Xe/^{132}Xe - INT	0.151	0.149	0.151
±	0.00050	-	-	±	0.001	0.013	0.001
^{22}Ne [in 10^{-8} cc/g]	0.019	-	-	^{131}Xe/^{132}Xe - INT	0.783	0.792	0.784
±	0.019	-	-	±	0.006	0.064	0.006
^{22}Ne [in 10^{-12} cc]	0.028	-	-	^{134}Xe/^{132}Xe - INT	0.388	0.348	0.387
±	0.026	-	-	±	0.003	0.035	0.003
^{20}Ne/^{22}Ne	-	-	-	^{136}Xe/^{132}Xe - INT	0.331	0.301	0.330
±	-	-	-	±	0.005	0.039	0.005
^{21}Ne/^{22}Ne	-	-	-	^{132}Xe - EXTa [in 10^{-8} cc/g]	0.1919	0.0051	0.1970
±	-	-	-	±	0.0035	0.0013	0.0037
^{21}Ne$_{cos}$ [in 10^{-8} cc/g]	< 0.005 (2σ)	-	-	^{132}Xe - EXTa [in 10^{-12} cc]	0.2731	0.0073	0.2804
±	-	-	-	±	0.0050	0.0018	0.0053
^{21}Ne$_{cos}$ [in 10^{-12} cc]	< 0.007 (2σ)	-	-	^{128}Xe/^{132}Xe - EXTa	0.069	0.043	0.069
±	-	-	-	±	0.002	0.020	0.002
^{20}Ne$_{trap}$ [in 10^{-8} cc/g]	< 0.006 (2σ)	-	-	^{129}Xe/^{132}Xe - EXTa	0.987	0.877	0.985
±	-	-	-	±	0.008	0.068	0.008
^{20}Ne$_{trap}$ [in 10^{-12} cc]	< 0.009 (2σ)	-	-	^{130}Xe/^{132}Xe - EXTa	0.150	0.139	0.150
±	-	-	-	±	0.002	0.015	0.002
^{36}Ar [in 10^{-8} cc/g]	1.14	1.20	2.34	^{131}Xe/^{132}Xe - EXTa	0.782	0.790	0.782
±	0.16	0.31	0.35	±	0.006	0.058	0.006
^{36}Ar [in 10^{-12} cc]	1.62	1.70	3.33	^{134}Xe/^{132}Xe - EXTa	0.387	0.394	0.387
±	0.23	0.45	0.50	±	0.003	0.027	0.003
^{38}Ar/^{36}Ar	0.192	0.187	0.189	^{136}Xe/^{132}Xe - EXTa	0.324	0.306	0.323
±	0.005	0.015	0.008	±	0.004	0.024	0.004
^{40}Ar/^{36}Ar	416.2	284.7	348.8	^{132}Xe - EXTb [in 10^{-8} cc/g]	0.1911	0.0054	0.1965
±	11.4	21.6	13.4	±	0.0067	0.0011	0.0068
^{40}Ar [in 10^{-8} cc/g]	484.2	343.8	828.0	^{132}Xe - EXTb [in 10^{-12} cc]	0.2719	0.0077	0.2797
±	58.6	88.7	106.3	±	0.0095	0.0015	0.0097
^{40}Ar [in 10^{-12} cc]	689.0	489.2	1178.2	^{128}Xe/^{132}Xe - EXTb	0.068	0.060	0.068
±	83.4	126.2	151.3	±	0.002	0.012	0.002
^{38}Ar$_{cos}$ [in 10^{-8} cc/g]	< 0.019 (2σ)	-	-	^{129}Xe/^{132}Xe - EXTb	0.988	0.890	0.985
±	-	-	-	±	0.008	0.054	0.008
^{38}Ar$_{cos}$ [in 10^{-12} cc]	< 0.026 (2σ)	-	-	^{130}Xe/^{132}Xe - EXTb	0.151	0.164	0.151
±	-	-	-	±	0.002	0.012	0.002
^{84}Kr [in 10^{-8} cc/g]	0.1626	0.0190	0.1816	^{131}Xe/^{132}Xe - EXTb	0.782	0.798	0.783
±	0.0135	0.0048	0.0143	±	0.004	0.026	0.004
^{84}Kr [in 10^{-12} cc]	0.2314	0.0271	0.2585	^{134}Xe/^{132}Xe - EXTb	0.390	0.375	0.390
±	0.0192	0.0068	0.0203	±	0.003	0.023	0.003
^{80}Kr/^{84}Kr	0.039	0.039	0.039	^{136}Xe/^{132}Xe - EXTb	0.332	0.350	0.333
±	0.001	0.007	0.001	±	0.003	0.024	0.003
^{82}Kr/^{84}Kr	0.201	0.194	0.200	^{21}Ne$_{cos}$/^{38}Ar$_{cos}$	-	-	-
±	0.004	0.020	0.004	±	-	-	-
^{83}Kr/^{84}Kr	0.204	0.202	0.204	^{36}Ar/^{132}Xe $_{(Int)}$	6.01	257.55	12.02
±	0.004	0.015	0.004	±	0.90	117.01	1.94
^{86}Kr/^{84}Kr	0.304	0.301	0.303	^{84}Kr/^{132}Xe $_{(Int)}$	0.86	4.10	0.93
±	0.005	0.023	0.005	±	0.09	1.83	0.09
^{83}Kr$_{cos}$ [in 10^{-8} cc/g]	< 0.0019 (2σ)	-	-				
±	-	-	-				
^{83}Kr$_{cos}$ [in 10^{-12} cc]	< 0.0027 (2σ)	-	-				
±	-	-	-				

Sample	45c.27_2						
Size [µm]	521 x 337						
Weight [µg]	38.0 ± 0.1						
Date of measurement	09/06/11	14/06/11	09+14/06/11	Date of measurement	09/06/11	14/06/11	09+14/06/11
Laser-Power	3 x 5 W	3 x 15 W		Laser-Power	3 x 5 W	3 x 15 W	
Laser-Beam	600 µm	360 µm		Laser-Beam	600 µm	360 µm	
Step(s)	1	2	total*	Step(s)	1	2	total*
^{4}He [in 10^{-8} cc/g]	< 12 (2σ)	-	-	^{132}Xe - INT [in 10^{-8} cc/g]	0.0204	< 0.003 (2σ)	-
±	-	-	-	±	0.0012	-	-
^{4}He [in 10^{-12} cc]	< 5 (2σ)	-	-	^{132}Xe - INT [in 10^{-12} cc]	0.0078	< 0.001 (2σ)	-
±	-	-	-	±	0.0005	-	-
^{3}He [in 10^{-12} cc/g]	< 20 (2σ)	-	-	^{128}Xe/^{132}Xe - INT	0.075	-	-
±	-	-	-	±	0.006	-	-
^{3}He [in 10^{-16} cc]	< 8 (2σ)	-	-	^{129}Xe/^{132}Xe - INT	0.941	-	-
±	-	-	-	±	0.034	-	-
^{3}He/^{4}He	-	-	-	^{130}Xe/^{132}Xe - INT	0.153	-	-
±	-	-	-	±	0.008	-	-
^{22}Ne [in 10^{-8} cc/g]	0.618	0.041	0.659	^{131}Xe/^{132}Xe - INT	0.793	-	-
±	0.039	0.037	0.054	±	0.037	-	-
^{22}Ne [in 10^{-12} cc]	0.235	0.016	0.250	^{134}Xe/^{132}Xe - INT	0.418	-	-
±	0.015	0.014	0.021	±	0.017	-	-
^{20}Ne/^{22}Ne	10.35	8.87	10.25	^{136}Xe/^{132}Xe - INT	0.328	-	-
±	0.34	2.76	0.36	±	0.021	-	-
^{21}Ne/^{22}Ne	0.063	0.047	0.062	^{132}Xe - EXTa [in 10^{-8} cc/g]	0.0204	< 0.003 (2σ)	-
±	0.005	0.028	0.005	±	0.0051	-	-
^{21}Ne$_{cos}$ [in 10^{-8} cc/g]	0.020	< 0.003 (2σ)	-	^{132}Xe - EXTa [in 10^{-12} cc]	0.0077	< 0.001 (2σ)	-
±	0.003	-	-	±	0.0019	-	-
^{21}Ne$_{cos}$ [in 10^{-12} cc]	0.007	< 0.001 (2σ)	-	^{128}Xe/^{132}Xe - EXTa	0.075	-	-
±	0.001	-	-	±	0.006	-	-
^{20}Ne$_{trap}$ [in 10^{-8} cc/g]	6.4	0.36	6.75	^{129}Xe/^{132}Xe - EXTa	0.941	-	-
±	0.6	0.34	0.67	±	0.033	-	-
^{20}Ne$_{trap}$ [in 10^{-12} cc]	2.4	0.14	2.56	^{130}Xe/^{132}Xe - EXTa	0.145	-	-
±	0.2	0.13	0.26	±	0.009	-	-
^{36}Ar [in 10^{-8} cc/g]	1.56	-	-	^{131}Xe/^{132}Xe - EXTa	0.793	-	-
±	0.24	-	-	±	0.037	-	-
^{36}Ar [in 10^{-12} cc]	0.59	-	-	^{134}Xe/^{132}Xe - EXTa	0.441	-	-
±	0.09	-	-	±	0.016	-	-
^{38}Ar/^{36}Ar	0.173	-	-	^{136}Xe/^{132}Xe - EXTa	0.365	-	-
±	0.007	-	-	±	0.014	-	-
^{40}Ar/^{36}Ar	224.6	-	-	^{132}Xe - EXTb [in 10^{-8} cc/g]	0.0195	< 0.003 (2σ)	-
±	7.1	-	-	±	0.0059	-	-
^{40}Ar [in 10^{-8} cc/g]	351.1	-	-	^{132}Xe - EXTb [in 10^{-12} cc]	0.0074	< 0.001 (2σ)	-
±	54.7	-	-	±	0.0022	-	-
^{40}Ar [in 10^{-12} cc]	133.4	-	-	^{128}Xe/^{132}Xe - EXTb	0.064	-	-
±	20.8	-	-	±	0.007	-	-
^{38}Ar$_{cos}$ [in 10^{-8} cc/g]	-	-	-	^{129}Xe/^{132}Xe - EXTb	0.940	-	-
±	-	-	-	±	0.033	-	-
^{38}Ar$_{cos}$ [in 10^{-12} cc]	-	-	-	^{130}Xe/^{132}Xe - EXTb	0.160	-	-
±	-	-	-	±	0.009	-	-
^{84}Kr [in 10^{-8} cc/g]	0.0814	< 0.010 (2σ)	-	^{131}Xe/^{132}Xe - EXTb	0.793	-	-
±	0.0062	-	-	±	0.011	-	-
^{84}Kr [in 10^{-12} cc]	0.0309	< 0.004 (2σ)	-	^{134}Xe/^{132}Xe - EXTb	0.438	-	-
±	0.0023	-	-	±	0.016	-	-
^{80}Kr/^{84}Kr	0.035	-	-	^{136}Xe/^{132}Xe - EXTb	0.365	-	-
±	0.004	-	-	±	0.015	-	-
^{82}Kr/^{84}Kr	0.182	-	-	^{21}Ne$_{cos}$/^{38}Ar$_{cos}$	-	-	-
±	0.009	-	-	±	-	-	-
^{83}Kr/^{84}Kr	0.199	-	-	^{36}Ar/^{132}Xe $_{(Int)}$	76.50	-	-
±	0.009	-	-	±	12.40	-	-
^{86}Kr/^{84}Kr	0.298	-	-	^{84}Kr/^{132}Xe $_{(Int)}$	3.98	-	-
±	0.012	-	-	±	0.38	-	-
^{83}Kr$_{cos}$ [in 10^{-8} cc/g]	-	-	-				
±	-	-	-				
^{83}Kr$_{cos}$ [in 10^{-12} cc]	-	-	-				
±	-	-	-				

Table X20. Noble gas data He to Xe for sample 45c.29_1 (corrected for blank)

Sample	45c.29_1			
Size [μm]	337 x 255			
Weight [μg]	22.1 ± 0.2			
Date of measurement	18/09/12	19/09/12	19/09/12	18+19/09/12
Laser-Power	3 x 0.91 W	2 x 5 W 1 x 30 W	3 x 5 - 30 W	
Laser-Beam	360-250 μm	250 μm	600-200 μm	
Step(s)	1	2	3	total*
^{4}He [in 10^{-8} cc/g]	340.5	54.6	-	395.1
±	25.2	19.6	-	31.9
^{4}He [in 10^{-12} cc]	75.2	12.1	-	87.3
±	5.5	4.3	-	7.0
^{3}He [in 10^{-12} cc/g]	43685.9	13755.0	1587.6	59028.4
±	1025.6	370.4	352.3	1146.0
^{3}He [in 10^{-16} cc]	9654.6	3039.8	350.9	13045.3
±	209.2	77.1	77.8	224.1
^{3}He/^{4}He	0.01283	0.02519	-	0.01494
±	0.00098	0.00904	-	0.00123
^{22}Ne [in 10^{-8} cc/g]	8.738	20.319	-	29.057
±	0.251	0.481	-	0.542
^{22}Ne [in 10^{-12} cc]	1.931	4.491	-	6.422
±	0.053	0.098	-	0.105
^{20}Ne/^{22}Ne	7.25	4.51	-	5.30
±	0.10	0.05	-	0.13
^{21}Ne/^{22}Ne	0.405	0.642	-	0.571
±	0.009	0.010	-	0.007
^{21}Ne$_{cos}$ [in 10^{-8} cc/g]	3.348	12.794	< 0.057 (2σ)	16.142
±	0.125	0.360	-	0.381
^{21}Ne$_{cos}$ [in 10^{-12} cc]	0.740	2.827	< 0.013 (2σ)	3.567
±	0.027	0.075	-	0.078
^{20}Ne$_{trap}$ [in 10^{-8} cc/g]	60.7	81.21	-	141.92
±	4.0	5.26	-	6.58
^{20}Ne$_{trap}$ [in 10^{-12} cc]	13.4	17.95	-	31.37
±	0.9	1.15	-	1.43
^{36}Ar [in 10^{-8} cc/g]	23.83	30.34	-	54.17
±	0.78	1.02	-	1.28
^{36}Ar [in 10^{-12} cc]	5.27	6.70	-	11.97
±	0.17	0.22	-	0.26
^{38}Ar/^{36}Ar	0.238	0.251	-	0.245
±	0.005	0.011	-	0.007
^{40}Ar/^{36}Ar	74.9	31.4	-	50.5
±	4.5	4.6	-	3.3
^{40}Ar [in 10^{-8} cc/g]	1829.3	1018.8	-	2848.1
±	148.8	147.5	-	209.5
^{40}Ar [in 10^{-12} cc]	404.3	225.1	-	629.4
±	32.7	32.5	-	46.0
^{38}Ar$_{cos}$ [in 10^{-8} cc/g]	1.346	2.166	-	3.512
±	0.130	0.323	-	0.348
^{38}Ar$_{cos}$ [in 10^{-12} cc]	0.297	0.479	-	0.776
±	0.029	0.071	-	0.077
^{84}Kr [in 10^{-8} cc/g]	0.6213	0.0987	-	0.7200
±	0.0249	0.0159	-	0.0296
^{84}Kr [in 10^{-12} cc]	0.1373	0.0218	-	0.1591
±	0.0054	0.0035	-	0.0064
^{80}Kr/^{84}Kr	0.037	0.080	-	0.043
±	0.002	0.008	-	0.002
^{82}Kr/^{84}Kr	0.196	0.199	-	0.197
±	0.010	0.018	-	0.009
^{83}Kr/^{84}Kr	0.203	0.191	-	0.201
±	0.008	0.014	-	0.007
^{86}Kr/^{84}Kr	0.330	0.345	-	0.332
±	0.015	0.026	-	0.014
^{83}Kr$_{cos}$ [in 10^{-8} cc/g]	< 0.0119 (2σ)	-	-	-
±	-	-	-	-
^{83}Kr$_{cos}$ [in 10^{-12} cc]	< 0.0026 (2σ)	-	-	-
±	-	-	-	-

Date of measurement	18/09/12	19/09/12	19/09/12	18+19/09/12
Laser-Power	3 x 0.91 W	2 x 5 W 1 x 30 W	3 x 5 - 30 W	
Laser-Beam	360-250 μm	250 μm	600-200 μm	
Step(s)	1	2	3	total*
^{132}Xe - INT [in 10^{-8} cc/g]	0.1473	0.0219	-	0.1693
±	0.0207	0.0052	-	0.0213
^{132}Xe - INT [in 10^{-12} cc]	0.0326	0.0048	-	0.0374
±	0.0046	0.0011	-	0.0047
^{128}Xe/^{132}Xe - INT	0.066	0.094	-	0.070
±	0.006	0.030	-	0.006
^{129}Xe/^{132}Xe - INT	0.903	1.393	-	0.967
±	0.025	0.081	-	0.025
^{130}Xe/^{132}Xe - INT	0.139	0.151	-	0.141
±	0.005	0.023	-	0.005
^{131}Xe/^{132}Xe - INT	0.786	0.762	-	0.783
±	0.023	0.077	-	0.022
^{134}Xe/^{132}Xe - INT	0.394	0.430	-	0.398
±	0.012	0.041	-	0.012
^{136}Xe/^{132}Xe - INT	0.360	0.398	-	0.365
±	0.014	0.055	-	0.014
^{132}Xe - EXTa [in 10^{-8} cc/g]	0.1407	0.0210	-	0.1616
±	0.0197	0.0049	-	0.0203
^{132}Xe - EXTa [in 10^{-12} cc]	0.0311	0.0046	-	0.0357
±	0.0043	0.0011	-	0.0045
^{128}Xe/^{132}Xe - EXTa	0.061	0.079	-	0.064
±	0.004	0.014	-	0.004
^{129}Xe/^{132}Xe - EXTa	0.896	1.385	-	0.960
±	0.025	0.084	-	0.025
^{130}Xe/^{132}Xe - EXTa	0.136	0.152	-	0.138
±	0.006	0.023	-	0.006
^{131}Xe/^{132}Xe - EXTa	0.783	0.751	-	0.779
±	0.024	0.086	-	0.023
^{134}Xe/^{132}Xe - EXTa	0.406	0.408	-	0.406
±	0.013	0.039	-	0.012
^{136}Xe/^{132}Xe - EXTa	0.379	0.378	-	0.379
±	0.018	0.039	-	0.017
^{132}Xe - EXTb [in 10^{-8} cc/g]	0.1379	0.0226	-	0.1604
±	0.0180	0.0040	-	0.0184
^{132}Xe - EXTb [in 10^{-12} cc]	0.0305	0.0050	-	0.0355
±	0.0040	0.0009	-	0.0041
^{128}Xe/^{132}Xe - EXTb	0.062	0.081	-	0.065
±	0.004	0.014	-	0.004
^{129}Xe/^{132}Xe - EXTb	0.896	1.366	-	0.962
±	0.025	0.077	-	0.024
^{130}Xe/^{132}Xe - EXTb	0.134	0.134	-	0.134
±	0.006	0.017	-	0.006
^{131}Xe/^{132}Xe - EXTb	0.785	0.768	-	0.783
±	0.007	0.039	-	0.008
^{134}Xe/^{132}Xe - EXTb	0.396	0.416	-	0.399
±	0.012	0.039	-	0.012
^{136}Xe/^{132}Xe - EXTb	0.376	0.373	-	0.375
±	0.015	0.033	-	0.014
^{21}Ne$_{cos}$/^{38}Ar$_{cos}$	2.49	5.91	-	4.60
±	0.26	0.90	-	0.47
^{36}Ar/^{132}Xe $_{(Int)}$	161.75	1382.68	-	320.01
±	23.20	328.85	-	40.78
^{84}Kr/^{132}Xe $_{(Int)}$	4.22	4.50	-	4.25
±	0.61	1.28	-	0.56

Table X21. Noble gas data He to Xe for sample 45c.29_2 (corrected for blank)

Sample	45c.29_2		
Size [µm]	305 x 187		
Weight [µg]	24.2 ± 0.2		
Date of measurement	12/06/12	13/06/12	12+13/06/12
Laser-Power	3 x 0.91 W	3 x 5 W	
Laser-Beam	360-250 µm	250 µm	
Step(s)	1	2	total*
^{4}He [in 10^{-8} cc/g]	4395.8	-	-
±	189.6	-	-
^{4}He [in 10^{-12} cc]	1063.8	-	-
±	45.0	-	-
^{3}He [in 10^{-12} cc/g]	26420.3	< 1003 (2σ)	
±	1168.4	-	-
^{3}He [in 10^{-16} cc]	6393.7	< 243 (2σ)	-
±	277.8	-	-
^{3}He/^{4}He	0.00060	-	-
±	0.00004	-	-
^{22}Ne [in 10^{-8} cc/g]	16.680	-	-
±	0.283	-	-
^{22}Ne [in 10^{-12} cc]	4.037	-	-
±	0.060	-	-
^{20}Ne/^{22}Ne	8.26	-	-
±	0.08	-	-
^{21}Ne/^{22}Ne	0.340	-	-
±	0.005	-	-
^{21}Ne$_{cos}$ [in 10^{-8} cc/g]	5.316	< 0.085 (2σ)	-
±	0.125	-	-
^{21}Ne$_{cos}$ [in 10^{-12} cc]	1.286	< 0.021 (2σ)	-
±	0.028	-	-
^{20}Ne$_{trap}$ [in 10^{-8} cc/g]	133.6	< 3.1 (2σ)	-
±	7.9	-	-
^{20}Ne$_{trap}$ [in 10^{-12} cc]	32.3	< 0.8 (2σ)	-
±	1.9	-	-
^{36}Ar [in 10^{-8} cc/g]	39.90	< 2.25 (2σ)	-
±	1.62	-	-
^{36}Ar [in 10^{-12} cc]	9.66	< 0.54 (2σ)	-
±	0.38	-	-
^{38}Ar/^{36}Ar	0.347	-	-
±	0.003	-	-
^{40}Ar/^{36}Ar	107.6	-	-
±	2.7	-	-
^{40}Ar [in 10^{-8} cc/g]	4574.8	-	-
±	154.6	-	-
^{40}Ar [in 10^{-12} cc]	1107.1	-	-
±	36.3	-	-
^{38}Ar$_{cos}$ [in 10^{-8} cc/g]	7.225	< 15.91 (2σ)	-
±	0.325	-	-
^{38}Ar$_{cos}$ [in 10^{-12} cc]	1.748	< 3.85 (2σ)	-
±	0.077	-	-
^{84}Kr [in 10^{-8} cc/g]	0.9403	-	-
±	0.0653	-	-
^{84}Kr [in 10^{-12} cc]	0.2275	-	-
±	0.0157	-	-
^{80}Kr/^{84}Kr	0.044	-	-
±	0.002	-	-
^{82}Kr/^{84}Kr	0.182	-	-
±	0.004	-	-
^{83}Kr/^{84}Kr	0.195	-	-
±	0.004	-	-
^{86}Kr/^{84}Kr	0.318	-	-
±	0.006	-	-
^{83}Kr$_{cos}$ [in 10^{-8} cc/g]	-	-	-
±	-	-	-
^{83}Kr$_{cos}$ [in 10^{-12} cc]	-	-	-
±	-	-	-

Date of measurement	12/06/12	13/06/12	12+13/06/12
Laser-Power	3 x 0.91 W	3 x 5 W	
Laser-Beam	360-250 µm	250 µm	
Step(s)	1	2	total*
^{132}Xe - INT [in 10^{-8} cc/g]	0.1294	-	-
±	0.0056	-	-
^{132}Xe - INT [in 10^{-12} cc]	0.0313	-	-
±	0.0013	-	-
^{128}Xe/^{132}Xe - INT	0.065	-	-
±	0.004	-	-
^{129}Xe/^{132}Xe - INT	1.060	-	-
±	0.023	-	-
^{130}Xe/^{132}Xe - INT	0.146	-	-
±	0.004	-	-
^{131}Xe/^{132}Xe - INT	0.798	-	-
±	0.016	-	-
^{134}Xe/^{132}Xe - INT	0.414	-	-
±	0.011	-	-
^{136}Xe/^{132}Xe - INT	0.396	-	-
±	0.013	-	-
^{132}Xe - EXTa [in 10^{-8} cc/g]	0.1282	-	-
±	0.0061	-	-
^{132}Xe - EXTa [in 10^{-12} cc]	0.0310	-	-
±	0.0015	-	-
^{128}Xe/^{132}Xe - EXTa	0.066	-	-
±	0.004	-	-
^{129}Xe/^{132}Xe - EXTa	1.056	-	-
±	0.023	-	-
^{130}Xe/^{132}Xe - EXTa	0.145	-	-
±	0.005	-	-
^{131}Xe/^{132}Xe - EXTa	0.799	-	-
±	0.016	-	-
^{134}Xe/^{132}Xe - EXTa	0.392	-	-
±	0.009	-	-
^{136}Xe/^{132}Xe - EXTa	0.345	-	-
±	0.009	-	-
^{132}Xe - EXTb [in 10^{-8} cc/g]	0.1302	-	-
±	0.0047	-	-
^{132}Xe - EXTb [in 10^{-12} cc]	0.0315	-	-
±	0.0011	-	-
^{128}Xe/^{132}Xe - EXTb	0.070	-	-
±	0.004	-	-
^{129}Xe/^{132}Xe - EXTb	1.050	-	-
±	0.022	-	-
^{130}Xe/^{132}Xe - EXTb	0.149	-	-
±	0.005	-	-
^{131}Xe/^{132}Xe - EXTb	0.797	-	-
±	0.006	-	-
^{134}Xe/^{132}Xe - EXTb	0.417	-	-
±	0.010	-	-
^{136}Xe/^{132}Xe - EXTb	0.376	-	-
±	0.008	-	-
^{21}Ne$_{cos}$/^{38}Ar$_{cos}$	0.74	-	-
±	0.04	-	-
^{36}Ar/^{132}Xe $_{(Int)}$	308.29	-	-
±	17.99	-	-
^{84}Kr/^{132}Xe $_{(Int)}$	7.27	-	-
±	0.59	-	-

Table X22. Noble gas data He to Xe for sample 45c.31_1 (corrected for blank)

Sample	45c.31_1						
Size [µm]	460 x 372						
Weight [µg]	33.2 ± 0.1						
Date of measurement	22/02/12	23/02/12	22+23/02/12	Date of measurement	22/02/12	23/02/12	22+23/02/12
Laser-Power	3 x 0.91 W	3 x 5 W		Laser-Power	3 x 0.91 W	3 x 5 W	
Laser-Beam	600 µm	360 µm		Laser-Beam	600 µm	360 µm	
Step(s)	1	2	total*	Step(s)	1	2	total*
^{4}He [in 10^{-8} cc/g]	756.4	176.5	932.9	^{132}Xe - INT [in 10^{-8} cc/g]	0.1496	0.0253	0.1749
±	23.4	17.9	29.5	±	0.0096	0.0072	0.0120
^{4}He [in 10^{-12} cc]	251.1	58.6	309.7	^{132}Xe - INT [in 10^{-12} cc]	0.0497	0.0084	0.0581
±	7.7	6.0	9.7	±	0.0032	0.0024	0.0040
^{3}He [in 10^{-12} cc/g]	2856.1	934.2	3790.3	^{128}Xe/^{132}Xe - INT	0.081	0.062	0.078
±	492.4	481.7	688.9	±	0.004	0.015	0.004
^{3}He [in 10^{-16} cc]	948.2	310.1	1258.4	^{129}Xe/^{132}Xe - INT	1.039	1.146	1.055
±	163.5	159.9	228.7	±	0.018	0.057	0.017
^{3}He/^{4}He	0.00038	0.00053	0.00041	^{130}Xe/^{132}Xe - INT	0.152	0.174	0.155
±	0.00007	0.00028	0.00007	±	0.003	0.012	0.003
^{22}Ne [in 10^{-8} cc/g]	4.370	9.452	13.822	^{131}Xe/^{132}Xe - INT	0.793	0.718	0.782
±	0.102	0.154	0.185	±	0.014	0.045	0.014
^{22}Ne [in 10^{-12} cc]	1.451	3.138	4.589	^{134}Xe/^{132}Xe - INT	0.398	0.375	0.395
±	0.034	0.050	0.060	±	0.008	0.029	0.008
^{20}Ne/^{22}Ne	11.83	11.86	11.85	^{136}Xe/^{132}Xe - INT	0.344	0.362	0.347
±	0.21	0.12	0.11	±	0.009	0.032	0.009
^{21}Ne/^{22}Ne	0.035	0.040	0.038	^{132}Xe - EXTa [in 10^{-8} cc/g]	0.1516	0.0253	0.1769
±	0.002	0.001	0.001	±	0.0261	0.0056	0.0267
^{21}Ne$_{cos}$ [in 10^{-8} cc/g]	0.021	0.087	0.108	^{132}Xe - EXTa [in 10^{-12} cc]	0.0503	0.0084	0.0587
±	0.007	0.011	0.013	±	0.0087	0.0019	0.0089
^{21}Ne$_{cos}$ [in 10^{-12} cc]	0.007	0.029	0.036	^{128}Xe/^{132}Xe - EXTa	0.081	0.062	0.078
±	0.002	0.004	0.004	±	0.003	0.015	0.004
^{20}Ne$_{trap}$ [in 10^{-8} cc/g]	51.7	112.00	163.68	^{129}Xe/^{132}Xe - EXTa	1.034	1.124	1.047
±	3.2	6.53	7.28	±	0.018	0.054	0.017
^{20}Ne$_{trap}$ [in 10^{-12} cc]	17.2	37.19	54.34	^{130}Xe/^{132}Xe - EXTa	0.153	0.169	0.155
±	1.1	2.17	2.41	±	0.004	0.014	0.004
^{36}Ar [in 10^{-8} cc/g]	16.43	9.49	25.92	^{131}Xe/^{132}Xe - EXTa	0.794	0.730	0.785
±	0.54	1.41	1.51	±	0.014	0.044	0.014
^{36}Ar [in 10^{-12} cc]	5.46	3.15	8.60	^{134}Xe/^{132}Xe - EXTa	0.386	0.372	0.384
±	0.18	0.47	0.50	±	0.007	0.025	0.007
^{38}Ar/^{36}Ar	0.193	0.203	0.197	^{136}Xe/^{132}Xe - EXTa	0.320	0.290	0.316
±	0.002	0.008	0.003	±	0.006	0.020	0.006
^{40}Ar/^{36}Ar	134.2	-	-	^{132}Xe - EXTb [in 10^{-8} cc/g]	0.1562	0.0273	0.1835
±	3.9	-	-	±	0.0064	0.0044	0.0078
^{40}Ar [in 10^{-8} cc/g]	2240.2	-	-	^{132}Xe - EXTb [in 10^{-12} cc]	0.0519	0.0091	0.0609
±	118.9	-	-	±	0.0021	0.0015	0.0026
^{40}Ar [in 10^{-12} cc]	743.7	-	-	^{128}Xe/^{132}Xe - EXTb	0.072	0.074	0.072
±	39.4	-	-	±	0.002	0.009	0.002
^{38}Ar$_{cos}$ [in 10^{-8} cc/g]	0.089	0.160	0.249	^{129}Xe/^{132}Xe - EXTb	1.033	1.113	1.045
±	0.055	0.090	0.106	±	0.017	0.047	0.016
^{38}Ar$_{cos}$ [in 10^{-12} cc]	0.030	0.053	0.083	^{130}Xe/^{132}Xe - EXTb	0.150	0.161	0.151
±	0.018	0.030	0.035	±	0.004	0.011	0.004
^{84}Kr [in 10^{-8} cc/g]	0.1940	0.0212	0.2152	^{131}Xe/^{132}Xe - EXTb	0.794	0.736	0.785
±	0.0427	0.0197	0.0470	±	0.005	0.022	0.005
^{84}Kr [in 10^{-12} cc]	0.0644	0.0070	0.0714	^{134}Xe/^{132}Xe - EXTb	0.395	0.391	0.394
±	0.0142	0.0065	0.0156	±	0.007	0.021	0.007
^{80}Kr/^{84}Kr	0.038	0.035	0.037	^{136}Xe/^{132}Xe - EXTb	0.330	0.359	0.334
±	0.003	0.014	0.003	±	0.007	0.021	0.007
^{82}Kr/^{84}Kr	0.193	0.179	0.191	^{21}Ne$_{cos}$/^{38}Ar$_{cos}$	0.24	0.55	0.44
±	0.009	0.053	0.010	±	0.17	0.32	0.19
^{83}Kr/^{84}Kr	0.196	0.132	0.189	^{36}Ar/^{132}Xe $_{(Int)}$	109.86	374.77	148.20
±	0.009	0.035	0.009	±	7.90	119.95	13.31
^{86}Kr/^{84}Kr	0.303	0.299	0.303	^{84}Kr/^{132}Xe $_{(Int)}$	1.30	0.84	1.23
±	0.014	0.053	0.014	±	0.30	0.81	0.28
^{83}Kr$_{cos}$ [in 10^{-8} cc/g]	-	-	-				
±	-	-	-				
^{83}Kr$_{cos}$ [in 10^{-12} cc]	-	-	-				
±	-	-	-				

Table X23. Noble gas data He to Xe for sample 45c.33_1 (corrected for blank)

Sample	45c.33_1		
Size [µm]	512 x 379		
Weight [µg]	58.7 ± 0.1		
Date of measurement	08/06/12	11/06/12	08+11/06/12
Laser-Power	3 x 0.91 W	3 x 5 W	
Laser-Beam	600-360 µm	360 µm	
Step(s)	1	2	total*

	1	2	total*
^{4}He [in 10^{-8} cc/g]	6133.7	55.7	6189.4
±	253.3	4.1	253.3
^{4}He [in 10^{-12} cc]	3600.5	32.7	3633.2
±	148.5	2.4	148.6
^{3}He [in 10^{-12} cc/g]	20049.6	1918.2	21967.7
±	884.6	255.9	920.9
^{3}He [in 10^{-16} cc]	11769.1	1126.0	12895.1
±	518.9	150.2	540.1
^{3}He/^{4}He	0.00033	0.00344	0.00035
±	0.00002	0.00052	0.00002
^{22}Ne [in 10^{-8} cc/g]	13.182	0.251	13.433
±	0.181	0.045	0.186
^{22}Ne [in 10^{-12} cc]	7.738	0.148	7.885
±	0.105	0.027	0.109
^{20}Ne/^{22}Ne	11.44	12.25	11.46
±	0.09	1.69	0.09
^{21}Ne/^{22}Ne	0.042	0.042	0.042
±	0.001	0.007	0.001
^{21}Ne$_{cos}$ [in 10^{-8} cc/g]	0.158	0.003	0.161
±	0.011	0.002	0.011
^{21}Ne$_{cos}$ [in 10^{-12} cc]	0.093	0.002	0.095
±	0.007	0.001	0.007
^{20}Ne$_{trap}$ [in 10^{-8} cc/g]	150.7	3.08	153.75
±	8.6	0.72	8.66
^{20}Ne$_{trap}$ [in 10^{-12} cc]	88.4	1.81	90.25
±	5.1	0.42	5.08
^{36}Ar [in 10^{-8} cc/g]	35.67	8.67	44.34
±	2.56	0.78	2.68
^{36}Ar [in 10^{-12} cc]	20.94	5.09	26.03
±	1.50	0.46	1.57
^{38}Ar/^{36}Ar	0.194	0.189	0.193
±	0.002	0.003	0.002
^{40}Ar/^{36}Ar	2.0	-	-
±	1.8	-	-
^{40}Ar [in 10^{-8} cc/g]	120.2	< 324.62 (2σ)	-
±	51.5	-	-
^{40}Ar [in 10^{-12} cc]	70.6	< 190.55 (2σ)	-
±	30.3	-	-
^{38}Ar$_{cos}$ [in 10^{-8} cc/g]	0.204	< 0.079 (2σ)	-
±	0.116	-	-
^{38}Ar$_{cos}$ [in 10^{-12} cc]	0.120	< 0.046 (2σ)	-
±	0.068	-	-
^{84}Kr [in 10^{-8} cc/g]	0.4776	0.1356	0.6132
±	0.0319	0.0161	0.0358
^{84}Kr [in 10^{-12} cc]	0.2804	0.0796	0.3600
±	0.0187	0.0095	0.0210
^{80}Kr/^{84}Kr	0.038	0.036	0.038
±	0.001	0.003	0.001
^{82}Kr/^{84}Kr	0.194	0.194	0.194
±	0.004	0.009	0.003
^{83}Kr/^{84}Kr	0.208	0.192	0.204
±	0.004	0.009	0.003
^{86}Kr/^{84}Kr	0.317	0.313	0.316
±	0.007	0.011	0.006
^{83}Kr$_{cos}$ [in 10^{-8} cc/g]	0.0027	-	-
±	0.0022	-	-
^{83}Kr$_{cos}$ [in 10^{-12} cc]	0.0016	-	-
±	0.0013	-	-

	1	2	total*
^{132}Xe - INT [in 10^{-8} cc/g]	0.4700	0.1168	0.5868
±	0.0055	0.0043	0.0069
^{132}Xe - INT [in 10^{-12} cc]	0.2759	0.0686	0.3444
±	0.0032	0.0025	0.0040
^{128}Xe/^{132}Xe - INT	0.083	0.076	0.081
±	0.001	0.003	0.001
^{129}Xe/^{132}Xe - INT	1.035	1.031	1.034
±	0.008	0.017	0.007
^{130}Xe/^{132}Xe - INT	0.163	0.163	0.163
±	0.001	0.003	0.001
^{131}Xe/^{132}Xe - INT	0.825	0.839	0.828
±	0.006	0.013	0.006
^{134}Xe/^{132}Xe - INT	0.386	0.393	0.388
±	0.003	0.007	0.003
^{136}Xe/^{132}Xe - INT	0.330	0.336	0.331
±	0.004	0.008	0.004
^{132}Xe - EXTa [in 10^{-8} cc/g]	0.4730	0.1204	0.5934
±	0.0130	0.0039	0.0136
^{132}Xe - EXTa [in 10^{-12} cc]	0.2777	0.0707	0.3483
±	0.0076	0.0023	0.0080
^{128}Xe/^{132}Xe - EXTa	0.082	0.076	0.081
±	0.001	0.002	0.001
^{129}Xe/^{132}Xe - EXTa	1.033	1.028	1.032
±	0.009	0.017	0.008
^{130}Xe/^{132}Xe - EXTa	0.164	0.164	0.164
±	0.002	0.003	0.002
^{131}Xe/^{132}Xe - EXTa	0.821	0.831	0.823
±	0.007	0.013	0.006
^{134}Xe/^{132}Xe - EXTa	0.380	0.382	0.380
±	0.003	0.007	0.003
^{136}Xe/^{132}Xe - EXTa	0.317	0.308	0.315
±	0.003	0.005	0.002
^{132}Xe - EXTb [in 10^{-8} cc/g]	0.4750	0.1219	0.5969
±	0.0120	0.0040	0.0127
^{132}Xe - EXTb [in 10^{-12} cc]	0.2788	0.0716	0.3504
±	0.0070	0.0023	0.0074
^{128}Xe/^{132}Xe - EXTb	0.079	0.080	0.079
±	0.003	0.003	0.002
^{129}Xe/^{132}Xe - EXTb	1.032	1.026	1.031
±	0.009	0.016	0.008
^{130}Xe/^{132}Xe - EXTb	0.161	0.161	0.161
±	0.002	0.003	0.002
^{131}Xe/^{132}Xe - EXTb	0.823	0.835	0.825
±	0.004	0.005	0.003
^{134}Xe/^{132}Xe - EXTb	0.385	0.393	0.387
±	0.004	0.005	0.003
^{136}Xe/^{132}Xe - EXTb	0.324	0.327	0.325
±	0.003	0.005	0.003
^{21}Ne$_{cos}$/^{38}Ar$_{cos}$	0.78	-	-
±	0.44	-	-
^{36}Ar/^{132}Xe (Int)	75.90	74.21	75.56
±	5.51	7.23	4.64
^{84}Kr/^{132}Xe (Int)	1.02	1.16	1.05
±	0.07	0.14	0.06

Table X24. Noble gas data He to Xe for sample 45c.34_1 (corrected for blank)

Sample		45c.34_1						
Size [µm]		428 x 318						
Weight [µg]		34.1 ± 0.1						
Date of measurement	08/10/12	16/10/12	08+16/10/12	**Date of measurement**	08/10/12	16/10/12	08+16/10/12	
Laser-Power	3 x 0.91 W	2 x 5W / 1 x 5 - 20 W		**Laser-Power**	3 x 0.91 W	2 x 5W / 1 x 5 - 20 W		
Laser-Beam	600-360 µm	360 µm		**Laser-Beam**	600-360 µm	360 µm		
Step(s)	1	2	total*	**Step(s)**	1	2	total*	
^{4}He [in 10^{-8} cc/g]	230.4	13.1	243.5	^{132}Xe - INT [in 10^{-8} cc/g]	0.1748	0.0317	0.2064	
±	13.3	12.5	18.2	±	0.0035	0.0025	0.0043	
^{4}He [in 10^{-12} cc]	78.6	4.5	83.0	^{132}Xe - INT [in 10^{-12} cc]	0.0596	0.0108	0.0704	
±	4.5	4.3	6.2	±	0.0012	0.0008	0.0015	
^{3}He [in 10^{-12} cc/g]	2376.3	1726.1	4102.3	^{128}Xe/^{132}Xe - INT	0.084	0.072	0.082	
±	180.0	187.7	260.0	±	0.003	0.013	0.003	
^{3}He [in 10^{-16} cc]	810.3	588.6	1398.9	^{129}Xe/^{132}Xe - INT	0.998	1.103	1.014	
±	61.3	64.0	88.6	±	0.020	0.048	0.019	
^{3}He/^{4}He	0.00103	0.01318	0.00168	^{130}Xe/^{132}Xe - INT	0.164	0.144	0.161	
±	0.00010	0.01266	0.00017	±	0.004	0.011	0.003	
^{22}Ne [in 10^{-8} cc/g]	0.363	0.072	0.435	^{131}Xe/^{132}Xe - INT	0.824	0.775	0.816	
±	0.070	0.069	0.098	±	0.015	0.039	0.014	
^{22}Ne [in 10^{-12} cc]	0.124	0.024	0.148	^{134}Xe/^{132}Xe - INT	0.388	0.397	0.389	
±	0.024	0.024	0.034	±	0.008	0.021	0.008	
^{20}Ne/^{22}Ne	10.84	8.85	10.51	^{136}Xe/^{132}Xe - INT	0.323	0.328	0.324	
±	1.38	8.06	1.76	±	0.009	0.026	0.009	
^{21}Ne/^{22}Ne	0.033	0.059	0.037	^{132}Xe - EXTa [in 10^{-8} cc/g]	0.1759	0.0319	0.2077	
±	0.007	0.051	0.010	±	0.0035	0.0025	0.0043	
^{21}Ne$_{cos}$ [in 10^{-8} cc/g]	< 0.011 (2σ)	< 0.011 (2σ)	-	^{132}Xe - EXTa [in 10^{-12} cc]	0.0600	0.0109	0.0708	
±	-	-	-	±	0.0012	0.0008	0.0015	
^{21}Ne$_{cos}$ [in 10^{-12} cc]	< 0.004 (2σ)	< 0.004 (2σ)	-	^{128}Xe/^{132}Xe - EXTa	0.082	0.076	0.081	
±	-	-	-	±	0.003	0.008	0.003	
^{20}Ne$_{trap}$ [in 10^{-8} cc/g]	3.9	< 2.3 (2σ)	-	^{129}Xe/^{132}Xe - EXTa	0.999	1.106	1.015	
±	0.9	-	-	±	0.018	0.047	0.017	
^{20}Ne$_{trap}$ [in 10^{-12} cc]	1.3	< 0.8 (2σ)	-	^{130}Xe/^{132}Xe - EXTa	0.163	0.140	0.159	
±	0.3	-	-	±	0.004	0.011	0.004	
^{36}Ar [in 10^{-8} cc/g]	10.84	3.79	14.62	^{131}Xe/^{132}Xe - EXTa	0.828	0.781	0.821	
±	0.44	0.39	0.59	±	0.016	0.037	0.014	
^{36}Ar [in 10^{-12} cc]	3.70	1.29	4.99	^{134}Xe/^{132}Xe - EXTa	0.378	0.355	0.375	
±	0.15	0.13	0.20	±	0.008	0.018	0.007	
^{38}Ar/^{36}Ar	0.182	0.169	0.178	^{136}Xe/^{132}Xe - EXTa	0.326	0.306	0.323	
±	0.004	0.006	0.003	±	0.007	0.016	0.006	
^{40}Ar/^{36}Ar	-	113.4	-	^{132}Xe - EXTb [in 10^{-8} cc/g]	0.1745	0.0305	0.2050	
±	-	12.8	-	±	0.0052	0.0019	0.0056	
^{40}Ar [in 10^{-8} cc/g]	< 245.47 (2σ)	440.4	-	^{132}Xe - EXTb [in 10^{-12} cc]	0.0595	0.0104	0.0699	
±	-	104.3	-	±	0.0018	0.0007	0.0019	
^{40}Ar [in 10^{-12} cc]	< 83.70 (2σ)	150.2	-	^{128}Xe/^{132}Xe - EXTb	0.086	0.085	0.086	
±	-	35.6	-	±	0.003	0.008	0.003	
^{38}Ar$_{cos}$ [in 10^{-8} cc/g]	-	-	-	^{129}Xe/^{132}Xe - EXTb	0.998	1.103	1.014	
±	-	-	-	±	0.018	0.047	0.017	
^{38}Ar$_{cos}$ [in 10^{-12} cc]	-	-	-	^{130}Xe/^{132}Xe - EXTb	0.163	0.159	0.162	
±	-	-	-	±	0.004	0.010	0.004	
^{84}Kr [in 10^{-8} cc/g]	0.1572	0.0410	0.1982	^{131}Xe/^{132}Xe - EXTb	0.828	0.781	0.821	
±	0.0154	0.0106	0.0187	±	0.005	0.018	0.005	
^{84}Kr [in 10^{-12} cc]	0.0536	0.0140	0.0676	^{134}Xe/^{132}Xe - EXTb	0.390	0.413	0.393	
±	0.0053	0.0036	0.0064	±	0.007	0.021	0.007	
^{80}Kr/^{84}Kr	0.044	0.050	0.045	^{136}Xe/^{132}Xe - EXTb	0.319	0.307	0.317	
±	0.003	0.008	0.003	±	0.006	0.018	0.006	
^{82}Kr/^{84}Kr	0.201	0.218	0.205	^{21}Ne$_{cos}$/^{38}Ar$_{cos}$	-	-	-	
±	0.010	0.021	0.009	±	-	-	-	
^{83}Kr/^{84}Kr	0.187	0.190	0.188	^{36}Ar/^{132}Xe $_{(Int)}$	62.02	119.59	70.85	
±	0.009	0.016	0.008	±	2.79	15.52	3.20	
^{86}Kr/^{84}Kr	0.310	0.221	0.292	^{84}Kr/^{132}Xe $_{(Int)}$	0.90	1.30	0.96	
±	0.013	0.031	0.012	±	0.09	0.35	0.09	
^{83}Kr$_{cos}$ [in 10^{-8} cc/g]	-	-	-					
±	-	-	-					
^{83}Kr$_{cos}$ [in 10^{-12} cc]	-	-	-					
±	-	-	-					

Table X25. Noble gas data He to Xe for sample X1 (45c.35_1) (corrected for blank)

Sample	X1 (45c.35_1)		
Size [µm]	427 x 315		
Weight [µg]	35.0 ± 0.1		

Date of measurement	03/11/11	04/11/11	03+04/11/11
Laser-Power	3 x 0.91 W	3 x 5 W	
Laser-Beam	600 µm	250 µm	
Step(s)	1	2	total*
^{4}He [in 10^{-8} cc/g]	3826.7	-	-
±	67.2	-	-
^{4}He [in 10^{-12} cc]	1339.4	-	-
±	23.2	-	-
^{3}He [in 10^{-12} cc/g]	17163.7	214.5	17378.2
±	380.1	79.1	388.2
^{3}He [in 10^{-16} cc]	6007.3	75.1	6082.4
±	131.9	27.7	134.8
^{3}He/^{4}He	0.00045	-	-
±	0.00001	-	-
^{22}Ne [in 10^{-8} cc/g]	34.295	0.338	34.633
±	0.484	0.092	0.492
^{22}Ne [in 10^{-12} cc]	12.003	0.118	12.122
±	0.166	0.032	0.169
^{20}Ne/^{22}Ne	10.12	10.84	10.13
±	0.21	1.21	0.21
^{21}Ne/^{22}Ne	0.050	0.082	0.050
±	0.001	0.012	0.001
^{21}Ne$_{cos}$ [in 10^{-8} cc/g]	0.710	0.017	0.727
±	0.075	0.006	0.075
^{21}Ne$_{cos}$ [in 10^{-12} cc]	0.249	0.006	0.255
±	0.026	0.002	0.026
^{20}Ne$_{trap}$ [in 10^{-8} cc/g]	346.5	3.68	350.14
±	21.2	1.10	21.20
^{20}Ne$_{trap}$ [in 10^{-12} cc]	121.3	1.29	122.55
±	7.4	0.39	7.41
^{36}Ar [in 10^{-8} cc/g]	43.93	5.15	49.08
±	0.84	0.39	0.93
^{36}Ar [in 10^{-12} cc]	15.38	1.80	17.18
±	0.29	0.14	0.32
^{38}Ar/^{36}Ar	0.196	0.183	0.195
±	0.002	0.004	0.002
^{40}Ar/^{36}Ar	29.1	267.4	54.1
±	0.3	6.6	0.8
^{40}Ar [in 10^{-8} cc/g]	1280.2	1376.5	2656.7
±	28.9	100.2	104.3
^{40}Ar [in 10^{-12} cc]	448.1	481.8	929.9
±	10.0	35.0	36.4
^{38}Ar$_{cos}$ [in 10^{-8} cc/g]	0.386	-	-
±	0.133	-	-
^{38}Ar$_{cos}$ [in 10^{-12} cc]	0.135	-	-
±	0.047	-	-
^{84}Kr [in 10^{-8} cc/g]	0.0886	0.0210	0.1095
±	0.0171	0.0141	0.0222
^{84}Kr [in 10^{-12} cc]	0.0310	0.0073	0.0383
±	0.0060	0.0049	0.0078
^{80}Kr/^{84}Kr	0.030	0.065	0.037
±	0.005	0.016	0.005
^{82}Kr/^{84}Kr	0.207	0.252	0.215
±	0.013	0.045	0.013
^{83}Kr/^{84}Kr	0.186	0.166	0.182
±	0.011	0.035	0.011
^{86}Kr/^{84}Kr	0.302	0.272	0.296
±	0.015	0.050	0.015
^{83}Kr$_{cos}$ [in 10^{-8} cc/g]	-	-	-
±	-	-	-
^{83}Kr$_{cos}$ [in 10^{-12} cc]	-	-	-
±	-	-	-

Date of measurement	03/11/11	04/11/11	03+04/11/11
Laser-Power	3 x 0.91 W	3 x 5 W	
Laser-Beam	600 µm	250 µm	
Step(s)	1	2	total*
^{132}Xe - INT [in 10^{-8} cc/g]	0.0281	-	-
±	0.0017	-	-
^{132}Xe - INT [in 10^{-12} cc]	0.0098	-	-
±	0.0006	-	-
^{128}Xe/^{132}Xe - INT	0.072	-	-
±	0.009	-	-
^{129}Xe/^{132}Xe - INT	1.009	-	-
±	0.045	-	-
^{130}Xe/^{132}Xe - INT	0.141	-	-
±	0.008	-	-
^{131}Xe/^{132}Xe - INT	0.775	-	-
±	0.033	-	-
^{134}Xe/^{132}Xe - INT	0.374	-	-
±	0.019	-	-
^{136}Xe/^{132}Xe - INT	0.357	-	-
±	0.024	-	-
^{132}Xe - EXTa [in 10^{-8} cc/g]	0.0283	-	-
±	0.0018	-	-
^{132}Xe - EXTa [in 10^{-12} cc]	0.0099	-	-
±	0.0006	-	-
^{128}Xe/^{132}Xe - EXTa	0.073	-	-
±	0.011	-	-
^{129}Xe/^{132}Xe - EXTa	1.007	-	-
±	0.046	-	-
^{130}Xe/^{132}Xe - EXTa	0.140	-	-
±	0.010	-	-
^{131}Xe/^{132}Xe - EXTa	0.774	-	-
±	0.034	-	-
^{134}Xe/^{132}Xe - EXTa	0.393	-	-
±	0.018	-	-
^{136}Xe/^{132}Xe - EXTa	0.334	-	-
±	0.017	-	-
^{132}Xe - EXTb [in 10^{-8} cc/g]	0.0276	-	-
±	0.0020	-	-
^{132}Xe - EXTb [in 10^{-12} cc]	0.0097	-	-
±	0.0007	-	-
^{128}Xe/^{132}Xe - EXTb	0.066	-	-
±	0.008	-	-
^{129}Xe/^{132}Xe - EXTb	1.007	-	-
±	0.055	-	-
^{130}Xe/^{132}Xe - EXTb	0.154	-	-
±	0.009	-	-
^{131}Xe/^{132}Xe - EXTb	0.774	-	-
±	0.017	-	-
^{134}Xe/^{132}Xe - EXTb	0.380	-	-
±	0.018	-	-
^{136}Xe/^{132}Xe - EXTb	0.382	-	-
±	0.018	-	-
^{21}Ne$_{cos}$/^{38}Ar$_{cos}$	1.84	-	-
±	0.67	-	-
^{36}Ar/^{132}Xe$_{(Int)}$	1565.45	-	-
±	101.43	-	-
^{84}Kr/^{132}Xe$_{(Int)}$	3.16	-	-
±	0.64	-	-

Table X26. Noble gas data He to Xe for sample 45c.35_2 (corrected for blank)

Sample	45c.35_2						
Size [µm]	152 x 135						
Weight [µg]	5.4 ± 0.1						
Date of measurement	13/02/12	14/02/12	13+14/02/12	**Date of measurement**	13/02/12	14/02/12	13+14/02/12
Laser-Power	3 x 0.91 W	3 x 5 W		**Laser-Power**	3 x 0.91 W	3 x 5 W	
Laser-Beam	200 µm	200 µm		**Laser-Beam**	200 µm	200 µm	
Step(s)	1	2	total*	**Step(s)**	1	2	total*
^{4}He [in 10^{-8} cc/g]	1198.4	-	-	^{132}Xe - INT [in 10^{-8} cc/g]	0.2138	-	-
±	111.8	-	-	±	0.0439	-	-
^{4}He [in 10^{-12} cc]	64.7	-	-	^{132}Xe - INT [in 10^{-12} cc]	0.0115	-	-
±	5.9	-	-	±	0.0024	-	-
^{3}He [in 10^{-12} cc/g]	17558.3	< 733 (2σ)	-	^{128}Xe/^{132}Xe - INT	0.070	-	-
±	3044.3	-	-	±	0.011	-	-
^{3}He [in 10^{-16} cc]	948.1	< 40 (2σ)	-	^{129}Xe/^{132}Xe - INT	1.000	-	-
±	163.5	-	-	±	0.042	-	-
^{3}He/^{4}He	0.00147	-	-	^{130}Xe/^{132}Xe - INT	0.166	-	-
±	0.00029	-	-	±	0.009	-	-
^{22}Ne [in 10^{-8} cc/g]	8.376	< 1.64 (2σ)	-	^{131}Xe/^{132}Xe - INT	0.729	-	-
±	0.673	-	-	±	0.038	-	-
^{22}Ne [in 10^{-12} cc]	0.452	< 0.09 (2σ)	-	^{134}Xe/^{132}Xe - INT	0.366	-	-
±	0.035	-	-	±	0.023	-	-
^{20}Ne/^{22}Ne	10.58	-	-	^{136}Xe/^{132}Xe - INT	0.317	-	-
±	0.57	-	-	±	0.025	-	-
^{21}Ne/^{22}Ne	0.100	-	-	^{132}Xe - EXTa [in 10^{-8} cc/g]	0.2289	-	-
±	0.007	-	-	±	0.0535	-	-
^{21}Ne$_{cos}$ [in 10^{-8} cc/g]	0.608	-	-	^{132}Xe - EXTa [in 10^{-12} cc]	0.0124	-	-
±	0.071	-	-	±	0.0029	-	-
^{21}Ne$_{cos}$ [in 10^{-12} cc]	0.033	-	-	^{128}Xe/^{132}Xe - EXTa	0.069	-	-
±	0.004	-	-	±	0.010	-	-
^{20}Ne$_{trap}$ [in 10^{-8} cc/g]	88.0	-	-	^{129}Xe/^{132}Xe - EXTa	0.984	-	-
±	9.8	-	-	±	0.039	-	-
^{20}Ne$_{trap}$ [in 10^{-12} cc]	4.7	-	-	^{130}Xe/^{132}Xe - EXTa	0.156	-	-
±	0.5	-	-	±	0.010	-	-
^{36}Ar [in 10^{-8} cc/g]	31.08	-	-	^{131}Xe/^{132}Xe - EXTa	0.739	-	-
±	2.97	-	-	±	0.035	-	-
^{36}Ar [in 10^{-12} cc]	1.68	-	-	^{134}Xe/^{132}Xe - EXTa	0.379	-	-
±	0.16	-	-	±	0.019	-	-
^{38}Ar/^{36}Ar	0.199	-	-	^{136}Xe/^{132}Xe - EXTa	0.318	-	-
±	0.006	-	-	±	0.017	-	-
^{40}Ar/^{36}Ar	162.3	-	-	^{132}Xe - EXTb [in 10^{-8} cc/g]	0.2331	-	-
±	9.4	-	-	±	0.0208	-	-
^{40}Ar [in 10^{-8} cc/g]	5261.2	3804.8	9066.0	^{132}Xe - EXTb [in 10^{-12} cc]	0.0126	-	-
±	703.8	698.0	991.2	±	0.0011	-	-
^{40}Ar [in 10^{-12} cc]	284.1	205.5	489.6	^{128}Xe/^{132}Xe - EXTb	0.073	-	-
±	37.6	37.5	52.8	±	0.006	-	-
^{38}Ar$_{cos}$ [in 10^{-8} cc/g]	0.379	-	-	^{129}Xe/^{132}Xe - EXTb	0.987	-	-
±	0.205	-	-	±	0.034	-	-
^{38}Ar$_{cos}$ [in 10^{-12} cc]	0.020	-	-	^{130}Xe/^{132}Xe - EXTb	0.157	-	-
±	0.011	-	-	±	0.009	-	-
^{84}Kr [in 10^{-8} cc/g]	1.4052	-	-	^{131}Xe/^{132}Xe - EXTb	0.743	-	-
±	0.1643	-	-	±	0.013	-	-
^{84}Kr [in 10^{-12} cc]	0.0759	-	-	^{134}Xe/^{132}Xe - EXTb	0.390	-	-
±	0.0088	-	-	±	0.016	-	-
^{80}Kr/^{84}Kr	0.039	-	-	^{136}Xe/^{132}Xe - EXTb	0.341	-	-
±	0.002	-	-	±	0.015	-	-
^{82}Kr/^{84}Kr	0.193	-	-	^{21}Ne$_{cos}$/^{38}Ar$_{cos}$	1.60	-	-
±	0.007	-	-	±	0.89	-	-
^{83}Kr/^{84}Kr	0.192	-	-	^{36}Ar/^{132}Xe $_{(Int)}$	145.37	-	-
±	0.007	-	-	±	32.73	-	-
^{86}Kr/^{84}Kr	0.330	-	-	^{84}Kr/^{132}Xe $_{(Int)}$	6.57	-	-
±	0.010	-	-	±	1.54	-	-
^{83}Kr$_{cos}$ [in 10^{-8} cc/g]	-	-	-				
±	-	-	-				
^{83}Kr$_{cos}$ [in 10^{-12} cc]	-	-	-				
±	-	-	-				

Table X27. Noble gas data He to Xe for sample 45c.35_3 (corrected for blank)

Sample	45c.35_3			
Size [µm]	428 x 245			
Weight [µg]	29.0 ± 0.1			
Date of measurement	02/09/11	05/09/11	06/09/11	02+05+06/09/11
Laser-Power	3 x 0.13 W	3 x 0.91 W	3 x 5 W	
Laser-Beam	250 µm	250 µm	250 µm	
Step(s)	1	2	3	total*
^{4}He [in 10^{-8} cc/g]	2161.7	10250.4	-	12412.1
±	48.2	169.9	-	176.6
^{4}He [in 10^{-12} cc]	626.9	2972.6	-	3599.5
±	13.8	48.2	-	49.7
^{3}He [in 10^{-12} cc/g]	2653.3	30849.2	-	33502.5
±	318.9	1416.6	-	1452.1
^{3}He [in 10^{-16} cc]	769.4	8946.3	-	9715.7
±	92.4	409.7	-	419.8
^{3}He/^{4}He	0.00012	0.00030	-	0.00027
±	0.00001	0.00001	-	0.00001
^{22}Ne [in 10^{-8} cc/g]	0.580	10.608	0.907	12.095
±	0.206	0.257	0.207	0.389
^{22}Ne [in 10^{-12} cc]	0.168	3.076	0.263	3.508
±	0.060	0.074	0.060	0.112
^{20}Ne/^{22}Ne	6.56	11.07	7.42	10.58
±	2.39	0.21	1.63	0.26
^{21}Ne/^{22}Ne	0.030	0.043	0.038	0.042
±	0.010	0.001	0.008	0.001
^{21}Ne$_{cos}$ [in 10^{-8} cc/g]	-	0.138	< 0.568 (2σ)	-
±	-	0.029	-	-
^{21}Ne$_{cos}$ [in 10^{-12} cc]	-	0.040	< 0.165 (2σ)	-
±	-	0.008	-	-
^{20}Ne$_{trap}$ [in 10^{-8} cc/g]	3.8	117.28	6.84	127.93
±	2.0	7.44	2.22	8.00
^{20}Ne$_{trap}$ [in 10^{-12} cc]	1.1	34.01	1.98	37.10
±	0.6	2.15	0.64	2.32
^{36}Ar [in 10^{-8} cc/g]	< 0.28 (2σ)	149.84	5.21	155.05
±	-	2.92	0.47	2.96
^{36}Ar [in 10^{-12} cc]	< 0.08 (2σ)	43.45	1.51	44.96
±	-	0.83	0.14	0.84
^{38}Ar/^{36}Ar	-	0.185	0.169	0.185
±	-	0.001	0.024	0.002
^{40}Ar/^{36}Ar	-	2.3	56.4	4.1
±	-	0.8	13.1	0.9
^{40}Ar [in 10^{-8} cc/g]	-	340.2	294.0	634.2
±	-	115.5	115.4	163.2
^{40}Ar [in 10^{-12} cc]	-	98.7	85.3	183.9
±	-	33.5	33.5	47.3
^{38}Ar$_{cos}$ [in 10^{-8} cc/g]	-	-	-	-
±	-	-	-	-
^{38}Ar$_{cos}$ [in 10^{-12} cc]	-	-	-	-
±	-	-	-	-
^{84}Kr [in 10^{-8} cc/g]	0.0164	0.6284	0.0557	0.7004
±	0.0156	0.0501	0.0164	0.0550
^{84}Kr [in 10^{-12} cc]	0.0047	0.1822	0.0161	0.2031
±	0.0045	0.0145	0.0047	0.0159
^{80}Kr/^{84}Kr	0.031	0.037	0.013	0.035
±	0.022	0.003	0.010	0.003
^{82}Kr/^{84}Kr	0.211	0.207	0.181	0.205
±	0.062	0.004	0.022	0.004
^{83}Kr/^{84}Kr	0.217	0.209	0.192	0.207
±	0.039	0.004	0.013	0.003
^{86}Kr/^{84}Kr	0.341	0.318	0.292	0.317
±	0.069	0.004	0.022	0.004
^{83}Kr$_{cos}$ [in 10^{-8} cc/g]	< 0.0017 (2σ)	0.0042	-	-
±	-	0.0030	-	-
^{83}Kr$_{cos}$ [in 10^{-12} cc]	< 0.0005 (2σ)	0.0012	-	-
±	-	0.0009	-	-

Date of measurement	02/09/11	05/09/11	06/09/11	02+05+06/09/11
Laser-Power	3 x 0.13 W	3 x 0.91 W	3 x 5 W	
Laser-Beam	250 µm	250 µm	250 µm	
Step(s)	1	2	3	total*
^{132}Xe - INT [in 10^{-8} cc/g]	0.0145	1.0528	0.0354	1.1027
±	0.0019	0.0377	0.0023	0.0378
^{132}Xe - INT [in 10^{-12} cc]	0.0042	0.3053	0.0103	0.3198
±	0.0005	0.0109	0.0007	0.0109
^{128}Xe/^{132}Xe - INT	0.127	0.084	0.100	0.085
±	0.021	0.001	0.009	0.001
^{129}Xe/^{132}Xe - INT	1.076	1.047	1.060	1.047
±	0.083	0.006	0.043	0.006
^{130}Xe/^{132}Xe - INT	0.189	0.165	0.173	0.166
±	0.014	0.001	0.008	0.001
^{131}Xe/^{132}Xe - INT	0.855	0.817	0.832	0.818
±	0.070	0.004	0.035	0.004
^{134}Xe/^{132}Xe - INT	0.354	0.379	0.359	0.378
±	0.037	0.003	0.021	0.003
^{136}Xe/^{132}Xe - INT	0.342	0.327	0.257	0.325
±	0.042	0.004	0.025	0.004
^{132}Xe - EXTa [in 10^{-8} cc/g]	0.0138	1.0520	0.0346	1.1004
±	0.0019	0.0376	0.0022	0.0378
^{132}Xe - EXTa [in 10^{-12} cc]	0.0040	0.3051	0.0100	0.3191
±	0.0005	0.0109	0.0007	0.0109
^{128}Xe/^{132}Xe - EXTa	0.108	0.082	0.086	0.082
±	0.025	0.001	0.011	0.001
^{129}Xe/^{132}Xe - EXTa	1.074	1.047	1.059	1.048
±	0.090	0.006	0.045	0.006
^{130}Xe/^{132}Xe - EXTa	0.185	0.164	0.160	0.165
±	0.018	0.001	0.010	0.001
^{131}Xe/^{132}Xe - EXTa	0.856	0.817	0.832	0.818
±	0.077	0.005	0.037	0.005
^{134}Xe/^{132}Xe - EXTa	0.391	0.375	0.399	0.376
±	0.035	0.002	0.019	0.002
^{136}Xe/^{132}Xe - EXTa	0.342	0.313	0.315	0.313
±	0.030	0.002	0.019	0.002
^{132}Xe - EXTb [in 10^{-8} cc/g]	0.0127	1.0477	0.0328	1.0932
±	0.0020	0.0409	0.0025	0.0411
^{132}Xe - EXTb [in 10^{-12} cc]	0.0037	0.3038	0.0095	0.3170
±	0.0006	0.0118	0.0007	0.0119
^{128}Xe/^{132}Xe - EXTb	0.065	0.079	0.077	0.079
±	0.018	0.001	0.007	0.001
^{129}Xe/^{132}Xe - EXTb	1.079	1.047	1.061	1.047
±	0.115	0.006	0.052	0.006
^{130}Xe/^{132}Xe - EXTb	0.197	0.162	0.180	0.163
±	0.020	0.001	0.010	0.001
^{131}Xe/^{132}Xe - EXTb	0.861	0.817	0.833	0.818
±	0.035	0.002	0.014	0.002
^{134}Xe/^{132}Xe - EXTb	0.373	0.382	0.388	0.382
±	0.037	0.002	0.021	0.002
^{136}Xe/^{132}Xe - EXTb	0.403	0.325	0.318	0.325
±	0.035	0.002	0.020	0.002
^{21}Ne$_{cos}$/^{38}Ar$_{cos}$	-	-	-	-
±	-	-	-	-
^{36}Ar/^{132}Xe $_{(Int)}$	-	142.32	147.28	140.60
±	-	5.76	16.23	5.47
^{84}Kr/^{132}Xe $_{(Int)}$	1.12	0.60	1.57	0.64
±	1.08	0.05	0.47	0.05

Table X28. Noble gas data He to Xe for sample 45c.37_2 (corrected for blank)

Sample	45c.37_2		
Size [µm]	498 x 379		
Weight [µg]	28.5 ± 0.1		
Date of measurement	14/02/12	15/02/12	14+15/02/12
Laser-Power	3 x 0.91 W	3 x 5 W	
Laser-Beam	600 µm	250 µm	
Step(s)	1	2	total*
^{4}He [in 10^{-8} cc/g]	473.9	< 58 (2σ)	-
±	22.5	-	-
^{4}He [in 10^{-12} cc]	135.1	< 16 (2σ)	-
±	6.4	-	-
^{3}He [in 10^{-12} cc/g]	1088.6	< 138 (2σ)	-
±	561.2	-	-
^{3}He [in 10^{-16} cc]	310.3	< 39 (2σ)	-
±	159.9	-	-
^{3}He/^{4}He	0.00023	-	-
±	0.00012	-	-
^{22}Ne [in 10^{-8} cc/g]	0.390	0.322	0.711
±	0.121	0.121	0.171
^{22}Ne [in 10^{-12} cc]	0.111	0.092	0.203
±	0.035	0.034	0.049
^{20}Ne/^{22}Ne	10.67	10.93	10.79
±	2.17	2.57	1.66
^{21}Ne/^{22}Ne	0.039	0.037	0.038
±	0.009	0.010	0.007
^{21}Ne$_{cos}$ [in 10^{-8} cc/g]	< 0.016 (2σ)	< 0.014 (2σ)	-
±	-	-	-
^{21}Ne$_{cos}$ [in 10^{-12} cc]	< 0.004 (2σ)	< 0.004 (2σ)	-
±	-	-	-
^{20}Ne$_{trap}$ [in 10^{-8} cc/g]	4.2	< 211.2 (2σ)	-
±	1.6	-	-
^{20}Ne$_{trap}$ [in 10^{-12} cc]	1.2	< 60.2 (2σ)	-
±	0.4	-	-
^{36}Ar [in 10^{-8} cc/g]	13.41	6.73	20.15
±	0.59	1.64	1.74
^{36}Ar [in 10^{-12} cc]	3.82	1.92	5.74
±	0.17	0.47	0.50
^{38}Ar/^{36}Ar	0.194	0.190	0.193
±	0.003	0.014	0.005
^{40}Ar/^{36}Ar	23.5	90.6	45.9
±	8.5	24.6	10.0
^{40}Ar [in 10^{-8} cc/g]	356.5	653.9	1010.4
±	131.2	426.7	446.4
^{40}Ar [in 10^{-12} cc]	101.6	186.4	288.0
±	37.4	121.6	127.2
^{38}Ar$_{cos}$ [in 10^{-8} cc/g]	0.078	< 0.223 (2σ)	-
±	0.052	-	-
^{38}Ar$_{cos}$ [in 10^{-12} cc]	0.022	< 0.064 (2σ)	-
±	0.015	-	-
^{84}Kr [in 10^{-8} cc/g]	0.1818	0.0533	0.2351
±	0.0548	0.0268	0.0610
^{84}Kr [in 10^{-12} cc]	0.0518	0.0152	0.0670
±	0.0156	0.0076	0.0174
^{80}Kr/^{84}Kr	0.036	0.052	0.040
±	0.004	0.009	0.003
^{82}Kr/^{84}Kr	0.212	0.205	0.210
±	0.013	0.027	0.012
^{83}Kr/^{84}Kr	0.203	0.184	0.199
±	0.014	0.021	0.012
^{86}Kr/^{84}Kr	0.314	0.326	0.316
±	0.022	0.035	0.018
^{83}Kr$_{cos}$ [in 10^{-8} cc/g]	-	-	-
±	-	-	-
^{83}Kr$_{cos}$ [in 10^{-12} cc]	-	-	-
±	-	-	-

Sample	45c.37_2		
Date of measurement	14/02/12	15/02/12	14+15/02/12
Laser-Power	3 x 0.91 W	3 x 5 W	
Laser-Beam	600 µm	250 µm	
Step(s)	1	2	total*
^{132}Xe - INT [in 10^{-8} cc/g]	0.3104	0.0566	0.3670
±	0.0100	0.0083	0.0130
^{132}Xe - INT [in 10^{-12} cc]	0.0885	0.0161	0.1046
±	0.0028	0.0024	0.0037
^{128}Xe/^{132}Xe - INT	0.081	0.070	0.079
±	0.003	0.008	0.003
^{129}Xe/^{132}Xe - INT	1.036	1.008	1.032
±	0.011	0.038	0.011
^{130}Xe/^{132}Xe - INT	0.161	0.150	0.159
±	0.002	0.006	0.002
^{131}Xe/^{132}Xe - INT	0.821	0.827	0.822
±	0.011	0.032	0.011
^{134}Xe/^{132}Xe - INT	0.381	0.375	0.380
±	0.005	0.018	0.005
^{136}Xe/^{132}Xe - INT	0.323	0.355	0.327
±	0.007	0.020	0.006
^{132}Xe - EXTa [in 10^{-8} cc/g]	0.3142	0.0590	0.3732
±	0.0672	0.0140	0.0686
^{132}Xe - EXTa [in 10^{-12} cc]	0.0896	0.0168	0.1064
±	0.0191	0.0040	0.0196
^{128}Xe/^{132}Xe - EXTa	0.076	0.071	0.075
±	0.002	0.009	0.003
^{129}Xe/^{132}Xe - EXTa	1.034	1.004	1.029
±	0.012	0.038	0.011
^{130}Xe/^{132}Xe - EXTa	0.157	0.147	0.156
±	0.003	0.007	0.003
^{131}Xe/^{132}Xe - EXTa	0.820	0.825	0.820
±	0.011	0.031	0.010
^{134}Xe/^{132}Xe - EXTa	0.384	0.365	0.381
±	0.005	0.014	0.005
^{136}Xe/^{132}Xe - EXTa	0.324	0.314	0.323
±	0.004	0.013	0.004
^{132}Xe - EXTb [in 10^{-8} cc/g]	0.3139	0.0615	0.3755
±	0.0119	0.0055	0.0131
^{132}Xe - EXTb [in 10^{-12} cc]	0.0895	0.0175	0.1070
±	0.0034	0.0016	0.0037
^{128}Xe/^{132}Xe - EXTb	0.078	0.077	0.078
±	0.002	0.005	0.002
^{129}Xe/^{132}Xe - EXTb	1.033	0.998	1.027
±	0.012	0.035	0.011
^{130}Xe/^{132}Xe - EXTb	0.154	0.157	0.155
±	0.002	0.008	0.002
^{131}Xe/^{132}Xe - EXTb	0.820	0.830	0.822
±	0.004	0.012	0.004
^{134}Xe/^{132}Xe - EXTb	0.385	0.370	0.383
±	0.005	0.013	0.004
^{136}Xe/^{132}Xe - EXTb	0.330	0.336	0.331
±	0.006	0.014	0.006
^{21}Ne$_{cos}$/^{38}Ar$_{cos}$	-	-	-
±	-	-	-
^{36}Ar/^{132}Xe $_{(Int)}$	43.22	118.92	54.90
±	2.34	33.74	5.11
^{84}Kr/^{132}Xe $_{(Int)}$	0.59	0.94	0.64
±	0.18	0.49	0.17

Table X29. Noble gas data He to Xe for sample 45c.37_3 (corrected for blank)

Sample	45c.37_3		
Size [µm]	322 x 205		
Weight [µg]	13.1 ± 0.1		
Date of measurement	16/02/12	16/02/12	16/02/12
Laser-Power	3 x 0.91 W	3 x 5 W	
Laser-Beam	360 µm	180 µm	
Step(s)	1	2	total*
^{4}He [in 10^{-8} cc/g]	340.0	< 106 (2σ)	-
±	44.8	-	-
^{4}He [in 10^{-12} cc]	44.5	< 14 (2σ)	-
±	5.9	-	-
^{3}He [in 10^{-12} cc/g]	< 2857 (2σ)	< 301 (2σ)	-
±	-	-	-
^{3}He [in 10^{-16} cc]	< 374 (2σ)	< 39 (2σ)	-
±	-	-	-
^{3}He/^{4}He	-	-	-
±	-	-	-
^{22}Ne [in 10^{-8} cc/g]	< 0.78 (2σ)	< 0.67 (2σ)	-
±	-	-	-
^{22}Ne [in 10^{-12} cc]	< 0.10 (2σ)	< 0.09 (2σ)	-
±	-	-	-
^{20}Ne/^{22}Ne	-	-	-
±	-	-	-
^{21}Ne/^{22}Ne	-	-	-
±	-	-	-
^{21}Ne$_{cos}$ [in 10^{-8} cc/g]	< 0.042 (2σ)	< 0.032 (2σ)	-
±	-	-	-
^{21}Ne$_{cos}$ [in 10^{-12} cc]	< 0.005 (2σ)	< 0.004 (2σ)	-
±	-	-	-
^{20}Ne$_{trap}$ [in 10^{-8} cc/g]	< 7.6 (2σ)	-	-
±	-	-	-
^{20}Ne$_{trap}$ [in 10^{-12} cc]	< 1.0 (2σ)	-	-
±	-	-	-
^{36}Ar [in 10^{-8} cc/g]	222.30	29.39	251.69
±	7.42	3.59	8.24
^{36}Ar [in 10^{-12} cc]	29.12	3.85	32.97
±	0.95	0.47	1.05
^{38}Ar/^{36}Ar	0.188	0.180	0.187
±	0.001	0.007	0.001
^{40}Ar/^{36}Ar	290.8	262.4	287.5
±	11.7	9.8	10.4
^{40}Ar [in 10^{-8} cc/g]	64732.3	7806.0	72538.4
±	2225.3	939.3	2415.4
^{40}Ar [in 10^{-12} cc]	8479.9	1022.6	9502.5
±	284.2	122.8	308.0
^{38}Ar$_{cos}$ [in 10^{-8} cc/g]	-	-	-
±	-	-	-
^{38}Ar$_{cos}$ [in 10^{-12} cc]	-	-	-
±	-	-	-
^{84}Kr [in 10^{-8} cc/g]	2.1161	0.3218	2.4378
±	0.5832	0.1010	0.5919
^{84}Kr [in 10^{-12} cc]	0.2772	0.0422	0.3194
±	0.0764	0.0132	0.0775
^{80}Kr/^{84}Kr	0.038	0.036	0.038
±	0.002	0.004	0.002
^{82}Kr/^{84}Kr	0.196	0.199	0.197
±	0.007	0.013	0.007
^{83}Kr/^{84}Kr	0.205	0.214	0.206
±	0.010	0.014	0.009
^{86}Kr/^{84}Kr	0.308	0.313	0.309
±	0.017	0.022	0.015
^{83}Kr$_{cos}$ [in 10^{-8} cc/g]	< 0.0541 (2σ)	< 0.0138 (2σ)	-
±	-	-	-
^{83}Kr$_{cos}$ [in 10^{-12} cc]	< 0.0071 (2σ)	< 0.0018 (2σ)	-
±	-	-	-

Date of measurement	16/02/12	16/02/12	16/02/12
Laser-Power	3 x 0.91 W	3 x 5 W	
Laser-Beam	360 µm	180 µm	
Step(s)	1	2	total*
^{132}Xe - INT [in 10^{-8} cc/g]	0.5220	0.0826	0.6046
±	0.0206	0.0180	0.0274
^{132}Xe - INT [in 10^{-12} cc]	0.0684	0.0108	0.0792
±	0.0027	0.0024	0.0035
^{128}Xe/^{132}Xe - INT	0.080	0.076	0.080
±	0.003	0.012	0.003
^{129}Xe/^{132}Xe - INT	1.023	1.016	1.022
±	0.013	0.051	0.013
^{130}Xe/^{132}Xe - INT	0.160	0.149	0.158
±	0.003	0.008	0.003
^{131}Xe/^{132}Xe - INT	0.792	0.834	0.798
±	0.012	0.044	0.012
^{134}Xe/^{132}Xe - INT	0.384	0.389	0.384
±	0.008	0.024	0.007
^{136}Xe/^{132}Xe - INT	0.323	0.322	0.323
±	0.008	0.027	0.008
^{132}Xe - EXTa [in 10^{-8} cc/g]	0.5277	0.0873	0.6150
±	0.1132	0.0230	0.1155
^{132}Xe - EXTa [in 10^{-12} cc]	0.0691	0.0114	0.0806
±	0.0148	0.0030	0.0151
^{128}Xe/^{132}Xe - EXTa	0.075	0.074	0.075
±	0.003	0.013	0.003
^{129}Xe/^{132}Xe - EXTa	1.021	1.010	1.019
±	0.013	0.051	0.013
^{130}Xe/^{132}Xe - EXTa	0.156	0.146	0.154
±	0.003	0.009	0.003
^{131}Xe/^{132}Xe - EXTa	0.791	0.831	0.796
±	0.011	0.041	0.011
^{134}Xe/^{132}Xe - EXTa	0.377	0.400	0.380
±	0.007	0.018	0.006
^{136}Xe/^{132}Xe - EXTa	0.316	0.343	0.320
±	0.005	0.017	0.005
^{132}Xe - EXTb [in 10^{-8} cc/g]	0.5259	0.0919	0.6177
±	0.0208	0.0114	0.0237
^{132}Xe - EXTb [in 10^{-12} cc]	0.0689	0.0120	0.0809
±	0.0027	0.0015	0.0030
^{128}Xe/^{132}Xe - EXTb	0.070	0.075	0.071
±	0.002	0.007	0.002
^{129}Xe/^{132}Xe - EXTb	1.019	1.001	1.016
±	0.013	0.044	0.013
^{130}Xe/^{132}Xe - EXTb	0.153	0.151	0.153
±	0.003	0.009	0.003
^{131}Xe/^{132}Xe - EXTb	0.792	0.838	0.799
±	0.005	0.017	0.005
^{134}Xe/^{132}Xe - EXTb	0.389	0.381	0.388
±	0.006	0.018	0.006
^{136}Xe/^{132}Xe - EXTb	0.323	0.327	0.324
±	0.006	0.019	0.006
^{21}Ne$_{cos}$/^{38}Ar$_{cos}$	-	-	-
±	-	-	-
^{36}Ar/^{132}Xe $_{(Int)}$	425.85	355.77	416.28
±	21.55	88.93	22.84
^{84}Kr/^{132}Xe $_{(Int)}$	4.05	3.90	4.03
±	1.13	1.49	0.99

Table X30. Noble gas data He to Xe for sample CP_9-1-1994_PL10-109D9 (corrected for blank)

Sample	CP_9-1-1994_PL10-109D9						
Size [μm]	252 x 188						
Weight [μg]	6.2 ± 0.1						
Date of measurement	07/11/11	08/11/11	07+08/11/11	**Date of measurement**	07/11/11	08/11/11	07+08/11/11
Laser-Power	3 x 0.91 W	3 x 5 W		**Laser-Power**	3 x 0.91 W	3 x 5 W	
Laser-Beam	250 μm	180 μm		**Laser-Beam**	250 μm	180 μm	
Step(s)	1	2	total*	**Step(s)**	1	2	total*
^{4}He [in 10^{-8} cc/g]	143.0	-	-	^{132}Xe - INT [in 10^{-8} cc/g]	0.1448	-	-
±	91.6	-	-	±	0.0099	-	-
^{4}He [in 10^{-12} cc]	8.9	-	-	^{132}Xe - INT [in 10^{-12} cc]	0.0090	-	-
±	5.7	-	-	±	0.0006	-	-
^{3}He [in 10^{-12} cc/g]	< 5218 (2σ)	< 4774 (2σ)	-	^{128}Xe/^{132}Xe - INT	0.077	-	-
±	-	-	-	±	0.010	-	-
^{3}He [in 10^{-16} cc]	< 324 (2σ)	< 296 (2σ)	-	^{129}Xe/^{132}Xe - INT	1.035	-	-
±	-	-	-	±	0.046	-	-
^{3}He/^{4}He	-	-	-	^{130}Xe/^{132}Xe - INT	0.158	-	-
±	-	-	-	±	0.009	-	-
^{22}Ne [in 10^{-8} cc/g]	2.893	< 1.25 (2σ)	-	^{131}Xe/^{132}Xe - INT	0.869	-	-
±	0.523	-	-	±	0.041	-	-
^{22}Ne [in 10^{-12} cc]	0.179	< 0.08 (2σ)	-	^{134}Xe/^{132}Xe - INT	0.362	-	-
±	0.032	-	-	±	0.024	-	-
^{20}Ne/^{22}Ne	11.94	-	-	^{136}Xe/^{132}Xe - INT	0.299	-	-
±	0.97	-	-	±	0.029	-	-
^{21}Ne/^{22}Ne	0.028	-	-	^{132}Xe - EXTa [in 10^{-8} cc/g]	0.1441	-	-
±	0.005	-	-	±	0.0099	-	-
^{21}Ne$_{cos}$ [in 10^{-8} cc/g]	< 0.044 (2σ)	< 0.019 (2σ)	-	^{132}Xe - EXTa [in 10^{-12} cc]	0.0089	-	-
±	-	-	-	±	0.0006	-	-
^{21}Ne$_{cos}$ [in 10^{-12} cc]	< 0.003 (2σ)	< 0.001 (2σ)	-	^{128}Xe/^{132}Xe - EXTa	0.074	-	-
±	-	-	-	±	0.012	-	-
^{20}Ne$_{trap}$ [in 10^{-8} cc/g]	34.5	< 13.2 (2σ)	-	^{129}Xe/^{132}Xe - EXTa	1.037	-	-
±	7.1	-	-	±	0.048	-	-
^{20}Ne$_{trap}$ [in 10^{-12} cc]	2.1	< 0.8 (2σ)	-	^{130}Xe/^{132}Xe - EXTa	0.159	-	-
±	0.4	-	-	±	0.010	-	-
^{36}Ar [in 10^{-8} cc/g]	18.75	-	-	^{131}Xe/^{132}Xe - EXTa	0.870	-	-
±	0.81	-	-	±	0.042	-	-
^{36}Ar [in 10^{-12} cc]	1.16	-	-	^{134}Xe/^{132}Xe - EXTa	0.370	-	-
±	0.05	-	-	±	0.023	-	-
^{38}Ar/^{36}Ar	0.172	-	-	^{136}Xe/^{132}Xe - EXTa	0.320	-	-
±	0.018	-	-	±	0.020	-	-
^{40}Ar/^{36}Ar	52.1	-	-	^{132}Xe - EXTb [in 10^{-8} cc/g]	0.1421	-	-
±	3.2	-	-	±	0.0114	-	-
^{40}Ar [in 10^{-8} cc/g]	977.1	-	-	^{132}Xe - EXTb [in 10^{-12} cc]	0.0088	-	-
±	86.6	-	-	±	0.0007	-	-
^{40}Ar [in 10^{-12} cc]	60.6	-	-	^{128}Xe/^{132}Xe - EXTb	0.094	-	-
±	5.3	-	-	±	0.009	-	-
^{38}Ar$_{cos}$ [in 10^{-8} cc/g]	-	< 0.261 (2σ)	-	^{129}Xe/^{132}Xe - EXTb	1.037	-	-
±	-	-	-	±	0.057	-	-
^{38}Ar$_{cos}$ [in 10^{-12} cc]	-	< 0.016 (2σ)	-	^{130}Xe/^{132}Xe - EXTb	0.165	-	-
±	-	-	-	±	0.011	-	-
^{84}Kr [in 10^{-8} cc/g]	-	-	-	^{131}Xe/^{132}Xe - EXTb	0.871	-	-
±	-	-	-	±	0.019	-	-
^{84}Kr [in 10^{-12} cc]	-	-	-	^{134}Xe/^{132}Xe - EXTb	0.359	-	-
±	-	-	-	±	0.022	-	-
^{80}Kr/^{84}Kr	-	-	-	^{136}Xe/^{132}Xe - EXTb	0.295	-	-
±	-	-	-	±	0.021	-	-
^{82}Kr/^{84}Kr	-	-	-	^{21}Ne$_{cos}$/^{38}Ar$_{cos}$	-	-	-
±	-	-	-	±	-	-	-
^{83}Kr/^{84}Kr	-	-	-	^{36}Ar/^{132}Xe (Int)	129.46	-	-
±	-	-	-	±	10.04	-	-
^{86}Kr/^{84}Kr	-	-	-	^{84}Kr/^{132}Xe (Int)	-	-	-
±	-	-	-	±	-	-	-
^{83}Kr$_{cos}$ [in 10^{-8} cc/g]	-	< 0.0090 (2σ)	-				
±	-	-	-				
^{83}Kr$_{cos}$ [in 10^{-12} cc]	-	< 0.0006 (2σ)	-				
±	-	-	-				

Table X31. Noble gas data He to Xe for sample DC 06_07_213 (corrected for blank)

Sample		DC 06_07_213	
Size [μm]		97 x 91	
Weight [μg]		~ 1.1	
Date of measurement	23/04/12	**Date of measurement**	23/04/12
Laser-Power	4 x 0.91 - 20 W	**Laser-Power**	4 x 0.91 - 20 W
Laser-Beam	180-600 μm	**Laser-Beam**	180-600 μm
Step(s)	1	**Step(s)**	1
^{4}He [in 10^{-8} cc/g]	1516.8	^{132}Xe - INT [in 10^{-8} cc/g]	0.8479
±	392.2	±	0.1941
^{4}He [in 10^{-12} cc]	16.2	^{132}Xe - INT [in 10^{-12} cc]	0.0091
±	3.9	±	0.0019
^{3}He [in 10^{-12} cc/g]	12194.9	^{128}Xe/^{132}Xe - INT	0.060
±	2987.8	±	0.011
^{3}He [in 10^{-16} cc]	130.5	^{129}Xe/^{132}Xe - INT	0.947
±	29.6	±	0.047
^{3}He/^{4}He	0.00080	^{130}Xe/^{132}Xe - INT	0.135
±	0.00027	±	0.008
^{22}Ne [in 10^{-8} cc/g]	77.585	^{131}Xe/^{132}Xe - INT	0.841
±	7.757	±	0.046
^{22}Ne [in 10^{-12} cc]	0.830	^{134}Xe/^{132}Xe - INT	0.412
±	0.029	±	0.024
^{20}Ne/^{22}Ne	11.17	^{136}Xe/^{132}Xe - INT	0.394
±	0.29	±	0.030
^{21}Ne/^{22}Ne	0.028	^{132}Xe - EXTa [in 10^{-8} cc/g]	0.9545
±	0.002	±	0.2458
^{21}Ne$_{cos}$ [in 10^{-8} cc/g]	-	^{132}Xe - EXTa [in 10^{-12} cc]	0.0102
±	-	±	0.0025
^{21}Ne$_{cos}$ [in 10^{-12} cc]	-	^{128}Xe/^{132}Xe - EXTa	0.075
±	-	±	0.008
^{20}Ne$_{trap}$ [in 10^{-8} cc/g]	866.7	^{129}Xe/^{132}Xe - EXTa	0.945
±	101.5	±	0.042
^{20}Ne$_{trap}$ [in 10^{-12} cc]	9.3	^{130}Xe/^{132}Xe - EXTa	0.143
±	0.7	±	0.009
^{36}Ar [in 10^{-8} cc/g]	261.02	^{131}Xe/^{132}Xe - EXTa	0.836
±	39.95	±	0.040
^{36}Ar [in 10^{-12} cc]	2.79	^{134}Xe/^{132}Xe - EXTa	0.395
±	0.34	±	0.018
^{38}Ar/^{36}Ar	0.184	^{136}Xe/^{132}Xe - EXTa	0.339
±	0.003	±	0.016
^{40}Ar/^{36}Ar	202.1	^{132}Xe - EXTb [in 10^{-8} cc/g]	0.8790
±	5.0	±	0.2668
^{40}Ar [in 10^{-8} cc/g]	54039.5	^{132}Xe - EXTb [in 10^{-12} cc]	0.0094
±	8428.3	±	0.0027
^{40}Ar [in 10^{-12} cc]	578.2	^{128}Xe/^{132}Xe - EXTb	0.063
±	72.2	±	0.009
^{38}Ar$_{cos}$ [in 10^{-8} cc/g]	-	^{129}Xe/^{132}Xe - EXTb	0.946
±	-	±	0.045
^{38}Ar$_{cos}$ [in 10^{-12} cc]	-	^{130}Xe/^{132}Xe - EXTb	0.148
±	-	±	0.010
^{84}Kr [in 10^{-8} cc/g]	2.5361	^{131}Xe/^{132}Xe - EXTb	0.844
±	0.6074	±	0.018
^{84}Kr [in 10^{-12} cc]	0.0271	^{134}Xe/^{132}Xe - EXTb	0.400
±	0.0060	±	0.018
^{80}Kr/^{84}Kr	0.035	^{136}Xe/^{132}Xe - EXTb	0.360
±	0.005	±	0.020
^{82}Kr/^{84}Kr	0.198	^{21}Ne$_{cos}$/^{38}Ar$_{cos}$	-
±	0.017	±	-
^{83}Kr/^{84}Kr	0.201	^{36}Ar/^{132}Xe $_{(Int)}$	307.83
±	0.012	±	74.37
^{86}Kr/^{84}Kr	0.331	^{84}Kr/^{132}Xe $_{(Int)}$	2.99
±	0.020	±	0.91
^{83}Kr$_{cos}$ [in 10^{-8} cc/g]	-		
±	-		
^{83}Kr$_{cos}$ [in 10^{-12} cc]	-		
±	-		

Table X32. Noble gas data He to Xe for sample DC 06_08_01 (corrected for blank)

Sample	DC 06_08_01							
Size [µm]	110 x 92							
Weight [µg]	~1.4							
Date of measurement	25/04/12	26/04/12	25+26/04/12	**Date of measurement**	25/04/12	26/04/12	25+26/04/12
Laser-Power	3 x 0.91 W	3 x 5 W		**Laser-Power**	3 x 0.91 W	3 x 5 W	
Laser-Beam	180 µm	180-250 µm		**Laser-Beam**	180 µm	180-250 µm	
Step(s)	1	2	total*	**Step(s)**	1	2	total*
^{4}He [in 10^{-8} cc/g]	1423.9	-	-	^{132}Xe - INT [in 10^{-8} cc/g]	0.2835	-	-
±	304.2	-	-	±	0.1353	-	-
^{4}He [in 10^{-12} cc]	19.5	-	-	^{132}Xe - INT [in 10^{-12} cc]	0.0039	-	-
±	3.9	-	-	±	0.0018	-	-
^{3}He [in 10^{-12} cc/g]	20110.5	-	-	^{128}Xe/^{132}Xe - INT	0.041	-	-
±	2710.1	-	-	±	0.023	-	-
^{3}He [in 10^{-16} cc]	275.5	-	-	^{129}Xe/^{132}Xe - INT	0.921	-	-
±	31.2	-	-	±	0.078	-	-
^{3}He/^{4}He	0.00141	-	-	^{130}Xe/^{132}Xe - INT	0.137	-	-
±	0.00033	-	-	±	0.016	-	-
^{22}Ne [in 10^{-8} cc/g]	234.853	-	-	^{131}Xe/^{132}Xe - INT	0.632	-	-
±	17.555	-	-	±	0.075	-	-
^{22}Ne [in 10^{-12} cc]	3.217	-	-	^{134}Xe/^{132}Xe - INT	0.431	-	-
±	0.052	-	-	±	0.048	-	-
^{20}Ne/^{22}Ne	11.43	-	-	^{136}Xe/^{132}Xe - INT	0.342	-	-
±	0.12	-	-	±	0.049	-	-
^{21}Ne/^{22}Ne	0.032	-	-	^{132}Xe - EXTa [in 10^{-8} cc/g]	0.3692	-	-
±	0.001	-	-	±	0.1201	-	-
^{21}Ne$_{cos}$ [in 10^{-8} cc/g]	0.523	-	-	^{132}Xe - EXTa [in 10^{-12} cc]	0.0051	-	-
±	0.201	-	-	±	0.0016	-	-
^{21}Ne$_{cos}$ [in 10^{-12} cc]	0.007	-	-	^{128}Xe/^{132}Xe - EXTa	0.049	-	-
±	0.003	-	-	±	0.013	-	-
^{20}Ne$_{trap}$ [in 10^{-8} cc/g]	2684.5	-	-	^{129}Xe/^{132}Xe - EXTa	0.926	-	-
±	250.8	-	-	±	0.061	-	-
^{20}Ne$_{trap}$ [in 10^{-12} cc]	36.8	-	-	^{130}Xe/^{132}Xe - EXTa	0.153	-	-
±	2.1	-	-	±	0.014	-	-
^{36}Ar [in 10^{-8} cc/g]	190.29	-	-	^{131}Xe/^{132}Xe - EXTa	0.670	-	-
±	27.15	-	-	±	0.054	-	-
^{36}Ar [in 10^{-12} cc]	2.61	-	-	^{134}Xe/^{132}Xe - EXTa	0.410	-	-
±	0.32	-	-	±	0.024	-	-
^{38}Ar/^{36}Ar	0.205	-	-	^{136}Xe/^{132}Xe - EXTa	0.292	-	-
±	0.004	-	-	±	0.022	-	-
^{40}Ar/^{36}Ar	19.7	-	-	^{132}Xe - EXTb [in 10^{-8} cc/g]	0.3061	-	-
±	10.8	-	-	±	0.1308	-	-
^{40}Ar [in 10^{-8} cc/g]	4746.2	-	-	^{132}Xe - EXTb [in 10^{-12} cc]	0.0042	-	-
±	2449.6	-	-	±	0.0018	-	-
^{40}Ar [in 10^{-12} cc]	65.0	-	-	^{128}Xe/^{132}Xe - EXTb	0.048	-	-
±	33.2	-	-	±	0.018	-	-
^{38}Ar$_{cos}$ [in 10^{-8} cc/g]	3.601	< 5.996 (2σ)	-	^{129}Xe/^{132}Xe - EXTb	0.923	-	-
±	1.034	-	-	±	0.073	-	-
^{38}Ar$_{cos}$ [in 10^{-12} cc]	0.049	< 0.082 (2σ)	-	^{130}Xe/^{132}Xe - EXTb	0.104	-	-
±	0.014	-	-	±	0.016	-	-
^{84}Kr [in 10^{-8} cc/g]	1.1513	-	-	^{131}Xe/^{132}Xe - EXTb	0.645	-	-
±	0.4392	-	-	±	0.041	-	-
^{84}Kr [in 10^{-12} cc]	0.0158	-	-	^{134}Xe/^{132}Xe - EXTb	0.412	-	-
±	0.0059	-	-	±	0.039	-	-
^{80}Kr/^{84}Kr	0.043	-	-	^{136}Xe/^{132}Xe - EXTb	0.293	-	-
±	0.008	-	-	±	0.033	-	-
^{82}Kr/^{84}Kr	0.226	-	-	^{21}Ne$_{cos}$/^{38}Ar$_{cos}$	0.15	-	-
±	0.027	-	-	±	0.07	-	-
^{83}Kr/^{84}Kr	0.186	-	-	^{36}Ar/^{132}Xe $_{(Int)}$	671.20	-	-
±	0.018	-	-	±	327.04	-	-
^{86}Kr/^{84}Kr	0.310	-	-	^{84}Kr/^{132}Xe $_{(Int)}$	4.06	-	-
±	0.027	-	-	±	2.45	-	-
^{83}Kr$_{cos}$ [in 10^{-8} cc/g]	-	-	-				
±	-	-	-				
^{83}Kr$_{cos}$ [in 10^{-12} cc]	-	-	-				
±	-	-	-				

Table X33. Noble gas data He to Xe for sample DC 06_09_11 (corrected for blank)

Sample		DC 06_09_11	
Size [μm]		137 x 111	
Weight [μg]		~1.3	
Date of measurement	26/04/12	**Date of measurement**	26/04/12
Laser-Power	3 x 0.91 W	**Laser-Power**	3 x 0.91 W
Laser-Beam	180 μm	**Laser-Beam**	180 μm
Step(s)	1	**Step(s)**	1
^{4}He [in 10^{-8} cc/g]	6714.2	^{132}Xe - INT [in 10^{-8} cc/g]	0.7811
±	614.2	±	0.1602
^{4}He [in 10^{-12} cc]	86.7	^{132}Xe - INT [in 10^{-12} cc]	0.0101
±	4.2	±	0.0019
^{3}He [in 10^{-12} cc/g]	21327.3	^{128}Xe/^{132}Xe - INT	0.083
±	4865.7	±	0.010
^{3}He [in 10^{-16} cc]	275.5	^{129}Xe/^{132}Xe - INT	1.033
±	59.1	±	0.044
^{3}He/^{4}He	0.00032	^{130}Xe/^{132}Xe - INT	0.166
±	0.00007	±	0.009
^{22}Ne [in 10^{-8} cc/g]	40.618	^{131}Xe/^{132}Xe - INT	0.783
±	3.820	±	0.040
^{22}Ne [in 10^{-12} cc]	0.525	^{134}Xe/^{132}Xe - INT	0.370
±	0.028	±	0.021
^{20}Ne/^{22}Ne	11.71	^{136}Xe/^{132}Xe - INT	0.333
±	0.45	±	0.024
^{21}Ne/^{22}Ne	0.033	^{132}Xe - EXTa [in 10^{-8} cc/g]	0.8687
±	0.002	±	0.2149
^{21}Ne$_{cos}$ [in 10^{-8} cc/g]	0.125	^{132}Xe - EXTa [in 10^{-12} cc]	0.0112
±	0.111	±	0.0026
^{21}Ne$_{cos}$ [in 10^{-12} cc]	0.002	^{128}Xe/^{132}Xe - EXTa	0.079
±	0.001	±	0.007
^{20}Ne$_{trap}$ [in 10^{-8} cc/g]	475.7	^{129}Xe/^{132}Xe - EXTa	1.023
±	55.0	±	0.039
^{20}Ne$_{trap}$ [in 10^{-12} cc]	6.1	^{130}Xe/^{132}Xe - EXTa	0.161
±	0.5	±	0.009
^{36}Ar [in 10^{-8} cc/g]	165.38	^{131}Xe/^{132}Xe - EXTa	0.782
±	24.72	±	0.034
^{36}Ar [in 10^{-12} cc]	2.14	^{134}Xe/^{132}Xe - EXTa	0.352
±	0.27	±	0.016
^{38}Ar/^{36}Ar	0.191	^{136}Xe/^{132}Xe - EXTa	0.314
±	0.004	±	0.015
^{40}Ar/^{36}Ar	107.4	^{132}Xe - EXTb [in 10^{-8} cc/g]	0.7573
±	9.1	±	0.2242
^{40}Ar [in 10^{-8} cc/g]	18833.7	^{132}Xe - EXTb [in 10^{-12} cc]	0.0098
±	3582.6	±	0.0028
^{40}Ar [in 10^{-12} cc]	243.3	^{128}Xe/^{132}Xe - EXTb	0.073
±	42.3	±	0.008
^{38}Ar$_{cos}$ [in 10^{-8} cc/g]	< 2.108 (2σ)	^{129}Xe/^{132}Xe - EXTb	1.034
±	-	±	0.044
^{38}Ar$_{cos}$ [in 10^{-12} cc]	< 0.027 (2σ)	^{130}Xe/^{132}Xe - EXTb	0.154
±	-	±	0.009
^{84}Kr [in 10^{-8} cc/g]	0.9102	^{131}Xe/^{132}Xe - EXTb	0.784
±	0.4613	±	0.017
^{84}Kr [in 10^{-12} cc]	0.0118	^{134}Xe/^{132}Xe - EXTb	0.384
±	0.0059	±	0.018
^{80}Kr/^{84}Kr	0.038	^{136}Xe/^{132}Xe - EXTb	0.312
±	0.011	±	0.017
^{82}Kr/^{84}Kr	0.274	^{21}Ne$_{cos}$/^{38}Ar$_{cos}$	-
±	0.036	±	-
^{83}Kr/^{84}Kr	0.209	^{36}Ar/^{132}Xe $_{(Int)}$	211.74
±	0.026	±	48.47
^{86}Kr/^{84}Kr	0.312	^{84}Kr/^{132}Xe $_{(Int)}$	1.17
±	0.037	±	0.62
^{83}Kr$_{cos}$ [in 10^{-8} cc/g]	< 0.0569 (2σ)		
±	-		
^{83}Kr$_{cos}$ [in 10^{-12} cc]	< 0.0007(2σ)		
±	-		

Table X34. Noble gas data He to Xe for sample DC 06_09_50 (corrected for blank)

Sample				DC 06_09_50			
Size [μm]				141 x 134			
Weight [μg]				~ 3.3			
Date of measurement	18/04/12	19/04/12	18+19/04/12	Date of measurement	18/04/12	19/04/12	18+19/04/12
Laser-Power	3 x 0.91 W	3 x 5 W		Laser-Power	3 x 0.91 W	3 x 5 W	
Laser-Beam	200 μm	180 μm		Laser-Beam	200 μm	180 μm	
Step(s)	1	2	total*	Step(s)	1	2	total*
^{4}He [in 10^{-8} cc/g]	368170.6	-	-	^{132}Xe - INT [in 10^{-8} cc/g]	0.8701	-	-
±	12532.8	-	-	±	0.0795	-	-
^{4}He [in 10^{-12} cc]	12149.6	-	-	^{132}Xe - INT [in 10^{-12} cc]	0.0287	-	-
±	188.4	-	-	±	0.0025	-	-
^{3}He [in 10^{-12} cc/g]	1098851.4	-	-	^{128}Xe/^{132}Xe - INT	0.072	-	-
±	56683.8	-	-	±	0.005	-	-
^{3}He [in 10^{-16} cc]	36262.1	-	-	^{129}Xe/^{132}Xe - INT	0.995	-	-
±	1513.8	-	-	±	0.023	-	-
^{3}He/^{4}He	0.00030	-	-	^{130}Xe/^{132}Xe - INT	0.162	-	-
±	0.00001	-	-	±	0.004	-	-
^{22}Ne [in 10^{-8} cc/g]	117.754	-	-	^{131}Xe/^{132}Xe - INT	0.784	-	-
±	3.983	-	-	±	0.019	-	-
^{22}Ne [in 10^{-12} cc]	3.886	-	-	^{134}Xe/^{132}Xe - INT	0.397	-	-
±	0.058	-	-	±	0.011	-	-
^{20}Ne/^{22}Ne	12.27	-	-	^{136}Xe/^{132}Xe - INT	0.349	-	-
±	0.11	-	-	±	0.013	-	-
^{21}Ne/^{22}Ne	0.032	-	-	^{132}Xe - EXTa [in 10^{-8} cc/g]	0.9007	-	-
±	0.001	-	-	±	0.1932	-	-
^{21}Ne$_{cos}$ [in 10^{-8} cc/g]	0.094	-	-	^{132}Xe - EXTa [in 10^{-12} cc]	0.0297	-	-
±	0.094	-	-	±	0.0063	-	-
^{21}Ne$_{cos}$ [in 10^{-12} cc]	0.003	-	-	^{128}Xe/^{132}Xe - EXTa	0.073	-	-
±	0.003	-	-	±	0.004	-	-
^{20}Ne$_{trap}$ [in 10^{-8} cc/g]	1445.4	-	-	^{129}Xe/^{132}Xe - EXTa	0.992	-	-
±	94.0	-	-	±	0.021	-	-
^{20}Ne$_{trap}$ [in 10^{-12} cc]	47.7	-	-	^{130}Xe/^{132}Xe - EXTa	0.161	-	-
±	2.7	-	-	±	0.005	-	-
^{36}Ar [in 10^{-8} cc/g]	568.71	26.90	595.61	^{131}Xe/^{132}Xe - EXTa	0.781	-	-
±	65.63	12.66	66.84	±	0.018	-	-
^{36}Ar [in 10^{-12} cc]	18.77	0.89	19.65	^{134}Xe/^{132}Xe - EXTa	0.379	-	-
±	2.09	0.42	2.12	±	0.009	-	-
^{38}Ar/^{36}Ar	0.193	0.195	0.193	^{136}Xe/^{132}Xe - EXTa	0.321	-	-
±	0.002	0.028	0.002	±	0.008	-	-
^{40}Ar/^{36}Ar	18.2	287.5	30.4	^{132}Xe - EXTb [in 10^{-8} cc/g]	0.8781	-	-
±	1.8	41.2	2.6	±	0.0603	-	-
^{40}Ar [in 10^{-8} cc/g]	10769.3	7855.4	18624.7	^{132}Xe - EXTb [in 10^{-12} cc]	0.0290	-	-
±	1585.9	3565.7	3902.5	±	0.0018	-	-
^{40}Ar [in 10^{-12} cc]	355.4	259.2	614.6	^{128}Xe/^{132}Xe - EXTb	0.072	-	-
±	51.2	117.4	127.4	±	0.004	-	-
^{38}Ar$_{cos}$ [in 10^{-8} cc/g]	3.172	< 1.886 (2σ)	-	^{129}Xe/^{132}Xe - EXTb	0.995	-	-
±	1.868	-	-	±	0.022	-	-
^{38}Ar$_{cos}$ [in 10^{-12} cc]	0.105	< 0.062 (2σ)	-	^{130}Xe/^{132}Xe - EXTb	0.160	-	-
±	0.062	-	-	±	0.005	-	-
^{84}Kr [in 10^{-8} cc/g]	1.1721	-	-	^{131}Xe/^{132}Xe - EXTb	0.780	-	-
±	0.1884	-	-	±	0.007	-	-
^{84}Kr [in 10^{-12} cc]	0.0387	-	-	^{134}Xe/^{132}Xe - EXTb	0.402	-	-
±	0.0061	-	-	±	0.010	-	-
^{80}Kr/^{84}Kr	0.038	-	-	^{136}Xe/^{132}Xe - EXTb	0.329	-	-
±	0.004	-	-	±	0.009	-	-
^{82}Kr/^{84}Kr	0.209	-	-	^{21}Ne$_{cos}$/^{38}Ar$_{cos}$	0.03	-	-
±	0.012	-	-	±	0.03	-	-
^{83}Kr/^{84}Kr	0.200	-	-	^{36}Ar/^{132}Xe $_{(Int)}$	653.61	-	-
±	0.009	-	-	±	92.02	-	-
^{86}Kr/^{84}Kr	0.288	-	-	^{84}Kr/^{132}Xe $_{(Int)}$	1.35	-	-
±	0.013	-	-	±	0.24	-	-
^{83}Kr$_{cos}$ [in 10^{-8} cc/g]	-	-	-				
±	-	-	-				
^{83}Kr$_{cos}$ [in 10^{-12} cc]	-	-	-				
±	-	-	-				

Table X35. Noble gas data He to Xe for sample DC 06_09_57 (1) (corrected for blank)

Sample		DC 06_09_57 (1)	
Size [μm]		74 x 36	
Weight [μg]		~ 0.15	
Date of measurement	24/10/12	**Date of measurement**	24/10/12
Laser-Power	1 x 0.91 W / 1 x 6.3 W / 1 x 6.3-30 W	**Laser-Power**	1 x 0.91 W / 1 x 6.3 W / 1 x 6.3-30 W
Laser-Beam	600 μm	**Laser-Beam**	600 μm
Step(s)	1	**Step(s)**	1
^{4}He [in 10^{-8} cc/g]	< 6411 (2σ)	^{132}Xe - INT [in 10^{-8} cc/g]	< 1.120 (2σ)
±	-	±	-
^{4}He [in 10^{-12} cc]	< 10 (2σ)	^{132}Xe - INT [in 10^{-12} cc]	< 0.002 (2σ)
±	-	±	-
^{3}He [in 10^{-12} cc/g]	< 36188 (2σ)	^{128}Xe/^{132}Xe - INT	-
±	-	±	-
^{3}He [in 10^{-16} cc]	< 54 (2σ)	^{129}Xe/^{132}Xe - INT	-
±	-	±	-
^{3}He/^{4}He	-	^{130}Xe/^{132}Xe - INT	-
±	-	±	-
^{22}Ne [in 10^{-8} cc/g]	< 46.91 (2σ)	^{131}Xe/^{132}Xe - INT	-
±	-	±	-
^{22}Ne [in 10^{-12} cc]	< 0.07 (2σ)	^{134}Xe/^{132}Xe - INT	-
±	-	±	-
^{20}Ne/^{22}Ne	-	^{136}Xe/^{132}Xe - INT	-
±	-	±	-
^{21}Ne/^{22}Ne	-	^{132}Xe - EXTa [in 10^{-8} cc/g]	< 1.120 (2σ)
±	-	±	-
^{21}Ne$_{cos}$ [in 10^{-8} cc/g]	-	^{132}Xe - EXTa [in 10^{-12} cc]	< 0.002 (2σ)
±	-	±	-
^{21}Ne$_{cos}$ [in 10^{-12} cc]	-	^{128}Xe/^{132}Xe - EXTa	-
±	-	±	-
^{20}Ne$_{trap}$ [in 10^{-8} cc/g]	< 863.9 (2σ)	^{129}Xe/^{132}Xe - EXTa	-
±	-	±	-
^{20}Ne$_{trap}$ [in 10^{-12} cc]	< 1.3 (2σ)	^{130}Xe/^{132}Xe - EXTa	-
±	-	±	-
^{36}Ar [in 10^{-8} cc/g]	199.37	^{131}Xe/^{132}Xe - EXTa	-
±	159.28	±	-
^{36}Ar [in 10^{-12} cc]	0.30	^{134}Xe/^{132}Xe - EXTa	-
±	0.13	±	-
^{38}Ar/^{36}Ar	0.173	^{136}Xe/^{132}Xe - EXTa	-
±	0.019	±	-
^{40}Ar/^{36}Ar	237.1	^{132}Xe - EXTb [in 10^{-8} cc/g]	< 0.818 (2σ)
±	34.4	±	-
^{40}Ar [in 10^{-8} cc/g]	53905.7	^{132}Xe - EXTb [in 10^{-12} cc]	< 0.001 (2σ)
±	41646.9	±	-
^{40}Ar [in 10^{-12} cc]	80.9	^{128}Xe/^{132}Xe - EXTb	-
±	31.6	±	-
^{38}Ar$_{cos}$ [in 10^{-8} cc/g]	-	^{129}Xe/^{132}Xe - EXTb	-
±	-	±	-
^{38}Ar$_{cos}$ [in 10^{-12} cc]	-	^{130}Xe/^{132}Xe - EXTb	-
±	-	±	-
^{84}Kr [in 10^{-8} cc/g]	< 8.356 (2σ)	^{131}Xe/^{132}Xe - EXTb	-
±	-	±	-
^{84}Kr [in 10^{-12} cc]	< 0.013 (2σ)	^{134}Xe/^{132}Xe - EXTb	-
±	-	±	-
^{80}Kr/^{84}Kr	-	^{136}Xe/^{132}Xe - EXTb	-
±	-	±	-
^{82}Kr/^{84}Kr	-	^{21}Ne$_{cos}$/^{38}Ar$_{cos}$	-
±	-	±	-
^{83}Kr/^{84}Kr	-	^{36}Ar/^{132}Xe $_{(Int)}$	-
±	-	±	-
^{86}Kr/^{84}Kr	-	^{84}Kr/^{132}Xe $_{(Int)}$	-
±	-	±	-
^{83}Kr$_{cos}$ [in 10^{-8} cc/g]	< 1.1382 (2σ)		
±	-		
^{83}Kr$_{cos}$ [in 10^{-12} cc]	< 0.0017 (2σ)		
±	-		

Table X36. Noble gas data He to Xe for sample DC 06_09_57 (2) (corrected for blank)

Sample		DC 06_09_57 (2)	
Size [μm]		19 x 18	
Weight [μg]		~ 0.05	
Date of measurement	25/10/12	**Date of measurement**	25/10/12
	1 x 0.91-18 W		1 x 0.91-18 W
Laser-Power	1 x 18 W	**Laser-Power**	1 x 18 W
	1 x 18-30 W		1 x 18-30 W
Laser-Beam	1000 / 180 / 2000 μm	**Laser-Beam**	1000 / 180 / 2000 μm
Step(s)	1	**Step(s)**	1
^{4}He [in 10^{-8} cc/g]	< 1829 (2σ)	^{132}Xe - INT [in 10^{-8} cc/g]	3.9241
±	-	±	2.2657
^{4}He [in 10^{-12} cc]	< 1 (2σ)	^{132}Xe - INT [in 10^{-12} cc]	0.0020
±	-	±	0.0011
^{3}He [in 10^{-12} cc/g]	1397290.0	^{128}Xe/^{132}Xe - INT	0.102
±	576893.0	±	0.064
^{3}He [in 10^{-16} cc]	698.6	^{129}Xe/^{132}Xe - INT	1.200
±	288.4	±	0.139
^{3}He/^{4}He	-	^{130}Xe/^{132}Xe - INT	0.135
±	-	±	0.048
^{22}Ne [in 10^{-8} cc/g]	< 12.60 (2σ)	^{131}Xe/^{132}Xe - INT	0.746
±	-	±	0.157
^{22}Ne [in 10^{-12} cc]	< 0.01 (2σ)	^{134}Xe/^{132}Xe - INT	0.312
±	-	±	0.078
^{20}Ne/^{22}Ne	-	^{136}Xe/^{132}Xe - INT	0.159
±	-	±	0.091
^{21}Ne/^{22}Ne	-	^{132}Xe - EXTa [in 10^{-8} cc/g]	3.9241
±	-	±	2.2657
^{21}Ne$_{cos}$ [in 10^{-8} cc/g]	-	^{132}Xe - EXTa [in 10^{-12} cc]	0.0020
±	-	±	0.0011
^{21}Ne$_{cos}$ [in 10^{-12} cc]	-	^{128}Xe/^{132}Xe - EXTa	0.104
±	-	±	0.031
^{20}Ne$_{trap}$ [in 10^{-8} cc/g]	< 252.6 (2σ)	^{129}Xe/^{132}Xe - EXTa	1.199
±	-	±	0.148
^{20}Ne$_{trap}$ [in 10^{-12} cc]	< 0.1 (2σ)	^{130}Xe/^{132}Xe - EXTa	0.119
±	-	±	0.045
^{36}Ar [in 10^{-8} cc/g]	5958.08	^{131}Xe/^{132}Xe - EXTa	0.747
±	2400.41	±	0.157
^{36}Ar [in 10^{-12} cc]	2.98	^{134}Xe/^{132}Xe - EXTa	0.346
±	1.20	±	0.068
^{38}Ar/^{36}Ar	0.150	^{136}Xe/^{132}Xe - EXTa	0.240
±	0.004	±	0.061
^{40}Ar/^{36}Ar	204.1	^{132}Xe - EXTb [in 10^{-8} cc/g]	3.8329
±	4.4	±	1.9463
^{40}Ar [in 10^{-8} cc/g]	1236210.0	^{132}Xe - EXTb [in 10^{-12} cc]	0.0019
±	499179.0	±	0.0010
^{40}Ar [in 10^{-12} cc]	618.1	^{128}Xe/^{132}Xe - EXTb	0.076
±	249.6	±	0.029
^{38}Ar$_{cos}$ [in 10^{-8} cc/g]	-	^{129}Xe/^{132}Xe - EXTb	1.196
±	-	±	0.148
^{38}Ar$_{cos}$ [in 10^{-12} cc]	-	^{130}Xe/^{132}Xe - EXTb	0.158
±	-	±	0.036
^{84}Kr [in 10^{-8} cc/g]	41.2497	^{131}Xe/^{132}Xe - EXTb	0.759
±	19.4745	±	0.095
^{84}Kr [in 10^{-12} cc]	0.0206	^{134}Xe/^{132}Xe - EXTb	0.342
±	0.0097	±	0.084
^{80}Kr/^{84}Kr	0.053	^{136}Xe/^{132}Xe - EXTb	0.244
±	0.007	±	0.054
^{82}Kr/^{84}Kr	0.215	^{21}Ne$_{cos}$/^{38}Ar$_{cos}$	-
±	0.023	±	-
^{83}Kr/^{84}Kr	0.201	^{36}Ar/^{132}Xe $_{(Int)}$	1518.31
±	0.018	±	1068.94
^{86}Kr/^{84}Kr	0.323	^{84}Kr/^{132}Xe $_{(Int)}$	10.51
±	0.030	±	7.84
^{83}Kr$_{cos}$ [in 10^{-8} cc/g]	-		
±	-		
^{83}Kr$_{cos}$ [in 10^{-12} cc]	-		
±	-		

Table X37. Noble gas data He to Xe for sample DC 06_09_63 (corrected for blank)

Sample			DC 06_09_63				
Size [μm]			198 x 141				
Weight [μg]			~ 3.3				
Date of measurement	16/01/12	17/01/12	16+17/01/12	**Date of measurement**	16/01/12	17/01/12	16+17/01/12
Laser-Power	3 x 0.91 W	3 x 5 W		**Laser-Power**	3 x 0.91 W	3 x 5 W	
Laser-Beam	250 μm	180 μm		**Laser-Beam**	250 μm	180 μm	
Step(s)	1	2	total*	**Step(s)**	1	2	total*
^{4}He [in 10^{-8} cc/g]	87331.4	8194.7	95526.0	^{132}Xe - INT [in 10^{-8} cc/g]	0.3326	0.2109	0.5435
±	3092.5	690.8	3168.7	±	0.0563	0.0553	0.0789
^{4}He [in 10^{-12} cc]	2881.9	270.4	3152.4	^{132}Xe - INT [in 10^{-12} cc]	0.0110	0.0070	0.0179
±	52.8	21.3	42.5	±	0.0018	0.0018	0.0025
^{3}He [in 10^{-12} cc/g]	384713.6	31454.7	416168.3	^{128}Xe/^{132}Xe - INT	0.091	0.072	0.084
±	56222.0	4739.8	56421.4	±	0.010	0.014	0.008
^{3}He [in 10^{-16} cc]	12695.6	1038.0	13733.6	^{129}Xe/^{132}Xe - INT	1.012	0.929	0.980
±	1815.0	153.2	1814.8	±	0.041	0.048	0.031
^{3}He/^{4}He	0.00044	0.00038	0.00044	^{130}Xe/^{132}Xe - INT	0.173	0.157	0.167
±	0.00006	0.00006	0.00006	±	0.008	0.011	0.006
^{22}Ne [in 10^{-8} cc/g]	53.216	3.535	56.751	^{131}Xe/^{132}Xe - INT	0.770	0.789	0.777
±	3.559	2.245	4.208	±	0.039	0.045	0.029
^{22}Ne [in 10^{-12} cc]	1.756	0.117	1.873	^{134}Xe/^{132}Xe - INT	0.370	0.365	0.368
±	0.105	0.074	0.127	±	0.019	0.027	0.016
^{20}Ne/^{22}Ne	11.88	11.11	11.83	^{136}Xe/^{132}Xe - INT	0.332	0.337	0.334
±	0.41	4.12	0.46	±	0.023	0.031	0.018
^{21}Ne/^{22}Ne	0.031	0.029	0.031	^{132}Xe - EXTa [in 10^{-8} cc/g]	0.3331	0.2112	0.5443
±	0.002	0.012	0.002	±	0.1120	0.0827	0.1392
^{21}Ne$_{cos}$ [in 10^{-8} cc/g]	< 0.252 (2σ)	< 0.251 (2σ)	-	^{132}Xe - EXTa [in 10^{-12} cc]	0.0110	0.0070	0.0180
±	-	-	-	±	0.0037	0.0027	0.0046
^{21}Ne$_{cos}$ [in 10^{-12} cc]	< 0.008 (2σ)	< 0.008 (2σ)	-	^{128}Xe/^{132}Xe - EXTa	0.082	0.073	0.078
±	-	-	-	±	0.008	0.013	0.007
^{20}Ne$_{trap}$ [in 10^{-8} cc/g]	628.4	< 1100.7 (2σ)	-	^{129}Xe/^{132}Xe - EXTa	1.006	0.922	0.973
±	58.5	-	-	±	0.044	0.055	0.034
^{20}Ne$_{trap}$ [in 10^{-12} cc]	20.7	< 36.3 (2σ)	-	^{130}Xe/^{132}Xe - EXTa	0.171	0.149	0.162
±	1.8	-	-	±	0.009	0.013	0.008
^{36}Ar [in 10^{-8} cc/g]	121.43	205.64	327.07	^{131}Xe/^{132}Xe - EXTa	0.773	0.796	0.782
±	10.28	11.76	15.62	±	0.039	0.045	0.029
^{36}Ar [in 10^{-12} cc]	4.01	6.79	10.79	^{134}Xe/^{132}Xe - EXTa	0.356	0.337	0.348
±	0.32	0.33	0.40	±	0.020	0.029	0.017
^{38}Ar/^{36}Ar	0.190	0.179	0.183	^{136}Xe/^{132}Xe - EXTa	0.320	0.321	0.320
±	0.004	0.002	0.002	±	0.016	0.023	0.013
^{40}Ar/^{36}Ar	41.9	246.0	170.2	^{132}Xe - EXTb [in 10^{-8} cc/g]	0.3071	0.1821	0.4891
±	12.9	3.1	6.0	±	0.0620	0.0511	0.0804
^{40}Ar [in 10^{-8} cc/g]	5085.3	50583.6	55668.9	^{132}Xe - EXTb [in 10^{-12} cc]	0.0101	0.0060	0.0161
±	2420.6	2984.9	3843.1	±	0.0020	0.0017	0.0026
^{40}Ar [in 10^{-12} cc]	167.8	1669.3	1837.1	^{128}Xe/^{132}Xe - EXTb	0.074	0.072	0.073
±	79.7	84.5	114.0	±	0.009	0.012	0.007
^{38}Ar$_{cos}$ [in 10^{-8} cc/g]	< 1.379 (2σ)	-	-	^{129}Xe/^{132}Xe - EXTb	0.999	0.898	0.961
±	-	-	-	±	0.051	0.072	0.042
^{38}Ar$_{cos}$ [in 10^{-12} cc]	< 0.045 (2σ)	-	-	^{130}Xe/^{132}Xe - EXTb	0.155	0.168	0.160
±	-	-	-	±	0.009	0.015	0.008
^{84}Kr [in 10^{-8} cc/g]	0.6333	1.4455	2.0787	^{131}Xe/^{132}Xe - EXTb	0.772	0.796	0.781
±	0.1497	0.1860	0.2387	±	0.018	0.029	0.016
^{84}Kr [in 10^{-12} cc]	0.0209	0.0477	0.0686	^{134}Xe/^{132}Xe - EXTb	0.363	0.370	0.366
±	0.0049	0.0060	0.0076	±	0.018	0.027	0.015
^{80}Kr/^{84}Kr	0.042	0.046	0.045	^{136}Xe/^{132}Xe - EXTb	0.340	0.361	0.348
±	0.006	0.003	0.003	±	0.018	0.027	0.015
^{82}Kr/^{84}Kr	0.210	0.217	0.215	^{21}Ne$_{cos}$/^{38}Ar$_{cos}$	-	-	-
±	0.016	0.009	0.008	±	-	-	-
^{83}Kr/^{84}Kr	0.200	0.209	0.206	^{36}Ar/^{132}Xe $_{(Int)}$	365.12	975.13	601.83
±	0.015	0.008	0.007	±	67.29	258.33	88.28
^{86}Kr/^{84}Kr	0.279	0.291	0.287	^{84}Kr/^{132}Xe $_{(Int)}$	1.90	6.85	3.83
±	0.020	0.011	0.010	±	0.55	1.98	0.69
^{83}Kr$_{cos}$ [in 10^{-8} cc/g]	-	< 0.0363 (2σ)	-				
±	-	-	-				
^{83}Kr$_{cos}$ [in 10^{-12} cc]	-	< 0.0012 (2σ)	-				
±	-	-	-				

Table X38. Noble gas data He to Xe for sample DC 06_09_141(1) (corrected for blank)

Sample		DC 06_09_141 (1)	
Size [µm]		84 x 79	
Weight [µg]		~ 0.7	
Date of measurement	24/10/12	**Date of measurement**	24/10/12
	1 x 0.91 W		1 x 0.91 W
Laser-Power	1 x 5 W	**Laser-Power**	1 x 5 W
	1 x 8-22 W		1 x 8-22 W
Laser-Beam	180 µm	**Laser-Beam**	180 µm
Step(s)	1	**Step(s)**	1
^{4}He [in 10^{-8} cc/g]	1241.5	^{132}Xe - INT [in 10^{-8} cc/g]	-
±	634.2	±	-
^{4}He [in 10^{-12} cc]	8.7	^{132}Xe - INT [in 10^{-12} cc]	-
±	4.3	±	-
^{3}He [in 10^{-12} cc/g]	62217.3	^{128}Xe/^{132}Xe - INT	-
±	13846.6	±	-
^{3}He [in 10^{-16} cc]	435.5	^{129}Xe/^{132}Xe - INT	-
±	74.3	±	-
^{3}He/^{4}He	0.00501	^{130}Xe/^{132}Xe - INT	-
±	0.00260	±	-
^{22}Ne [in 10^{-8} cc/g]	31.660	^{131}Xe/^{132}Xe - INT	-
±	5.690	±	-
^{22}Ne [in 10^{-12} cc]	0.222	^{134}Xe/^{132}Xe - INT	-
±	0.024	±	-
^{20}Ne/^{22}Ne	11.14	^{136}Xe/^{132}Xe - INT	-
±	0.85	±	-
^{21}Ne/^{22}Ne	0.025	^{132}Xe - EXTa [in 10^{-8} cc/g]	-
±	0.004	±	-
^{21}Ne$_{cos}$ [in 10^{-8} cc/g]	-	^{132}Xe - EXTa [in 10^{-12} cc]	-
±	-	±	-
^{21}Ne$_{cos}$ [in 10^{-12} cc]	-	^{128}Xe/^{132}Xe - EXTa	-
±	-	±	-
^{20}Ne$_{trap}$ [in 10^{-8} cc/g]	352.8	^{129}Xe/^{132}Xe - EXTa	-
±	71.7	±	-
^{20}Ne$_{trap}$ [in 10^{-12} cc]	2.5	^{130}Xe/^{132}Xe - EXTa	-
±	0.4	±	-
^{36}Ar [in 10^{-8} cc/g]	73.19	^{131}Xe/^{132}Xe - EXTa	-
±	21.55	±	-
^{36}Ar [in 10^{-12} cc]	0.51	^{134}Xe/^{132}Xe - EXTa	-
±	0.13	±	-
^{38}Ar/^{36}Ar	0.173	^{136}Xe/^{132}Xe - EXTa	-
±	0.012	±	-
^{40}Ar/^{36}Ar	141.6	^{132}Xe - EXTb [in 10^{-8} cc/g]	-
±	22.8	±	-
^{40}Ar [in 10^{-8} cc/g]	11781.9	^{132}Xe - EXTb [in 10^{-12} cc]	-
±	4816.4	±	-
^{40}Ar [in 10^{-12} cc]	82.5	^{128}Xe/^{132}Xe - EXTb	-
±	31.6	±	-
^{38}Ar$_{cos}$ [in 10^{-8} cc/g]	-	^{129}Xe/^{132}Xe - EXTb	-
±	-	±	-
^{38}Ar$_{cos}$ [in 10^{-12} cc]	-	^{130}Xe/^{132}Xe - EXTb	-
±	-	±	-
^{84}Kr [in 10^{-8} cc/g]	< 1.486 (2σ)	^{131}Xe/^{132}Xe - EXTb	-
±	-	±	-
^{84}Kr [in 10^{-12} cc]	< 0.010 (2σ)	^{134}Xe/^{132}Xe - EXTb	-
±	-	±	-
^{80}Kr/^{84}Kr	-	^{136}Xe/^{132}Xe - EXTb	-
±	-	±	-
^{82}Kr/^{84}Kr	-	^{21}Ne$_{cos}$/^{38}Ar$_{cos}$	-
±	-	±	-
^{83}Kr/^{84}Kr	-	^{36}Ar/^{132}Xe$_{(Int)}$	-
±	-	±	-
^{86}Kr/^{84}Kr	-	^{84}Kr/^{132}Xe$_{(Int)}$	-
±	-	±	-
^{83}Kr$_{cos}$ [in 10^{-8} cc/g]	-		
±	-		
^{83}Kr$_{cos}$ [in 10^{-12} cc]	-		
±	-		

Table X39. Noble gas data He to Xe for sample DC 06_09_149 (corrected for blank)

Sample		DC 06_09_149	
Size [μm]		85 x 60	
Weight [μg]		~ 0.3	
Date of measurement	23/10/12	**Date of measurement**	23/10/12
	1 x 0.91 W		1 x 0.91 W
Laser-Power	1 x 8 W	**Laser-Power**	1 x 8 W
	1 x 5-22 W		1 x 5-22 W
Laser-Beam	180 / 1000 / 180 μm	**Laser-Beam**	180 / 1000 / 180 μm
Step(s)	1	**Step(s)**	1
^{4}He [in 10^{-8} cc/g]	15973.0	^{132}Xe - INT [in 10^{-8} cc/g]	0.3535
±	5517.0	±	0.2957
^{4}He [in 10^{-12} cc]	47.9	^{132}Xe - INT [in 10^{-12} cc]	0.0011
±	4.3	±	0.0008
^{3}He [in 10^{-12} cc/g]	404248.9	^{128}Xe/^{132}Xe - INT	-
±	136585.3	±	-
^{3}He [in 10^{-16} cc]	1212.7	^{129}Xe/^{132}Xe - INT	0.911
±	67.0	±	0.210
^{3}He/^{4}He	0.00253	^{130}Xe/^{132}Xe - INT	0.124
±	0.00027	±	0.086
^{22}Ne [in 10^{-8} cc/g]	688.004	^{131}Xe/^{132}Xe - INT	0.898
±	229.749	±	0.254
^{22}Ne [in 10^{-12} cc]	2.064	^{134}Xe/^{132}Xe - INT	0.384
±	0.041	±	0.134
^{20}Ne/^{22}Ne	11.65	^{136}Xe/^{132}Xe - INT	0.513
±	0.14	±	0.182
^{21}Ne/^{22}Ne	0.032	^{132}Xe - EXTa [in 10^{-8} cc/g]	0.3535
±	0.001	±	0.2957
^{21}Ne$_{cos}$ [in 10^{-8} cc/g]	< 3.536 (2σ)	^{132}Xe - EXTa [in 10^{-12} cc]	0.0011
±	-	±	0.0008
^{21}Ne$_{cos}$ [in 10^{-12} cc]	< 0.023 (2σ)	^{128}Xe/^{132}Xe - EXTa	-
±	-	±	-
^{20}Ne$_{trap}$ [in 10^{-8} cc/g]	8015.0	^{129}Xe/^{132}Xe - EXTa	0.911
±	2714.5	±	0.230
^{20}Ne$_{trap}$ [in 10^{-12} cc]	24.0	^{130}Xe/^{132}Xe - EXTa	0.150
±	1.4	±	0.079
^{36}Ar [in 10^{-8} cc/g]	2881.42	^{131}Xe/^{132}Xe - EXTa	0.900
±	963.04	±	0.254
^{36}Ar [in 10^{-12} cc]	8.64	^{134}Xe/^{132}Xe - EXTa	0.278
±	0.21	±	0.111
^{38}Ar/^{36}Ar	0.186	^{136}Xe/^{132}Xe - EXTa	0.211
±	0.004	±	0.094
^{40}Ar/^{36}Ar	5.6	^{132}Xe - EXTb [in 10^{-8} cc/g]	0.4485
±	3.8	±	0.2440
^{40}Ar [in 10^{-8} cc/g]	19510.6	^{132}Xe - EXTb [in 10^{-12} cc]	0.0013
±	12370.0	±	0.0006
^{40}Ar [in 10^{-12} cc]	58.5	^{128}Xe/^{132}Xe - EXTb	0.108
±	31.6	±	0.039
^{38}Ar$_{cos}$ [in 10^{-8} cc/g]	-	^{129}Xe/^{132}Xe - EXTb	0.922
±	-	±	0.191
^{38}Ar$_{cos}$ [in 10^{-12} cc]	-	^{130}Xe/^{132}Xe - EXTb	0.095
±	-	±	0.046
^{84}Kr [in 10^{-8} cc/g]	3.1330	^{131}Xe/^{132}Xe - EXTb	0.907
±	2.0019	±	0.135
^{84}Kr [in 10^{-12} cc]	0.0094	^{134}Xe/^{132}Xe - EXTb	0.329
±	0.0051	±	0.115
^{80}Kr/^{84}Kr	0.062	^{136}Xe/^{132}Xe - EXTb	0.373
±	0.013	±	0.078
^{82}Kr/^{84}Kr	0.250	^{21}Ne$_{cos}$/^{38}Ar$_{cos}$	-
±	0.038	±	-
^{83}Kr/^{84}Kr	0.219	^{36}Ar/^{132}Xe $_{(Int)}$	8151.56
±	0.027	±	6257.76
^{86}Kr/^{84}Kr	0.333	^{84}Kr/^{132}Xe $_{(Int)}$	8.86
±	0.044	±	8.34
^{83}Kr$_{cos}$ [in 10^{-8} cc/g]	< 0.2479 (2σ)		
±	-		
^{83}Kr$_{cos}$ [in 10^{-12} cc]	< 0.0007 (2σ)		
±	-		

Table X40. Noble gas data He to Xe for sample DC 06_09_189 (corrected for blank)

Sample		DC 06_09_189	
Size [μm]		93 x 92	
Weight [μg]		~ 1.0	
Date of measurement	18/10/12	**Date of measurement**	18/10/12
	1 x 0.91 W		1 x 0.91 W
Laser-Power	1 x 25 W	**Laser-Power**	1 x 25 W
	1 x 21 W		1 x 21 W
Laser-Beam	180 / 1850 / 250 μm	**Laser-Beam**	180 / 1850 / 250 μm
Step(s)	1	**Step(s)**	1
^{4}He [in 10^{-8} cc/g]	479919.3	^{132}Xe - INT [in 10^{-8} cc/g]	17.2706
±	48471.5	±	1.7471
^{4}He [in 10^{-12} cc]	4799.2	^{132}Xe - INT [in 10^{-12} cc]	0.1727
±	68.0	±	0.0026
^{3}He [in 10^{-12} cc/g]	1562556.0	^{128}Xe/^{132}Xe - INT	0.073
±	159464.8	±	0.002
^{3}He [in 10^{-16} cc]	15625.6	^{129}Xe/^{132}Xe - INT	0.991
±	318.3	±	0.014
^{3}He/^{4}He	0.00033	^{130}Xe/^{132}Xe - INT	0.153
±	0.00001	±	0.002
^{22}Ne [in 10^{-8} cc/g]	309.073	^{131}Xe/^{132}Xe - INT	0.782
±	31.382	±	0.009
^{22}Ne [in 10^{-12} cc]	3.091	^{134}Xe/^{132}Xe - INT	0.386
±	0.054	±	0.005
^{20}Ne/^{22}Ne	11.89	^{136}Xe/^{132}Xe - INT	0.318
±	0.11	±	0.005
^{21}Ne/^{22}Ne	0.032	^{132}Xe - EXTa [in 10^{-8} cc/g]	17.3777
±	0.001	±	1.7577
^{21}Ne$_{cos}$ [in 10^{-8} cc/g]	0.480	^{132}Xe - EXTa [in 10^{-12} cc]	0.1738
±	0.358	±	0.0026
^{21}Ne$_{cos}$ [in 10^{-12} cc]	0.005	^{128}Xe/^{132}Xe - EXTa	0.071
±	0.004	±	0.002
^{20}Ne$_{trap}$ [in 10^{-8} cc/g]	3675.0	^{129}Xe/^{132}Xe - EXTa	0.991
±	425.7	±	0.011
^{20}Ne$_{trap}$ [in 10^{-12} cc]	36.7	^{130}Xe/^{132}Xe - EXTa	0.151
±	2.1	±	0.002
^{36}Ar [in 10^{-8} cc/g]	1458.11	^{131}Xe/^{132}Xe - EXTa	0.786
±	149.01	±	0.009
^{36}Ar [in 10^{-12} cc]	14.58	^{134}Xe/^{132}Xe - EXTa	0.385
±	0.31	±	0.004
^{38}Ar/^{36}Ar	0.185	^{136}Xe/^{132}Xe - EXTa	0.316
±	0.004	±	0.004
^{40}Ar/^{36}Ar	217.9	^{132}Xe - EXTb [in 10^{-8} cc/g]	17.0686
±	2.1	±	1.7737
^{40}Ar [in 10^{-8} cc/g]	318697.1	^{132}Xe - EXTb [in 10^{-12} cc]	0.1707
±	32722.3	±	0.0048
^{40}Ar [in 10^{-12} cc]	3187.0	^{128}Xe/^{132}Xe - EXTb	0.073
±	74.2	±	0.002
^{38}Ar$_{cos}$ [in 10^{-8} cc/g]	-	^{129}Xe/^{132}Xe - EXTb	0.991
±	-	±	0.011
^{38}Ar$_{cos}$ [in 10^{-12} cc]	-	^{130}Xe/^{132}Xe - EXTb	0.151
±	-	±	0.002
^{84}Kr [in 10^{-8} cc/g]	71.5792	^{131}Xe/^{132}Xe - EXTb	0.786
±	7.8362	±	0.004
^{84}Kr [in 10^{-12} cc]	0.7158	^{134}Xe/^{132}Xe - EXTb	0.391
±	0.0319	±	0.005
^{80}Kr/^{84}Kr	0.038	^{136}Xe/^{132}Xe - EXTb	0.324
±	0.001	±	0.004
^{82}Kr/^{84}Kr	0.195	^{21}Ne$_{cos}$/^{38}Ar$_{cos}$	-
±	0.007	±	-
^{83}Kr/^{84}Kr	0.196	^{36}Ar/^{132}Xe $_{(Int)}$	84.43
±	0.006	±	2.20
^{86}Kr/^{84}Kr	0.293	^{84}Kr/^{132}Xe $_{(Int)}$	4.14
±	0.008	±	0.20
^{83}Kr$_{cos}$ [in 10^{-8} cc/g]	-		
±	-		
^{83}Kr$_{cos}$ [in 10^{-12} cc]	-		
±	-		

C. Noble gas data for measured micrometeorites - not corrected for blank, corrected for isobaric interferences

Data tables for He to Xe - isotopic analysis for all measured micrometeorites.

Table X41. Noble gas data He to Xe for sample 45b.08_1 (not corrected for blank)

Sample	45b.08_1
Size [µm]	654 x 374
Weight [µg]	119.3 ± 0.1

Date of measure	24/10/11	25/10/11	26/10/11	24-27/10/11#
Laser-Power	3 x 0.13 W	3 x 0.91 W	3 x 5 W	
Laser-Beam	250 µm	600 µm	600 µm	
Step(s)	1	2	3	total*
^{4}He [in 10^{-8} cc/g]	27.7	174.7	14.5	216.9
±	0.5	3.4	0.3	3.4
^{4}He [in 10^{-12} cc]	33.0	208.4	17.3	258.7
±	0.6	4.0	0.3	4.1
^{3}He [in 10^{-12} cc/g]	-	343.8	458.6	802.4
±	-	115.1	92.4	147.6
^{3}He [in 10^{-16} cc]	-	410.1	547.1	957.2
±	-	137.3	110.3	176.1
^{3}He/^{4}He	-	0.00020	0.00316	0.00037
±	-	0.00007	0.00064	0.00007
^{22}Ne [in 10^{-8} cc/g]	0.039	0.129	1.612	1.779
±	0.014	0.013	0.027	0.033
^{22}Ne [in 10^{-12} cc]	0.047	0.153	1.923	2.123
±	0.016	0.015	0.032	0.039
^{20}Ne/^{22}Ne	7.37	7.49	5.29	5.49
±	2.56	0.73	0.08	0.10
^{21}Ne/^{22}Ne	0.017	0.264	0.545	0.513
±	0.008	0.027	0.009	0.009
^{21}Ne$_{cos}$ [in 10^{-8} cc/g]	-	0.031	0.855	0.886
±	-	0.004	0.020	0.021
^{21}Ne$_{cos}$ [in 10^{-12} cc]	-	0.037	1.020	1.058
±	-	0.005	0.024	0.025
^{20}Ne$_{trap}$ [in 10^{-8} cc/g]	-	0.93	7.81	8.74
±	-	0.14	0.49	0.51
^{20}Ne$_{trap}$ [in 10^{-12} cc]	-	1.11	9.32	10.43
±	-	0.17	0.58	0.60
^{36}Ar [in 10^{-8} cc/g]	0.78	1.60	1.15	3.53
±	0.02	0.04	0.03	0.05
^{36}Ar [in 10^{-12} cc]	0.93	1.91	1.37	4.21
±	0.02	0.04	0.03	0.06
^{38}Ar/^{36}Ar	0.179	0.195	0.221	0.200
±	0.004	0.002	0.003	0.002
^{40}Ar/^{36}Ar	262.2	315.0	173.2	257.1
±	2.3	1.9	1.3	1.1
^{40}Ar [in 10^{-8} cc/g]	203.6	504.0	199.3	906.9
±	4.7	11.5	4.6	13.3
^{40}Ar [in 10^{-12} cc]	242.9	601.3	237.7	1082.0
±	5.6	13.8	5.5	15.8
^{38}Ar$_{cos}$ [in 10^{-8} cc/g]	-	0.011	0.042	0.053
±	-	0.006	0.005	0.007
^{38}Ar$_{cos}$ [in 10^{-12} cc]	-	0.013	0.050	0.063
±	-	0.007	0.005	0.009
^{84}Kr [in 10^{-8} cc/g]	0.0314	0.3263	0.0289	0.3865
±	0.0032	0.0329	0.0029	0.0332
^{84}Kr [in 10^{-12} cc]	0.0374	0.3892	0.0344	0.4611
±	0.0038	0.0393	0.0035	0.0396
^{80}Kr/^{84}Kr	0.041	0.032	0.036	0.033
±	0.003	0.001	0.003	0.001
^{82}Kr/^{84}Kr	0.189	0.180	0.190	0.182
±	0.008	0.003	0.007	0.002
^{83}Kr/^{84}Kr	0.202	0.191	0.191	0.191
±	0.009	0.002	0.008	0.002
^{86}Kr/^{84}Kr	0.307	0.335	0.319	0.332
±	0.014	0.004	0.011	0.004
^{83}Kr$_{cos}$ [in 10^{-8} cc/g]	-	-	-	-
±	-	-	-	-
^{83}Kr$_{cos}$ [in 10^{-12} cc]	-	-	-	-
±	-	-	-	-

Date of measure	24/10/11	25/10/11	26/10/11	24-27/10/11#
Laser-Power	3 x 0.13 W	3 x 0.91 W	3 x 5 W	
Laser-Beam	250 µm	600 µm	600 µm	
Step(s)	1	2	3	total*
^{132}Xe - INT [in 10^{-8} cc/g]	-	0.0699	-	-
±	-	0.0031	-	-
^{132}Xe - INT [in 10^{-12} cc]	-	0.0833	-	-
±	-	0.0037	-	-
^{128}Xe/^{132}Xe - INT	-	0.065	-	-
±	-	0.002	-	-
^{129}Xe/^{132}Xe - INT	-	0.893	-	-
±	-	0.011	-	-
^{130}Xe/^{132}Xe - INT	-	0.145	-	-
±	-	0.002	-	-
^{131}Xe/^{132}Xe - INT	-	0.753	-	-
±	-	0.009	-	-
^{134}Xe/^{132}Xe - INT	-	0.408	-	-
±	-	0.006	-	-
^{136}Xe/^{132}Xe - INT	-	0.372	-	-
±	-	0.008	-	-
^{132}Xe - EXTa [in 10^{-8} cc/g]	-	0.0698	-	-
±	-	0.0019	-	-
^{132}Xe - EXTa [in 10^{-12} cc]	-	0.0833	-	-
±	-	0.0023	-	-
^{128}Xe/^{132}Xe - EXTa	-	0.063	-	-
±	-	0.001	-	-
^{129}Xe/^{132}Xe - EXTa	-	0.893	-	-
±	-	0.011	-	-
^{130}Xe/^{132}Xe - EXTa	-	0.145	-	-
±	-	0.003	-	-
^{131}Xe/^{132}Xe - EXTa	-	0.753	-	-
±	-	0.009	-	-
^{134}Xe/^{132}Xe - EXTa	-	0.406	-	-
±	-	0.005	-	-
^{136}Xe/^{132}Xe - EXTa	-	0.360	-	-
±	-	0.005	-	-
^{132}Xe - EXTb [in 10^{-8} cc/g]	-	0.0699	-	-
±	-	0.0022	-	-
^{132}Xe - EXTb [in 10^{-12} cc]	-	0.0833	-	-
±	-	0.0026	-	-
^{128}Xe/^{132}Xe - EXTb	-	0.063	-	-
±	-	0.002	-	-
^{129}Xe/^{132}Xe - EXTb	-	0.893	-	-
±	-	0.011	-	-
^{130}Xe/^{132}Xe - EXTb	-	0.143	-	-
±	-	0.003	-	-
^{131}Xe/^{132}Xe - EXTb	-	0.753	-	-
±	-	0.002	-	-
^{134}Xe/^{132}Xe - EXTb	-	0.410	-	-
±	-	0.005	-	-
^{136}Xe/^{132}Xe - EXTb	-	0.372	-	-
±	-	0.005	-	-
^{21}Ne$_{cos}$/^{38}Ar$_{cos}$	-	2.80	20.341	16.66
±	-	1.44	2.280	2.28
^{36}Ar/^{132}Xe $_{(Int)}$	-	22.91	-	-
±	-	1.13	-	-
^{84}Kr/^{132}Xe $_{(Int)}$	-	4.67	-	-
±	-	0.51	-	-

Table X42. Noble gas data He to Xe for sample 45b.09_1 (not corrected for blank)

Sample				45b.09_1			
Size [µm]				626 x 557			
Weight [µg]				126.9 ± 0.1			
Date of measure	18/07/11	18/07/11	18/07/11	**Date of measure**	18/07/11	18/07/11	18/07/11
Laser-Power	4 x 5 W	3 x 15 W		**Laser-Power**	4 x 5 W	3 x 15 W	
Laser-Beam	600 µm	600 µm		**Laser-Beam**	600 µm	600 µm	
Step(s)	1	2	total*	**Step(s)**	1	2	total*
^{4}He [in 10^{-8} cc/g]	26.7	3.1	29.8	^{132}Xe - INT [in 10^{-8} cc/g]	0.0829	0.0016	0.0844
±	1.3	0.2	1.3	±	0.0004	0.0001	0.0004
^{4}He [in 10^{-12} cc]	33.9	3.9	37.8	^{132}Xe - INT [in 10^{-12} cc]	0.1052	0.0020	0.1071
±	1.7	0.2	1.7	±	0.0005	0.0001	0.0005
^{3}He [in 10^{-12} cc/g]	< 3.9 (2σ)	-	-	^{128}Xe/^{132}Xe - INT	0.069	0.063	0.069
±	-	-	-	±	0.001	0.010	0.001
^{3}He [in 10^{-16} cc]	< 5.0 (2σ)	-	-	^{129}Xe/^{132}Xe - INT	0.932	0.960	0.933
±	-	-	-	±	0.010	0.063	0.010
^{3}He/^{4}He	-	-	-	^{130}Xe/^{132}Xe - INT	0.150	0.135	0.150
±	-	-	-	±	0.002	0.012	0.002
^{22}Ne [in 10^{-8} cc/g]	6.319	0.063	6.382	^{131}Xe/^{132}Xe - INT	0.769	0.741	0.769
±	0.105	0.007	0.105	±	0.008	0.054	0.008
^{22}Ne [in 10^{-12} cc]	8.019	0.080	8.099	^{134}Xe/^{132}Xe - INT	0.401	0.304	0.399
±	0.133	0.009	0.133	±	0.004	0.028	0.004
^{20}Ne/^{22}Ne	10.45	5.36	10.40	^{136}Xe/^{132}Xe - INT	0.356	0.230	0.354
±	0.16	0.58	0.16	±	0.005	0.029	0.005
^{21}Ne/^{22}Ne	0.128	0.027	0.127	^{132}Xe - EXTa [in 10^{-8} cc/g]	0.0811	0.0015	0.0826
±	0.001	0.008	0.001	±	0.0237	0.0005	0.0237
^{21}Ne$_{cos}$ [in 10^{-8} cc/g]	0.640	-	-	^{132}Xe - EXTa [in 10^{-12} cc]	0.1029	0.0020	0.1048
±	0.018	-	-	±	0.0300	0.0006	0.0301
^{21}Ne$_{cos}$ [in 10^{-12} cc]	0.812	-	-	^{128}Xe/^{132}Xe - EXTa	0.067	0.075	0.067
±	0.023	-	-	±	0.001	0.012	0.001
^{20}Ne$_{trap}$ [in 10^{-8} cc/g]	65.6	0.34	65.90	^{129}Xe/^{132}Xe - EXTa	0.934	0.961	0.935
±	3.9	0.06	3.92	±	0.009	0.063	0.009
^{20}Ne$_{trap}$ [in 10^{-12} cc]	83.2	0.43	83.62	^{130}Xe/^{132}Xe - EXTa	0.148	0.132	0.147
±	5.0	0.07	4.97	±	0.002	0.015	0.002
^{36}Ar [in 10^{-8} cc/g]	4.98	0.16	5.14	^{131}Xe/^{132}Xe - EXTa	0.776	0.747	0.775
±	0.20	0.01	0.20	±	0.008	0.054	0.008
^{36}Ar [in 10^{-12} cc]	6.32	0.20	6.52	^{134}Xe/^{132}Xe - EXTa	0.401	0.356	0.400
±	0.26	0.01	0.26	±	0.004	0.027	0.004
^{38}Ar/^{36}Ar	0.194	0.180	0.193	^{136}Xe/^{132}Xe - EXTa	0.355	0.343	0.355
±	0.003	0.010	0.002	±	0.004	0.027	0.004
^{40}Ar/^{36}Ar	71.5	251.7	77.0	^{132}Xe - EXTb [in 10^{-8} cc/g]	0.0804	0.0015	0.0819
±	1.5	7.3	1.4	±	0.0237	0.0005	0.0237
^{40}Ar [in 10^{-8} cc/g]	356.3	39.7	395.9	^{132}Xe - EXTb [in 10^{-12} cc]	0.1020	0.0019	0.1039
±	16.2	1.8	16.3	±	0.0301	0.0006	0.0301
^{40}Ar [in 10^{-12} cc]	452.1	50.3	502.4	^{128}Xe/^{132}Xe - EXTb	0.067	0.059	0.067
±	20.6	2.3	20.7	±	0.001	0.010	0.001
^{38}Ar$_{cos}$ [in 10^{-8} cc/g]	0.028	-	-	^{129}Xe/^{132}Xe - EXTb	0.935	0.962	0.936
±	0.018	-	-	±	0.009	0.063	0.009
^{38}Ar$_{cos}$ [in 10^{-12} cc]	0.036	-	-	^{130}Xe/^{132}Xe - EXTb	0.147	0.163	0.147
±	0.023	-	-	±	0.002	0.019	0.002
^{84}Kr [in 10^{-8} cc/g]	0.1898	0.0047	0.1944	^{131}Xe/^{132}Xe - EXTb	0.776	0.747	0.775
±	0.0082	0.0003	0.0082	±	0.002	0.002	0.002
^{84}Kr [in 10^{-12} cc]	0.2408	0.0060	0.2468	^{134}Xe/^{132}Xe - EXTb	0.406	0.310	0.404
±	0.0104	0.0003	0.0105	±	0.004	0.028	0.004
^{80}Kr/^{84}Kr	0.035	0.051	0.035	^{136}Xe/^{132}Xe - EXTb	0.361	0.275	0.360
±	0.001	0.009	0.001	±	0.004	0.028	0.004
^{82}Kr/^{84}Kr	0.186	0.193	0.186	^{21}Ne$_{cos}$/^{38}Ar$_{cos}$	22.49	-	-
±	0.003	0.019	0.003	±	14.51	-	-
^{83}Kr/^{84}Kr	0.199	0.208	0.199	^{36}Ar/^{132}Xe $_{(Int)}$	60.12	100.14	60.86
±	0.003	0.018	0.003	±	2.46	5.87	2.42
^{86}Kr/^{84}Kr	0.327	0.283	0.326	^{84}Kr/^{132}Xe $_{(Int)}$	2.29	2.98	2.30
±	0.004	0.026	0.004	±	0.10	0.20	0.10
^{83}Kr$_{cos}$ [in 10^{-8} cc/g]	-	-	-				
±	-	-	-				
^{83}Kr$_{cos}$ [in 10^{-12} cc]	-	-	-				
±	-	-	-				

Table X43. *Noble gas data He to Xe for sample 45b.10_2 (not corrected for blank)*

Sample				45b.10_2			
Size [µm]				494 x 418			
Weight [µg]				95.5 ± 0.1			
Date of measure	17/10/12	18/10/12	17+18/10/12	**Date of measure**	17/10/12	18/10/12	17+18/10/12
Laser-Power	3 x 0.91 W	2 x 15 W 1 x 5-20 W		**Laser-Power**	3 x 0.91 W	2 x 15 W 1 x 5-20 W	
Laser-Beam	360 µm	360 µm		**Laser-Beam**	360 µm	360 µm	
Step(s)	1	2	total*	**Step(s)**	1	2	total*
^{4}He [in 10^{-8} cc/g]	23.8	5.1	28.9	^{132}Xe - INT [in 10^{-8} cc/g]	0.0410	-	-
±	0.5	0.2	0.5	±	0.0006	-	-
^{4}He [in 10^{-12} cc]	22.7	4.9	27.6	^{132}Xe - INT [in 10^{-12} cc]	0.0392	-	-
±	0.4	0.2	0.5	±	0.0006	-	-
^{3}He [in 10^{-12} cc/g]	680.6	< 58.0 (2σ)	-	^{128}Xe/^{132}Xe - INT	0.062	-	-
±	72.0	-	-	±	0.002	-	-
^{3}He [in 10^{-16} cc]	650.0	< 55.4 (2σ)	-	^{129}Xe/^{132}Xe - INT	0.919	-	-
±	68.8	-	-	±	0.016	-	-
^{3}He/^{4}He	0.00287	-	-	^{130}Xe/^{132}Xe - INT	0.147	-	-
±	0.00031	-	-	±	0.003	-	-
^{22}Ne [in 10^{-8} cc/g]	0.163	0.037	0.200	^{131}Xe/^{132}Xe - INT	0.806	-	-
±	0.009	0.007	0.012	±	0.016	-	-
^{22}Ne [in 10^{-12} cc]	0.156	0.036	0.191	^{134}Xe/^{132}Xe - INT	0.403	-	-
±	0.009	0.007	0.011	±	0.009	-	-
^{20}Ne/^{22}Ne	7.63	6.86	7.49	^{136}Xe/^{132}Xe - INT	0.361	-	-
±	0.41	1.28	0.41	±	0.011	-	-
^{21}Ne/^{22}Ne	0.240	0.014	0.198	^{132}Xe - EXTa [in 10^{-8} cc/g]	0.0410	-	-
±	0.019	0.007	0.016	±	0.0006	-	-
^{21}Ne$_{cos}$ [in 10^{-8} cc/g]	0.035	-	-	^{132}Xe - EXTa [in 10^{-12} cc]	0.0392	-	-
±	0.004	-	-	±	0.0006	-	-
^{21}Ne$_{cos}$ [in 10^{-12} cc]	0.034	-	-	^{128}Xe/^{132}Xe - EXTa	0.063	-	-
±	0.003	-	-	±	0.002	-	-
^{20}Ne$_{trap}$ [in 10^{-8} cc/g]	1.2	0.26	1.47	^{129}Xe/^{132}Xe - EXTa	0.919	-	-
±	0.1	0.07	0.14	±	0.015	-	-
^{20}Ne$_{trap}$ [in 10^{-12} cc]	1.2	0.24	1.40	^{130}Xe/^{132}Xe - EXTa	0.143	-	-
±	0.1	0.07	0.13	±	0.004	-	-
^{36}Ar [in 10^{-8} cc/g]	12.57	0.41	12.98	^{131}Xe/^{132}Xe - EXTa	0.806	-	-
±	0.24	0.01	0.24	±	0.016	-	-
^{36}Ar [in 10^{-12} cc]	12.00	0.39	12.39	^{134}Xe/^{132}Xe - EXTa	0.390	-	-
±	0.23	0.01	0.23	±	0.008	-	-
^{38}Ar/^{36}Ar	0.177	0.176	0.177	^{136}Xe/^{132}Xe - EXTa	0.339	-	-
±	0.005	0.005	0.004	±	0.009	-	-
^{40}Ar/^{36}Ar	312.0	282.6	311.0	^{132}Xe - EXTb [in 10^{-8} cc/g]	0.0404	-	-
±	2.9	4.4	2.8	±	0.0012	-	-
^{40}Ar [in 10^{-8} cc/g]	3921.1	115.1	4036.2	^{132}Xe - EXTb [in 10^{-12} cc]	0.0386	-	-
±	82.7	2.6	82.8	±	0.0011	-	-
^{40}Ar [in 10^{-12} cc]	3744.6	109.9	3854.5	^{128}Xe/^{132}Xe - EXTb	0.072	-	-
±	78.9	2.5	79.0	±	0.003	-	-
^{38}Ar$_{cos}$ [in 10^{-8} cc/g]	-	-	-	^{129}Xe/^{132}Xe - EXTb	0.919	-	-
±	-	-	-	±	0.016	-	-
^{38}Ar$_{cos}$ [in 10^{-12} cc]	-	-	-	^{130}Xe/^{132}Xe - EXTb	0.155	-	-
±	-	-	-	±	0.004	-	-
^{84}Kr [in 10^{-8} cc/g]	0.4358	0.0097	0.4455	^{131}Xe/^{132}Xe - EXTb	0.806	-	-
±	0.0193	0.0005	0.0194	±	0.004	-	-
^{84}Kr [in 10^{-12} cc]	0.4162	0.0093	0.4254	^{134}Xe/^{132}Xe - EXTb	0.412	-	-
±	0.0185	0.0005	0.0185	±	0.008	-	-
^{80}Kr/^{84}Kr	0.035	0.056	0.036	^{136}Xe/^{132}Xe - EXTb	0.355	-	-
±	0.001	0.009	0.001	±	0.008	-	-
^{82}Kr/^{84}Kr	0.188	0.225	0.189	^{21}Ne$_{cos}$/^{38}Ar$_{cos}$	-	-	-
±	0.007	0.020	0.006	±	-	-	-
^{83}Kr/^{84}Kr	0.196	0.205	0.197	^{36}Ar/^{132}Xe $_{(Int)}$	306.43	-	-
±	0.006	0.019	0.006	±	7.50	-	-
^{86}Kr/^{84}Kr	0.299	0.289	0.298	^{84}Kr/^{132}Xe $_{(Int)}$	10.62	-	-
±	0.009	0.029	0.009	±	0.50	-	-
^{83}Kr$_{cos}$ [in 10^{-8} cc/g]	-	-	-				
±	-	-	-				
^{83}Kr$_{cos}$ [in 10^{-12} cc]	-	-	-				
±	-	-	-				

Table X44. Noble gas data He to Xe for sample 45b.13_1 (not corrected for blank)

Sample	45b.13_1						
Size [µm]	547 x 455						
Weight [µg]	137.6 ± 0.1						
Date of measure	20/07/11	21/07/11	20+21/07/12	**Date of measure**	20/07/11	21/07/11	20+21/07/12
Laser-Power	3 x 5 W	3 x 15 W		**Laser-Power**	3 x 5 W	3 x 15 W	
Laser-Beam	600 µm	600 µm		**Laser-Beam**	600 µm	600 µm	
Step(s)	1	2	total*	**Step(s)**	1	2	total*
^{4}He [in 10^{-8} cc/g]	9.1	3.2	12.4	^{132}Xe - INT [in 10^{-8} cc/g]	0.2953	0.0017	0.2970
±	0.5	0.2	0.5	±	0.0225	0.0001	0.0225
^{4}He [in 10^{-12} cc]	12.6	4.4	17.0	^{132}Xe - INT [in 10^{-12} cc]	0.4063	0.0023	0.4086
±	0.6	0.2	0.7	±	0.0310	0.0002	0.0310
^{3}He [in 10^{-12} cc/g]	6.1	-	-	^{128}Xe/^{132}Xe - INT	0.067	0.104	0.067
±	2.3	-	-	±	0.001	0.014	0.001
^{3}He [in 10^{-16} cc]	8.4	-	-	^{129}Xe/^{132}Xe - INT	0.931	0.985	0.931
±	3.1	-	-	±	0.007	0.065	0.007
^{3}He/^{4}He	0.00007	-	-	^{130}Xe/^{132}Xe - INT	0.148	0.158	0.148
±	0.00003	-	-	±	0.001	0.011	0.001
^{22}Ne [in 10^{-8} cc/g]	2.554	0.049	2.602	^{131}Xe/^{132}Xe - INT	0.764	0.699	0.764
±	0.043	0.006	0.044	±	0.005	0.053	0.005
^{22}Ne [in 10^{-12} cc]	3.514	0.067	3.581	^{134}Xe/^{132}Xe - INT	0.397	0.436	0.397
±	0.060	0.008	0.060	±	0.002	0.030	0.002
^{20}Ne/^{22}Ne	12.02	6.23	11.91	^{136}Xe/^{132}Xe - INT	0.349	0.408	0.349
±	0.19	0.77	0.19	±	0.003	0.039	0.003
^{21}Ne/^{22}Ne	0.032	0.018	0.032	^{132}Xe - EXTa [in 10^{-8} cc/g]	0.2889	0.0016	0.2905
±	0.001	0.004	0.001	±	0.0844	0.0005	0.0844
^{21}Ne$_{cos}$ [in 10^{-8} cc/g]	0.004	-	-	^{132}Xe - EXTa [in 10^{-12} cc]	0.3975	0.0022	0.3997
±	0.002	-	-	±	0.1161	0.0007	0.1161
^{21}Ne$_{cos}$ [in 10^{-12} cc]	0.006	-	-	^{128}Xe/^{132}Xe - EXTa	0.066	0.091	0.066
±	0.003	-	-	±	0.001	0.010	0.001
^{20}Ne$_{trap}$ [in 10^{-8} cc/g]	30.7	0.30	31.00	^{129}Xe/^{132}Xe - EXTa	0.931	0.986	0.932
±	1.8	0.06	1.83	±	0.006	0.065	0.006
^{20}Ne$_{trap}$ [in 10^{-12} cc]	42.2	0.42	42.65	^{130}Xe/^{132}Xe - EXTa	0.147	0.146	0.147
±	2.5	0.08	2.52	±	0.001	0.014	0.001
^{36}Ar [in 10^{-8} cc/g]	18.53	0.50	19.03	^{131}Xe/^{132}Xe - EXTa	0.771	0.705	0.770
±	0.75	0.02	0.75	±	0.005	0.053	0.005
^{36}Ar [in 10^{-12} cc]	25.49	0.69	26.18	^{134}Xe/^{132}Xe - EXTa	0.399	0.367	0.399
±	1.04	0.03	1.04	±	0.002	0.024	0.002
^{38}Ar/^{36}Ar	0.190	0.174	0.190	^{136}Xe/^{132}Xe - EXTa	0.356	0.333	0.355
±	0.002	0.004	0.002	±	0.002	0.024	0.002
^{40}Ar/^{36}Ar	217.4	258.8	218.4	^{132}Xe - EXTb [in 10^{-8} cc/g]	0.2882	0.0015	0.2897
±	4.5	5.6	4.4	±	0.0850	0.0004	0.0850
^{40}Ar [in 10^{-8} cc/g]	4026.7	129.3	4156.0	^{132}Xe - EXTb [in 10^{-12} cc]	0.3965	0.0021	0.3986
±	183.3	5.9	183.4	±	0.1170	0.0006	0.1170
^{40}Ar [in 10^{-12} cc]	5540.8	177.9	5718.6	^{128}Xe/^{132}Xe - EXTb	0.066	0.067	0.066
±	252.2	8.1	252.4	±	0.001	0.011	0.001
^{38}Ar$_{cos}$ [in 10^{-8} cc/g]	< 0.164 (2σ)	-	-	^{129}Xe/^{132}Xe - EXTb	0.932	0.987	0.933
±	-	-	-	±	0.006	0.065	0.006
^{38}Ar$_{cos}$ [in 10^{-12} cc]	< 0.226 (2σ)	-	-	^{130}Xe/^{132}Xe - EXTb	0.147	0.150	0.147
±	-	-	-	±	0.001	0.013	0.001
^{84}Kr [in 10^{-8} cc/g]	1.0656	0.0103	1.0759	^{131}Xe/^{132}Xe - EXTb	0.771	0.705	0.770
±	0.0460	0.0005	0.0460	±	0.002	0.002	0.002
^{84}Kr [in 10^{-12} cc]	1.4663	0.0141	1.4804	^{134}Xe/^{132}Xe - EXTb	0.399	0.472	0.400
±	0.0633	0.0007	0.0633	±	0.003	0.029	0.003
^{80}Kr/^{84}Kr	0.036	0.047	0.036	^{136}Xe/^{132}Xe - EXTb	0.354	0.372	0.354
±	0.000	0.006	0.000	±	0.002	0.027	0.002
^{82}Kr/^{84}Kr	0.190	0.202	0.190	^{21}Ne$_{cos}$/^{38}Ar$_{cos}$	-	-	-
±	0.001	0.011	0.001	±	-	-	-
^{83}Kr/^{84}Kr	0.196	0.198	0.196	^{36}Ar/^{132}Xe $_{(Int)}$	62.73	301.94	64.07
±	0.001	0.012	0.001	±	5.42	27.83	5.48
^{86}Kr/^{84}Kr	0.326	0.297	0.326	^{84}Kr/^{132}Xe $_{(Int)}$	3.61	6.20	3.62
±	0.002	0.014	0.002	±	0.32	0.59	0.32
^{83}Kr$_{cos}$ [in 10^{-8} cc/g]	-	-	-				
±	-	-	-				
^{83}Kr$_{cos}$ [in 10^{-12} cc]	-	-	-				
±	-	-	-				

Table X45. Noble gas data He to Xe for sample 45b.14_1 (not corrected for blank)

Sample				45b.14_1			
Size [µm]				514 x 432			
Weight [µg]				56.5 ± 0.1			
Date of measure	03/10/12	04/10/12	03+04/10/12	**Date of measure**	03/10/12	04/10/12	03+04/10/12
Laser-Power	3 x 0.91 W	2 x 5 W / 1 x 5 - 27 W		**Laser-Power**	3 x 0.91 W	2 x 5 W / 1 x 5 - 27 W	
Laser-Beam	600 µm	600 µm		**Laser-Beam**	600 µm	600 µm	
Step(s)	1	2	total*	**Step(s)**	1	2	total*
^{4}He [in 10^{-8} cc/g]	10.0	12.6	22.5	^{132}Xe - INT [in 10^{-8} cc/g]	$	$	-
±	0.5	0.2	0.5	±	$	$	-
^{4}He [in 10^{-12} cc]	5.6	7.1	12.7	^{132}Xe - INT [in 10^{-12} cc]	0.0084	0.0020	0.0103
±	0.3	0.1	0.3	±	0.0002	0.0001	0.0002
^{3}He [in 10^{-12} cc/g]	-	542.9	-	^{128}Xe/^{132}Xe - INT	0.066	0.103	0.073
±	-	146.8	-	±	0.006	0.017	0.006
^{3}He [in 10^{-16} cc]	-	306.7	-	^{129}Xe/^{132}Xe - INT	0.971	0.987	0.974
±	-	82.9	-	±	0.048	0.096	0.043
^{3}He/^{4}He	-	0.00432	-	^{130}Xe/^{132}Xe - INT	0.130	0.147	0.133
±	-	0.00117	-	±	0.007	0.015	0.006
^{22}Ne [in 10^{-8} cc/g]	0.088	0.080	0.168	^{131}Xe/^{132}Xe - INT	0.798	0.620	0.765
±	0.018	0.016	0.024	±	0.037	0.058	0.032
^{22}Ne [in 10^{-12} cc]	0.050	0.045	0.095	^{134}Xe/^{132}Xe - INT	0.378	0.366	0.375
±	0.010	0.009	0.013	±	0.020	0.038	0.017
^{20}Ne/^{22}Ne	5.80	6.12	5.95	^{136}Xe/^{132}Xe - INT	0.319	0.328	0.321
±	1.18	1.20	0.84	±	0.022	0.043	0.020
^{21}Ne/^{22}Ne	0.022	0.021	0.021	^{132}Xe - EXTa [in 10^{-8} cc/g]	0.0148	0.0035	0.0183
±	0.007	0.006	0.005	±	0.0004	0.0001	0.0004
^{21}Ne$_{cos}$ [in 10^{-8} cc/g]	-	< 1.947 (2σ)	-	^{132}Xe - EXTa [in 10^{-12} cc]	0.0084	0.0020	0.0103
±	-	-	-	±	0.0002	0.0001	0.0002
^{21}Ne$_{cos}$ [in 10^{-12} cc]	-	< 1.100 (2σ)	-	^{128}Xe/^{132}Xe - EXTa	0.072	0.104	0.078
±	-	-	-	±	0.007	0.015	0.006
^{20}Ne$_{trap}$ [in 10^{-8} cc/g]	0.5	0.47	0.98	^{129}Xe/^{132}Xe - EXTa	0.971	0.988	0.974
±	0.2	0.14	0.21	±	0.048	0.096	0.043
^{20}Ne$_{trap}$ [in 10^{-12} cc]	0.3	0.27	0.55	^{130}Xe/^{132}Xe - EXTa	0.128	0.128	0.128
±	0.1	0.08	0.12	±	0.009	0.018	0.008
^{36}Ar [in 10^{-8} cc/g]	0.96	0.56	1.52	^{131}Xe/^{132}Xe - EXTa	0.802	0.623	0.768
±	0.02	0.01	0.02	±	0.037	0.058	0.032
^{36}Ar [in 10^{-12} cc]	0.54	0.32	0.86	^{134}Xe/^{132}Xe - EXTa	0.388	0.339	0.379
±	0.01	0.01	0.01	±	0.017	0.034	0.015
^{38}Ar/^{36}Ar	0.179	0.180	0.179	^{136}Xe/^{132}Xe - EXTa	0.341	0.277	0.329
±	0.005	0.006	0.004	±	0.017	0.029	0.015
^{40}Ar/^{36}Ar	294.3	278.8	288.6	^{132}Xe - EXTb [in 10^{-8} cc/g]	0.0149	0.0032	0.0181
±	4.1	5.4	3.3	±	0.0005	0.0002	0.0005
^{40}Ar [in 10^{-8} cc/g]	281.9	155.5	437.4	^{132}Xe - EXTb [in 10^{-12} cc]	0.0084	0.0018	0.0102
±	6.2	3.7	7.2	±	0.0003	0.0001	0.0003
^{40}Ar [in 10^{-12} cc]	159.3	87.9	247.2	^{128}Xe/^{132}Xe - EXTb	0.075	0.071	0.074
±	3.5	2.1	4.1	±	0.007	0.014	0.006
^{38}Ar$_{cos}$ [in 10^{-8} cc/g]	-	-	-	^{129}Xe/^{132}Xe - EXTb	0.971	0.987	0.974
±	-	-	-	±	0.048	0.096	0.043
^{38}Ar$_{cos}$ [in 10^{-12} cc]	-	-	-	^{130}Xe/^{132}Xe - EXTb	0.146	0.176	0.151
±	-	-	-	±	0.009	0.020	0.008
^{84}Kr [in 10^{-8} cc/g]	0.0287	0.0094	0.0380	^{131}Xe/^{132}Xe - EXTb	0.802	0.623	0.771
±	0.0014	0.0006	0.0015	±	0.004	0.003	0.003
^{84}Kr [in 10^{-12} cc]	0.0162	0.0053	0.0215	^{134}Xe/^{132}Xe - EXTb	0.379	0.401	0.383
±	0.0008	0.0003	0.0009	±	0.018	0.037	0.017
^{80}Kr/^{84}Kr	0.049	0.078	0.056	^{136}Xe/^{132}Xe - EXTb	0.333	0.342	0.335
±	0.006	0.012	0.005	±	0.016	0.032	0.014
^{82}Kr/^{84}Kr	0.221	0.198	0.216	^{21}Ne$_{cos}$/^{38}Ar$_{cos}$	-	-	-
±	0.015	0.020	0.012	±	-	-	-
^{83}Kr/^{84}Kr	0.197	0.193	0.196	^{36}Ar/^{132}Xe $_{(Int)}$	64.64	160.86	82.88
±	0.013	0.018	0.011	±	2.08	7.72	2.20
^{86}Kr/^{84}Kr	0.279	0.252	0.272	^{84}Kr/^{132}Xe $_{(Int)}$	1.93	2.70	2.08
±	0.023	0.036	0.020	±	0.11	0.20	0.10
^{83}Kr$_{cos}$ [in 10^{-8} cc/g]	-	-	-				
±	-	-	-				
^{83}Kr$_{cos}$ [in 10^{-12} cc]	-	-	-				
±	-	-	-				

Table X46. Noble gas data He to Xe for sample 45b.15_1 (not corrected for blank)

Sample	45b.15_1		
Size [µm]	422 x 300		
Weight [µg]	30.3 ± 0.1		
Date of measure	17/09/12	18/09/12	17+18/09/12
Laser-Power	3 x 0.91 W	3 x 5 W	
Laser-Beam	600-360 µm	360 µm	
Step(s)	1	2	total*
^{4}He [in 10^{-8} cc/g]	236.8	15.9	252.6
±	9.3	0.9	9.3
^{4}He [in 10^{-12} cc]	71.7	4.8	76.5
±	2.8	0.3	2.8
^{3}He [in 10^{-12} cc/g]	386.7	< 182.2 (2σ)	-
±	61.4	-	-
^{3}He [in 10^{-16} cc]	117.2	< 55.2 (2σ)	-
±	18.6	-	-
^{3}He/^{4}He	0.00016	-	-
±	0.00003	-	-
^{22}Ne [in 10^{-8} cc/g]	0.503	0.261	0.765
±	0.045	0.043	0.063
^{22}Ne [in 10^{-12} cc]	0.153	0.079	0.232
±	0.014	0.013	0.019
^{20}Ne/^{22}Ne	8.83	8.23	8.63
±	0.79	1.35	0.70
^{21}Ne/^{22}Ne	0.029	0.031	0.029
±	0.005	0.007	0.004
^{21}Ne$_{cos}$ [in 10^{-8} cc/g]	-	< 0.011 (2σ)	-
±	-	-	-
^{21}Ne$_{cos}$ [in 10^{-12} cc]	-	< 0.003 (2σ)	-
±	-	-	-
^{20}Ne$_{trap}$ [in 10^{-8} cc/g]	4.4	2.10	6.55
±	0.6	0.52	0.81
^{20}Ne$_{trap}$ [in 10^{-12} cc]	1.3	0.64	1.98
±	0.2	0.16	0.24
^{36}Ar [in 10^{-8} cc/g]	23.65	1.16	24.81
±	0.46	0.03	0.46
^{36}Ar [in 10^{-12} cc]	7.17	0.35	7.52
±	0.14	0.01	0.14
^{38}Ar/^{36}Ar	0.187	0.204	0.188
±	0.003	0.009	0.003
^{40}Ar/^{36}Ar	27.3	163.3	33.7
±	0.3	3.1	0.3
^{40}Ar [in 10^{-8} cc/g]	646.0	189.2	835.2
±	14.3	4.0	14.9
^{40}Ar [in 10^{-12} cc]	195.7	57.3	253.1
±	4.3	1.2	4.4
^{38}Ar$_{cos}$ [in 10^{-8} cc/g]	-	0.020	-
±	-	0.011	-
^{38}Ar$_{cos}$ [in 10^{-12} cc]	-	0.006	-
±	-	0.003	-
^{84}Kr [in 10^{-8} cc/g]	0.5048	0.0187	0.5235
±	0.0374	0.0016	0.0374
^{84}Kr [in 10^{-12} cc]	0.1530	0.0057	0.1586
±	0.0113	0.0005	0.0113
^{80}Kr/^{84}Kr	0.042	0.091	0.044
±	0.002	0.016	0.002
^{82}Kr/^{84}Kr	0.201	0.268	0.203
±	0.012	0.034	0.011
^{83}Kr/^{84}Kr	0.197	0.205	0.198
±	0.009	0.021	0.009
^{86}Kr/^{84}Kr	0.305	0.309	0.305
±	0.016	0.042	0.015
^{83}Kr$_{cos}$ [in 10^{-8} cc/g]	-	-	-
±	-	-	-
^{83}Kr$_{cos}$ [in 10^{-12} cc]	-	-	-
±	-	-	-

Date of measure	17/09/12	18/09/12	17+18/09/12
Laser-Power	3 x 0.91 W	3 x 5 W	
Laser-Beam	600-360 µm	360 µm	
Step(s)	1	2	total*
^{132}Xe - INT [in 10^{-8} cc/g]	0.7735	$	-
±	0.0109	$	-
^{132}Xe - INT [in 10^{-12} cc]	0.2344	0.0039	0.2344
±	0.0032	0.0001	0.0032
^{128}Xe/^{132}Xe - INT	0.080	0.137	0.080
±	0.002	0.017	0.002
^{129}Xe/^{132}Xe - INT	1.036	0.955	1.036
±	0.011	0.061	0.011
^{130}Xe/^{132}Xe - INT	0.158	0.137	0.158
±	0.002	0.015	0.002
^{131}Xe/^{132}Xe - INT	0.797	0.879	0.797
±	0.010	0.056	0.010
^{134}Xe/^{132}Xe - INT	0.384	0.416	0.384
±	0.004	0.025	0.004
^{136}Xe/^{132}Xe - INT	0.330	0.373	0.330
±	0.005	0.033	0.005
^{132}Xe - EXTa [in 10^{-8} cc/g]	0.8744	0.0147	0.8891
±	0.0963	0.0017	0.0963
^{132}Xe - EXTa [in 10^{-12} cc]	0.2649	0.0044	0.2694
±	0.0292	0.0005	0.0292
^{128}Xe/^{132}Xe - EXTa	0.078	0.097	0.078
±	0.002	0.010	0.002
^{129}Xe/^{132}Xe - EXTa	1.026	0.946	1.025
±	0.014	0.061	0.014
^{130}Xe/^{132}Xe - EXTa	0.155	0.180	0.155
±	0.003	0.017	0.003
^{131}Xe/^{132}Xe - EXTa	0.795	0.877	0.797
±	0.010	0.056	0.010
^{134}Xe/^{132}Xe - EXTa	0.376	0.359	0.376
±	0.006	0.024	0.006
^{136}Xe/^{132}Xe - EXTa	0.325	0.328	0.325
±	0.013	0.025	0.013
^{132}Xe - EXTb [in 10^{-8} cc/g]	0.8095	0.0136	0.8231
±	0.1040	0.0018	0.1040
^{132}Xe - EXTb [in 10^{-12} cc]	0.2453	0.0041	0.2494
±	0.0315	0.0005	0.0315
^{128}Xe/^{132}Xe - EXTb	0.076	0.098	0.077
±	0.003	0.012	0.003
^{129}Xe/^{132}Xe - EXTb	1.027	0.947	1.026
±	0.014	0.061	0.014
^{130}Xe/^{132}Xe - EXTb	0.159	0.145	0.158
±	0.003	0.015	0.003
^{131}Xe/^{132}Xe - EXTb	0.795	0.877	0.797
±	0.004	0.004	0.004
^{134}Xe/^{132}Xe - EXTb	0.393	0.443	0.394
±	0.006	0.024	0.006
^{136}Xe/^{132}Xe - EXTb	0.334	0.345	0.334
±	0.011	0.026	0.011
^{21}Ne$_{cos}$/^{38}Ar$_{cos}$	-	-	-
±	-	-	-
^{36}Ar/^{132}Xe $_{(Int)}$	30.57	89.17	32.07
±	0.72	3.59	0.73
^{84}Kr/^{132}Xe $_{(Int)}$	0.65	1.44	0.68
±	0.05	0.13	0.05

Table X47. Noble gas data He to Xe for sample 45b.16 (not corrected for blank)

Sample	45b.16						
Size [µm]	572 x 463						
Weight [µg]	138.3 ± 0.1						
Date of measure	18/06/12	19/06/12	18+19/06/12	**Date of measure**	18/06/12	19/06/12	18+19/06/12
Laser-Power	3 x 0.91 W	3 x 5 - 8 W		**Laser-Power**	3 x 0.91 W	3 x 5 - 8 W	
Laser-Beam	600-360 µm	360 µm		**Laser-Beam**	600-360 µm	360 µm	
Step(s)	1	2	total*	**Step(s)**	1	2	total*
^{4}He [in 10^{-8} cc/g]	24.8	7.9	32.7	^{132}Xe - INT [in 10^{-8} cc/g]	0.0305	0.0084	0.0390
±	1.1	0.3	1.2	±	0.0006	0.0002	0.0006
^{4}He [in 10^{-12} cc]	34.4	10.9	45.3	^{132}Xe - INT [in 10^{-12} cc]	0.0423	0.0117	0.0539
±	1.5	0.5	1.6	±	0.0008	0.0003	0.0008
^{3}He [in 10^{-12} cc/g]	< 308.8 (2σ)	617.7	-	^{128}Xe/^{132}Xe - INT	0.076	0.103	0.082
±	-	106.3	-	±	0.003	0.007	0.003
^{3}He [in 10^{-16} cc]	< 427.1 (2σ)	854.3	-	^{129}Xe/^{132}Xe - INT	0.931	1.046	0.956
±	-	147.0	-	±	0.015	0.033	0.014
^{3}He/^{4}He	< 0.0012 (2σ)	0.00784	-	^{130}Xe/^{132}Xe - INT	0.153	0.164	0.155
±	-	0.00139	-	±	0.003	0.006	0.003
^{22}Ne [in 10^{-8} cc/g]	0.964	10.862	11.826	^{131}Xe/^{132}Xe - INT	0.766	0.823	0.778
±	0.052	0.581	0.583	±	0.014	0.026	0.012
^{22}Ne [in 10^{-12} cc]	1.333	15.022	16.356	^{134}Xe/^{132}Xe - INT	0.389	0.382	0.388
±	0.072	0.803	0.806	±	0.007	0.015	0.007
^{20}Ne/^{22}Ne	11.34	11.26	11.26	^{136}Xe/^{132}Xe - INT	0.335	0.326	0.333
±	0.14	0.09	0.08	±	0.009	0.017	0.008
^{21}Ne/^{22}Ne	0.035	0.040	0.039	^{132}Xe - EXTa [in 10^{-8} cc/g]	0.0303	0.0084	0.0387
±	0.001	0.001	0.001	±	0.0008	0.0003	0.0009
^{21}Ne$_{cos}$ [in 10^{-8} cc/g]	0.005	0.109	0.115	^{132}Xe - EXTa [in 10^{-12} cc]	0.0420	0.0116	0.0536
±	0.001	0.010	0.010	±	0.0012	0.0004	0.0012
^{21}Ne$_{cos}$ [in 10^{-12} cc]	0.007	0.151	0.158	^{128}Xe/^{132}Xe - EXTa	0.068	0.087	0.072
±	0.002	0.013	0.014	±	0.002	0.006	0.002
^{20}Ne$_{trap}$ [in 10^{-8} cc/g]	10.9	122.15	133.08	^{129}Xe/^{132}Xe - EXTa	0.928	1.045	0.954
±	0.9	9.44	9.48	±	0.016	0.034	0.015
^{20}Ne$_{trap}$ [in 10^{-12} cc]	15.1	168.94	184.05	^{130}Xe/^{132}Xe - EXTa	0.152	0.158	0.153
±	1.2	13.05	13.10	±	0.004	0.007	0.004
^{36}Ar [in 10^{-8} cc/g]	1.52	12.97	14.49	^{131}Xe/^{132}Xe - EXTa	0.767	0.826	0.780
±	0.03	0.24	0.25	±	0.015	0.027	0.013
^{36}Ar [in 10^{-12} cc]	2.11	17.94	20.05	^{134}Xe/^{132}Xe - EXTa	0.390	0.369	0.385
±	0.04	0.34	0.34	±	0.008	0.013	0.007
^{38}Ar/^{36}Ar	0.196	0.199	0.199	^{136}Xe/^{132}Xe - EXTa	0.327	0.299	0.321
±	0.002	0.002	0.002	±	0.007	0.012	0.006
^{40}Ar/^{36}Ar	124.6	36.5	45.8	^{132}Xe - EXTb [in 10^{-8} cc/g]	0.0303	0.0081	0.0384
±	0.8	0.4	0.4	±	0.0008	0.0002	0.0008
^{40}Ar [in 10^{-8} cc/g]	190.0	473.8	663.8	^{132}Xe - EXTb [in 10^{-12} cc]	0.0419	0.0112	0.0531
±	3.6	9.4	10.0	±	0.0011	0.0003	0.0011
^{40}Ar [in 10^{-12} cc]	262.8	655.2	918.0	^{128}Xe/^{132}Xe - EXTb	0.066	0.076	0.068
±	4.9	12.9	13.8	±	0.003	0.006	0.003
^{38}Ar$_{cos}$ [in 10^{-8} cc/g]	0.014	0.159	0.172	^{129}Xe/^{132}Xe - EXTb	0.928	1.045	0.953
±	0.005	0.040	0.041	±	0.016	0.033	0.014
^{38}Ar$_{cos}$ [in 10^{-12} cc]	0.019	0.219	0.238	^{130}Xe/^{132}Xe - EXTb	0.139	0.146	0.141
±	0.007	0.056	0.056	±	0.004	0.008	0.004
^{84}Kr [in 10^{-8} cc/g]	0.0431	0.0488	0.0919	^{131}Xe/^{132}Xe - EXTb	0.767	0.826	0.779
±	0.0027	0.0031	0.0041	±	0.004	0.004	0.003
^{84}Kr [in 10^{-12} cc]	0.0596	0.0675	0.1271	^{134}Xe/^{132}Xe - EXTb	0.394	0.397	0.395
±	0.0038	0.0043	0.0057	±	0.006	0.014	0.006
^{80}Kr/^{84}Kr	0.043	0.046	0.045	^{136}Xe/^{132}Xe - EXTb	0.340	0.328	0.338
±	0.003	0.003	0.002	±	0.006	0.012	0.006
^{82}Kr/^{84}Kr	0.179	0.202	0.192	^{21}Ne$_{cos}$/^{38}Ar$_{cos}$	0.39	0.69	0.66
±	0.006	0.006	0.005	±	0.17	0.19	0.17
^{83}Kr/^{84}Kr	0.191	0.214	0.203	^{36}Ar/^{132}Xe $_{(Int)}$	49.92	1536.05	371.71
±	0.007	0.007	0.005	±	1.29	45.22	8.47
^{86}Kr/^{84}Kr	0.301	0.286	0.293	^{84}Kr/^{132}Xe $_{(Int)}$	1.41	5.78	2.36
±	0.009	0.008	0.006	±	0.09	0.39	0.11
^{83}Kr$_{cos}$ [in 10^{-8} cc/g]	-	0.0006	-				
±	-	0.0004	-				
^{83}Kr$_{cos}$ [in 10^{-12} cc]	-	0.0008	-				
±	-	0.0005	-				

Table X48. Noble gas data He to Xe for sample 45b.17_1 (not corrected for blank)

Sample		45b.17_1	
Size [µm]		416 x 283	
Weight [µg]		56.2 ± 0.1	
Date of measure	20/06/12	**Date of measure**	20/06/12
Laser-Power	3 x 0.91 W	**Laser-Power**	3 x 0.91 W
Laser-Beam	600 µm	**Laser-Beam**	600 µm
Step(s)	1	**Step(s)**	1
^{4}He [in 10^{-8} cc/g]	1097.9	^{132}Xe - INT [in 10^{-8} cc/g]	0.0533
±	49.0	±	0.0010
^{4}He [in 10^{-12} cc]	617.0	^{132}Xe - INT [in 10^{-12} cc]	0.0299
±	27.5	±	0.0006
^{3}He [in 10^{-12} cc/g]	26099.3	^{128}Xe/^{132}Xe - INT	0.067
±	1132.3	±	0.003
^{3}He [in 10^{-16} cc]	14667.8	^{129}Xe/^{132}Xe - INT	0.905
±	635.8	±	0.021
^{3}He/^{4}He	0.00238	^{130}Xe/^{132}Xe - INT	0.144
±	0.00015	±	0.003
^{22}Ne [in 10^{-8} cc/g]	11.716	^{131}Xe/^{132}Xe - INT	0.779
±	0.626	±	0.015
^{22}Ne [in 10^{-12} cc]	6.584	^{134}Xe/^{132}Xe - INT	0.392
±	0.352	±	0.010
^{20}Ne/^{22}Ne	7.13	^{136}Xe/^{132}Xe - INT	0.346
±	0.05	±	0.011
^{21}Ne/^{22}Ne	0.396	^{132}Xe - EXTa [in 10^{-8} cc/g]	0.0529
±	0.005	±	0.0015
^{21}Ne$_{cos}$ [in 10^{-8} cc/g]	4.412	^{132}Xe - EXTa [in 10^{-12} cc]	0.0297
±	0.243	±	0.0008
^{21}Ne$_{cos}$ [in 10^{-12} cc]	2.480	^{128}Xe/^{132}Xe - EXTa	0.066
±	0.137	±	0.003
^{20}Ne$_{trap}$ [in 10^{-8} cc/g]	79.9	^{129}Xe/^{132}Xe - EXTa	0.903
±	6.3	±	0.022
^{20}Ne$_{trap}$ [in 10^{-12} cc]	44.9	^{130}Xe/^{132}Xe - EXTa	0.141
±	3.5	±	0.004
^{36}Ar [in 10^{-8} cc/g]	10.52	^{131}Xe/^{132}Xe - EXTa	0.780
±	0.39	±	0.016
^{36}Ar [in 10^{-12} cc]	5.91	^{134}Xe/^{132}Xe - EXTa	0.404
±	0.22	±	0.009
^{38}Ar/^{36}Ar	0.224	^{136}Xe/^{132}Xe - EXTa	0.342
±	0.001	±	0.007
^{40}Ar/^{36}Ar	116.7	^{132}Xe - EXTb [in 10^{-8} cc/g]	0.0520
±	1.3	±	0.0014
^{40}Ar [in 10^{-8} cc/g]	1227.8	^{132}Xe - EXTb [in 10^{-12} cc]	0.0292
±	47.4	±	0.0008
^{40}Ar [in 10^{-12} cc]	690.0	^{128}Xe/^{132}Xe - EXTb	0.067
±	26.6	±	0.004
^{38}Ar$_{cos}$ [in 10^{-8} cc/g]	0.424	^{129}Xe/^{132}Xe - EXTb	0.903
±	0.034	±	0.021
^{38}Ar$_{cos}$ [in 10^{-12} cc]	0.238	^{130}Xe/^{132}Xe - EXTb	0.146
±	0.019	±	0.005
^{84}Kr [in 10^{-8} cc/g]	0.2918	^{131}Xe/^{132}Xe - EXTb	0.780
±	0.0184	±	0.004
^{84}Kr [in 10^{-12} cc]	0.1640	^{134}Xe/^{132}Xe - EXTb	0.402
±	0.0103	±	0.009
^{80}Kr/^{84}Kr	0.034	^{136}Xe/^{132}Xe - EXTb	0.367
±	0.001	±	0.008
^{82}Kr/^{84}Kr	0.184	^{21}Ne$_{cos}$/^{38}Ar$_{cos}$	10.40
±	0.004	±	1.02
^{83}Kr/^{84}Kr	0.191	^{36}Ar/^{132}Xe $_{(Int)}$	197.52
±	0.004	±	8.24
^{86}Kr/^{84}Kr	0.319	^{84}Kr/^{132}Xe $_{(Int)}$	5.48
±	0.006	±	0.36
^{83}Kr$_{cos}$ [in 10^{-8} cc/g]	-		
±	-		
^{83}Kr$_{cos}$ [in 10^{-12} cc]	-		
±	-		

Table X49. Noble gas data He to Xe for sample 45b.18_1 (not corrected for blank)

Sample	45b.18_1		
Size [µm]	253 x 235		
Weight [µg]	5.3 ± 0.1		
Date of measure	11/11/11	17/11/11	11+17/11/11
Laser-Power	3 x 0.91 W	3 x 5 W	
Laser-Beam	250 µm	200 µm	
Step(s)	1	2	total*

	1	2	total*		1	2	total*
^{4}He [in 10^{-8} cc/g]	549.1	171.8	720.9	^{132}Xe - INT [in 10^{-8} cc/g]	-	-	-
±	14.4	4.5	15.1	±	-	-	-
^{4}He [in 10^{-12} cc]	29.1	9.1	38.2	^{132}Xe - INT [in 10^{-12} cc]	-	-	-
±	0.5	0.2	0.3	±	-	-	-
^{3}He [in 10^{-12} cc/g]	4153.0	4151.7	8304.7	^{128}Xe/^{132}Xe - INT	-	-	-
±	2606.1	2606.1	3685.5	±	-	-	-
^{3}He [in 10^{-16} cc]	220.1	220.0	440.2	^{129}Xe/^{132}Xe - INT	-	-	-
±	138.1	138.1	195.2	±	-	-	-
^{3}He/^{4}He	0.00076	0.00242	0.00115	^{130}Xe/^{132}Xe - INT	-	-	-
±	0.00047	0.00152	0.00051	±	-	-	-
^{22}Ne [in 10^{-8} cc/g]	7.709	1.075	8.784	^{131}Xe/^{132}Xe - INT	-	-	-
±	0.349	0.268	0.440	±	-	-	-
^{22}Ne [in 10^{-12} cc]	0.409	0.057	0.466	^{134}Xe/^{132}Xe - INT	-	-	-
±	0.017	0.014	0.022	±	-	-	-
^{20}Ne/^{22}Ne	11.36	8.00	10.95	^{136}Xe/^{132}Xe - INT	-	-	-
±	0.45	1.96	0.47	±	-	-	-
^{21}Ne/^{22}Ne	0.039	0.026	0.037	^{132}Xe - EXTa [in 10^{-8} cc/g]	-	-	-
±	0.003	0.008	0.003	±	-	-	-
^{21}Ne$_{cos}$ [in 10^{-8} cc/g]	0.072	< 0.036 (2σ)	-	^{132}Xe - EXTa [in 10^{-12} cc]	-	-	-
±	0.025	-	-	±	-	-	-
^{21}Ne$_{cos}$ [in 10^{-12} cc]	0.004	< 0.002 (2σ)	-	^{128}Xe/^{132}Xe - EXTa	-	-	-
±	0.001	-	-	±	-	-	-
^{20}Ne$_{trap}$ [in 10^{-8} cc/g]	87.6	8.31	95.87	^{129}Xe/^{132}Xe - EXTa	-	-	-
±	7.2	2.95	7.76	±	-	-	-
^{20}Ne$_{trap}$ [in 10^{-12} cc]	4.6	0.44	5.08	^{130}Xe/^{132}Xe - EXTa	-	-	-
±	0.4	0.16	0.40	±	-	-	-
^{36}Ar [in 10^{-8} cc/g]	13.34	2.25	15.59	^{131}Xe/^{132}Xe - EXTa	-	-	-
±	0.38	0.13	0.40	±	-	-	-
^{36}Ar [in 10^{-12} cc]	0.71	0.12	0.83	^{134}Xe/^{132}Xe - EXTa	-	-	-
±	0.01	0.01	0.01	±	-	-	-
^{38}Ar/^{36}Ar	0.190	0.197	0.191	^{136}Xe/^{132}Xe - EXTa	-	-	-
±	0.005	0.026	0.006	±	-	-	-
^{40}Ar/^{36}Ar	191.5	252.3	200.3	^{132}Xe - EXTb [in 10^{-8} cc/g]	-	-	-
±	2.2	12.7	2.6	±	-	-	-
^{40}Ar [in 10^{-8} cc/g]	2554.5	567.1	3121.7	^{132}Xe - EXTb [in 10^{-12} cc]	-	-	-
±	70.4	15.3	72.1	±	-	-	-
^{40}Ar [in 10^{-12} cc]	135.4	30.1	165.4	^{128}Xe/^{132}Xe - EXTb	-	-	-
±	2.7	0.6	2.2	±	-	-	-
^{38}Ar$_{cos}$ [in 10^{-8} cc/g]	< 0.181 (2σ)	< 0.151 (2σ)	-	^{129}Xe/^{132}Xe - EXTb	-	-	-
±	-	-	-	±	-	-	-
^{38}Ar$_{cos}$ [in 10^{-12} cc]	< 0.010 (2σ)	< 0.008 (2σ)	-	^{130}Xe/^{132}Xe - EXTb	-	-	-
±	-	-	-	±	-	-	-
^{84}Kr [in 10^{-8} cc/g]	0.3844	0.0493	0.4337	^{131}Xe/^{132}Xe - EXTb	-	-	-
±	0.0442	0.0061	0.0446	±	-	-	-
^{84}Kr [in 10^{-12} cc]	0.0204	0.0026	0.0230	^{134}Xe/^{132}Xe - EXTb	-	-	-
±	0.0023	0.0003	0.0023	±	-	-	-
^{80}Kr/^{84}Kr	0.046	0.101	0.052	^{136}Xe/^{132}Xe - EXTb	-	-	-
±	0.005	0.021	0.005	±	-	-	-
^{82}Kr/^{84}Kr	0.210	0.226	0.212	^{21}Ne$_{cos}$/^{38}Ar$_{cos}$	-	-	-
±	0.012	0.034	0.012	±	-	-	-
^{83}Kr/^{84}Kr	0.206	0.228	0.209	^{36}Ar/^{132}Xe$_{(Int)}$	-	-	-
±	0.010	0.030	0.010	±	-	-	-
^{86}Kr/^{84}Kr	0.277	0.277	0.277	^{84}Kr/^{132}Xe$_{(Int)}$	-	-	-
±	0.016	0.043	0.015	±	-	-	-
^{83}Kr$_{cos}$ [in 10^{-8} cc/g]	-	-	-				
±	-	-	-				
^{83}Kr$_{cos}$ [in 10^{-12} cc]	-	-	-				
±	-	-	-				

Table X50. Noble gas data He to Xe for sample 45b.19_1 (not corrected for blank)

Sample	45b.19_1		
Size [µm]	450 x 292		
Weight [µg]	55.9 ± 0.1		
Date of measure	19/01/12	**Date of measure**	19/01/12
Laser-Power	3 x 0.91 W	**Laser-Power**	3 x 0.91 W
Laser-Beam	250 µm	**Laser-Beam**	250 µm
Step(s)	1	**Step(s)**	1
^{4}He [in 10^{-8} cc/g]	977.1	^{132}Xe - INT [in 10^{-8} cc/g]	0.0368
±	15.5	±	0.0010
^{4}He [in 10^{-12} cc]	546.2	^{132}Xe - INT [in 10^{-12} cc]	0.0206
±	8.6	±	0.0006
^{3}He [in 10^{-12} cc/g]	1072.3	^{128}Xe/^{132}Xe - INT	0.076
±	271.8	±	0.004
^{3}He [in 10^{-16} cc]	599.4	^{129}Xe/^{132}Xe - INT	0.985
±	151.9	±	0.023
^{3}He/^{4}He	0.00011	^{130}Xe/^{132}Xe - INT	0.147
±	0.00003	±	0.004
^{22}Ne [in 10^{-8} cc/g]	0.441	^{131}Xe/^{132}Xe - INT	0.767
±	0.028	±	0.018
^{22}Ne [in 10^{-12} cc]	0.247	^{134}Xe/^{132}Xe - INT	0.370
±	0.016	±	0.011
^{20}Ne/^{22}Ne	10.67	^{136}Xe/^{132}Xe - INT	0.319
±	0.56	±	0.012
^{21}Ne/^{22}Ne	0.028	^{132}Xe - EXTa [in 10^{-8} cc/g]	0.0366
±	0.003	±	0.0107
^{21}Ne$_{cos}$ [in 10^{-8} cc/g]	< 0.008 (2σ)	^{132}Xe - EXTa [in 10^{-12} cc]	0.0205
±	-	±	0.0060
^{21}Ne$_{cos}$ [in 10^{-12} cc]	< 0.004 (2σ)	^{128}Xe/^{132}Xe - EXTa	0.073
±	-	±	0.004
^{20}Ne$_{trap}$ [in 10^{-8} cc/g]	4.7	^{129}Xe/^{132}Xe - EXTa	0.984
±	0.5	±	0.023
^{20}Ne$_{trap}$ [in 10^{-12} cc]	2.6	^{130}Xe/^{132}Xe - EXTa	0.144
±	0.3	±	0.006
^{36}Ar [in 10^{-8} cc/g]	2.41	^{131}Xe/^{132}Xe - EXTa	0.766
±	0.04	±	0.018
^{36}Ar [in 10^{-12} cc]	1.34	^{134}Xe/^{132}Xe - EXTa	0.374
±	0.02	±	0.010
^{38}Ar/^{36}Ar	0.186	^{136}Xe/^{132}Xe - EXTa	0.323
±	0.005	±	0.009
^{40}Ar/^{36}Ar	263.1	^{132}Xe - EXTb [in 10^{-8} cc/g]	0.0362
±	2.9	±	0.0050
^{40}Ar [in 10^{-8} cc/g]	632.8	^{132}Xe - EXTb [in 10^{-12} cc]	0.0202
±	11.3	±	0.0028
^{40}Ar [in 10^{-12} cc]	353.7	^{128}Xe/^{132}Xe - EXTb	0.073
±	6.3	±	0.003
^{38}Ar$_{cos}$ [in 10^{-8} cc/g]	-	^{129}Xe/^{132}Xe - EXTb	0.984
±	-	±	0.023
^{38}Ar$_{cos}$ [in 10^{-12} cc]	-	^{130}Xe/^{132}Xe - EXTb	0.146
±	-	±	0.005
^{84}Kr [in 10^{-8} cc/g]	0.0838	^{131}Xe/^{132}Xe - EXTb	0.766
±	0.0067	±	0.004
^{84}Kr [in 10^{-12} cc]	0.0468	^{134}Xe/^{132}Xe - EXTb	0.376
±	0.0037	±	0.010
^{80}Kr/^{84}Kr	0.044	^{136}Xe/^{132}Xe - EXTb	0.328
±	0.003	±	0.010
^{82}Kr/^{84}Kr	0.215	^{21}Ne$_{cos}$/^{38}Ar$_{cos}$	-
±	0.007	±	-
^{83}Kr/^{84}Kr	0.205	^{36}Ar/^{132}Xe $_{(Int)}$	65.42
±	0.007	±	2.13
^{86}Kr/^{84}Kr	0.317	^{84}Kr/^{132}Xe $_{(Int)}$	2.28
±	0.010	±	0.19
^{83}Kr$_{cos}$ [in 10^{-8} cc/g]	-		
±	-		
^{83}Kr$_{cos}$ [in 10^{-12} cc]	-		
±	-		

Table X51. Noble gas data He to Xe for sample 45b.20_2 (not corrected for blank)

Sample		45b.20_2	
Size [µm]		613 x 482	
Weight [µg]		77.3 ± 0.1	

Date of measure	25/09/12	26/09/12	25+26/09/12
Laser-Power	1 x 0.91-11W / 2 x 3.3 W	2 x 5 W / 1 x 11-33W	
Laser-Beam	600- 250 µm	250 µm	
Step(s)	1	2	total*
^{4}He [in 10^{-8} cc/g]	55.1	9.2	64.2
±	1.0	0.2	1.0
^{4}He [in 10^{-12} cc]	42.6	7.1	49.6
±	0.8	0.1	0.8
^{3}He [in 10^{-12} cc/g]	873.2	620.1	1493.4
±	122.7	136.7	183.7
^{3}He [in 10^{-16} cc]	675.0	479.4	1154.4
±	94.8	105.7	142.0
^{3}He/^{4}He	0.00159	0.00677	0.00233
±	0.00022	0.00150	0.00029
^{22}Ne [in 10^{-8} cc/g]	0.537	0.057	0.594
±	0.021	0.013	0.024
^{22}Ne [in 10^{-12} cc]	0.415	0.044	0.459
±	0.016	0.010	0.019
^{20}Ne/^{22}Ne	10.89	7.30	10.55
±	0.32	1.66	0.33
^{21}Ne/^{22}Ne	0.062	0.018	0.058
±	0.004	0.007	0.004
^{21}Ne$_{cos}$ [in 10^{-8} cc/g]	0.018	-	-
±	0.003	-	-
^{21}Ne$_{cos}$ [in 10^{-12} cc]	0.014	-	-
±	0.002	-	-
^{20}Ne$_{trap}$ [in 10^{-8} cc/g]	5.8	< 68.5 (2σ)	-
±	0.4	-	-
^{20}Ne$_{trap}$ [in 10^{-12} cc]	4.5	< 53.0 (2σ)	-
±	0.3	-	-
^{36}Ar [in 10^{-8} cc/g]	1.26	0.34	1.61
±	0.03	0.01	0.03
^{36}Ar [in 10^{-12} cc]	0.98	0.26	1.24
±	0.02	0.01	0.02
^{38}Ar/^{36}Ar	0.182	0.177	0.180
±	0.004	0.007	0.004
^{40}Ar/^{36}Ar	187.3	282.2	207.5
±	2.2	5.8	2.1
^{40}Ar [in 10^{-8} cc/g]	236.8	96.4	333.2
±	5.1	2.2	5.6
^{40}Ar [in 10^{-12} cc]	183.1	74.5	257.6
±	3.9	1.7	4.3
^{38}Ar$_{cos}$ [in 10^{-8} cc/g]	-	-	-
±	-	-	-
^{38}Ar$_{cos}$ [in 10^{-12} cc]	-	-	-
±	-	-	-
^{84}Kr [in 10^{-8} cc/g]	0.0913	0.0081	0.0994
±	0.0068	0.0007	0.0068
^{84}Kr [in 10^{-12} cc]	0.0706	0.0063	0.0768
±	0.0053	0.0005	0.0053
^{80}Kr/^{84}Kr	0.046	0.068	0.048
±	0.003	0.011	0.003
^{82}Kr/^{84}Kr	0.209	0.236	0.211
±	0.013	0.025	0.012
^{83}Kr/^{84}Kr	0.210	0.202	0.209
±	0.011	0.023	0.010
^{86}Kr/^{84}Kr	0.318	0.356	0.321
±	0.018	0.041	0.017
^{83}Kr$_{cos}$ [in 10^{-8} cc/g]	-	-	-
±	-	-	-
^{83}Kr$_{cos}$ [in 10^{-12} cc]	-	-	-
±	-	-	-

Date of measure	25/09/12	26/09/12	25+26/09/12
Laser-Power	1 x 0.91 - 11 W / 2 x 3.3 W	2 x 5 W / 1 x 11 - 33 W	
Laser-Beam	600 - 250 µm	250 µm	
Step(s)	1	2	total*
^{132}Xe - INT [in 10^{-8} cc/g]	0.1076	0.0023	0.1099
±	0.0016	0.0001	0.0016
^{132}Xe - INT [in 10^{-12} cc]	0.0832	0.0018	0.0850
±	0.0012	0.0001	0.0012
^{128}Xe/^{132}Xe - INT	0.079	0.094	0.079
±	0.002	0.017	0.002
^{129}Xe/^{132}Xe - INT	0.987	1.057	0.988
±	0.013	0.082	0.013
^{130}Xe/^{132}Xe - INT	0.158	0.185	0.158
±	0.003	0.018	0.003
^{131}Xe/^{132}Xe - INT	0.770	0.864	0.772
±	0.011	0.080	0.011
^{134}Xe/^{132}Xe - INT	0.387	0.419	0.388
±	0.006	0.041	0.006
^{136}Xe/^{132}Xe - INT	0.341	0.380	0.341
±	0.007	0.048	0.007
^{132}Xe - EXTa [in 10^{-8} cc/g]	0.1076	0.0023	0.1099
±	0.0016	0.0001	0.0016
^{132}Xe - EXTa [in 10^{-12} cc]	0.0832	0.0018	0.0850
±	0.0012	0.0001	0.0012
^{128}Xe/^{132}Xe - EXTa	0.075	0.076	0.075
±	0.002	0.014	0.002
^{129}Xe/^{132}Xe - EXTa	0.989	1.060	0.991
±	0.013	0.082	0.013
^{130}Xe/^{132}Xe - EXTa	0.155	0.187	0.155
±	0.003	0.021	0.003
^{131}Xe/^{132}Xe - EXTa	0.775	0.870	0.777
±	0.011	0.080	0.010
^{134}Xe/^{132}Xe - EXTa	0.375	0.441	0.376
±	0.005	0.040	0.005
^{136}Xe/^{132}Xe - EXTa	0.324	0.303	0.324
±	0.006	0.032	0.006
^{132}Xe - EXTb [in 10^{-8} cc/g]	0.1064	0.0024	0.1088
±	0.0117	0.0003	0.0117
^{132}Xe - EXTb [in 10^{-12} cc]	0.0823	0.0019	0.0841
±	0.0090	0.0002	0.0090
^{128}Xe/^{132}Xe - EXTb	0.069	0.102	0.070
±	0.002	0.018	0.002
^{129}Xe/^{132}Xe - EXTb	0.987	1.057	0.988
±	0.014	0.082	0.014
^{130}Xe/^{132}Xe - EXTb	0.153	0.146	0.153
±	0.003	0.019	0.003
^{131}Xe/^{132}Xe - EXTb	0.770	0.864	0.772
±	0.004	0.004	0.004
^{134}Xe/^{132}Xe - EXTb	0.394	0.429	0.395
±	0.006	0.036	0.005
^{136}Xe/^{132}Xe - EXTb	0.336	0.416	0.338
±	0.005	0.036	0.005
^{21}Ne$_{cos}$/^{38}Ar$_{cos}$	-	-	-
±	-	-	-
^{36}Ar/^{132}Xe $_{(Int)}$	11.75	147.05	14.61
±	0.29	8.23	0.32
^{84}Kr/^{132}Xe $_{(Int)}$	0.85	3.49	0.90
±	0.06	0.34	0.06

Table X52. Noble gas data He to Xe for sample 45b.21 (not corrected for blank)

Sample	45b.21						
Size [µm]	571 x 212						
Weight [µg]	24.8 ± 0.1						
Date of measure	18/01/12	19/01/12	18+19/01/12	Date of measure	18/01/12	19/01/12	18+19/01/12
Laser-Power	3 x 0.91 W	3 x 5 W		Laser-Power	3 x 0.91 W	3 x 5 W	
Laser-Beam	250 µm	250 µm		Laser-Beam	250 µm	250 µm	
Step(s)	1	2	total*	Step(s)	1	2	total*
^{4}He [in 10^{-8} cc/g]	4850.6	768.3	5618.9	^{132}Xe - INT [in 10^{-8} cc/g]	0.4883	0.2642	0.7525
±	81.6	12.3	82.6	±	0.0126	0.0069	0.0144
^{4}He [in 10^{-12} cc]	1203.0	190.5	1393.5	^{132}Xe - INT [in 10^{-12} cc]	0.1211	0.0655	0.1866
±	19.7	3.0	19.7	±	0.0031	0.0017	0.0035
^{3}He [in 10^{-12} cc/g]	12362.9	1126.4	13489.3	^{128}Xe/^{132}Xe - INT	0.078	0.086	0.081
±	1785.0	723.8	1926.2	±	0.002	0.002	0.001
^{3}He [in 10^{-16} cc]	3066.0	279.4	3345.3	^{129}Xe/^{132}Xe - INT	1.019	1.035	1.025
±	442.5	179.5	477.5	±	0.010	0.014	0.008
^{3}He/^{4}He	0.00025	0.00015	0.00024	^{130}Xe/^{132}Xe - INT	0.158	0.163	0.160
±	0.00004	0.00009	0.00003	±	0.002	0.003	0.002
^{22}Ne [in 10^{-8} cc/g]	5.722	0.792	6.514	^{131}Xe/^{132}Xe - INT	0.807	0.816	0.810
±	0.255	0.056	0.262	±	0.008	0.011	0.007
^{22}Ne [in 10^{-12} cc]	1.419	0.196	1.616	^{134}Xe/^{132}Xe - INT	0.385	0.378	0.382
±	0.063	0.014	0.065	±	0.004	0.006	0.004
^{20}Ne/^{22}Ne	11.23	11.03	11.20	^{136}Xe/^{132}Xe - INT	0.333	0.322	0.329
±	0.26	0.66	0.24	±	0.006	0.008	0.005
^{21}Ne/^{22}Ne	0.028	0.030	0.029	^{132}Xe - EXTa [in 10^{-8} cc/g]	0.4891	0.2646	0.7537
±	0.001	0.003	0.001	±	0.1427	0.0772	0.1622
^{21}Ne$_{cos}$ [in 10^{-8} cc/g]	< 0.057 (2σ)	0.004	-	^{132}Xe - EXTa [in 10^{-12} cc]	0.1213	0.0656	0.1869
±	-	0.003	-	±	0.0354	0.0191	0.0402
^{21}Ne$_{cos}$ [in 10^{-12} cc]	< 0.014 (2σ)	0.001	-	^{128}Xe/^{132}Xe - EXTa	0.077	0.085	0.080
±	-	0.001	-	±	0.001	0.002	0.001
^{20}Ne$_{trap}$ [in 10^{-8} cc/g]	63.9	8.68	72.57	^{129}Xe/^{132}Xe - EXTa	1.018	1.035	1.024
±	4.8	0.94	4.85	±	0.010	0.014	0.008
^{20}Ne$_{trap}$ [in 10^{-12} cc]	15.8	2.15	18.00	^{130}Xe/^{132}Xe - EXTa	0.157	0.163	0.159
±	1.2	0.23	1.20	±	0.002	0.003	0.002
^{36}Ar [in 10^{-8} cc/g]	35.00	30.35	65.35	^{131}Xe/^{132}Xe - EXTa	0.805	0.815	0.808
±	0.58	0.51	0.77	±	0.008	0.011	0.007
^{36}Ar [in 10^{-12} cc]	8.68	7.53	16.21	^{134}Xe/^{132}Xe - EXTa	0.376	0.375	0.376
±	0.14	0.12	0.18	±	0.004	0.006	0.003
^{38}Ar/^{36}Ar	0.192	0.189	0.190	^{136}Xe/^{132}Xe - EXTa	0.318	0.325	0.321
±	0.001	0.001	0.001	±	0.004	0.006	0.003
^{40}Ar/^{36}Ar	38.5	77.0	56.4	^{132}Xe - EXTb [in 10^{-8} cc/g]	0.4888	0.2645	0.7533
±	0.2	0.4	0.3	±	0.0675	0.0365	0.0768
^{40}Ar [in 10^{-8} cc/g]	1345.8	2337.5	3683.3	^{132}Xe - EXTb [in 10^{-12} cc]	0.1212	0.0656	0.1868
±	23.6	40.8	47.1	±	0.0167	0.0091	0.0190
^{40}Ar [in 10^{-12} cc]	333.8	579.7	913.5	^{128}Xe/^{132}Xe - EXTb	0.076	0.079	0.077
±	5.7	9.8	11.1	±	0.002	0.002	0.001
^{38}Ar$_{cos}$ [in 10^{-8} cc/g]	0.122	< 0.184 (2σ)	-	^{129}Xe/^{132}Xe - EXTb	1.018	1.035	1.024
±	0.094	-	-	±	0.011	0.015	0.009
^{38}Ar$_{cos}$ [in 10^{-12} cc]	0.030	< 0.046 (2σ)	-	^{130}Xe/^{132}Xe - EXTb	0.156	0.162	0.158
±	0.023	-	-	±	0.002	0.003	0.002
^{84}Kr [in 10^{-8} cc/g]	0.3922	0.2769	0.6691	^{131}Xe/^{132}Xe - EXTb	0.806	0.816	0.809
±	0.0309	0.0219	0.0379	±	0.004	0.004	0.003
^{84}Kr [in 10^{-12} cc]	0.0973	0.0687	0.1659	^{134}Xe/^{132}Xe - EXTb	0.385	0.379	0.383
±	0.0077	0.0054	0.0094	±	0.004	0.006	0.004
^{80}Kr/^{84}Kr	0.039	0.039	0.039	^{136}Xe/^{132}Xe - EXTb	0.326	0.321	0.324
±	0.002	0.002	0.002	±	0.004	0.005	0.003
^{82}Kr/^{84}Kr	0.201	0.200	0.200	^{21}Ne$_{cos}$/^{38}Ar$_{cos}$	-	-	-
±	0.005	0.006	0.004	±	-	-	-
^{83}Kr/^{84}Kr	0.195	0.203	0.198	^{36}Ar/^{132}Xe $_{(Int)}$	71.67	114.88	86.84
±	0.005	0.006	0.004	±	2.16	3.51	1.89
^{86}Kr/^{84}Kr	0.312	0.302	0.308	^{84}Kr/^{132}Xe $_{(Int)}$	0.80	1.05	0.89
±	0.006	0.008	0.005	±	0.07	0.09	0.05
^{83}Kr$_{cos}$ [in 10^{-8} cc/g]	-	-	-				
±	-	-	-				
^{83}Kr$_{cos}$ [in 10^{-12} cc]	-	-	-				
±	-	-	-				

Table X53. Noble gas data He to Xe for sample 45b.22_2 (not corrected for blank)

Sample				45b.22_2			
Size [μm]				268 x 191			
Weight [μg]				9.2 ± 0.2			
Date of measure	04/05/11	04/05/11	04/05/11	**Date of measure**	04/05/11	04/05/11	04/05/11
Laser-Power	3 x 5 W	3 x 15 W		**Laser-Power**	3 x 5 W	3 x 15 W	
Laser-Beam	1000 μm	1000 μm		**Laser-Beam**	1000 μm	1000 μm	
Step(s)	1	2	total*	**Step(s)**	1	2	total*
^{4}He [in 10^{-8} cc/g]	69.4	39.2	108.5	^{132}Xe - INT [in 10^{-8} cc/g]	-	-	-
±	8.5	4.8	9.8	^{132}Xe - INT [in 10^{-12} cc]	-	-	-
^{4}He [in 10^{-12} cc]	6.4	3.6	10.0	^{128}Xe/^{132}Xe - INT	-	-	-
±	0.8	0.4	0.9	^{129}Xe/^{132}Xe - INT	-	-	-
^{3}He [in 10^{-12} cc/g]	-	-	-	^{130}Xe/^{132}Xe - INT	-	-	-
±	-	-	-	^{131}Xe/^{132}Xe - INT	-	-	-
^{3}He [in 10^{-16} cc]	-	-	-	^{134}Xe/^{132}Xe - INT	-	-	-
±	-	-	-	^{136}Xe/^{132}Xe - INT	-	-	-
^{3}He/^{4}He	-	-	-	^{132}Xe - EXTa [in 10^{-8} cc/g]	-	-	-
±	-	-	-	^{132}Xe - EXTa [in 10^{-12} cc]	-	-	-
^{22}Ne [in 10^{-8} cc/g]	5.291	0.927	6.218	^{128}Xe/^{132}Xe - EXTa	-	-	-
±	0.181	0.116	0.215	^{129}Xe/^{132}Xe - EXTa	-	-	-
^{22}Ne [in 10^{-12} cc]	0.487	0.085	0.572	^{130}Xe/^{132}Xe - EXTa	-	-	-
±	0.013	0.011	0.015	^{131}Xe/^{132}Xe - EXTa	-	-	-
^{20}Ne/^{22}Ne	10.75	7.93	10.33	^{134}Xe/^{132}Xe - EXTa	-	-	-
±	0.30	0.98	0.30	^{136}Xe/^{132}Xe - EXTa	-	-	-
^{21}Ne/^{22}Ne	0.064	0.021	0.058	^{132}Xe - EXTb [in 10^{-8} cc/g]	-	-	-
±	0.003	0.005	0.003	^{132}Xe - EXTb [in 10^{-12} cc]	-	-	-
^{21}Ne$_{cos}$ [in 10^{-8} cc/g]	0.181	-	-	^{128}Xe/^{132}Xe - EXTb	-	-	-
±	0.019	-	-	^{129}Xe/^{132}Xe - EXTb	-	-	-
^{21}Ne$_{cos}$ [in 10^{-12} cc]	0.017	-	-	^{130}Xe/^{132}Xe - EXTb	-	-	-
±	0.002	-	-	^{131}Xe/^{132}Xe - EXTb	-	-	-
^{20}Ne$_{trap}$ [in 10^{-8} cc/g]	56.7	7.11	63.82	^{134}Xe/^{132}Xe - EXTb	-	-	-
±	4.0	1.31	4.23	^{136}Xe/^{132}Xe - EXTb	-	-	-
^{20}Ne$_{trap}$ [in 10^{-12} cc]	5.2	0.65	5.87	±	-	-	-
±	0.4	0.12	0.37	^{21}Ne$_{cos}$/^{38}Ar$_{cos}$	2.88	-	-
^{36}Ar [in 10^{-8} cc/g]	5.44	2.34	7.78	±	2.12	-	-
±	0.27	0.13	0.30	^{36}Ar/^{132}Xe $_{(Int)}$	-	-	-
^{36}Ar [in 10^{-12} cc]	0.50	0.22	0.72	±	-	-	-
±	0.02	0.01	0.02	^{84}Kr/^{132}Xe $_{(Int)}$	-	-	-
^{38}Ar/^{36}Ar	0.199	0.207	0.201	±	-	-	-
±	0.007	0.016	0.007				
^{40}Ar/^{36}Ar	128.7	237.0	161.3				
±	4.0	8.1	3.8				
^{40}Ar [in 10^{-8} cc/g]	699.6	555.0	1254.5				
±	37.9	26.7	46.4				
^{40}Ar [in 10^{-12} cc]	64.4	51.1	115.4				
±	3.2	2.2	3.5				
^{38}Ar$_{cos}$ [in 10^{-8} cc/g]	0.063	0.049	0.112				
±	0.046	0.039	0.060				
^{38}Ar$_{cos}$ [in 10^{-12} cc]	0.006	0.005	0.010				
±	0.004	0.004	0.006				
^{84}Kr [in 10^{-8} cc/g]	-	-	-				
±	-	-	-				
^{84}Kr [in 10^{-12} cc]	-	-	-				
±	-	-	-				
^{80}Kr/^{84}Kr	-	-	-				
±	-	-	-				
^{82}Kr/^{84}Kr	-	-	-				
±	-	-	-				
^{83}Kr/^{84}Kr	-	-	-				
±	-	-	-				
^{86}Kr/^{84}Kr	-	-	-				
±	-	-	-				
^{83}Kr$_{cos}$ [in 10^{-8} cc/g]	-	-	-				
±	-	-	-				
^{83}Kr$_{cos}$ [in 10^{-12} cc]	-	-	-				
±	-	-	-				

Table X54. Noble gas data He to Xe for sample 45c.16_2 (not corrected for blank)

Sample				45c.16_2			
Size [μm]				465 x 324			
Weight [μg]				105.1 ± 0.2			
Date of measure	02/05/11	02/05/11	02/05/11	**Date of measure**	02/05/11	02/05/11	02/05/11
Laser-Power	3 x 5 W	3 x 15 W		**Laser-Power**	3 x 5 W	3 x 15 W	
Laser-Beam	1000 μm	1000 μm		**Laser-Beam**	1000 μm	1000 μm	
Step(s)	1	2	total*	**Step(s)**	1	2	total*
^{4}He [in 10^{-8} cc/g]	7.6	3.4	11.0	^{132}Xe - INT [in 10^{-8} cc/g]	-	-	-
±	0.9	0.4	1.0	±	-	-	-
^{4}He [in 10^{-12} cc]	8.0	3.6	11.6	^{132}Xe - INT [in 10^{-12} cc]	-	-	-
±	1.0	0.4	1.1	±	-	-	-
^{3}He [in 10^{-12} cc/g]	6.9	3.4	10.3	^{128}Xe/^{132}Xe - INT	-	-	-
±	2.9	3.1	4.2	±	-	-	-
^{3}He [in 10^{-16} cc]	7.2	3.6	10.8	^{129}Xe/^{132}Xe - INT	-	-	-
±	3.0	3.3	4.5	±	-	-	-
^{3}He/^{4}He	0.00009	0.00010	0.00009	^{130}Xe/^{132}Xe - INT	-	-	-
±	0.00004	0.00009	0.00004	±	-	-	-
^{22}Ne [in 10^{-8} cc/g]	0.190	0.084	0.275	^{131}Xe/^{132}Xe - INT	-	-	-
±	0.014	0.011	0.018	±	-	-	-
^{22}Ne [in 10^{-12} cc]	0.200	0.089	0.289	^{134}Xe/^{132}Xe - INT	-	-	-
±	0.015	0.012	0.019	±	-	-	-
^{20}Ne/^{22}Ne	9.26	6.95	8.55	^{136}Xe/^{132}Xe - INT	-	-	-
±	0.65	0.93	0.53	±	-	-	-
^{21}Ne/^{22}Ne	0.028	0.014	0.024	^{132}Xe - EXTa [in 10^{-8} cc/g]	-	-	-
±	0.003	0.004	0.003	±	-	-	-
^{21}Ne$_{cos}$ [in 10^{-8} cc/g]	< 0.007 (2σ)	-	-	^{132}Xe - EXTa [in 10^{-12} cc]	-	-	-
±	-	-	-	±	-	-	-
^{21}Ne$_{cos}$ [in 10^{-12} cc]	< 0.007 (2σ)	-	-	^{128}Xe/^{132}Xe - EXTa	-	-	-
±	-	-	-	±	-	-	-
^{20}Ne$_{trap}$ [in 10^{-8} cc/g]	1.8	0.57	2.33	^{129}Xe/^{132}Xe - EXTa	-	-	-
±	0.2	0.11	0.24	±	-	-	-
^{20}Ne$_{trap}$ [in 10^{-12} cc]	1.9	0.60	2.45	^{130}Xe/^{132}Xe - EXTa	-	-	-
±	0.2	0.12	0.25	±	-	-	-
^{36}Ar [in 10^{-8} cc/g]	0.45	0.22	0.67	^{131}Xe/^{132}Xe - EXTa	-	-	-
±	0.02	0.01	0.02	±	-	-	-
^{36}Ar [in 10^{-12} cc]	0.47	0.23	0.70	^{134}Xe/^{132}Xe - EXTa	-	-	-
±	0.02	0.01	0.02	±	-	-	-
^{38}Ar/^{36}Ar	0.191	0.221	0.200	^{136}Xe/^{132}Xe - EXTa	-	-	-
±	0.009	0.016	0.008	±	-	-	-
^{40}Ar/^{36}Ar	287.4	240.8	272.3	^{132}Xe - EXTb [in 10^{-8} cc/g]	-	-	-
±	6.3	8.4	5.1	±	-	-	-
^{40}Ar [in 10^{-8} cc/g]	129.5	52.0	181.5	^{132}Xe - EXTb [in 10^{-12} cc]	-	-	-
±	5.6	2.2	6.0	±	-	-	-
^{40}Ar [in 10^{-12} cc]	136.1	54.6	190.7	^{128}Xe/^{132}Xe - EXTb	-	-	-
±	5.8	2.3	6.3	±	-	-	-
^{38}Ar$_{cos}$ [in 10^{-8} cc/g]	< 0.011 (2σ)	0.008	-	^{129}Xe/^{132}Xe - EXTb	-	-	-
±	-	0.004	-	±	-	-	-
^{38}Ar$_{cos}$ [in 10^{-12} cc]	< 0.012 (2σ)	0.008	-	^{130}Xe/^{132}Xe - EXTb	-	-	-
±	-	0.004	-	±	-	-	-
^{84}Kr [in 10^{-8} cc/g]	-	-	-	^{131}Xe/^{132}Xe - EXTb	-	-	-
±	-	-	-	±	-	-	-
^{84}Kr [in 10^{-12} cc]	-	-	-	^{134}Xe/^{132}Xe - EXTb	-	-	-
±	-	-	-	±	-	-	-
^{80}Kr/^{84}Kr	-	-	-	^{136}Xe/^{132}Xe - EXTb	-	-	-
±	-	-	-	±	-	-	-
^{82}Kr/^{84}Kr	-	-	-	^{21}Ne$_{cos}$/^{38}Ar$_{cos}$	-	-	-
±	-	-	-	±	-	-	-
^{83}Kr/^{84}Kr	-	-	-	^{36}Ar/^{132}Xe $_{(Int)}$	-	-	-
±	-	-	-	±	-	-	-
^{86}Kr/^{84}Kr	-	-	-	^{84}Kr/^{132}Xe $_{(Int)}$	-	-	-
±	-	-	-	±	-	-	-
^{83}Kr$_{cos}$ [in 10^{-8} cc/g]	-	-	-				
±	-	-	-				
^{83}Kr$_{cos}$ [in 10^{-12} cc]	-	-	-				
±	-	-	-				

Table X55. Noble gas data He to Xe for sample 45c.17 (not corrected for blank)

Sample	45c.17						
Size [μm]	630 x 476						
Weight [μg]	126.3 ± 0.2						
Date of measure	31/03/11	31/03/11	31/03/11	**Date of measure**	31/03/11	31/03/11	31/03/11
Laser-Power	3 x 5 W	3 x 15 W		**Laser-Power**	3 x 5 W	3 x 15 W	
Laser-Beam	1000 μm	1000 μm		**Laser-Beam**	1000 μm	1000 μm	
Step(s)	1	2	total*	**Step(s)**	1	2	total*
^{4}He [in 10^{-8} cc/g]	18.1	2.7	20.8	^{132}Xe - INT [in 10^{-8} cc/g]	-	-	-
±	2.4	0.4	2.4	±	-	-	-
^{4}He [in 10^{-12} cc]	22.9	3.4	26.3	^{132}Xe - INT [in 10^{-12} cc]	-	-	-
±	3.1	0.5	3.1	±	-	-	-
^{3}He [in 10^{-12} cc/g]	29.2	5.5	34.6	^{128}Xe/^{132}Xe - INT	-	-	-
±	8.3	3.0	8.9	±	-	-	-
^{3}He [in 10^{-16} cc]	36.8	6.9	43.7	^{129}Xe/^{132}Xe - INT	-	-	-
±	10.5	3.8	11.2	±	-	-	-
^{3}He/^{4}He	0.00016	0.00020	0.00017	^{130}Xe/^{132}Xe - INT	-	-	-
±	0.00005	0.00011	0.00005	±	-	-	-
^{22}Ne [in 10^{-8} cc/g]	0.110	0.063	0.173	^{131}Xe/^{132}Xe - INT	-	-	-
±	0.012	0.011	0.017	±	-	-	-
^{22}Ne [in 10^{-12} cc]	0.138	0.080	0.218	^{134}Xe/^{132}Xe - INT	-	-	-
±	0.015	0.014	0.021	±	-	-	-
^{20}Ne/^{22}Ne	10.18	9.92	10.09	^{136}Xe/^{132}Xe - INT	-	-	-
±	1.10	1.75	0.94	±	-	-	-
^{21}Ne/^{22}Ne	0.041	0.023	0.035	^{132}Xe - EXTa [in 10^{-8} cc/g]	-	-	-
±	0.006	0.006	0.004	±	-	-	-
^{21}Ne$_{cos}$ [in 10^{-8} cc/g]	0.001	-	-	^{132}Xe - EXTa [in 10^{-12} cc]	-	-	-
±	0.001	-	-	±	-	-	-
^{21}Ne$_{cos}$ [in 10^{-12} cc]	0.002	-	-	^{128}Xe/^{132}Xe - EXTa	-	-	-
±	0.001	-	-	±	-	-	-
^{20}Ne$_{trap}$ [in 10^{-8} cc/g]	1.1	0.63	1.74	^{129}Xe/^{132}Xe - EXTa	-	-	-
±	0.2	0.16	0.24	±	-	-	-
^{20}Ne$_{trap}$ [in 10^{-12} cc]	1.4	0.79	2.20	^{130}Xe/^{132}Xe - EXTa	-	-	-
±	0.2	0.20	0.31	±	-	-	-
^{36}Ar [in 10^{-8} cc/g]	1.04	0.23	1.27	^{131}Xe/^{132}Xe - EXTa	-	-	-
±	0.15	0.03	0.15	±	-	-	-
^{36}Ar [in 10^{-12} cc]	1.31	0.29	1.60	^{134}Xe/^{132}Xe - EXTa	-	-	-
±	0.19	0.04	0.19	±	-	-	-
^{38}Ar/^{36}Ar	0.192	0.216	0.196	^{136}Xe/^{132}Xe - EXTa	-	-	-
±	0.007	0.022	0.007	±	-	-	-
^{40}Ar/^{36}Ar	270.3	199.6	257.6	^{132}Xe - EXTb [in 10^{-8} cc/g]	-	-	-
±	6.6	12.0	5.8	±	-	-	-
^{40}Ar [in 10^{-8} cc/g]	281.4	45.4	326.7	^{132}Xe - EXTb [in 10^{-12} cc]	-	-	-
±	40.7	6.8	41.2	±	-	-	-
^{40}Ar [in 10^{-12} cc]	355.4	57.3	412.7	^{128}Xe/^{132}Xe - EXTb	-	-	-
±	51.3	8.5	52.0	±	-	-	-
^{38}Ar$_{cos}$ [in 10^{-8} cc/g]	< 0.020 (2σ)	0.007	-	^{129}Xe/^{132}Xe - EXTb	-	-	-
±	-	0.005	-	±	-	-	-
^{38}Ar$_{cos}$ [in 10^{-12} cc]	< 0.026 (2σ)	0.009	-	^{130}Xe/^{132}Xe - EXTb	-	-	-
±	-	0.006	-	±	-	-	-
^{84}Kr [in 10^{-8} cc/g]	0.0634	-	-	^{131}Xe/^{132}Xe - EXTb	-	-	-
±	0.0079	-	-	±	-	-	-
^{84}Kr [in 10^{-12} cc]	0.0801	-	-	^{134}Xe/^{132}Xe - EXTb	-	-	-
±	0.0100	-	-	±	-	-	-
^{80}Kr/^{84}Kr	0.038	-	-	^{136}Xe/^{132}Xe - EXTb	-	-	-
±	0.002	-	-	±	-	-	-
^{82}Kr/^{84}Kr	0.199	-	-	^{21}Ne$_{cos}$/^{38}Ar$_{cos}$	-	-	-
±	0.005	-	-	±	-	-	-
^{83}Kr/^{84}Kr	0.208	-	-	^{36}Ar/^{132}Xe $_{(Int)}$	-	-	-
±	0.005	-	-	±	-	-	-
^{86}Kr/^{84}Kr	0.296	-	-	^{84}Kr/^{132}Xe $_{(Int)}$	-	-	-
±	0.007	-	-	±	-	-	-
^{83}Kr$_{cos}$ [in 10^{-8} cc/g]	< 0.0011 (2σ)	-	-				
±	-	-	-				
^{83}Kr$_{cos}$ [in 10^{-12} cc]	< 0.0014 (2σ)	-	-				
±	-	-	-				

Table X56. Noble gas data He to Xe for sample 45c.21 (not corrected for blank)

Sample	45c.21						
Size [μm]	720 x 556						
Weight [μg]	337.9 ± 0.2						
Date of measure	28/04/11	28/04/11	28/04/11	**Date of measure**	28/04/11	28/04/11	28/04/11
Laser-Power	3 x 5 W	3 x 15 W		**Laser-Power**	3 x 5 W	3 x 15 W	
Laser-Beam	1000 μm	1000 μm		**Laser-Beam**	1000 μm	1000 μm	
Step(s)	1	2	total*	**Step(s)**	1	2	total*
^{4}He [in 10^{-8} cc/g]	1.3	1.1	2.4	^{132}Xe - INT [in 10^{-8} cc/g]	-	-	-
±	0.0	0.0	0.1	±	-	-	-
^{4}He [in 10^{-12} cc]	4.4	3.6	8.1	^{132}Xe - INT [in 10^{-12} cc]	-	-	-
±	0.2	0.1	0.2	±	-	-	-
^{3}He [in 10^{-12} cc/g]	725.1	< 2.8 (2σ)	-	^{128}Xe/^{132}Xe - INT	-	-	-
±	35.2	-	-	±	-	-	-
^{3}He [in 10^{-16} cc]	2450.7	< 9.6 (2σ)	-	^{129}Xe/^{132}Xe - INT	-	-	-
±	119.1	-	-	±	-	-	-
^{3}He/^{4}He	0.05532	-	-	^{130}Xe/^{132}Xe - INT	-	-	-
±	0.00339	-	-	±	-	-	-
^{22}Ne [in 10^{-8} cc/g]	0.118	0.026	0.144	^{131}Xe/^{132}Xe - INT	-	-	-
±	0.006	0.004	0.007	±	-	-	-
^{22}Ne [in 10^{-12} cc]	0.397	0.089	0.486	^{134}Xe/^{132}Xe - INT	-	-	-
±	0.019	0.012	0.023	±	-	-	-
^{20}Ne/^{22}Ne	9.44	7.29	9.05	^{136}Xe/^{132}Xe - INT	-	-	-
±	0.33	0.96	0.32	±	-	-	-
^{21}Ne/^{22}Ne	0.030	0.011	0.026	^{132}Xe - EXTa [in 10^{-8} cc/g]	-	-	-
±	0.002	0.003	0.002	±	-	-	-
^{21}Ne$_{cos}$ [in 10^{-8} cc/g]	< 0.002 (2σ)	-	-	^{132}Xe - EXTa [in 10^{-12} cc]	-	-	-
±	-	-	-	±	-	-	-
^{21}Ne$_{cos}$ [in 10^{-12} cc]	< 0.007 (2σ)	-	-	^{128}Xe/^{132}Xe - EXTa	-	-	-
±	-	-	-	±	-	-	-
^{20}Ne$_{trap}$ [in 10^{-8} cc/g]	1.1	0.19	1.30	^{129}Xe/^{132}Xe - EXTa	-	-	-
±	0.1	0.04	0.10	±	-	-	-
^{20}Ne$_{trap}$ [in 10^{-12} cc]	3.8	0.63	4.38	^{130}Xe/^{132}Xe - EXTa	-	-	-
±	0.3	0.12	0.33	±	-	-	-
^{36}Ar [in 10^{-8} cc/g]	0.06	0.04	0.09	^{131}Xe/^{132}Xe - EXTa	-	-	-
±	0.01	0.00	0.01	±	-	-	-
^{36}Ar [in 10^{-12} cc]	0.19	0.12	0.31	^{134}Xe/^{132}Xe - EXTa	-	-	-
±	0.03	0.02	0.03	±	-	-	-
^{38}Ar/^{36}Ar	0.174	0.353	0.243	^{136}Xe/^{132}Xe - EXTa	-	-	-
±	0.024	0.037	0.021	±	-	-	-
^{40}Ar/^{36}Ar	315.7	204.0	272.7	^{132}Xe - EXTb [in 10^{-8} cc/g]	-	-	-
±	15.0	13.1	10.7	±	-	-	-
^{40}Ar [in 10^{-8} cc/g]	17.8	7.2	25.0	^{132}Xe - EXTb [in 10^{-12} cc]	-	-	-
±	2.2	0.9	2.4	±	-	-	-
^{40}Ar [in 10^{-12} cc]	60.1	24.3	84.4	^{128}Xe/^{132}Xe - EXTb	-	-	-
±	7.5	3.0	8.1	±	-	-	-
^{38}Ar$_{cos}$ [in 10^{-8} cc/g]	-	0.007	-	^{129}Xe/^{132}Xe - EXTb	-	-	-
±	-	0.001	-	±	-	-	-
^{38}Ar$_{cos}$ [in 10^{-12} cc]	-	0.022	-	^{130}Xe/^{132}Xe - EXTb	-	-	-
±	-	0.005	-	±	-	-	-
^{84}Kr [in 10^{-8} cc/g]	-	-	-	^{131}Xe/^{132}Xe - EXTb	-	-	-
±	-	-	-	±	-	-	-
^{84}Kr [in 10^{-12} cc]	-	-	-	^{134}Xe/^{132}Xe - EXTb	-	-	-
±	-	-	-	±	-	-	-
^{80}Kr/^{84}Kr	-	-	-	^{136}Xe/^{132}Xe - EXTb	-	-	-
±	-	-	-	±	-	-	-
^{82}Kr/^{84}Kr	-	-	-	^{21}Ne$_{cos}$/^{38}Ar$_{cos}$	-	-	-
±	-	-	-	±	-	-	-
^{83}Kr/^{84}Kr	-	-	-	^{36}Ar/^{132}Xe $_{(Int)}$	-	-	-
±	-	-	-	±	-	-	-
^{86}Kr/^{84}Kr	-	-	-	^{84}Kr/^{132}Xe $_{(Int)}$	-	-	-
±	-	-	-	±	-	-	-
^{83}Kr$_{cos}$ [in 10^{-8} cc/g]	-	-	-				
±	-	-	-				
^{83}Kr$_{cos}$ [in 10^{-12} cc]	-	-	-				
±	-	-	-				

Table X57. Noble gas data He to Xe for sample 45c.24 (not corrected for blank)

Sample				45c.24			
Size [μm]				489 x 330			
Weight [μg]				34.0 ± 0.1			
Date of measure	27/09/12	02/10/12	27/09/ + 02/10/12	Date of measure	27/09/12	02/10/12	27/09/ + 02/10/12
Laser-Power	3 x 0.91 W	2 x 5W 1 x 9.8W		Laser-Power	3 x 0.91 W	2 x 5W 1 x 9.8W	
Laser-Beam	600-250 μm	250 μm		Laser-Beam	600-250 μm	250 μm	
Step(s)	1	2	total*	Step(s)	1	2	total*
^{4}He [in 10^{-8} cc/g]	489.9	21.3	511.3	^{132}Xe - INT [in 10^{-8} cc/g]	0.5657	0.0095	0.5752
±	8.4	0.4	8.4	±	0.0084	0.0003	0.0084
^{4}He [in 10^{-12} cc]	166.6	7.3	173.8	^{132}Xe - INT [in 10^{-12} cc]	0.1924	0.0032	0.1956
±	2.8	0.1	2.8	±	0.0028	0.0001	0.0028
^{3}He [in 10^{-12} cc/g]	2972.0	1059.0	4031.0	^{128}Xe/^{132}Xe - INT	0.079	0.090	0.080
±	175.1	255.2	309.5	±	0.002	0.012	0.002
^{3}He [in 10^{-16} cc]	1010.5	360.1	1370.6	^{129}Xe/^{132}Xe - INT	1.029	0.931	1.028
±	59.5	86.7	105.1	±	0.014	0.059	0.014
^{3}He/^{4}He	0.00061	0.00497	0.00079	^{130}Xe/^{132}Xe - INT	0.158	0.153	0.158
±	0.00004	0.00120	0.00006	±	0.002	0.012	0.002
^{22}Ne [in 10^{-8} cc/g]	1.062	0.186	1.248	^{131}Xe/^{132}Xe - INT	0.814	0.697	0.812
±	0.041	0.028	0.049	±	0.010	0.056	0.009
^{22}Ne [in 10^{-12} cc]	0.361	0.063	0.424	^{134}Xe/^{132}Xe - INT	0.384	0.390	0.384
±	0.014	0.009	0.017	±	0.005	0.032	0.005
^{20}Ne/^{22}Ne	11.21	6.89	10.57	^{136}Xe/^{132}Xe - INT	0.325	0.350	0.325
±	0.37	1.02	0.35	±	0.005	0.036	0.005
^{21}Ne/^{22}Ne	0.025	0.011	0.023	^{132}Xe - EXTa [in 10^{-8} cc/g]	0.5692	0.0095	0.5788
±	0.004	0.005	0.003	±	0.0085	0.0003	0.0085
^{21}Ne$_{cos}$ [in 10^{-8} cc/g]	-	-	-	^{132}Xe - EXTa [in 10^{-12} cc]	0.1935	0.0032	0.1968
±	-	-	-	±	0.0028	0.0001	0.0028
^{21}Ne$_{cos}$ [in 10^{-12} cc]	-	-	-	^{128}Xe/^{132}Xe - EXTa	0.081	0.086	0.081
±	-	-	-	±	0.001	0.011	0.001
^{20}Ne$_{trap}$ [in 10^{-8} cc/g]	11.9	1.35	13.26	^{129}Xe/^{132}Xe - EXTa	1.030	0.931	1.028
±	0.9	0.44	1.00	±	0.010	0.059	0.010
^{20}Ne$_{trap}$ [in 10^{-12} cc]	4.0	0.46	4.51	^{130}Xe/^{132}Xe - EXTa	0.158	0.143	0.157
±	0.3	0.15	0.34	±	0.002	0.013	0.002
^{36}Ar [in 10^{-8} cc/g]	24.59	1.10	25.69	^{131}Xe/^{132}Xe - EXTa	0.817	0.699	0.815
±	0.47	0.02	0.47	±	0.009	0.056	0.009
^{36}Ar [in 10^{-12} cc]	8.36	0.37	8.74	^{134}Xe/^{132}Xe - EXTa	0.373	0.365	0.373
±	0.16	0.01	0.16	±	0.004	0.030	0.004
^{38}Ar/^{36}Ar	0.183	0.184	0.183	^{136}Xe/^{132}Xe - EXTa	0.316	0.289	0.315
±	0.004	0.005	0.004	±	0.004	0.022	0.004
^{40}Ar/^{36}Ar	10.7	216.8	19.6	^{132}Xe - EXTb [in 10^{-8} cc/g]	0.5669	0.0089	0.5758
±	0.2	4.2	0.2	±	0.0164	0.0004	0.0164
^{40}Ar [in 10^{-8} cc/g]	264.2	238.6	502.8	^{132}Xe - EXTb [in 10^{-12} cc]	0.1927	0.0030	0.1958
±	6.3	5.9	8.6	±	0.0056	0.0001	0.0056
^{40}Ar [in 10^{-12} cc]	89.8	81.1	171.0	^{128}Xe/^{132}Xe - EXTb	0.082	0.063	0.081
±	2.1	2.0	2.9	±	0.001	0.010	0.001
^{38}Ar$_{cos}$ [in 10^{-8} cc/g]	-	-	-	^{129}Xe/^{132}Xe - EXTb	1.029	0.931	1.028
±	-	-	-	±	0.010	0.059	0.010
^{38}Ar$_{cos}$ [in 10^{-12} cc]	-	-	-	^{130}Xe/^{132}Xe - EXTb	0.162	0.159	0.162
±	-	-	-	±	0.002	0.015	0.002
^{84}Kr [in 10^{-8} cc/g]	0.3293	0.0258	0.3551	^{131}Xe/^{132}Xe - EXTb	0.816	0.698	0.814
±	0.0244	0.0021	0.0245	±	0.004	0.003	0.004
^{84}Kr [in 10^{-12} cc]	0.1120	0.0088	0.1207	^{134}Xe/^{132}Xe - EXTb	0.383	0.423	0.384
±	0.0083	0.0007	0.0083	±	0.004	0.028	0.004
^{80}Kr/^{84}Kr	0.043	0.052	0.044	^{136}Xe/^{132}Xe - EXTb	0.317	0.362	0.317
±	0.003	0.008	0.002	±	0.003	0.026	0.003
^{82}Kr/^{84}Kr	0.217	0.209	0.217	^{21}Ne$_{cos}$/^{38}Ar$_{cos}$	-	-	-
±	0.013	0.023	0.012	±	-	-	-
^{83}Kr/^{84}Kr	0.202	0.174	0.200	^{36}Ar/^{132}Xe $_{(Int)}$	43.47	116.17	44.67
±	0.010	0.019	0.009	±	1.04	4.85	1.04
^{86}Kr/^{84}Kr	0.323	0.275	0.319	^{84}Kr/^{132}Xe $_{(Int)}$	0.58	2.72	0.62
±	0.017	0.030	0.016	±	0.04	0.24	0.04
^{83}Kr$_{cos}$ [in 10^{-8} cc/g]	-	-	-				
±	-	-	-				
^{83}Kr$_{cos}$ [in 10^{-12} cc]	-	-	-				
±	-	-	-				

Table X58. Noble gas data He to Xe for sample 45c.25_2 (not corrected for blank)

Sample	45c.25_2						
Size [µm]	580 x 528						
Weight [µg]	142.3 ± 0.1						
Date of measure	19/04/12	20/04/12	19+20/04/12	**Date of measure**	19/04/12	20/04/12	19+20/04/12
Laser-Power	3 x 0.91 W	3 x 5 W		**Laser-Power**	3 x 0.91 W	3 x 5 W	
Laser-Beam	600 µm	600 µm		**Laser-Beam**	600 µm	600 µm	
Step(s)	1	2	total*	**Step(s)**	1	2	total*
^{4}He [in 10^{-8} cc/g]	26.8	1.0	27.9	^{132}Xe - INT [in 10^{-8} cc/g]	0.1924	0.0085	0.2009
±	0.5	0.0	0.5	±	0.0112	0.0005	0.0112
^{4}He [in 10^{-12} cc]	38.2	1.5	39.6	^{132}Xe - INT [in 10^{-12} cc]	0.2738	0.0121	0.2858
±	0.7	0.0	0.7	±	0.0159	0.0007	0.0159
^{3}He [in 10^{-12} cc/g]	407.1	< 30.1 (2σ)	-	^{128}Xe/^{132}Xe - INT	0.072	0.069	0.072
±	103.3	-	-	±	0.002	0.005	0.002
^{3}He [in 10^{-16} cc]	579.3	< 42.8 (2σ)	-	^{129}Xe/^{132}Xe - INT	0.989	0.923	0.987
±	147.0	-	-	±	0.008	0.029	0.008
^{3}He/^{4}He	0.00152	-	-	^{130}Xe/^{132}Xe - INT	0.151	0.149	0.151
±	0.00039	-	-	±	0.001	0.006	0.001
^{22}Ne [in 10^{-8} cc/g]	0.045	0.029	0.073	^{131}Xe/^{132}Xe - INT	0.784	0.794	0.784
±	0.006	0.005	0.007	±	0.006	0.030	0.006
^{22}Ne [in 10^{-12} cc]	0.064	0.041	0.104	^{134}Xe/^{132}Xe - INT	0.388	0.370	0.387
±	0.008	0.007	0.011	±	0.003	0.014	0.003
^{20}Ne/^{22}Ne	10.51	10.27	10.41	^{136}Xe/^{132}Xe - INT	0.331	0.313	0.330
±	1.29	1.79	1.05	±	0.005	0.017	0.005
^{21}Ne/^{22}Ne	0.038	0.022	0.032	^{132}Xe - EXTa [in 10^{-8} cc/g]	0.1945	0.0086	0.2030
±	0.008	0.008	0.006	±	0.0033	0.0002	0.0033
^{21}Ne$_{cos}$ [in 10^{-8} cc/g]	0.0004	-	-	^{132}Xe - EXTa [in 10^{-12} cc]	0.2767	0.0122	0.2889
±	0.0004	-	-	±	0.0047	0.0003	0.0047
^{21}Ne$_{cos}$ [in 10^{-12} cc]	0.001	-	-	^{128}Xe/^{132}Xe - EXTa	0.070	0.070	0.070
±	0.001	-	-	±	0.002	0.005	0.002
^{20}Ne$_{trap}$ [in 10^{-8} cc/g]	0.5	0.29	0.76	^{129}Xe/^{132}Xe - EXTa	0.987	0.922	0.985
±	0.1	0.07	0.11	±	0.007	0.029	0.007
^{20}Ne$_{trap}$ [in 10^{-12} cc]	0.7	0.42	1.09	^{130}Xe/^{132}Xe - EXTa	0.150	0.148	0.150
±	0.1	0.11	0.16	±	0.002	0.008	0.002
^{36}Ar [in 10^{-8} cc/g]	1.38	2.05	3.43	^{131}Xe/^{132}Xe - EXTa	0.782	0.794	0.783
±	0.15	0.23	0.27	±	0.006	0.030	0.006
^{36}Ar [in 10^{-12} cc]	1.97	2.91	4.88	^{134}Xe/^{132}Xe - EXTa	0.387	0.397	0.387
±	0.22	0.32	0.39	±	0.003	0.014	0.003
^{38}Ar/^{36}Ar	0.190	0.185	0.187	^{136}Xe/^{132}Xe - EXTa	0.324	0.316	0.324
±	0.002	0.002	0.002	±	0.004	0.013	0.004
^{40}Ar/^{36}Ar	391.4	279.1	324.4	^{132}Xe - EXTb [in 10^{-8} cc/g]	0.1937	0.0085	0.2022
±	4.1	2.9	3.5	±	0.0067	0.0003	0.0067
^{40}Ar [in 10^{-8} cc/g]	541.1	571.4	1112.4	^{132}Xe - EXTb [in 10^{-12} cc]	0.2756	0.0121	0.2877
±	60.4	63.7	87.8	±	0.0095	0.0005	0.0096
^{40}Ar [in 10^{-12} cc]	770.0	813.0	1583.0	^{128}Xe/^{132}Xe - EXTb	0.068	0.066	0.068
±	85.9	90.7	124.9	±	0.002	0.005	0.002
^{38}Ar$_{cos}$ [in 10^{-8} cc/g]	< 0.012 (2σ)	-	-	^{129}Xe/^{132}Xe - EXTb	0.988	0.923	0.985
±	-	-	-	±	0.008	0.029	0.008
^{38}Ar$_{cos}$ [in 10^{-12} cc]	< 0.017 (2σ)	-	-	^{130}Xe/^{132}Xe - EXTb	0.151	0.157	0.151
±	-	-	-	±	0.002	0.007	0.002
^{84}Kr [in 10^{-8} cc/g]	0.1743	0.0326	0.2069	^{131}Xe/^{132}Xe - EXTb	0.782	0.794	0.783
±	0.0136	0.0026	0.0138	±	0.004	0.004	0.004
^{84}Kr [in 10^{-12} cc]	0.2481	0.0464	0.2944	^{134}Xe/^{132}Xe - EXTb	0.390	0.376	0.389
±	0.0194	0.0037	0.0197	±	0.003	0.013	0.003
^{80}Kr/^{84}Kr	0.039	0.042	0.039	^{136}Xe/^{132}Xe - EXTb	0.332	0.344	0.333
±	0.001	0.003	0.001	±	0.003	0.012	0.003
^{82}Kr/^{84}Kr	0.200	0.195	0.200	^{21}Ne$_{cos}$/^{38}Ar$_{cos}$	-	-	-
±	0.003	0.007	0.003	±	-	-	-
^{83}Kr/^{84}Kr	0.204	0.204	0.204	^{36}Ar/^{132}Xe$_{(Int)}$	7.19	241.67	17.07
±	0.003	0.008	0.003	±	0.90	30.53	1.66
^{86}Kr/^{84}Kr	0.303	0.298	0.302	^{84}Kr/^{132}Xe$_{(Int)}$	0.91	3.85	1.03
±	0.004	0.011	0.004	±	0.09	0.38	0.09
^{83}Kr$_{cos}$ [in 10^{-8} cc/g]	< 0.0020 (2σ)	< 0.0006 (2σ)	-				
±	-	-	-				
^{83}Kr$_{cos}$ [in 10^{-12} cc]	< 0.0028 (2σ)	< 0.0009 (2σ)	-				
±	-	-	-				

Table X59. Noble gas data He to Xe for sample 45c.27_2 (not corrected for blank)

Sample	45c.27_2						
Size [μm]	521 x 337						
Weight [μg]	38.0 ± 0.1						
Date of measure	09/06/11	14/06/11	09+14/06/11	Date of measure	09/06/11	14/06/11	09+14/06/11
Laser-Power	3 x 5 W	3 x 15 W		Laser-Power	3 x 5 W	3 x 15 W	
Laser-Beam	600 μm	360 μm		Laser-Beam	600 μm	360 μm	
Step(s)	1	2	total*	Step(s)	1	2	total*
^{4}He [in 10^{-8} cc/g]	14.4	-	-	^{132}Xe - INT [in 10^{-8} cc/g]	0.0250	0.0050	0.0300
±	0.7	-	-	±	0.0006	0.0002	0.0007
^{4}He [in 10^{-12} cc]	5.5	-	-	^{132}Xe - INT [in 10^{-12} cc]	0.0095	0.0019	0.0114
±	0.3	-	-	±	0.0002	0.0001	0.0003
^{3}He [in 10^{-12} cc/g]	< 22.2 (2σ)	-		^{128}Xe/^{132}Xe - INT	0.078	0.087	0.079
±	-	-	-	±	0.005	0.012	0.004
^{3}He [in 10^{-16} cc]	< 8.4 (2σ)	-		^{129}Xe/^{132}Xe - INT	0.948	0.979	0.953
±	-	-	-	±	0.025	0.065	0.023
^{3}He/^{4}He	-	-	-	^{130}Xe/^{132}Xe - INT	0.154	0.131	0.150
±	-	-	-	±	0.005	0.011	0.005
^{22}Ne [in 10^{-8} cc/g]	0.778	0.201	0.979	^{131}Xe/^{132}Xe - INT	0.793	0.857	0.803
±	0.027	0.024	0.036	±	0.029	0.064	0.027
^{22}Ne [in 10^{-12} cc]	0.296	0.077	0.372	^{134}Xe/^{132}Xe - INT	0.415	0.436	0.418
±	0.010	0.009	0.014	±	0.013	0.032	0.012
^{20}Ne/^{22}Ne	9.66	7.38	9.19	^{136}Xe/^{132}Xe - INT	0.336	0.353	0.339
±	0.33	0.89	0.32	±	0.014	0.037	0.013
^{21}Ne/^{22}Ne	0.052	0.018	0.045	^{132}Xe - EXTa [in 10^{-8} cc/g]	0.0249	0.0050	0.0299
±	0.004	0.004	0.003	±	0.0061	0.0012	0.0062
^{21}Ne$_{cos}$ [in 10^{-8} cc/g]	0.018	-	-	^{132}Xe - EXTa [in 10^{-12} cc]	0.0095	0.0019	0.0114
±	0.003	-	-	±	0.0023	0.0005	0.0024
^{21}Ne$_{cos}$ [in 10^{-12} cc]	0.007	-	-	^{128}Xe/^{132}Xe - EXTa	0.076	0.099	0.080
±	0.001	-	-	±	0.004	0.012	0.004
^{20}Ne$_{trap}$ [in 10^{-8} cc/g]	7.5	1.44	8.93	^{129}Xe/^{132}Xe - EXTa	0.948	0.979	0.953
±	0.6	0.26	0.61	±	0.025	0.065	0.023
^{20}Ne$_{trap}$ [in 10^{-12} cc]	2.8	0.55	3.39	^{130}Xe/^{132}Xe - EXTa	0.149	0.139	0.147
±	0.2	0.10	0.23	±	0.006	0.015	0.006
^{36}Ar [in 10^{-8} cc/g]	1.96	0.33	2.29	^{131}Xe/^{132}Xe - EXTa	0.793	0.857	0.803
±	0.08	0.02	0.08	±	0.029	0.064	0.027
^{36}Ar [in 10^{-12} cc]	0.75	0.13	0.87	^{134}Xe/^{132}Xe - EXTa	0.428	0.404	0.424
±	0.03	0.01	0.03	±	0.012	0.027	0.011
^{38}Ar/^{36}Ar	0.177	0.225	0.184	^{136}Xe/^{132}Xe - EXTa	0.361	0.343	0.358
±	0.005	0.020	0.005	±	0.011	0.027	0.010
^{40}Ar/^{36}Ar	227.9	250.1	231.1	^{132}Xe - EXTb [in 10^{-8} cc/g]	0.0241	0.0053	0.0293
±	5.0	11.1	4.6	±	0.0072	0.0016	0.0073
^{40}Ar [in 10^{-8} cc/g]	447.1	82.3	529.4	^{132}Xe - EXTb [in 10^{-12} cc]	0.0091	0.0020	0.0111
±	20.4	3.8	20.8	±	0.0027	0.0006	0.0028
^{40}Ar [in 10^{-12} cc]	169.9	31.3	201.2	^{128}Xe/^{132}Xe - EXTb	0.067	0.069	0.068
±	7.7	1.4	7.9	±	0.004	0.011	0.004
^{38}Ar$_{cos}$ [in 10^{-8} cc/g]	-	0.014	-	^{129}Xe/^{132}Xe - EXTb	0.948	0.979	0.953
±	-	0.007	-	±	0.025	0.065	0.024
^{38}Ar$_{cos}$ [in 10^{-12} cc]	-	0.005	-	^{130}Xe/^{132}Xe - EXTb	0.157	0.142	0.154
±	-	0.003	-	±	0.007	0.014	0.006
^{84}Kr [in 10^{-8} cc/g]	0.0962	0.0151	0.1113	^{131}Xe/^{132}Xe - EXTb	0.793	0.857	0.804
±	0.0043	0.0009	0.0043	±	0.002	0.002	0.002
^{84}Kr [in 10^{-12} cc]	0.0366	0.0057	0.0423	^{134}Xe/^{132}Xe - EXTb	0.429	0.412	0.426
±	0.0016	0.0003	0.0016	±	0.012	0.028	0.011
^{80}Kr/^{84}Kr	0.040	0.070	0.044	^{136}Xe/^{132}Xe - EXTb	0.359	0.309	0.350
±	0.003	0.010	0.003	±	0.011	0.024	0.010
^{82}Kr/^{84}Kr	0.189	0.217	0.192	^{21}Ne$_{cos}$/^{38}Ar$_{cos}$	-	-	-
±	0.007	0.019	0.006	±	-	-	-
^{83}Kr/^{84}Kr	0.197	0.201	0.197	^{36}Ar/^{132}Xe $_{(Int)}$	78.53	66.09	76.46
±	0.006	0.018	0.006	±	3.81	4.60	3.25
^{86}Kr/^{84}Kr	0.293	0.281	0.292	^{84}Kr/^{132}Xe $_{(Int)}$	3.85	3.03	3.72
±	0.009	0.027	0.009	±	0.20	0.21	0.17
^{83}Kr$_{cos}$ [in 10^{-8} cc/g]	-	-	-				
±	-	-	-				
^{83}Kr$_{cos}$ [in 10^{-12} cc]	-	-	-				
±	-	-	-				

Table X60. Noble gas data He to Xe for sample 45c.29_1 (not corrected for blank)

Sample					45c.29_1				
Size [µm]					337 x 255				
Weight [µg]					22.1 ± 0.2				
Date of measure	18/09/12	19/09/12	19/09/12	18/09/ + 19/09/12	Date of measure	18/09/12	19/09/12	19/09/12	18/09/ + 19/09/12
Laser-Power	3 x 0.91 W	2 x 5 W 1 x 30 W	3 x 5-30 W		Laser-Power	3 x 0.91 W	2 x 5 W 1 x 30 W	3 x 5-30 W	
Laser-Beam	360-250 µm	250 µm	600-200 µm		Laser-Beam	360-250 µm	250 µm	600-200 µm	
Step(s)	1	2	3	total*	Step(s)	1	2	3	total*
^{4}He [in 10^{-8} cc/g]	372.3	86.4	28.8	487.4	^{132}Xe - INT [in 10^{-8} cc/g]	0.1581	0.0327	-	0.1908
±	16.4	3.5	0.7	16.8	±	0.0217	0.0045	-	0.0222
^{4}He [in 10^{-12} cc]	82.3	19.1	6.4	107.7	^{132}Xe - INT [in 10^{-12} cc]	0.0349	0.0072	-	0.0422
±	3.5	0.8	0.1	3.6	±	0.0048	0.0010	-	0.0049
^{3}He [in 10^{-12} cc/g]	43765.8	13834.9	1667.6	59268.3	^{128}Xe/^{132}Xe - INT	0.070	0.102	-	0.075
±	1023.6	361.9	342.1	1138.3	±	0.003	0.010	-	0.003
^{3}He [in 10^{-16} cc]	9672.2	3057.5	368.5	13098.3	^{129}Xe/^{132}Xe - INT	0.909	1.259	-	0.969
±	208.6	75.0	75.5	221.9	±	0.024	0.047	-	0.021
^{3}He/^{4}He	0.01176	0.01601	0.00580	0.01216	^{130}Xe/^{132}Xe - INT	0.141	0.158	-	0.144
±	0.00057	0.00074	0.00119	0.00045	±	0.004	0.009	-	0.004
^{22}Ne [in 10^{-8} cc/g]	8.968	20.595	0.280	29.843	^{131}Xe/^{132}Xe - INT	0.790	0.791	-	0.790
±	0.218	0.467	0.069	0.520	±	0.020	0.042	-	0.018
^{22}Ne [in 10^{-12} cc]	1.982	4.551	0.062	6.595	^{134}Xe/^{132}Xe - INT	0.394	0.420	-	0.399
±	0.045	0.095	0.015	0.098	±	0.011	0.022	-	0.010
^{20}Ne/^{22}Ne	7.25	4.56	4.20	5.36	^{136}Xe/^{132}Xe - INT	0.358	0.379	-	0.362
±	0.09	0.04	1.45	0.04	±	0.013	0.029	-	0.012
^{21}Ne/^{22}Ne	0.395	0.634	-	0.562	^{132}Xe - EXTa [in 10^{-8} cc/g]	0.1509	0.0312	-	0.1822
±	0.008	0.009	-	0.007	±	0.0207	0.0043	-	0.0211
^{21}Ne$_{cos}$ [in 10^{-8} cc/g]	3.347	12.793	< 0.018 (2σ)	16.140	^{132}Xe - EXTa [in 10^{-12} cc]	0.0334	0.0069	-	0.0403
±	0.105	0.340	-	0.356	±	0.0046	0.0010	-	0.0047
^{21}Ne$_{cos}$ [in 10^{-12} cc]	0.740	2.827	< 0.004 (2σ)	3.567	^{128}Xe/^{132}Xe - EXTa	0.065	0.093	-	0.070
±	0.022	0.071	-	0.072	±	0.004	0.009	-	0.004
^{20}Ne$_{trap}$ [in 10^{-8} cc/g]	62.4	83.25	1.17	146.78	^{129}Xe/^{132}Xe - EXTa	0.901	1.249	-	0.961
±	3.9	5.32	0.53	6.63	±	0.023	0.047	-	0.021
^{20}Ne$_{trap}$ [in 10^{-12} cc]	13.8	18.40	0.26	32.44	^{130}Xe/^{132}Xe - EXTa	0.139	0.161	-	0.143
±	0.9	1.16	0.12	1.44	±	0.006	0.012	-	0.005
^{36}Ar [in 10^{-8} cc/g]	25.33	32.07	-	57.40	^{131}Xe/^{132}Xe - EXTa	0.789	0.789	-	0.789
±	0.54	0.87	-	1.02	±	0.020	0.042	-	0.018
^{36}Ar [in 10^{-12} cc]	5.60	7.09	-	12.68	^{134}Xe/^{132}Xe - EXTa	0.406	0.411	-	0.407
±	0.11	0.18	-	0.19	±	0.011	0.021	-	0.010
^{38}Ar/^{36}Ar	0.235	0.248	-	0.242	^{136}Xe/^{132}Xe - EXTa	0.378	0.373	-	0.377
±	0.004	0.011	-	0.006	±	0.018	0.027	-	0.015
^{40}Ar/^{36}Ar	86.3	44.7	-	63.0	^{132}Xe - EXTb [in 10^{-8} cc/g]	0.1476	0.0323	-	0.1798
±	0.8	0.9	-	0.6	±	0.0190	0.0042	-	0.0195
^{40}Ar [in 10^{-8} cc/g]	2184.5	1433.2	-	3617.7	^{132}Xe - EXTb [in 10^{-12} cc]	0.0326	0.0071	-	0.0397
±	50.4	33.0	-	60.2	±	0.0042	0.0009	-	0.0043
^{40}Ar [in 10^{-12} cc]	482.8	316.7	-	799.5	^{128}Xe/^{132}Xe - EXTb	0.064	0.081	-	0.067
±	10.2	6.7	-	11.2	±	0.004	0.008	-	0.003
^{38}Ar$_{cos}$ [in 10^{-8} cc/g]	1.337	2.157	-	3.494	^{129}Xe/^{132}Xe - EXTb	0.901	1.249	-	0.964
±	0.128	0.331	-	0.354	±	0.023	0.047	-	0.021
^{38}Ar$_{cos}$ [in 10^{-12} cc]	0.295	0.477	-	0.772	^{130}Xe/^{132}Xe - EXTb	0.136	0.144	-	0.137
±	0.028	0.073	-	0.078	±	0.005	0.011	-	0.005
^{84}Kr [in 10^{-8} cc/g]	0.6521	0.1295	-	0.7816	^{131}Xe/^{132}Xe - EXTb	0.789	0.789	-	0.789
±	0.0206	0.0048	-	0.0211	±	0.004	0.004	-	0.003
^{84}Kr [in 10^{-12} cc]	0.1441	0.0286	-	0.1727	^{134}Xe/^{132}Xe - EXTb	0.396	0.412	-	0.399
±	0.0044	0.0010	-	0.0044	±	0.011	0.020	-	0.009
^{80}Kr/^{84}Kr	0.037	0.071	-	0.043	^{136}Xe/^{132}Xe - EXTb	0.374	0.367	-	0.373
±	0.002	0.006	-	0.002	±	0.015	0.022	-	0.013
^{82}Kr/^{84}Kr	0.196	0.198	-	0.196	^{21}Ne$_{cos}$/^{38}Ar$_{cos}$	2.50	5.93	-	4.62
±	0.010	0.014	-	0.009	±	0.25	0.92	-	0.48
^{83}Kr/^{84}Kr	0.203	0.195	-	0.202	^{36}Ar/^{132}Xe $_{(Int)}$	160.19	980.60	-	300.82
±	0.008	0.012	-	0.007	±	22.17	138.27	-	35.17
^{86}Kr/^{84}Kr	0.328	0.331	-	0.328	^{84}Kr/^{132}Xe $_{(Int)}$	4.12	3.96	-	4.10
±	0.015	0.020	-	0.013	±	0.58	0.57	-	0.49
^{83}Kr$_{cos}$ [in 10^{-8} cc/g]	< 0.0125 (2σ)	-	-	-					
±	-	-	-	-					
^{83}Kr$_{cos}$ [in 10^{-12} cc]	< 0.0028 (2σ)	-	-	-					
±	-	-	-	-					

Table X61. Noble gas data He to Xe for sample 45c.29_2 (not corrected for blank)

Sample				45c.29_2			
Size [µm]				305 x 187			
Weight [µg]				24.2 ± 0.2			
Date of measure	12/06/12	13/06/12	12+13/06/12	Date of measure	12/06/12	13/06/12	12+13/06/12
Laser-Power	3 x 0.91 W	3 x 5 W		Laser-Power	3 x 0.91 W	3 x 5 W	
Laser-Beam	360-250 µm	250 µm		Laser-Beam	360-250 µm	250 µm	
Step(s)	1	2	total*	Step(s)	1	2	total*
^{4}He [in 10^{-8} cc/g]	4403.8	4.8	4408.5	^{132}Xe - INT [in 10^{-8} cc/g]	0.1419	$	$
±	189.7	0.2	189.7	±	0.0028	$	$
^{4}He [in 10^{-12} cc]	1065.7	1.2	1066.9	^{132}Xe - INT [in 10^{-12} cc]	0.0343	0.0023	0.0366
±	45.1	0.1	45.1	±	0.0006	0.0001	0.0013
^{3}He [in 10^{-12} cc/g]	26476.3	< 1057.9 (2σ)	-	^{128}Xe/^{132}Xe - INT	0.068	-	-
±	1170.7	-	-	±	0.003	-	-
^{3}He [in 10^{-16} cc]	6407.3	< 256.0 (2σ)	-	^{129}Xe/^{132}Xe - INT	1.053	1.030	1.053
±	278.3	-	-	±	0.020	0.074	0.020
^{3}He/^{4}He	0.00060	-	-	^{130}Xe/^{132}Xe - INT	0.146	0.169	0.146
±	0.00004	-	-	±	0.003	0.014	0.003
^{22}Ne [in 10^{-8} cc/g]	16.857	0.205	17.062	^{131}Xe/^{132}Xe - INT	0.798	1.057	0.798
±	0.266	0.034	0.268	±	0.014	0.068	0.014
^{22}Ne [in 10^{-12} cc]	4.079	0.050	4.129	^{134}Xe/^{132}Xe - INT	0.413	0.359	0.413
±	0.055	0.008	0.055	±	0.010	0.031	0.010
^{20}Ne/^{22}Ne	8.27	11.31	8.31	^{136}Xe/^{132}Xe - INT	0.390	0.263	0.390
±	0.06	1.86	0.07	±	0.011	0.032	0.011
^{21}Ne/^{22}Ne	0.337	0.095	0.334	^{132}Xe - EXTa [in 10^{-8} cc/g]	0.1406	0.0094	0.1500
±	0.005	0.018	0.005	±	0.0039	0.0004	0.0039
^{21}Ne$_{cos}$ [in 10^{-8} cc/g]	5.317	0.013	5.330	^{132}Xe - EXTa [in 10^{-12} cc]	0.0340	0.0023	0.0363
±	0.117	0.004	0.117	±	0.0009	0.0001	0.0009
^{21}Ne$_{cos}$ [in 10^{-12} cc]	1.287	0.003	1.290	^{128}Xe/^{132}Xe - EXTa	0.067	-	-
±	0.026	0.001	0.026	±	0.003	-	-
^{20}Ne$_{trap}$ [in 10^{-8} cc/g]	135.3	2.32	137.63	^{129}Xe/^{132}Xe - EXTa	1.050	1.029	1.049
±	8.0	0.56	7.98	±	0.021	0.074	0.020
^{20}Ne$_{trap}$ [in 10^{-12} cc]	32.7	0.56	33.31	^{130}Xe/^{132}Xe - EXTa	0.145	0.154	0.146
±	1.9	0.14	1.91	±	0.004	0.015	0.004
^{36}Ar [in 10^{-8} cc/g]	41.55	2.22	43.77	^{131}Xe/^{132}Xe - EXTa	0.800	1.061	0.816
±	1.58	0.09	1.58	±	0.015	0.068	0.014
^{36}Ar [in 10^{-12} cc]	10.05	0.54	10.59	^{134}Xe/^{132}Xe - EXTa	0.392	0.402	0.393
±	0.37	0.02	0.37	±	0.008	0.029	0.008
^{38}Ar/^{36}Ar	0.341	0.207	0.334	^{136}Xe/^{132}Xe - EXTa	0.344	0.278	0.340
±	0.002	0.004	0.002	±	0.008	0.025	0.008
^{40}Ar/^{36}Ar	114.3	245.8	121.0	^{132}Xe - EXTb [in 10^{-8} cc/g]	0.1390	0.0087	0.1478
±	1.2	3.6	1.1	±	0.0039	0.0004	0.0039
^{40}Ar [in 10^{-8} cc/g]	4925.4	566.6	5492.1	^{132}Xe - EXTb [in 10^{-12} cc]	0.0336	0.0021	0.0358
±	100.5	12.1	101.2	±	0.0009	0.0001	0.0009
^{40}Ar [in 10^{-12} cc]	1192.0	137.1	1329.1	^{128}Xe/^{132}Xe - EXTb	0.071	0.085	0.072
±	22.2	2.7	21.9	±	0.003	0.012	0.003
^{38}Ar$_{cos}$ [in 10^{-8} cc/g]	7.209	0.047	7.256	^{129}Xe/^{132}Xe - EXTb	1.051	1.030	1.050
±	0.301	0.012	0.301	±	0.021	0.074	0.020
^{38}Ar$_{cos}$ [in 10^{-12} cc]	1.745	0.011	1.756	^{130}Xe/^{132}Xe - EXTb	0.149	0.155	0.149
±	0.071	0.003	0.071	±	0.005	0.016	0.004
^{84}Kr [in 10^{-8} cc/g]	1.0130	0.0793	1.0923	^{131}Xe/^{132}Xe - EXTb	0.801	1.062	0.816
±	0.0642	0.0053	0.0645	±	0.004	0.005	0.004
^{84}Kr [in 10^{-12} cc]	0.2451	0.0192	0.2643	^{134}Xe/^{132}Xe - EXTb	0.417	0.408	0.416
±	0.0154	0.0013	0.0154	±	0.009	0.030	0.008
^{80}Kr/^{84}Kr	0.044	0.049	0.044	^{136}Xe/^{132}Xe - EXTb	0.372	0.338	0.370
±	0.001	0.006	0.001	±	0.008	0.027	0.007
^{82}Kr/^{84}Kr	0.183	0.221	0.186	^{21}Ne$_{cos}$/^{38}Ar$_{cos}$	0.74	0.29	0.73
±	0.003	0.012	0.003	±	0.03	0.11	0.03
^{83}Kr/^{84}Kr	0.196	0.214	0.197	^{36}Ar/^{132}Xe $_{(Int)}$	292.78	234.16	289.11
±	0.004	0.011	0.004	±	12.10	12.98	14.56
^{86}Kr/^{84}Kr	0.317	0.277	0.314	^{84}Kr/^{132}Xe $_{(Int)}$	7.14	8.36	7.22
±	0.005	0.017	0.005	±	0.47	0.65	0.50
^{83}Kr$_{cos}$ [in 10^{-8} cc/g]	-	0.0010	-				
±	-	0.0009	-				
^{83}Kr$_{cos}$ [in 10^{-12} cc]	-	0.0002	-				
±	-	0.0002	-				

Table X62. Noble gas data He to Xe for sample 45c.31_1 (not corrected for blank)

Sample			45c.31_1				
Size [µm]			460 x 372				
Weight [µg]			33.2 ± 0.1				
Date of measure	22/02/12	23/02/12	22+23/02/12	Date of measure	22/02/12	23/02/12	22+23/02/12
Laser-Power	3 x 0.91 W	3 x 5 W		Laser-Power	3 x 0.91 W	3 x 5 W	
Laser-Beam	600 µm	360 µm		Laser-Beam	600 µm	360 µm	
Step(s)	1	2	total*	Step(s)	1	2	total*
^{4}He [in 10^{-8} cc/g]	791.3	211.4	1002.7	^{132}Xe - INT [in 10^{-8} cc/g]	0.1655	0.0412	0.2067
±	16.0	4.6	16.7	±	0.0072	0.0019	0.0074
^{4}He [in 10^{-12} cc]	262.7	70.2	332.9	^{132}Xe - INT [in 10^{-12} cc]	0.0549	0.0137	0.0686
±	5.3	1.5	5.4	±	0.0024	0.0006	0.0024
^{3}He [in 10^{-12} cc/g]	2880.1	958.0	3838.1	^{128}Xe/^{132}Xe - INT	0.082	0.076	0.081
±	492.6	481.8	689.0	±	0.003	0.005	0.002
^{3}He [in 10^{-16} cc]	956.2	318.0	1274.2	^{129}Xe/^{132}Xe - INT	1.034	1.082	1.043
±	163.5	160.0	228.7	±	0.016	0.027	0.014
^{3}He/^{4}He	0.00036	0.00045	0.00038	^{130}Xe/^{132}Xe - INT	0.152	0.165	0.154
±	0.00006	0.00023	0.00007	±	0.003	0.006	0.002
^{22}Ne [in 10^{-8} cc/g]	4.526	9.608	14.133	^{131}Xe/^{132}Xe - INT	0.794	0.751	0.786
±	0.072	0.139	0.156	±	0.012	0.022	0.011
^{22}Ne [in 10^{-12} cc]	1.503	3.190	4.692	^{134}Xe/^{132}Xe - INT	0.398	0.384	0.395
±	0.023	0.045	0.050	±	0.007	0.013	0.006
^{20}Ne/^{22}Ne	11.73	11.81	11.78	^{136}Xe/^{132}Xe - INT	0.343	0.350	0.345
±	0.13	0.10	0.08	±	0.008	0.016	0.007
^{21}Ne/^{22}Ne	0.034	0.039	0.038	^{132}Xe - EXTa [in 10^{-8} cc/g]	0.1657	0.0413	0.2070
±	0.001	0.001	0.001	±	0.0283	0.0071	0.0291
^{21}Ne$_{cos}$ [in 10^{-8} cc/g]	0.019	0.086	0.105	^{132}Xe - EXTa [in 10^{-12} cc]	0.0550	0.0137	0.0687
±	0.007	0.011	0.013	±	0.0094	0.0023	0.0097
^{21}Ne$_{cos}$ [in 10^{-12} cc]	0.006	0.029	0.035	^{128}Xe/^{132}Xe - EXTa	0.081	0.071	0.079
±	0.002	0.004	0.004	±	0.002	0.004	0.002
^{20}Ne$_{trap}$ [in 10^{-8} cc/g]	53.1	113.47	166.55	^{129}Xe/^{132}Xe - EXTa	1.032	1.082	1.042
±	3.1	6.53	7.22	±	0.016	0.027	0.014
^{20}Ne$_{trap}$ [in 10^{-12} cc]	17.6	37.67	55.30	^{130}Xe/^{132}Xe - EXTa	0.153	0.161	0.154
±	1.0	2.16	2.39	±	0.003	0.007	0.003
^{36}Ar [in 10^{-8} cc/g]	17.62	13.19	30.81	^{131}Xe/^{132}Xe - EXTa	0.793	0.751	0.785
±	0.29	0.22	0.36	±	0.013	0.022	0.011
^{36}Ar [in 10^{-12} cc]	5.85	4.38	10.23	^{134}Xe/^{132}Xe - EXTa	0.387	0.378	0.385
±	0.10	0.07	0.12	±	0.006	0.013	0.006
^{38}Ar/^{36}Ar	0.192	0.198	0.194	^{136}Xe/^{132}Xe - EXTa	0.320	0.301	0.317
±	0.001	0.001	0.001	±	0.005	0.010	0.005
^{40}Ar/^{36}Ar	143.0	46.4	101.7	^{132}Xe - EXTb [in 10^{-8} cc/g]	0.1668	0.0401	0.2069
±	0.8	0.3	0.5	±	0.0061	0.0015	0.0063
^{40}Ar [in 10^{-8} cc/g]	2520.2	612.0	3132.2	^{132}Xe - EXTb [in 10^{-12} cc]	0.0554	0.0133	0.0687
±	43.4	10.8	44.7	±	0.0020	0.0005	0.0021
^{40}Ar [in 10^{-12} cc]	836.7	203.2	1039.9	^{128}Xe/^{132}Xe - EXTb	0.072	0.072	0.072
±	14.2	3.5	14.5	±	0.002	0.004	0.002
^{38}Ar$_{cos}$ [in 10^{-8} cc/g]	0.066	0.139	0.205	^{129}Xe/^{132}Xe - EXTb	1.032	1.082	1.042
±	0.050	0.038	0.063	±	0.016	0.027	0.014
^{38}Ar$_{cos}$ [in 10^{-12} cc]	0.022	0.046	0.068	^{130}Xe/^{132}Xe - EXTb	0.150	0.158	0.151
±	0.017	0.013	0.021	±	0.004	0.007	0.003
^{84}Kr [in 10^{-8} cc/g]	0.2362	0.0634	0.2997	^{131}Xe/^{132}Xe - EXTb	0.793	0.751	0.785
±	0.0464	0.0125	0.0480	±	0.004	0.004	0.003
^{84}Kr [in 10^{-12} cc]	0.0784	0.0211	0.0995	^{134}Xe/^{132}Xe - EXTb	0.395	0.394	0.395
±	0.0154	0.0041	0.0159	±	0.006	0.013	0.006
^{80}Kr/^{84}Kr	0.038	0.040	0.039	^{136}Xe/^{132}Xe - EXTb	0.331	0.354	0.335
±	0.002	0.003	0.002	±	0.007	0.012	0.006
^{82}Kr/^{84}Kr	0.193	0.189	0.192	^{21}Ne$_{cos}$/^{38}Ar$_{cos}$	0.30	0.62	0.51
±	0.007	0.012	0.006	±	0.25	0.19	0.17
^{83}Kr/^{84}Kr	0.197	0.181	0.194	^{36}Ar/^{132}Xe $_{(Int)}$	106.49	320.27	149.11
±	0.008	0.010	0.006	±	4.91	15.51	5.59
^{86}Kr/^{84}Kr	0.303	0.301	0.302	^{84}Kr/^{132}Xe $_{(Int)}$	1.43	1.54	1.45
±	0.013	0.016	0.011	±	0.29	0.31	0.24
^{83}Kr$_{cos}$ [in 10^{-8} cc/g]	-	-	-				
±	-	-	-				
^{83}Kr$_{cos}$ [in 10^{-12} cc]	-	-	-				
±	-	-	-				

Table X63. Noble gas data He to Xe for sample 45c.33_1 (not corrected for blank)

Sample	45c.33_1						
Size [µm]	512 x 379						
Weight [µg]	58.7 ± 0.1						
Date of measure	08/06/12	11/06/12	08+11/06/12	Date of measure	08/06/12	11/06/12	08+11/06/12
Laser-Power	3 x 0.91 W	3 x 5 W		Laser-Power	3 x 0.91 W	3 x 5 W	
Laser-Beam	600-360 µm	360 µm		Laser-Beam	600-360 µm	360 µm	
Step(s)	1	2	total*	Step(s)	1	2	total*
^{4}He [in 10^{-8} cc/g]	6137.1	59.0	6196.1	^{132}Xe - INT [in 10^{-8} cc/g]	0.4751	0.1260	0.6010
±	253.4	2.5	253.4	±	0.0051	0.0014	0.0053
^{4}He [in 10^{-12} cc]	3602.4	34.7	3637.1	^{132}Xe - INT [in 10^{-12} cc]	0.2789	0.0739	0.3528
±	148.6	1.5	148.6	±	0.0030	0.0008	0.0031
^{3}He [in 10^{-12} cc/g]	20072.6	1941.0	22013.6	^{128}Xe/^{132}Xe - INT	0.083	0.077	0.082
±	885.6	256.2	921.9	±	0.001	0.002	0.001
^{3}He [in 10^{-16} cc]	11782.6	1139.4	12922.0	^{129}Xe/^{132}Xe - INT	1.034	1.028	1.033
±	519.4	150.4	540.7	±	0.008	0.015	0.007
^{3}He/^{4}He	0.00033	0.00329	0.00036	^{130}Xe/^{132}Xe - INT	0.163	0.162	0.163
±	0.00002	0.00046	0.00002	±	0.001	0.002	0.001
^{22}Ne [in 10^{-8} cc/g]	13.255	0.353	13.607	^{131}Xe/^{132}Xe - INT	0.825	0.836	0.827
±	0.177	0.015	0.177	±	0.006	0.011	0.005
^{22}Ne [in 10^{-12} cc]	7.780	0.207	7.988	^{134}Xe/^{132}Xe - INT	0.386	0.393	0.388
±	0.103	0.009	0.103	±	0.003	0.006	0.003
^{20}Ne/^{22}Ne	11.43	11.37	11.43	^{136}Xe/^{132}Xe - INT	0.330	0.335	0.331
±	0.08	0.46	0.08	±	0.004	0.007	0.004
^{21}Ne/^{22}Ne	0.042	0.039	0.042	^{132}Xe - EXTa [in 10^{-8} cc/g]	0.4771	0.1265	0.6036
±	0.001	0.004	0.001	±	0.0130	0.0035	0.0134
^{21}Ne$_{cos}$ [in 10^{-8} cc/g]	0.159	0.003	0.162	^{132}Xe - EXTa [in 10^{-12} cc]	0.2801	0.0743	0.3543
±	0.011	0.001	0.011	±	0.0076	0.0020	0.0079
^{21}Ne$_{cos}$ [in 10^{-12} cc]	0.093	0.002	0.095	^{128}Xe/^{132}Xe - EXTa	0.082	0.077	0.081
±	0.007	0.001	0.007	±	0.001	0.002	0.001
^{20}Ne$_{trap}$ [in 10^{-8} cc/g]	151.5	4.01	155.49	^{129}Xe/^{132}Xe - EXTa	1.033	1.028	1.032
±	8.7	0.32	8.67	±	0.009	0.016	0.008
^{20}Ne$_{trap}$ [in 10^{-12} cc]	88.9	2.35	91.27	^{130}Xe/^{132}Xe - EXTa	0.164	0.162	0.164
±	5.1	0.19	5.09	±	0.002	0.003	0.002
^{36}Ar [in 10^{-8} cc/g]	36.37	9.61	45.98	^{131}Xe/^{132}Xe - EXTa	0.821	0.834	0.824
±	2.60	0.69	2.69	±	0.007	0.012	0.006
^{36}Ar [in 10^{-12} cc]	21.35	5.64	26.99	^{134}Xe/^{132}Xe - EXTa	0.380	0.381	0.380
±	1.53	0.40	1.58	±	0.003	0.006	0.003
^{38}Ar/^{36}Ar	0.193	0.188	0.192	^{136}Xe/^{132}Xe - EXTa	0.317	0.307	0.315
±	0.002	0.002	0.002	±	0.003	0.005	0.002
^{40}Ar/^{36}Ar	7.3	33.1	12.7	^{132}Xe - EXTb [in 10^{-8} cc/g]	0.4787	0.1268	0.6055
±	0.1	0.4	0.1	±	0.0120	0.0033	0.0125
^{40}Ar [in 10^{-8} cc/g]	264.8	318.5	583.2	^{132}Xe - EXTb [in 10^{-12} cc]	0.2810	0.0744	0.3554
±	19.1	23.0	29.9	±	0.0071	0.0019	0.0073
^{40}Ar [in 10^{-12} cc]	155.4	186.9	342.4	^{128}Xe/^{132}Xe - EXTb	0.079	0.080	0.079
±	11.2	13.5	17.6	±	0.003	0.003	0.002
^{38}Ar$_{cos}$ [in 10^{-8} cc/g]	0.198	-	-	^{129}Xe/^{132}Xe - EXTb	1.033	1.028	1.032
±	0.117	-	-	±	0.009	0.016	0.008
^{38}Ar$_{cos}$ [in 10^{-12} cc]	0.116	-	-	^{130}Xe/^{132}Xe - EXTb	0.161	0.161	0.161
±	0.069	-	-	±	0.002	0.003	0.002
^{84}Kr [in 10^{-8} cc/g]	0.5076	0.1765	0.6841	^{131}Xe/^{132}Xe - EXTb	0.823	0.836	0.826
±	0.0319	0.0111	0.0338	±	0.004	0.004	0.003
^{84}Kr [in 10^{-12} cc]	0.2980	0.1036	0.4016	^{134}Xe/^{132}Xe - EXTb	0.385	0.394	0.387
±	0.0187	0.0065	0.0198	±	0.004	0.005	0.003
^{80}Kr/^{84}Kr	0.039	0.038	0.039	^{136}Xe/^{132}Xe - EXTb	0.324	0.326	0.325
±	0.001	0.002	0.001	±	0.003	0.005	0.003
^{82}Kr/^{84}Kr	0.194	0.194	0.194	^{21}Ne$_{cos}$/^{38}Ar$_{cos}$	0.80	-	-
±	0.003	0.005	0.003	±	0.48	-	-
^{83}Kr/^{84}Kr	0.208	0.196	0.205	^{36}Ar/^{132}Xe $_{(Int)}$	76.57	76.30	76.51
±	0.003	0.006	0.003	±	5.53	5.52	4.52
^{86}Kr/^{84}Kr	0.316	0.308	0.314	^{84}Kr/^{132}Xe $_{(Int)}$	1.07	1.40	1.14
±	0.006	0.008	0.005	±	0.07	0.09	0.06
^{83}Kr$_{cos}$ [in 10^{-8} cc/g]	0.0029	-	-				
±	0.0023	-	-				
^{83}Kr$_{cos}$ [in 10^{-12} cc]	0.0017	-	-				
±	0.0013	-	-				

Table X64. Noble gas data He to Xe for sample 45c.34_1 (not corrected for blank)

Sample	45c.34_1		
Size [μm]	428 x 318		
Weight [μg]	34.1 ± 0.1		
Date of measure	08/10/12	16/10/12	08+16/10/12
Laser-Power	3 x 0.91 W	2 x 5W / 1 x 5 - 20 W	
Laser-Beam	600-360 μm	360 μm	
Step(s)	1	2	total*
^{4}He [in 10^{-8} cc/g]	251.1	33.7	284.8
±	4.6	0.6	4.7
^{4}He [in 10^{-12} cc]	85.6	11.5	97.1
±	1.6	0.2	1.6
^{3}He [in 10^{-12} cc/g]	2428.1	1777.9	4206.0
±	171.6	179.6	248.4
^{3}He [in 10^{-16} cc]	828.0	606.3	1434.2
±	58.5	61.2	84.6
^{3}He/^{4}He	0.00097	0.00527	0.00148
±	0.00007	0.00054	0.00009
^{22}Ne [in 10^{-8} cc/g]	0.456	0.193	0.649
±	0.028	0.024	0.037
^{22}Ne [in 10^{-12} cc]	0.155	0.066	0.221
±	0.009	0.008	0.013
^{20}Ne/^{22}Ne	10.34	8.12	9.68
±	0.63	1.02	0.54
^{21}Ne/^{22}Ne	0.032	0.038	0.034
±	0.005	0.008	0.004
^{21}Ne$_{cos}$ [in 10^{-8} cc/g]	< 0.014 (2σ)	< 0.005 (2σ)	-
±	-	-	-
^{21}Ne$_{cos}$ [in 10^{-12} cc]	< 0.005 (2σ)	< 0.002 (2σ)	-
±	-	-	-
^{20}Ne$_{trap}$ [in 10^{-8} cc/g]	4.7	1.57	6.28
±	0.5	0.29	0.57
^{20}Ne$_{trap}$ [in 10^{-12} cc]	1.6	0.53	2.14
±	0.2	0.10	0.19
^{36}Ar [in 10^{-8} cc/g]	11.81	4.79	16.60
±	0.23	0.09	0.25
^{36}Ar [in 10^{-12} cc]	4.03	1.63	5.66
±	0.08	0.03	0.08
^{38}Ar/^{36}Ar	0.182	0.172	0.179
±	0.004	0.004	0.003
^{40}Ar/^{36}Ar	24.6	147.9	60.2
±	0.4	1.6	0.6
^{40}Ar [in 10^{-8} cc/g]	290.7	709.0	999.7
±	6.9	15.5	16.9
^{40}Ar [in 10^{-12} cc]	99.1	241.8	340.9
±	2.3	5.2	5.7
^{38}Ar$_{cos}$ [in 10^{-8} cc/g]	-	-	-
±	-	-	-
^{38}Ar$_{cos}$ [in 10^{-12} cc]	-	-	-
±	-	-	-
^{84}Kr [in 10^{-8} cc/g]	0.1774	0.0612	0.2387
±	0.0131	0.0046	0.0139
^{84}Kr [in 10^{-12} cc]	0.0605	0.0209	0.0814
±	0.0044	0.0016	0.0047
^{80}Kr/^{84}Kr	0.043	0.047	0.044
±	0.003	0.005	0.003
^{82}Kr/^{84}Kr	0.200	0.209	0.202
±	0.009	0.013	0.007
^{83}Kr/^{84}Kr	0.189	0.195	0.191
±	0.008	0.011	0.007
^{86}Kr/^{84}Kr	0.307	0.241	0.290
±	0.011	0.020	0.010
^{83}Kr$_{cos}$ [in 10^{-8} cc/g]	-	-	-
±	-	-	-
^{83}Kr$_{cos}$ [in 10^{-12} cc]	-	-	-
±	-	-	-

Date of measure	08/10/12	16/10/12	08+16/10/12
Laser-Power	3 x 0.91 W	2 x 5W / 1 x 5 - 20 W	
Laser-Beam	600-360 μm	360 μm	
Step(s)	1	2	total*
^{132}Xe - INT [in 10^{-8} cc/g]	0.1809	0.0378	0.2187
±	0.0027	0.0008	0.0028
^{132}Xe - INT [in 10^{-12} cc]	0.0617	0.0129	0.0746
±	0.0009	0.0003	0.0009
^{128}Xe/^{132}Xe - INT	0.085	0.080	0.084
±	0.003	0.006	0.002
^{129}Xe/^{132}Xe - INT	0.998	1.084	1.013
±	0.020	0.039	0.018
^{130}Xe/^{132}Xe - INT	0.164	0.149	0.162
±	0.003	0.006	0.003
^{131}Xe/^{132}Xe - INT	0.825	0.787	0.818
±	0.015	0.029	0.013
^{134}Xe/^{132}Xe - INT	0.388	0.398	0.390
±	0.008	0.016	0.007
^{136}Xe/^{132}Xe - INT	0.323	0.330	0.324
±	0.008	0.019	0.008
^{132}Xe - EXTa [in 10^{-8} cc/g]	0.1820	0.0380	0.2201
±	0.0027	0.0008	0.0028
^{132}Xe - EXTa [in 10^{-12} cc]	0.0621	0.0130	0.0750
±	0.0009	0.0003	0.0009
^{128}Xe/^{132}Xe - EXTa	0.083	0.082	0.083
±	0.002	0.006	0.002
^{129}Xe/^{132}Xe - EXTa	0.998	1.084	1.013
±	0.018	0.038	0.016
^{130}Xe/^{132}Xe - EXTa	0.163	0.143	0.159
±	0.004	0.008	0.003
^{131}Xe/^{132}Xe - EXTa	0.829	0.791	0.822
±	0.015	0.029	0.013
^{134}Xe/^{132}Xe - EXTa	0.380	0.365	0.377
±	0.007	0.013	0.006
^{136}Xe/^{132}Xe - EXTa	0.327	0.314	0.325
±	0.006	0.012	0.006
^{132}Xe - EXTb [in 10^{-8} cc/g]	0.1804	0.0364	0.2168
±	0.0051	0.0012	0.0053
^{132}Xe - EXTb [in 10^{-12} cc]	0.0615	0.0124	0.0739
±	0.0017	0.0004	0.0018
^{128}Xe/^{132}Xe - EXTb	0.086	0.085	0.086
±	0.003	0.006	0.002
^{129}Xe/^{132}Xe - EXTb	0.998	1.084	1.012
±	0.017	0.038	0.016
^{130}Xe/^{132}Xe - EXTb	0.163	0.160	0.162
±	0.004	0.008	0.003
^{131}Xe/^{132}Xe - EXTb	0.829	0.791	0.823
±	0.004	0.004	0.003
^{134}Xe/^{132}Xe - EXTb	0.390	0.410	0.393
±	0.007	0.015	0.006
^{136}Xe/^{132}Xe - EXTb	0.320	0.314	0.319
±	0.006	0.014	0.005
^{21}Ne$_{cos}$/^{38}Ar$_{cos}$	-	-	-
±	-	-	-
^{36}Ar/^{132}Xe $_{(Int)}$	65.27	126.83	75.91
±	1.57	3.57	1.45
^{84}Kr/^{132}Xe $_{(Int)}$	0.98	1.62	1.09
±	0.07	0.13	0.06

Table X65. Noble gas data He to Xe for sample X1 (45c.35_1) (not corrected for blank)

Sample				X1 (45c.35_1)			
Size [µm]				427 x 315			
Weight [µg]				35.0 ± 0.1			
Date of measure	03/11/11	04/11/11	03+04/11/11	**Date of measure**	03/11/11	04/11/11	03+04/11/11
Laser-Power	3 x 0.91 W	3 x 5 W		**Laser-Power**	3 x 0.91 W	3 x 5 W	
Laser-Beam	600 µm	250 µm		**Laser-Beam**	600 µm	250 µm	
Step(s)	1	2	total*	**Step(s)**	1	2	total*
^{4}He [in 10^{-8} cc/g]	3859.1	32.5	3891.7	^{132}Xe - INT [in 10^{-8} cc/g]	0.0371	-	-
±	65.7	0.6	65.7	±	0.0014	-	-
^{4}He [in 10^{-12} cc]	1350.7	11.4	1362.1	^{132}Xe - INT [in 10^{-12} cc]	0.0130	-	-
±	22.7	0.2	22.7	±	0.0005	-	-
^{3}He [in 10^{-12} cc/g]	17183.4	234.2	17417.6	^{128}Xe/^{132}Xe - INT	0.081	-	-
±	380.3	79.0	388.5	±	0.005	-	-
^{3}He [in 10^{-16} cc]	6014.2	82.0	6096.2	^{129}Xe/^{132}Xe - INT	1.003	-	-
±	132.0	27.7	134.8	±	0.030	-	-
^{3}He/^{4}He	0.00045	0.00072	0.00045	^{130}Xe/^{132}Xe - INT	0.143	-	-
±	0.00001	0.00024	0.00001	±	0.005	-	-
^{22}Ne [in 10^{-8} cc/g]	34.433	0.477	34.910	^{131}Xe/^{132}Xe - INT	0.782	-	-
±	0.480	0.047	0.482	±	0.023	-	-
^{22}Ne [in 10^{-12} cc]	12.052	0.167	12.218	^{134}Xe/^{132}Xe - INT	0.385	-	-
±	0.164	0.016	0.165	±	0.013	-	-
^{20}Ne/^{22}Ne	10.11	9.91	10.11	^{136}Xe/^{132}Xe - INT	0.361	-	-
±	0.21	0.96	0.21	±	0.017	-	-
^{21}Ne/^{22}Ne	0.050	0.065	0.050	^{132}Xe - EXTa [in 10^{-8} cc/g]	0.0378	-	-
±	0.001	0.008	0.001	±	0.0014	-	-
^{21}Ne$_{cos}$ [in 10^{-8} cc/g]	0.710	0.017	0.727	^{132}Xe - EXTa [in 10^{-12} cc]	0.0132	-	-
±	0.078	0.004	0.078	±	0.0005	-	-
^{21}Ne$_{cos}$ [in 10^{-12} cc]	0.248	0.006	0.254	^{128}Xe/^{132}Xe - EXTa	0.083	-	-
±	0.027	0.001	0.027	±	0.005	-	-
^{20}Ne$_{trap}$ [in 10^{-8} cc/g]	347.5	4.71	352.21	^{129}Xe/^{132}Xe - EXTa	1.003	-	-
±	21.2	0.70	21.23	±	0.030	-	-
^{20}Ne$_{trap}$ [in 10^{-12} cc]	121.6	1.65	123.27	^{130}Xe/^{132}Xe - EXTa	0.144	-	-
±	7.4	0.25	7.42	±	0.007	-	-
^{36}Ar [in 10^{-8} cc/g]	44.03	6.03	50.06	^{131}Xe/^{132}Xe - EXTa	0.782	-	-
±	0.84	0.12	0.85	±	0.023	-	-
^{36}Ar [in 10^{-12} cc]	15.41	2.11	17.52	^{134}Xe/^{132}Xe - EXTa	0.396	-	-
±	0.29	0.04	0.29	±	0.012	-	-
^{38}Ar/^{36}Ar	0.197	0.185	0.196	^{136}Xe/^{132}Xe - EXTa	0.334	-	-
±	0.001	0.002	0.001	±	0.012	-	-
^{40}Ar/^{36}Ar	29.4	264.5	57.7	^{132}Xe - EXTb [in 10^{-8} cc/g]	0.0375	-	-
±	0.1	1.6	0.2	±	0.0015	-	-
^{40}Ar [in 10^{-8} cc/g]	1295.4	1595.2	2890.6	^{132}Xe - EXTb [in 10^{-12} cc]	0.0131	-	-
±	25.3	31.1	40.1	±	0.0005	-	-
^{40}Ar [in 10^{-12} cc]	453.4	558.3	1011.7	^{128}Xe/^{132}Xe - EXTb	0.069	-	-
±	8.7	10.8	13.7	±	0.005	-	-
^{38}Ar$_{cos}$ [in 10^{-8} cc/g]	0.431	-	-	^{129}Xe/^{132}Xe - EXTb	1.003	-	-
±	0.118	-	-	±	0.030	-	-
^{38}Ar$_{cos}$ [in 10^{-12} cc]	0.151	-	-	^{130}Xe/^{132}Xe - EXTb	0.148	-	-
±	0.041	-	-	±	0.006	-	-
^{84}Kr [in 10^{-8} cc/g]	0.1194	0.0518	0.1713	^{131}Xe/^{132}Xe - EXTb	0.782	-	-
±	0.0134	0.0059	0.0146	±	0.005	-	-
^{84}Kr [in 10^{-12} cc]	0.0418	0.0181	0.0599	^{134}Xe/^{132}Xe - EXTb	0.384	-	-
±	0.0047	0.0021	0.0051	±	0.011	-	-
^{80}Kr/^{84}Kr	0.034	0.053	0.040	^{136}Xe/^{132}Xe - EXTb	0.372	-	-
±	0.003	0.005	0.003	±	0.012	-	-
^{82}Kr/^{84}Kr	0.205	0.222	0.211	^{21}Ne$_{cos}$/^{38}Ar$_{cos}$	1.65	-	-
±	0.008	0.012	0.007	±	0.49	-	-
^{83}Kr/^{84}Kr	0.193	0.194	0.194	^{36}Ar/^{132}Xe $_{(Int)}$	1188.29	-	-
±	0.008	0.012	0.007	±	49.94	-	-
^{86}Kr/^{84}Kr	0.305	0.297	0.302	^{84}Kr/^{132}Xe $_{(Int)}$	3.22	-	-
±	0.010	0.017	0.009	±	0.38	-	-
^{83}Kr$_{cos}$ [in 10^{-8} cc/g]	-	-	-				
±	-	-	-				
^{83}Kr$_{cos}$ [in 10^{-12} cc]	-	-	-				
±	-	-	-				

Table X66. Noble gas data He to Xe for sample 45c.35_2 (not corrected for blank)

Sample	45c.35_2							
Size [µm]	152 x 135							
Weight [µg]	5.4 ± 0.1							
Date of measure	13/02/12	14/02/12	13+14/02/12	**Date of measure**	13/02/12	14/02/12	13+14/02/12	
Laser-Power	3 x 0.91 W	3 x 5 W		**Laser-Power**	3 x 0.91 W	3 x 5 W		
Laser-Beam	200 µm	200 µm		**Laser-Beam**	200 µm	200 µm		
Step(s)	1	2	total*	**Step(s)**	1	2	total*	
^{4}He [in 10^{-8} cc/g]	1412.8	152.4	1565.2	^{132}Xe - INT [in 10^{-8} cc/g]	0.3115	-	-	
±	36.5	3.9	36.7	±	0.0088	-	-	
^{4}He [in 10^{-12} cc]	76.3	8.2	84.5	^{132}Xe - INT [in 10^{-12} cc]	0.0168	-	-	
±	1.4	0.1	1.2	±	0.0004	-	-	
^{3}He [in 10^{-12} cc/g]	17706.0	< 876.6 (2σ)	-	^{128}Xe/^{132}Xe - INT	0.079	-	-	
±	3045.6	-	-	±	0.005	-	-	
^{3}He [in 10^{-16} cc]	956.1	< 47.3 (2σ)	-	^{129}Xe/^{132}Xe - INT	0.994	-	-	
±	163.5	-	-	±	0.024	-	-	
^{3}He/^{4}He	0.00125	-	-	^{130}Xe/^{132}Xe - INT	0.161	-	-	
±	0.00022	-	-	±	0.005	-	-	
^{22}Ne [in 10^{-8} cc/g]	9.064	1.055	10.119	^{131}Xe/^{132}Xe - INT	0.753	-	-	
±	0.283	0.160	0.325	±	0.022	-	-	
^{22}Ne [in 10^{-12} cc]	0.489	0.057	0.546	^{134}Xe/^{132}Xe - INT	0.377	-	-	
±	0.012	0.009	0.014	±	0.013	-	-	
^{20}Ne/^{22}Ne	10.62	10.10	10.56	^{136}Xe/^{132}Xe - INT	0.322	-	-	
±	0.24	1.51	0.27	±	0.014	-	-	
^{21}Ne/^{22}Ne	0.094	0.029	0.087	^{132}Xe - EXTa [in 10^{-8} cc/g]	0.3174	-	-	
±	0.004	0.008	0.004	±	0.0668	-	-	
^{21}Ne$_{cos}$ [in 10^{-8} cc/g]	0.593	< 0.129 (2σ)	-	^{132}Xe - EXTa [in 10^{-12} cc]	0.0171	-	-	
±	0.039	-	-	±	0.0036	-	-	
^{21}Ne$_{cos}$ [in 10^{-12} cc]	0.032	< 0.007 (2σ)	-	^{128}Xe/^{132}Xe - EXTa	0.074	-	-	
±	0.002	-	-	±	0.004	-	-	
^{20}Ne$_{trap}$ [in 10^{-8} cc/g]	95.8	< 509.4 (2σ)	-	^{129}Xe/^{132}Xe - EXTa	0.992	-	-	
±	6.5	-	-	±	0.024	-	-	
^{20}Ne$_{trap}$ [in 10^{-12} cc]	5.2	< 27.5 (2σ)	-	^{130}Xe/^{132}Xe - EXTa	0.153	-	-	
±	0.3	-	-	±	0.006	-	-	
^{36}Ar [in 10^{-8} cc/g]	38.38	-	-	^{131}Xe/^{132}Xe - EXTa	0.751	-	-	
±	0.95	-	-	±	0.022	-	-	
^{36}Ar [in 10^{-12} cc]	2.07	-	-	^{134}Xe/^{132}Xe - EXTa	0.381	-	-	
±	0.03	-	-	±	0.012	-	-	
^{38}Ar/^{36}Ar	0.194	-	-	^{136}Xe/^{132}Xe - EXTa	0.318	-	-	
±	0.002	-	-	±	0.011	-	-	
^{40}Ar/^{36}Ar	181.9	-	-	^{132}Xe - EXTb [in 10^{-8} cc/g]	0.2984	-	-	
±	1.2	-	-	±	0.0124	-	-	
^{40}Ar [in 10^{-8} cc/g]	6982.6	9542.6	16525.2	^{132}Xe - EXTb [in 10^{-12} cc]	0.0161	-	-	
±	175.7	239.8	297.2	±	0.0006	-	-	
^{40}Ar [in 10^{-12} cc]	377.1	515.3	892.4	^{128}Xe/^{132}Xe - EXTb	0.072	-	-	
±	6.4	8.8	9.1	±	0.004	-	-	
^{38}Ar$_{cos}$ [in 10^{-8} cc/g]	0.234	-	-	^{129}Xe/^{132}Xe - EXTb	0.993	-	-	
±	0.121	-	-	±	0.024	-	-	
^{38}Ar$_{cos}$ [in 10^{-12} cc]	0.013	-	-	^{130}Xe/^{132}Xe - EXTb	0.156	-	-	
±	0.007	-	-	±	0.007	-	-	
^{84}Kr [in 10^{-8} cc/g]	1.6649	-	-	^{131}Xe/^{132}Xe - EXTb	0.752	-	-	
±	0.1350	-	-	±	0.004	-	-	
^{84}Kr [in 10^{-12} cc]	0.0899	-	-	^{134}Xe/^{132}Xe - EXTb	0.392	-	-	
±	0.0071	-	-	±	0.012	-	-	
^{80}Kr/^{84}Kr	0.040	-	-	^{136}Xe/^{132}Xe - EXTb	0.342	-	-	
±	0.002	-	-	±	0.010	-	-	
^{82}Kr/^{84}Kr	0.193	-	-	^{21}Ne$_{cos}$/^{38}Ar$_{cos}$	2.53	-	-	
±	0.005	-	-	±	1.31	-	-	
^{83}Kr/^{84}Kr	0.194	-	-	^{36}Ar/^{132}Xe $_{(Int)}$	123.22	-	-	
±	0.005	-	-	±	3.31	-	-	
^{86}Kr/^{84}Kr	0.326	-	-	^{84}Kr/^{132}Xe $_{(Int)}$	5.34	-	-	
±	0.008	-	-	±	0.44	-	-	
^{83}Kr$_{cos}$ [in 10^{-8} cc/g]	-	-	-					
±	-	-	-					
^{83}Kr$_{cos}$ [in 10^{-12} cc]	-	-	-					
±	-	-	-					

Table X67. Noble gas data He to Xe for sample 45c.35_3 (not corrected for blank)

Sample	45c.35_3			
Size [µm]	428 x 245			
Weight [µg]	29.0 ± 0.1			

Date of measure	02/09/11	05/09/11	06/09/11	02/+05/+06/09/11
Laser-Power	3 x 0.13 W	3 x 0.91 W	3 x 5 W	
Laser-Beam	250 µm	250 µm	250 µm	
Step(s)	1	2	3	total*
^{4}He [in 10^{-8} cc/g]	2200.8	10289.6	37.8	12528.1
±	44.6	169.4	23.4	176.7
^{4}He [in 10^{-12} cc]	638.2	2984.0	11.0	3633.1
±	12.7	48.0	6.8	49.7
^{3}He [in 10^{-12} cc/g]	2676.4	30872.3	104.7	33653.3
±	319.2	1417.6	17.0	1453.2
^{3}He [in 10^{-16} cc]	776.1	8953.0	30.3	9759.5
±	92.5	410.0	4.9	420.1
^{3}He/^{4}He	0.00012	0.00030	0.00028	0.00027
±	0.00001	0.00001	0.00018	0.00001
^{22}Ne [in 10^{-8} cc/g]	0.691	10.719	1.018	12.428
±	0.108	0.192	0.106	0.245
^{22}Ne [in 10^{-12} cc]	0.200	3.108	0.295	3.604
±	0.031	0.055	0.031	0.070
^{20}Ne/^{22}Ne	8.82	11.17	8.87	10.85
±	1.37	0.15	0.91	0.17
^{21}Ne/^{22}Ne	0.033	0.043	0.039	0.042
±	0.006	0.001	0.005	0.001
^{21}Ne$_{cos}$ [in 10^{-8} cc/g]	< 0.018 (2σ)	0.145	0.009	0.154
±	-	0.028	0.006	0.028
^{21}Ne$_{cos}$ [in 10^{-12} cc]	< 0.005 (2σ)	0.042	0.003	0.045
±	-	0.008	0.002	0.008
^{20}Ne$_{trap}$ [in 10^{-8} cc/g]	6.1	119.58	9.03	134.70
±	1.4	7.14	1.42	7.41
^{20}Ne$_{trap}$ [in 10^{-12} cc]	1.8	34.68	2.62	39.06
±	0.4	2.07	0.41	2.15
^{36}Ar [in 10^{-8} cc/g]	0.12	150.98	6.36	157.46
±	0.05	2.91	0.13	2.91
^{36}Ar [in 10^{-12} cc]	0.03	43.79	1.84	45.66
±	0.01	0.83	0.04	0.83
^{38}Ar/^{36}Ar	0.990	0.186	0.183	0.186
±	0.479	0.001	0.004	0.001
^{40}Ar/^{36}Ar	75.7	4.2	91.6	7.8
±	32.9	0.0	0.9	0.1
^{40}Ar [in 10^{-8} cc/g]	8.8	628.9	582.7	1220.4
±	0.2	12.8	11.6	17.3
^{40}Ar [in 10^{-12} cc]	2.5	182.4	169.0	353.9
±	0.1	3.6	3.3	4.9
^{38}Ar$_{cos}$ [in 10^{-8} cc/g]	0.106	-	-	-
±	0.070	-	-	-
^{38}Ar$_{cos}$ [in 10^{-12} cc]	0.031	-	-	-
±	0.020	-	-	-
^{84}Kr [in 10^{-8} cc/g]	0.0514	0.6634	0.0907	0.8055
±	0.0041	0.0503	0.0075	0.0510
^{84}Kr [in 10^{-12} cc]	0.0149	0.1924	0.0263	0.2336
±	0.0012	0.0146	0.0022	0.0148
^{80}Kr/^{84}Kr	0.055	0.039	0.033	0.039
±	0.003	0.003	0.004	0.002
^{82}Kr/^{84}Kr	0.205	0.206	0.189	0.204
±	0.006	0.003	0.008	0.003
^{83}Kr/^{84}Kr	0.206	0.208	0.196	0.207
±	0.006	0.003	0.005	0.003
^{86}Kr/^{84}Kr	0.323	0.318	0.301	0.317
±	0.010	0.003	0.007	0.003
^{83}Kr$_{cos}$ [in 10^{-8} cc/g]	< 0.0010 (2σ)	0.0041	-	-
±	-	0.0030	-	-
^{83}Kr$_{cos}$ [in 10^{-12} cc]	< 0.0003 (2σ)	0.0012	-	-
±	-	0.0009	-	-

Date of measure	02/09/11	05/09/11	06/09/11	02/+05/+06/09/11
Laser-Power	3 x 0.13 W	3 x 0.91 W	3 x 5 W	
Laser-Beam	250 µm	250 µm	250 µm	
Step(s)	1	2	3	total*
^{132}Xe - INT [in 10^{-8} cc/g]	0.0247	1.0629	0.0455	1.1331
±	0.0013	0.0380	0.0019	0.0381
^{132}Xe - INT [in 10^{-12} cc]	0.0072	0.3082	0.0132	0.3286
±	0.0004	0.0110	0.0006	0.0110
^{128}Xe/^{132}Xe - INT	0.115	0.084	0.100	0.085
±	0.009	0.001	0.006	0.001
^{129}Xe/^{132}Xe - INT	1.036	1.046	1.042	1.046
±	0.040	0.006	0.030	0.006
^{130}Xe/^{132}Xe - INT	0.173	0.165	0.168	0.165
±	0.007	0.001	0.006	0.001
^{131}Xe/^{132}Xe - INT	0.833	0.817	0.825	0.818
±	0.038	0.004	0.026	0.004
^{134}Xe/^{132}Xe - INT	0.380	0.380	0.371	0.379
±	0.018	0.002	0.015	0.002
^{136}Xe/^{132}Xe - INT	0.356	0.327	0.283	0.326
±	0.022	0.004	0.018	0.004
^{132}Xe - EXTa [in 10^{-8} cc/g]	0.0247	1.0629	0.0455	1.1331
±	0.0013	0.0380	0.0019	0.0381
^{132}Xe - EXTa [in 10^{-12} cc]	0.0072	0.3082	0.0132	0.3286
±	0.0004	0.0110	0.0006	0.0110
^{128}Xe/^{132}Xe - EXTa	0.110	0.082	0.093	0.083
±	0.007	0.001	0.005	0.001
^{129}Xe/^{132}Xe - EXTa	1.037	1.046	1.043	1.046
±	0.040	0.005	0.030	0.005
^{130}Xe/^{132}Xe - EXTa	0.172	0.164	0.159	0.164
±	0.009	0.001	0.007	0.001
^{131}Xe/^{132}Xe - EXTa	0.833	0.817	0.825	0.818
±	0.038	0.005	0.026	0.005
^{134}Xe/^{132}Xe - EXTa	0.396	0.376	0.400	0.377
±	0.017	0.002	0.014	0.002
^{136}Xe/^{132}Xe - EXTa	0.338	0.313	0.320	0.314
±	0.015	0.002	0.014	0.002
^{132}Xe - EXTb [in 10^{-8} cc/g]	0.0238	1.0588	0.0440	1.1265
±	0.0012	0.0413	0.0020	0.0414
^{132}Xe - EXTb [in 10^{-12} cc]	0.0069	0.3071	0.0127	0.3267
±	0.0003	0.0119	0.0006	0.0120
^{128}Xe/^{132}Xe - EXTb	0.070	0.079	0.076	0.079
±	0.007	0.001	0.004	0.001
^{129}Xe/^{132}Xe - EXTb	1.037	1.046	1.042	1.046
±	0.040	0.005	0.030	0.005
^{130}Xe/^{132}Xe - EXTb	0.166	0.162	0.167	0.162
±	0.009	0.001	0.007	0.001
^{131}Xe/^{132}Xe - EXTb	0.833	0.817	0.825	0.818
±	0.002	0.002	0.002	0.002
^{134}Xe/^{132}Xe - EXTb	0.383	0.382	0.390	0.382
±	0.016	0.002	0.014	0.002
^{136}Xe/^{132}Xe - EXTb	0.375	0.325	0.324	0.326
±	0.015	0.002	0.014	0.002
^{21}Ne$_{cos}$/^{38}Ar$_{cos}$	-	-	-	-
±	-	-	-	-
^{36}Ar/^{132}Xe (Int)	4.70	142.04	139.73	138.96
±	2.08	5.73	6.58	5.29
^{84}Kr/^{132}Xe (Int)	2.08	0.62	1.99	0.71
±	0.20	0.05	0.18	0.05

Table X68. Noble gas data He to Xe for sample 45c.37_2 (not corrected for blank)

Sample	45c.37_2						
Size [µm]	498 x 379						
Weight [µg]	28.5 ± 0.1						
Date of measure	14/02/12	15/02/12	14+15/02/12	Date of measure	14/02/12	15/02/12	14+15/02/12
Laser-Power	3 x 0.91 W	3 x 5 W		Laser-Power	3 x 0.91 W	3 x 5 W	
Laser-Beam	600 µm	250 µm		Laser-Beam	600 µm	250 µm	
Step(s)	1	2	total*	Step(s)	1	2	total*
^{4}He [in 10^{-8} cc/g]	514.5	57.9	572.4	^{132}Xe - INT [in 10^{-8} cc/g]	0.3300	0.0753	0.4053
±	10.1	1.0	10.2	±	0.0060	0.0016	0.0062
^{4}He [in 10^{-12} cc]	146.6	16.5	163.1	^{132}Xe - INT [in 10^{-12} cc]	0.0940	0.0215	0.1155
±	2.8	0.3	2.8	±	0.0017	0.0005	0.0017
^{3}He [in 10^{-12} cc/g]	1116.6	< 165.3 (2σ)	-	^{128}Xe/^{132}Xe - INT	0.082	0.077	0.081
±	561.2	-	-	±	0.002	0.004	0.002
^{3}He [in 10^{-16} cc]	318.2	< 47.1 (2σ)	-	^{129}Xe/^{132}Xe - INT	1.033	1.001	1.027
±	160.0	-	-	±	0.011	0.026	0.010
^{3}He/^{4}He	0.00022	-	-	^{130}Xe/^{132}Xe - INT	0.160	0.150	0.158
±	0.00011	-	-	±	0.002	0.004	0.002
^{22}Ne [in 10^{-8} cc/g]	0.520	0.452	0.972	^{131}Xe/^{132}Xe - INT	0.821	0.821	0.821
±	0.031	0.037	0.048	±	0.010	0.022	0.009
^{22}Ne [in 10^{-12} cc]	0.148	0.129	0.277	^{134}Xe/^{132}Xe - INT	0.382	0.381	0.382
±	0.009	0.010	0.014	±	0.005	0.011	0.004
^{20}Ne/^{22}Ne	10.76	10.95	10.85	^{136}Xe/^{132}Xe - INT	0.323	0.349	0.328
±	0.63	0.87	0.53	±	0.006	0.013	0.005
^{21}Ne/^{22}Ne	0.034	0.032	0.033	^{132}Xe - EXTa [in 10^{-8} cc/g]	0.3307	0.0755	0.4062
±	0.004	0.005	0.003	±	0.0704	0.0161	0.0722
^{21}Ne$_{cos}$ [in 10^{-8} cc/g]	< 0.009 (2σ)	-	-	^{132}Xe - EXTa [in 10^{-12} cc]	0.0943	0.0215	0.1158
±	-	-	-	±	0.0201	0.0046	0.0206
^{21}Ne$_{cos}$ [in 10^{-12} cc]	< 0.003 (2σ)	-	-	^{128}Xe/^{132}Xe - EXTa	0.078	0.080	0.078
±	-	-	-	±	0.002	0.003	0.002
^{20}Ne$_{trap}$ [in 10^{-8} cc/g]	< 6.7 (2σ)	-	-	^{129}Xe/^{132}Xe - EXTa	1.032	1.001	1.026
±	-	-	-	±	0.010	0.026	0.010
^{20}Ne$_{trap}$ [in 10^{-12} cc]	< 1.9 (2σ)	-	-	^{130}Xe/^{132}Xe - EXTa	0.158	0.151	0.156
±	-	-	-	±	0.003	0.005	0.002
^{36}Ar [in 10^{-8} cc/g]	14.80	11.05	25.85	^{131}Xe/^{132}Xe - EXTa	0.819	0.821	0.819
±	0.25	0.19	0.31	±	0.010	0.022	0.009
^{36}Ar [in 10^{-12} cc]	4.22	3.15	7.37	^{134}Xe/^{132}Xe - EXTa	0.385	0.372	0.383
±	0.07	0.05	0.08	±	0.005	0.010	0.004
^{38}Ar/^{36}Ar	0.191	0.186	0.189	^{136}Xe/^{132}Xe - EXTa	0.325	0.317	0.323
±	0.002	0.002	0.001	±	0.004	0.009	0.004
^{40}Ar/^{36}Ar	46.1	157.5	93.8	^{132}Xe - EXTb [in 10^{-8} cc/g]	0.3263	0.0764	0.4027
±	0.4	1.0	0.6	±	0.0118	0.0028	0.0121
^{40}Ar [in 10^{-8} cc/g]	682.6	1741.1	2423.7	^{132}Xe - EXTb [in 10^{-12} cc]	0.0930	0.0218	0.1148
±	12.3	30.3	32.7	±	0.0033	0.0008	0.0034
^{40}Ar [in 10^{-12} cc]	194.5	496.2	690.7	^{128}Xe/^{132}Xe - EXTb	0.077	0.075	0.077
±	3.4	8.5	9.0	±	0.002	0.003	0.002
^{38}Ar$_{cos}$ [in 10^{-8} cc/g]	0.050	-	-	^{129}Xe/^{132}Xe - EXTb	1.032	1.001	1.026
±	0.043	-	-	±	0.011	0.026	0.010
^{38}Ar$_{cos}$ [in 10^{-12} cc]	0.014	-	-	^{130}Xe/^{132}Xe - EXTb	0.154	0.156	0.155
±	0.012	-	-	±	0.002	0.006	0.002
^{84}Kr [in 10^{-8} cc/g]	0.2310	0.1025	0.3335	^{131}Xe/^{132}Xe - EXTb	0.819	0.821	0.819
±	0.0635	0.0282	0.0695	±	0.004	0.004	0.003
^{84}Kr [in 10^{-12} cc]	0.0658	0.0292	0.0950	^{134}Xe/^{132}Xe - EXTb	0.386	0.376	0.384
±	0.0181	0.0080	0.0198	±	0.004	0.009	0.004
^{80}Kr/^{84}Kr	0.038	0.048	0.041	^{136}Xe/^{132}Xe - EXTb	0.330	0.338	0.332
±	0.003	0.004	0.002	±	0.006	0.010	0.005
^{82}Kr/^{84}Kr	0.210	0.202	0.207	^{21}Ne$_{cos}$/^{38}Ar$_{cos}$	-	-	-
±	0.010	0.011	0.008	±	-	-	-
^{83}Kr/^{84}Kr	0.204	0.196	0.202	^{36}Ar/^{132}Xe $_{(Int)}$	44.84	146.73	63.78
±	0.012	0.012	0.009	±	1.09	3.94	1.20
^{86}Kr/^{84}Kr	0.312	0.317	0.314	^{84}Kr/^{132}Xe $_{(Int)}$	0.70	1.36	0.82
±	0.020	0.021	0.015	±	0.19	0.38	0.17
^{83}Kr$_{cos}$ [in 10^{-8} cc/g]	< 0.0069 (2σ)	-	-				
±	-	-	-				
^{83}Kr$_{cos}$ [in 10^{-12} cc]	< 0.0020 (2σ)	-	-				
±	-	-	-				

Table X69. Noble gas data He to Xe for sample 45c.37_3 (not corrected for blank)

Sample				45c.37_3			
Size [µm]				322 x 205			
Weight [µg]				13.1 ± 0.1			
Date of measure	16/02/12	16/02/12	16/02/12	**Date of measure**	16/02/12	16/02/12	16/02/12
Laser-Power	3 x 0.91 W	3 x 5 W		**Laser-Power**	3 x 0.91 W	3 x 5 W	
Laser-Beam	360 µm	180 µm		**Laser-Beam**	360 µm	180 µm	
Step(s)	1	2	total*	**Step(s)**	1	2	total*
^{4}He [in 10^{-8} cc/g]	428.4	105.6	534.0	^{132}Xe - INT [in 10^{-8} cc/g]	0.5623	0.1229	0.6852
±	8.4	1.9	8.6	±	0.0110	0.0028	0.0114
^{4}He [in 10^{-12} cc]	56.1	13.8	70.0	^{132}Xe - INT [in 10^{-12} cc]	0.0737	0.0161	0.0898
±	1.0	0.2	1.0	±	0.0013	0.0003	0.0013
^{3}He [in 10^{-12} cc/g]	< 2917.5 (2σ)	< 360.2 (2σ)	-	^{128}Xe/^{132}Xe - INT	0.082	0.084	0.082
±	-	-	-	±	0.002	0.005	0.002
^{3}He [in 10^{-16} cc]	< 382.2 (2σ)	< 47.2 (2σ)	-	^{129}Xe/^{132}Xe - INT	1.020	1.004	1.017
±	-	-	-	±	0.011	0.030	0.011
^{3}He/^{4}He	-	-	-	^{130}Xe/^{132}Xe - INT	0.159	0.149	0.157
±	-	-	-	±	0.003	0.005	0.002
^{22}Ne [in 10^{-8} cc/g]	0.542	0.435	0.977	^{131}Xe/^{132}Xe - INT	0.793	0.824	0.799
±	0.069	0.091	0.114	±	0.010	0.026	0.010
^{22}Ne [in 10^{-12} cc]	0.071	0.057	0.128	^{134}Xe/^{132}Xe - INT	0.385	0.392	0.386
±	0.009	0.012	0.015	±	0.007	0.013	0.006
^{20}Ne/^{22}Ne	9.15	11.33	10.13	^{136}Xe/^{132}Xe - INT	0.324	0.325	0.324
±	1.14	2.34	1.22	±	0.007	0.015	0.006
^{21}Ne/^{22}Ne	0.030	0.035	0.032	^{132}Xe - EXTa [in 10^{-8} cc/g]	0.5636	0.1231	0.6867
±	0.006	0.009	0.005	±	0.1200	0.0263	0.1229
^{21}Ne$_{cos}$ [in 10^{-8} cc/g]	-	< 0.014 (2σ)	-	^{132}Xe - EXTa [in 10^{-12} cc]	0.0738	0.0161	0.0900
±	-	-	-	±	0.0157	0.0034	0.0161
^{21}Ne$_{cos}$ [in 10^{-12} cc]	-	< 0.002 (2σ)	-	^{128}Xe/^{132}Xe - EXTa	0.078	0.085	0.079
±	-	-	-	±	0.002	0.004	0.002
^{20}Ne$_{trap}$ [in 10^{-8} cc/g]	5.0	-	-	^{129}Xe/^{132}Xe - EXTa	1.019	1.004	1.016
±	0.9	-	-	±	0.011	0.030	0.011
^{20}Ne$_{trap}$ [in 10^{-12} cc]	0.6	-	-	^{130}Xe/^{132}Xe - EXTa	0.156	0.151	0.155
±	0.1	-	-	±	0.003	0.006	0.003
^{36}Ar [in 10^{-8} cc/g]	225.31	38.79	264.10	^{131}Xe/^{132}Xe - EXTa	0.792	0.824	0.797
±	7.35	0.70	7.38	±	0.010	0.026	0.010
^{36}Ar [in 10^{-12} cc]	29.52	5.08	34.60	^{134}Xe/^{132}Xe - EXTa	0.378	0.400	0.382
±	0.94	0.08	0.93	±	0.006	0.011	0.005
^{38}Ar/^{36}Ar	0.187	0.179	0.186	^{136}Xe/^{132}Xe - EXTa	0.317	0.339	0.321
±	0.001	0.002	0.001	±	0.005	0.011	0.004
^{40}Ar/^{36}Ar	290.4	262.2	286.3	^{132}Xe - EXTb [in 10^{-8} cc/g]	0.5528	0.1241	0.6769
±	11.5	1.5	9.8	±	0.0203	0.0048	0.0209
^{40}Ar [in 10^{-8} cc/g]	65441.9	10171.3	75613.2	^{132}Xe - EXTb [in 10^{-12} cc]	0.0724	0.0163	0.0887
±	2214.1	188.8	2222.2	±	0.0026	0.0006	0.0026
^{40}Ar [in 10^{-12} cc]	8572.9	1332.4	9905.3	^{128}Xe/^{132}Xe - EXTb	0.070	0.074	0.071
±	282.6	22.6	281.1	±	0.002	0.004	0.002
^{38}Ar$_{cos}$ [in 10^{-8} cc/g]	-	-	-	^{129}Xe/^{132}Xe - EXTb	1.019	1.004	1.016
±	-	-	-	±	0.012	0.030	0.011
^{38}Ar$_{cos}$ [in 10^{-12} cc]	-	-	-	^{130}Xe/^{132}Xe - EXTb	0.153	0.151	0.153
±	-	-	-	±	0.003	0.006	0.003
^{84}Kr [in 10^{-8} cc/g]	2.2231	0.4288	2.6520	^{131}Xe/^{132}Xe - EXTb	0.792	0.824	0.798
±	0.6106	0.1179	0.6219	±	0.004	0.004	0.003
^{84}Kr [in 10^{-12} cc]	0.2912	0.0562	0.3474	^{134}Xe/^{132}Xe - EXTb	0.389	0.387	0.389
±	0.0800	0.0154	0.0814	±	0.006	0.012	0.005
^{80}Kr/^{84}Kr	0.038	0.038	0.038	^{136}Xe/^{132}Xe - EXTb	0.324	0.332	0.326
±	0.002	0.003	0.002	±	0.006	0.013	0.005
^{82}Kr/^{84}Kr	0.197	0.199	0.197	^{21}Ne$_{cos}$/^{38}Ar$_{cos}$	-	-	-
±	0.007	0.009	0.006	±	-	-	-
^{83}Kr/^{84}Kr	0.205	0.213	0.206	^{36}Ar/^{132}Xe $_{(Int)}$	400.71	315.67	385.46
±	0.010	0.012	0.009	±	14.62	8.54	11.82
^{86}Kr/^{84}Kr	0.308	0.311	0.309	^{84}Kr/^{132}Xe $_{(Int)}$	3.95	3.49	3.87
±	0.017	0.019	0.015	±	1.09	0.96	0.91
^{83}Kr$_{cos}$ [in 10^{-8} cc/g]	< 0.0572 (2σ)	< 0.0163 (2σ)	-				
±	-	-	-				
^{83}Kr$_{cos}$ [in 10^{-12} cc]	< 0.0075 (2σ)	< 0.0021 (2σ)	-				
±	-	-	-				

Table X70. Noble gas data He to Xe for sample CP9-1-1994_PL10-109D9 (not corrected for blank)

Sample				CP_9-1-1994_PL10-109D9			
Size [µm]				252 x 188			
Weight [µg]				6.2 ± 0.1			
Date of measure	07/11/11	08/11/11	07+08/11/11	**Date of measure**	07/11/11	08/11/11	07+08/11/11
Laser-Power	3 x 0.91 W	3 x 5 W		**Laser-Power**	3 x 0.91 W	3 x 5 W	
Laser-Beam	250 µm	180 µm		**Laser-Beam**	250 µm	180 µm	
Step(s)	1	2	total*	**Step(s)**	1	2	total*
^{4}He [in 10^{-8} cc/g]	325.9	131.4	457.3	^{132}Xe - INT [in 10^{-8} cc/g]	0.1962	-	-
±	7.9	4.1	8.9	±	0.0080	-	-
^{4}He [in 10^{-12} cc]	20.2	8.1	28.3	^{132}Xe - INT [in 10^{-12} cc]	0.0122	-	-
±	0.4	0.2	0.3	±	0.0005	-	-
^{3}He [in 10^{-12} cc/g]	< 5328.9 (2σ)	< 4884.6 (2σ)	-	^{128}Xe/^{132}Xe - INT	0.085	-	-
±	-	-	-	±	0.005	-	-
^{3}He [in 10^{-16} cc]	< 330.4 (2σ)	< 302.8 (2σ)	-	^{129}Xe/^{132}Xe - INT	1.024	-	-
±	-	-	-	±	0.029	-	-
^{3}He/^{4}He	-	-	-	^{130}Xe/^{132}Xe - INT	0.156	-	-
±	-	-	-	±	0.006	-	-
^{22}Ne [in 10^{-8} cc/g]	3.674	0.996	4.669	^{131}Xe/^{132}Xe - INT	0.852	-	-
±	0.255	0.244	0.353	±	0.028	-	-
^{22}Ne [in 10^{-12} cc]	0.228	0.062	0.290	^{134}Xe/^{132}Xe - INT	0.376	-	-
±	0.015	0.015	0.021	±	0.017	-	-
^{20}Ne/^{22}Ne	11.02	8.18	10.42	^{136}Xe/^{132}Xe - INT	0.318	-	-
±	0.73	1.99	0.72	±	0.020	-	-
^{21}Ne/^{22}Ne	0.027	0.026	0.027	^{132}Xe - EXTa [in 10^{-8} cc/g]	0.1979	-	-
±	0.004	0.008	0.003	±	0.0081	-	-
^{21}Ne$_{cos}$ [in 10^{-8} cc/g]	< 0.057 (2σ)	< 0.027 (2σ)	-	^{132}Xe - EXTa [in 10^{-12} cc]	0.0123	-	-
±	-	-	-	±	0.0005	-	-
^{21}Ne$_{cos}$ [in 10^{-12} cc]	< 0.004 (2σ)	< 0.002 (2σ)	-	^{128}Xe/^{132}Xe - EXTa	0.085	-	-
±	-	-	-	±	0.005	-	-
^{20}Ne$_{trap}$ [in 10^{-8} cc/g]	40.5	7.91	48.42	^{129}Xe/^{132}Xe - EXTa	1.025	-	-
±	4.5	2.78	5.29	±	0.029	-	-
^{20}Ne$_{trap}$ [in 10^{-12} cc]	2.5	0.49	3.00	^{130}Xe/^{132}Xe - EXTa	0.157	-	-
±	0.3	0.17	0.32	±	0.007	-	-
^{36}Ar [in 10^{-8} cc/g]	19.27	3.61	22.88	^{131}Xe/^{132}Xe - EXTa	0.852	-	-
±	0.49	0.13	0.51	±	0.028	-	-
^{36}Ar [in 10^{-12} cc]	1.19	0.22	1.42	^{134}Xe/^{132}Xe - EXTa	0.379	-	-
±	0.02	0.01	0.02	±	0.016	-	-
^{38}Ar/^{36}Ar	0.184	0.199	0.186	^{136}Xe/^{132}Xe - EXTa	0.324	-	-
±	0.003	0.014	0.004	±	0.014	-	-
^{40}Ar/^{36}Ar	55.1	223.1	81.6	^{132}Xe - EXTb [in 10^{-8} cc/g]	0.1981	-	-
±	0.7	5.9	1.1	±	0.0085	-	-
^{40}Ar [in 10^{-8} cc/g]	1062.9	804.4	1867.3	^{132}Xe - EXTb [in 10^{-12} cc]	0.0123	-	-
±	28.7	20.2	35.1	±	0.0005	-	-
^{40}Ar [in 10^{-12} cc]	65.9	49.9	115.8	^{128}Xe/^{132}Xe - EXTb	0.089	-	-
±	1.4	1.0	1.1	±	0.005	-	-
^{38}Ar$_{cos}$ [in 10^{-8} cc/g]	-	< 0.152 (2σ)	-	^{129}Xe/^{132}Xe - EXTb	1.025	-	-
±	-	-	-	±	0.029	-	-
^{38}Ar$_{cos}$ [in 10^{-12} cc]	-	< 0.009 (2σ)	-	^{130}Xe/^{132}Xe - EXTb	0.155	-	-
±	-	-	-	±	0.007	-	-
^{84}Kr [in 10^{-8} cc/g]	0.0974	0.0728	0.1703	^{131}Xe/^{132}Xe - EXTb	0.852	-	-
±	0.0116	0.0089	0.0146	±	0.006	-	-
^{84}Kr [in 10^{-12} cc]	0.0060	0.0045	0.0106	^{134}Xe/^{132}Xe - EXTb	0.370	-	-
±	0.0007	0.0005	0.0009	±	0.014	-	-
^{80}Kr/^{84}Kr	0.061	0.043	0.053	^{136}Xe/^{132}Xe - EXTb	0.309	-	-
±	0.010	0.012	0.008	±	0.014	-	-
^{82}Kr/^{84}Kr	0.205	0.198	0.202	^{21}Ne$_{cos}$/^{38}Ar$_{cos}$	-	-	-
±	0.018	0.023	0.014	±	-	-	-
^{83}Kr/^{84}Kr	0.161	0.236	0.193	^{36}Ar/^{132}Xe $_{(Int)}$	98.23	-	-
±	0.020	0.025	0.016	±	4.18	-	-
^{86}Kr/^{84}Kr	0.267	0.265	0.266	^{84}Kr/^{132}Xe $_{(Int)}$	0.50	-	-
±	0.027	0.033	0.021	±	0.06	-	-
^{83}Kr$_{cos}$ [in 10^{-8} cc/g]	-	0.0026	-				
±	-	0.0018	-				
^{83}Kr$_{cos}$ [in 10^{-12} cc]	-	0.0002	-				
±	-	0.0001	-				

Table X71. Noble gas data He to Xe for sample DC 06_07_213 (not corrected for blank)

Sample		DC 06_07_213	
Size [μm]		97 x 91	
Weight [μg]		~ 1.1	
Date of measure	23/04/12	**Date of measure**	23/04/12
Laser-Power	4 x 0.91 - 20 W	**Laser-Power**	4 x 0.91 - 20 W
Laser-Beam	180-600 μm	**Laser-Beam**	180-600 μm
Step(s)	1	**Step(s)**	1
^{4}He [in 10^{-8} cc/g]	2063.5	^{132}Xe - INT [in 10^{-8} cc/g]	1.1866
±	196.4	±	0.1317
^{4}He [in 10^{-12} cc]	22.1	^{132}Xe - INT [in 10^{-12} cc]	0.0127
±	0.4	±	0.0008
^{3}He [in 10^{-12} cc/g]	< 40726.6 (2σ)	^{128}Xe/^{132}Xe - INT	0.071
±	-	±	0.005
^{3}He [in 10^{-16} cc]	< 435.8 (2σ)	^{129}Xe/^{132}Xe - INT	0.957
±	-	±	0.030
^{3}He/^{4}He	-	^{130}Xe/^{132}Xe - INT	0.139
±	-	±	0.005
^{22}Ne [in 10^{-8} cc/g]	80.949	^{131}Xe/^{132}Xe - INT	0.828
±	7.698	±	0.031
^{22}Ne [in 10^{-12} cc]	0.866	^{134}Xe/^{132}Xe - INT	0.408
±	0.015	±	0.015
^{20}Ne/^{22}Ne	11.21	^{136}Xe/^{132}Xe - INT	0.375
±	0.16	±	0.019
^{21}Ne/^{22}Ne	0.029	^{132}Xe - EXTa [in 10^{-8} cc/g]	1.1788
±	0.002	±	0.2698
^{21}Ne$_{cos}$ [in 10^{-8} cc/g]	< 0.627 (2σ)	^{132}Xe - EXTa [in 10^{-12} cc]	0.0126
±	-	±	0.0026
^{21}Ne$_{cos}$ [in 10^{-12} cc]	< 0.007 (2σ)	^{128}Xe/^{132}Xe - EXTa	0.077
±	-	±	0.005
^{20}Ne$_{trap}$ [in 10^{-8} cc/g]	907.2	^{129}Xe/^{132}Xe - EXTa	0.954
±	100.6	±	0.030
^{20}Ne$_{trap}$ [in 10^{-12} cc]	9.7	^{130}Xe/^{132}Xe - EXTa	0.144
±	0.6	±	0.007
^{36}Ar [in 10^{-8} cc/g]	293.24	^{131}Xe/^{132}Xe - EXTa	0.829
±	42.58	±	0.031
^{36}Ar [in 10^{-12} cc]	3.14	^{134}Xe/^{132}Xe - EXTa	0.394
±	0.35	±	0.014
^{38}Ar/^{36}Ar	0.184	^{136}Xe/^{132}Xe - EXTa	0.336
±	0.002	±	0.012
^{40}Ar/^{36}Ar	210.1	^{132}Xe - EXTb [in 10^{-8} cc/g]	1.2131
±	2.2	±	0.3183
^{40}Ar [in 10^{-8} cc/g]	61605.8	^{132}Xe - EXTb [in 10^{-12} cc]	0.0130
±	8966.2	±	0.0032
^{40}Ar [in 10^{-12} cc]	659.2	^{128}Xe/^{132}Xe - EXTb	0.067
±	73.5	±	0.004
^{38}Ar$_{cos}$ [in 10^{-8} cc/g]	-	^{129}Xe/^{132}Xe - EXTb	0.956
±	-	±	0.030
^{38}Ar$_{cos}$ [in 10^{-12} cc]	-	^{130}Xe/^{132}Xe - EXTb	0.147
±	-	±	0.006
^{84}Kr [in 10^{-8} cc/g]	3.9576	^{131}Xe/^{132}Xe - EXTb	0.829
±	0.4093	±	0.002
^{84}Kr [in 10^{-12} cc]	0.0423	^{134}Xe/^{132}Xe - EXTb	0.394
±	0.0019	±	0.012
^{80}Kr/^{84}Kr	0.038	^{136}Xe/^{132}Xe - EXTb	0.352
±	0.002	±	0.012
^{82}Kr/^{84}Kr	0.197	^{21}Ne$_{cos}$/^{38}Ar$_{cos}$	-
±	0.007	±	-
^{83}Kr/^{84}Kr	0.204	^{36}Ar/^{132}Xe $_{(Int)}$	247.12
±	0.007	±	31.19
^{86}Kr/^{84}Kr	0.318	^{84}Kr/^{132}Xe $_{(Int)}$	3.34
±	0.010	±	0.25
^{83}Kr$_{cos}$ [in 10^{-8} cc/g]	< 0.0689 (2σ)		
±	-		
^{83}Kr$_{cos}$ [in 10^{-12} cc]	< 0.0007 (2σ)		
±	-		

Table X72. Noble gas data He to Xe for sample DC 06_08_01 (not corrected for blank)

Sample				DC 06_08_01			
Size [µm]				110 x 92			
Weight [µg]				~1.4			
Date of measure	25/04/12	26/04/12	25+26/04/12	**Date of measure**	25/04/12	26/04/12	25+26/04/12
Laser-Power	3 x 0.91 W	3 x 5 W		**Laser-Power**	3 x 0.91 W	3 x 5 W	
Laser-Beam	180 µm	180-250 µm		**Laser-Beam**	180 µm	180-250 µm	
Step(s)	1	2	total*	**Step(s)**	1	2	total*
^{4}He [in 10^{-8} cc/g]	1850.9	94.7	1945.6	^{132}Xe - INT [in 10^{-8} cc/g]	0.5480	-	-
±	138.9	7.2	139.1	±	0.0521	-	-
^{4}He [in 10^{-12} cc]	25.4	1.3	26.7	^{132}Xe - INT [in 10^{-12} cc]	0.0075	-	-
±	0.4	0.0	0.2	±	0.0005	-	-
^{3}He [in 10^{-12} cc/g]	21117.1	< 3139.4 (2σ)	-	^{128}Xe/^{132}Xe - INT	0.068	-	-
±	10731.3	-	-	±	0.006	-	-
^{3}He [in 10^{-16} cc]	289.3	< 43.0 (2σ)	-	^{129}Xe/^{132}Xe - INT	0.949	-	-
±	145.5	-	-	±	0.033	-	-
^{3}He/^{4}He	0.00114	-	-	^{130}Xe/^{132}Xe - INT	0.143	-	-
±	0.00057	-	-	±	0.006	-	-
^{22}Ne [in 10^{-8} cc/g]	237.480	1.979	239.459	^{131}Xe/^{132}Xe - INT	0.714	-	-
±	17.649	0.502	17.656	±	0.032	-	-
^{22}Ne [in 10^{-12} cc]	3.253	0.027	3.281	^{134}Xe/^{132}Xe - INT	0.414	-	-
±	0.045	0.007	0.034	±	0.020	-	-
^{20}Ne/^{22}Ne	11.44	11.38	11.44	^{136}Xe/^{132}Xe - INT	0.336	-	-
±	0.10	2.72	0.10	±	0.021	-	-
^{21}Ne/^{22}Ne	0.032	0.016	0.032	^{132}Xe - EXTa [in 10^{-8} cc/g]	0.5444	-	-
±	0.001	0.008	0.001	±	0.1206	-	-
^{21}Ne$_{cos}$ [in 10^{-8} cc/g]	0.546	-	-	^{132}Xe - EXTa [in 10^{-12} cc]	0.0075	-	-
±	0.194	-	-	±	0.0016	-	-
^{21}Ne$_{cos}$ [in 10^{-12} cc]	0.007	-	-	^{128}Xe/^{132}Xe - EXTa	0.061	-	-
±	0.003	-	-	±	0.005	-	-
^{20}Ne$_{trap}$ [in 10^{-8} cc/g]	2716.5	22.51	2739.04	^{129}Xe/^{132}Xe - EXTa	0.948	-	-
±	252.4	7.96	252.51	±	0.032	-	-
^{20}Ne$_{trap}$ [in 10^{-12} cc]	37.2	0.31	37.52	^{130}Xe/^{132}Xe - EXTa	0.151	-	-
±	2.1	0.11	2.11	±	0.009	-	-
^{36}Ar [in 10^{-8} cc/g]	215.45	29.89	245.34	^{131}Xe/^{132}Xe - EXTa	0.711	-	-
±	28.65	3.98	28.92	±	0.032	-	-
^{36}Ar [in 10^{-12} cc]	2.95	0.41	3.36	^{134}Xe/^{132}Xe - EXTa	0.404	-	-
±	0.33	0.05	0.31	±	0.015	-	-
^{38}Ar/^{36}Ar	0.202	0.199	0.202	^{136}Xe/^{132}Xe - EXTa	0.301	-	-
±	0.002	0.005	0.002	±	0.012	-	-
^{40}Ar/^{36}Ar	49.5	284.0	78.0	^{132}Xe - EXTb [in 10^{-8} cc/g]	0.5671	-	-
±	0.6	4.1	0.9	±	0.1452	-	-
^{40}Ar [in 10^{-8} cc/g]	10655.6	8486.8	19142.4	^{132}Xe - EXTb [in 10^{-12} cc]	0.0078	-	-
±	1421.8	1132.8	1817.9	±	0.0019	-	-
^{40}Ar [in 10^{-12} cc]	146.0	116.3	262.3	^{128}Xe/^{132}Xe - EXTb	0.061	-	-
±	16.3	13.0	15.9	±	0.006	-	-
^{38}Ar$_{cos}$ [in 10^{-8} cc/g]	3.394	0.347	3.741	^{129}Xe/^{132}Xe - EXTb	0.949	-	-
±	0.882	0.172	0.898	±	0.032	-	-
^{38}Ar$_{cos}$ [in 10^{-12} cc]	0.046	0.005	0.051	^{130}Xe/^{132}Xe - EXTb	0.122	-	-
±	0.012	0.002	0.012	±	0.007	-	-
^{84}Kr [in 10^{-8} cc/g]	2.2615	-	-	^{131}Xe/^{132}Xe - EXTb	0.711	-	-
±	0.1940	-	-	±	0.002	-	-
^{84}Kr [in 10^{-12} cc]	0.0310	-	-	^{134}Xe/^{132}Xe - EXTb	0.396	-	-
±	0.0014	-	-	±	0.018	-	-
^{80}Kr/^{84}Kr	0.044	-	-	^{136}Xe/^{132}Xe - EXTb	0.311	-	-
±	0.003	-	-	±	0.013	-	-
^{82}Kr/^{84}Kr	0.212	-	-	^{21}Ne$_{cos}$/^{38}Ar$_{cos}$	0.16	-	-
±	0.008	-	-	±	0.07	-	-
^{83}Kr/^{84}Kr	0.197	-	-	^{36}Ar/^{132}Xe $_{(Int)}$	393.13	-	-
±	0.007	-	-	±	49.84	-	-
^{86}Kr/^{84}Kr	0.303	-	-	^{84}Kr/^{132}Xe $_{(Int)}$	4.13	-	-
±	0.010	-	-	±	0.31	-	-
^{83}Kr$_{cos}$ [in 10^{-8} cc/g]	-	-	-				
±	-	-	-				
^{83}Kr$_{cos}$ [in 10^{-12} cc]	-	-	-				
±	-	-	-				

Table X73. Noble gas data He to Xe for sample DC 06_09_11 (not corrected for blank)

Sample		DC 06_09_11	
Size [μm]		137 x 111	
Weight [μg]		~1.3	
Date of measure	26/04/12	Date of measure	26/04/12
Laser-Power	3 x 0.91 W	Laser-Power	3 x 0.91 W
Laser-Beam	180 μm	Laser-Beam	180 μm
Step(s)	1	Step(s)	1
^{4}He [in 10^{-8} cc/g]	7167.0	^{132}Xe - INT [in 10^{-8} cc/g]	1.0616
±	570.3	±	0.1040
^{4}He [in 10^{-12} cc]	92.6	^{132}Xe - INT [in 10^{-12} cc]	0.0137
±	1.7	±	0.0008
^{3}He [in 10^{-12} cc/g]	22394.6	^{128}Xe/^{132}Xe - INT	0.087
±	11393.8	±	0.005
^{3}He [in 10^{-16} cc]	289.3	^{129}Xe/^{132}Xe - INT	1.019
±	145.5	±	0.030
^{3}He/^{4}He	0.00031	^{130}Xe/^{132}Xe - INT	0.162
±	0.00016	±	0.006
^{22}Ne [in 10^{-8} cc/g]	43.404	^{131}Xe/^{132}Xe - INT	0.788
±	3.487	±	0.027
^{22}Ne [in 10^{-12} cc]	0.561	^{134}Xe/^{132}Xe - INT	0.377
±	0.012	±	0.014
^{20}Ne/^{22}Ne	11.73	^{136}Xe/^{132}Xe - INT	0.332
±	0.22	±	0.016
^{21}Ne/^{22}Ne	0.034	^{132}Xe - EXTa [in 10^{-8} cc/g]	1.0544
±	0.002	±	0.2349
^{21}Ne$_{cos}$ [in 10^{-8} cc/g]	0.148	^{132}Xe - EXTa [in 10^{-12} cc]	0.0136
±	0.094	±	0.0028
^{21}Ne$_{cos}$ [in 10^{-12} cc]	0.002	^{128}Xe/^{132}Xe - EXTa	0.080
±	0.001	±	0.004
^{20}Ne$_{trap}$ [in 10^{-8} cc/g]	509.3	^{129}Xe/^{132}Xe - EXTa	1.017
±	50.5	±	0.029
^{20}Ne$_{trap}$ [in 10^{-12} cc]	6.6	^{130}Xe/^{132}Xe - EXTa	0.159
±	0.4	±	0.007
^{36}Ar [in 10^{-8} cc/g]	192.07	^{131}Xe/^{132}Xe - EXTa	0.785
±	26.01	±	0.027
^{36}Ar [in 10^{-12} cc]	2.48	^{134}Xe/^{132}Xe - EXTa	0.359
±	0.28	±	0.013
^{38}Ar/^{36}Ar	0.189	^{136}Xe/^{132}Xe - EXTa	0.316
±	0.002	±	0.011
^{40}Ar/^{36}Ar	130.7	^{132}Xe - EXTb [in 10^{-8} cc/g]	1.0340
±	1.4	±	0.2658
^{40}Ar [in 10^{-8} cc/g]	25099.9	^{132}Xe - EXTb [in 10^{-12} cc]	0.0134
±	3408.5	±	0.0033
^{40}Ar [in 10^{-12} cc]	324.3	^{128}Xe/^{132}Xe - EXTb	0.074
±	36.2	±	0.004
^{38}Ar$_{cos}$ [in 10^{-8} cc/g]	< 1.506 (2σ)	^{129}Xe/^{132}Xe - EXTb	1.019
±	-	±	0.029
^{38}Ar$_{cos}$ [in 10^{-12} cc]	< 0.019 (2σ)	^{130}Xe/^{132}Xe - EXTb	0.151
±	-	±	0.006
^{84}Kr [in 10^{-8} cc/g]	2.0874	^{131}Xe/^{132}Xe - EXTb	0.785
±	0.1881	±	0.002
^{84}Kr [in 10^{-12} cc]	0.0270	^{134}Xe/^{132}Xe - EXTb	0.382
±	0.0012	±	0.012
^{80}Kr/^{84}Kr	0.042	^{136}Xe/^{132}Xe - EXTb	0.317
±	0.004	±	0.010
^{82}Kr/^{84}Kr	0.231	^{21}Ne$_{cos}$/^{38}Ar$_{cos}$	-
±	0.009	±	-
^{83}Kr/^{84}Kr	0.209	^{36}Ar/^{132}Xe $_{(Int)}$	180.93
±	0.009	±	22.85
^{86}Kr/^{84}Kr	0.303	^{84}Kr/^{132}Xe $_{(Int)}$	1.97
±	0.012	±	0.15
^{83}Kr$_{cos}$ [in 10^{-8} cc/g]	< 0.0572 (2σ)		
±	-		
^{83}Kr$_{cos}$ [in 10^{-12} cc]	< 0.0007 (2σ)		
±	-		

Table X74. Noble gas data He to Xe for sample DC 06_09_50 (not corrected for blank)

Sample				DC 06_09_50			
Size [µm]				141 x 134			
Weight [µg]				~ 3.3			
Date of measure	18/04/12	19/04/12	18+19/04/12	Date of measure	18/04/12	19/04/12	18+19/04/12
Laser-Power	3 x 0.91 W	3 x 5 W		Laser-Power	3 x 0.91 W	3 x 5 W	
Laser-Beam	200 µm	180 µm		Laser-Beam	200 µm	180 µm	
Step(s)	1	2	total*	Step(s)	1	2	total*
^{4}He [in 10^{-8} cc/g]	368347.9	43.9	368391.8	^{132}Xe - INT [in 10^{-8} cc/g]	0.9799	-	-
±	12538.3	1.6	12538.3	±	0.0646	-	-
^{4}He [in 10^{-12} cc]	12155.5	1.4	12156.9	^{132}Xe - INT [in 10^{-12} cc]	0.0323	-	-
±	188.5	0.0	188.4	±	0.0019	-	-
^{3}He [in 10^{-12} cc/g]	1099269.3	< 1308.9 (2σ)	-	^{128}Xe/^{132}Xe - INT	0.075	-	-
±	56705.1	-	-	±	0.003	-	-
^{3}He [in 10^{-16} cc]	36275.9	< 43.2 (2σ)	-	^{129}Xe/^{132}Xe - INT	0.993	-	-
±	1514.3	-	-	±	0.020	-	-
^{3}He/^{4}He	0.00030	-	-	^{130}Xe/^{132}Xe - INT	0.161	-	-
±	0.00001	-	-	±	0.004	-	-
^{22}Ne [in 10^{-8} cc/g]	118.845	1.628	120.473	^{131}Xe/^{132}Xe - INT	0.786	-	-
±	3.943	0.234	3.949	±	0.016	-	-
^{22}Ne [in 10^{-12} cc]	3.922	0.054	3.976	^{134}Xe/^{132}Xe - INT	0.397	-	-
±	0.053	0.008	0.050	±	0.009	-	-
^{20}Ne/^{22}Ne	12.27	10.53	12.25	^{136}Xe/^{132}Xe - INT	0.347	-	-
±	0.09	1.48	0.10	±	0.011	-	-
^{21}Ne/^{22}Ne	0.032	0.020	0.032	^{132}Xe - EXTa [in 10^{-8} cc/g]	0.9734	-	-
±	0.001	0.006	0.001	±	0.2051	-	-
^{21}Ne$_{cos}$ [in 10^{-8} cc/g]	0.104	-	-	^{132}Xe - EXTa [in 10^{-12} cc]	0.0321	-	-
±	0.091	-	-	±	0.0067	-	-
^{21}Ne$_{cos}$ [in 10^{-12} cc]	0.003	-	-	^{128}Xe/^{132}Xe - EXTa	0.074	-	-
±	0.003	-	-	±	0.003	-	-
^{20}Ne$_{trap}$ [in 10^{-8} cc/g]	1458.5	16.94	1475.43	^{129}Xe/^{132}Xe - EXTa	0.992	-	-
±	94.1	3.53	94.20	±	0.019	-	-
^{20}Ne$_{trap}$ [in 10^{-12} cc]	48.1	0.56	48.69	^{130}Xe/^{132}Xe - EXTa	0.160	-	-
±	2.7	0.12	2.74	±	0.005	-	-
^{36}Ar [in 10^{-8} cc/g]	910.10	99.83	1009.93	^{131}Xe/^{132}Xe - EXTa	0.783	-	-
±	110.02	12.07	110.68	±	0.016	-	-
^{36}Ar [in 10^{-12} cc]	30.03	3.29	33.33	^{134}Xe/^{132}Xe - EXTa	0.380	-	-
±	3.51	0.39	3.51	±	0.008	-	-
^{38}Ar/^{36}Ar	0.193	0.188	0.193	^{136}Xe/^{132}Xe - EXTa	0.321	-	-
±	0.002	0.002	0.002	±	0.008	-	-
^{40}Ar/^{36}Ar	22.8	278.1	48.1	^{132}Xe - EXTb [in 10^{-8} cc/g]	0.9887	-	-
±	0.2	2.9	0.5	±	0.0460	-	-
^{40}Ar [in 10^{-8} cc/g]	20778.3	27765.1	48543.4	^{132}Xe - EXTb [in 10^{-12} cc]	0.0326	-	-
±	2520.7	3368.2	4206.9	±	0.0012	-	-
^{40}Ar [in 10^{-12} cc]	685.7	916.2	1601.9	^{128}Xe/^{132}Xe - EXTb	0.073	-	-
±	80.5	107.6	130.1	±	0.004	-	-
^{38}Ar$_{cos}$ [in 10^{-8} cc/g]	4.850	-	-	^{129}Xe/^{132}Xe - EXTb	0.994	-	-
±	2.960	-	-	±	0.019	-	-
^{38}Ar$_{cos}$ [in 10^{-12} cc]	0.160	-	-	^{130}Xe/^{132}Xe - EXTb	0.158	-	-
±	0.098	-	-	±	0.004	-	-
^{84}Kr [in 10^{-8} cc/g]	1.6330	-	-	^{131}Xe/^{132}Xe - EXTb	0.781	-	-
±	0.0874	-	-	±	0.004	-	-
^{84}Kr [in 10^{-12} cc]	0.0539	-	-	^{134}Xe/^{132}Xe - EXTb	0.399	-	-
±	0.0024	-	-	±	0.008	-	-
^{80}Kr/^{84}Kr	0.040	-	-	^{136}Xe/^{132}Xe - EXTb	0.329	-	-
±	0.003	-	-	±	0.008	-	-
^{82}Kr/^{84}Kr	0.206	-	-	^{21}Ne$_{cos}$/^{38}Ar$_{cos}$	0.02	-	-
±	0.007	-	-	±	0.02	-	-
^{83}Kr/^{84}Kr	0.203	-	-	^{36}Ar/^{132}Xe $_{(Int)}$	928.74	-	-
±	0.006	-	-	±	121.51	-	-
^{86}Kr/^{84}Kr	0.290	-	-	^{84}Kr/^{132}Xe $_{(Int)}$	1.67	-	-
±	0.008	-	-	±	0.12	-	-
^{83}Kr$_{cos}$ [in 10^{-8} cc/g]	-	-	-				
±	-	-	-				
^{83}Kr$_{cos}$ [in 10^{-12} cc]	-	-	-				
±	-	-	-				

Table X75. Noble gas data He to Xe for sample DC 06_09_57(1) (not corr. for blank)

Sample		DC 06_09_57 (1)	
Size [μm]		74 x 36	
Weight [μg]		~ 0.15	
Date of measure	24/10/12	Date of measure	24/10/12
	1 x 0.91 W		1 x 0.91 W
Laser-Power	1 x 6.3 W	Laser-Power	1 x 6.3 W
	1 x 6.3-30 W		1 x 6.3-30 W
Laser-Beam	600 μm	Laser-Beam	600 μm
Step(s)	1	Step(s)	1
^{4}He [in 10^{-8} cc/g]	5348.7	^{132}Xe - INT [in 10^{-8} cc/g]	1.4328
±	3566.7	±	0.9577
^{4}He [in 10^{-12} cc]	8.0	^{132}Xe - INT [in 10^{-12} cc]	0.0021
±	0.1	±	0.0001
^{3}He [in 10^{-12} cc/g]	< 42569.4 (2σ)	^{128}Xe/^{132}Xe - INT	0.112
±	-	±	0.018
^{3}He [in 10^{-16} cc]	< 63.9 (2σ)	^{129}Xe/^{132}Xe - INT	0.945
±	-	±	0.077
^{3}He/^{4}He	-	^{130}Xe/^{132}Xe - INT	0.152
±	-	±	0.015
^{22}Ne [in 10^{-8} cc/g]	32.702	^{131}Xe/^{132}Xe - INT	0.728
±	22.495	±	0.063
^{22}Ne [in 10^{-12} cc]	0.049	^{134}Xe/^{132}Xe - INT	0.392
±	0.008	±	0.036
^{20}Ne/^{22}Ne	6.06	^{136}Xe/^{132}Xe - INT	0.318
±	1.03	±	0.042
^{21}Ne/^{22}Ne	0.020	^{132}Xe - EXTa [in 10^{-8} cc/g]	1.4328
±	0.006	±	0.9577
^{21}Ne$_{cos}$ [in 10^{-8} cc/g]	-	^{132}Xe - EXTa [in 10^{-12} cc]	0.0021
±	-	±	0.0001
^{21}Ne$_{cos}$ [in 10^{-12} cc]	-	^{128}Xe/^{132}Xe - EXTa	0.091
±	-	±	0.013
^{20}Ne$_{trap}$ [in 10^{-8} cc/g]	198.7	^{129}Xe/^{132}Xe - EXTa	0.944
±	141.5	±	0.076
^{20}Ne$_{trap}$ [in 10^{-12} cc]	0.3	^{130}Xe/^{132}Xe - EXTa	0.140
±	0.1	±	0.019
^{36}Ar [in 10^{-8} cc/g]	419.62	^{131}Xe/^{132}Xe - EXTa	0.730
±	279.87	±	0.063
^{36}Ar [in 10^{-12} cc]	0.63	^{134}Xe/^{132}Xe - EXTa	0.401
±	0.01	±	0.030
^{38}Ar/^{36}Ar	0.178	^{136}Xe/^{132}Xe - EXTa	0.316
±	0.004	±	0.037
^{40}Ar/^{36}Ar	253.2	^{132}Xe - EXTb [in 10^{-8} cc/g]	1.4129
±	2.8	±	0.9562
^{40}Ar [in 10^{-8} cc/g]	106242.7	^{132}Xe - EXTb [in 10^{-12} cc]	0.0021
±	70864.0	±	0.0002
^{40}Ar [in 10^{-12} cc]	159.4	^{128}Xe/^{132}Xe - EXTb	0.066
±	3.4	±	0.012
^{38}Ar$_{cos}$ [in 10^{-8} cc/g]	-	^{129}Xe/^{132}Xe - EXTb	0.943
±	-	±	0.076
^{38}Ar$_{cos}$ [in 10^{-12} cc]	-	^{130}Xe/^{132}Xe - EXTb	0.136
±	-	±	0.016
^{84}Kr [in 10^{-8} cc/g]	8.1152	^{131}Xe/^{132}Xe - EXTb	0.730
±	5.4211	±	0.003
^{84}Kr [in 10^{-12} cc]	0.0122	^{134}Xe/^{132}Xe - EXTb	0.406
±	0.0005	±	0.033
^{80}Kr/^{84}Kr	0.045	^{136}Xe/^{132}Xe - EXTb	0.342
±	0.006	±	0.033
^{82}Kr/^{84}Kr	0.210	^{21}Ne$_{cos}$/^{38}Ar$_{cos}$	-
±	0.018	±	-
^{83}Kr/^{84}Kr	0.227	^{36}Ar/^{132}Xe $_{(Int)}$	292.87
±	0.018	±	15.26
^{86}Kr/^{84}Kr	0.278	^{84}Kr/^{132}Xe $_{(Int)}$	5.66
±	0.023	±	0.36
^{83}Kr$_{cos}$ [in 10^{-8} cc/g]	0.2178		
±	0.2078		
^{83}Kr$_{cos}$ [in 10^{-12} cc]	0.0003		
±	0.0003		

Table X76. Noble gas data He to Xe for sample DC 06_09_57(2) (not corr. for blank)

Sample		DC 06_09_57 (2)	
Size [µm]		19 x 18	
Weight [µg]		~ 0.05	
Date of measure	25/10/12	**Date of measure**	25/10/12
	1 x 0.91-18 W		1 x 0.91-18 W
Laser-Power	1 x 18 W	**Laser-Power**	1 x 18 W
	1 x 18-30 W		1 x 18-30 W
Laser-Beam	1000 / 180 / 2000 µm	**Laser-Beam**	1000 / 180 / 2000 µm
Step(s)	1	**Step(s)**	1
^{4}He [in 10^{-8} cc/g]	15281.1	^{132}Xe - INT [in 10^{-8} cc/g]	8.1101
±	6116.7	±	3.2571
^{4}He [in 10^{-12} cc]	7.6	^{132}Xe - INT [in 10^{-12} cc]	0.0041
±	0.1	±	0.0001
^{3}He [in 10^{-12} cc/g]	1432634.1	^{128}Xe/^{132}Xe - INT	0.110
±	589427.0	±	0.013
^{3}He [in 10^{-16} cc]	716.3	^{129}Xe/^{132}Xe - INT	1.090
±	69.0	±	0.062
^{3}He/^{4}He	0.00938	^{130}Xe/^{132}Xe - INT	0.154
±	0.00091	±	0.012
^{22}Ne [in 10^{-8} cc/g]	91.380	^{131}Xe/^{132}Xe - INT	0.799
±	39.486	±	0.060
^{22}Ne [in 10^{-12} cc]	0.046	^{134}Xe/^{132}Xe - INT	0.358
±	0.007	±	0.028
^{20}Ne/^{22}Ne	7.38	^{136}Xe/^{132}Xe - INT	0.252
±	1.20	±	0.025
^{21}Ne/^{22}Ne	0.013	^{132}Xe - EXTa [in 10^{-8} cc/g]	8.1101
±	0.005	±	3.2571
^{21}Ne$_{cos}$ [in 10^{-8} cc/g]	-	^{132}Xe - EXTa [in 10^{-12} cc]	0.0041
±	-	±	0.0001
^{21}Ne$_{cos}$ [in 10^{-12} cc]	-	^{128}Xe/^{132}Xe - EXTa	0.109
±	-	±	0.010
^{20}Ne$_{trap}$ [in 10^{-8} cc/g]	676.4	^{129}Xe/^{132}Xe - EXTa	1.088
±	315.3	±	0.061
^{20}Ne$_{trap}$ [in 10^{-12} cc]	0.3	^{130}Xe/^{132}Xe - EXTa	0.147
±	0.1	±	0.014
^{36}Ar [in 10^{-8} cc/g]	6618.85	^{131}Xe/^{132}Xe - EXTa	0.801
±	2650.56	±	0.060
^{36}Ar [in 10^{-12} cc]	3.31	^{134}Xe/^{132}Xe - EXTa	0.383
±	0.06	±	0.026
^{38}Ar/^{36}Ar	0.153	^{136}Xe/^{132}Xe - EXTa	0.302
±	0.003	±	0.033
^{40}Ar/^{36}Ar	210.5	^{132}Xe - EXTb [in 10^{-8} cc/g]	7.8589
±	2.0	±	3.2674
^{40}Ar [in 10^{-8} cc/g]	1393220.6	^{132}Xe - EXTb [in 10^{-12} cc]	0.0039
±	558071.3	±	0.0004
^{40}Ar [in 10^{-12} cc]	696.6	^{128}Xe/^{132}Xe - EXTb	0.080
±	14.8	±	0.011
^{38}Ar$_{cos}$ [in 10^{-8} cc/g]	-	^{129}Xe/^{132}Xe - EXTb	1.087
±	-	±	0.061
^{38}Ar$_{cos}$ [in 10^{-12} cc]	-	^{130}Xe/^{132}Xe - EXTb	0.163
±	-	±	0.015
^{84}Kr [in 10^{-8} cc/g]	61.6497	^{131}Xe/^{132}Xe - EXTb	0.801
±	24.7567	±	0.003
^{84}Kr [in 10^{-12} cc]	0.0308	^{134}Xe/^{132}Xe - EXTb	0.371
±	0.0011	±	0.026
^{80}Kr/^{84}Kr	0.049	^{136}Xe/^{132}Xe - EXTb	0.296
±	0.004	±	0.020
^{82}Kr/^{84}Kr	0.208	^{21}Ne$_{cos}$/^{38}Ar$_{cos}$	-
±	0.015	±	-
^{83}Kr/^{84}Kr	0.203	^{36}Ar/^{132}Xe $_{(Int)}$	816.12
±	0.012	±	33.24
^{86}Kr/^{84}Kr	0.311	^{84}Kr/^{132}Xe $_{(Int)}$	7.60
±	0.021	±	0.38
^{83}Kr$_{cos}$ [in 10^{-8} cc/g]	< 0.1772 (2σ)		
±	-		
^{83}Kr$_{cos}$ [in 10^{-12} cc]	< 0.0001 (2σ)		
±	-		

Table X77. Noble gas data He to Xe for sample DC 06_09_63 (not corrected for blank)

Sample			DC 06_09_63			
Size [µm]			198 x 141			
Weight [µg]			~ 3.3			
Date of measure	16/01/12	17/01/12	16+17/01/12			
Laser-Power	3 x 0.91 W	3 x 5 W				
Laser-Beam	250 µm	180 µm				
Step(s)	1	2	total*			

Left block:

	1	2	total*
^{4}He [in 10^{-8} cc/g]	90285.9	12331.0	102616.9
±	3133.7	475.4	3169.6
^{4}He [in 10^{-12} cc]	2979.4	406.9	3386.4
±	50.4	9.7	20.3
^{3}He [in 10^{-12} cc/g]	384984.1	31719.9	416704.0
±	56261.4	4777.0	56463.9
^{3}He [in 10^{-16} cc]	12704.5	1046.8	13751.2
±	1816.3	154.4	1816.1
^{3}He/^{4}He	0.00043	0.00026	0.00041
±	0.00006	0.00004	0.00005
^{22}Ne [in 10^{-8} cc/g]	55.006	5.325	60.331
±	2.874	0.451	2.909
^{22}Ne [in 10^{-12} cc]	1.815	0.176	1.991
±	0.077	0.014	0.075
^{20}Ne/^{22}Ne	11.85	11.06	11.78
±	0.26	0.77	0.25
^{21}Ne/^{22}Ne	0.031	0.026	0.031
±	0.001	0.004	0.001
^{21}Ne$_{cos}$ [in 10^{-8} cc/g]	< 0.184 (2σ)	-	-
±	-	-	-
^{21}Ne$_{cos}$ [in 10^{-12} cc]	< 0.006 (2σ)	-	-
±	-	-	-
^{20}Ne$_{trap}$ [in 10^{-8} cc/g]	648.6	-	-
±	51.1	-	-
^{20}Ne$_{trap}$ [in 10^{-12} cc]	21.4	-	-
±	1.6	-	-
^{36}Ar [in 10^{-8} cc/g]	139.94	224.15	364.09
±	4.82	7.71	9.09
^{36}Ar [in 10^{-12} cc]	4.62	7.40	12.01
±	0.08	0.12	0.03
^{38}Ar/^{36}Ar	0.191	0.180	0.184
±	0.001	0.001	0.001
^{40}Ar/^{36}Ar	69.9	246.6	178.7
±	0.5	1.3	1.5
^{40}Ar [in 10^{-8} cc/g]	9779.9	55278.2	65058.1
±	340.9	1918.5	1948.6
^{40}Ar [in 10^{-12} cc]	322.7	1824.2	2146.9
±	5.6	30.9	35.9
^{38}Ar$_{cos}$ [in 10^{-8} cc/g]	< 1.127 (2σ)	-	-
±	-	-	-
^{38}Ar$_{cos}$ [in 10^{-12} cc]	< 0.037 (2σ)	-	-
±	-	-	-
^{84}Kr [in 10^{-8} cc/g]	0.9424	1.7546	2.6969
±	0.0806	0.1491	0.1695
^{84}Kr [in 10^{-12} cc]	0.0311	0.0579	0.0890
±	0.0025	0.0046	0.0049
^{80}Kr/^{84}Kr	0.042	0.046	0.044
±	0.004	0.002	0.002
^{82}Kr/^{84}Kr	0.205	0.213	0.210
±	0.008	0.007	0.005
^{83}Kr/^{84}Kr	0.202	0.208	0.206
±	0.009	0.006	0.005
^{86}Kr/^{84}Kr	0.287	0.293	0.291
±	0.012	0.009	0.007
^{83}Kr$_{cos}$ [in 10^{-8} cc/g]	-	< 0.0367 (2σ)	-
±	-	-	-
^{83}Kr$_{cos}$ [in 10^{-12} cc]	-	< 0.0012 (2σ)	-
±	-	-	-

Right block:

	1	2	total*
^{132}Xe - INT [in 10^{-8} cc/g]	0.4415	0.3198	0.7613
±	0.0182	0.0134	0.0226
^{132}Xe - INT [in 10^{-12} cc]	0.0146	0.0106	0.0251
±	0.0004	0.0003	0.0003
^{128}Xe/^{132}Xe - INT	0.093	0.081	0.088
±	0.005	0.006	0.004
^{129}Xe/^{132}Xe - INT	1.004	0.946	0.980
±	0.028	0.027	0.020
^{130}Xe/^{132}Xe - INT	0.167	0.154	0.162
±	0.005	0.006	0.004
^{131}Xe/^{132}Xe - INT	0.779	0.794	0.785
±	0.027	0.026	0.019
^{134}Xe/^{132}Xe - INT	0.377	0.376	0.376
±	0.012	0.014	0.009
^{136}Xe/^{132}Xe - INT	0.331	0.334	0.332
±	0.016	0.018	0.012
^{132}Xe - EXTa [in 10^{-8} cc/g]	0.4422	0.3203	0.7624
±	0.1298	0.0940	0.1603
^{132}Xe - EXTa [in 10^{-12} cc]	0.0146	0.0106	0.0252
±	0.0043	0.0031	0.0052
^{128}Xe/^{132}Xe - EXTa	0.086	0.081	0.084
±	0.005	0.006	0.004
^{129}Xe/^{132}Xe - EXTa	1.003	0.946	0.979
±	0.028	0.027	0.020
^{130}Xe/^{132}Xe - EXTa	0.167	0.150	0.160
±	0.006	0.008	0.005
^{131}Xe/^{132}Xe - EXTa	0.778	0.794	0.784
±	0.027	0.026	0.019
^{134}Xe/^{132}Xe - EXTa	0.379	0.376	0.378
±	0.011	0.012	0.008
^{136}Xe/^{132}Xe - EXTa	0.322	0.324	0.323
±	0.011	0.012	0.008
^{132}Xe - EXTb [in 10^{-8} cc/g]	0.4389	0.3139	0.7528
±	0.0622	0.0446	0.0766
^{132}Xe - EXTb [in 10^{-12} cc]	0.0145	0.0104	0.0248
±	0.0020	0.0014	0.0024
^{128}Xe/^{132}Xe - EXTb	0.076	0.075	0.076
±	0.005	0.005	0.004
^{129}Xe/^{132}Xe - EXTb	1.003	0.946	0.979
±	0.028	0.027	0.020
^{130}Xe/^{132}Xe - EXTb	0.155	0.162	0.158
±	0.006	0.008	0.005
^{131}Xe/^{132}Xe - EXTb	0.778	0.794	0.784
±	0.004	0.004	0.003
^{134}Xe/^{132}Xe - EXTb	0.377	0.386	0.381
±	0.012	0.014	0.009
^{136}Xe/^{132}Xe - EXTb	0.334	0.343	0.338
±	0.011	0.013	0.009
^{21}Ne$_{cos}$/^{38}Ar$_{cos}$	-	-	-
±	-	-	-
^{36}Ar/^{132}Xe$_{(Int)}$	316.97	700.91	478.25
±	10.24	23.32	5.71
^{84}Kr/^{132}Xe$_{(Int)}$	2.13	5.49	3.54
±	0.18	0.46	0.20

Table X78. Noble gas data He to Xe for sample DC 06_09 141 (1) (not corr. for blank)

Sample		DC 06_09_141 (1)	
Size [µm]		84 x 79	
Weight [µg]		~ 0.7	
Date of measure	24/10/12	**Date of measure**	24/10/12
	1 x 0.91 W		1 x 0.91 W
Laser-Power	1 x 5 W	**Laser-Power**	1 x 5 W
	1 x 8-22 W		1 x 8-22 W
Laser-Beam	180 µm	**Laser-Beam**	180 µm
Step(s)	1	**Step(s)**	1
^{4}He [in 10^{-8} cc/g]	2245.6	^{132}Xe - INT [in 10^{-8} cc/g]	0.2700
±	322.5	±	0.0407
^{4}He [in 10^{-12} cc]	15.7	^{132}Xe - INT [in 10^{-12} cc]	0.0019
±	0.2	±	0.0001
^{3}He [in 10^{-12} cc/g]	64741.9	^{128}Xe/^{132}Xe - INT	0.106
±	13825.8	±	0.019
^{3}He [in 10^{-16} cc]	453.2	^{129}Xe/^{132}Xe - INT	0.919
±	71.9	±	0.068
^{3}He/^{4}He	0.00288	^{130}Xe/^{132}Xe - INT	0.155
±	0.00046	±	0.015
^{22}Ne [in 10^{-8} cc/g]	36.067	^{131}Xe/^{132}Xe - INT	0.800
±	5.308	±	0.081
^{22}Ne [in 10^{-12} cc]	0.252	^{134}Xe/^{132}Xe - INT	0.380
±	0.009	±	0.040
^{20}Ne/^{22}Ne	10.81	^{136}Xe/^{132}Xe - INT	0.257
±	0.35	±	0.035
^{21}Ne/^{22}Ne	0.026	^{132}Xe - EXTa [in 10^{-8} cc/g]	0.2700
±	0.003	±	0.0407
^{21}Ne$_{cos}$ [in 10^{-8} cc/g]	-	^{132}Xe - EXTa [in 10^{-12} cc]	0.0019
±	-	±	0.0001
^{21}Ne$_{cos}$ [in 10^{-12} cc]	-	^{128}Xe/^{132}Xe - EXTa	0.103
±	-	±	0.016
^{20}Ne$_{trap}$ [in 10^{-8} cc/g]	389.8	^{129}Xe/^{132}Xe - EXTa	0.919
±	62.6	±	0.067
^{20}Ne$_{trap}$ [in 10^{-12} cc]	2.7	^{130}Xe/^{132}Xe - EXTa	0.144
±	0.2	±	0.019
^{36}Ar [in 10^{-8} cc/g]	120.39	^{131}Xe/^{132}Xe - EXTa	0.802
±	17.36	±	0.081
^{36}Ar [in 10^{-12} cc]	0.84	^{134}Xe/^{132}Xe - EXTa	0.460
±	0.02	±	0.036
^{38}Ar/^{36}Ar	0.177	^{136}Xe/^{132}Xe - EXTa	0.274
±	0.004	±	0.035
^{40}Ar/^{36}Ar	191.0	^{132}Xe - EXTb [in 10^{-8} cc/g]	0.2638
±	2.3	±	0.0492
^{40}Ar [in 10^{-8} cc/g]	22997.0	^{132}Xe - EXTb [in 10^{-12} cc]	0.0018
±	3324.1	±	0.0002
^{40}Ar [in 10^{-12} cc]	161.0	^{128}Xe/^{132}Xe - EXTb	0.069
±	3.5	±	0.014
^{38}Ar$_{cos}$ [in 10^{-8} cc/g]	-	^{129}Xe/^{132}Xe - EXTb	0.918
±	-	±	0.067
^{38}Ar$_{cos}$ [in 10^{-12} cc]	-	^{130}Xe/^{132}Xe - EXTb	0.166
±	-	±	0.019
^{84}Kr [in 10^{-8} cc/g]	1.4837	^{131}Xe/^{132}Xe - EXTb	0.802
±	0.2207	±	0.003
^{84}Kr [in 10^{-12} cc]	0.0104	^{134}Xe/^{132}Xe - EXTb	0.400
±	0.0004	±	0.034
^{80}Kr/^{84}Kr	0.054	^{136}Xe/^{132}Xe - EXTb	0.339
±	0.007	±	0.031
^{82}Kr/^{84}Kr	0.224	^{21}Ne$_{cos}$/^{38}Ar$_{cos}$	-
±	0.019	±	-
^{83}Kr/^{84}Kr	0.206	^{36}Ar/^{132}Xe $_{(Int)}$	445.89
±	0.016	±	23.31
^{86}Kr/^{84}Kr	0.288	^{84}Kr/^{132}Xe $_{(Int)}$	5.49
±	0.027	±	0.35
^{83}Kr$_{cos}$ [in 10^{-8} cc/g]	< 0.0588 (2σ)		
±	-		
^{83}Kr$_{cos}$ [in 10^{-12} cc]	< 0.0004 (2σ)		
±	-		

Sample		DC 06_09_149	
Size [µm]		85 x 60	
Weight [µg]		~ 0.3	
Date of measure	23/10/12	**Date of measure**	23/10/12
Laser-Power	1 x 0.91 W	**Laser-Power**	1 x 0.91 W
	1 x 8 W		1 x 8 W
	1 x 5-22 W		1 x 5-22 W
Laser-Beam	180 / 1000 / 180 µm	**Laser-Beam**	180 / 1000 / 180 µm
Step(s)	1	**Step(s)**	1
^{4}He [in 10^{-8} cc/g]	18316.0	^{132}Xe - INT [in 10^{-8} cc/g]	1.0511
±	6112.6	±	0.3528
^{4}He [in 10^{-12} cc]	54.9	^{132}Xe - INT [in 10^{-12} cc]	0.0032
±	0.9	±	0.0001
^{3}He [in 10^{-12} cc/g]	410139.5	^{128}Xe/^{132}Xe - INT	0.087
±	138387.1	±	0.013
^{3}He [in 10^{-16} cc]	1230.4	^{129}Xe/^{132}Xe - INT	0.961
±	64.4	±	0.063
^{3}He/^{4}He	0.00224	^{130}Xe/^{132}Xe - INT	0.156
±	0.00012	±	0.012
^{22}Ne [in 10^{-8} cc/g]	698.250	^{131}Xe/^{132}Xe - INT	0.866
±	233.047	±	0.061
^{22}Ne [in 10^{-12} cc]	2.095	^{134}Xe/^{132}Xe - INT	0.395
±	0.035	±	0.031
^{20}Ne/^{22}Ne	11.60	^{136}Xe/^{132}Xe - INT	0.398
±	0.11	±	0.041
^{21}Ne/^{22}Ne	0.032	^{132}Xe - EXTa [in 10^{-8} cc/g]	1.0511
±	0.001	±	0.3528
^{21}Ne$_{cos}$ [in 10^{-8} cc/g]	1.446	^{132}Xe - EXTa [in 10^{-12} cc]	0.0032
±	1.035	±	0.0001
^{21}Ne$_{cos}$ [in 10^{-12} cc]	0.004	^{128}Xe/^{132}Xe - EXTa	0.079
±	0.003	±	0.012
^{20}Ne$_{trap}$ [in 10^{-8} cc/g]	8101.1	^{129}Xe/^{132}Xe - EXTa	0.960
±	2741.5	±	0.062
^{20}Ne$_{trap}$ [in 10^{-12} cc]	24.3	^{130}Xe/^{132}Xe - EXTa	0.165
±	1.4	±	0.015
^{36}Ar [in 10^{-8} cc/g]	2991.54	^{131}Xe/^{132}Xe - EXTa	0.867
±	998.81	±	0.061
^{36}Ar [in 10^{-12} cc]	8.97	^{134}Xe/^{132}Xe - EXTa	0.371
±	0.17	±	0.027
^{38}Ar/^{36}Ar	0.186	^{136}Xe/^{132}Xe - EXTa	0.310
±	0.004	±	0.034
^{40}Ar/^{36}Ar	15.3	^{132}Xe - EXTb [in 10^{-8} cc/g]	1.1195
±	0.2	±	0.3944
^{40}Ar [in 10^{-8} cc/g]	45679.1	^{132}Xe - EXTb [in 10^{-12} cc]	0.0034
±	15261.1	±	0.0004
^{40}Ar [in 10^{-12} cc]	137.0	^{128}Xe/^{132}Xe - EXTb	0.093
±	3.1	±	0.012
^{38}Ar$_{cos}$ [in 10^{-8} cc/g]	-	^{129}Xe/^{132}Xe - EXTb	0.959
±	-	±	0.062
^{38}Ar$_{cos}$ [in 10^{-12} cc]	-	^{130}Xe/^{132}Xe - EXTb	0.138
±	-	±	0.015
^{84}Kr [in 10^{-8} cc/g]	6.5330	^{131}Xe/^{132}Xe - EXTb	0.867
±	2.1903	±	0.003
^{84}Kr [in 10^{-12} cc]	0.0196	^{134}Xe/^{132}Xe - EXTb	0.371
±	0.0007	±	0.028
^{80}Kr/^{84}Kr	0.052	^{136}Xe/^{132}Xe - EXTb	0.357
±	0.006	±	0.024
^{82}Kr/^{84}Kr	0.221	^{21}Ne$_{cos}$/^{38}Ar$_{cos}$	-
±	0.016	±	-
^{83}Kr/^{84}Kr	0.214	^{36}Ar/^{132}Xe $_{(Int)}$	2846.15
±	0.013	±	124.29
^{86}Kr/^{84}Kr	0.309	^{84}Kr/^{132}Xe $_{(Int)}$	6.22
±	0.021	±	0.33
^{83}Kr$_{cos}$ [in 10^{-8} cc/g]	< 0.2736 (2σ)		
±	-		
^{83}Kr$_{cos}$ [in 10^{-12} cc]	< 0.0008 (2σ)		
±	-		

Table X80. Noble gas data He to Xe for sample DC 06_09_189 (not corrected for blank)

Sample		DC 06_09_189	
Size [µm]		93 x 92	
Weight [µg]		~ 1.0	
Date of measure	18/10/12	**Date of measure**	18/10/12
	1 x 0.91 W		1 x 0.91 W
Laser-Power	1 x 25 W	**Laser-Power**	1 x 25 W
	1 x 21 W		1 x 21 W
Laser-Beam	180 / 1850 / 250 µm	**Laser-Beam**	180 / 1850 / 250 µm
Step(s)	1	**Step(s)**	1
^{4}He [in 10^{-8} cc/g]	480622.2	^{132}Xe - INT [in 10^{-8} cc/g]	17.4799
±	48540.6	±	1.7662
^{4}He [in 10^{-12} cc]	4806.2	^{132}Xe - INT [in 10^{-12} cc]	0.1748
±	68.0	±	0.0025
^{3}He [in 10^{-12} cc/g]	1564323.2	^{128}Xe/^{132}Xe - INT	0.074
±	159632.9	±	0.002
^{3}He [in 10^{-16} cc]	15643.2	^{129}Xe/^{132}Xe - INT	0.991
±	318.1	±	0.014
^{3}He/^{4}He	0.00033	^{130}Xe/^{132}Xe - INT	0.153
±	0.00001	±	0.002
^{22}Ne [in 10^{-8} cc/g]	312.159	^{131}Xe/^{132}Xe - INT	0.782
±	31.619	±	0.009
^{22}Ne [in 10^{-12} cc]	3.122	^{134}Xe/^{132}Xe - INT	0.386
±	0.050	±	0.005
^{20}Ne/^{22}Ne	11.86	^{136}Xe/^{132}Xe - INT	0.318
±	0.09	±	0.005
^{21}Ne/^{22}Ne	0.032	^{132}Xe - EXTa [in 10^{-8} cc/g]	17.5883
±	0.001	±	1.7770
^{21}Ne$_{cos}$ [in 10^{-8} cc/g]	0.489	^{132}Xe - EXTa [in 10^{-12} cc]	0.1759
±	0.351	±	0.0025
^{21}Ne$_{cos}$ [in 10^{-12} cc]	0.005	^{128}Xe/^{132}Xe - EXTa	0.071
±	0.003	±	0.002
^{20}Ne$_{trap}$ [in 10^{-8} cc/g]	3700.8	^{129}Xe/^{132}Xe - EXTa	0.991
±	427.6	±	0.011
^{20}Ne$_{trap}$ [in 10^{-12} cc]	37.0	^{130}Xe/^{132}Xe - EXTa	0.151
±	2.1	±	0.002
^{36}Ar [in 10^{-8} cc/g]	1491.15	^{131}Xe/^{132}Xe - EXTa	0.786
±	151.79	±	0.009
^{36}Ar [in 10^{-12} cc]	14.91	^{134}Xe/^{132}Xe - EXTa	0.385
±	0.28	±	0.004
^{38}Ar/^{36}Ar	0.185	^{136}Xe/^{132}Xe - EXTa	0.316
±	0.004	±	0.004
^{40}Ar/^{36}Ar	219.0	^{132}Xe - EXTb [in 10^{-8} cc/g]	17.2699
±	2.0	±	1.7937
^{40}Ar [in 10^{-8} cc/g]	326547.7	^{132}Xe - EXTb [in 10^{-12} cc]	0.1727
±	33372.3	±	0.0048
^{40}Ar [in 10^{-12} cc]	3265.5	^{128}Xe/^{132}Xe - EXTb	0.073
±	68.8	±	0.002
^{38}Ar$_{cos}$ [in 10^{-8} cc/g]	-	^{129}Xe/^{132}Xe - EXTb	0.991
±	-	±	0.011
^{38}Ar$_{cos}$ [in 10^{-12} cc]	-	^{130}Xe/^{132}Xe - EXTb	0.151
±	-	±	0.002
^{84}Kr [in 10^{-8} cc/g]	72.2592	^{131}Xe/^{132}Xe - EXTb	0.786
±	7.9030	±	0.004
^{84}Kr [in 10^{-12} cc]	0.7226	^{134}Xe/^{132}Xe - EXTb	0.391
±	0.0320	±	0.005
^{80}Kr/^{84}Kr	0.038	^{136}Xe/^{132}Xe - EXTb	0.324
±	0.001	±	0.004
^{82}Kr/^{84}Kr	0.195	^{21}Ne$_{cos}$/^{38}Ar$_{cos}$	-
±	0.007	±	-
^{83}Kr/^{84}Kr	0.196	^{36}Ar/^{132}Xe $_{(Int)}$	85.31
±	0.006	±	2.04
^{86}Kr/^{84}Kr	0.293	^{84}Kr/^{132}Xe $_{(Int)}$	4.13
±	0.008	±	0.19
^{83}Kr$_{cos}$ [in 10^{-8} cc/g]	-		
±	-		
^{83}Kr$_{cos}$ [in 10^{-12} cc]	-		
±	-		

D.　Figures showing micrometeorites examined for noble gases - Micrometeorites are from Miller Butte, Transantarctic Mountains, Antartica.

- Basic information and SEM pictures of micrometeorites - SEM picture taken October 2010 at University of Siena / MNA with courtesy of L. Folco and C. Cordier.

- Mineralogical and petrological information (where available) by C. Cordier (2010 at MNA, University of Siena, Italy - now at ISTerre, University of Grenoble, France); in personal communication 2013/14.

Table X81. Overall petrography of micrometeorite 45b.08
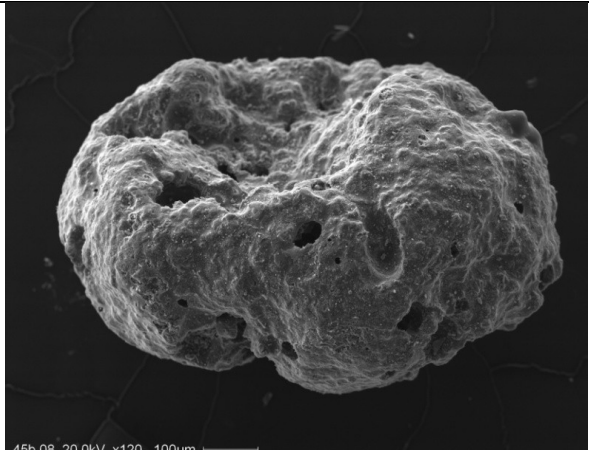
Sample	45b.08
Size [μm]	850 x 540
Elongation ratio (1 = round spherule)	1.57

Mineralogical and petrological information (C. Cordier, ISTerre, University of Grenoble, France; personal communication 2013).

- **The MM 45b.08 is scoriaceous, microporphyritic and fresh**.
- Observable are a few relict grains of olivine, low Ca pyroxene and chromite with sizes up to 50 μm.
    - ○ Analysis of the olivine relict grains:
        - ▪ The grains are homogenous throughout the core of the MM - $Fa_{0.8-5.2}$.
        - ▪ Minor element concentrations:
            - • CaO = 0.21 to 0.63 wt.% (avg. 0.38 wt.%)
            - • MnO = 0.01 to 0.35 wt.% (avg. 0.16 wt.%)
            - • Cr_2O_3 = 0.10 to 0.59 wt.% (avg. 0.37 wt.%)
            - • NiO < 0.03 wt.%
        - ▪ At the rim they show overgrowth due to crystallization during atmospheric entry heating - Fa_9.
- Also visible are interstitial olivine, microphenocrysts, magnetite grains and glass. The microphenocrysts show higher Fa contents (up to $Fa_{24.1}$), lower CaO contents (0.15 to 0.23 wt.%), higher MnO (0.31 to 0.66 wt.%) and similar Cr_2O_3 contents (0.29 to 0.52 wt.%). The NiO content does not show significant differences between microphenocrysts and relict grains. The microphenocrysts are surrounded by a thin Fe-rich rim. Some show an Mg-poor core and are equivalent in composition to large olivine relict grains.
- A magnetite rim is formed continuously around the whole MM and shows the meteoritic origin (see Genge et al. (2008)).
- Near the rim, numerous olivines show a dusty habit and are speckled with very small opaque grains.
- Dusty olivines near the MM rim show Fa_{18-20} and are observed in other particles. This value is presumably due to contamination with very small FeNi metal grains.
- The low Ca pyroxene in the relict grains shows a heterogeneous composition throughout the section with $Fs_{1.8-20.9}$ and $Wo_{0.5-22}$.
    - ○ They show a significant range of minor element concentrations:
        - ▪ MnO = 0.05 to 0.66 wt.% (avg. 0.40 wt.%)
        - ▪ Cr_2O_3 = 0.38 to 1.29 wt.% (avg. 0.82 wt.%).
- The relict chromite grains are rounded and possess MgO of about 7.8 wt.%.
    - ○ The $\frac{Cr}{Cr+Al}$ ratio shows a value of 0.82. The $\frac{Fe}{Fe+Mg}$ ratio gives a result of 0.65 which is lower than in OC material (0.8-0.9).
- Visible in the thin section are to metal blebs - one is small, Ni-poor, possesses around 1wt% phosphate and is imbedded in a forsteritic relict grain (upper middle), the other bleb (below middle) is bigger, Ni-rich (70.6 wt.%) and has S = 26.1 wt.%, Fe = 2.5 wt.%.

Conclusion:

Presumably 45b.08 is a **Type-3 ordinary chondrite (OC) (type IA chondrules)**

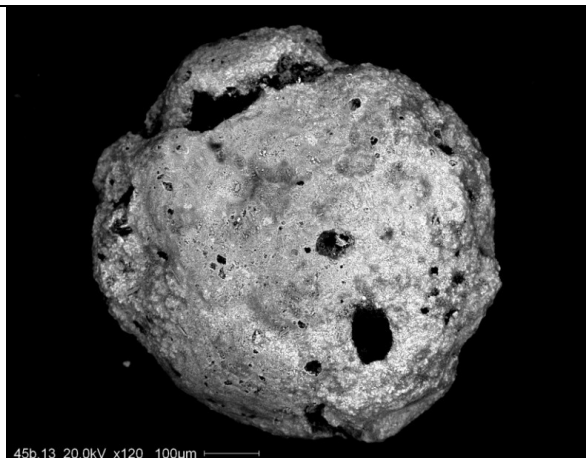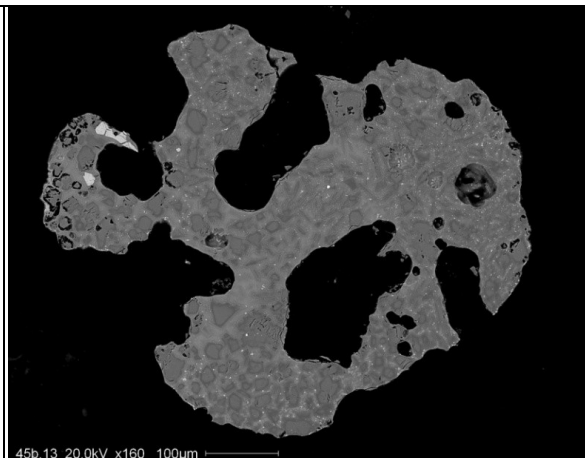**Figure 90 SEM image (Back-scattered electron (BSE) mode) showing the whole MM 45b.08.**

Figure 91 SEM image (BSE mode) showing a sectioned portion of MM 45b.08. The analysis (see text in Table X81) is suggesting a scoriaceous, microporphyritic and fresh micrometeorite origin.

Table X82. Overall petrography of micrometeorite 45b.09
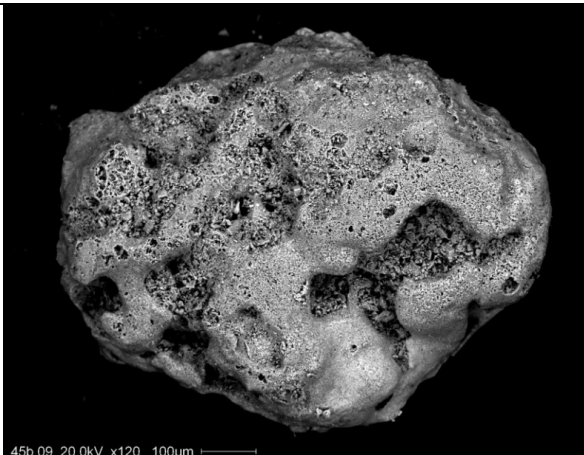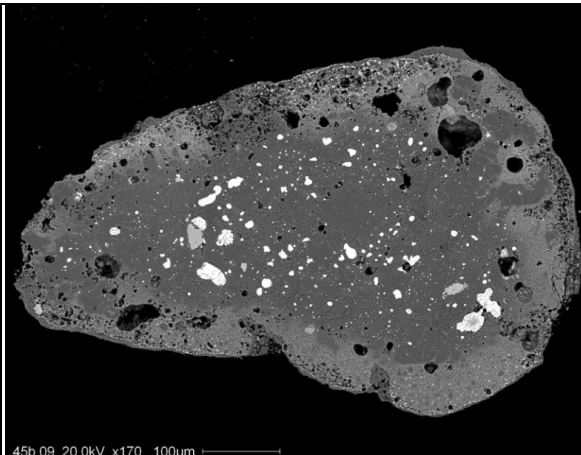
Sample	45b.09
Size [μm]	830 x 660
Elongation ratio (1 = round spherule)	1.26

Mineralogical and petrological information (C. Cordier, ISTerre, University of Grenoble, France; personal communication 2013).

- **45b.09 is a fine grained, fresh, micro porphyritic and relict grain bearing micrometeorite.**

- Visible are relict grains of olivine, low Ca pyroxene and chromite. Olivine and low Ca pyroxene are set in a Na_2O-rich glass. Numerous numbers of sulfide and (oxidized) metal blebs are visible. Fe-Mg minerals in the particle core are surrounded by a melt and suffered dissolution and digestion.

- A thick igneous rim (Genge (2006)) with a higher abundance of vesicles is observable. The rim is up to 75 μm thick and contains out of glass, olivine microphenocrysts and magnetite. The igneous rim itself is surrounded by a magnetite rim and both rims suggest a meteoritic origin of the sample (see Genge et al. (2008)).

- The MM shows a differing glass composition from the core to the igneous rim:
  - Na_2O, MgO, Al_2O_3, SiO_2 contents <u>decrease</u> from 7 to 3.5 wt%, 7 to 3 wt.%, 15 to 10 wt.% and 60 to 50 wt.%
  - The CaO and FeO contents <u>increase</u> from 2.5 to 6 wt.% and 6 to 26 wt.%

- The olivine relict grains possess of a homogenous composition throughout the section with $Fa_{16.8-17.1}$.
  - Minor elemental concentrations:
    - CaO = 0.02 to 0.04 wt.% (avg. 0.03 wt.%)
    - MnO = 0.47 wt.%
    - Cr_2O_3 = 0.02 to 0.03 wt.% (avg. 0.02 wt.%)
    - NiO < 0.03 wt.%

- Some microphenocrysts have an Mg-poor core and are mostly found in the igneous rim. The Mg-poor core is equivalent in composition to large olivine relict grains. The microphenocrysts in the igneous rim are different to the relict grains. They show higher Fa contents with up to $Fa_{39.3}$, higher CaO contents (0.05 to 0.38 wt.%), lower MnO (0.31 to 0.45 wt.%), higher Cr_2O_3 contents (0.06 to 0.32 wt.%) and higher NiO contents (0.31 to 0.45 wt.%).

- The low Ca pyroxenes are homogenous in composition throughout the section with $Fs_{15.2-16.8}$ and $Wo_{0.8-1.2}$.
  - They show a range of minor element concentrations:
    - MnO = 0.49 to 0.52 wt.% (avg. 0.49 wt.%)
    - Cr_2O_3 = 0.09 to 0.14 wt.% (avg. 0.13 wt.%).

- Also, chromite relict grains are distributed uniformly throughout the section with 3.6 wt.% MgO:
  - The $\frac{Cr}{Cr+Al}$ ratio shows a value of 0.87. The $\frac{Fe}{Fe+Mg}$ ratio gives a result of 0.81

- Abundant metal and sulfide grains form intergrowth or assemblages, whereas metal is surrounded by sulfide. The metal consists out of FeNi with Ni from 1.7 to 22.2 wt.%. Further the metal is poor on P and Si. The sulfide consists of 1 - 7.8 wt.% of Ni and contain often spherical voids.

<u>Conclusion:</u>

Presumably 45b.09 is an **equilibrated ordinary chondrite (EOC) (H4-6)**
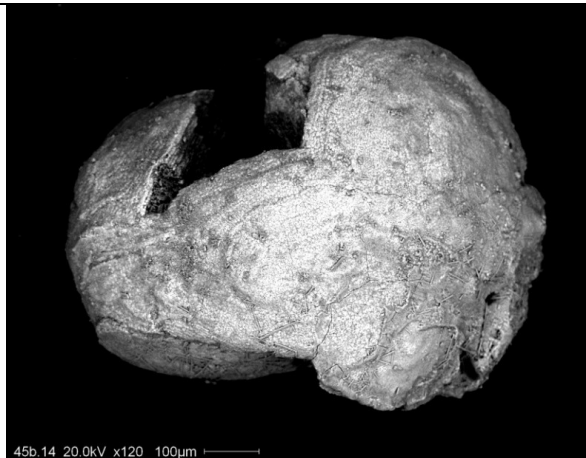

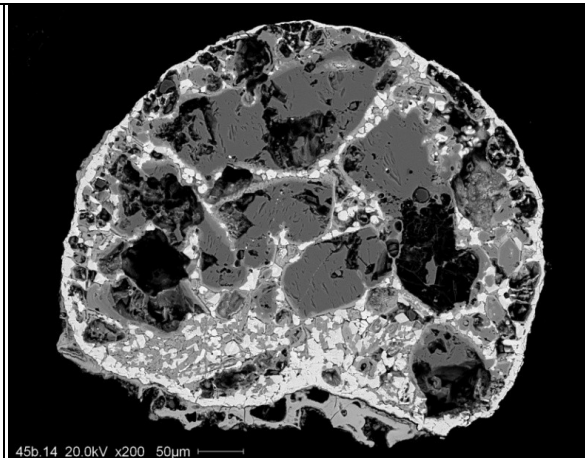|	
Figure 92 SEM image (BSE mode) showing the whole MM 45b.09.	**Figure 93 SEM image (BSE mode) showing a sectioned portion of MM 45b.09. The analysis (see text in Table X82) is suggesting a fine grained, microporphyritic, relict grain bearing and fresh MM.**

Table X83. Overall petrography of micrometeorite 45b.10

Sample	45b.10
Size [μm]	720 x 540
Elongation ratio (1 = round spherule)	1.33

Mineralogical and petrological information (C. Cordier, ISTerre, University of Grenoble, France; personal communication 2013).

- **45b.10 is a coarse grained, fresh and relict grain bearing micrometeorite.**

- The MM consists out of up to 100 μm in size olivine relict grains with metal inclusions, olivine microphenocrysts and magnetite grains embedded in a glassy mesostasis. Observable is a microphenocrysts bearing igneous rim (Genge (2006)), which is well developed along one edge of the MM. Its magnetite content increases towards the rims exterior. Detectable interstitial glass shows less MgO and SiO_2 but more FeO contents than the igneous rim.

- The olivine relict grains possess of a homogenous composition throughout the section and are highly magnesian with $Fa_{1.4-2.3}$. Furthermore the relict grains are surrounded by a FeO-rich rim.
  - The minor elemental concentrations show a homogenous pattern:
    - CaO = 0.23 wt.%
    - MnO = 0.12 wt.%
    - Cr_2O_3 = 0.61 wt.%
    - NiO = below detection limit

- Available olivine microphenocrysts are Fe-rich (Fa_{20-40}) and do not show a detectable amount of Ni. The rim of the microphenocrysts is richer on Fe than the core. Compositions with highest Fe amounts are observed in the igneous rim. Some of the microphenocrysts show core compositions similar to relict grains.

- Additionally observable are olivine relict grains which contain spherical metal blebs with the following composition:
  - Fe: 89.7 wt.%
  - Ni: 6.5 wt.%
  - Co: 0.3 wt.%
  - P: 0.07-0.2 wt.%

- These blebs are sometimes oxidized – assumedly due to weathering or oxidation during atmospheric entry. In this context metal grains are only observed in inclusions in olivines.

Conclusion:

Presumably 45b.10 is an **unequilibrated carbonaceous chondrite (CR)**

Figure 94 SEM image (BSE mode) showing the whole MM 45b.10.
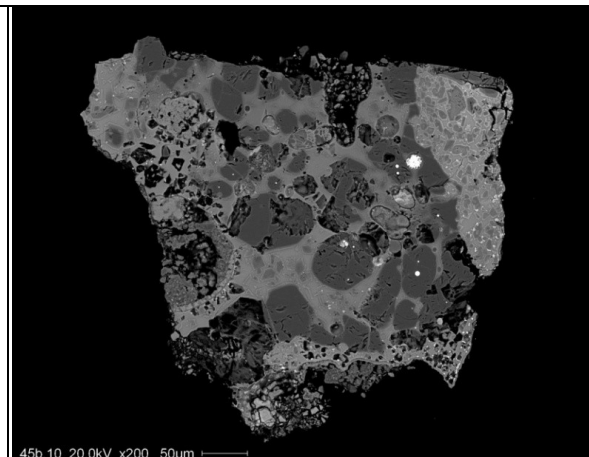
Figure 95 SEM image (BSE mode) showing a sectioned portion of MM 45b.10. The analysis (see text in Table X83) presumes a coarse-grained relict grains bearing fresh MM.

Table X84. Overall petrography of micrometeorite 45b.13

Sample	45b.13
Size [µm]	710 x 650
Elongation ratio (1 = round spherule)	1.09

Mineralogical and petrological information (C. Cordier, ISTerre, University of Grenoble, France; personal communication 2013).

- **45b.13 is a scoriaceous, microporphyritic, highly vesicular and fresh micrometeorite.**
- The MM consists of olivine microphenocrysts and olivine relict grains with interstitial feathered olivines, dendritic magnetite and glass. An igneous rim and/or magnetite rim is not observable.
- The olivine relict grains are homogeneous throughout the section with Fa_{23-24}. The grains are surrounded by a more Mg-rich rim with Fa_{14-20}, indicating reverse zoning. The zoning has the same composition as microphenocrysts and crystallized during atmospheric entry heating.
    - The minor element contents in the relict grains are:
        - CaO = 0.18 to 0.23 wt.% (avg. = 0.21 wt.%)
        - MnO = 0.35 to 0.48 wt.% (avg. = 0.42)
        - Cr_2O_3 = 0.10 to 0.23 wt.% (avg. = 0.15 wt.%)
        - NiO = below detection limit
        - The rims contain less CaO (0.13 wt.%) and MnO (0.26 wt.%) but more Cr_2O_3 (0.42 wt.%) and NiO (0.01 to 0.08 wt.%).
- Large relict grains of chromite are observed on the left upper side of the particle along with smaller grains on the whole section. The large grain composition contains 5.5 to 6.5 wt.% MgO, low Al_2O_3 contents of 0.07 to 0.26 wt.%, $\frac{Fe}{Fe+Mg}$ = 0.68 to 0.72 and $\frac{Cr}{Cr+Al}$ = 0.8 to 0.9 (slightly lower than for OC material).
- Additionally observable are sulfide blebs with both Ni-poor (6.8 wt.%) and Ni-rich (38%) contents.
- Minor elements in olivine relict grains - along with high MnO and lower but distinctly measureable CaO and Cr_2O_3 - suggest an unequilibrated ordinary chondrite precursor, similar to Type 3 L or LL chondrites (petrologic type < 3.5, after Bunch et al. (2012)).

Conclusion:

Presumably 45b.13 is an **unequilibrated ordinary chondrite (UOC) (L-LL3 - 3.1 to 3.5)**

Figure 96 SEM image (BSE mode) showing the whole MM 45b.13.

Figure 97 SEM image (BSE mode) showing a sectioned portion of MM 45b.13. The analysis (see text in Table X84) is suggesting a scoriaceous, microporphyritic, highly vesicular and fresh MM.

Table X85. Overall petrography of micrometeorite 45b.14

Sample	45b.14
Size [μm]	815 x 540
Elongation ratio (1 = round spherule)	1.51

Mineralogical and petrological information (C. Cordier, ISTerre, University of Grenoble, France; personal communication 2013).

- **45b.14 is a coarse-grained scoriaceous and fresh micrometeorite.**
- The MM consists of large (up to 250 μm in lenght) olivine relict grains in a mesostasis of Fe-rich olivine microphenocrysts and subhedral magnetite grains.
- The particle is rimmed by a thick and continuous magnetite layer and locally encrusted by weathering products (Fe, S and Cl rich). The completeness of the magnetite rim indicates that this particle is a micrometeorite and not a fragment of larger meteorite (Genge et al. (2008)).
  - The olivine relict grains are homogenous throughout the section and show a $Fa_{18.6-18.9}$ composition.
  - The minor element contents in the relict grains are:
    - CaO = 0.04 wt.%
    - MnO = 0.49 wt.%
    - Cr_2O_3 = 0.02 wt.%
    - NiO is below detection limit
- Relict grains are surrounded by a Fe-rich rim (~Fa_{34}) with composition close to that of microphenocrysts, constituting the mesostasis (analyzed by SEM). Some of the largest microphenocrysts have grown from relict grains, their cores having the same composition as the relict grains.
- Within the magnetite rims, a few bright crystals of Cu-Zn-Fe metal are observable along with Cu = 60.1 wt.%, Zn = 36.2 wt.% and Fe = 5 wt.%.
- The olivine composition and homogeneity suggest an equilibrated (Fe) precursor, similar to H ordinary chondrites. This is consistent with the large amount of Fe-oxide.

Conclusion:
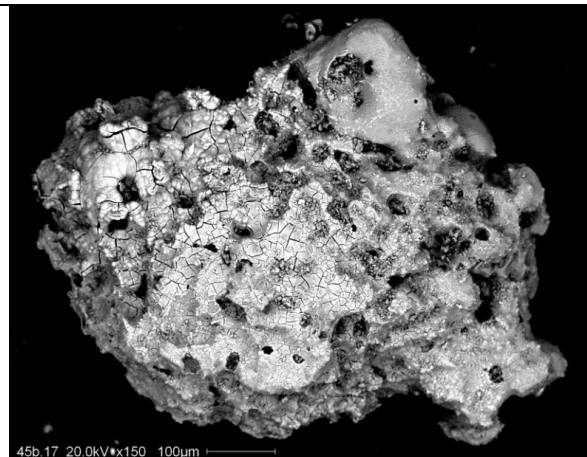Presumably 45b.14 is an **ordinary chondrite (OC) (H4-6)**

Figure 98 SEM image (BSE mode) showing the whole MM 45b.14.

Figure 99 SEM image (BSE mode) showing a sectioned portion of MM 45b.14. The analysis (see text in Table X85) is suggesting a scoriaceous, coarse grained and fresh MM.

Table X86. Overall petrography of micrometeorite 45b.15
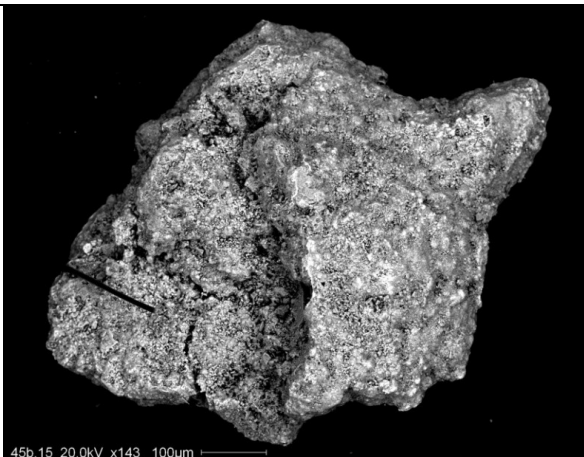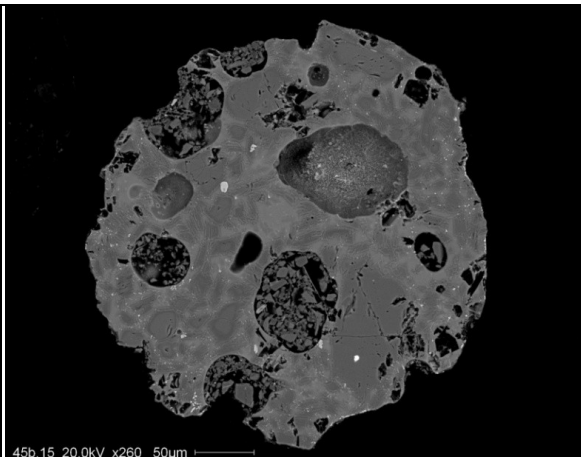
Sample	45b.15
Size [µm]	800 x 500
Elongation ratio (1 = round spherule)	1.60

Mineralogical and petrological information (C. Cordier, ISTerre, University of Grenoble, France; personal communication 2013).

- **45b.15 is a scoriaceous, porphyritic and fresh micrometeorite.**
- The MM consists of large (up to 100 µm in lenght) olivine relict grains, along with a few rounded relict chromite grains.
- The melted part crystallized as olivine µ-phenocrysts, magnetite and glass. A discontinuous and thin magnetite rim is locally observed. Abundant rounded vesicles are observable.
  - o The olivine relict grains show a $Fa_{15.3-18.6}$ composition (average of 16.3). These grains are surrounded by a Fe-poor rim with Fa_{14}.
  - o The minor element contents in the relict grains are:
    - CaO = 0.02-0.05 wt.%
    - MnO = 0.45-0.49 wt.%
    - Cr_2O_3 = 0.01-0.12 wt.%
    - NiO is below detection limit
  - o The minor element contents in the rims are:
    - high CaO = 0.25-0.27 wt.%
    - low MnO = 0.27-0.38 wt.%
    - Cr_2O_3 = 0.26-0.45 wt.%
    - higher NiO = 0.05-0.12 wt.%
- Some olivine microphenocrysts show oscillatory zoning, with a Fe-rich core (as relict grains) surrounded by a more MgO-rich mantle (as relict rim) followed by a very FeO-rich rim.
- One of the relict grains includes a Fe-Ni-S bleb with S = 32.0 wt.%, Fe = 55.3 wt.% and Ni = 4.2 wt.%.
- Chromite relicts grains contain 8.3 wt.% of MgO and $\frac{Fe}{Fe+Mg}$ as well as $\frac{Cr}{Cr+Al}$ ratios of 0.6 and 0.87 respectively. The $\frac{Fe}{Fe+Mg}$ ratio is not consistent with any chondritic chromite, which can be explained possibly with an analytical bias.
- The olivine composition and homogeneity throughout the section, along with chromite in the $\frac{Cr}{Cr+Al}$ ratio is consistent with an equilibrated ordinary chondrite parentage (4-6). However, the Fa contents suggest a H source.

Conclusion:

Presumably 45b.15 is an **equilibrated ordinary chondrite (EOC) (H4-6)**
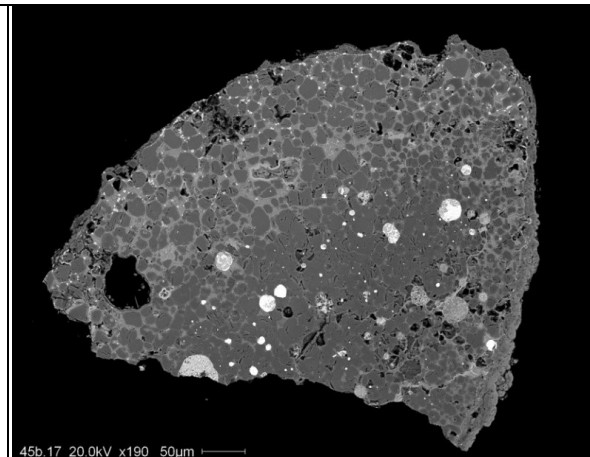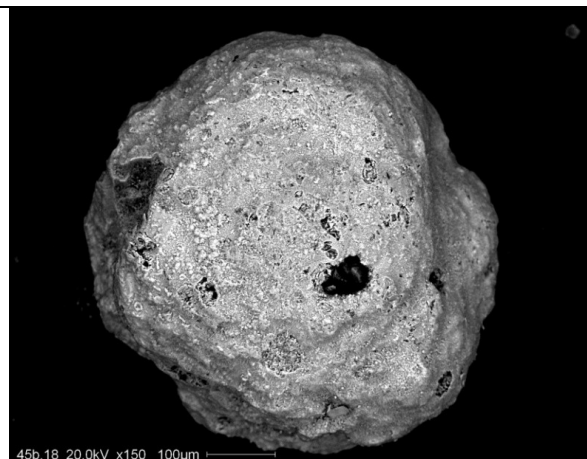

Figure 100 SEM image (BSE mode) showing the whole MM 45b.15.

Figure 101 SEM image (BSE mode) showing a sectioned portion of MM 45b.15. The analysis (see text in Table X86) is suggesting a scoriaceous, porphyritic and fresh MM.

Table X87. Overall petrography of micrometeorite 45b.16
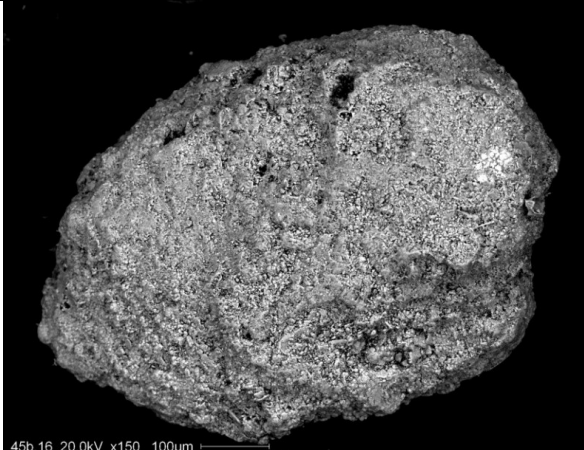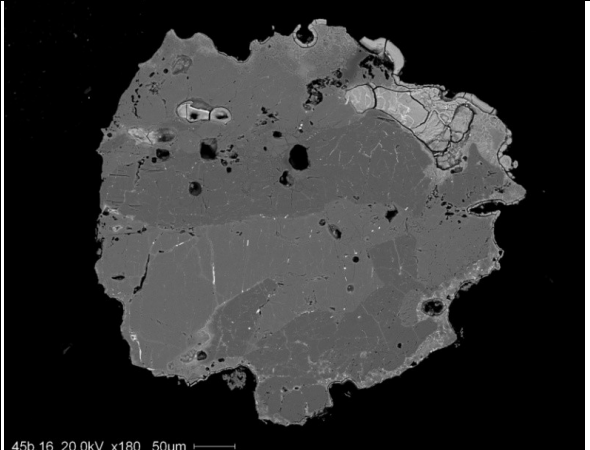
Sample	45b.16
Size [μm]	750 x 495
Elongation ratio (1 = round spherule)	1.52

Mineralogical and petrological information (C. Cordier, ISTerre, University of Grenoble, France; personal communication 2013).

- **45b.16 is a coarse-grained micrometeorite** made of imbricated olivine and pyroxene grains with size up to about 400 x 150 μm.
- A thin igneous rim (Genge (2006)) is observed on two opposite sides of the MM, one with small olivine microphenocrysts set in a glass mesostasis and the other one richer in magnetite dendrites. The MM is encrusted with jarosite.
- Olivine and pyroxene relict grains are crosscut by a network of fractures (maybe shock veinlets), locally filled with oxidized Fe-Ni metal and sulfide.
    - Olivine relict grains show a homogeneous composition with $Fa_{23.7-24.3}$ (in average $Fa_{23.9}$).
    - The minor element contents in the relict grains are:
        - CaO = 0.02 wt.%
        - MnO = 0.46-0.49 wt.%
        - Cr_2O_3 = 0.02-0.04 wt.%
        - NiO = 0.004-0.06 wt.%
    - Pyroxene relict grains have homogeneous composition with $Fs_{21.2}Wo_{1.7}$.
    - Minor element contents are:
        - Cr_2O_3 = 0.10 to 0.17 wt.% (avg. = 0.14 wt.%)
        - MnO = 0.47-0.48 wt.% (avg. = 0.47 wt.%)
- Olivine microphenocrysts show a Fa_{40} composition, along with higher NiO contents than relict grains (NiO = 1.28 to 1.68 wt.%), higher CaO = 0.06-0.08 wt.%, Cr_2O_3 = 0.04-0.08 wt.% and lower MnO = 0.26-0.29 wt.%.

Conclusion:

- Presumably 45b.16 is an **ordinary chondrite (OC) (L4-6)**

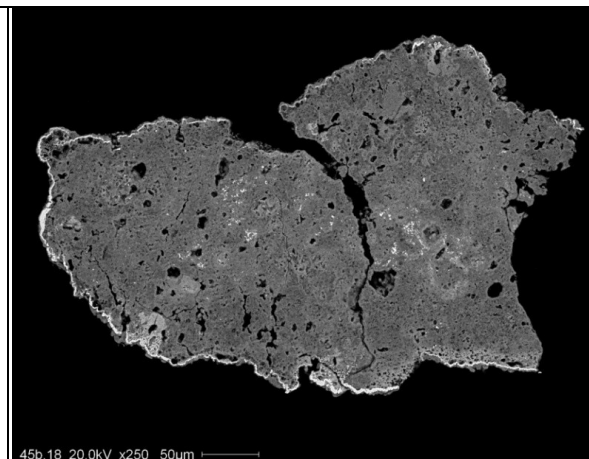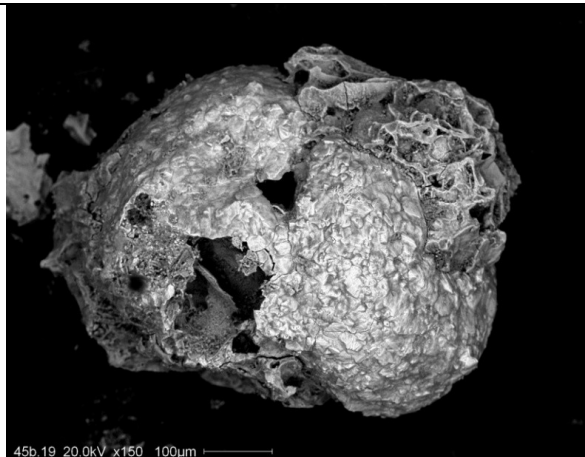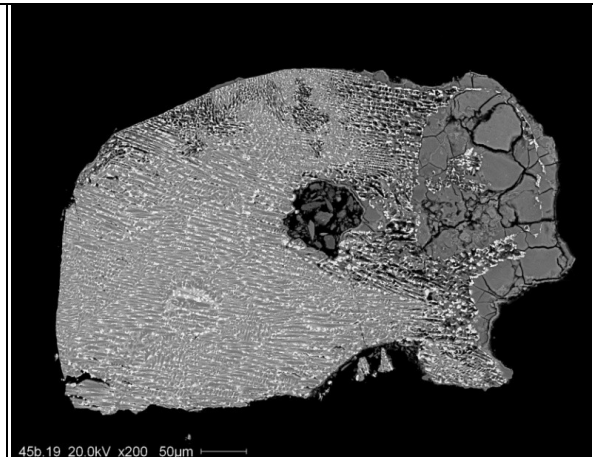**Figure 102 SEM image (BSE mode) showing the whole MM 45b.16.**

Figure 103 SEM image (BSE mode) showing a sectioned portion of MM 45b.16. The analysis (see text in Table X87) is suggesting a coarse grained MM.

Table X88. Overall petrography of micrometeorite 45b.17

Sample	45b.17
Size [μm]	655 x 470
Elongation ratio (1 = round spherule)	1.39

Mineralogical and petrological information (C. Cordier, ISTerre, University of Grenoble, France; personal communication 2013).

- **45b.17 is a coarse-grained and fresh micrometeorite** consisting of olivine relict grains, set in a glassy mesostasis which increases towards the particle exterior.
- Also magnetite grains are increasingly abundant towards the particle edge, locally forming a discontinuous magnetite rim. Numerous metal (both Ni-poor and Ni-rich) and sulfide blebs are observed in the particle interior, either in the mesostasis or included within the olivine grains. The MM is encrusted with jarosite.
  - Olivine relict grains show a composition in the range of $Fa_{11.2}$ to $Fa_{19.1}$ (average $Fa_{16.1}$).
  - Minor element contents are:
    - CaO = 0.23 to 0.43 wt.% (av = 0.32 wt.%)
    - Cr_2O_3 = 0.42 to 0.90 wt.% (av = 0.60 wt.%)
    - MnO = 0.46 to 0.56 wt.% (av = 0.5 wt.%)
    - NiO is below detection limit.
  - Fe/Mn ratios range from 20 to 38 (avg. = 29).
  - Relict grains in the particle core and rim show similar compositions.
- Also, metal and sulfide intergrowth have been analyzed. The disequilibrium of the sulfide part (indicated by abundant voids) impedes a reliable analysis. Metals are both, Ni-poor (~1 wt.%) and Ni-rich (~12 wt.%). Metal grains are P- and Si-poor.

Conclusion:

- Presumably 45b.17 is an **unequilibrated ordinary chondrite (UOC) (H3)**

Figure 104 SEM image (BSE mode) showing the whole MM 45b.17.

Figure 105 SEM image (BSE mode) showing a sectioned portion of MM 45b.17. The analysis (see text in Table X88) is suggesting a coarse grained and fresh MM.

Table X89. Overall petrography of micrometeorite 45b.18

Sample	45b.18
Size [µm]	560 x 550
Elongation ratio (1 = round spherule)	1.02

Mineralogical and petrological information (C. Cordier, ISTerre, University of Grenoble, France; personal communication 2013).

- **45b.18 is a fine-grained and porous MM** consisting of speckled magnetite.
- The continuous thin magnetite rim along the particle edge suggests a "real" MM rather than an origin as a larger meteorite fragment (Genge et al. (2008)). The MM is heavily weathered and no primary mineral phases can be observed at present.
- Weathering is proven by abundant contents of Na_2O (0.7 to 1.6 wt%), SO_3 (17 to 30 wt%) and K_2O (3.1 to 6.5 wt %), which suggests the presence of jarosite ($KFe^{3+}_3(OH)_6(SO_4)_2$).
- Numerous cracks crosscut the particle, which may correspond to degassing pathways.
- The texture of this particle is similar to that of the fresh UnMM #2.1c described by van Ginneken et al. (2012), which is porous and shows a fine grained texture with dehydration cracks. However, in contrast to 45b.18, $SiO2$ enrichment is observed in #2.1c. The observed dehydration cracks have been interpreted as a result of the decomposition of phyllosilicates (van Ginneken et al. (2012)).
- Overall the 45b.18 MM is a CI-like fine-grained particle. To decipher between C1 and C2 parentage is challenging.

Conclusion:

- Presumably 45b.18 is a **carbonaceous chondrite**

Figure 106 SEM image (BSE mode) showing the whole MM 45b.18.	**Figure 107 SEM image (BSE mode) showing a sectioned portion of MM 45b.18. The analysis (see text in Table X89) is suggesting a fine-grained and porous MM.**

Table X90. Overall petrography of micrometeorite 45b.19

Sample	45b.19
Size [µm]	610 x 450
Elongation ratio (1 = round spherule)	1.36

Mineralogical and petrological information (C. Cordier, ISTerre, University of Grenoble, France; personal communication 2013).

- **45b.19 is presumably similar to barred olivine Cosmic Spherules.**
- The MM morphology is sub-rounded.
- The MM shows weathering.
- The texture shows thin olivine hopper bars along with two rounded stuctures delineated by magnetite and very little interstitial glass.
- A single vesicle is observable.
- Also visible are Si-rich encrustations at the external side.
- At the right side, possibly a previous metal bead is completely replaced by alteration minerals.

Conclusion:

- At present, no detailed analysis of 45b.19 is available.
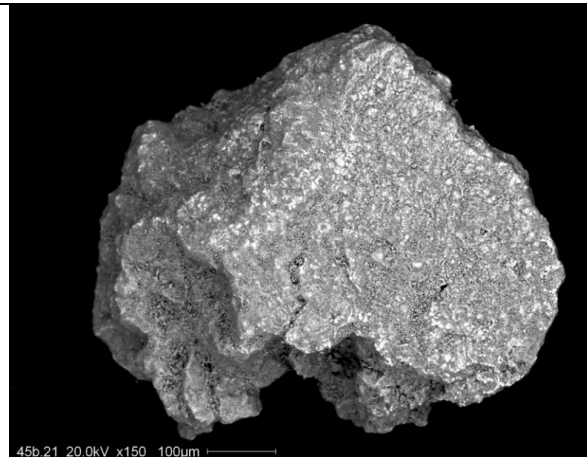

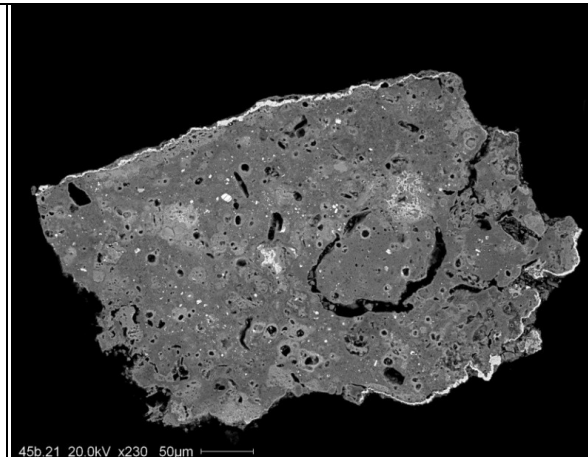|	
Figure 108 SEM image (BSE mode) showing the whole MM 45b.19.	**Figure 109 SEM image (BSE mode) showing a sectioned portion of MM 45b.19. The analysis (see text in Table X90) is suggesting a possible Cosmic Spherule origin.**

Table X91. Overall petrography of micrometeorite 45b.20
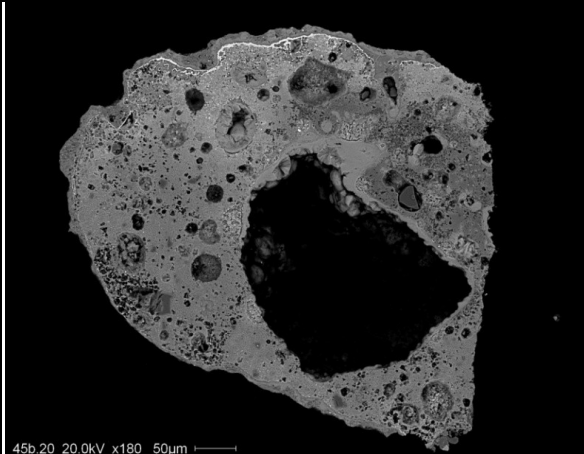
Sample	45b.20
Size [µm]	1000 x 500
Elongation ratio (1 = round spherule)	2.00

Mineralogical and petrological information (C. Cordier, ISTerre, University of Grenoble, France; personal communication 2013).

- **45b.20 is a scoriaceous, fine-grained micrometeorite** with rare and small olivine relict grains.
- The mesostasis is cryptocrystalline with Fe-rich olivine microphenocrysts, glass and sparse oxide (chromite) grains. The particle shows a high porosity, along with numerous, small vesicles dispersed in the mesostasis. A very large vesicle is observable in the center of this MM with a diameter of ~260µm.
- An almost continuous magnetite rim is apparent along one edge of the particle. The MM is encrusted by jarosite and Si-rich material (both along the particle rim and around vesicles). Some of the dark areas in the particle interior seem to consist of weathered glass.
  - Olivine relict grains show a $Fa_{1.1-5.7}$ composition (avg. = $Fa_{2.7}$). These grains form the core (often < 10 µm) of microphenocrysts, and are surrounded by a Fe-rich rim.
  - Minor element contents in relict grains are:
    - CaO = 0.18 to 0.30 wt.% (avg. = 0.23 wt.%)
    - Cr_2O_3 = 0.34 to 0.53 wt.% (avg. = 0.47 wt.%)
    - MnO = 0.09 to 0.47 wt.% (avg. = 0.21 wt.%)
    - NiO is below detection limit
- Olivine microphenocrysts show Fa_{30-33} compositions. These grains contain lower amounts of CaO (0.11 to 0.18 wt.%), Cr_2O_3 (0.31 to 0.32 wt.%) and MnO = 0.2 wt.% in the lower range of the relict grains and NiO = 0.04 to 0.34 wt.%.
- The high MgO contents of olivine relict grains suggest an unequilibrated precursor. The MnO contents rule out a CV precursor.

Conclusion:

- Presumably 45b.20 is a **unequilibrated chondritic MM** originated from **type 3 ordinary chondrites, CM, CO or CR carbonaceous chondrites.**

Figure 110 SEM image (BSE mode) showing the whole MM 45b.20.

Figure 111 SEM image (BSE mode) showing a sectioned portion of MM 45b.20. The analysis (see text in Table X91) is suggesting a scoriaceous and fine grained MM.

Table X92. Overall petrography of micrometeorite 45b.21

Sample	45b.21
Size [μm]	630 x 450
Elongation ratio (1 = round spherule)	1.40

Mineralogical and petrological information (C. Cordier, ISTerre, University of Grenoble, France; personal communication 2013).

- **45b.21 is a fine-grained unmelted micrometeorite** with high porosity, small rounded to elongated vesicles and some dehydration cracks.

- Direct obvious Fe-Mg relict grains can not be identified. The Relict grains consist of ilmenite, along with FeNi and FeS grains. The sample is heavily weathered, at which the fine-grained mesostasis is rich on Na_2O, K_2O, SO_3 and Cl).

- Small dark areas in the mesostasis consist of Si-rich material.

- The almost continuous rim of magnetite rules out an origin as a meteorite fragment (Genge et al. (2008)).

- Observable bright grains mainly consist of FeS with a fraction 0.4 to 1.7 wt.% of Si. One grain contains FeNi (5 wt.% Ni), along with 0.9 wt.% Si. The grains have a rounded to elongated shape, along with high Si contents.

- Observable ilmenite ($FeTiO_3$) grains are Mn-rich (3 wt% to 5 wt%). Furthermore two bright blebs are visible, which show an interesting opaque phase made of Ag (35 wt %) and I (50 wt %).

- The high Si contents in sulfide and metal suggest an unequilibrated precursor. The cracks could be formed due to dehydration, resulting from the decomposition of phyllosilicates (see particle 45b.18).

Conclusion:

- Presumably 45b.21 is originated from an **unequilibrated carbonaceous chondrite** or **an equilibrated ordinary chondrite.**
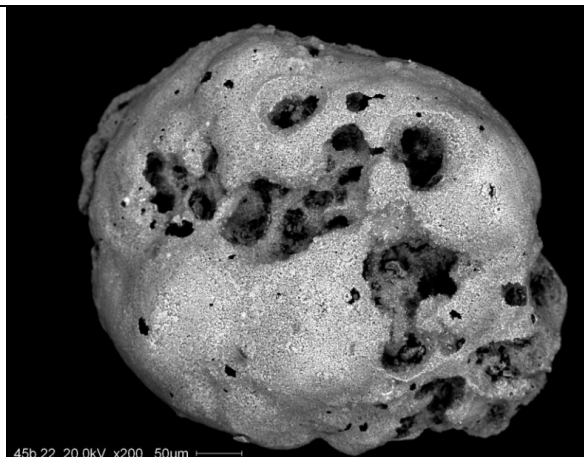

Figure 112 SEM image (BSE mode) showing the whole MM 45b.21.

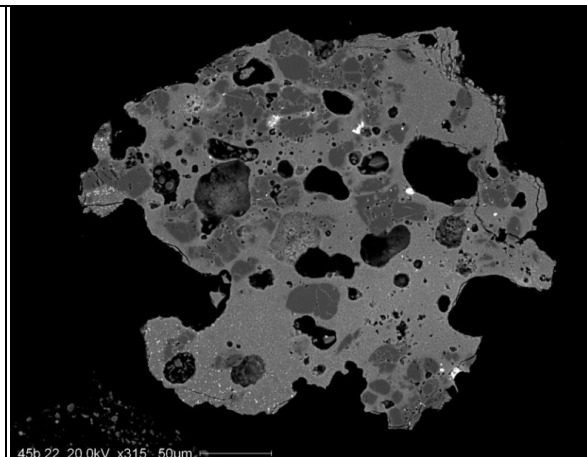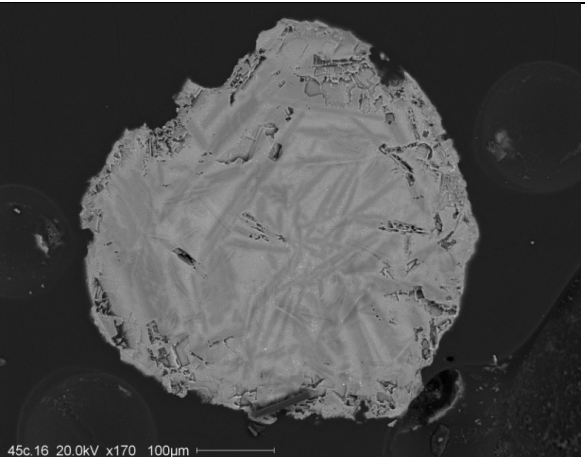**Figure 113 SEM image (BSE mode) showing a sectioned portion of MM 45b.21. The analysis (see text in Table X92) is suggesting a fine-grained unmelted MM.**

Table X93. Overall petrography of micrometeorite 45b.22

Sample	45b.22
Size [μm]	490 x 400
Elongation ratio (1 = round spherule)	1.23

Mineralogical and petrological information (C. Cordier, ISTerre, University of Grenoble, France; personal communication 2013).

- **45b.22 is a scoriaceous, porphyritic and fresh micrometeorite.**
- Olivine and pyroxene relict grains are in a cryptocrystalline, more Fe-rich mesostasis (small cristals of olivine and/or pyroxene and magnetite).
- An igneous or magnetite rim is not observable.
- A few sulfide grains and blebs are disseminated in the mesostasis.
  - Olivine relict grains show a fayalitic composition. These grains are surrounded by a Fe-rich rim.
  - The minor element contents of these grains are:
    - CaO = 0.18 to 0.23 wt.% (avg. = 0.21 wt.%)
    - Cr2O3 = 0.41 to 0.48 wt.% (avg. = 0.45 wt.%)
    - MnO = 0.09 to 0.19 wt.% (avg. = 0.12 wt.%)
    - NiO = < 0.01 wt.%
  - Pyroxene relict grains have $Fs_{0.9-2.8}Wo_{0.9-4.7}$ (avg. = $Fs_{1.4}Wo_{1.7}$).
  - Minor element contents are
    - Cr2O3 = 0.44 to 0.79 wt.%
    - MnO = 0.04 to 0.18 wt.%.
- The high MgO contents of olivine and pyroxene suggest an unequilibrated precursor (similar to type I chondrules in type 3 OC or to CM, CV, CO carbonaceous chondrites).

Conclusion:

Presumably 45b.20 is originated from an **unequilibrated chondrite**.

Figure 114 SEM image (BSE mode) showing the whole MM 45b.22.

Figure 115 SEM image (BSE mode) showing a sectioned portion of MM 45b.22. The analysis (see text in Table X93) is suggesting a scoriaceous, porphyritic and fresh MM.

Table X94. Overall petrography of micrometeorite 45c.16

Sample	45c.16
Size [µm]	930 x 920
Elongation ratio (1 = round spherule)	1.01

Mineralogical and petrological information (C. Cordier, ISTerre, University of Grenoble, France; personal communication 2013).

- **45c.16 is presumably similar to porphyritic olivine Cosmic Spherules.**
- The MM morphology is oblate.
- The MM surface is highly irregular along with striation.
- The MM shows white encrustations, probably alteration of olivine.
- Within the thin section long olivine hopper bars with abundant interstitial feathered olivine are observable
- Dendritic magnetite, glass and heteorgeneous abundance of the interstitial phases are visible.
- 5 vesicles are observable.

Conclusion:

- At present, no detailed analysis of 45c.16 is available.

Not available	
	Figure 116 SEM image (BSE mode) showing a sectioned portion of MM 45c.16. The analysis (see text in Table X94) is suggesting a possible Cosmic Spherule origin.

Table X95. Overall petrography of micrometeorite 45c.17
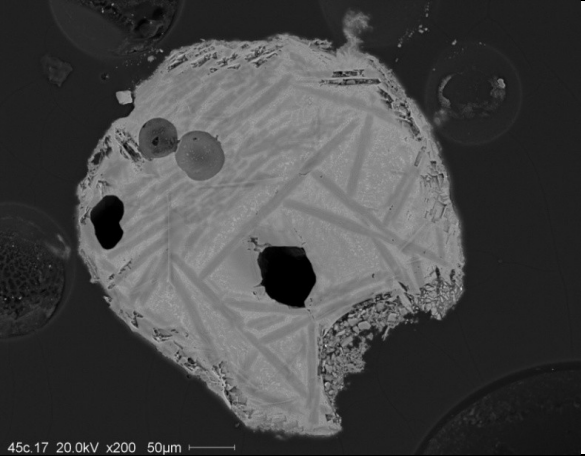
Sample	45c.17
Size [μm]	680 x 630
Elongation ratio (1 = round spherule)	1.08

Mineralogical and petrological information (C. Cordier, ISTerre, University of Grenoble, France; personal communication 2013).

- **45c.17 is presumably similar to porphyritic olivine Cosmic Spherules.**
- The MM morphology is spherical.
- The MM surface is highly irregular with striation.
- The MM shows white and orange alteration minerals within abundant vesicles.
- The texture shows long olivine hopper bars with abundant interstitial feathered olivine, dendritic magnetite and glass, along with heteorgeneous abundance of the interstitial phases.
- 5 larger vesicles are observable.
- Also visible is exterior encrustation, along with negative crystals of olivine, though a fresh interior.

Conclusion:

- At present, no detailed analysis of 45c.17 is available.

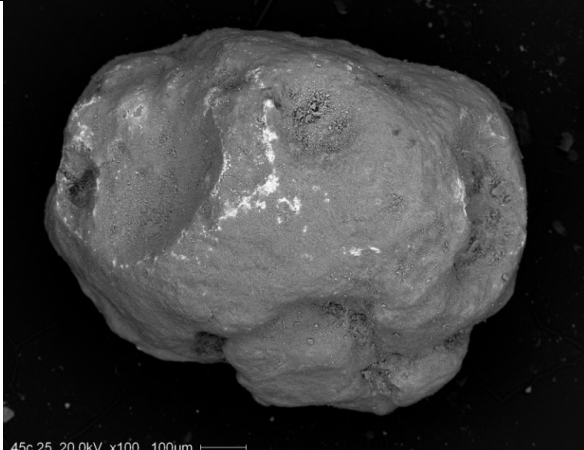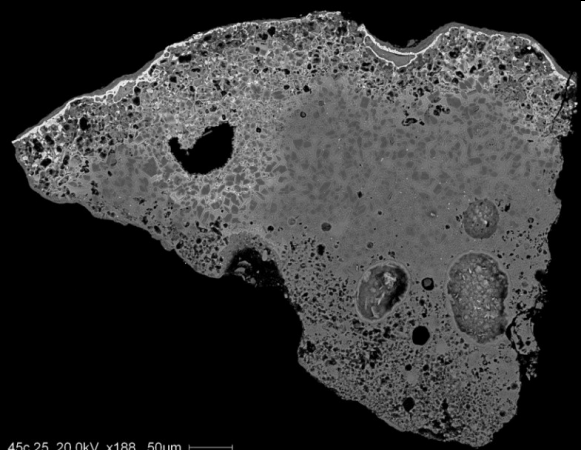|	
Not available	
Figure 117 SEM image (BSE mode) showing the whole MM 45c.17.	**Figure 118 SEM image (BSE mode) showing a sectioned portion of MM 45c.17. The analysis (see text in Table X95) is suggesting a possible Cosmic Spherule origin.**

Table X96. Overall petrography of micrometeorite 45c.21

Sample	45c.21
Size [µm]	730 x 570
Elongation ratio (1 = round spherule)	1.28

Mineralogical and petrological information (C. Cordier, ISTerre, University of Grenoble, France; personal communication 2013).

- **45c.21 is presumably similar to glassy Cosmic Spherules.**
- The MM morphology is higly oblate.
- The MM surface is smooth along with striation near the metal bead.

Conclusion:

- At present, no detailed analysis of 45c.21 is available.

Figure not available	Figure Not available

Table X97. Overall petrography of micrometeorite 45c.24
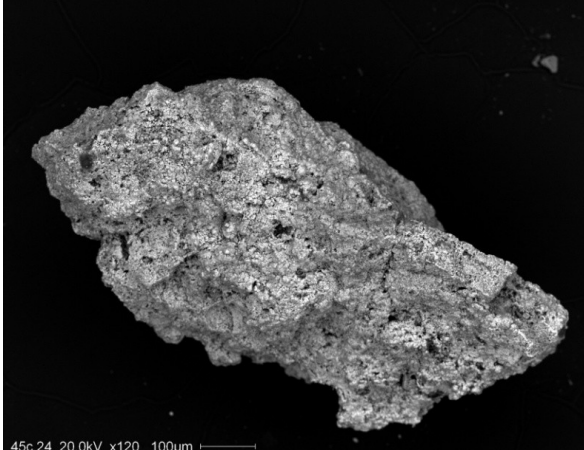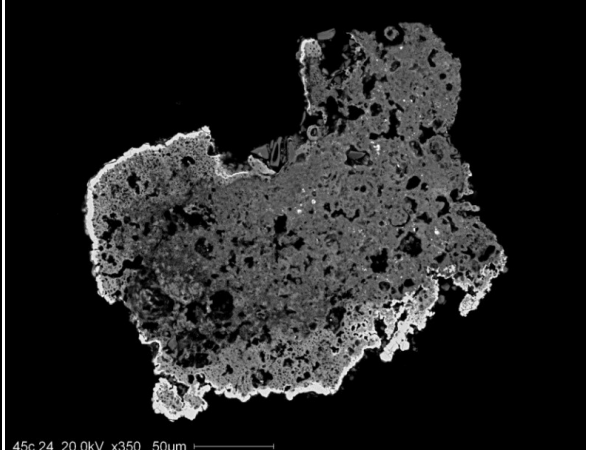
Sample	45c.24
Size [µm]	955 x 430
Elongation ratio (1 = round spherule)	2.22

Mineralogical and petrological information (C. Cordier, ISTerre, University of Grenoble, France; personal communication 2013).

- **45c.24 is presumably similar to fine grained unmelted micrometeorites.**
- The MM morphology is angular.
- The MM surface weathered.
- The MM is porous and fresh.
- An almost continuous igneous and magnetite rim is an evidence for a micrometeorite (Genge et al. (2008)).

Conclusion:

- At present, no detailed analysis of 45c.24 is available.

Figure 119 SEM image (BSE mode) showing the whole MM 45c.24.

Figure 120 SEM image (BSE mode) showing a sectioned portion of MM 45c.24. The analysis (see text in Table X97) is suggesting a possible fine grained MM origin.

Table X98. Overall petrography of micrometeorite 45c.25

Sample	45c.25
Size [µm]	970 x 660
Elongation ratio (1 = round spherule)	1.47

Mineralogical and petrological information (C. Cordier, ISTerre, University of Grenoble, France and L. Folco, Dipartimento di Scienze della Terra, University of Pisa, Italy; personal communication 2013).

- **45c.25 seems to be in between porphyritic scoriaceous MMs and porphyritic Cosmic Spherules.**
- The MM morphology is sub-rounded.
- The MM surface is weathered.
- Numerous small vesicles are observable.
- Partially a magnetite rim is clearly present.
- The interior of the micrometeorite is fresh and shows negative crystals in the circumference.
- In terms of mineralogy and texture, the MM shows rounded olivine relict grains surrounded by euhedral olivines, which are crystallized during atmospheric entry along with little interstitial glass and magnetite.
- In further detail, the euhedral olivine microphenocrysts, the glass and other the opaque particles are all the products of the crystallization/solidification from a melt.

Conclusion:

- At present, no detailed (microprobe) analysis of 45c.25 is available. However, this particle underwent nearly complete melting and should be related to relict bearing porphyritic cosmic spherules in terms of interaction with atmospheric air. In terms of classification (which is descriptive) it is a kind of border line between a CS and a ScMM.

Figure 121 SEM image (BSE mode) showing the whole MM 45c.25.

Figure 122 SEM image (BSE mode) showing a sectioned portion of MM 45c.25. The analysis (see text in Table X98) is suggesting a a kind of border line between a Cosmic Spherule and a scoriaceous MM.

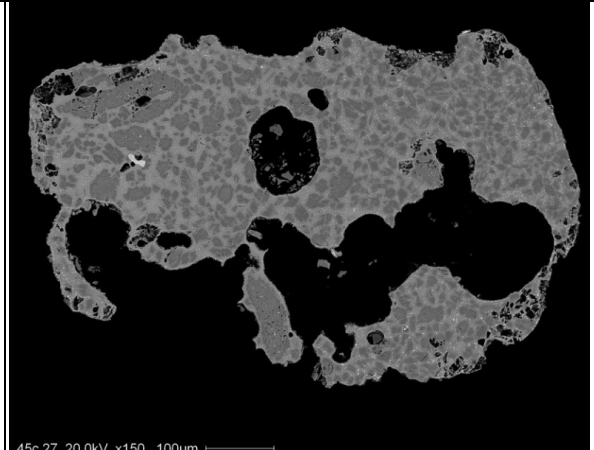*Table X99. Overall petrography of micrometeorite 45c.27*

Sample	45c.27
Size [μm]	780 x 660
Elongation ratio (1 = round spherule)	1.18

Mineralogical and petrological information (C. Cordier, ISTerre, University of Grenoble, France; personal communication 2013).

- **45c.27 is a scoriaceous, microporphyritic and fresh MM,** with high porosity (numerous and coalescent vesicles) and with olivine relict grains in a mesostasis made of olivine microphenocrysts, glass, and sparse oxide.
- No magnetite rim on the sample is observable.
- Two large (up to 150 μm in length) and elongated (L/l = 3.4 to 5.4) olivine relict grains ($Fa_{21.9}$) contain numerous sulfide blebs (FeNiS) and voids.
- These are surrounded by a Fe-poor mantle (Fa_{14}) and a Fe-rich rim. The Fe-rich rim also surrounds the voids within the crystals. The mantle and rim have similar composition, similar to microphenocrysts and crystallized during the atmospheric entry.
  - The relict cores have variable but low CaO and Cr_2O_3 contents (0.05 to 0.23 wt.%, av. 0.08 ± 0.06 wt.% and 0.03 to 0.12 wt.%, av. 0.06 wt.% ± 0.03 wt.%, respectively), significant MnO contents (0.39 to 0.49 wt.%, av. 0.44 wt.% ± 0.04 wt%).
  - The rims are characterized by higher CaO and Cr_2O_3 contents (0.10 to 0.37 wt.% and 0.12 to 0.26 wt.%, respectively), lower MnO (0.21 to 0.37 wt.%) and higher NiO contents (0.15 to 0.38 wt.% vs < 0.08 wt.%).
- The microphenocrysts comprise higher Fa mole contents ($Fa_{16.7}$), higher Cr_2O_3 contents of 0.36 wt.% and NiO contents of 0.32 wt.%, along with lower MnO contents (0.25 wt.%) than relict grains. The microphenocrysts are surrounded by a thin Fe-rich rim. Some of the microphenocrysts show a Mg-poor core, equivalent in composition to large olivine relict grains ($Fa_{22.3}$).
- The large (20 μm in lenght) chromite relict grain has a MgO content of 5.9 wt.% and a $\frac{Fe}{Fe+Mg}$ ratio of 0.72 along with a $\frac{Cr}{Cr+Al}$ ratio of 0.87.

Conclusion:

- Presumably 45c.27 is originated from an **equilibrated ordinary chondrite (L4-6).**

Figure 123 SEM image (BSE mode) showing the whole MM 45c.27.

Figure 124 SEM image (BSE mode) showing a sectioned portion of MM 45c.27. The analysis (see text in Table X99) is suggesting a scoriaceous, microporphyritic and fresh MM.

Table X100. Overall petrography of micrometeorite 45c.29

Sample	45c.29
Size [μm]	710 x 590
Elongation ratio (1 = round spherule)	1.20

Mineralogical and petrological information (C. Cordier, ISTerre, University of Grenoble, France; personal communication 2014).

- **45c.29 is a fine-grained unmelted (possibly scoriaceous) micrometeorite**

- The internal part of the particle shows an igneous texture with resorbed (possibly partially melted) olivine (43 vol.%) and pyroxene (8 vol.%) grains. Olivine and pyroxene usually form aggregates set in a fine-grained crystalline mesostasis (42 vol.%) consisting of radiating laths of plagioclase, interstitial pyroxene, Fe-oxides and glass.

- The edge of the particle consists of an igneous rim (in parts well-developed – 5 wt.%), surrounded by a μm-thick magnetite rim (as defined by Genge (2006)). The igneous rim consists of abundant glass along with crystallites of pyroxene and magnetite as well as relict olivine grains speckled with tiny Fe-To oxide grains (dusty olivine, 2 vol.%). Additionally, the rim is speckled with abundant and very small Fe-oxide grains.

- **Mineral composition:**
  - Ca-rich plagioclase in the mesostasis ranges from An_{87} to An_{95}.
  - Olivines:
    - $Fa_{26.5 \pm 1.6}$, Fe/Mn = 117.5 ± 3.8 (n=15).
    - High Ni contents (0.67 wt.%, > 5000 ppm)
    - Low MnO contents (0.2 wt.%, ~1550 ppm),
    - Cr_2O_3 (0.06 wt.%, ~250 ppm; except for two Cr-rich grains)
    - Dusty olivines are so far not completely analyzed, but their composition is more Mg-rich (~Fa_8)
  - Pyroxenes:
    - Ca-poor cores are overgrown by Ca-rich rims.
    - "Low-Ca" pyroxene = $Fs_{3.8 \pm 1.2}Wo_{8.1 \pm 1.3}$, Fe/Mn = 16.4 ± 5.5 (n=8)
    - "High-Ca" pyroxenes = $Fs_{5.1 \pm 3.8}Wo_{37.3 \pm 5.1}$, Fe/Mn = 22.2 ± 19.9 (n=9)
    - Ca-rich pyroxenes show a relatively large Fs variation:
      - Minimum: $Fs_{1.9}Wo_{37.9}$, Fe/Mn = 4.8
      - Maximum: $Fs_{12.1}Wo_{29.7}$, Fe/Mn = 55.8 (n=2)

Conclusion:

- At present, it is not sure whether 45c.29 does have a chondritic or achondritic origin. Even an unknown parent body material is possible.
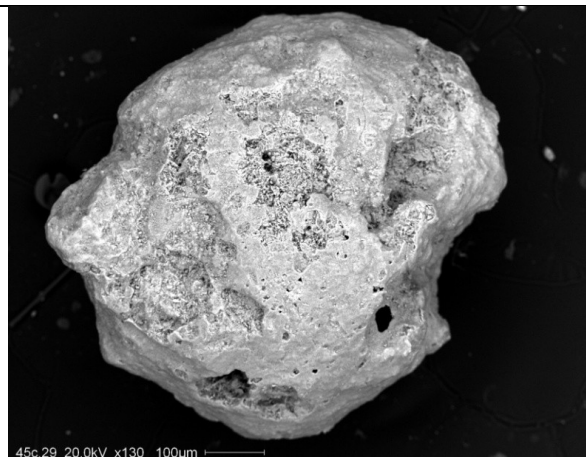

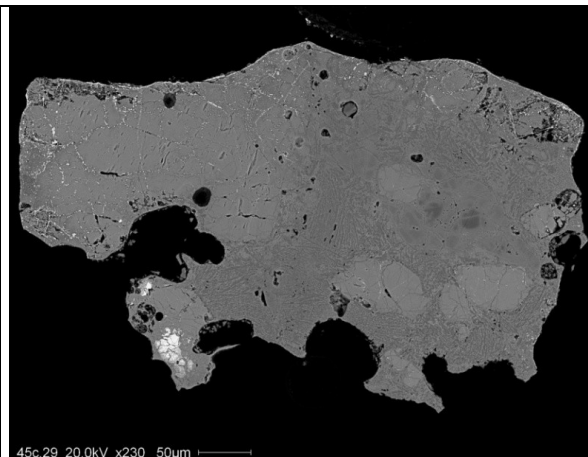**Figure 125 SEM image (BSE mode) showing the whole MM 45c.29.**

Figure 126 SEM image (BSE mode) showing a sectioned portion of MM 45c.29. The analysis (see text in Table X100) is suggesting a fine grained unmelted (possibly scoriaceous) MM.

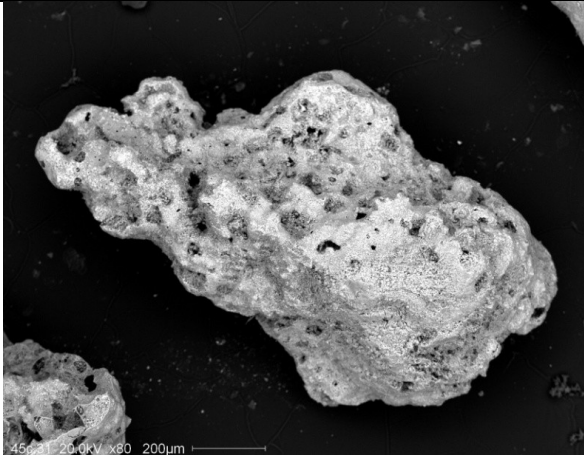*Table X101. Overall petrography of micrometeorite 45c.31*

Sample	45c.31
Size [μm]	1350 x 620
Elongation ratio (1 = round spherule)	2.18

Mineralogical and petrological information (C. Cordier, ISTerre, University of Grenoble, France; personal communication 2013).

- 45c.31 is presumably similar to porphyritic scoriaceous micrometeorites.
- The MM morphology is sub-rounded.
- The MM surface is fresh.
- Several small to large vesicles are clearly present. The MM is porous.
- An almost continuous magnetite rim is visible and an evidence for a micrometeorite (Genge et al. (2008)).
- Rounded olivine relict grains are surrounded by euhedral olivines, which crystallized during atmospheric entry.
- Smaller amounts of interstitial glass and magnetite is observable.

Conclusion:

- At present, no detailed analysis of 45c.31 is available.

Figure 127 SEM image (BSE mode) showing the whole MM 45c.31.

Figure 128 SEM image (BSE mode) showing a sectioned portion of MM 45c.31. The analysis (see text in Table X101) is suggesting a possible porphyritic, scoriaceous MM.

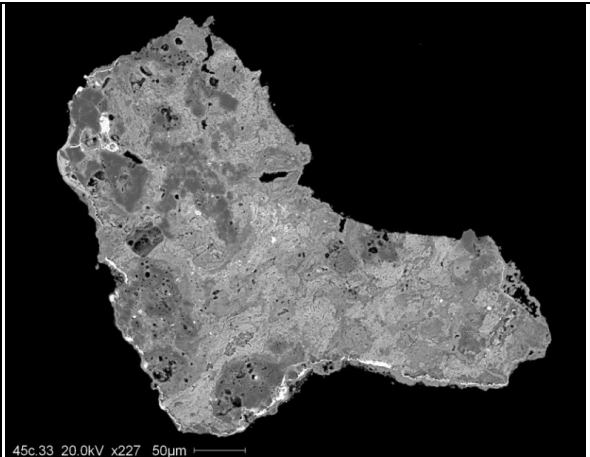*Table X102. Overall petrography of micrometeorite 45c.33*

Sample	45c.33
Size [μm]	820 x 730
Elongation ratio (1 = round spherule)	1.12

Mineralogical and petrological information (C. Cordier, ISTerre, University of Grenoble, France; personal communication 2013).

- **45c.33 is a fine grained unmelted micrometeorite**, containing pyroxene relict grains.
- The MM is heavily weathered, due to observed jarosite and SiO_2-rich weathering product.
- The MM is surrounded by an almost continuous magnetite rim, which rules out an meteoritic origin.
- Numerous metal/sulfide blebs are present.
- Observed pyroxene relict grains show a disequilibrium texture, probably due to their incipient melting.
  - Within these, a large range of variations in $Fs_{2-11}Wo_{1-9}$ is detected.
  - Some grains show higher Fs contents, this is in correlation with an increase of the sulphur contents, which therefore is due to alteration of the relict grains.
- Concerning metals and sulfide, most of the grains contain FeNi meta, whereas only some of them are Si- and/or P-rich (up to 0.6 wt.% and 0.5 wt.%, respectively).
- Furthermore observed is a single bright bleb consisting of Ag (40 wt.%) and I (50 wt.%). This may indicates weathering or is due to contamination during laboratory preparations.

Conclusion:

- Presumably 45c.33 is originated from an **unequilibrated chondrite.**

Figure 129 SEM image (BSE mode) showing the whole MM 45c.33.	**Figure 130 SEM image (BSE mode) showing a sectioned portion of MM 45c.33. The analysis (see text in Table X102) is suggesting a fine grained unmelted MM.**

Table X103. Overall petrography of micrometeorite 45c.34

Sample	45c.34
Size [µm]	660 x 545
Elongation ratio (1 = round spherule)	1.21

Mineralogical and petrological information (C. Cordier, ISTerre, University of Grenoble, France; personal communication 2013).

- **45c.34 is a fine grained unmelted micrometeorite**, along with relict grains (probably olivine).
- The MM is surrounded by an almost continuous magnetite rim, which rules out an origin as a meteorite fragment (Genge et al. (2008)).
- The porosity is high, with vesicles and dehydration cracks.
- Distinction between relict grains and mesostasis is - so far - ambiguous from a textural and chemical point of view. Here, the term relict grains is used for the areas mainly devoid of small vesicles. In contrast, the mesostasis has a "dirty" aspect, punctured with numerous small to large vesicles. The mesostasis contains Na_2O with 0.26 wt.%.
- Observable relict grains are not homogeneous distributed, moreover they show complex zoning and sometimes are enriched in bright, very small metal/sulfide blebs.
- The fine silicate-opaque intergrowth are interesting and should be resolved to understand this particle.
- The relict grains show a homogeneous composition, close to that of Fe-rich olivine (Fa_{46}). However, they are anomalously rich in Al_2O_3 (2.6 wt.%).
- The mean "olivine" composition measured with the SEM is as follows:
    - MgO = 22.40
    - Al_2O_3 = 2.46
    - SiO_2 = 40.21
    - CaO = 0.51
    - FeO = 34.63

Conclusion:

- At present, the parentage of 45c.34 is not clarified.

Figure 131 SEM image (BSE mode) showing the whole MM 45c.33.

Figure 132 SEM image (BSE mode) showing a sectioned portion of MM 45c.34. The analysis (see text in Table X103) is suggesting a fine grained unmelted MM.

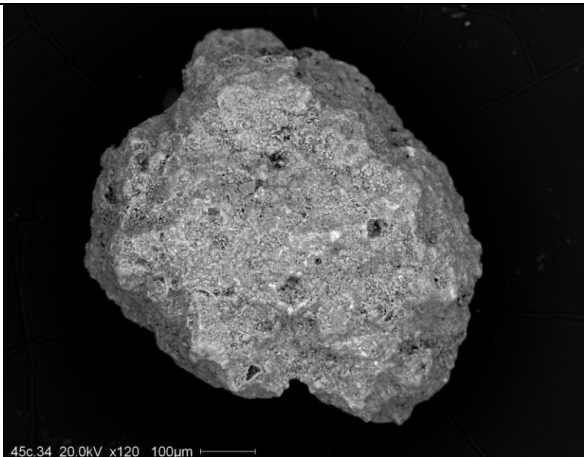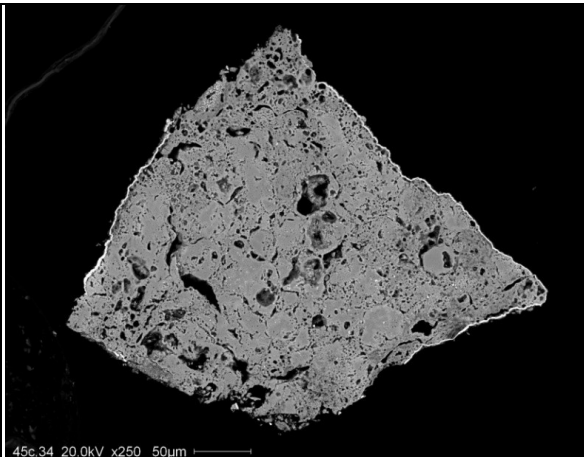*Table X104. Overall petrography of micrometeorite 45c.35*

Sample	45c.35
Size [μm]	460 x 300
Elongation ratio (1 = round spherule)	1.53

Mineralogical and petrological information (C. Cordier, ISTerre, University of Grenoble, France; personal communication 2013).

- **45c.35 is a coarse-grained, unmelted micrometeorite**, along with pyroxene and plagioclase relict grains.
- Observable is a thick and layered weathering rim, rich in Fe, Ni and S. This rim is crosscut by magnetite veins.
- A plagioclase grain analyzed within the weathered rim is rich in K (Or_{26}). This may reflects a terrestrial origin. Very likely is that a terrestrial bedrock fragment is embedded in the large weathered rim.
- Locally, fresh FeNi metal grains occur, consist of Fe=95 % and Ni = 5 %.
- The fresh core of the MM is a coarse-grained assemblage of homogeneous low Ca-pyroxenes ($Fs_{15}Wo_{1.5}$) and large (up to 40 μm in length) oligoclase ($Ab_{89}An_7$) grains
- Enclosed in the core of a single pyroxene grain is a brighter crystal. Non stoichiometric analyze suggest that this might be olivine (Fa_{16}).
- The weathering rim impedes to observe the particle periphery for the search of an igneous and/or magnetite rim.

Conclusion:

- Presumably 45c.35 is originated from an **ordinary chondrite (H6).**

Figure 133 SEM image (BSE mode) showing the whole MM 45c.33.	**Figure 134 SEM image (BSE mode) showing a sectioned portion of MM 45c.35. The analysis (see text in Table X104) is suggesting a fine grained unmelted MM.**

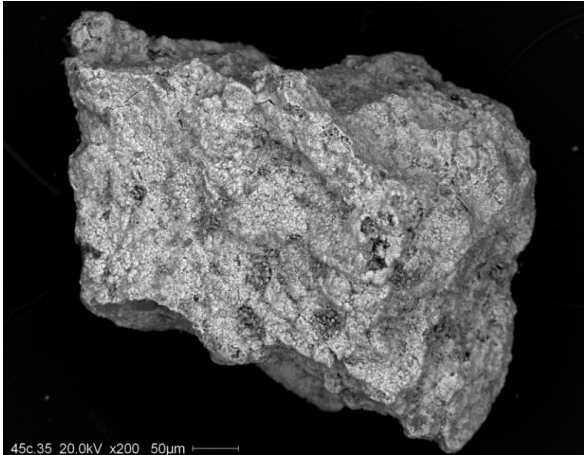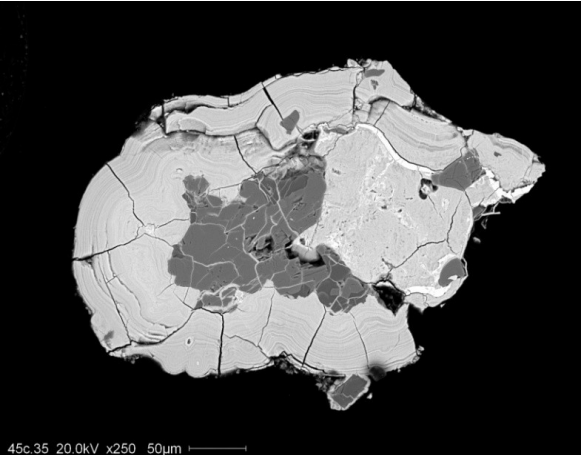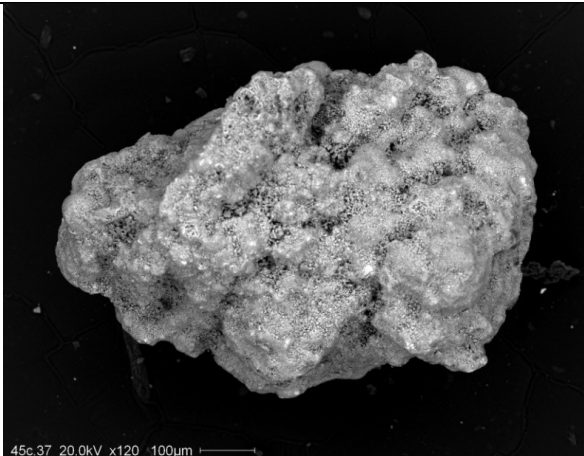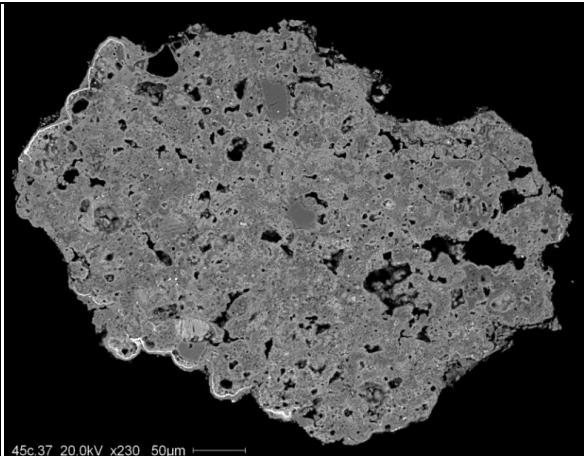*Table X105. Overall petrography of micrometeorite 45c.37*

Sample	45c.37
Size [μm]	825 x 500
Elongation ratio (1 = round spherule)	1.65

Mineralogical and petrological information (C. Cordier, ISTerre, University of Grenoble, France; personal communication 2013).

- **45c.37 is a fine grained unmelted micrometeorite,** along with small pyroxene relict grains.
- An almost continue magnetite rim is observed (discontinuities are probably linked to the encrustation), which proofs the MM origin (Genge et al. (2008)).
- The particle is heavily weathered, containing jarosite and Si-rich material.
- Numerous irregularly shaped vesicles are observable throughout the sample.
- Pyroxene relict grains show $Fs_{5-16}Wo_{1-5}$. Additionally, they are rich in Cr_2O_3 (0.9 to 1.8 wt %), what, however, has to be proven using EPMA. The pyroxene grains are surrounded by Fe-rich rims.
- To relate this MM to carbonaceous or ordinary chondrites, additional EPMA analyses are required, especially on minor elements like Ca, Al, Cr and Mn in pyroxenes.

Conclusion:

- Presumably 45c.37 is originated from an **unequilibrated chondrite.**

Figure 135 SEM image (BSE mode) showing the whole MM 45c.33.

Figure 136 SEM image (BSE mode) showing a sectioned portion of MM 45c.37. The analysis (see text in Table X105) is suggesting a fine grained unmelted MM.

E.   Figures showing micrometeorites examined for noble gases - Micrometeorites are from the CONCORDIA collection, Dome C and from Cap Prudhomme, Antarctica.

- SEM images of micrometeorites were taken at the University of South Paris, Orsay, France. With courtesy of J. Duprat, C. Engrand, M. Maurette and colleagues at CSNSM, University of South Paris, Orsay, France.

- Mineralogical and petrological information by J. Duprat, C. Engrand, M. Maurette and colleagues at CSNSM, University of South Paris, Orsay, France; in personal communication 2010.

Table X106. SEM and basic information of sample CP 9-1-1994 - PL10-109-D9
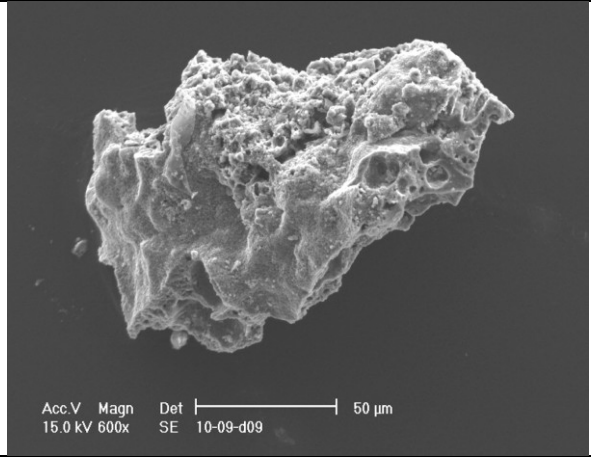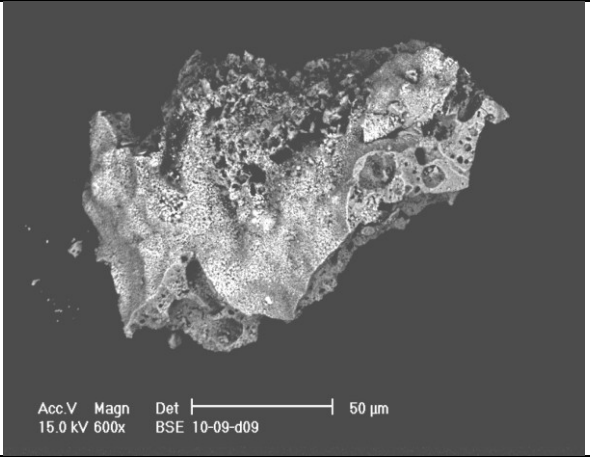
Sample	CP 9-1-1994_PL10-109-D9
Size [µm]	252 x 188
Weight [µg]	6.2 ± 0.1

Mineralogical and petrological information by J. Duprat, C. Engrand, M. Maurette and colleagues at CSNSM, University of South Paris, Orsay, France.

- Particle extracted from blue ice near Cap Prudhomme, Antarctica (Maurette et al. (1991)).
- Scoriaceous (Sc) micrometeroite particle.

Figure 137 SEM image showing the micrometeroite CP 9-1-1994 - PL 10-109-D9 (with courtesy of J. Duprat, C. Engrand, M. Maurette and colleagues).	**Figure 138 Backscatter SEM image showing the micrometeroite CP 9-1-1994 - PL 10-109-D9 (with courtesy of J. Duprat, C. Engrand, M. Maurette and colleagues).**

Table X107. SEM and basic information of sample DC 06_07_213 - PL09-20-4

Sample	DC 06_07_213 - PL09-20-4
Size [µm]	97 x 91
Weight [µg]	~ 1.1

Mineralogical and petrological information by J. Duprat, C. Engrand, M. Maurette and colleagues at CSNSM, University of South Paris, Orsay, France.

- Particle extracted from snow near the CONCORDIA station at Dome C, Central Antarctica (Duprat et al. (2007)).
- Crystalline (Xtal) micrometeorite particle.

Figure 139 SEM image showing a similar but not identical micrometeorite to particle DC 06_07_213 - PL09-20-4 - the same group finding (with courtesy of J. Duprat, C. Engrand, M. Maurette and colleagues).	**Figure 140 Backscatter SEM image showing a similar but not identical micrometeorite to particle DC 06_07_213 - PL09-20-4 - the same group finding (with courtesy of J. Duprat, C. Engrand, M. Maurette and colleagues).**

Table X108. SEM and basic information of sample DC 06_08_01 - PL06-09A-1

Sample	DC 06_08_01 - PL06-09A-1
Size [µm]	110 x 92
Weight [µg]	~1.4

Mineralogical and petrological information by J. Duprat, C. Engrand, M. Maurette and colleagues at CSNSM, University of South Paris, Orsay, France.

- Particle extracted from snow near the CONCORDIA station at Dome C, Central Antarctica (Duprat et al. (2007).
- Crystalline (Xtal) micrometeorite particle.

Figure 141 Backscatter SEM image showing a similar but not identical micrometeorite to particle DC 06_08_01 - PL06-09A-1 - the same group finding (with courtesy of J. Duprat, C. Engrand, M. Maurette and colleagues).

Figure 142 Backscatter SEM image showing a similar but not identical micrometeorite to particle DC 06_08_01 - PL06-09A-1 - the same group finding (with courtesy of J. Duprat, C. Engrand, M. Maurette and colleagues).

Table X109. SEM and basic information of sample DC 06_09_11 - PL07-01A-11

Sample	DC 06_09_11 - PL07-01A-11
Size [µm]	137 x 111
Weight [µg]	~1.3

Mineralogical and petrological information by J. Duprat, C. Engrand, M. Maurette and colleagues at CSNSM, University of South Paris, Orsay, France.

- Particle extracted from snow near the CONCORDIA station at Dome C, Central Antarctica (Duprat et al. (2007).
- Fine-grained carbonaceous (FgC) to scoriaceous (Sc) micrometeorite particle.

Figure 143 SEM image showing a similar but not identical micrometeorite to particle DC 06_09_11 - PL07-01A-11 - the same group finding (with courtesy of J. Duprat, C. Engrand, M. Maurette and colleagues).

Figure 144 Backscatter SEM image showing a similar but not identical micrometeorite to particle DC 06_09_11 - PL07-01A-11 - the same group finding (with courtesy of J. Duprat, C. Engrand, M. Maurette and colleagues).

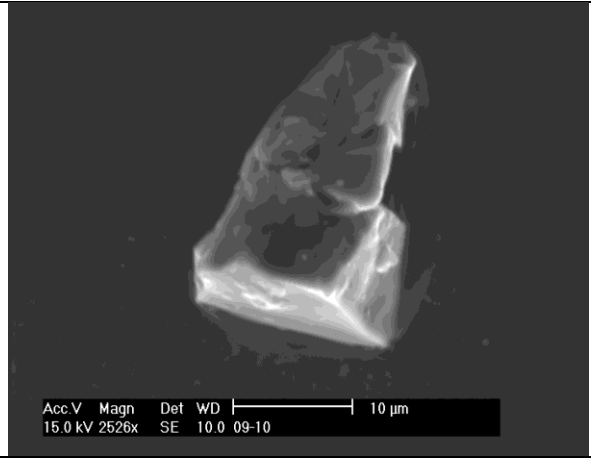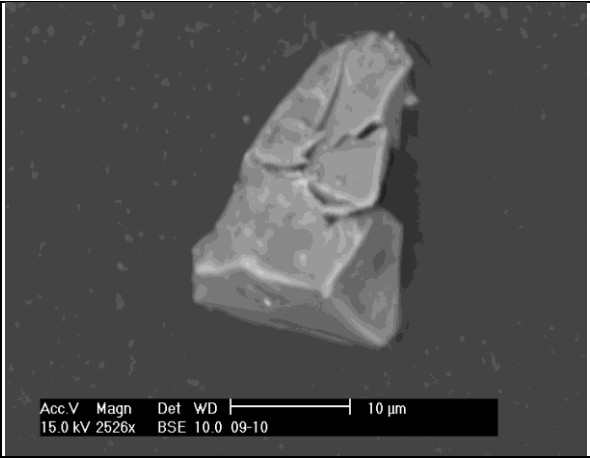*Table X110. SEM and basic information of sample DC 06_09_50 - PL07-02B-2*

Sample	DC 06_09_50 - PL07-02B-2
Size [µm]	141 x 134
Weight [µg]	~ 3.3

Mineralogical and petrological information by J. Duprat, C. Engrand, M. Maurette and colleagues at CSNSM, University of South Paris, Orsay, France.

- Particle extracted from snow near the CONCORDIA station at Dome C, Central Antarctica (Duprat et al. (2007).
- Fine-grained carbonaceous (FgC) micrometeorite particle.

Figure 145 SEM image showing a similar but not identical micrometeorite to particle DC 06_09_50 - PL07-02B-2 - the same group finding (with courtesy of J. Duprat, C. Engrand, M. Maurette and colleagues).

Figure 146 Backscatter SEM image showing a similar but not identical micrometeorite to particle DC 06_09_50 - PL07-02B-2 - the same group finding (with courtesy of J. Duprat, C. Engrand, M. Maurette and colleagues).

Table X111. SEM and basic information of sample DC 06_09_57 (1) - PL07-02B-9

Sample	DC 06_09_57 (1) - PL07-02B-9
Size [µm]	74 x 36
Weight [µg]	~ 0.15

Mineralogical and petrological information by J. Duprat, C. Engrand, M. Maurette and colleagues at CSNSM, University of South Paris, Orsay, France.

- Particle extracted from snow near the CONCORDIA station at Dome C, Central Antarctica (Duprat et al. (2007).
- Fine-grained carbonaceous (FgC) micrometeorite particle.

Figure 147 SEM image showing a similar but not identical micrometeorite to particle DC 06_09_57 (1) - PL07-02B-9 - the same group finding (with courtesy of J. Duprat, C. Engrand, M. Maurette and colleagues).

Figure 148 Backscatter SEM image showing a similar but not identical micrometeorite to particle DC 06_09_57 (1) - PL07-02B-9 - the same group finding (with courtesy of J. Duprat, C. Engrand, M. Maurette and colleagues).

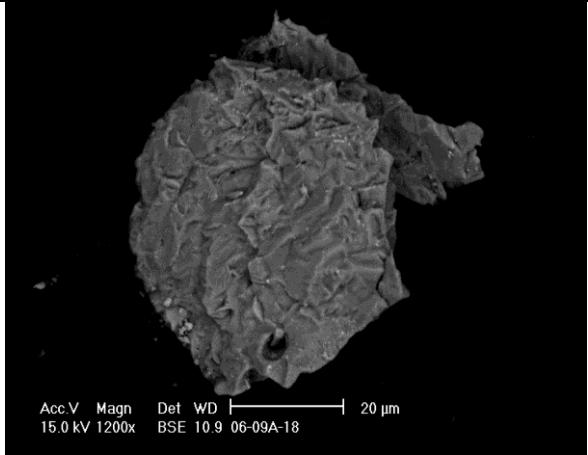*Table X112. SEM and basic information of sample DC 06_09_57 (2) - PL07-02B-9*

Sample	DC 06_09_57 (2) - PL07-02B-9
Size [μm]	19 x 18
Weight [μg]	~ 0.05

Mineralogical and petrological information by J. Duprat, C. Engrand, M. Maurette and colleagues at CSNSM, University of South Paris, Orsay, France.

- Particle extracted from snow near the CONCORDIA station at Dome C, Central Antarctica (Duprat et al. (2007).
- Fine-grained carbonaceous (FgC) micrometeorite particle.

Figure 149 SEM image showing a similar but not identical micrometeorite to particle DC 06_09_57 (2) - PL07-02B-9 - the same group finding (with courtesy of J. Duprat, C. Engrand, M. Maurette and colleagues).

Figure 150 Backscatter SEM image showing a similar but not identical micrometeorite to particle DC 06_09_57 (2) - PL07-02B-9 - the same group finding (with courtesy of J. Duprat, C. Engrand, M. Maurette and colleagues).

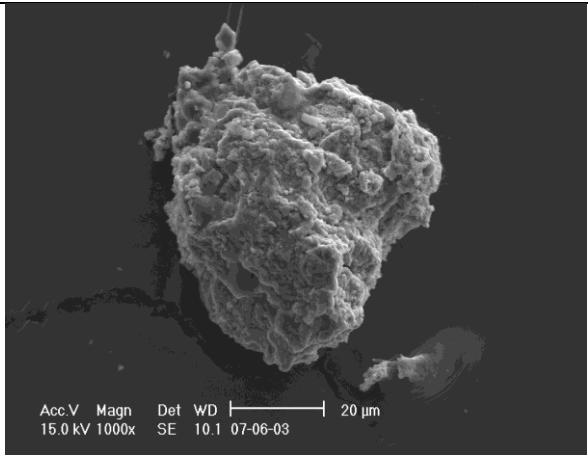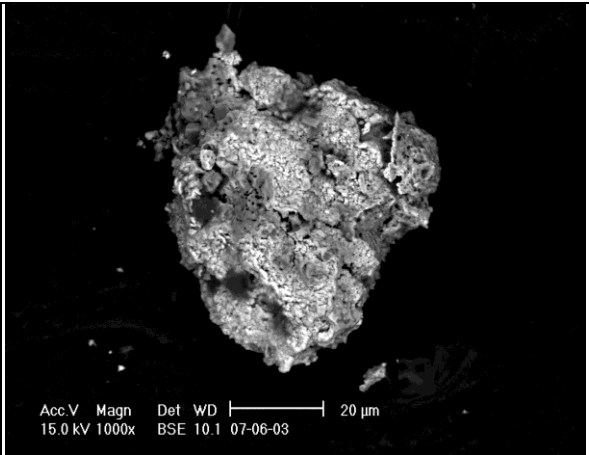*Table X113. SEM and basic information of sample DC 06_09_63 - PL07-02C-3*
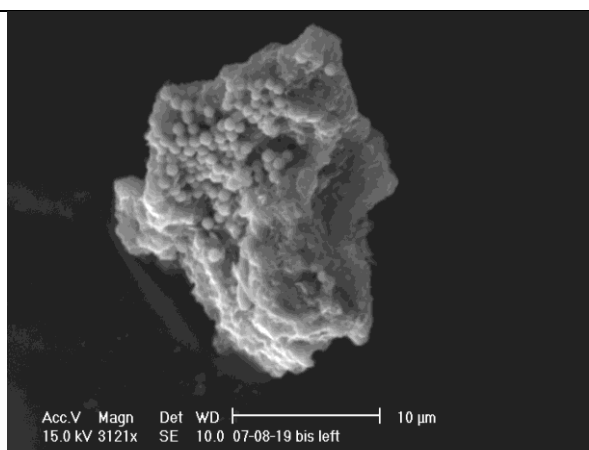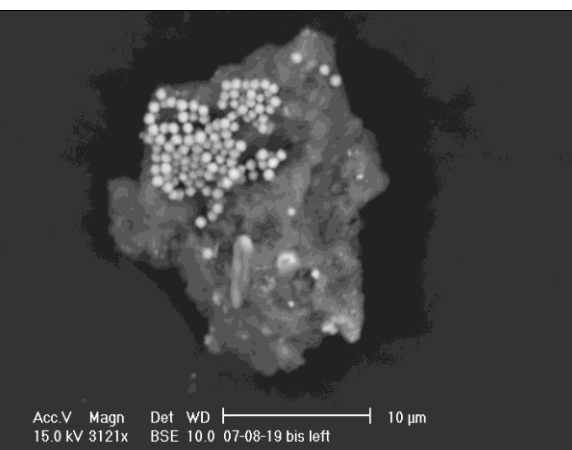
Sample	DC 06_09_63 - PL07-02C-3
Size [μm]	198 x 141
Weight [μg]	~ 3.3

Mineralogical and petrological information by J. Duprat, C. Engrand, M. Maurette and colleagues at CSNSM, University of South Paris, Orsay, France.

- Particle extracted from snow near the CONCORDIA station at Dome C, Central Antarctica (Duprat et al. (2007).
- Fine-grained carbonaceous (FgC) to crystalline (Xtal) micrometeorite particle.

Figure 151 SEM image showing a similar but not identical micrometeorite to particle DC 06_09_63 - PL07-02C-3 - the same group finding (with courtesy of J. Duprat, C. Engrand, M. Maurette and colleagues).

Figure 152 Backscatter SEM image showing a similar but not identical micrometeorite to particle DC 06_09_63 - PL07-02C-3 - the same group finding (with courtesy of J. Duprat, C. Engrand, M. Maurette and colleagues).

Table X114. SEM and basic information of sample DC 06_09_141 (1) - PL07-04C-9
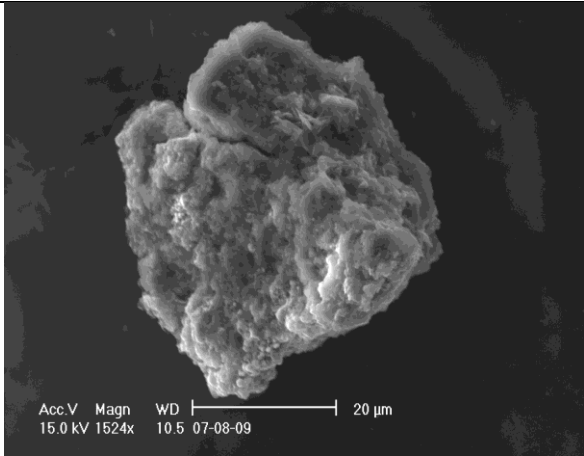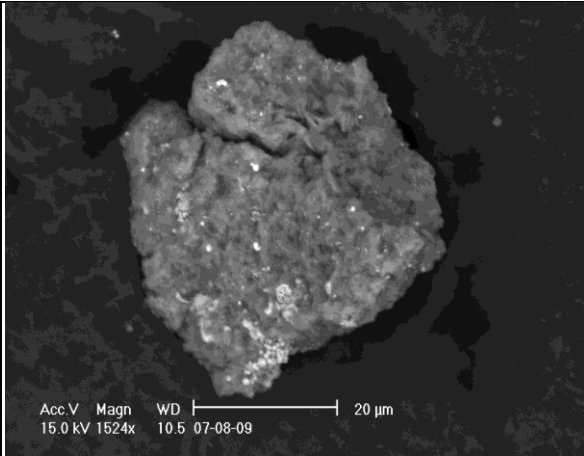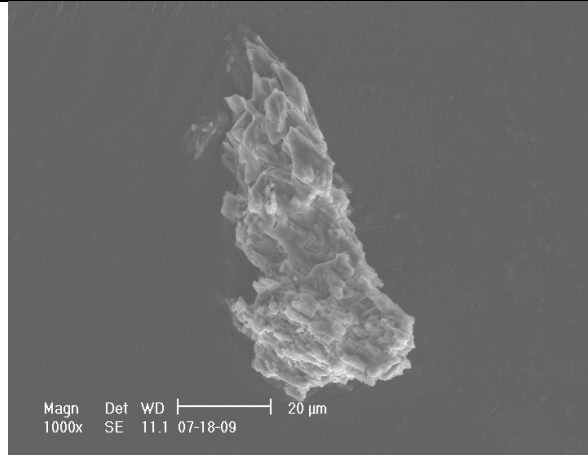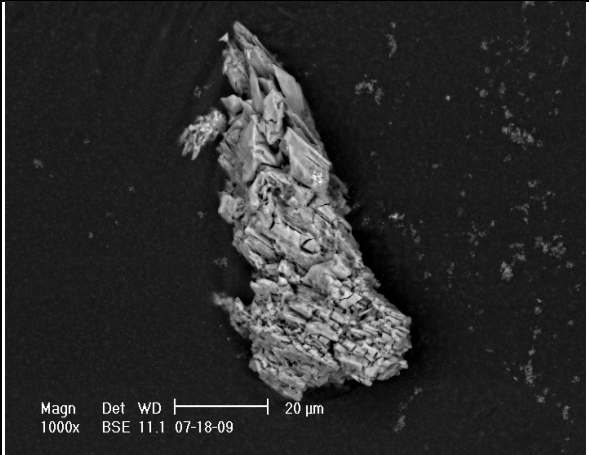
Sample	DC 06_09_141 (1) - PL07-04C-9
Size [μm]	84 x 79
Weight [μg]	~ 0.7

Mineralogical and petrological information by J. Duprat, C. Engrand, M. Maurette and colleagues at CSNSM, University of South Paris, Orsay, France.

- Particle extracted from snow near the CONCORDIA station at Dome C, Central Antarctica (Duprat et al. (2007).
- Crystalline (Xtal) micrometeorite particle.

Figure 153 SEM image showing a similar but not identical micrometeorite to particle DC 06_09_141 (1) - PL07-04C-9 - the same group finding (with courtesy of J. Duprat, C. Engrand, M. Maurette and colleagues).

Figure 154 Backscatter SEM image showing a similar but not identical micrometeorite to particle DC 06_09_141 (1) - PL07-04C-9 - the same group finding (with courtesy of J. Duprat, C. Engrand, M. Maurette and colleagues).

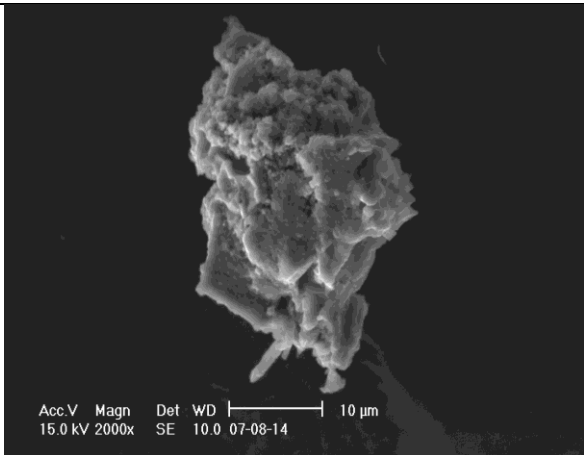*Table X115. SEM and basic information of sample DC 06_09_149 - PL07-05A-5*
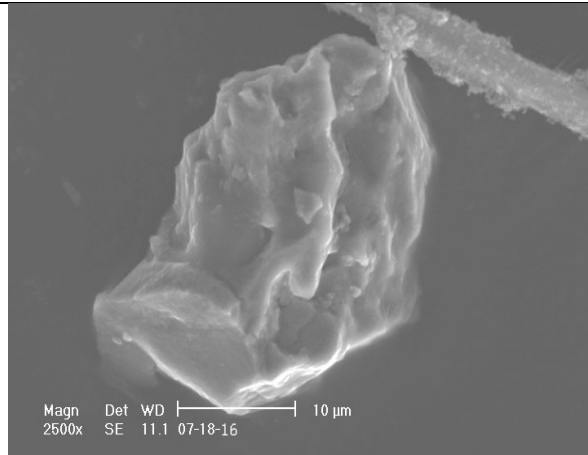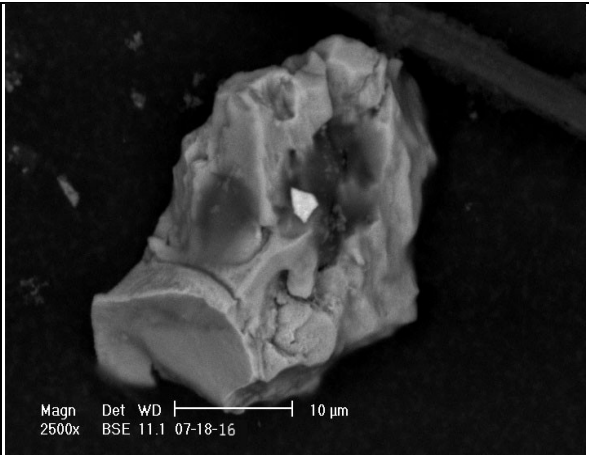
Sample	DC 06_09_149 - PL07-05A-5
Size [μm]	85 x 60
Weight [μg]	~ 0.3

Mineralogical and petrological information by J. Duprat, C. Engrand, M. Maurette and colleagues at CSNSM, University of South Paris, Orsay, France.

- Particle extracted from snow near the CONCORDIA station at Dome C, Central Antarctica (Duprat et al. (2007).
- Crystalline (Xtal) micrometeorite particle.

Figure 155 SEM image showing a similar but not identical micrometeorite to particle DC 06_09_149 - PL07-05A-5 - the same group finding (with courtesy of J. Duprat, C. Engrand, M. Maurette and colleagues).

Figure 156 Backscatter SEM image showing a similar but not identical micrometeorite to particle DC 06_09_149 - PL07-05A-5 - the same group finding (with courtesy of J. Duprat, C. Engrand, M. Maurette and colleagues).

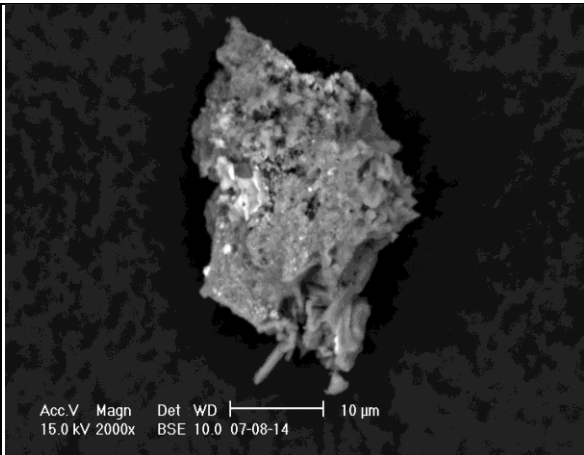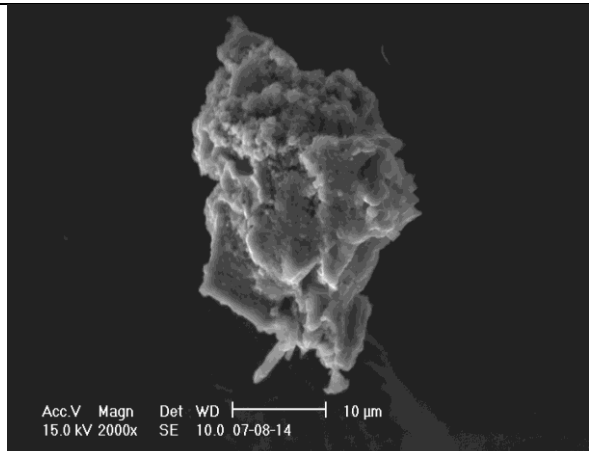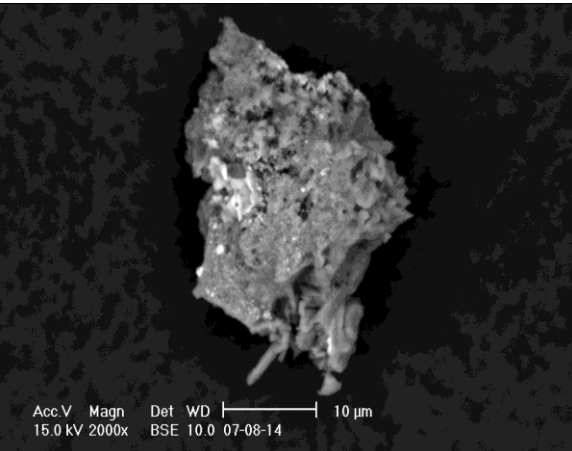*Table X116. SEM and basic information of sample DC 06_09_189 - PL07-06A-9*

Sample	DC 06_09_189 - PL07-06A-9
Size [μm]	93 x 92
Weight [μg]	~ 1.0

Mineralogical and petrological information by J. Duprat, C. Engrand, M. Maurette and colleagues at CSNSM, University of South Paris, Orsay, France.

- Particle extracted from snow near the CONCORDIA station at Dome C, Central Antarctica (Duprat et al. (2007).
- Fine-grained carbonaceous (FgC) to scoriaceous (Sc) micrometeorite particle.

Figure 157 SEM image showing a similar but not identical micrometeorite to particle DC 06_09_189 - PL07-06A-9 - the same group finding (with courtesy of J. Duprat, C. Engrand, M. Maurette and colleagues).

Figure 158 Backscatter SEM image showing a similar but not identical micrometeorite to particle DC 06_09_189 - PL07-06A-9 - the same group finding (with courtesy of J. Duprat, C. Engrand, M. Maurette and colleagues).

F. Calculation specifications used for noble gas measurements on the "Noblesse". Hard-coded using the "NICE" application provided along with the "Noblesse" software from Nu Instruments.

Helium – ^{4}He, ^{3}He and HD/H$_3$ measured on the channeltrons:

```
"Total Number Of Answers ",3
"He4"
"He3"
"HD"
"Spare "
"Spare "
"Spare "
"Spare "
     Dim He4, He3, HD

     He4 = Mass(1,4) - Zero(1,4)
     He3 = Mass(2,4) - Zero(1,4)
     HD = Mass(3,4) - Zero(1,4)

     Result(0) = He4
     Result(1) = He3
     Result(2) = HD
```

Helium – ^{4}He measured on the Faraday detector; ^{3}He and HD/H$_3$ measured on the channeltrons:

```
"Total Number Of Answers ",3
"He4"
"He3"
"HD"
"Spare "
"Spare "
"Spare "
"Spare "
     Dim He4, He3, HD


     He4 = Mass(1,0) - Zero(1,0)
     He3 = Mass(2,4) - Zero(1,4)
     HD = Mass(3,4) - Zero(1,4)

     Result(0) = He4
     Result(1) = He3
     Result(2) = HD
```

Helium gain measured between the Faraday detector and the channeltrons:

```
"Total Number Of Answers ",3
"He4 far"
"He4 count"
"He4 count/far cts/V"
"Spare "
"Spare "
"Spare "
"Spare "
     Dim He4far, He4count

     He4far = Mass(1,0) - Zero(1,0)
     He4count = Mass(2,4) - Zero(1,4)

     Result(0) = He4far
     Result(1) = He4count
     Result(2) = He4count / He4far
```

Neon – ^{20}Ne, ^{21}Ne, ^{22}Ne and interference masses measured on the channeltrons:

```
"Total Number Of Answers ",8
"Ne20"
"Ne21"
"Ne22"
"Ne21/Ne22"
"Ne20/Ne22"
"Ms18"
"Ms40"
"Ms44"
"Spare "
"Spare "
"Spare "
"Spare "
     Dim Ms18, Ne20, Ne21, Ne22, Ms44, Ms40

     Ms18 = Mass(1,4) - Zero(1,4)
     Ne20 = Mass(2,4) - Zero(1,4)
     Ne21 = Mass(3,4) - Zero(1,4)
     Ne22 = Mass(4,4) - Zero(1,4)
     Ms44 = Mass(5,1) - Zero(1,4)
     Ms40 = Mass(5,7) - Zero(1,4)


     Result(0) = Ne20
     Result(1) = Ne21
     Result(2) = Ne22
     Result(3) = Ne21 / Ne22
     Result(4) = Ne20 / Ne22
     Result(5) = Ms18
     Result(6) = Ms40
     Result(7) = Ms44
```

Argon – ^{40}Ar, ^{38}Ar and ^{36}Ar measured on the Faraday detector:

```
"Total Number Of Answers ",5
"Ar40"
"Ar38"
"Ar36"
"Ar40/Ar36"
"Ar38/Ar36"
"Spare "
"Spare "
"Spare "
"Spare "
     Dim Ar40, Ar38, Ar36

     Ar40 = Mass(1,0) - Zero(1,0)
     Ar38 = Mass(2,0) - Zero(1,0)
     Ar36 = Mass(3,0) - Zero(1,0)

     Result(0) = Ar40
     Result(1) = Ar38
     Result(2) = Ar36
     Result(3) = Ar40 / Ar36
     Result(4) = Ar38 / Ar36
```

Argon – ^{40}Ar measured on the Faraday detector; ^{38}Ar, ^{36}Ar measured on the channeltrons:

```
"Total Number Of Answers ",5
"Ar40"
"Ar38"
"Ar36"
"Ar38/Ar36"
"Ar40/Ar36"
"Spare "
"Spare "
"Spare "
"Spare "
     Dim Ar40, Ar38, Ar36


     Ar40 = Mass(1,0) - Zero(1,0)
     Ar38 = Mass(2,4) - Zero(1,4)
     Ar36 = Mass(3,4) - Zero(1,4)

     Result(0) = Ar40
     Result(1) = Ar38
     Result(2) = Ar36
     Result(3) = Ar38 / Ar36
     Result(4) = (Ar40 * 7.12E7) / Ar36
```

Argon – ^{40}Ar and ^{36}Ar measured on the Faraday detector; ^{38}Ar measured on the channeltrons:

```
"Total Number Of Answers ",5
"Ar40"
"Ar38"
"Ar36"
"Ar38/Ar36"
"Ar40/Ar36"
"Spare "
"Spare "
"Spare "
"Spare "
Dim Ar40, Ar38, Ar36


    Ar40 = Mass(1,0) - Zero(1,0)
    Ar38 = Mass(2,4) - Zero(1,4)
    Ar36 = Mass(3,0) - Zero(1,0)

    Result(0) = Ar40
    Result(1) = Ar38
    Result(2) = Ar36
    Result(3) = Ar38 / (Ar36 * 7.12E7)
    Result(4) = Ar40 / Ar36
```

Argon – ^{40}Ar, ^{38}Ar and ^{36}Ar measured on the channeltrons:

```
"Total Number Of Answers ",6
"Ar36"
"Ar38"
"Ar40"
"Ar40/Ar36"
"Ar40/Ar38"
"Ar38/Ar36"
"Spare "
"Spare "
"Spare "
"Spare "
    Dim Ar36, Ar38, Ar40

    Ar36 = Mass(1,4) - Zero(1,4)
    Ar38 = Mass(2,4) - Zero(1,4)
    Ar40 = Mass(3,4) - Zero(1,4)

    Result(0) = Ar36
    Result(1) = Ar38
    Result(2) = Ar40
    Result(3) = Ar40 / Ar36
    Result(4) = Ar40 / Ar38
    Result(5) = Ar38 / Ar36
```

<u>Argon</u> gain measured between the Faraday detector and the channeltrons:

```
"Total Number Of Answers ",3
"Ar_Far"
"Ar_IC"
"Ar_IC/Ar_Far"
"Spare "
"Spare "
"Spare "
"Spare "
    Dim Ar_Far, Ar_IC

    Ar_Far = Mass(1,0) - Zero(1,0)
    Ar_IC = Mass(2,4) - Zero(1,4)

    Result(0) = Ar_Far
    Result(1) = Ar_IC
    Result(2) = Ar_IC / Ar_Far
```

<u>Argon</u> interference masses measured on the channeltrons:

```
"Total Number Of Answers ",3
"Ms35"
"Ms37"
"Ms39"
"Spare "
"Spare "
"Spare "
"Spare "
    Dim Ms35, Ms37, Ms39

    Ms35 = Mass(1,4) - Zero(1,4)
    Ms37 = Mass(2,4) - Zero(1,4)
    Ms39 = Mass(3,4) - Zero(1,4)

    Result(0) = Ms35
    Result(1) = Ms37
    Result(2) = Ms39
```

Krypton - ^{78}Kr, ^{79}Kr, ^{80}Kr, ^{81}Kr, ^{82}Kr, ^{83}Kr, ^{84}Kr a, ^{84}Kr b and ^{86}Kr measured on the channeltrons:

```
"Total Number Of Answers ",9
"Kr84a"
"Kr84b"
"Kr86/Kr84a"
"Kr83/Kr84a"
"Kr82/Kr84a"
"Kr80/Kr84a"
"Kr78b/Kr84b"
"Kr81"
"Kr79"
"Spare "
"Spare "
"Spare "
"Spare "
     Dim Kr86, Kr84a, Kr84b, Kr83, Kr82, Kr81, Kr80, Kr79,
Kr78b


     Kr86 = Mass(1,2) - Zero(1,2)
     Kr84a = Mass(1,4) - Zero(1,4)
     Kr84b = Mass(2,2) - Zero(1,4)
     Kr83 = Mass(1,5) - Zero(1,5)
     Kr82 = Mass(1,6) - Zero(1,6)
     Kr81 = Mass(2,5) - Zero(1,5)
     Kr80 = Mass(1,8) - Zero(1,8)
     Kr79 = Mass(2,7) - Zero(1,7)
     Kr78b = Mass(2,8) - Zero(1,8)



     Result(0) = Kr84a
     Result(1) = Kr84b
     Result(2) = Kr86 / Kr84a
     Result(3) = Kr83 / Kr84a
     Result(4) = Kr82 / Kr84a
     Result(5) = Kr80 / Kr84a
     Result(6) = Kr78b / Kr84b
     Result(7) = Kr81
     Result(8) = Kr79
```

Xenon - ^{124}Xe, ^{126}Xe, ^{128}Xe, ^{129}Xe, ^{130}Xe, ^{131}Xe, ^{132}Xe, ^{134}Xe and ^{136}Xe measured on the channeltrons:

```
"Total Number Of Answers ",18
"X132a"
"X132b"
"X136/X132a"
"X134/X132a"
"X131 / X132a"
"X130 / X132b"
"X129 / X132b"
"X128 / X132b"
"X126 / X132b"
"X124 / X132b"
"X136a / X132a"
"X134a / X132a"
"X131c / X132a"
"X130a / X132a"
"X129 c/ X132a"
"X128a / X132a"
"X126a / X132a"
"X124a / X132a"
"Spare "
"Spare "
"Spare "
"Spare "
Dim X136a, X136b, X134a, X134b, X132a, X132b, X131c, X130a, X130b,
X129c, X128a, X128b, X126a, X126b, X124a, X124b

     X136a = Mass(1,1) - Zero(1,1)
     X136b = Mass(2,2) - Zero(1,2)
     X134a = Mass(1,2) - Zero(1,2)
     X134b = Mass(2,3) - Zero(1,3)
     X132a = Mass(1,3) - Zero(1,3)
     X132b = Mass(2,4) - Zero(1,4)
     X131c = Mass(3,3) - Zero(1,3)
     X130a = Mass(1,4) - Zero(1,4)
     X130b = Mass(2,5) - Zero(1,5)
     X129c = Mass(3,4) - Zero(1,4)
     X128a = Mass(1,5) - Zero(1,5)
     X128b = Mass(2,6) - Zero(1,6)
     X126a = Mass(1,6) - Zero(1,6)
     X126b = Mass(2,7) - Zero(1,7)
     X124a = Mass(1,7) - Zero(1,7)
     X124b = Mass(2,8) - Zero(1,8)

     Result(0) = X132a
     Result(1) = X132b
     Result(2) = (X136b / X132a) * (X134b / X134a)
     Result(3) = X134b / X132a
     Result(4) = X131c / X132a
     Result(5) = X130a / X132b
     Result(6) = X129c / X132b
     Result(7) = (X128a / X132b) * (X130a / X130b)
     Result(8) = (X126a / X132b) * (X128a / X128b) * (X130a / X130b)
     Result(9) = (X124a / X132b) * (X126a / X126b) * (X128a / X128b)
* ( X130a / X130b)
     Result(10) = X136a / X132a
     Result(11) = X134a / X132a
     Result(12) = X131c / X132a
     Result(13) = X130a / X132a
     Result(14) = X129c / X132a
```

```
        Result(15) = X128a / X132a
        Result(16) = X126a / X132a
        Result(17) = X124a / X132a


Total Number Of Answers ",15
"X136 b/ X132b"
"X134b / X132b"
"X131c / X132b"
"X130b/ X132b"
"X129c/ X132b"
" X128 b/ X132b"
" X126b/ X132b"
"X124b/ X132b"
"X136b/ X136a"
"X134b/ X134a"
"X132b/ X132a"
"X130b / X130a"
"X128b / X128a"
"X126b/ X126a"
"X124b / X124a"
"Spare "
"Spare "
"Spare "
"Spare "
Dim X136a, X136b, X134a, X134b, X132a, X132b, X131c, X130a, X130b,
X129c, X128a, X128b, X126a, X126b, X124a, X124b


        X136a = Mass(1,1) - Zero(1,1)
        X136b = Mass(2,2) - Zero(1,2)
        X134a = Mass(1,2) - Zero(1,2)
        X134b = Mass(2,3) - Zero(1,3)
        X132a = Mass(1,3) - Zero(1,3)
        X132b = Mass(2,4) - Zero(1,4)
        X131c = Mass(3,3) - Zero(1,3)
        X130a = Mass(1,4) - Zero(1,4)
        X130b = Mass(2,5) - Zero(1,5)
        X129c = Mass(3,4) - Zero(1,4)
        X128a = Mass(1,5) - Zero(1,5)
        X128b = Mass(2,6) - Zero(1,6)
        X126a = Mass(1,6) - Zero(1,6)
        X126b = Mass(2,7) - Zero(1,7)
        X124a = Mass(1,7) - Zero(1,7)
        X124b = Mass(2,8) - Zero(1,8)


        Result(0) = X136b / X132b
        Result(1) = X134b / X132b
        Result(2) = X131c / X132b
        Result(3) = X130b / X132b
        Result(4) = X129c / X132b
        Result(5) = X128b / X132b
        Result(6) = X126b / X132b
        Result(7) = X124b / X132b


        Result(8) = X136b / X136a
        Result(9) = X134b / X134a
        Result(10) = X132b / X132a
        Result(11) = X130b / X130a
        Result(12) = X128b / X128a
        Result(13) = X126b / X126a
        Result(14) = X124b / X124a
```

References

Ahrens L., Willis J., and Erlank A. (1973) The chemical composition of Kainsaz and Efremovka. *Meteoritics* **8**(2), 133-139.

Alaerts L., Lewis R., and Anders E. (1979) Isotopic anomalies of noble gases in meteorites and their origins--III. LL-chondrites. *Geochimica et Cosmochimica Acta* **43**(9), 1399-1415.

Albrecht A., Schnabel C., Vogt S., Xue S., Herzog G., Begemann F., Weber H., Middleton R., Fink D., and Klein J. (2000) Light noble gases and cosmogenic radionuclides in Estherville, Budulan, and other mesosiderites: Implications for exposure histories and production rates. *Meteoritics & Planetary Science* **35**(5), 975-986.

Alexander E., Lewis R., Reynolds J., and Michel M. (1971) Plutonium-244: Confirmation as an extinct radioactivity. *Science* **172**(3985), 837-840.

Allen J. S. (1947) An Improved Electron Multiplier Particle Counter. *Review of Scientific Instruments* **18(10)**, 739-749.

Amari S., Lewis R. S., and Anders E. (1995) Interstellar grains in meteorites: III. Graphite and its noble gases. *Geochimica et Cosmochimica Acta* **59**(7), 1411-1426.

Amari S. and Ozima M. (1985) Search for the origin of exotic helium in deep-sea sediments. *Nature* **317**(6037), 520-522.

Amari S. and Ozima M. (1988) Extra-terrestrial noble gases in deep sea sediments. *Geochimica et Cosmochimica Acta* **52**(5), 1087-1095.

Amelin Y., Krot A. N., Hutcheon I. D., and Ulyanov A. A. (2002) Lead isotopic ages of chondrules and calcium-aluminum-rich inclusions. *Science* **297**(5587), 1678-1683.

Anders E. (1971) Meteorites and the early solar system. *Annual Review of Astronomy and Astrophysics* **9**, 1-34.

Axford W. (1965) Anisotropic diffusion of solar cosmic rays. *Planetary and Space Science* **13**(12), 1301-1309.

Badjukov D., Brandstätter F., Raitala J., and Kurat G. (2010) Basaltic micrometeorites from the Novaya Zemlya glacier. *Meteoritics & Planetary Science* **45**(9), 1502-1512.

Basford, J. R., Dragon, J. C., Pepin, R. O., Coscio, Jr., M. R., & Murthy, V. R. (1973) Krypton and xenon in lunar fines. *Proceedings of the Lunar and Planetary Science Conference*, Vol. 4, 1915-1955.

Baur H. (1999) A noble-gas mass spectrometer compressor source with two orders of magnitude improvement in sensitivity. *EOS Trans., American Geophysical Union* **46**, Abstract F1118.

Beckerling W., Bischoff A., and Klock W. (1992) Mineralogy and chemistry of micrometeorites from Greenland and Antarctica. *Meteoritics* **27**, 200.

Benkert J. P., Baur H., Signer P., and Wieler R. (1993) He, Ne, and Ar from the solar wind and solar energetic particles in lunar ilmenites and pyroxenes. *Journal of Geophysical Research* **98**(E7), 13147-13162.

Bernatowicz T. J., Croat T. K., and Daulton T. L. (2006) Origin and evolution of carbonaceous presolar grains in stellar environments. In *Meteorites and the early solar system II,* edited by Lauretta D. S. and McSween Jr. H. Y. University of Arizona Press, Tucson. pp. 109–126. ISBN 978-0816525621.

Bischoff A. (2001) Meteorite classification and the definition of new chondrite classes as a result of successful meteorite search in hot and cold deserts. *Planetary and Space Science* **49**(8), 769-776.

Black D. C. and Pepin R. O. (1969) Trapped neon in meteorites--II. *Earth and Planetary Science Letters* **6**(5), 395-405.

Black D. C. (1972a) On the origins of trapped helium, neon and argon isotopic variations in meteorites--I. Gas-rich meteorites, lunar soil and breccia. *Geochimica et Cosmochimica Acta* **36**(3), 347-375.

Black D. C. (1972b) On the origins of trapped helium, neon and argon isotopic variations in meteorites--II. Carbonaceous meteorites. *Geochimica et Cosmochimica Acta* **36**(3), 377-394.

Blanchard M. B., Brownlee D. E., Bunch T. E., Hodge P. W., and Kyte F. T. (1980) Meteoroid ablation spheres from deep-sea sediments. *Earth and Planetary Science Letters* **46**(2), 178-190.

Boss A. P. and Goswami J. N. (2006) Presolar cloud collapse and the formation and early evolution of the solar nebula. In *Meteorites and the early solar system II*, edited by Lauretta D. S. and McSween Jr. H. Y. University of Arizona Press, Tucson. pp. 171-186. ISBN 978-0816525621.

Boss A. P. and Vanhala H. A. (2000) Triggering protostellar collapse, injection, and disk formation. *Space Science Reviews* **92**(1-2), 13-22.

Bouvier A. and Wadhwa M. (2010) The age of the Solar System redefined by the oldest Pb–Pb age of a meteoritic inclusion. *Nature geoscience* **3**(9), 637-641.

Brearley A. J. and Jones R. H. (1998) Chondritic meteorites. In *Planetary Materials*, edited by J. J. Papike. *Reviews in Mineralogy and Geochemistry* **36**(1), 3-1-3-398. ISBN 978-0939950461.

Brinkmann R. (1970) Departures from Jeans' escape rate for H and He in the Earth's atmosphere. *Planetary and Space Science* **18**(4), 449-478.

Britt D. T. and Consolmagno G. J. S. J. (2003) Stony meteorite porosities and densities: A review of the data through 2001. *Meteoritics & Planetary Science* **38**(8), 1161-1180.

Brown H. (1952) Rare gases and the formation of the Earth's atmosphere. In *The Atmospheres of the Earth and Planets,* edited by Kuiper G. P. University of Chicago Press, Chicago. pp. 258-66

Brownlee D. E. (1979) Interplanetary dust. *Reviews of Geophysics* **17**(7), 1735-1743.

Brownlee D. E. (1985) Cosmic dust: Collection and research. *Annual Review of Earth and Planetary Sciences* **13**(1), 147-173.

Brownlee D. E., Olszewski E., and Wheelock M. (1982) A working taxonomy for micrometeorites (abstract). In *Lunar and Planetary Science XIII*. The Lunar and Planetary Institute, Houston. pp.71-72.

Bunch T. E., Wittke J. H., Irving A. J., and Kuehner S. M. (2012) Estimation of Petrologic Subtypes of Unequilibrated Ordinary Chondrites from Systematics of Chromium Distribution in Ferroan Olivine (abstract). In *Lunar and Planetary Science XLIII.* The Lunar and Planetary Institute, Houston. # 2193.

Burnard P., Zimmermann L., and Sano Y. (2013) The Noble Gases as geochemical tracers: History and Backround. In *The Noble Gases as geochemical tracers, Advances in Isotope Geochemistry,* edited by Burnard P. Springer-Verlag Berlin Heidelberg. pp. 1-6. ISBN 978-3642288364.

Busemann H., Baur H., and Wieler R. (2000) Primordial noble gases in "phase Q" in carbonaceous and ordinary chondrites studied by closed system stepped etching. *Meteoritics & Planetary Science* **35**(5), 949-973.

Busemann H., Baur H., and Wieler R. (2001b) Subsolar noble gases in an acid-resistant residue of the EH5 chondrite St. Mark's (abstract). *Meteoritics and Planetary Science Supplement* **36**, #A34.

Busemann H. and Eugster O. (2002) The trapped noble gas component in achondrites. *Meteoritics and Planetary Science* **37**, 1865-1891.

Busemann H., Nguyen A. N., Cody G. D., Hoppe P., Kilcoyne A. L., Stroud R. M., Zega T. J., and Nittler L. R. (2009) Ultra-primitive interplanetary dust particles from the comet 26P/Grigg–Skjellerup dust stream collection. *Earth and Planetary Science Letters* **288**(1), 44-57.

Cameron A. G. W. and Truran J. W. (1977) The supernova trigger for formation of the solar system. *Icarus* **30**(3), 447-461.

Capitaine N., Guinot B., and Klioner S. (2010) Proposal for the re-definition of the astronomical unit of length through a fixed relation to the SI metre. In *Proceedings of the Journées 2010 Systèmes de référence spatio-temporels,* edited by Capitaine N., Observatoire de Paris. pp. 20-23.

Cartwright J. A., Ott U., Mittlefehldt D. W., Herrin J. S., Herrmann S., Mertzman S. A., Mertzman K. R., Peng Z. X., and Quinn J. E. (2013) The Quest for Regolithic Howardites Part 1: Two Trends Uncovered using Noble Gases. *Geochimica et Cosmochimica Acta* **105**, 395-421.

Castagnoli G. and Lal D. (1980) Solar modulation effects in terrestrial production of carbon-14. *Radiocarbon* **22**(2), 133-158.

Chambers, J. E. (2005) Planet Formation. In *Meteorites, Comets and Planets: Treatise on Geochemistry,* Vol. 1, edited by Davis A. M. Executive Editors: Holland H.D. and Turekian K.K. Elsevier-Pergamon, Oxford. pp. 461-475. ISBN 0-08-044720-1.

Chambers J. E. and Wetherill G. W. (1998) Making the terrestrial planets: N-body integrations of planetary embryos in three dimensions. *Icarus* **136**(2), 304-327.

Clayton D. D. (1984) *Principles of stellar evolution and nucleosynthesis*. University of Chicago Press, Chicago. 634 p. ISBN 0-226-10953-4.

Cordier C., Folco L., Suavet C., Sonzogni C., and Rochette P. (2011) Major, trace element and oxygen isotope study of glass cosmic spherules of chondritic composition: The record of their source material and atmospheric entry heating. *Geochimica et Cosmochimica Acta*, **75**(18), 5203-5218.

Cordier C., Folco L., and Taylor S. (2010) Vestoid cosmic spherules from the South Pole Water Well and Transantarctic Mountains (Antarctica): A major and trace element study. *Geochimica et Cosmochimica Acta,***75**(5), 1199-1215.

Cordier C., Suavet C., Folco L., Rochette P., and Sonzogni C. (2012) HED-like cosmic spherules from the Transantarctic Mountains, Antarctica: Major and trace element abundances and oxygen isotopic compositions. *Geochimica et Cosmochimica Acta,* **77**, 515-529.

Cowan II R. L. and Tedmon Jr. C. S. (1973) Intergranular corrosion of iron-nickel-chromium alloys. In *Advances in Corrosion Science and Technology Vol. 3*, edited by Fontana M. G. and Staehle R.W. Springer-Verlag, US. pp. 293-400. ISBN 978-1461582588

Crabb J. and Anders E. (1981) Noble gases in E-chondrites. *Geochimica et Cosmochimica Acta* **45**(12), 2443-2464.

Cremonese G., Borin P., Martellato E., Marzari F., and Bruno M. (2012) New Calibration of the Micrometeoroid Flux on Earth. *The Astrophysical Journal Letters* **749**(2), L40.

Croat T. K., Stadermann F. J., and Bernatowicz T. J. (2005) Presolar graphite from AGB stars: Microstructure and s-process enrichment. *The Astrophysical Journal* **631**(2), 976.

Crowther S. A., Mohapatra R. K., Turner G., Blagburn D. J., Kehm K., and Gilmour J. D. (2008) Characteristics and applications of RELAX, an ultrasensitive resonance ionization mass spectrometer for xenon. *Journal of Analytical Atomic Spectrometry.* **23**(7), 938-947.

Dai Z. R., Bradley J. P., Joswiak D. J., Brownlee D. E., and Genge M. J. (2002) Nano-diamonds in interplanetary dust particles (IDPs), micrometeorites, and meteorites (abstract). In *Lunar and Planetary Science XXXIII.* The Lunar and Planetary Institute, Houston. # 1321.

Demange M. A. (2012) *Mineralogy for Petrologists: Optics, Chemistry, and Occurrences of Rock-forming Minerals.* CRC Press/Balkema, Taylor & Francis Group, London. 218 p. ISBN 978-0415684217.

Dinda G. P., Dasgupta A. K., and Mazumder J. (2009) Laser aided direct metal deposition of Inconel 625 superalloy: Microstructural evolution and thermal stability. *Materials Science and Engineering: A* **509**(1), 98-104.

Dobrică E., Engrand C., Leroux H., and Duprat J. (2010) Investigation of Ultracarbonaceous Antarctic Micrometeorites by Analytical Transmission Electron Microscopy (abstract). In *Lunar and Planetary Science XLI.* The Lunar and Planetary Institute, Houston. # 1613.

Dobrică E., Engrand C., Leroux H., Rouzaud J. N., and Duprat J. (2012) Transmission Electron Microscopy of CONCORDIA UltraCarbonaceous Antarctic MicroMeteorites (UCAMMs): Mineralogical properties. *Geochimica et Cosmochimica Acta*, **76**, 68-82.

Dobrică E., Engrand C., Quirico E., Montagnac G., and Duprat J. (2011) Raman characterization of carbonaceous matter in CONCORDIA Antarctic micrometeorites. *Meteoritics & Planetary Science* **46**(9), 1363-1375.

Dodds D., Strong A. W., and Wolfendale A. W. (1975) Galactic gamma-rays and cosmic ray origin. *Monthly Notices of the Royal Astronomical Society* **171**, 569-577.

Dohnanyi J. S. (1978) Particle dynamics. In *Cosmic Dust,* edited by McDonnell J. A. M. Wiley-Interscience, Chichester. pp. 527-605.

Dones L., Weissman P. R., Levison H. F., and Duncan M. J. (2004) Oort cloud formation and dynamics. In *Comets II (Space Science Series),* edited by Festou M. C., Keller H. U. and Weaver, H. A. University of Arizona Press. pp. 153-174. ISBN 978-0816524501.

Downard K. M. (2004) *Mass spectrometry: a foundation course.* Royal Society of Chemistry, Cambridge. 210 p. ISBN 978-0854046096.

Drozd R. J., Morgan C. J., Podosek F. A., Poupeau G., Shirck J. R., and Taylor G. T. (1977) Plutonium-244 in the early solar system. *The Astrophysical Journal* **212**, 567-569.

Duckworth, H. E., Barber, R. C., and Venkatasubramanian, V. S. (1990). *Mass Spectroscopy Second Editon.* Cambridge University Press, Cambridge. 354 p. ISBN 978-0521386890.

Duprat J., Dobrica E., Engrand C., Aléon J., Marrocchi Y., Mostefaoui S., Meibom A., Leroux H., Rouzaud J. N., Gounelle M., and Robert F. (2010) Extreme Deuterium Excesses in Ultracarbonaceous Micrometeorites from Central Antarctic Snow. *Science* **328**(5979), 742-745.

Duprat J., Engrand C., Maurette M., Kurat G., Gounelle M., and Hammer C. (2007) Micrometeorites from central Antarctic snow: The CONCORDIA collection. *Advances in Space Research* **39**(4), 605-611.

Eberhardt, P., Eugster, O., and Marti, K. (1965). A Redetermination of the Isotopic Composition of Atmospheric Neon. Zeitschrift Naturforschung Teil A **20**, 623.

Ehmann W. and Kohman T. (1958) Cosmic-ray-induced radioactivities in meteorites - II. ^{26}Al, ^{10}Be and ^{60}Co, aerolites, siderites and tektites. *Geochimica et Cosmochimica Acta* **14**(4), 364-379.

Endress M., Keil K., and Bischoff A. (1992) Dark Clasts in the ACFER 059/El Djouf 001 Meteorite (CR) from the Sahara: Implications for their Origins. *Meteoritics* **27**, 218.

Engrand C. and Maurette M. (1998) Carbonaceous micrometeorites from Antarctica. *Meteoritics & Planetary Science* **33**(4), 565-580.

Eugster O. (1988) Cosmic-ray production rates for ^{3}He, ^{21}Ne, ^{38}Ar, ^{83}Kr, and ^{126}Xe in chondrites based on ^{81}Kr-Kr exposure ages. *Geochimica et Cosmochimica Acta* **52**, 1649-1662.

Eugster O., Eberhardt P., and Geiss J. (1967) ^{81}Kr in Meteorites and ^{81}Kr radiation ages. *Earth and Planetary Science Letters* **2**(2), 77-82.

Eugster O., Herzog G., Marti K., and Caffee M. (2006) Irradiation records, cosmic-ray exposure ages, and transfer times of meteorites. In *Meteorites and the early solar system II,* edited by Lauretta D. S. and McSween Jr. H. Y. University of Arizona Press, Tucson. pp. 829-851. ISBN 978-0816525621.

Eugster O. and Michel T. (1995) Common asteroid break-up events of eucrites, diogenites, and howardites and cosmic-ray production rates for noble gases in achondrites. *Geochimica et Cosmochimica Acta* **59**(1), 177-199.

Eugster O., Michel T., Niedermann S., Wang D., and Yi W. (1993) The record of cosmogenic, radiogenic, fissiogenic, and trapped noble gases in recently recovered Chinese and other chondrites. *Geochimica et Cosmochimica Acta* **57**(5), 1115-1142.

Fichtel C. E. (1971) Solar cosmic rays. *Philosophical Transactions of the Royal Society of London. Series A, Mathematical and Physical Sciences* **270**(1202), 167-174.

Fields B. D. and Olive K. A. (2006) Big bang nucleosynthesis. *Nuclear Physics A* **777**, 208-225.

Floss C., Noguchi T., and Yada T. (2012) Ultracarbonaceous Antarctic Micrometeorites: Origins and Relationships to Other Primitive Extraterrestrial Materials (abstract). In *Lunar and Planetary Science XLIII*. The Lunar and Planetary Institute, Houston. # 1217.

Flynn G. J. and McKay D. S. (1988) Meteorites on Mars. In *Workshop on Mars Sample Return Science.* The Lunar and Planetary Institute, Houston. pp. 77-78.

Folco L., Rochette P., Perchiazzi N., D'Orazio M., Laurenzi M. A., and Tiepolo M. (2008) Microtektites from Victoria Land Transantarctic Mountains. *Geology* **36**(4), 291-294.

Fraundorf P. (1980) The distribution of temperature maxima for micrometeorites decelerated in the Earth's atmosphere without melting. *Geophysical Research Letters* **7**(10), 765-768.

Fraundorf P., Flynn G. J., Walker R. M., and Shirck J. (1980) Interplanetary dust collected in the earth's stratosphere-The question of solar flare tracks. In *Proceedings of the Lunar and Planetary Science Conference,* Vol. 11, 1235-1249.

Fuchs L. H., Olsen E., and Jensen K. J. (1973) Mineralogy, mineral-chemistry, and composition of the Murchison (C2) meteorite. *Smithsonian Contributions to the Earth Sciences* **10**, 1-38.

Füri E., Aléon-Toppani A., Marty B., Libourel G., and Zimmermann L. (2013) Effects of atmospheric entry heating on the noble gas and nitrogen content of micrometeorites. *Earth and Planetary Science Letters* **377**, 1-12.

Garrison D., Rao M., and Bogard D. (1995) Solar-proton-produced neon in shergottite meteorites and implications for their origin. *Meteoritics* **30**(6), 738-747.

Genge M. J. (1998) Micrometeorites: Little rocks with a big message. *Geology Today* **14**(5), 177-181.

Genge M. J., Engrand C., Gounelle M., and Taylor S. (2008) The classification of micrometeorites. *Meteoritics & Planetary Science* **43**(3), 497-515.

Genge M. J., Engrand C., and Grady M. M. (2000) The parent bodies of thermally altered fine-grained micrometeorites: comparisons with CI and CM fusion crusts (abstract). *Meteoritics and Planetary Science Supplement***35**, #59.

Genge M. J., Gileski A., and Grady M. M. (2005) Chondrules in Antarctic micrometeorites. *Meteoritics & Planetary Science* **40**(2), 225-238.

Genge M. J., Grady M. M., and Hutchison R. (1996a) Atmospheric alteration in fine-grained Antarctic micrometeorites (abstract). In *Lunar and Planetary Science XXVII*. The Lunar and Planetary Institute, Houston. # 399.

Genge M. J., Hutchison R., and Grady M. M. (1996b) Atmospheric alteration of coarse-grained Antarctic micrometeorites (abstract). *Meteoritics and Planetary Science Supplement* **31**, #49.

Genge M. J. (2006) Igneous rims on micrometeorites. *Geochimica et Cosmochimica Acta* **70**(10), 2603-2621.

Genge M. J., Grady M. M., and Hutchison R. (1997) The textures and compositions of fine-grained Antarctic micrometeorites: Implications for comparisons with meteorites. *Geochimica et Cosmochimica Acta* **61**(23), 5149-5162.

Gerling E. K. and Levskii L. K. (1956) On the origin of the rare gases in stony meteorites. In *Dokl. Akad. Nauk SSS, Vol. 110*, 750-753.

Gilmour J. D., Lyon I. C., Johnston W. A., and Turner G. (1994) RELAX: An ultrasensitive, resonance ionization mass spectrometer for xenon. *Review of scientific instruments* **65**(3), 617-625.

Gleeson L. J. and Axford W. I. (1968) Solar modulation of galactic cosmic rays. *The Astrophysical Journal* **154**, 1011.

Göbel R., Begemann F., and Ott U. (1982) On neutron-induced and other noble gases in Allende inclusions. *Geochimica et Cosmochimica Acta* **46**(10), 1777-1792.

Göbel R., Ott U., and Begemann F. (1978) On Trapped Noble Gases in Ureilites. *Journal of Geophysical Research* **83**(B2), 855-867.

Goldreich P. and Ward W. R. (1973) The formation of planetesimals. *The Astrophysical Journal* **183**, 1051-1062.

Goodrich G. W. and Wiley W. C. (1962) Continuous channel electron multiplier. *Review of Scientific Instruments* **33**(7), 761-762.

Goswami J. N., McGuire R. E., Reedy R. C., Lal D., and Jha R. (1988) Solar flare protons and alpha particles during the last three solar cycles. *Journal of Geophysical Research: Space Physics (1978–2012)* **93**(A7), 7195-7205.

Gounelle M., Chaussidon M., Morbidelli A., Barrat J. A., Engrand C., Zolensky M. E., and McKeegan K. D. (2009) A unique basaltic micrometeorite expands the inventory of solar system planetary crusts. *Proceedings of the National Academy of Sciences* **106**(17), 6904-6909.

Graf T., Baur H., and Signer P. (1990) A model for the production of cosmogenic nuclides in chondrites. *Geochimica et Cosmochimica Acta* **54**(9), 2521-2534.

Greenberg R. and Chapman C. R. (1983) Asteroids and meteorites: Parent bodies and delivered samples. *Icarus* **55**(3), 455-481.

Greenberg R., Wacker J. F., Hartmann W. K., and Chapman C. R. (1978) Planetesimals to planets: Numerical simulation of collisional evolution. *Icarus* **35**(1), 1-26.

Greshake A., Kloeck W., Arndt P., Maetz M., Flynn G. J., Bajt S., and Bischoff A. (1998) Heating experiments simulating atmospheric entry heating of micrometeorites: Clues to their parent body sources. *Meteoritics & Planetary Science* **33**(2), 267-290.

Grimberg A., Baur H., Bochsler P., Bühler F., Burnett D. S., Hays C. C., Heber V. S., Jurewicz A. J. G., and Wieler R. (2006) Solar wind neon from genesis: implications for the lunar noble gas record. *Science* **314**(5802), 1133-1135.

Grossman J. N., Rubin A. E., Nagahara H., and King E. A. (1988) Properties of chondrules. In *Meteorites and the early solar system,* edited by Kerridge J. F. and Matthews M. S. University of Arizona Press, Tucson. pp. 619–659.

Hartquist T. W. and Williams D. A. (1995) *The chemically controlled cosmos: astronomical molecules from the big bang to exploding stars*. Cambridge University Press, Cambridge. 185 p. ISBN 978-0521419833.

Harvey R. P. and Maurette M. (1991) The origin and significance of cosmic dust from the Walcott Névé, Antarctica. In *Proceedings of the Lunar and Planetary Science Conference,* Vol. 21, 569-578.

Haynes W. M., Lide D. R., and Bruno T. J. (Eds.) (2012) *CRC Handbook of Chemistry and Physics 2012-2013*. CRC Press, Taylor & Francis Group Ltd., Boca Raton. 2584 p. ISBN 978-1439880494

Heber V. S., Baur H., Bochsler P., McKeegan K. D., Neugebauer M., Reisenfeld D. B., Wieler R., and Wiens R. C. (2012) Isotopic Mass Fractionation of Solar Wind: Evidence from Fast and Slow Solar Wind Collected by the Genesis mission. *The Astrophysical Journal* **759**(2), 121.

Heber V. S., Wieler R., Baur H., Olinger C., Friedmann T. A., and Burnett D. S. (2009) Noble gas composition of the solar wind as collected by the Genesis mission. *Geochimica et Cosmochimica Acta* **73**(24), 7414-7432.

Heck P. R., Schmitz B., Baur H., and Wieler R. (2008) Noble gases in fossil micrometeorites and meteorites from 470 Myr old sediments from southern Sweden, and new evidence for the L-chondrite parent body breakup event. *Meteoritics & Planetary Science* **43**(3), 517-528.

Heck P. R., Schmitz B., Baur H., Halliday A. N., and Wieler R. (2004) Fast delivery of meteorites to Earth after a major asteroid collision. *Nature* **430**(6997), 323-325.

Hemenway C. L., Soberman R. K., Fullam E. F., Balsamo J. J., Cole J., Hallgren D., Yedinak P., Goodman A., and Hoff G. (1963) Micrometeorite collection from a recoverable sounding rocket. II. *Smithsonian Contributions to Astrophysics* **7**, 93.

Hohenberg C. M., Hudson B., Kennedy B. M., and Podosek F. A. (1981) Xenon spallation systernatics in Angra dos Reis. *Geochimica et Cosmochimica Acta* **45**(10), 1909-1915.

Hohenberg C. M., Podosek F. A., and Reynolds J. H. (1967) Xenon-iodine dating: Sharp isochronism in chondrites. *Science* **156**(3772), 233-236.

Hohenberg C. M., Podosek F. A., Shirck J. R., Marti K., and Reedy R. C. (1978) Comparisons between observed and predicted cosmogenic noble gases in lunar samples. In *Proceedings of the Lunar and Planetary Science Conference,* Vol. 9, 2311-2344.

Hoppe P. and Zinner E. (2000) Presolar dust grains from meteorites and their stellar sources. *Journal of Geophysical Research: Space Physics (1978–2012)* **105**(A5), 10371-10385.

Hörz F., Hartung J. B., and Gault D. E. (1971) Micrometeorite craters on lunar rock surfaces. *Journal of Geophysical Research* **76**(23), 5770-5798.

Hudson G. B., Kennedy B. M., Podosek F. A., and Hohenberg C. M. (1989) The early solar system abundance of Pu-244 as inferred from the St. Severin chondrite. In *Proceedings of the Lunar and Planetary Science Conference*, Vol. 19, 547-557.

Huss G. R. and Lewis R. S. (1994a) Noble gases in presolar diamonds I: Three distinct components and their implications for diamond origins. *Meteoritics* **29**(6), 791-810.

Huss G. R. and Lewis R. S. (1994b) Noble gases in presolar diamonds II: Component abundances reflect thermal processing. *Meteoritics* **29**(6), 811-829.

Iwata N. and Imae N. (2002) Antarctic micrometeorite collection at a bare ice region near Syowa Station by JARE-41 in 2000. *Antarctic Meteorite Research* **15**, 25-37.

Jessberger E. K., Dominik B., Staudacher T., and Herzog G. F. (1980) Ar-40-Ar-39 ages of Allende. *Icarus* **42**, 380-405.

Johnson H. E. and Axford W. I. (1969) Production and loss of He^3 in the Earth's atmosphere. *Journal of Geophysical Research* **74**(9), 2433-2438.

Jousten K. (Ed.) (2008) *Handbook of vacuum technology*. Wiley-VCH Verlag GmbH & Co. KGaA, Weinheim. 1040 p. ISBN 978-3527407231

Kallemeyn G. W., Rubin A. E., Wang D., and Wasson J. T. (1989) Ordinary chondrites: Bulk compositions, classification, lithophile-element fractionations and composition-petrographic type relationships. *Geochimica et Cosmochimica Acta* **53**(10), 2747-2767.

Kallemeyn G. W. and Wasson J. T. (1981) The compositional classification of chondrites—I. The carbonaceous chondrite groups. *Geochimica et Cosmochimica Acta* **45**(7), 1217-1230.

Kehm K., Flynn G. J., Sutton S. R., and Hohenberg C. M. (2002) Combined noble gas and trace element measurements on individual stratospheric interplanetary dust particles. *Meteoritics and Planetary Science* **37**(10), 1323-1335.

Kelley S. (2002) K-Ar and Ar-Ar dating. *Reviews in Mineralogy and Geochemistry* **47**(1), 785-818.

Kimura H., Okamoto H., and Mukai T. (2002) Radiation pressure and the Poynting–Robertson effect for fluffy dust particles. *Icarus* **157**(2), 349-361.

Klačka J. (1992) Poynting-Robertson effect I. Equation of motion. *Earth, Moon, and Planets* **59**(1), 41-59.

Klačka J. (1993) Poynting-Robertson effect: general case. *Earth, Moon, and Planets* **61**(2), 119-124.

Kneubühl F. and Sigrist M. (2008) *Laser.* 7.Auflage. Vieweg+Teubner, GWV Fachverlage GmbH, Wiesbaden. pp. 447. ISBN 978-3835101456.

Koeberl C., Hagen E. H., and Faure G. (1989) Extraterrestrial Spherules from Glacial Sediment in Antarctica: Internal Structure, Mineralogy, and Chemical Composition (abstract). In *Lunar and Planetary Science **XX***. The Lunar and Planetary Institute, Houston. # 528.

König H., Keil K., Hintenberger H., Wlotzka F., and Begemann F. (1961) Investigations on stone meteorites with extremely high inert gas contents, 1, The chondrite Pantar. *Zeitschrift Naturforschung Teil* **16a**, 1124.

Korschinek G., Bergmaier A., Faestermann T., Gerstmann U. C., Knie K., Rugel G., Wallner A., Dillmann I., Dollinger G., Von Gostomski C. L., Kossert K., Maiti M., Poutivtsev M., and Remmert, A. (2010) A new value for the half-life of ^{10}Be by Heavy-Ion Elastic Recoil Detection and liquid scintillation counting. *Nuclear Instruments and Methods in Physics Research Section B: Beam Interactions with Materials and Atoms* **268**(2), 187-191.

Krasinsky G. A., Pitjeva E. V., Vasilyev M., and Yagudina E. (2002) Hidden mass in the asteroid belt. *Icarus* **158**(1), 98-105.

Kruijer T. S., Sprung P., Kleine T., Leya I., Burkhardt C., and Wieler R. (2012) Hf-W chronometry of core formation in planetesimals inferred from weakly irradiated iron meteorites. *Geochimica et Cosmochimica Acta* **99**, 287-304.

Kurat G., Koeberl C., Presper T., Brandstätter F., and Maurette M. (1994) Petrology and geochemistry of Antarctic micrometeorites. *Geochimica et Cosmochimica Acta* **58**(18), 3879-3904.

Lattanzio J. and Forestini M. (1999) Nucleosynthesis in AGB stars. In *Asymptotic Giant Branch Stars,* edited by Le Bertre T., Lebre A. and Waelkens C. - I.A.U. Symposium **191**, 31-40.

Lee J. Y., Marti K., Severinghaus J. P., Kawamura K., Yoo H. S., Lee J. B., and Kim J. S. (2006) A redetermination of the isotopic abundances of atmospheric Ar. *Geochimica et Cosmochimica Acta* **70**(17), 4507-4512.

Levison H. F., Morbidelli A., Dones L., Jedicke R., Wiegert P. A., and Bottke Jr W. F. (2002) The mass disruption of Oort cloud comets. *Science* **296**(5576), 2212-2215.

Lewis R. S., Amari S., and Anders E. (1994) Interstellar grains in meteorites: II. SiC and its noble gases. *Geochimica et Cosmochimica Acta* **58**(1), 471-494.

Leya I., Lange H. J., Neumann S., Wieler R., and Michel R. (2000) The production of cosmogenic nuclides in stony meteoroids by galactic cosmic-ray particles. *Meteoritics & Planetary Science* **35**(2), 259-286.

Leya I. and Masarik J. (2009) Cosmogenic nuclides in stony meteorites revisited. *Meteoritics & Planetary Science* **44**(7), 1061-1086.

Leya I., Neumann S., Wieler R., and Michel R. (2001) The production of cosmogenic nuclides by galactic cosmic-ray particles for 2π exposure geometries. *Meteoritics & Planetary Science* **36**(11), 1547-1561.

Lodders K. (2003) Solar system abundances and condensation temperatures of the elements. *The Astrophysical Journal* **591**(2), 1220-1247.

Love S. G. and Brownlee D. E. (1991) Heating and thermal transformation of micrometeoroids entering the Earth's atmosphere. *Icarus* **89**(1), 26-43.

Love S. G. and Brownlee D. E. (1993) A direct measurement of the terrestrial mass accretion rate of cosmic dust. *Science* **262**(5133), 550-553.

Love S. G. and Brownlee D. E. (1994) Peak atmospheric entry temperature of micrometeorites. *Meteoritics* **29**(1), 69-70.

Lugmair G. W. (1974) Sm-Nd ages: a new dating method. *Meteoritics* **9**, 369.

MacPherson G. J. (2003) Calcium-aluminum-rich inclusions in chondritic meteorites. In *Meteorites, Comets and Planets: Treatise on Geochemistry*, Vol. 1, edited by Davis A. M. Executive Editors: Holland H.D. and Turekian K.K. Elsevier-Pergamon, Oxford. pp. 201-246. ISBN 0-08-044720-1.

Marrocchi Y. and Marty B. (2013) Experimental determination of the xenon isotopic fractionation during adsorption. *Geophysical Research Letters* **40**(16), 4165-4170.

Marti K. (1967) Trapped xenon and the classification of chondrites. *Earth and Planetary Science Letters* **2**(3), 193-196.

Marty B., Matrajt G., Zimmermann L., Engrand C., and Duprat J. (2002) Nitrogen and noble gas isotopes in Antarctic micrometeorites (abstract). In *Lunar and Planetary Science XXXIII*. The Lunar and Planetary Institute, Houston. # 1578.

Marty B., Palma R. L., Pepin R. O., Zimmermann L., Schlutter D. J., Burnard P. G., Westphal A. J., Snead C. J, Bajt S., Becker R. H., and Simones J. E. (2008) Helium and neon abundances and compositions in cometary matter. *Science* **319**(5859), 75-78.

Marty B., Robert P., and Zimmermann L. (2005) Nitrogen and noble gases in micrometeorites. *Meteoritics & Planetary Science* **40**(6), 881-894.

Marvin U. B. and Einaudi M. T. (1967) Black, magnetic spherules from Pleistocene and recent beach sands. *Geochimica et Cosmochimica Acta* **31**(10), 1871-1884.

Maurette M. (2006) *Micrometeorites and the mysteries of our origins*. Springer Verlag Berlin, Heidelberg, New York. 330 p. ISBN 978-3540258162

Maurette M., Brack A., Kurat G., Perreau M., and Engrand C. (1995) Were micrometeorites a source of prebiotic molecules on the early earth? *Advances in Space Research* **15**(3), 113-126.

Maurette M., Duprat J., Engrand C., Gounelle M., Kurat G., Matrajt G., and Toppani A. (2000) Accretion of neon, organics, CO_2, nitrogen and water from large interplanetary dust particles on the early Earth. *Planetary and Space Science* **48**(11), 1117-1137.

Maurette M., Jehanno C., Robin E., and Hammer C. (1987) Characteristics and mass distribution of extraterrestrial dust from the Greenland ice cap. *Nature* **328**, 699-702.

Maurette M., Olinger C., Michel-Levy M. C., Kurat G., Pourchet M., Brandstätter F., and Bourot-Denise M. (1991) A collection of diverse micrometeorites recovered from 100 tonnes of Antarctic blue ice. *Nature* **351**, 44-47.

McGuff P. E., Bushnell D., Soroff H. S., and Deterling Jr R. A. (1963) Studies of the surgical applications of laser (light amplification by stimulated emission of radiation). In *Surgical Forum* **14**. Tufts-New England Center Hospital, Boston. 143-145.

McGuire R. E. and Von Rosenvinge T. T. (1984) The energy spectra of solar energetic particles. *Advances in Space Research* **4**(2), 117-125.

Meier M. M. M., Schmitz B., Baur H., and Wieler R. (2010) Noble gases in individual L chondritic micrometeorites preserved in an Ordovician limestone. *Earth and Planetary Science Letters* **290**(1), 54-63.

Mellon F. (1989) *Chapter 3 - Development and Trends in Instrumentation*. In *Mass Spectrometry,*Vol. 10, edited by Rose M.E. Royal Society of Chemistry. pp. 75-117.

Melosh H. J. (1984) Impact ejection, spallation, and the origin of meteorites. *Icarus* **59**(2), 234-260.

Meshik A., Hohenberg C., Pravdivtseva O., and Burnett D. (2012) Measuring the Isotopic Composition of Solar Wind Noble Gases. In *Exploring the Solar Wind*, edited by Dr. Marian Lazar. InTech. 93-120. ISBN: 978-9535103394. Available from: http://www.intechopen.com/books/exploring-the-solar-wind/measuring-the-isotopic-composition-of-solar-wind-noble-gases.

Messenger S., Keller L., Nakamura-Messenger K., and Ito M. (2007) The Abundance and Distribution of Presolar Materials in Cluster IDPs (abstract). In *Lunar and Planetary Science XXXVIII*. The Lunar and Planetary Institute, Houston. *# 2122*

Michel R. and Neumann S. (1998) Interpretation of cosmogenic nuclides in meteorites on the basis of accelerator experiments and physical model calculations. *Proceedings of the Indian Academy of Sciences-Earth and Planetary Sciences* **107**(4), 441-457.

Mittlefehldt D. W., McCoy T. J., Goodrich C. A., and Kracher A. (1998) Non-chondritic meteorites from asteroidal bodies. In *Planetary Materials*, edited by J. J. Papike. Reviews in Mineralogy and Geochemistry **36**(1), 4-1-4-195. ISBN 978-0939950461.

Modest M. F. (2013) *Radiative heat transfer (3rd edition).* Academic Press/Elsevier, Amsterdam/Oxford. 904 p. ISBN 978-0123869449.

Mohapatra R. K., Schwenzer S. P., and Ott U. (2002) Krypton and Xenon in Martian Meteorites from Hot Deserts--The Low Temperature Component (abstract). In *Lunar and Planetary Science XXXIII*. The Lunar and Planetary Institute, Houston. # 1532.

Mohapatra R. K., Schwenzer S. P., Herrmann S., Murty S. V. S., Ott U., and Gilmour J. D. (2009) Noble gases and nitrogen in Martian meteorites Dar al Gani 476, Sayh al Uhaymir 005 and Lewis Cliff 88516: EFA and extra neon. *Geochimica et Cosmochimica Acta***73**(5), 1505-1522.

Montmerle T., Augereau J. C., Chaussidon M., Gounelle M., Marty B., and Morbidelli A. (2006) Solar system formation and early evolution: the first 100 million years. In *From Suns to Life: A Chronological Approach to the History of Life on Earth,* edited by Gargaud M., Claeys P., López-Garcia P., Martin H., Montmerle T., Pascal R. and Reisse J. Springer-Verlag New York. pp. 39-95. ISBN 978-0387450834

Morbidelli A. and Gladman B. (1998) Orbital and temporal distributions of meteorites originating in the asteroid belt. *Meteoritics & Planetary Science* **33**(5), 999-1016.

Murray J., Renard A. F., and Gibson J. (1891) *Report on deep-sea deposits based on the specimens collected during the voyage of HMS Challenger in the years 1872 to 1876*. Printed for HM Stationery off., by Neill and company.

Nagel K., Neukum G., Fechtig H., and Gentner W. (1976) Density and composition of interplanetary dust particles. *Earth and Planetary Science Letters* **30**(2), 234-240.

Nagy B., Meinschein W. G., and Hennessy D. J. (1961) Mass spectroscopic analysis of the Orgueil meteorite: evidence for biogenic hydrocarbons. *Annals of the New York Academy of Sciences* **93**(2), 27-35.

Nakamura T., Imae N., Nakai I., Noguchi T., Yano H., Terada K., Murakami T., Fukuoka T., Nogami K., and Ohashi H. (1999) Antarctic micrometeorites collected at the Dome Fuji Station. *Antarctic Meteorite Research* **12**, 183-198.

Nakamura T., Noguchi T., Ozono Y., Osawa T., and Nagao K. (2005) Mineralogy of ultracarbonaceous large micrometeorites (abstract). *Meteoritics and Planetary Science Supplement* **40**, #5046.

Nakamura T. and Takaoka N. (2000) Solar-wind derived light noble gases in micrometeorites collected at the Dome Fuji Station: Characterization by stepped pyrolysis. *Antarctic meteorite research* **13**, 311-321.

Neukum G., Mehl A., Fechtig H., and Zähringer J. (1970) Impact phenomena of micrometeorites on lunar surface material. *Earth and Planetary Science Letters* **8**(1), 31-35.

Nguyen A. N. and Messenger S. (2011) Presolar history recorded in extraterrestrial materials. *Elements* **7**(1), 17-22.

Nier A. O. and Schlutter D. J. (1993) The thermal history of interplanetary dust particles collected in the Earth's stratosphere. *Meteoritics* **28**(5), 675-681.

Oetliker M., Klecker B., Hovestadt D., Mason G. M., Mazur J. E., Leske R. A., Mewaldt R. A., Blake J. B., and Looper M. D. (1997) The ionic charge of solar energetic particles with energies of 0.3-70 MeV per nucleon. *The Astrophysical Journal* **477**(1), 495-501.

Olinger C. (1990) Isotopic measurements of solar noble gases in individual micrometeorites from Greenland and Antarctica. *Ph.D. thesis*. Washington University, Seattle, WA (United States), 236 p.

Olinger C. T., Maurette M., Walker R. M., and Hohenberg C. M. (1990) Neon measurements of individual Greenland sediment particles: Proof of an extraterrestrial origin and comparison with EDX and morphological analyses. *Earth and Planetary Science Letters* **100**(1), 77-93.

Osawa T. (2012) Solar Wind Noble Gases in Micrometeorites. In *Exploring the Solar Wind*, edited by Dr. Marian Lazar. InTech. 121-140. ISBN: 978-9535103394. Available from: http://www.intechopen.com/books/exploring-the-solar-wind/solar-wind-noble-gases-in-micrometeorites.

Osawa T. and Nagao K. (2002) Noble gas compositions of Antarctic micrometeorites collected at the Dome Fuji Station in 1996 and 1997. *Meteoritics and Planetary Science* **37**(7), 911-936.

Osawa T., Nagao K., Nakamura T., and Takaoka N. (2000) Noble gas measurement in individual micrometeorites using laser gas-extraction system. *Antarctic Meteorite Research* **13**, 322-341.

Ott U. (1988) Noble gases in SNC meteorites: Shergotty, Nakhla, Chassigny. *Geochimica et Cosmochimica Acta* **52**(7), 1937-1948.

Ott U. (2002) Noble gases in meteorites-trapped components. *Reviews in Mineralogy and Geochemistry* **47**(1), 71-100.

Ott U. and Begemann F. (1985) Are all the 'martian' meteorites from Mars? *Nature* **317**, 509-512.

Ott U., Haubold R., Herrmann S., and Sudek C. (2010) Ureilite Noble Gases Measured by Multiple Ion Counting Mass Spectrometry (abstract). *Meteoritics and Planetary Science Supplement* **73**, #5096.

Ott U. and Hoppe P. (2007) Pre-solar grains in meteorites and interplanetary dust: an overview. *Highlights of Astronomy* **14**, 341-344.

Ott U., Löhr H. P., and Begemann F. (1985) Trapped neon in ureilites: A new component. *Isotopic Ratios in the Solar System* **1**, 129-136.

Ozima M. and Podosek F. A. (2002) *Noble Gas Geochemistry*. Cambridge University Press, Cambridge, UK. pp. 300. ISBN 978-0521803663.

Palme H. and Jones A. (2003) Solar System Abundances of the Elements. In *Meteorites, Comets and Planets: Treatise on Geochemistry*, Vol. 1, edited by Davis A. M. Executive Editors: Holland H.D. and Turekian K.K. Elsevier-Pergamon, Oxford. pp. 41-61. ISBN 0-08-044720-1.

Partington J. (1957) Discovery of radon. *Nature* **179**. 912

Patchett P. J., Vervoort J. D., Söderlund U., and Salters V. J. M. (2004) Lu–Hf and Sm–Nd isotopic systematics in chondrites and their constraints on the Lu–Hf properties of the Earth. *Earth and Planetary Science Letters* **222**(1), 29-41.

Patel C. K. N. (1964) *Continuous-wave laser action on vibrational-rotational transitions of CO_2. Physical review*, **136(**5A), A1187.

Patzer A. and Schultz L. (2002) Noble gases in enstatite chondrites II: The trapped component. *Meteoritics & Planetary Science* **37**(4), 601-612.

Pepin R. O. (1991) On the origin and early evolution of terrestrial planet atmospheres and meteoritic volatiles. *Icarus* **92**(1), 2-79.

Pepin R. O. (2006) Atmospheres on the terrestrial planets: Clues to origin and evolution. *Earth and Planetary Science Letters* **252**(1), 1-14.

Pepin R. O., Becker R. H., and Rider P. E. (1995) Xenon and krypton isotopes in extraterrestrial regolith soils and in the solar wind. *Geochimica et Cosmochimica Acta* **59**(23), 4997-5022.

Pepin R. O., Palma R. L., and Schlutter D. J. (2000) Noble gases in interplanetary dust particles, I: The excess helium-3 problem and estimates of the relative fluxes of solar wind and solar energetic particles in interplanetary space. *Meteoritics & Planetary Science* **35**(3), 495-504.

Pepin R. O. and Signer P. (1994) Memorial to AOC Nier. *Meteoritics* **29**, 747.

Pepin R. O. and Porcelli D. (2002) Origin of noble gases in the terrestrial planets. *Reviews in Mineralogy and Geochemistry* **47**(1), 191-246.

Pepin R. O. and Signer P. (1965) Primordial rare gases in meteorites. *Science* **149**(3681), 253-265.

Podosek F. and Swindle T. (1988) Extinct radionuclides. In *Meteorites and the early solar system*, edited by Kerridge J. F. and Matthews M. S. University of Arizona Press, Tucson. pp. 1093-1113.

Porcelli D., Ballentine C. J., and Wieler R. (2002) An overview of noble gas geochemistry and cosmochemistry. *Reviews in Mineralogy and Geochemistry* **47**(1), 1-19.

Prantzos N. (2012) On the origin and composition of Galactic cosmic rays. *Astronomy and Astrophysics* **538**, 80.

Preibisch T. and Zinnecker H. (1999) The history of low-mass star formation in the upper Scorpius OB association. *The Astronomical Journal* **117**(5), 2381.

Presper T., Kurat G., Koeberl C., Palme H., and Maurette M. (1993) Elemental depletions in Antarctic micrometeorites and Arctic cosmic spherules: Comparison and relationships (abstract). In *Lunar and Planetary Science XXIV*. The Lunar and Planetary Institute, Houston. pp. 1177-1178.

Rai V. K., Murty S. V. S., and Ott U. (2003) Noble gases in ureilites: cosmogenic, radiogenic, and trapped components. *Geochimica et Cosmochimica Acta* **67**(22), 4435-4456.

Raisbeck G. M. and Yiou F. (1987) 10Be and 26Al in micrometeorites from Greenland ice. *Meteoritics* **22**, 485.

Raisbeck G. M. and Yiou F. (1989) Cosmic ray exposure ages of cosmic spherules. *Meteoritics* **24**, 318.

Reedy R. C. (1981) Cosmic-ray-produced stable nuclides: Various production rates and their implications (abstract). In *Lunar and Planetary Science XII*. The Lunar and Planetary Institute, Houston. pp. 871-873.

Reedy R. C. (1985) A model for GCR-particle fluxes in stony meteorites and production rates of cosmogenic nuclides. *Journal of Geophysical Research: Solid Earth (1978–2012)* **90**(S02), C722-C728.

Reedy R. C. (1992) Solar-proton production of neon and argon (abstract). In *Lunar and Planetary Science XXIII*. The Lunar and Planetary Institute, Houston. #1133.

Reedy R. C. and Arnold J. R. (1972) Interaction of solar and galactic cosmic-ray particles with the Moon. *Journal of Geophysical Research* **77**(4), 537-555.

Reedy R. C., Arnold J. R., and Lal D. (1983) Cosmic-ray record in solar system matter. *Annual Review of Nuclear and Particle Science* **33**(1), 505-538.

Reimold W. U., Grieve R. A. F., and Palme H. (1981) Rb-Sr dating of the impact melt from East Clearwater, Quebec. *Contributions to Mineralogy and Petrology* **76**(1), 73-76.

Reynolds J. H. (1960a) I-Xe dating of meteorites. *Journal of Geophysical Research* **65**(11), 3843-3846.

Reynolds J. H. (1960b) Isotopic composition of primordial xenon. *Physical Review Letters* **4**(7), 351.

Richter S., Ott U., and Begemann F. (1994) Multiple ion counting in isotope abundance mass spectrometry. *International Journal of Mass Spectrometry and Ion Processes* **136**(1), 91-100.

Rietmeijer F. J. M., Schramm L. S., Barrett R. A., McKay D. S., and Zook H. A. (1986) An inadvertent capture cell for orbital debris and micrometeorites; The main electronics box thermal blanket of the solar maximum satellite. *Advances in Space Research* **6**(7), 145-149.

Robertson H. P. (1937) Dynamical effects of radiation in the solar system. *Monthly Notices of the Royal Astronomical Society* **97**, 423.

Rochette P., Folco L., Suavet C., Van Ginneken M., Gattacceca J., Perchiazzi N., Braucher R., and Harvey R. P. (2008) Micrometeorites from the Transantarctic Mountains. *Proceedings of the National Academy of Sciences* **105**(47), 18206-18211.

Rudraswami N. G., Parashar K., and Shyam Prasad M. (2011) Micrometer- and nanometer-sized platinum group nuggets in micrometeorites from deep-sea sediments of the Indian Ocean. *Meteoritics & Planetary Science* **46**(3), 470-491.

Rudraswami N. G., Shyam Prasad M., Babu E. V. S. S. K., Vijaya Kumar T., Feng W., and Plane J. M. C. (2012) Fractionation and fragmentation of glass cosmic spherules during atmospheric entry. *Geochimica et Cosmochimica Acta* **99**, 110-127.

Russell H. N. (1916) On the albedo of the planets and their satellites. *Proceedings of the National Academy of Sciences of the United States of America* **2**(2), 74.

Sarda P., Staudacher T., and Allegre C. J. (1991) Complete Rare Gas Study of a Very Large Unmelted Cosmic Dust Particle from Greenland (abstract). In *Lunar and Planetary Science XXII*. The Lunar and Planetary Institute, Houston. #1165.

Scherer P., Schultz L., and Loeken T. (1994) Weathering and atmospheric noble gases in chondrites. In *Noble gas geochemistry and cosmochemistry,* edited by Matsuda J., Tokyo, Terrapub. pp. 43-53.

Schneider E. (1986) Micrometeorite impact on solar panels. In *Photovoltaic generators in space.* European symposium **5**, 171-174.

Schramm L. S., Brownlee D. E., and Wheelock M. M. (1989) Major element composition of stratospheric micrometeorites. *Meteoritics* **24**(2), 99-112.

Schramm L. S., McKay D. S., Zook H. A., and Robinson G. A. (1985) Analysis of micrometeorite material captured by the solar max satellite (abstract). In *Lunar and Planetary Science XVI*. The Lunar and Planetary Institute, Houston. pp. 736-737.

Schultz L. and Franke L. (2004) Helium, neon, and argon in meteorites: A data collection. *Meteoritics & Planetary Science* **39**(11), 1889-1890.

Schultz L., Weber H. W., and Franke L. (2005) Rumuruti chondrites: Noble gases, exposure ages, pairing, and parent body history. *Meteoritics & Planetary Science* **40**(4), 557-571.

Schwenzer S. P., Colindes M., Herrmann S., and Ott U. (2007) Cold Desert's Fingerprints: Terrestrial Nitrogen and Noble Gas Signatures, Which Might be Confused with (Martian) Meteorites Signatures (abstract). In *Lunar and Planetary Science XXXVIII*. The Lunar and Planetary Institute, Houston. #1150.

Scott E. R. D. and Wasson J. T. (1975) Classification and properties of iron meteorites. *Reviews of Geophysics* **13**(4), 527-546.

Shea M. A. and Smart D. F. (1990) A summary of major solar proton events. *Solar Physics* **127**(2), 297-320.

Signer P. and Suess H. (1963) Rare gases in the sun, in the atmosphere, and in meteorites. In *Earth Science and Meteoritics*, edited by Geiss J. and Goldberg E. D. North Holland Publ. Co., Amsterdam. pp. 241-272.

Simpson J. A. (1983) Elemental and isotopic composition of the galactic cosmic rays. *Annual Review of Nuclear and Particle Science* **33**(1), 323-382.

Soberman R. K. and Hemenway C. L. (1963) Micrometeorite collection from a recoverable sounding rocket. III. *Smithsonian Contributions to Astrophysics* **7**, 99.

Soberman R. K., Hemenway C. L., Ryan T. G., Chrest S. A., Frissora J., and Fullam E. F. (1963) Micrometeorite collection from a recoverable sounding rocket. I. *Smithsonian Contributions to Astrophysics* **7**, 89.

Stauffer H. (1961) Primordial argon and neon in carbonaceous chondrites and ureilites. *Geochimica et Cosmochimica Acta* **24**(1), 70-82.

Stern S. A. and Colwell J. E. (1997) Collisional erosion in the primordial Edgeworth-Kuiper belt and the generation of the 30-50 AU Kuiper gap. *The Astrophysical Journal* **490**(2), 879.

Stuart F. M., Harrop P. J., Knott S., and Turner G. (1999) Laser extraction of helium isotopes from Antarctic micrometeorites: Source of He and implications for the flux of extraterrestrial [3]He to earth. *Geochimica et Cosmochimica Acta* **63**(17), 2653-2665.

Suavet C., Alexandre A., Franchi I. A., Gattacceca J., Sonzoghi C., Greenwood R. C., Folco L., and Rochette P. (2009) Oxygen isotope ratios of large cosmic spherules: Carbonaceous and ordinary chondrite parent bodies (abstract). In Lunar and Planetary Science XL. The Lunar and Planetary Institute, Houston. #1776.

Suavet C., Alexandre A., Franchi I. A., Gattacceca J., Sonzogni C., Greenwood R. C., Folco L., and Rochette P. (2010) Identification of the parent bodies of micrometeorites with high-precision oxygen isotope ratios. *Earth and Planetary Science Letters,* **293**(3), 313-320.

Swindle T. D. (2002a) Martian noble gases. *Reviews in Mineralogy and Geochemistry* **47**(1), 171-190.

Swindle T. D. (2002b) Noble gases in the Moon and meteorites: Radiogenic components and early volatile chronologies. *Reviews in Mineralogy and Geochemistry* **47**(1), 101-124.

Swindle T. D. (1988) Trapped noble gases in meteorites. In *Meteorites and the early solar system*, edited by Kerridge J. F. and Matthews M. S. University of Arizona Press, Tucson. pp. 535-564.

Sylvester P. J., Simon S. B., and Grossman L. (1993) Refractory inclusions from the Leoville, Efremovka, and Vigarano C3V chondrites: Major element differences between Types A and B, and extraordinary refractory siderophile element compositions. *Geochimica et cosmochimica acta* **57**(15), 3763-3784.

Taylor S., Herzog G. F., and Delaney J. S. (2007) Crumbs from the crust of Vesta: Achondritic cosmic spherules from the South Pole water well. *Meteoritics & Planetary Science* **42**(2), 223-233.

Taylor S., Lever J. H., and Harvey R. P. (1998) Accretion rate of cosmic spherules measured at the South Pole. *Nature* **392**(6679), 899-903.

Taylor S., Lever J. H., and Harvey R. P. (2000) Numbers, types, and compositions of an unbiased collection of cosmic spherules. *Meteoritics & Planetary Science* **35**(4), 651-666.

Tera F. and Wasserburg G. J. (1972) U-Th-Pb systematics in three Apollo 14 basalts and the problem of initial Pb in lunar rocks. *Earth and Planetary Science Letters* **14**(3), 281-304.

Tonkov E. Y. and Ponyatovsky E. G. (2005) Phase transformations of elements under high pressure. In *Advances in Metallic Alloys Vol. 4,* edited by Fridlyander J. N. and Eskin D. G. CRC press LLC, Boca Raton, FL, USA. 392 p. ISBN 978-0849333675.

Toppani A., Libourel G., Engrand C., and Maurette M. (2001) Experimental simulation of atmospheric entry of micrometeorites. *Meteoritics & Planetary Science* **36**(10), 1377-1396.

Trappitsch R. and Leya I. (2013) Cosmogenic production rates and recoil loss effects in micrometeorites and interplanetary dust particles. *Meteoritics & Planetary Science* **48**, 195-210.

Urey H. C. and Craig H. (1953) The composition of the stone meteorites and the origin of the meteorites. *Geochimica et Cosmochimica Acta* **4**(1), 36-82.

Van Ginneken M., Folco L., Cordier C., and Rochette P. (2012) Chondritic micrometeorites from the Transantarctic Mountains. *Meteoritics & Planetary Science* **47**(2), 228-247.

Van Schmus W. R. and Wood J. A. (1967) A chemical-petrologic classification for the chondritic meteorites. *Geochimica et Cosmochimica Acta* **31**(5), 747-765.

Vogel N., Heber V. S., Baur H., Burnett D. S., and Wieler R. (2011) Argon, Krypton, and Xenon in the bulk solar wind as collected by the Genesis mission. *Geochimica et Cosmochimica Acta* **75**(11), 3057-3071.

Vokrouhlický D. and Farinella P. (2000) Efficient delivery of meteorites to the Earth from a wide range of asteroid parent bodies. *Nature* **407**(6804), 606-608.

Wasson J. T. (1974) Meteorites: Classification and properties. *Minerals and Rocks Vol. 10, Springer-Verlag New York. 327 p.*

Wasson J. T. and Kallemeyn G. W. (1988) Compositions of chondrites. *Philosophical Transactions of the Royal Society of London. Series A, Mathematical and Physical Sciences* **325**(1587), 535-544.

Wasson J. T. and Kimbeblin J. (1967) The chemical classification of iron meteorites—II. Irons and pallasites with germanium concentrations between 8 and 100 ppm. *Geochimica et Cosmochimica Acta* **31**(10), 2065-2093.

Weigel A., Eugster O., Koeberl C., Michel R., Krahenbuhl U., and Neumann S. (1999) Relationships among lodranites and acapulcoites: noble gas isotopic abundances, chemical composition, cosmic-ray exposure ages, and solar cosmic ray effects. *Geochimica et Cosmochimica Acta* **63**(2), 175-192.

Weisberg M. K., McCoy T. J., and Krot A. N. (2006) Systematics and evaluation of meteorite classification. In *Meteorites and the early solar system II*, edited by Lauretta D. S. and McSween Jr. H. Y. University of Arizona Press, Tucson. pp. 19-52. ISBN 978-0816525621.

Westphal A. J., Price P. B., Weaver B. A., and Afanasiev V. G. (1998) Evidence against stellar chromospheric origin of galactic cosmic rays. *Nature* **396**(6706), 50-52.

Whipple F. L. (1949) The theory of micrometeorites. *Popular Astronomy* **57**, 517.

Whipple F. L. (1950) The Theory of Micro-Meteorites: Part I. In an Isothermal Atmosphere*. *Proceedings of the National Academy of Sciences of the United States of America* **36**(12), 687.

Whipple F. L. (1951) The Theory of Micro-Meteorites: Part II. In Heterothermal Atmospheres*. *Proceedings of the National Academy of Sciences of the United States of America* **37**(1), 19.

Whipple F. L. and Wyatt S. P. (1949) The Poynting-Robertson effect on meteor orbits. *The Astronomical Journal* **54**, 138.

Wieler R. (1998) The solar noble gas record in lunar samples and meteorites. *Space Science Reviews* **85**(1), 303-314.

Wieler R. (2002a) Cosmic-ray-produced noble gases in meteorites. *Reviews in Mineralogy and Geochemistry* **47**(1), 125-170.

Wieler R. (2002b) Noble gases in the solar system. *Reviews in Mineralogy and Geochemistry* **47**(1), 21-70.

Wieler R., Anders E., Baur H., Lewis R. S., and Signer P. (1992) Characterisation of Q-gases and other noble gas components in the Murchison meteorite. *Geochimica et Cosmochimica Acta* **56**(7), 2907-2921.

Wieler R. and Baur H. (1994) Krypton and xenon from the solar wind and solar energetic particles in two lunar ilmenites of different antiquity. *Meteoritics* **29**(5), 570-580.

Wieler R., Anders E., Baur H., Lewis R. S., and Signer P. (1991) Noble gases in 'phase Q': Closed-system etching of an Allende residue. *Geochimica et Cosmochimica Acta* **55**(6), 1709-1722.

Wieler R., Grimberg A., and Heber V. S. (2007) Consequences of the non-existence of the "SEP" component for noble gas geo-and cosmochemistry. *Chemical Geology* **244**(3), 382-390.

Wiik H. B. (1956) The chemical composition of some stony meteorites. *Geochimica et Cosmochimica Acta* **9**(5), 279-289.

Wyatt S. P. and Whipple F. L. (1950) The Poynting-Robertson effect on meteor orbits. *The Astrophysical Journal* **111**, 134-141.

Yada T., Floss C., Stadermann F. J., Zinner E., Nakamura T., Noguchi T., and Lea A. S. (2008) Stardust in Antarctic micrometeorites. *Meteoritics & Planetary Science* **43**(8), 1287-1298.

Yada T. and Kojima H. (2000) The collection of micrometeorites in the Yamato meteorite ice field of Antarctica in 1998. *Antarctic Meteorite Research* **13**, 9-18.

Yada T., Nakamura T., Noguchi T., Matsumoto N., Kusakabe M., Hiyagon H., Ushikubo T., Sugiura N., Kojima H., and Takaoka N. (2005) Oxygen isotopic and chemical compositions of cosmic spherules collected from the Antarctic ice sheet: Implications for their precursor materials. *Geochimica et Cosmochimica Acta* **69**(24), 5789-5804.

Zähringer J. and Gentner W. (1960) Uredelgase in einigen Steinmeteoriten. *Zeitschrift Naturforschung Teil* **15A**, 600.

Zeilik M. and Gregory S. A.(1998) Introductory Astronomy and Astrophysics. Saunders Golden Sunburst Series. Cengage Learning, 4th edition. 672 p. ISBN 978-0030062285.

Eidesstattliche Versicherung gemäß § 8 der Promotionsordnung der Naturwissenschaftlich-Mathematischen Gesamtfakultät der Universität Heidelberg

1. Bei der eingereichten Dissertation zu dem Thema

Primordial and other noble gases in micrometeorites
_____

_____

_____

handelt es sich um meine eigenständig erbrachte Leistung.

2. Ich habe nur die angegebenen Quellen und Hilfsmittel benutzt und mich keiner unzulässigen Hilfe Dritter bedient. Insbesondere habe ich wörtlich oder sinngemäß aus anderen Werken übernommene Inhalte als solche kenntlich gemacht.

3. Die Arbeit oder Teile davon habe ich ~~wie folgt~~/bislang nicht[1] an einer Hochschule des In- oder Auslands als Bestandteil einer Prüfungs- oder Qualifikationsleistung vorgelegt.

Titel der Arbeit:_____

_____

Hochschule und Jahr:_____

Art der Prüfungs- oder Qualifikationsleistung:_____

4. Die Richtigkeit der vorstehenden Erklärungen bestätige ich.

5. Die Bedeutung der eidesstattlichen Versicherung und die strafrechtlichen Folgen einer unrichtigen oder unvollständigen eidesstattlichen Versicherung sind mir bekannt.

Ich versichere an Eides statt, dass ich nach bestem Wissen die reine Wahrheit erklärt und nichts verschwiegen habe.

_____   _____
Ort und Datum   Unterschrift

[1] Nicht Zutreffendes streichen. Bei Bejahung sind anzugeben: der Titel der andernorts vorgelegten Arbeit, die Hochschule, das Jahr der Vorlage und die Art der Prüfungs- oder Qualifikationsleistung.

12/2012